ANL-7325
Chemical Separations Processes
for Plutonium and Uranium (TID-4500)
AEC Research and
Development Report

Argonne National Laboratory
9700 South Cass Avenue
Argonne, Illinois 60439

CHEMICAL ENGINEERING DIVISION SEMIANNUAL REPORT

July-December 1966

R. C. Vogel, Division Director
Milton Levenson, Associate Division Director
E. R. Proud, Assistant Division Director
J. Royal

April 1967

Preceding Semiannual Reports:

ANL-7055	January-June, 1965
ANL-7125	July-December, 1965
ANL-7225	January-June, 1966

DISCLAIMER

Table of Contents

SUMMARY

Chemical Engineering Division Semiannual Report

I. Compact Pyrochemical Processes (pages 19 to 49)

Compact pyrochemical processes continue to be developed for the recovery of uranium and plutonium from fast breeder reactor fuels. They possess utility for the recovery of ceramic (oxide and carbide) and metal reactor fuels. In present process concepts, the basic separations are accomplished through differences in the partition behavior of the fuel constituents between liquid metal and salt solvents. Pyrochemical processes incorporating a salt transport separations step are currently under development. Salt transport separations are based on the selective transfer of solutes (fissile and fertile materials) from one liquid metal solution (donor) to another metal solution (acceptor) by cycling a molten salt phase which acts as a carrier between the two metal solutions. A conceptual flowsheet (see Figure I-1) employing a salt transport step for the separation of plutonium from uranium is currently under investigation. Processes utilizing salt transport separations show promise of providing good fission product removal together with high recoveries of plutonium and uranium.

Supporting Chemical Studies of Pyrochemical Processes. In support of development of liquid metal and salt systems for pyrochemical processes, chemical investigations have included (1) measurements of the distribution of uranium, zirconium, and thorium between liquid magnesium alloys and fused salts containing $MgCl_2$, (2) measurements of the solubilities of uranium and zirconium in liquid alloys and (3) the interactions of UO_2 and U_3O_8 with various fused salt mixtures.

The distribution coefficient of uranium (w/o uranium in salt/w/o uranium in metal) between a molten ternary salt mixture containing 50 m/o $MgCl_2$, 30 m/o NaCl and 20 m/o KCl and a liquid Cu-5 w/o Mg alloy was measured as a function of the uranium concentration in the alloy at 750, 800, and 850°C. It was found that the distribution coefficient was independent of the uranium concentration in the liquid alloy from about 0.1 w/o to the solubility limit. These data indicate that the effectiveness of this alloy for use as a uranium donor alloy in the salt transport process will not decrease when the uranium concentration reaches low levels, as it does toward the end of the transfer.

Distribution coefficients were also obtained for uranium between molten 50 m/o $MgCl_2$-30 m/o NaCl-20 m/o KCl and liquid zinc-magnesium alloys saturated with uranium at 600, 700, and 800°C. The results indicate that the distribution coefficients decrease as the magnesium concentration of the alloy is increased; the coefficients reach a minimum value of the order of 10^{-4} and then increase. The minimum value of the distribution coefficient coincides with the maximum value for the solubility of uranium in the liquid alloy. The results indicate that zinc-magnesium alloys would be good acceptor alloys for uranium in a salt transport separation.

Preliminary measurements were made of the distribution coefficients for zirconium between molten $MgCl_2$ and liquid copper-magnesium alloys at 800°C. The magnesium concentration in the alloys varied from 30 to 50 w/o. The distribution coefficient is less than 10^{-4}, and therefore zirconium is not expected to transfer in a salt transport process when copper-magnesium alloys are used as the donor alloys.

A preliminary study was made of the distribution of thorium between molten 50 m/o $MgCl_2$-30 m/o NaCl-20 m/o KCl and liquid magnesium-based alloys, Cu-8 w/o Mg and Zn-10 w/o Mg. The distribution coefficient was about 10^{-3} for the Cu-Mg alloy and about 10^{-4} for the Zn-Mg alloy. These results indicate that uranium could probably be separated from thorium using a salt transport process.

The solubility of uranium in liquid zinc-magnesium alloys was measured at 600, 700, and 800°C. The solubility was found to increase with increasing magnesium concentration to a maximum and then decrease. The values of the maximum uranium solubility at each temperature were as follows: 4.6 w/o U at 600°C and 24.8 w/o Mg; 11.0 w/o U at 700°C and 16.7 w/o Mg; and 18.0 w/o U at 800°C and 10.8 w/o Mg. The maximum in the solubility corresponds to the equilibrium between a solid uranium-zinc intermetallic compound, solid uranium metal and the saturated liquid phase.

The solubility of zirconium in liquid copper-magnesium alloys was measured at 800°C. The solubility

varied from 2.7 w/o Zr in a Cu-49 w/o Mg alloy to 3.9 w/o Zr in a Cu-37.5 w/o Mg alloy.

The effect of small zinc additions on the solubility of uranium in liquid cadmium was studied. At 500°C, where α-uranium is the equilibrium solid phase, the solubility varies from 2.4 w/o U at 0 w/o Zn to 3.0 w/o U at 2.1 w/o Zn. At 470°C, where a uranium-cadmium intermetallic compound is the equilibrium solid phase, the solubility varies from 2.4 w/o U at 0 w/o Zn to 2.0 w/o U at 2.1 w/o Zn. Evidence was found for the substitution of zinc atoms for cadmium atoms in the cadmium-uranium intermetallic phase.

The interaction of UO_2 and U_3O_8 with a variety of molten salts was studied at 800°C. The salts investigated were pure $MgCl_2$, 50 m/o $MgCl_2$-30 m/o NaCl-20 m/o KCl, $MgCl_2$-50 m/o $CaCl_2$ and LiCl-49 m/o KCl eutectic. Uranium dioxide was found to be very insoluble in all salts examined; the uranium content varied from about 5×10^{-3} w/o in LiCl-49 m/o KCl eutectic to 2.9×10^{-2} w/o in pure molten $MgCl_2$. The addition of 5 m/o MgF_2 to each of these systems did not significantly change the uranium concentrations in the salts: 3×10^{-3} w/o in the LiCl-KCl salt and $\sim 1.5 \times 10^{-2}$ w/o in pure $MgCl_2$ and the $MgCl_2$-based salts. The U_3O_8 reacted with the various chloride salts tested to produce UO_2. In the U_3O_8 experiments, the initial uranium content in all the salt mixtures was higher than that found for UO_2; however, as the reaction progressed the uranium content of the salt decreased.

Supporting Engineering Studies of Pyrochemical Processes. The development of the engineering technology required for the separation of plutonium and uranium from fission products by extractions between liquid metal and molten salt phases was continued. Process concepts are being developed on a pilot-plant scale, with the present emphasis on the development of a pyrochemical process which incorporates a salt transport separation step (Figure I-1), which is based on the selective transfer of solutes between two liquid metals in contact with a molten salt.

In this reporting period, engineering feasibility experiments to demonstrate the salt transport separation technique were completed. All of the experiments utilized a batch transfer method* and were carried out with unirradiated feeds consisting of uranium (2 to 5 kg) and selected fission product elements (zirconium, molybdenum, palladium, ruthenium, and niobium; totaling about 0.5 kg). In the last of the experiments (USTP-5), a uranium recovery of about 99% was achieved. The overall removals of fission product elements were as follows: zirconium, 99.7%; molybdenum, 99.9%; palladium and ruthenium, 99.99% (each); and niobium, 99.999%. A product purity of 99.87% was achieved with the major impurities being copper and zirconium. These experiments successfully demonstrated the engineering feasibility of the salt transport separation method. Plans are in progress to conduct similar experiments with plutonium. Calculations indicate that salt transport techniques are especially promising for the processing of plutonium-bearing fuels; in batch contact systems plutonium recoveries exceeding 99.9% may be achieved in a few cycles for high salt/metal ratios.

Multistage extractions between liquid metals and molten salts are required in various future pyrochemical processes to separate rare earth fission products from uranium and plutonium. As a means of effecting this separation, continuous operations offer some potential advantages. In current work, countercurrent, liquid-liquid extraction in a multistage packed column is being investigated. The hydrodynamic behavior of a liquid metal-molten salt system in a packed column has been simulated with a system consisting of water (continuous phase) and a metal alloy (discontinuous phase) melting at a low temperature (71°C). The column was operated at temperatures of 85–90°C. Measurements of the pressure drop of the continuous phase, limiting flows and hold-up of the discontinuous phase were made with a column that was fabricated of glass pipe* and was packed with $\frac{3}{16}$-in. perforated metal saddles to a height (nominal) of 24 in. The pressure drop of the continuous phase, at constant water rate, was found to increase linearly with metal rate until the flooding point was approached at which point the pressure drop suddenly increased. Published flooding correlations for aqueous-organic systems in packed columns were found to give unreliable predictions of the limiting flow rates actually observed in the metal-water system. The hold-up data are being evaluated.

The information obtained from the low-temperature metal-water studies has been used to design a high-temperature column in which the liquids will be a metal and a salt; this information will also be useful in the interpretation of results from the high-temperature studies.

During this reporting period, operation was completed of a loop utilized for testing equipment and instruments in an environment of flowing molten chloride salt (50 m/o $MgCl_2$-30 m/o NaCl-20 m/o KCl). The equipment in the loop included a centrifugal pump,

* In this method, the liquid alloys are in adjacent vessels and the molten salt is cycled between the two vessels by alternately pressuring the bulk of the molten salt through a heated transfer line from one alloy to another.

* The packed portion of the column consisted of a 1-in. ID by 24-in. long section with expanded sections (to 2-in. ID) at the top and bottom.

pressure sensor to measure the pump discharge pressure, a bellows-sealed throttle valve, an orifice flow meter, and a freeze valve. The total operating time accumulated was 1000 hr: 150 hr at 515°C, 550 hr at 550°C, and 300 hr at 600°C. The molten salt was circulated at an average flow rate of 1 gpm; however, flow rates up to 3.5 gpm were reached. With few exceptions, the loop and its components have performed satisfactorily. Design features of the pump are being incorporated into experimental pumps being developed for pyrochemical process equipment. The quantity of corrosion products (iron, nickel, and chromium) and contaminants (oxygen and carbon) in the salt from the loop was undetectable or small.

A materials testing program is being conducted to determine the suitability of various materials of construction for application in pyrochemical flowsheets employing systems consisting of liquid Cu-Mg-U or Zn-Mg-U in combination with molten $MgCl_2$ or $MgCl_2$-based chloride salts.

Several ferrous alloys were tested in these systems at temperatures of 800 and 850°C. The alloys and the test results were as follows:

1. Cast iron and CB-30 cast stainless steel are being tested as potential container materials for Cu-Mg-U/halide salt systems. Previously it was shown that when both materials were exposed to Cu-9.7 w/o Mg-2 w/o U and $MgCl_2$ or 50 m/o $MgCl_2$-30 m/o NaCl-20 m/o KCl, they exhibited low enough corrosion rates to allow service in this system (ANL-7225, pp. 37–39). However, they reacted with the solute uranium to form an adherent surface film. In recent work, this film was identified. The film from the cast iron was identified as uranium phosphide (either UP or U_3P_4) which resulted from the reaction between the solute uranium and the phosphorus in the cast iron. The film from the CB-30 stainless steel showed the presence of a minor phase, U_6Fe, and a major phase, UN, which had formed from the reaction of the uranium with the nitrogen present in the steel. Such reactions are undesirable because they can cause excessive processing losses. The magnitude of the losses that would probably be encountered in process applications has not yet been accurately determined. However, work on these two alloys has been temporarily suspended pending testing of other materials which, at this time, appear more promising.

2. Croloy 16-1, a ferritic stainless steel, and Croloy 9M, which is similar to Croloy 16-1 except for a lower chromium content (9 w/o vs 16 w/o) are under consideration for use in the fabrication of transfer lines for these systems. In recently completed salt transport process demonstration runs, a Croloy 16-1 transfer line was exposed to Cu-Mg-U/$MgCl_2$ and Zn-Mg-U/$MgCl_2$ systems for about 60 hr at 800°C. The line was used for about 200 molten salt transfers between the two liquid alloy phases. The inside of the pipe showed very little corrosion as a result of exposure to the molten salt. However, the ends exposed to the alloy phases did show corrosion (36 mils in Cu-Mg-U, 80 mils in Zn-Mg-U). Despite the corrosion of Croloy 16-1 when exposed to the metal phases, it appears to possess adequate corrosion resistance for limited use in exploratory process runs. Croloy 9M, in the form of agitator blades, was exposed to an Mg-35 w/o Zn-2 w/o U and $MgCl_2$ system at 850°C for 100 hr. The samples exposed to the metal phase and metal-salt interface showed poor resistance (penetrations of 1.1 and 0.9 mm, respectively), whereas the salt and vapor phase samples indicated acceptable corrosion resistance (penetrations of 0.04 and 0.03 mm, respectively). These results suggest that Croloy 9M is an acceptable material for use with molten $MgCl_2$ but not for liquid zinc-magnesium alloys, except for very short periods of time.

3. Both type 304 stainless steel and Tenelon* steel, which are austenitic in structure, were significantly attacked when tested in a Cu-Mg-U/$MgCl_2$ system at 850°C. Specimens of type 304 stainless steel evidenced disintegration (metal phase and metal/salt interface), and formation of a nonadherent reaction film (salt and vapor phases). The Tenelon steel coupons showed extensive attack, probably because of dissolution of contained manganese, in the metal phase (penetrations up to 12 mils in 192 hr) and little or no detectable attack in the other phases. These results suggest that Tenelon possesses some usefulness in containing Cu-Mg-U/$MgCl_2$ systems.

In other work, TZM alloy (0.5 w/o Ti, 0.08 w/o Zr, balance Mo) and molybdenum of low carbon content (0.003 w/o) have been tested for corrosion resistance to these systems at temperatures from 700 to 850°C. When exposed to 66–89 w/o Cu-Mg-1 w/o U and $MgCl_2$ or $MgCl_2$-based chloride salt, the two materials generally showed good corrosion resistance. Further tests with these alloys in the Cu-Mg-U/salt system are planned. In the Zn-Mg-U/salt system tests, TZM alloy exhibited good corrosion resistance, when exposed to Zn-Mg-U/$MgCl_2$ systems at 750–850°C at zinc concentrations below 87 w/o. Molybdenum showed poor corrosion resistance in a test with Zn-5 w/o Mg-1 w/o U and $MgCl_2$-30 m/o NaCl-20 m/o KCl at 700°C. It was also observed in the Zn-Mg-U tests that TZM alloy and molybdenum had lost their normal room-temperature ductility. Possible causes of the high corrosion rate observed for molybdenum and the loss in ductility noted for both TZM alloy and molybdenum are being evaluated.

* Product of U.S. Steel Corporation.

Skull Reclamation Process. After the fuel pins discharged from the EBR-II reactor are melt refined, a residue or skull containing uranium (about 5 to 10% of the melt refining charge) remains in the crucible. To recover and purify this uranium, a skull reclamation process has been developed and successfully demonstrated (ANL-7225, pp. 42–53). This process consists of the following operations. The skull is first oxidized to a free flowing powder, after which the skull oxides are subjected to noble metal extraction, uranium oxide reduction, and uranium metal redissolution steps. The redissolved uranium is retorted to evaporate solvent metals (magnesium and zinc), and the resulting uranium sponge is melted. The recovered uranium is then returned to the melt refining process as makeup material.

Plant equipment for the process has been built and consists of three major equipment items: (1) a skull oxidation furnace, (2) a reduction furnace that utilizes a tungsten crucible and (3) a retorting furnace that utilizes a beryllia crucible. The latter two furnaces are sized for operation on about 5.8 kg of skull oxide (~5 kg of uranium oxide) and have been tested and remotely operated in a large argon-atmosphere enclosure (volume, ~4000 cu ft). The skull oxidation furnace is now in use in the EBR-II Fuel Cycle Facility. As previously reported, the installation of the other two furnaces in the Fuel Cycle Facility has been postponed (ANL-7225, p. 46). The retorting furnace will be used at Argonne, Illinois, however, to investigate retorting operations in other pyrochemical processes.

Following the completion of the second set of skull oxide reduction runs (SRR-11 through SRR-18; ANL-7225, pp. 44–47) an attempt was made to remove accumulated oxide and metal by a technique which would be suitable for remote operation. The furnace was charged with Zn-13 w/o Mg alloy (30 kg) and sufficient salt (70 kg of 47.5 m/o $MgCl_2$-47.5 m/o $CaCl_2$-5 m/o CaF_2) to almost fill the tungsten crucible so as to provide contact with most of the interior surface of the crucible. After agitating the mixture at 800°C the contents of the furnace were discharged. It was subsequently discovered that during the run, some of the salt foamed out of the crucible and partially filled the annular space between the crucible and the Hastelloy C furnace wall. Direct examination revealed cracks in the furnace wall and in the sintered tungsten crucible. The cracking is attributed to stresses resulting from the presence of the solid salt layer and the greater contraction of the Hastelloy C compared with tungsten when the furnace cooled.

Approximately 350 g of uranium had been removed from the furnace in the zinc-magnesium alloy, an amount which represented about 1.1% of the total uranium charged in the last series of runs. An equivalent amount was subsequently removed during direct cleanup of the furnace. Overall accountability of the 32.8 kg uranium charged in the eight runs was about 97.8%.

The performance of the reduction furnace and auxiliaries was considered to have been adequately established in the eighteen process runs (SRR-1 through SRR-18). The failure of the furnace and crucible during the cleanup operation was the result of operating difficulties under nonstandard conditions. Since a decision had been made earlier to postpone the installation of the skull reclamation process in the EBR-II Fuel Cycle Facility, the reduction furnace is not being rebuilt at the present time.

The final step in the skull reclamation process consists of retorting, or solvent evaporation, to recover the product uranium from a zinc-magnesium solution. This product solution has the nominal composition Zn-12 w/o Mg-12 w/o U, weighs about 36 kg (volume, 8 liters), and contains approximately 4 kg of uranium. Plant retorting equipment is being developed to recover the uranium in a form suitable for use as make-up feed material for the melt refining process. Twenty-two additional retorting runs have been completed and have demonstrated high retention of zinc-magnesium vapors within the apparatus, ready release of the uranium product from the crucible and high durability of the beryllia crucibles. Individual crucibles were reused from six to ten times without failure and are considered suitable for additional uses. Although a slight seepage of process solution through the crucible wall is still observed, this is not considered to be a significant deficiency in the present use of the retort. The uranium found in the secondary container is about 0.3% of the retorted product and could be recovered if necessary.

Investigation of Pyrochemical Operations. In the pyrochemical process under development for fast reactor fuels (see Figure I-1) the large quantity of uranium contained in the fuel which is fed to the process is accumulated in a crucible as a uranium-magnesium mixture. Removal and recovery of the uranium by dissolution in a zinc-magnesium solution would require retorting large quantities of magnesium and zinc. Previous experiments (see ANL-7055, p. 67–71) showed that it is possible to break up precipitated uranium in a zinc-magnesium matrix by hydriding the uranium. Equipment is being set up to investigate the use of a hydriding procedure to facilitate the removal of the uranium-magnesium mixture.

An alumina-silica fiber material (Fiberfrax) has been used successfully in the skull reclamation process

to remove residual salt from molten metal product solutions as they are transferred from the reduction furnace. The liquid metal does not wet the Fiberfrax, whereas the molten salt does wet the Fiberfrax and is absorbed. Experiments have been conducted which have demonstrated a high capacity of Fiberfrax for molten salt absorption. This phenomenon is expected to find an application in the removal of a residual salt layer from the surface of a molten metal.

Fuel Cycle Facility Operations. During the current reporting period, 83 irradiated fuel subassemblies from the Experimental Breeder Reactor-II were transferred to the Fuel Cycle Facility (FCF) after short cooling periods, cleaned of sodium, disassembled, and reprocessed by melt refining in 47 batches. From the recovered ingots, 8000 fuel pin castings were made by injection casting, from which 70 new fuel subassemblies were fabricated, almost wholly from reprocessed fuel, for return to the reactor. In order to facilitate accelerated operations, additional subassembly storage capacity was provided in the Air Cell storage pits by the remote installation of pit inserts and cooling manifolds.

In studies of fission product removal from irradiated fuel effected by the melt refining operation, it was determined that over 99.9% of the cesium and barium was removed by a 2-hr liquation period at 1350°C. Removal of cerium, however, is somewhat less effective, and 2.5 to 3 hr at 1400°C are required to assure greater than 98% removal.

The injection casting operation yields a waste stream consisting of crushed Vycor glass molds containing a small amount of fissium alloy from the casting operation. Material accumulated over the past two years (about 24 to 25 kg of refined alloy) has been transferred to the Idaho Chemical Processing Plant for recovery of the uranium by HNO_3 leaching and disposal of leached glass.

The extent of fuel swelling has been determined for Mark IA EBR-II fuel subassemblies [13.5-in. long fuel pin, enriched uranium (~52 a/o ^{235}U)-fissium alloy] after periods of reactor irradiation corresponding to a maximum atom percent burnup of up to 1.2%. The average swelling at this maximum burnup ranged from 10 to 14 v/o, compared to 4.5 to 7 v/o for average Mark I fuel [14.22-in. long fuel pin, enriched uranium (~48 a/o ^{235}U)-fissium alloy] at the same maximum burnup. However, it has also been observed that considerable variations in swelling occur for both Mark I and Mark IA fuel. Some correlation appears to exist between swelling and process operations to which the recycle fuel has been subjected. Fuel which has been melt refined, cast, rejected (for dimensional or similar reasons), and consolidated for recasting appears to swell less than fuel which is accepted for reuse after melt refining. Causes for this behavior are not yet understood but various possibilities are being examined.

A review of the operation of the eight electromechanical manipulators located in the Air Cell and Argon Cell of the FCF for the past four years indicates relatively extensive and satisfactory operation and ease of maintenance. Remote repair or replacement of drive units, power pickup brushes, and grips and forearm has been readily accomplished, and drive units have been overhauled satisfactorily. The carriages have also been removed from the cells for partial decontamination and repair of limit switches, telescoping tubes, and minor mechanical defects.

II. Fluidization and Volatility Processes (pages 50 to 98)

Laboratory Studies—Volatility Processing. Fluorination studies are being carried out in a 2-in. dia. fluid-bed reactor to determine conditions for fluorinating UO_2-PuO_2-fission product pellets that would result in a minimum retention of uranium and plutonium in a fluidized bed of alumina particles. Two fluorinating agents are being evaluated: fluorine and bromine pentafluoride (BrF_5). Fluorination of the pellets is carried out in three steps: In the first step the pellets are oxidized to fines which in the second step are contacted at low temperatures (~300°C) with either fluorine or BrF_5 to remove most of the uranium. In the third step, the fluorination is carried out at higher temperatures (up to 550°C) with 90 v/o fluorine to effect recovery of plutonium and uranium.

The pellets used in this work contained approximately 0.4 w/o plutonium as PuO_2, 86 w/o uranium as UO_2 and 1 w/o fission products as the oxides. In most runs, the charge consisted of 650 g of UO_2-PuO_2-fission product pellets, corresponding to a 2-in. deep pellet bed, and 1100 g of nominal 48 to 100 mesh alumina, corresponding to a static-bed depth of 12 in. Also, 0.6 g CsF was added to the alumina bed in all runs while in several runs with BrF_5 reagent RbF was also added to the alumina bed. In all runs the pellets were initially oxidized with 20 v/o O_2 in nitrogen for 4 hr at 450°C.

The reuse of the alumina bed to process several batches of fuel pellets was evaluated in an effort to reduce plutonium losses in waste solids from a fluid-bed fluoride volatility process. Two techniques were investigated: (1) the use of oxygen, fluorine, and a recycle-fluorination for each of several batches of fuel processed in the same alumina bed, and (2) the use of oxidation followed by uranium fluorination with BrF_5 for each batch of fuel and then a single recycle-

fluorination with fluorine to recover the accumulated plutonium from the alumina bed.

The first technique was evaluated in a series of three runs (Pure-19, -20, and -21). The fluorination sequence for each batch of fuel charge was carried out as follows: 2 hr of fluorination at 350°C with 5 to 16 v/o F_2 was followed by recycle-fluorination for 3 hr at 350°C, 6 hr from 350 to 550°C, and 1 hr at 550°C (in run Pure-21, 4 hr at 550°C was used), giving a total recycle-fluorination period of 33 hr for three batches of fuel pellets. The final bed from run Pure-21 contained 0.009 w/o uranium and 0.009 w/o plutonium; thus, on the basis of 1200 g alumina charged for runs Pure-19, -20, and -21, the final uranium and plutonium concentrations corresponded to fluorination from the alumina bed of more than 99.9% of the uranium and 99% of the plutonium charged to the reactor.

In the alternative alumina reuse scheme, uranium from three successive batches of pellets (runs Purse-10, -11, and -12) was selectively fluorinated with 8 to 10 v/o BrF_5 in nitrogen for 2 hr at 300°C and then plutonium which had accumulated in the bed was fluorinated in 20 hr of recycle-fluorination consisting of 10 hr at 300°C, 5 hr from 300 to 550°C, and 3 hr at 550°C. The final bed from run Purse-12 contained 0.003 w/o U and 0.009 w/o Pu. Based on 1200 g of alumina charged to the reactor for the three runs, these results correspond to removal of 99.9% of the uranium charge and 99% of the plutonium charge. Analyses of bed samples taken during the run showed that the final plutonium content of the bed could have been achieved in only 11 hr of recycle-fluorination rather than the 20 hr actually used.

These results show that the two alternative schemes for the reuse of an alumina bed represent promising methods for minimizing total plutonium losses and reducing the quantity of solid wastes from a fluid-bed fluoride volatility process.

Several experiments were performed to determine the feasibility of recovering plutonium from the alumina bed material by aqueous techniques after the uranium had been recovered by fluorination with BrF_5. Samples of alumina beds resulting from reaction of pulverized pellets with BrF_5 at 300°C were leached with 6*N* HNO_3 at 100°C. More than 99% of the uranium and plutonium was dissolved in 2 hr and 99.9% was dissolved in 5 hr, demonstrating that uranium and plutonium can be readily leached from alumina.

The temperature of uranium fluorination with BrF_5 was shown to affect the extent of plutonium removal during fluorination with fluorine. Using similar recycle-fluorination sequences, final plutonium concentrations of 0.009, 0.007, and 0.012 w/o were obtained when the uranium was fluorinated with BrF_5 at 200, 300, and 400°C, respectively. Based on currently available information, 300°C appears to be the best temperature for fluorination of uranium with BrF_5.

The fluorination of neptunium as well as uranium and plutonium was monitored during reaction with BrF_5 and the subsequent recycle-fluorination with fluorine in run Purse-9. After a BrF_5 fluorination step at 300°C for 2.1 hr, a recycle-fluorination sequence of 3 hr at 300°C, 5 hr from 300 to 550°C, and 3 hr at 550°C was used. The final alumina bed from run Purse-9 contained 0.002 w/o Np, 0.003 w/o U, and 0.005 w/o Pu. These results, together with data taken during the run, indicated that one-half of the original neptunium was volatilized with the uranium hexafluoride during fluorination with BrF_5, while the remainder was recovered with plutonium hexafluoride during fluorination with fluorine.

Rate data for the reaction of U_3O_8 with BrF_5 in the fluid-bed reactor were compared with data previously obtained with a thermobalance. Reaction rate constants at 200, 300, and 400°C were in reasonably good agreement with the data from thermobalance experiments.

Plutonium material balances for nine runs ranged from 87 to 126% with an overall average of about 98%. The sampling procedure for the major source of plutonium, the sodium fluoride traps, was evaluated and shown to give duplicate analyses for uranium and plutonium within the known analytical error.

In experiments performed using the BrF_5 fluorination step, it has been observed that fine particles containing plutonium remain within the fluid-bed reactor after fluorination. In order to determine if plutonium could be recovered from these fines if they were present in the fluid bed during fluorination with fluorine, a sample of the fines was fluorinated in a boat reactor test, using a recycle-fluorination sequence similar to that used in runs Purse-10, -11, and -12. Preliminary results indicate that the plutonium concentration in the fines was reduced from 6.7 to 0.2 w/o, indicating that only 0.4% of the plutonium charge for runs Purse-10, -11, and -12 would have remained in the fines if they had been effectively returned to the reaction zone.

The study of the reaction of BrF_5 with uranium compounds has been concluded with the determination of the kinetics of the reactions with UO_2 and UO_3. Experiments were performed in the temperature range 220 to 300°C and in the BrF_5 partial pressure range 70 to 370 torr. Values of the activation energy of 7.5 and 7.7 kcal mole^{-1} were calculated for the UO_2-BrF_5 and UO_3-BrF_5 reactions, respectively. For UO_2, the coefficient, n, of the pressure term in the equation $k' = Ae^{-E/RT}P^n$ was found to be 0.84 and for UO_3 its

value was 1.05. The following equations were derived to express the dependence on temperature and BrF_5 partial pressure for these reactions.

UO_2-BrF_5:

$$\log k' = 0.84 \log P - 1630/T - 0.270$$

UO_3-BrF_5:

$$\log k' = 1.05 \log P - 1680/T - 0.767$$

A summary of the rate equations derived for the reactions of BrF_5 with UF_4, UO_2F_2, U_3O_8, UO_2, and UO_3 is presented.

The sorption of pure tellurium hexafluoride on various solids was studied at different temperatures in order to identify suitable materials for the removal of TeF_6 from off-gas streams. Sorption rates, capacity of the sorbents for TeF_6, and retention of TeF_6 on the solids under vacuum were determined at various temperatures. Results indicate that activated alumina, Linde type 13X Molecular Sieve, BPL activated charcoal, magnesium fluoride, and copper turnings are promising reagents for the removal of TeF_6 from gas streams. Soda lime, copper (II) oxide, metallic nickel, metallic tellurium, cocoanut charcoal and type 10X Molecular Sieve were shown to be unsuitable. Surface area changes during the sorption process were determined for activated alumina and type 13X Molecular Sieve.

An investigation of instrumental methods of analysis for use with fluoride volatility processes has been initiated. A water-moderated neutron detector using helium-3 proportional counters has been constructed and has been tested with plutonium fluorides. Although the detector exhibits a specific neutron counting rate of 20,800 ± 400 counts per min per g PuF_4, which is sufficiently sensitive and accurate for some process uses, it is desirable to extend the applicability of the detector.

The rate of reaction of NpF_4 with a mixture of 33 v/o BrF_5-67 v/o N_2 has been studied at 300, 325, 350, and 400°C using a boat reactor. The rate of reaction at 300, 325, and 350°C can be described by the diminishing sphere model. Results of rate experiments at 400°C might be better correlated by some other model. The rate of reaction of NpF_4 is lower than the rate of reaction of UF_4 with BrF_5. The activation energy derived from experiments at 300, 325, and 350°C is 26 kcal/mole.

Chemical and X-ray analyses indicate that the solid residue after partial reaction of NpF_4 with BrF_5 is NpF_4. The volatile neptunium product of the reaction is presumed to be NpF_6, but it has not been identified.

A nonvolatile solid is produced by the reaction of NpF_6 with elemental bromine at $\leq$30°C.

Boat reactor experiments have shown that NpF_4 reacts with BrF_3 at 400°C to produce a volatile neptunium compound.

The rates of corrosion of nickel-200, Monel, Duranickel-301, and nickel-200 coupons containing areas of nickel-200 weld or nickel-61 weld, in equimolar solutions of uranium hexafluoride-antimony pentafluoride or uranium hexafluoride-bromine trifluoride were determined for exposures of about 7 hr at 105°C. The results of these experiments indicate that Monel would probably be the best choice of the material of construction for equipment which is to be exposed to uranium hexafluoride-antimony pentafluoride mixtures at temperatures to 100°C. In the presence of uranium hexafluoride-bromine trifluoride mixtures at 100°C, all of the metals examined showed excellent corrosion resistance. No intergranular penetration was found in any of the coupons after exposure to these fluorides.

Engineering-Scale Investigations. Engineering-scale development work is in progress on a fluid-bed fluoride volatility process for the recovery of uranium and plutonium from spent uranium dioxide fuels. Recent emphasis has been placed on the development of a processing scheme involving the use of interhalogens, such as BrF_5, to effect of a separation of the uranium from the plutonium. This step is followed by fluorination with fluorine for plutonium recovery. The steps in the new flowsheet are basically the same as in the previous flowsheet in which both uranium and plutonium were simultaneously converted to volatile hexafluorides by fluorination with fluorine. The processing steps are: decladding, oxidative pulverization of the fuel, fluorination with BrF_5 to separate the uranium as the volatile hexafluoride, and fluorination with fluorine to effect the recovery of the plutonium as the hexafluoride. Subsequent steps for final purification of the PuF_6 and UF_6 may include distillation, thermal decomposition, and selective sorption techniques. Process studies are being demonstrated with nonirradiated uranium-plutonium materials in an engineering-scale alpha facility comprising two large alpha boxes. The larger box contains the main process equipment, and the smaller box houses auxiliary equipment.

A fluorination pilot plant and a converter pilot plant have been installed in the facility and several tests have been performed with plutonium materials. A third unit, a distillation column, has been erected and tested in a mock-up area.

Major emphasis of work has been directed towards development of the fluorination step and gaining an understanding of the behavior of PuF_6 in engineering-scale equipment. The initial fluorinations with 0.5 w/o PuO_2-UO_2-fission product pellets reported in the previous summary report were followed by a cleanup to

remove residual plutonium from the equipment. These cleanup fluorination operations were conducted with all parts of the system (fluorinator, filter sections, secondary filter, lines, cold-traps, and hexafluoride transfer vessels) maintained at temperatures of 300 to 350°C while near-100% fluorine was circulated through the system for periods ranging from 10 to 60 hr. The cleanup was carried out systematically so that the quantity of plutonium from each equipment item could be recovered separately. This was achieved by using several NaF sorption traps to collect the PuF_6. Sorption served as an expedient to avoid the problems associated with cold-trapping and transferring small quantities of PuF_6.

The results of the cleanup operations showed that:

(1) Small (gram) quantities of plutonium were recovered from process lines and the secondary filter, possibly indicating some slight interaction of PuF_6 with construction materials.

(2) Intermediate (several-gram) quantities were recovered from product receivers and from primary filters of the fluorinator. Retention of plutonium within the product receivers was due in part to alpha decomposition and in part to interaction of PuF_6 with the nickel surfaces. Accumulation of plutonium at the primary filters of the fluorinator is associated with the collection of fine particles in this section of the reactor. The temperature of this portion of the reactor during fluorination of oxide fuel is too low to allow conversion of the plutonium in the fines to PuF_6.

(3) Relatively large (decagram) quantities were found only in the primary cold-traps. The holdup of plutonium in the cold-traps is attributed to interaction between the plutonium and a relatively high boiling molybdenum compound, possibly an oxyfluoride. The molybdenum (~1000 ppm as MoO_3) was present in the oxide fuel pellets as a synthetic fission product.

(4) Neutron surveys of the equipment indicated that a complete recovery of the plutonium had been achieved in the cleanup fluorination.

A series of experiments have been performed to develop basic information on the behavior of PuF_6 in the fluorination pilot plant. The experiments were each made with ~135 g of powdered PuF_4 to simulate the plutonium fluorination step of the interhalogen reference flowsheet. The general procedure involved an initial low-temperature (200°C or 300°C) fluorination period, fluorination while the temperature increased to 550°C, and recycle fluorination at 550°C with 100% fluorine. Experiments were of about 20-hr or 50-hr duration. Low gas velocities were employed in the 50-hr experiment. Approximately equal amounts of fluorine were used in the two cases. Towards the end of each experiment, the filter section temperature was increased from the normal 125°C to 300°C to effect recovery of plutonium from the fines accumulated in the filter region.

The initial experiment showed a plutonium recovery of 99%; the value for residual plutonium in alumina was only 0.005 w/o, and represented about 0.25 g of plutonium. Plutonium accounted for was 99.3%. Sorption of the PuF_6 on NaF was employed rather than cold-trapping.

Two subsequent experiments in which CsF was added with the PuF_4 indicated that CsF interfered with plutonium removal from the alumina bed. The residual plutonium concentration in the bed was about 0.08 w/o. Studies on the behavior of plutonium in systems containing CsF are being carried out in laboratory experiments. At the end of this series of experiments it was found that the two sintered Monel metal filters in the fluorinator were badly corroded. Failure had probably occurred during a cleanup period when the temperature in the vicinity of the filters was increased to 375°C. Both filters showed evidence of nickel-fluorine reaction. A limit of 300°C has now been set for plutonium fluorination from the filter sections.

Successful transfers of UF_6 and PuF_6 were carried out between a small supply vessel and a large inverted-U shaped cold trap. Quantities involved were 160.2 g of UF_6 and 89.4 g of PuF_6. Recoveries were 99% and 98.4% for the two materials, respectively. These results indicate that the transport of PuF_6 in engineering-scale equipment is feasibile provided that the equipment has been properly conditioned (prefluorinated with fluorine or, perhaps, even with PuF_6).

An engineering-scale fluid-bed reactor facility has been modified to handle BrF_5 as the fluorinating agent for the processing of UO_2 fuels. Two runs were completed in which fragmented UO_2 fuel was oxidized in a fluid bed of alumina particles to U_3O_8 fines, and the U_3O_8 was fluorinated with BrF_5 to UF_6. The average rates of UF_6 production were 65 and 86 lb UF_6/(hr)(sq ft of reactor cross section) and the average utilization efficiency of BrF_5 was ~60% over the entire period of fluorination. These results are considered highly satisfactory for process application.

Preliminary results have been obtained for the distribution of actinides and fission products in two experiments in which irradiated UO_2 was processed by an O_2-BrF_5-F_2 scheme. These results show that only minor amounts of activities are volatilized during the UO_2 oxidation. The principal activity volatilized was krypton; 17% of the total krypton released during the entire processing sequence was released during this step. In addition to krypton, ^{106}Ru was present in the stack discharge at a concentration that was about 0.6% of the recommended upper limit. During the uranium

volatilization by reaction with BrF_5, about 83% of the krypton, 61% of the ruthenium, and 76% of the molybdenum volatilized with the UF_6. The ruthenium and molybdenum collected with the uranium on soda lime and activated alumina traps. Also, trace amounts of cerium, cesium, niobium, and zirconium volatilized from the fluid-bed reactor. Only very small amounts of ^{106}Ru and ^{125m}Te were detected along with krypton in the stack discharge. During the step in which plutonium was volatilized by reaction with fluorine, about 0.8% of the gross beta and gamma was also volatilized. About 3.5% of the ruthenium and 1.8% of the niobium were collected with the plutonium on a NaF trap. Small amounts (less than 0.1%) of the cesium, cerium, and zirconium were found in an activated alumina trap downstream from the NaF trap. The stack effluent during the plutonium fluorination step contained 3% and 0.001% of the recommended limiting concentrations for ^{106}Ru and ^{125m}Te, respectively.

A fluid-bed process has been developed for the disposal of fluorine using activated alumina (A.A.) as the reactive solid. The process is highly effective, removing greater than 99.9% of the fluorine from a gas stream and utilizing activated alumina to near the theoretical maximum conversion. The process has a capability for high fluorine disposal rates and produces a free-flowing solid product for waste disposal. The reaction between fluorine and activated alumina is characterized by a long initial period during which the fluorine concentration in the reactor off-gas remains at a relatively constant value, less than 50 ppm, and by a breakthrough period in which the concentration of fluorine in the off-gas increases rapidly to greater than 50 ppm. The results of a factorially designed set of experiments indicated that increasing the bed temperature from 300 to 400°C, increasing the bed depth-to-bed diameter ratio from 3 to 6, and decreasing the mean particle size from 399 microns to 183 microns were all effective in increasing the capacity (g fluorine/g A.A.) of activated alumina for fluorine removal. There were no significant effects of varying the fluorine concentration between 5 and 75 v/o or of changing the gas velocity from 1.25 to 1.65 times the minimum fluidizing velocity (V_{mf}). Increasing the gas velocity to 3.0 V_{mf} appeared to decrease the capacity slightly. Other solids reactants, which are less expensive than activated alumina, were given preliminary evaluation. Soda ash appears especially promising.

Basic Mechanisms of Fluidization. The effect of column width on fluidized particle movement during the passage of a gas bubble through the bed is being investigated theoretically and experimentally. The theoretical treatment, based on an ideal fluid, describes the particle movement as being downward near the walls but looping with a net upward displacement in the center of the column. Experimentally, it was observed that the extent of downward movement decreased with an increase in the distance from the bubble to the particle. Particles in the center of the column were initially pushed upwards by the bubble and then fell through the bubble and were collected in the wake of the bubble. It is concluded from both the theoretical and experimental studies that downward particle movement near the walls increases with increasing bubble size and that particle movement is primarily in the vertical direction with negligible horizontal movement.

Theoretical models proposed to predict heat transfer coefficients from a gas-fluidized bed to the wall require knowledge of the residence times of the fluidized particles at the wall. An experimental apparatus has been operated to measure both the particle residence times and the coefficients of heat transfer at the same section of the wall of a fluidized bed. Mean particle residence times were calculated from an analysis of motion picture films. The data obtained in these experiments indicate that heat transfer coefficients increase as the particle residence times decrease.

III. Materials Chemistry and Thermodynamics
(pages 99 to 105)

High Temperature Materials Development. Several manuscripts have been prepared for journal publication on the uranium-urania system, namely, on the phase diagram, on the equilibria between vapor and condensed phases, and on the oxidation-reduction equilibria of urania. The specific objective of these studies was to obtain comprehensive thermodynamic data for compositions ranging from nearly pure uranium to slightly hyperstoichiometric urania; correlation of the experimental results in terms of theoretical concepts is continuing. The composition of congruently vaporizing urania has been measured. It varies from UO_{1997} at 2000°C to $UO_{1.953}$ at 2400°C.

The experimental capacities of the high-temperature materials laboratory are being extended to handling plutonium-bearing systems. Redesign of equipment and ordering of new equipment are now about 90% complete. Projected studies of the U-Pu-O system will include: transpiration measurements of oxygen partial pressures and total vapor pressures as a function of temperature and composition (especially of nonstoichiometric compositions); determination of the hyper- and hypostoichiometric phase boundaries; mass spectrometric investigation of the Pu-O system to clarify uncertainties in the relative importance of the PuO and PuO_2 species; and determination of the congruently effusing composition(s) of plutonia. Plans for carrying

out similar studies of the U-Pu-C system are also under consideration.

A study of the Re-O system has been undertaken in connection with the selection of container materials for plutonia-bearing systems. Results thus far show that rhenium containers will be more stable to oxidation than the tungsten containers used in previous studies. Mass spectrometric analysis of the vapor over rhenium dioxide heated to 850°C and examination of the solid residue indicated that vaporization proceeds mainly by disproportionation according to the equation

$$7\ ReO_2(c) \rightarrow 2\ Re_2O_7(g) + 3\ Re(c).$$

Mass-spectrometric effusion studies of uranium monophosphide have been carried out. The preliminary results give no indication that single-phase uranium monophosphide vaporizes congruently. Instead, they suggest that on vaporization UP tends progressively toward a hypostoichiometric composition until uranium liquid precipitates within the uranium monophosphide matrix. Tentative equations for the partial pressures over hypostoichiometric UP between 1800 and 2150°C were derived from mass spectrometric and weight loss measurements:

$$\log p_U(\text{atm}) = 5.891 - 26{,}270/T;$$

$$\log p_P(\text{atm}) = 8.284 - 31{,}490/T;$$

$$\log p_{P_2}(\text{atm}) = 10.145 - 37{,}350/T.$$

The corresponding partial molar enthalpies of vaporization are (in kcal/mole): $\Delta H(U) = 120.2 \pm 0.3$; $\Delta H(P) = 144.1 \pm 1.5$; $\Delta H(P_2) = 170.9 \pm 4.2$. The enthalpy of formation of uranium monophosphide, $\Delta Hf^\circ_{298}(UP,c)$, was estimated to be -77 ± 5 kcal/mole.

Chemistry of Fast Reactor Fuels. The Chemistry of Fast Reactor Fuels program was initiated as a separate group in July, 1966. A major effort has gone into the organization of the program and studies leading to the selection and generation of detailed specifications for a cave-instrument complex to carry out the program. Work on the extensive modifications of M-4 cell in the Chemistry Division cave facilities is now scheduled to begin in January 1967. Detailed specifications have been generated for the major instruments needed. These include a spark source mass spectrometer, a solid-state radiation analyzer system, a metallograph, and a shielded electron probe analyzer.

The program requires studies of the microstructure of both newly fabricated fuel and the changes which occur in this microstructure with irradiation. Therefore, emphasis has been placed on procedures which are capable of microsampling or microanalysis directly. Microsampling for the spark source mass spectrometer and solid-state radiation analyzers has been achieved with an optically restricted laser pulse. Holes as small as 5 microns in diameter by about 5 microns deep have been obtained with a single pulse.

Other methods of microsampling and analyzing inside the cave facility (e.g., microdrilling, radiographic methods and solid state track detectors) are being evaluated for application to this program. Also, the procedures and equipment for cutting, grinding, polishing, and mounting fuel specimens in the helium atmosphere are being developed.

The first electron probe experiments with irradiated material have been completed. The purpose of these experiments was to find the limitations of the unshielded probe in analyzing irradiated specimens with a minimum mounted sample volume. The conclusion was that the radiation associated with 1 a/o burnup, 1-year-cooled fuel had a negligible effect on the instrument detectors and was not a hazard to the instrument operators. Increased radiation levels will be evaluated and it is expected that an increase by a factor of ten or more can be tolerated. A limited, but significant amount of work undoubtably can be accomplished on the unshielded probe in this manner.

Preparation of Reactor Materials—Ceramic Fuels. The preparation of ceramic fuels is being studied to develop processes which economically fit into appropriate fuel cycles, and to make well-defined fuel compounds for further experimental studies, particularly irradiation studies. At the present time, efforts are being directed toward procedures for preparing uranium and uranium-plutonium carbide fuels.

A series of twelve runs has been conducted to demonstrate the preparation of high purity (U, 15 w/o Pu)C by the fluidized-bed technique. In each run 300 g of U-Pu alloy ($\frac{3}{8}$-in. dia. rods) was hydrided at 250°C to form a powder; this in turn was fluidized and reacted, usually at 800°C, with methane-hydrogen gas mixtures to form the monocarbide. The rate of carburization was determined from the difference between the inlet and outlet methane concentrations and from the gas flow rate. It was found that the operating conditions of pressure, temperature, and methane concentration should be chosen such that free carbon would not form, since formation of free carbon inhibits carbiding. After a carbon content of about 4.2 w/o is reached, the rate of carbiding decreases, but it can be increased by treating the bed with pure hydrogen either at lower temperatures (below 400°C) to cause rehydriding, or at the carbiding temperature to remove a higher carbide (sesquicarbide) reaction layer. It was demonstrated that (U,Pu)C containing less than 1000 ppm oxygen and less than 2[illegible] ppm nitrogen can be produced by the fluidized-bed method at a satisfactory rate for scale-up to an economically feasible process.

Equipment design and operational concepts that would be applicable to a large-scale, remotely operated fluidized-bed process are being tested in the preparation of UC on a scale of 1 kg per batch. The fluidized bed for this work is operated at 10 atm pressure with recirculation of the fluidizing gas, automatic methane concentration control, and product discharge by pneumatic conveying directly from the reactor to a receiver.

Thermobalance experiments using U-20 w/o Pu carbide samples with methane-hydrogen gas mixtures have indicated that the free energy change is less than −7 kcal/mole of (U, 20 w/o Pu)$_2$C$_3$ at 750°C for the reaction:

$$2\ (\mathrm{U,\ 20\ w/o\ Pu})\mathrm{C} + \mathrm{C} \rightleftarrows (\mathrm{U,\ 20\ w/o\ Pu})_2\mathrm{C}_3\ .$$

Calorimetry. The enthalpy of formation of carbon tetrafluoride (tetrafluoromethane) is being determined by fluorine combustion of graphite in a heavy-walled, two-chambered bomb. Quartz thermometry is used in conjunction with automatic print-out of time and temperature data. The calorimetric system has been calibrated by combustions of benzoic acid in oxygen with a precision of 0.02 %. Combustions of both natural and pyrolytic graphites appear to be yielding reliable results.

The energy of the all-gas reaction of phosphorus trifluoride with fluorine to form phosphorus pentafluoride has been measured. From this study, the value $\Delta Hf^{\circ}_{298.15}(\mathrm{PF_3}, \mathrm{g}) = -228.8 \pm 0.4$ kcal mol^{-1} was calculated.

In connection with the study of the reactions of PF_3 with fluorine, and gas reactions generally, a new separation and analytical technique, which combines certain features of both gas chromatography and fractional volatilization, has been developed. The gas mixture is swept through a metal-packed column at low temperatures by a carrier gas. Because of a temperature gradient along the column, the components of the mixture are repeatedly condensed and volatilized according to their vapor pressures and, thereby, fractionated. The fractionated gas then enters a detector (thermal conductivity cell) which, together with the separation column, can be calibrated to identify components of an unknown mixture. For example, minor components in various mixtures were detected at concentrations as low as 0.01 %.

For calorimetric studies of plutonium and its compounds, a rotating bomb calorimeter, gas-charging and -discharging manifold, balances, and other auxiliary equipment have been installed within a glovebox, and solution calorimeter is being built for later installation.

A series of electrical-energy calibration experiments with the flow calorimetric system was carried out. The standard deviation of the mean of the series was 0.01 %. Combustions of uranium monosulfide are now being performed in the system.

As part of a comprehensive effort to examine the nature of chemical bonding in inorganic fluorides, the bond energies of all the chalcogen fluorides have been systematically calculated from experimental data. The peculiarly weak bonding of selenium to fluorine, noticed before in a comparison of the hexafluorides of sulfur, selenium, and tellurium, has now become apparent also in the tetrafluorides and difluorides.

The furnace for the 1500°C drop-type enthalpy calorimeter has been reassembled with tantalum-sheathed heaters and thermocouples, and the 2500°C enthalpy calorimetric system has been completely assembled. Both are undergoing final testing.

Chemistry of Liquid Metals. The chemistry of liquid metals and alloys is being studied to provide basic data for the development and testing of theories of the metallic liquid state. In addition, liquid sodium is under intensive study as a practical contribution to its use as a heat transfer medium in reactors.

Thermodynamic activities of alkali metals in their binary liquid solutions are being measured by atomic absorption spectrophotometry. For the Rb-Cs system at 111°C, the activity coefficients of rubidium in alloys containing 20.3, 35.5, and 51.9 a/o Rb are 0.98, 1.02, and 1.03, respectively. Study of this system was discontinued because the deviation of the activity coefficients from unity, if it exists at all, is expected to be smaller than the experimental uncertainty (±0.03) over the entire composition range.

Solubility of the rare gases in liquid sodium is being determined. The solubility (x) of argon in liquid sodium was remeasured and found to vary between 10^{-9} and 10^{-7} atom fraction over the temperature and pressure ranges 330–530°C and 1–7 atm according to the equation $\log (x/P) = -2.130 - 4542\ T^{-1}$. The enthalpy of solution of argon in liquid sodium was 20.8 ± 2.0 kcal/mole. Preliminary calculations show that a hard-sphere model can account for the magnitude of the solubility and the enthalpy of solution.

Evidence for the existence or nonexistence of molecular complexes in liquid alloys is being sought by ultrasonic investigation. Apparatus has been developed for measuring the velocity of sound in liquid metals. The observed velocity of sound in cadmium at 362°C (2247 m/sec) is in good agreement with literature values. Measurements of sound velocity in mercury were extended over the temperature range from 20 to 330°C. The temperature coefficient of sound velocity was constant over this range, being equal to −0.46 ± 0.02 m/sec/deg.

To gain some insight into the physical and chemical

nature of carbon in liquid sodium, its solubility was measured by the use of radiocarbon-14. The true solubility of elemental carbon in sodium at temperatures up to 450°C is less than 0.005 ppm, in marked contrast to earlier reported values of 5 to 50 ppm.

Radial and vertical segregation of the carbon impurity was observed in a column of sodium subjected to repeated, unidirectional, zone melting. Reduction in the number of zone-melting cycles, from 240 to 25, did not significantly alter the tendency of carbon to segregate either radially or vertically. Subsequently, by means of some simple experiments, it was found that strong radial segregation of the carbon impurity on casting in small-diameter tubes is commonplace.

IV. Reactor Safety (pages 136 to 178)

Thermal Reactor Safety Studies. The experimental program to determine rates and extents of reaction of molten fuel and cladding metals with water is continuing. Experimental studies of the stainless steel-steam reaction were carried out in the high-pressure furnace. Experiments at 1300°C confirmed a previous conclusion that the reaction rate decreased as the effective heat-up time of the sample was increased. The reaction rates at 1300°C were linear. Experiments performed with molten stainless steel at 1500 and 1600°C were accompanied by sample swelling and foaming, resulting in reaction rates that were not reproducible. High rates were associated with an oxide which had a smooth foamy texture, while lower rates were associated with an oxide product which was nodular in appearance.

A brief study of the kinetics of the nickel-steam reaction was also carried out in the high-pressure furnace. The reaction rate of solid nickel at 1400°C was too low to measure accurately; a nominal average rate for a 100-min experiment was 0.11 ml H_2 (STP)/(cm^2)(min). The reaction at 1500 and 1600°C followed an approximately parabolic rate law and was independent of total pressure over the range 1 to 16 atm. The oxide formed during the reaction was NiO, which was observed to be somewhat volatile in steam.

Experiments designed to simulate the environment of the fuel in a water-cooled power reactor following a loss-of-coolant accident were continued. Four experiments were performed in the high-pressure furnace in an attempt to simulate the loss-of-coolant accident under limited steam flow rate conditions. The Zircaloy-2-clad, UO_2-core fuel rods, oxidized under limited steam conditions, showed the development of a zone of concentrated reaction about ⅓ of the way down from the top of the fuel rod. This was believed to be caused by a combination of a vertical temperature gradient (hotter at the top), which promoted reaction at the upper end of the rod, and the limited steam availability, which promoted reaction toward the lower end of the rod (steam flow directly upward). An experiment was also performed by induction heating of a single Zircaloy-2-clad, UO_2-core fuel rod in an attempt to observe some of the features of the meltdown and collapse of the fuel rod. Although preliminary in nature, the experiment indicated that there was no tendency for the molten Zircaloy to drip from the fuel rod. The residue from the experiment indicated that there was some interaction between the molten Zircaloy and the UO_2.

The calculational study to demonstrate the application of metal-water reaction data to the analysis of a loss-of-coolant accident in a reactor was continued. The development of a new computer program (CHEMLOC-I) was completed. The program describes the core heating and chemical reaction up to the time of fuel melting and takes into consideration the effects of evaluating the temperatures of the gas, cladding, and fuel separately. Also considered are the effects of heat transfer by axial conduction in the cladding and fuel, by radial conduction between cladding and fuel, by radial radiation from cladding to cladding, and by convection between the cladding and the flowing gas. The LOFT reactor core was used as a model for the initial CHEMLOC-I calculations. A range of constant steam flow rates through the core from 100 to 10,000 lb/hr and one decreasing steam flow rate were considered. The results indicated that core heatup was prevented for the case of an initial core temperature of 285°C when the steam flow rate was 7500 lb/hr or greater. Fuel melting begins at times from 100 sec to over 1000 sec in every other case calculated. Development of a meltdown calculational model (CHEMLOC-II) is in progress.

A series of three experiments in the Transient Reactor Test Facility (TREAT) were completed which were designed to simulate the meltdown phase of the loss-of-coolant accident. A cluster of three Zircaloy-2-clad, UO_2-core fuel rods was located above a pool of water and subjected to a "flat-top" transient in TREAT during each experiment. Fission heating remained reasonably constant over periods of 12, 32, and 50 sec, respectively, for the three experiments. Fuel failure occurred in each experiment and the total metal-water reaction for the three experiments varied from 30 to 44%. An encouraging result of the experiments was the absence of "spike" pressure rises. This observation indicates that no steam explosions occurred

as the partially molten fuel and cladding material entered the water pool.

The series of photographic experiments in TREAT was extended to include stainless steel-clad and Zircaloy-2-clad, UO_2-core fuel. High speed motion pictures recorded the response of single fuel rods, submerged in water in transparent autoclaves, to destructive neutron bursts in TREAT. One experiment was performed with a stainless steel-clad fuel rod in which the fission energy generation was 290 cal/g UO_2. The fuel rod retained its cylindrical form; however, extensive cladding failure occurred. The motion pictures indicated that cladding surface heating was very irregular. This was confirmed by the final appearance of the fuel rod which showed that cladding-water reaction and oxide foaming had occurred in patches. Three transient experiments were performed with a single Zircaloy-2-clad, UO_2-core fuel rod. The pulsed irradiations resulted in fission energy inputs of 165, 305, and 347 cal/g UO_2. Indications were that only minor damage to the fuel rod was produced during the first two transients. Extensive cladding damage and the release of some molten fuel occurred as a result of the third transient. The results of the experiments indicated that both stainless steel and Zircaloy-2 cladding are very effective in containing molten UO_2 in an environment of subcooled water.

Fast Reactor Safety Studies. The program of studies of potential problems in the field of fast reactor safety has continued. As part of this program, studies are in progress of transient heat transfer from heated metal spheres to sodium and to water. Such data are required in order to analyze adequately the consequences of an incident in a reactor (either fast or thermal) in which hot fuel materials may be dispersed into the liquid coolant and thus cause explosive vapor generation. A theoretical equation was developed for the special case of highly subcooled liquid where nearly all of the heat is transferred into the bulk liquid. A method for estimating the thickness of the vapor film surrounding the hot spheres was also derived from theoretical considerations.

Experimental determinations of heat fluxes from a heated ½-in. dia. tantalum sphere to liquid sodium were completed for sphere velocities of 6 and 10 ft/sec and sodium temperatures of 300 and 450°C. Initial sphere temperatures ranged up to 1980°C. A computer program was developed to reduce the experimental temperature-time data to yield instantaneous heat flux-surface temperature data points. Instantaneous values of heat flux as high as 2700 cal/(cm²)(sec) have been calculated. The experimental heat flux data were compared with the theoretical expression. It was found that the data could best be accounted for in terms of liquid superheating. Thickness of the vapor film separating the hot sphere from the superheated liquid was determined to be negligibly small.

Experimental studies of the heat flux from heated ¼-in. dia. spheres to water were performed with silver spheres in a new motor-driven swinging-arm apparatus. Experiments employed very short immersion times of 19 to 31 msec at velocities of 12 to 19 ft/sec. Values of heat flux as high as 450 cal/(cm²)(sec) were obtained. Within a scatter band up to surface temperatures of the order of 300 to 400°C, the experimental results were described by the same theoretical expression employed to describe the sodium experiments. Above surface temperatures of the order of 300 to 400°C, the heat flux decreased, indicating the formation of a vapor film.

Preparations are continuing for a forthcoming series of energetic fuel meltdown tests in a sodium environment in TREAT. Design and construction of the in-pile assembly has been completed. Nine rods, 5 of which are fueled with 10%-enriched UO_2 pellets, are located in an environment of liquid sodium. A piston which is coupled to a linear motion transducer is located directly above the liquid level. The liquid sodium is coupled directly to a pressure transducer. Records from the linear motion transducer and the pressure transducer are expected to yield the detailed course of the development of the pressure pulse resulting from fuel destruction.

Work is proceeding on the program to measure the heat capacity of liquid uranium dioxide. Experiments have been made to test materials, fabrication methods, and design of sample capsules. In addition, design and construction of an appropriate calorimeter system is under way.

Calculation of the effects of plutonium migration in initially homogeneous PuO_2-UO_2 fuels under a thermal gradient indicates that significant alteration of the Doppler shutdown capability is not likely in the cases considered; however, changes in the local composition because of the migration could lower the melting point of such regions. These regions might then be at a temperature near their melting point in certain situations. Preliminary experiments to test the thermal gradient furnace for extended use are in progress. Pellets of UO_2-CeO_2 are being heated continuously for periods up to 500 hr. In a gradient of approximately 1000°C/cm, pore migration toward the hotter end of the pellets was observed; columnar grain growth also occurred in this area.

The experimental study of the transient pressure and the aerosol produced by the liquid sodium-air reac-

tion in simulated spray-type accidents is continuing. An apparatus has been constructed in which a pneumatically operated piston will spray sodium through suitable orifices into a reaction chamber of known volume. Preliminary tests of the apparatus using water as the driven fluid have been made.

V. Energy Conversion (pages 179 to 196)

Lithium Hydride Cells. Basic studies associated with the lithium hydride cell have continued, with emphasis on the fused salt electrolyte. The phase diagrams for the ternary system LiH-LiCl-LiI and its component binaries have been determined. All of these systems exhibit simple eutectic behavior. Of particular interest is the fact that the ternary eutectic has a melting point of 332.9°C. This low temperature aids in the maximization of the Carnot cycle efficiency for the total system.

A thermodynamic analysis of the LiH-LiCl phase diagram has indicated that the large deviations from ideality found for this system were consistent with an association of the LiCl to form such species as $LiCl_2^-$. Such an association would be accompanied by a decrease of the ionic conductance. With this in mind, the conductivity of the LiH-LiCl system is being investigated. The results now available indicate that the conductance of LiH-LiCl mixtures is much lower than would be expected from the values of the two components. This result is consistent with the idea of association.

Because of the thermodynamic indications of the possible existence of such species as $LiCl_2^-$ in the LiH-LiCl system, it is appropriate that an attempt be made to observe the presence of such a species by a relatively direct method such as spectroscopy. A laser-excited Raman spectroscope has been constructed and tested on fused salts. Only preliminary results have been obtained on the LiH-LiCl system. It is still too early to tell whether or not $LiCl_2^-$ or some similar species exists in this system at concentrations high enough to yield a detectable Raman spectrum.

Bimetallic Cells. The research work on bimetallic cells has been concerned with emf measurements of candidate couples, electrolyte phase diagrams, and vapor pressure studies for evaluation of thermal regeneration problems. All of these three programs yield basic thermodynamic data, highly useful in their own right.

Because of the fact that lithium metal is not very soluble in its halides, there is only an insignificant error in the emf measurements due to the electronic conduction associated with dissolved lithium. The emf values for several lithium-containing couples have been measured and were reported previously. Currently, the emf's for lithium-selenium and lithium-tellurium cells are being determined. Sodium metal, however, has a high enough solubility in its halides that special experimental techniques are necessary in order to avoid the errors caused by the electronic conduction associated with the dissolved sodium. These techniques are being developed.

In order to establish the compositions of the lowest-melting fused salt electrolytes for bimetallic cells, the phase diagrams of promising lithium and sodium halide systems have been determined. For cells with sodium anodes, the NaF-NaCl-NaI system is appropriate, with a eutectic temperature of 529.4°C. For lithium anode cells, significantly lower temperatures are available because of the lower melting points of various eutectic and minimum-melting compositions. Experiments have begun on the LiBr-LiI and LiF-LiCl-LiI systems.

Vapor pressure and vapor phase compositions have been determined for the sodium-bismuth and sodium-lead systems. The thermodynamic analysis of the sodium-bismuth system has uncovered some interesting features which are consistent with the existence of NaBi and Na_3Bi in the liquid phase. Good agreement is obtained between the experimentally determined activity coefficients and those calculated on the basis of a quasi-ideal thermodynamic model for the system, including NaBi and Na_3Bi as species. Analysis of the results for the sodium-lead system is proceeding.

Laboratory-scale engineering studies on the sodium-bismuth and sodium-lead cells have continued. The sodium-bismuth cell which was accidentally shut down after over 17 months of continuous operation has been cleaned, inspected for corrosion, and reassembled with minor modifications for further operation. The corrosion of the stainless steel cell housing during the 17 months of operation at 535 to 650°C was only 50 μ.

The sodium-lead cell with regenerator was operated for a total of only about 150 hr because of difficulties in the circulation of the cathode alloy between the cell and regenerator. Separate studies on a regenerator with no cell attached resulted in an improved regenerator which operated smoothly for about 1000 hr before the experiment was terminated. A new cell-regenerator unit is now being built incorporating the new regenerator design.

Corrosion studies of refractory metal alloys in liquid anode and cathode metals are continuing in order to provide the information necessary for the selection of materials for apparatus construction. Tantalum and molybdenum-30 w/o tungsten have both shown excellent static resistance to tin and lithium-tin mixtures at 1300°C for periods of at least 150 hr. Dynamic corrosion tests of molybdenum-30 w/o tungsten in liquid bismuth at 700 to 1050°C showed excellent resistance for

up to 2488 hr. Tantalum showed good dynamic corrosion resistance to lead-30 a/o sodium at 750 to 1050°C for 932.5 hr. Experiments on lithium-tin in both tantalum and molybdenum-30 w/o tungsten are in progress. Preliminary results are encouraging.

VI. Nuclear Constants (pages 197 to 200)

Measurements of neutron cross sections of materials important to the fast reactor program are continuing. Radiative capture cross sections of ^{41}K, ^{55}Mn, ^{85}Rb, and ^{237}Np are presented for monoenergetic neutrons in the fast reactor energy region. Experimental results are compared with calculations based on theoretical considerations. Samples of uranium and plutonium isotopes are undergoing irradiation in EBR-II in preparation for experiments designed to measure the capture-to-fission ratios of these isotopes. The irradiations will be completed by February 1967; the samples will then be returned to Argonne for analysis.

VII. Analytical Research and Development (pages 201 to 203)

The program for the development of analytical methods for the determination of burnup of fast reactor fuels and for the measurement of fast fission yields is continuing. A method for determining burnup by a total rare earth analysis is being developed. After separation from interferences by precipitation and ion exchange, the rare earths are determined by a complexiometric titration. Using lanthanum as a stand-in for the rare earth fission products, the compatibility of the separation procedure and titration has been demonstrated.

A neutron activation method for the determination of fission product praseodymium-141 in irradiated nuclear fuels has been developed. Separation from uranium and other fission products is effected by precipitation and ion exchange; the assay is accomplished by neutron activation using manganese-55 as an internal flux monitor.

ARGONNE NATIONAL LABORATORY

Chemical Engineering Division Semiannual Report

U of C-AUA-USAEC

July-December 1966

SEMIANNUAL REPORT

I

Compact Pyrochemical Processes[1]

Compact pyrochemical processes are nonaqueous processes that are being developed for the recovery and purification of both ceramic (oxide and carbide) and metallic fuels discharged from power reactors. The pyrochemical processes currently under investigation make extensive use of liquid metal and molten salt systems as the processing media. The metal solvent systems are usually binary alloys of magnesium with zinc, cadmium, or copper. The salt systems consist of $MgCl_2$ alone or in combination with alkali and/or alkaline earth chlorides.

Pyrochemical processes possess certain technological and economical features which should be particularly beneficial in fast reactor fuel cycles. Among these features are: (1) the ability to accommodate short-cooled, high-burnup fuels with a consequent reduction in out-of-reactor fuel inventories, (2) the avoidance or simplification of chemical conversions, (3) the use of small process volumes (and, hence, compact processing equipment which requires a minimum of shielded space), (4) the direct production of solid radioactive wastes, and (5) the alleviation of criticality problems because of the absence of aqueous solutions. In the case of metal fuels, the valuable alloying elements in the fuel can be recovered.

Pyrochemical processing has as its objectives the following: (1) removal of the bulk of the fission products, (2) extraction of the bred plutonium from the blanket, (3) enrichment of the core with plutonium, and (4) repair of irradiation damage. These objectives are achieved through separations of cladding material, uranium, plutonium, and fission products from one another. Because of the buildup of radioactive isotopes of uranium and plutonium in recycled fuel, it is unlikely that direct refabrication of the fuel will be possible, even with complete removal of the fission products. Present indications are that the same pyrochemical process, with little or no change in the sequence of operations, could handle both core fuel containing about 10 to 20 w/o plutonium and blanket material containing 5 w/o or less plutonium. Such a process would be suitable for small processing plants serving one or several reactors.

Pyrochemical processes that incorporate a salt transport separations step are currently being investigated. In the salt transport step, fissile and fertile materials are selectively transferred from one liquid metal solution (donor solvent) to another metal solution (acceptor solvent). A molten salt phase serves as a carrier for the transfer of solutes between the two liquid metal solutions. Such processes show promise of good separations of fission products from plutonium and uranium and high recoveries of plutonium and uranium.

A. LABORATORY-SCALE INVESTIGATIONS (I. Johnson, R. K. Steunenberg, P. Fineman)

Laboratory-scale investigations are being conducted to provide basic chemical data of process importance and to originate and evaluate new process concepts. During the period covered by this report the major effort has been devoted to the further development of a pyrochemical process for fast breeder reactor fuels which employs a salt transport separation. Salt transport separations (see ANL-7225, pp. 24–25) are based on the selective transfer of solutes between two liquid alloys of different compositions by the circulation of a fused salt between the two alloys. Chemical studies in support of salt transport separations include (1) measurements of the distribution of uranium, zirconium, and thorium between liquid alloys and fused salts and

[1] A summary of this section is given on pages 1 to 5.

(2) measurements of the solubilities of uranium and zirconium in liquid alloys. Studies were also conducted on the interaction of UO_2 and U_3O_8 with molten salt mixtures.

1. Conceptual Pyrochemical Process for Fast Reactor Fuels

A conceptual pyrochemical process flowsheet for fast breeder reactor oxide core and blanket fuels is outlined in Figure I-1. This flowsheet differs from the one presented in the preceding report (ANL-7225, Fig. I-1, p. 24) in the following two ways: First, a decladding step is shown in which the fuel or blanket cladding is selectively dissolved in liquid zinc, after which the oxide fuel is separated from the waste zinc solution. Secondly, after the plutonium salt transport separation step, a uranium recovery step is presented in which the Cu-Mg alloy is decanted from the uranium. The uranium is then washed with liquid magnesium and the residual magnesium is removed from the uranium by retorting. The process is designed to achieve the following objectives: (1) plutonium recoveries of 99+%, (2) overall fission product decontamination of from 10^3 to 10^4, (3) plutonium-to-uranium ratio in the plutonium product of unity or greater, and (4) uranium recoveries of the order of 99%. The process can be used for core or blanket fuel either separately or together and, with modifications, is also applicable to carbide or metallic fuels. The oxide preparation step would be replaced by a carbide preparation step in the case of carbide fuels.

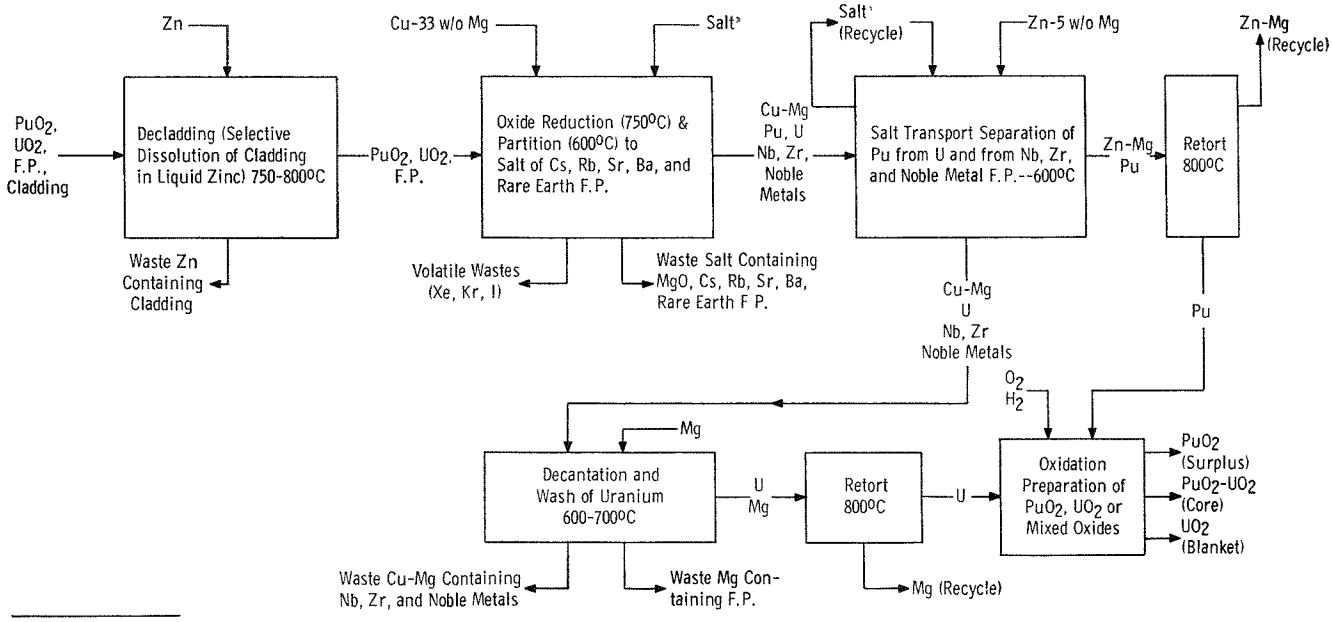

*For example, a 42.5 m/o NaCl-42.5 m/o $CaCl_2$-15 m/o $MgCl_2$.
**For example, a 50 m/o $MgCl_2$-30 m/o NaCl-20 m/o KCl salt.

308-120

FIG. I-1. Reference Pyrochemical Process Flowsheet for Fast Breeder Reactor Oxide Core and Blanket Fuel. (Cladding material: stainless steel.)

2. Distribution of Elements Between Liquid Alloys and Molten Salts

In the pyrochemical processes currently under investigation, the basic separations of plutonium, uranium, and fission product elements are effected through differences in the distribution behavior of these elements between liquid alloys of magnesium and molten salts containing $MgCl_2$. Two types of liquid alloys are required in the process as currently envisioned, a reduction-partition-donor alloy and an acceptor alloy. The potential utility of a given alloy for either of these uses can be determined from a knowledge of the distribution coefficients of plutonium, uranium, and representative fission product elements between a molten salt and the liquid alloy. Two molten salts have been used, pure $MgCl_2$ and a ternary mixture com-

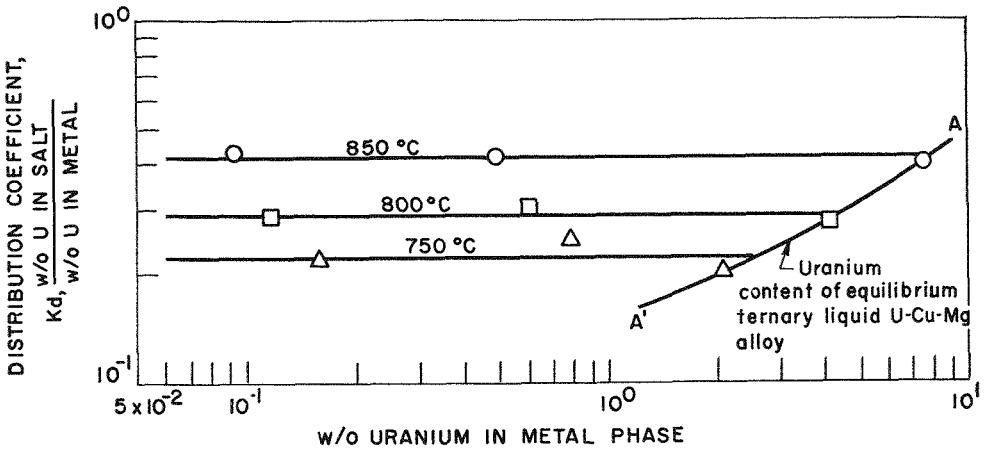

308-405

FIG. I-2. Effect of Uranium Content upon Uranium Distribution between Magnesium Chloride and Cu-~5 w/o Mg Alloy of Controlled Magnesium Composition.

posed of 50 m/o $MgCl_2$, 30 m/o NaCl, and 20 m/o KCl.

Distribution coefficients are experimentally determined by the following procedure: (a) the liquid alloy containing the solute under study (e.g., plutonium, uranium) and the molten salt are mixed together at a given temperature until equilibrium has been established and (b) after allowing the two liquid phases to separate, filtered samples of each phase are taken for chemical analysis. This procedure is repeated after changing the temperature, alloy composition, or solute concentration to obtain the dependence of the distribution coefficient on these variables.

a. DISTRIBUTION OF URANIUM BETWEEN COPPER-MAGNESIUM ALLOY AND MOLTEN MAGNESIUM CHLORIDE—EFFECT OF URANIUM CONCENTRATION AND TEMPERATURE (J. B. KNIGHTON, R. WOLSON)

As previously indicated (ANL-7225, pp. 25–30), a good separation of uranium from the refractory and noble metal fission products can be achieved by the salt transport of uranium from a copper-magnesium donor alloy to a high magnesium-low zinc acceptor alloy. To predict the effectiveness of the salt transport separation as the uranium concentration reaches low levels in the donor alloy, as it would toward the end of the transfer, it is necessary to know the distribution coefficient of uranium between the transport salt and the donor alloy at low uranium concentrations.

An experiment has been performed to determine the dependence of the uranium distribution coefficient on uranium concentration. A liquid Cu-Mg alloy (Cu-~5 w/o Mg)[2] was used as the uranium donor and molten $MgCl_2$ as the transport salt. Three uranium loadings in the copper-magnesium alloy were used: 0.1 w/o, 0.5 w/o and the uranium saturation limit for the donor alloy at the temperature of interest. Equilibrations were made at 750, 800, and 850°C at each uranium concentration.

Results of this experiment are presented in Figure I-2. The distribution coefficients were found to have the values: 0.22, 0.29, and 0.42 at 750, 800, and 850°C, respectively, and to be independent of the uranium concentration in the metal phase. The curved line A'—A (Figure I-2) represents the uranium content of the equilibrium ternary liquid U-Cu-Mg alloy as a function of temperature.

b. DISTRIBUTION OF URANIUM BETWEEN 50 m/o $MgCl_2$-30 m/o NaCl-20 m/o KCl SALT AND Zn-Mg ALLOYS (J. B. KNIGHTON, R. TIFFANY, K. TOBIAS)

Zinc-magnesium alloys have been selected as uranium and plutonium acceptors for the salt transport process. Although the present reference flowsheet (Figure I-1) does not include a uranium salt transport step, it is essential to know the uranium distribution between the transport salt and uranium-saturated acceptor alloys.

An experiment was conducted to determine uranium distribution between 50 m/o $MgCl_2$-30 m/o NaCl-20 m/o KCl and uranium-saturated zinc-magnesium alloys at 600, 700, and 800°C. In the course of this experiment, the uranium solubility in the liquid alloy was also determined. These solubility data are reported below (subsection 3a).

The effects of temperature and magnesium concen-

[2] The magnesium content of this alloy was maintained constant at each temperature by having an excess of solid copper-magnesium solid solution present; thus the liquid remained at the liquidus composition (see ANL-7225, p. 26).

TABLE I-1. DISTRIBUTION OF URANIUM BETWEEN MOLTEN 50 m/o $MgCl_2$-30 m/o NaCl-20 m/o KCl AND LIQUID ZINC-MAGNESIUM ALLOY

	600°C	700°C	800°C
Zn-5 w/o Mg[a]			
U solubility, w/o	0.17	1.3	6.0
K_d[b]	1.3×10^{-3}	8×10^{-4}	2.6×10^{-3}
Zn-60 w/o Mg[c]			
U solubility, w/o	0.04	0.09	0.16
K_d[b]	5.8×10^{-3}	6.6×10^{-3}	1.5×10^{-2}
Zn-Mg Alloy with Minimum K_d[b]			
Mg conc., w/o	24.8	16.7	10.8
K_d[b]	1.3×10^{-4}	2.8×10^{-4}	3.6×10^{-4}
U solubility, w/o	4.6	11.0	18.0

[a] An alloy of this composition may be used as both a uranium and plutonium acceptor alloy in a salt transport separation.

[b] K_d = (w/o U in salt)/(w/o U in metal).

[c] An alloy of this composition may be used as either a plutonium donor alloy or a uranium acceptor alloy in a salt transport separation.

TABLE I-2. ZIRCONIUM DISTRIBUTION BETWEEN $MgCl_2$ AND Cu-Mg ALLOY AT 800°C

Sample Number	Metal		Salt[a]	K_d[b, c]
	w/o Mg	w/o Zr	w/o Zr	
1	30.66	3.66[d]	3.5×10^{-4}	1×10^{-4}
2	37.52	3.90	1.3×10^{-3}	3×10^{-4}
3	42.51	3.28	7×10^{-4}	2×10^{-4}
4	49.07	2.67	1.2×10^{-3}	4×10^{-4}

[a] Probably represents an upper limit of zirconium concentration in salt phase.

[b] K_d = (w/o Zr in salt)/(w/o Zr in metal).

[c] Actual K_d probably less than reported number.

[d] Zirconium concentration in alloy believed to be below solubility limit.

tration upon uranium solubility and distribution are presented in Table I-1 for three alloys: Zn-5 w/o Mg (plutonium and uranium acceptor), Zn-60 w/o Mg (uranium acceptor or plutonium donor), and the Zn-Mg alloy for which the distribution coefficient at each temperature is a minimum. This minimum occurs at the alloy composition that provides maximum uranium solubility.

c. DISTRIBUTION OF ZIRCONIUM BETWEEN $MgCl_2$ AND Cu-Mg ALLOY (J. B. KNIGHTON, K. R. TOBIAS)

Data for the distribution of zirconium between $MgCl_2$ and zirconium-saturated copper-magnesium alloy at 800°C have been obtained. These data (Table I-2), taken at alloy compositions of 30 to 50 w/o magnesium, show zirconium distributing preferentially to the metal phase. Zirconium concentrations in the $MgCl_2$ are near or below the limit of detection and thus the zirconium distribution coefficients of about 10^{-4} represent an upper limit. Zirconium concentrations in the copper-magnesium alloy are believed to represent the solubility limits. The low distribution coefficients are very encouraging and provide a basis for a separation of plutonium from zirconium (along with uranium, niobium, and the noble metals) by the salt transport process.

Additional experimental work using ^{95}Zr tracer ($T_{1/2}$ = 65 days) will be conducted to: (1) determine more accurately the zirconium distribution coefficient between salt-metal systems used in the reference flowsheet and (2) obtain additional zirconium solubility data at temperatures and alloy compositions of process interest.

d. DISTRIBUTION OF THORIUM BETWEEN MOLTEN $MgCl_2$-NaCl-KCl AND LIQUID MAGNESIUM ALLOYS (J. FISCHER, J. J. HEIBERGER)

The potential use of thorium as a fertile material in a thorium-uranium fuel cycle prompted a preliminary examination of the distribution behavior of thorium between a typical uranium donor alloy (copper-magnesium alloy) and a salt and a typical uranium acceptor alloy (zinc-magnesium alloy) and a salt.

The distribution of thorium between 50 m/o $MgCl_2$-30 m/o NaCl-20 m/o KCl and Cu-8 w/o Mg alloy and the distribution of thorium between the ternary salt of the same composition and Zn-10 w/o Mg at 800°C have been determined. In all these experiments, as shown in Table I-3, thorium distributes strongly in favor of the metal phase. The distribution coefficients

TABLE I-3. DISTRIBUTION OF THORIUM BETWEEN MOLTEN 50 m/o $MgCl_2$-30 m/o NaCl-20 m/o KCl AND Cu-Mg ALLOY OR Zn-Mg ALLOY AT 800°C

Thorium (w/o)			Distribution Coefficient[b] (K_d)
Salt[a]	Metal Alloy		
	Cu-8 w/o Mg	Zn-10 w/o Mg	
2.5×10^{-3}	1.51 ± 0.08	—	1.7×10^{-3}
2.6×10^{-3}	1.51 ± 0.08	—	1.7×10^{-3}
2.0×10^{-3}	1.51 ± 0.08	—	1.3×10^{-3}
4.0×10^{-5}	—	0.82 ± 0.04	4.9×10^{-5}
1.7×10^{-4}	—	2.08 ± 0.10	8.2×10^{-5}

[a] Thorium in salt determined by emission spectrography; estimated accuracy, ±2 times the value.

[b] K_d = (w/o Th in salt)/(w/o Th in metal).

(w/o Th in salt/w/o Th in alloy) at this temperature are about 10^{-4} for the Zn-Mg alloy and about 10^{-3} for the Cu-Mg alloy.

These preliminary results indicate that uranium could probably be effectively separated from thorium using a salt transport process.

3. Solubilities in Liquid Alloys

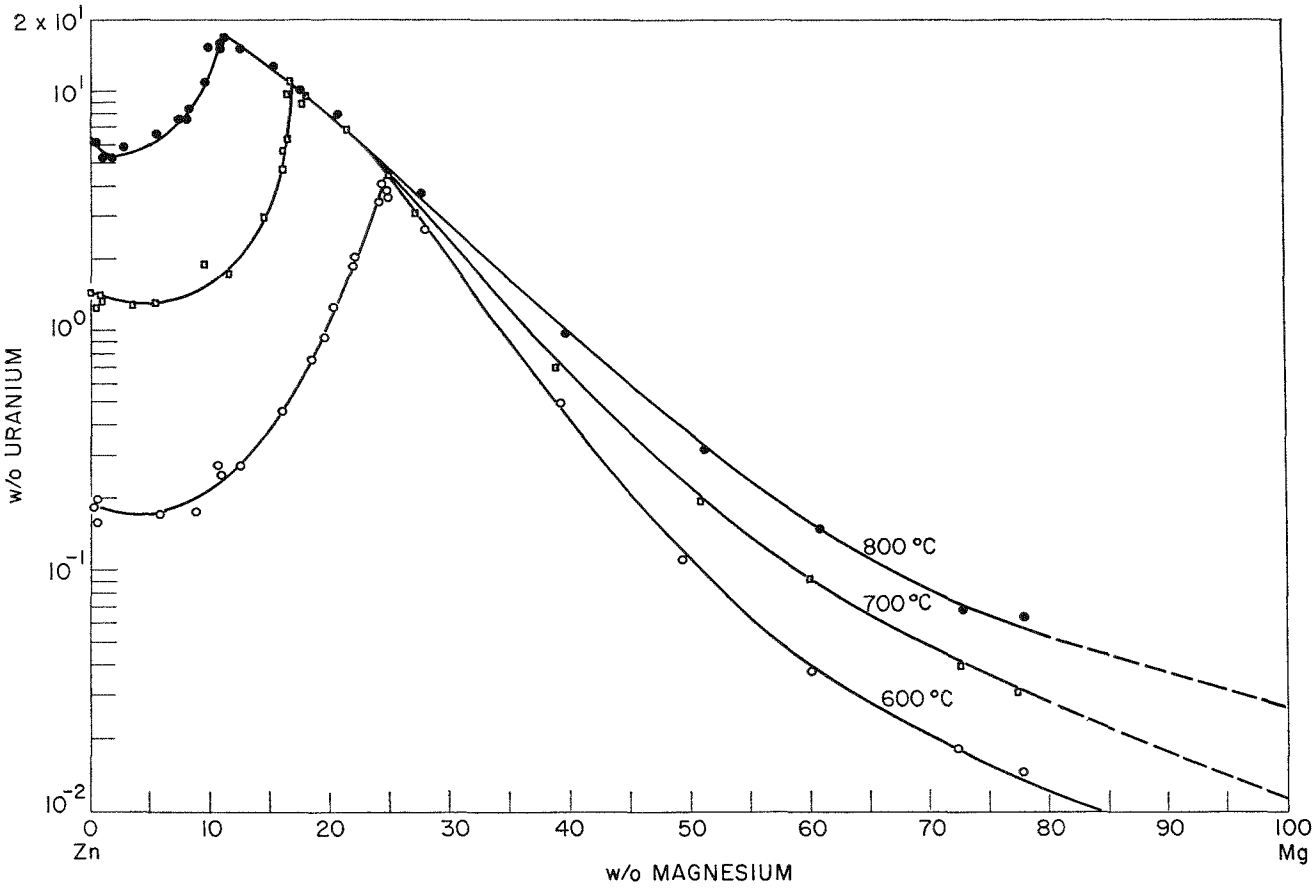

308-423

Fig. I-3. Solubility of Uranium in Zinc-Magnesium Alloys.

The solubilities of plutonium, uranium, fission product elements and structural metals in liquid alloys are of importance in the choice of suitable donor and acceptor alloys for the salt transport process, in the determination of the volumes of process streams, and in the evaluation of corrosion data. Data are presented on the solubility of uranium in liquid zinc-magnesium alloys and in liquid cadmium-zinc alloys.

a. SOLUBILITY OF URANIUM IN ZINC-MAGNESIUM (J. B. Knighton, R. Tiffany, K. Tobias)

In the course of determining uranium distribution coefficients (see subsection 2b above) between molten 50 m/o $MgCl_2$-30 m/o NaCl-20 m/o KCl and liquid Zn-Mg alloy saturated with uranium, the solubility of uranium in Zn-Mg alloys of various compositions was determined at 600, 700, and 800°C. These data are presented in Figure I-3, where uranium solubility in the alloy is plotted as a function of magnesium content of the alloy; the zinc content can be calculated by difference. The magnitude of the maximum uranium solubility increases with temperature; the point of maximum solubility occurs at lower magnesium concentrations as the temperature increases.

These data are in agreement with the results of Martin et al[3, 4] and Johnson et al.[5] Extrapolation of these data to 100% magnesium gives a uranium solubility in magnesium of about 0.027 w/o at 800°C and

[3] A. E. Martin, C. Wach, and R. Uhle, ANL-6101, p. 66.
[4] A. E. Martin and C. Wach, ANL-6648, p. 118.
[5] I. Johnson, K. E. Anderson, and J. Bartos, ANL-6569, p. 83.

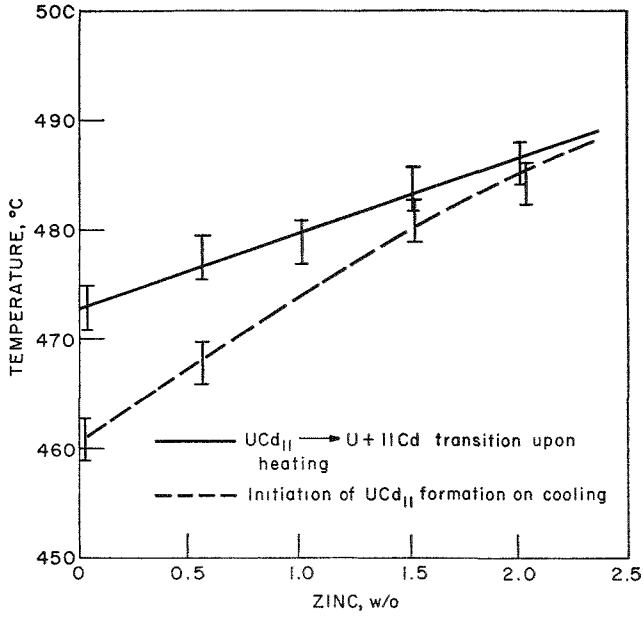

308-422

FIG. I-4. Peritectic Transition for U-Cd-Zn System. $UCd_{11} \rightarrow U + 11\ Cd$

TABLE I-4. SOLUBILITY OF URANIUM IN THE U-Cd-Zn SYSTEM

Four experimental mixtures were tested. Initially, each mixture weighed about 400 g and contained about 4 w/o uranium.

Temperature (±2°C) (°C)	Composition of Liquid Phases (w/o)		Solid Phases
	U	Zn[a]	
507	2.25 ± 0.14[b]	0.0[c]	U
480	2.68[d]		U + $UCd_{11-x}Zn_x$
502	2.71 ± 0.04[b]	1.1 ± 0.06[e]	U
528	2.65 ± 0.03[b]		U
493	2.89 ± 0.03[b]	1.3 ± 0.0[b]	U
476	2.37 ± 0.03[b]		U + $Cd_{11-r}Zn_x$
485	2.72 ± 0.06[b]	2.1 ± 0.1[f]	U
500	3.20 ± 0.02[b]		U
528	2.94 ± 0.06[b]		U

[a] Zinc analysis by atomic absorption.

[b] Average deviation of duplicate samples.

[c] Zinc analysis by atomic absorption (limit of detection, 3.8×10^{-3} w/o.

[d] One sample.

[e] Average deviation of six samples, duplicates at each temperature.

[f] Average deviation of eight samples, duplicates at each temperature.

0.011 w/o at 700°C compared to values of 0.023 w/o at 800°C and 0.007 w/o at 700°C reported by Chiotti et al.[6]

[6] P. Chiotti and H. E. Shoemaker, Ind. Eng. Chem. **50,** 137 (1958).

No attempt was made to isolate and identify the equilibrium uranium solid phases as this was not within the scope of the experiment. However, it is believed that the solid phase in equilibrium with alloys to the right of the maximum uranium solubility peak is α-uranium at 600°C, β-uranium at 700°C, and γ-uranium at 800°C. The equilibrium solid phase to the left of the maximum uranium solubility peak is believed to be a uranium-zinc intermetallic compound.

b. SOLUBILITY OF URANIUM IN THE U-Cd-Zn SYSTEM AT LOW ZINC CONCENTRATIONS

(J. FISCHER, J. J. HEIBERGER)

A cadmium-zinc-magnesium alloy is being considered as a potential liquid metal solvent for various pyrochemical separations. In recent work, a portion of the uranium-cadmium-zinc system was investigated to obtain information about the solubility of uranium[7] in the ternary system at low zinc concentrations. The solubility of uranium in pure cadmium has been studied by Martin et al;[8] in the present investigation similar experimental methods and equipment[9] were used. The results of thermal analyses showed that the temperature for the peritectic decomposition of UCd_{11} increased from 472 ± 2°C to 485 ± 2°C as the zinc concentration was increased from 0.0 to 2.0 w/o, as shown in Figure I-4. The increase in the peritectic transition temperature may be attributed to an increase in the free energy brought about by the substitution of zinc for cadmium in UCd_{11} to produce $UCd_{11-x}Zn_x$. The intermetallic phase was examined by X-ray diffraction. The lattice parameters were found to be different from those of UCd_{11} to an extent which suggests that a solid solution $UCd_{11-x}Zn_x$ is formed at low zinc concentrations. When the liquid phase was supercooled to initiate the reaction of α-uranium with cadmium to form UCd_{11}, the degree of supercooling decreased with increasing zinc concentration of the mixture as shown in Figure I-4. The change in degree of supercooling probably results from the introduction of zinc into the solid phase and that the smaller zinc atom enhances nucleation and brings about an onset of crystallization of the solid phase at a higher temperature than that for pure UCd_{11}.

[7] In discussing the solubility of uranium in the ternary system, it is necessary to refer to two liquidus fields in the region of low zinc concentration. In one field, which is below the uranium transition temperature, the solid in equilibrium with the liquid is UCd_{11}. In the other field, which is above transition temperature, α-uranium is the solid.

[8] A. E. Martin, I. Johnson, and H. M. Feder, Trans. Met. Soc., AIME **221,** 789 (1961).

[9] An exception was the use of tantalum containers, and tantalum sampling tubes and filters for obtaining liquid samples.

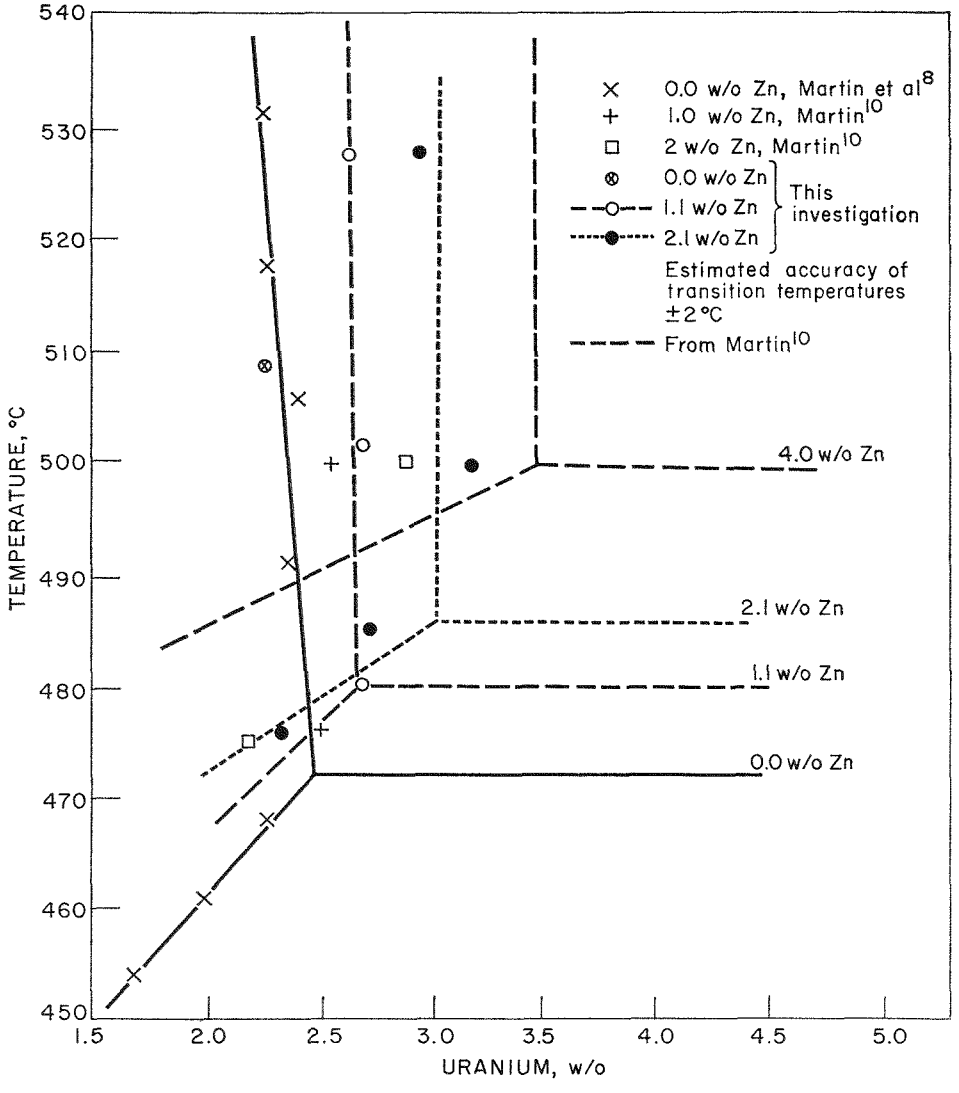

308-482

FIG. I-5. Uranium-Cadmium-Zinc System.

The data of the present investigation are shown in Table I-4 and are plotted in Figure I-5 along with data previously obtained by Martin, Johnson, and Feder[8] and Martin.[10] The combined results of the several investigations show that the solubility of α-uranium varied at 500°C from 2.4 w/o uranium at 0.0 w/o zinc to 3.0 w/o uranium at 2.1 w/o zinc. Below the transition temperature, for example at 470°C, the solubility of uranium (solution in equilibrium with UCd_{11} or $UCd_{11-x}Zn_x$) decreases on adding zinc, and varies from 2.4 w/o uranium at 0.0 w/o zinc to 2.0 w/o uranium at 2.1 w/o zinc. The retrograde solubility of α-uranium found in the U-Cd system[8] continues in the ternary system up to at least 2 w/o zinc.

4. Chemical Interactions of Uranium Oxides with Molten Salts (D. A. WENZ, R. D. WOLSON)

Measurements of the concentration of uranium in molten salts in equilibrium with solid UO_2 and U_3O_8 have been performed in order to help in the understanding of the mechanism of the reduction of these oxides in molten salt-metal systems.

Approximately 5 g of uranium oxide and 200 g of chloride salt were equilibrated in a crucible under a helium atmosphere at 800°C with moderate stirring. Baffled tantalum crucibles and tantalum stirrers were used in the UO_2 experiments whereas alumina crucibles and quartz stirrers were used in the U_3O_8 experi-

[10] A. Martin, ANL-6029, p. 53.

TABLE I-5. URANIUM CONTENTS OF MOLTEN SALTS AFTER CONTACT WITH UO_2 AND U_3O_8 AT 800°C

Salt Composition (m/o)	Uranium Content of Salt (w/o)	
	UO_2[a]	U_3O_8[b]
100 $MgCl_2$	0.029	1.0
Above salt + 5 MgF_2	0.015	—
50 $MgCl_2$-30 NaCl-20 KCl	0.023	0.4
Above salt + 5 MgF_2	0.015	—
50 $MgCl_2$-50 $CaCl_2$	0.025	0.4
Above salt + 5 MgF_2	0.014	0.4
59 LiCl-41 KCl	0.005	0.2
Above salt + 5 MgF_2	0.003	—

[a] Equilibrium concentration of uranium in salt.

[b] Compositions of salt after 1 hr contact with U_3O_8, which decreased to lower values with longer contact time.

ments. The salt phases were sampled at equilibration times of 1, 2, and 4 hr with quartz tubes having porous graphite filters. After each of the chloride-salt experiments was completed, 5 m/o MgF_2 was added to determine the effect of fluoride on the interaction of the salt with UO_2. The results are given in Table I-5.

The data for UO_2 show that the concentration of uranium is essentially the same in the pure $MgCl_2$ and the two magnesium chloride-containing melts in equilibrium with UO_2. The addition of 5 m/o MgF_2 decreases the uranium concentration to the same level in all three salts. The uranium concentration in the LiCl-49 m/o KCl eutectic is much less and is also lowered by the addition of MgF_2. These results are in agreement with previous measurements which showed about 0.01 w/o uranium in $MgCl_2$-NaCl-KCl salt in equilibrium with UO_2 at 500°C.[11]

The uranium contents of the salts in contact with U_3O_8 are given only for the first sample, taken at 1 hr, because the uranium content dropped to low values in later samples. Microscopic and X-ray observations showed that the solid in equilibrium with the salts at the end of the experiments was UO_2. Thus, it is apparent that U_3O_8 dissolves to give uranium concentrations in the salts that are initially higher than those obtained with UO_2, then slowly decomposes to UO_2. The following sequence of reactions, based on previous work on uranium oxide chemistry[12] is postulated to explain these results.

$$U_3O_8 + 4\,MCl = UO_2Cl_2 + 2\,UO_2Cl + 2\,M_2O \quad (1)$$

$$UO_2Cl_2 = UO_2Cl + \tfrac{1}{2}\,Cl_2 \quad (2)$$

$$UO_2Cl = UO_2 + \tfrac{1}{2}\,Cl_2 \quad (3)$$

In these reactions, M is an alkali cation; however, similar reactions are postulated for the alkaline earth chlorides.

Future studies are planned on the interactions between plutonium dioxide and molten salts.

B. ENGINEERING-SCALE INVESTIGATIONS (R. D. PIERCE, R. K. STEUNENBERG, P. FINEMAN)

Engineering studies are being conducted to develop the technology required for plant-scale application of pyrochemical processes. The major portion of this effort is devoted to investigations of process concepts on a pilot-plant scale, the present emphasis being on salt transport separations (Figure I-1). These separations are based on the selective transfer of solutes between two liquid metal solutions in contact with a molten salt. Exploratory experiments on salt transport separations are being performed, pilot-scale equipment is being developed, and materials of construction are being evaluated. These investigations are expected to lead to the design and operation of a pilot plant for the recovery of plutonium and uranium from simulated fast breeder reactor fuel.

1. Engineering Studies of Salt Transport Separations (W. J. WALSH, I. O. WINSCH, T. F. CANNON, J. D. ARNTZEN, F. G. TEATS)

The engineering development of salt transport separations is currently in progress. Recently completed salt transport experiments continued to be of an exploratory nature (ANL-7225, pp. 32–35). These tests had the following objectives: (1) to demonstrate the feasibility of salt transport separations, (2) to identify the major engineering problems involved, (3) to determine the fission product decontamination obtainable, and (4) to provide a clearer understanding of the

[11] M. D. Adams, Argonne National Laboratory, private communication.

[12] D. A. Wenz, M. D. Adams, and R. K. Steunenberg, Inorg. Chem. **3**, 989 (1964).

salt transport step. The five experiments in this preliminary investigation were conducted in pilot-plant equipment originally used in the studies of the EBR-II skull reclamation process (ANL-6875, p. 20). Since this facility was not designed for experimentation with plutonium, the experiments were restricted to the transport of uranium.

The feed preparation and the experimental procedure for the experiment were as follows. The feed charges, containing from 2 to 5 kg of uranium, were prepared by one of the two following methods: (1) unirradiated oxides of uranium and inactive representative fission product elements (zirconium, molybdenum, palladium, ruthenium, and niobium) were charged as a suspension in a $MgCl_2$-based salt and then reduced by a Cu-10 w/o Mg alloy (the magnesium concentration of the alloy, after the reduction, was ~5 w/o), or (2) unirradiated elemental uranium and inactive fission product elements were dissolved in liquid Cu-5 w/o Mg alloy at an elevated temperature of 925°C. In each case, the bulk of the uranium appeared as a finely divided precipitate in contact with the copper-magnesium donor alloy, thereby simulating process conditions prior to the transport step. The uranium was incrementally transferred (batch-transfer method) at 845°C to a liquid Mg-35 w/o Zn acceptor alloy by alternately contacting the two metal alloys with a charge of molten $MgCl_2$ which was pressure transferred through a heated transfer line (ANL-7225, Figure I-10, p. 33). Both alloys were contained in tungsten crucibles. Prior to each salt transfer, the salt and metal phases were mixed for 4 to 6 min to promote chemical equilibration and the phases were then allowed to separate by settling for 5 to 10 min. After the uranium transfer to the acceptor alloy was about 99% complete, the alloy was separated from the precipitated uranium, and the uranium product was washed with Mg-30 w/o Zn for additional removal of soluble noble and refractory metals. Following separation of the wash solution, the uranium product was dissolved in a Zn-13 w/o Mg solution which was then retorted to evaporate the zinc and magnesium for recovery of the uranium.

Since these five experiments were the first large-scale salt transport tests attempted, the first few runs served primarily to provide experience and to allow the improvement of experimental techniques. The last experiment of the five, run USTP-5, is believed to be the most meaningful. The results of this run are given in Figure I-6, in which the uranium recovery is shown as a function of the number of cycles completed. The uranium transferred at a constant rate until the 5th

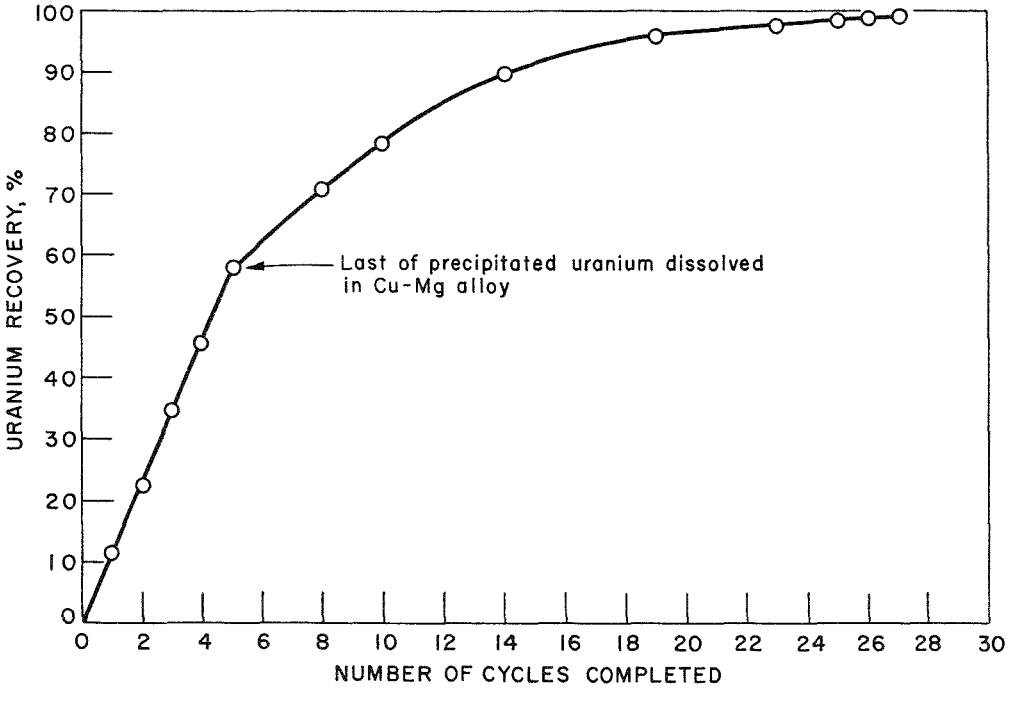

8-479

FIG. I-6. Rate of Uranium Recovery in Salt Transport Experiment USTP-5.
System: Cu-Mg/$MgCl_2$/Zn-Mg
Donor alloy: Cu-5 w/o Mg
Acceptor alloy: Mg-35 w/o Zn
Salt: 100% $MgCl_2$

cycle when the last of the uranium precipitate in the copper-magnesium alloy dissolved. The transfer rate then decreased steadily, and a uranium recovery of about 99% was achieved after a total of 27 cycles. A similar behavior had been observed in the preceding runs (ANL-7225, p. 34). The overall removals of fission product elements were as follows: zirconium, 99.7%; molybdenum, 99.9%; palladium and ruthenium, 99.99% (each); and niobium, 99.999%. The removals are superior to those achieved in the previously reported skull reclamation processing studies (ANL-7125, pp. 44 and 45 and ANL-7225, pp. 46–47).

Washing of the precipitated uranium product was effective in removing most of the transferred copper and fission product elements, except for zirconium. The small amount of zirconium that had transferred coprecipitated with the uranium and was not appreciably removed by the washes. (Laboratory data indicate that zirconium would not coprecipitate with uranium below the γ-transition temperature (775°C) for uranium.) The highest purity of uranium product (99.87%) was achieved in the fifth run; the major impurities were copper and zirconium.

In the earlier experiments of this series, two major engineering problems were encountered (ANL-7225, pp. 34–35). The first one was the control of the magnesium concentration in the donor alloy. Effective magnesium control was accomplished by maintaining an excess of copper in the system until most of the uranium had been transported (ANL-7225, p. 26). The other problem was the cross-contamination of the two metal alloys (via entrainment or other mechanisms). An experiment to study the entrainment phenomenon revealed that the metal alloy settled rapidly from the salt phase; however, some uncoalesced droplets may have accumulated at the metal-salt interface. Entrainment was minimized in the later runs by locating the transfer tube inlet to decrease vortexing near the metal-salt interface.

In these experiments, the rate of uranium transport was limited by the small volumes of the tungsten crucibles used. If 100-liter vessels were used, 99% of a 10-kg charge of uranium could be transported in less than 10 cycles, which would require a period of less than 4 hr. Moreover, in a full-scale processing plant, the uranium transfer would be managed such that most of the transfer would be at the maximum possible rate and the diminishing rate period would be minimized. Cal-

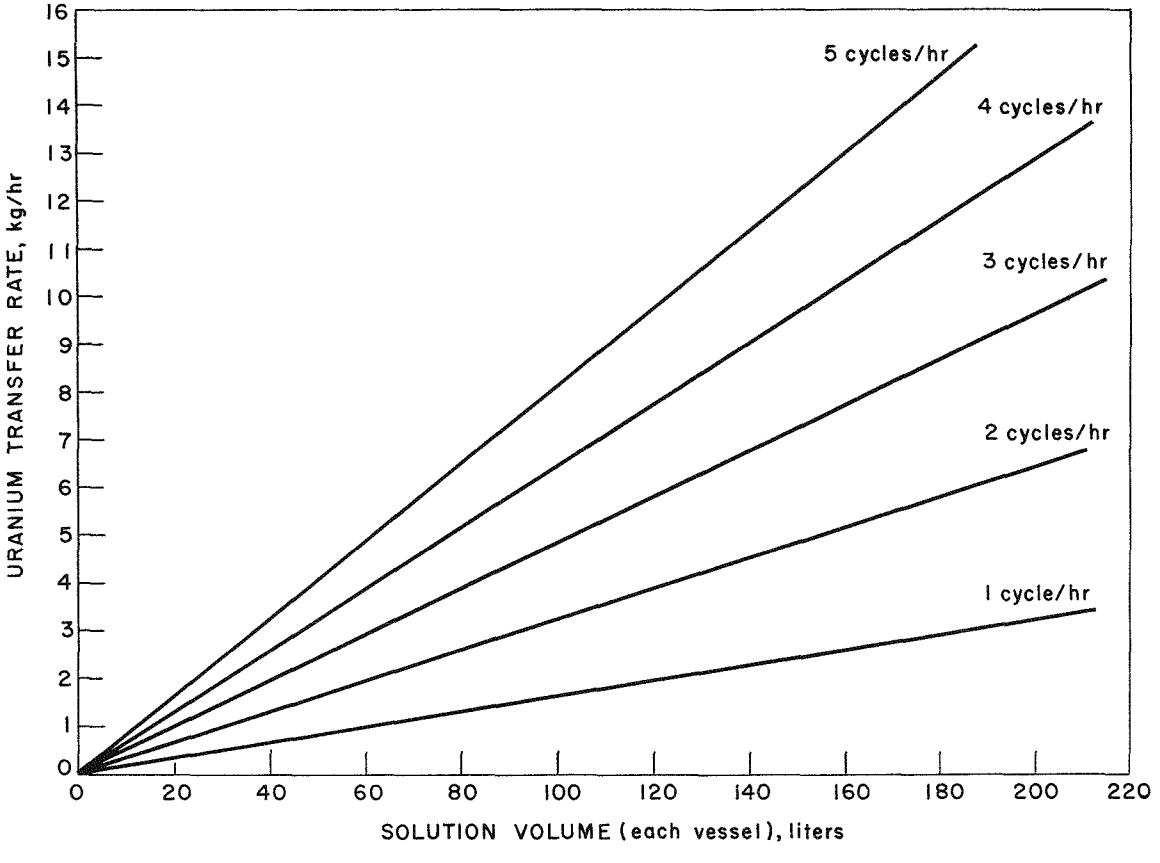

308-408

FIG. I-7. Calculated Rates of Uranium Transfer for Batch-Transfer System.

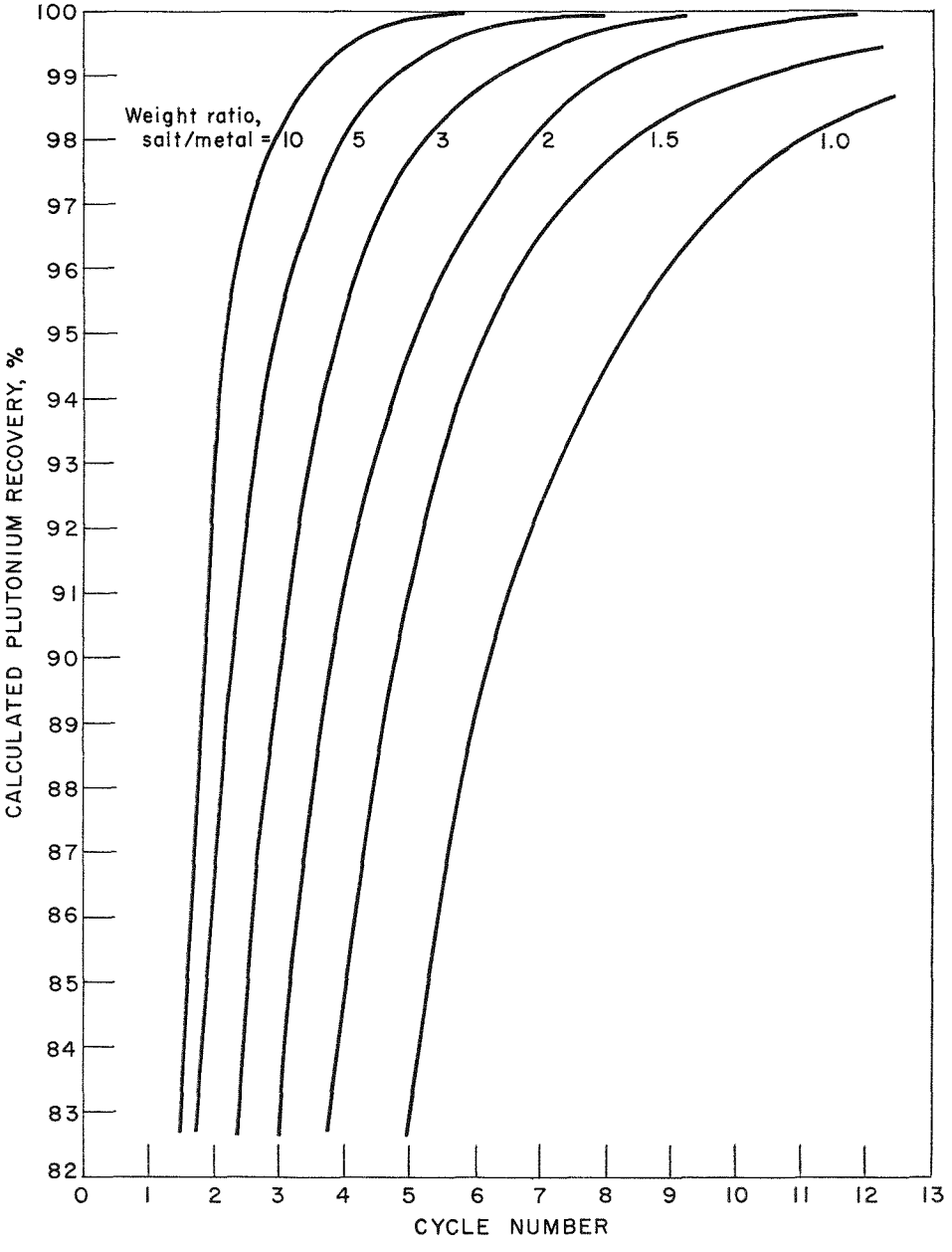

308-407

FIG. I-8. Calculated Rates of Plutonium Transport for Batch-Transfer Systems.
Calculations are based on the following:

99% completion of donor equilibrations
99% completion of acceptor equilibrations
90% salt transfer efficiency

culated uranium transfer rates (for a saturated donor alloy) as functions of solution volume and cycle frequency for the batch-transfer method are shown in Figure I-7. If a continuous salt circulation method is used, higher uranium processing rates appear feasible (ANL-7225, p. 35).

Since these experiments have successfully demonstrated the engineering feasibility of salt transport separations, no additional uranium transport experiments are planned at this time. Equipment is being constructed for a series of plutonium transport experiments using the batch-transfer method. In the current reference flowsheet which incorporates a plutonium transport step (Figure I-1), a Cu-33 w/o Mg alloy at 600°C is the proposed plutonium donor alloy. Since all of the plutonium is assumed to be in solution

in the donor alloy prior to the transport step, no constant rate period (as observed in the uranium experiments) will be encountered, and the plutonium transport rate will be primarily dependent on the distribution coefficient and the salt/metal ratio in the donor system. This can be seen in Figure I-8 where theoretical plutonium recoveries for batch contacts are shown as functions of the number of cycles and the salt/metal weight ratio for the case of 90% salt transfer efficiency and 99% completion of the equilibration reactions. As indicated, plutonium recoveries exceeding 99.9% may be achieved in a few cycles for high salt/metal ratios. The percent recovery achieved is independent of the amount of plutonium processed for all cases in which the solubility of plutonium in the donor alloy is not exceeded.

2. Studies of Extraction Columns (T. R. Johnson, F. G. Teats, D. R. Gorth,[13] P. J. Mack)

Although batch processing methods are being considered for current pyrochemical processes, continuous operations in these and future pyrochemical processes offer some potential advantages. Continuous equipment generally is smaller and requires fewer manipulations than batch equipment. Countercurrent, liquid-liquid extraction in multistage, packed columns is being investigated because this unit operation has utility in a number of pyrochemical flowsheets. Previously reported preliminary studies of mass transfer rates in metal-salt systems indicated that countercurrent, packed columns can be employed in pyrochemical processes (ANL-7055, pp. 44–45; ANL-7125, pp. 35–36).

In recent work, a study was made of a countercurrent, liquid-liquid, packed column in which the discontinuous phase was a low-melting metal alloy (50 w/o Bi-29 w/o Pb-13 w/o Sn-8 w/o Cd; m.p., 71°C) and the continuous phase was water. The objective of this work was the simulation of a high-temperature extraction column in which the liquid phases are metal and salt. Although no mass transfer takes place in the system being tested, the operation of this column is useful for two reasons: (1) the system has physical properties similar to those of a liquid metal-molten salt system and (2) the low operating temperature permits use of a glass column that allows visual observation of the flow of the two phases. Very few investigations of extractive processes have been reported with systems that have large density differences and high interfacial tensions. Metal-salt and metal-water systems have these properties.

The experimental column was fabricated of glass pipe and was maintained at an operating temperature of 85–90°C in a heated glass enclosure. The packed portion of the column consisted of a 1-in. ID by 24-in. long section with expanded sections[14] (to 2-in. ID) at the top and bottom. The column packing was $\frac{3}{16}$-in. perforated metal saddles which were held rigidly i

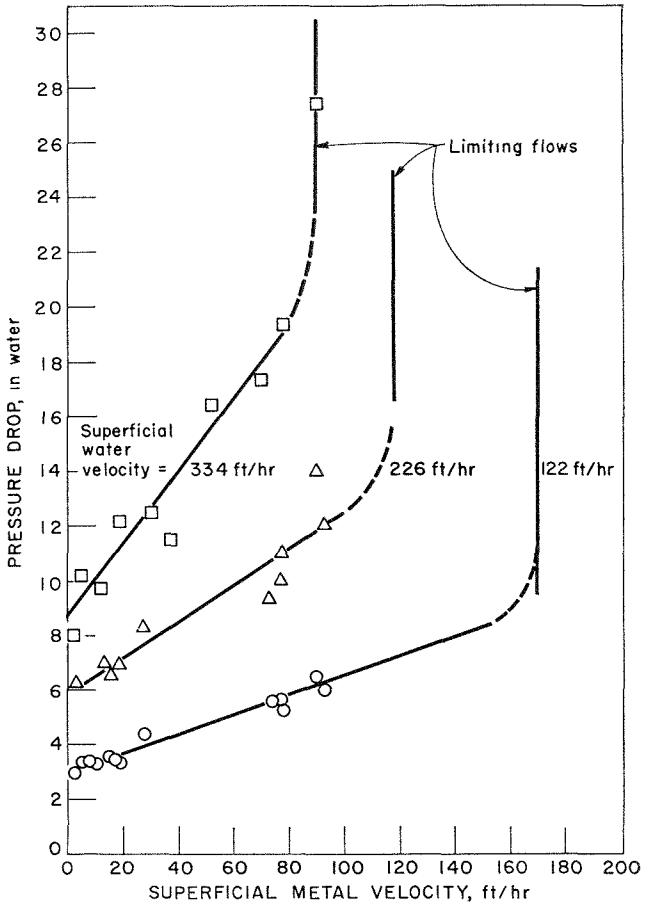

308-431

Fig. I-9. Pressure Drop in Countercurrent, Metal-Water System, Packed Column.
Continuous phase: Water
Discontinuous phase: Metal (50 w/o Bi-29 w/o Pb-13 w/o Sn-8 w/o Cd)
Column (glass pipe): 1 in. ID, 24-in. packed height (nominal)
Packing: $\frac{3}{16}$-in. perforated metal saddles
Temperature: 85–90°C

[13] Cooperative Plan student, University of Detroit.

[14] The expanded sections are made up of a short transition fitting and 2-in. ID pipe in which the retainer screen is located. The expanded sections were added to eliminate flooding that had occurred in initial tests at the packing-retainer screens originally installed in the 1-in. ID pipe.

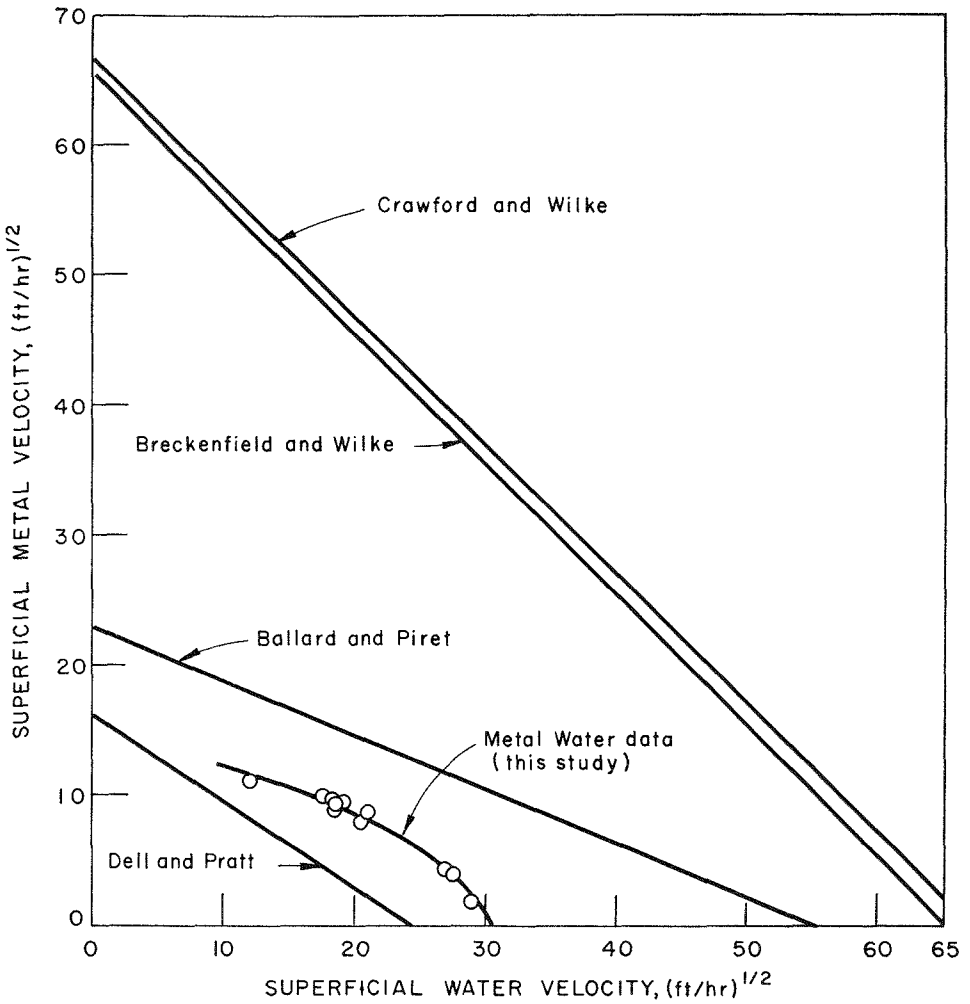

FIG. I-10. Flooding in Metal-Water Column. A Comparison with Published Correlations.
Continuous phase: Water
Discontinuous phase: Metal (50 w/o Bi-29 w/o Pb-13 w/o Sn-8 w/o Cd)
Column (glass pipe): 1-in. ID, 24-in. packed height (nominal)
Packing: $\frac{3}{16}$-in. perforated metal saddles
Temperature: 85–90°C

the column by retainer screens. The screens prevented the formation of large voids in the packing that were found to cause premature flooding. Associated equipment items included supply and receiver tanks for each phase, and a gas pressure control system for the gas (nitrogen) used to push the fluids from the supply tanks, through the column, and into the receiver tanks. The lines and tanks for the metal and water phases were heated to 85 to 95°C with resistance wire and the glass enclosure for the column was heated with resistance heaters. The metal phase entered the top of the column through a ¼-in. dia. tube that released the metal just above the top packing-retainer screen. To prevent water from entering the metal phase receiver tank, the liquid-liquid interface at the bottom of the column was maintained at a constant level by controlling the gas pressure in a jack-leg. The interface level was monitored by means of a mutual inductance coil that surrounded the bottom section of the column.

Measurements of the pressure drop of the continuous phase[15] and the limiting flow conditions were completed. Results of these measurements are summarized in Figures I-9 and I-10. As shown in Figure I-9, at constant water flow rate, the pressure drop of the continuous phase increased linearly with metal flow rate and then increased rapidly as the limiting flow rate (flooding point) was approached. In Figure I-10, experimentally determined limiting flow rates are com-

[15] The pressure drop data were based on a nominal packing height of 24 in. (1-in. ID portion of column) and have not been corrected for the small amount of packing in the expanded sections. Future tests will determine what this correction should be.

pared to limiting flow rates predicted[16] by several published correlations[17-20] that were developed to describe flooding in water-organic systems. The results indicate that extrapolations of such correlations to metal-water systems and presumably to metal-salt systems are not reliable. Initial measurements of the holdup of the discontinuous phase have been made and are being evaluated.

This study is being continued to extend extraction technology into liquid metal-molten salt systems and to obtain data pertinent to the operation of a liquid metal-molten salt extraction column. A facility is being built in which countercurrent metal-salt extractions will be investigated at high temperatures. The metal-water studies have outlined practical flow rates, have indicated considerations in the column design, and should assist in the interpretation of results from the metal-salt studies.

3. Salt Pump Loop (T. R. Johnson, F. G. Teats, P. J. Mack)

The salt pump loop described in the previous report (ANL-7225, pp. 35–37) has been further operated to obtain information on the behavior of the pump and other loop components when exposed to a molten chloride salt having the nominal composition of 50 m/o $MgCl_2$-30 m/o NaCl-20 m/o KCl. The loop consists of a centrifugal pump (obtained from Oak Ridge National Laboratory), a pressure sensor to measure the discharge pressure of the pump, a bellows-sealed valve to throttle the salt flow, an orifice flow meter to measure the flow rate, and a freeze valve (the molten salt passes this valve when the loop is filled or drained). Except for the pump, which is made of INOR-8,[21] the loop and loop components are made of type 304 stainless steel.

During this reporting period, the loop was operated for an additional 850 hr (a total of 1000 hr). In the 1000 hr of loop operation, the average flow rate for the circulated molten salt was 1 gpm, but flow rates up to 3.5 gpm have been obtained. The operating temperature during the first 150 hr was 515°C; during the next 550 hr, about 550°C; and during the last 300 hr, 600°C. With few exceptions the loop and its components have performed satisfactorily and routinely.

The design features of the pump are being incorporated into experimental pumps being developed for pyrochemical process equipment. Although the operating principle of the induction pressure sensor was proven, the various designs tried to date have not been completely satisfactory, and this instrument was omitted from the loop during the last 600 hr of operation. The freeze valve has been opened and closed approximately 40 times, and, although the response time has increased significantly with operating time, the valve performs satisfactorily.

Chemical analyses of salt samples taken from the loop have shown that the iron and nickel contents were below the level of detection of 50 and 10 ppm, respectively. The chromium content of the circulated salt appeared to increase slowly during each run to an equilibrium level of 60 to 100 ppm. (Chromium was the corrosion product that was most likely to be found in the salt because its chloride is thermodynamically more stable than the chlorides of iron and nickel.) These values represent a negligible amount of corrosion in this loop.

Carbon analyses were made of the circulating salt to determine whether the oil which served as the pump lubricant and coolant had leaked into the salt. Apparently, the salt was contaminated only once by oil from the pump, and this was caused by overfilling the loop with molten salt. However, as the salt circulated through the loop, the carbon content of the salt decreased gradually from a high value of about 200 ppm to a level of 10 to 20 ppm. The oxygen content of the salt also decreased as the salt was pumped through the loop.

[16] The following physical properties were used in the calculations: density (lb/cu ft), metal (586) and water (62); water viscosity, 0.32 cp; surface tension (dyne/cm), metal (450) and water (61); packing surface area, 545 sq ft/cu ft; and packing void fraction, 0.94.

[17] F. R. Dell and H. R. C. Pratt, Trans. Inst. Chem. Engrs. (London) **29**, 89 (1951).

[18] J. H. Ballard and E. L. Piret, Ind. Eng. Chem. **42**, 1088 (1950).

[19] R. R. Breckenfeld and C. R. Wilke, Chem. Eng. Progr. **46**(4), 187 (1950).

[20] J. W. Crawford and C. R. Wilke, Chem. Eng. Progr. **47**, 423 (1951).

[21] INOR-8 is a nickel alloy containing 17 w/o Mo, 7 w/o Cr and 5 w/o Fe.

4. Materials Testing (M. L. Kyle, A. Chandler, L. F. Dorsey, A. Rashinskas, A. Sanders[22])

Liquid copper-magnesium, zinc-magnesium and cadmium-zinc-magnesium alloys in combination with molten chloride salts are being investigated as potential solvent systems for pyrochemical processes. A materials testing program is being conducted to evaluate the solubility of various materials of construction for process applications (see ANL-7225, p. 37). Such items as crucibles, transfer lines, agitators, and associated equipment will be required, and the materials selected for each application may not necessarily be the same. The emphasis is currently placed on liquid copper-magnesium and zinc-magnesium alloys, which are used as donor and acceptor alloys, respectively, in salt transport separations (see Figure I-1). Corrosion rates of various materials are being obtained, and the interactions between candidate container materials and solute uranium in liquid metals and molten salts are also being studied. Although an acceptable corrosion rate is an essential requirement for the process equipment, it is also necessary to avoid losses of uranium and plutonium resulting from interactions with the process equipment.

a. CONTAINMENT OF Cu-Mg-U/HALIDE SALT SYSTEMS

Corrosion Resistance of Cast Iron to Cu-Mg-U/Salt Systems. Cast iron[23] is being tested for corrosion resistance to Cu-Mg-U/halide salt systems[24] at temperatures from 600 to 850°C and copper concentrations from 60 to 90 w/o. The results of three previously reported preliminary tests indicated that although the corrosion rate of cast iron at 800–850°C was acceptable, uranium was apparently being lost from solution by reaction with the crucible (see ANL-7225, p. 38). The analyses of these initial tests have been extended in an attempt to identify the mechanism and severity of uranium losses since it might be possible to reduce these losses to an acceptable level by techniques such as repeated reuse of the crucible or modification of the alloy composition.

In these preliminary tests, two cast iron crucibles were exposed to Cu-9.7 w/o Mg-2 w/o U/halide salt systems at 800 and 850°C. One crucible was exposed to Cu-Mg-U/50 m/o $MgCl_2$-30 m/o NaCl-20 m/o KCl for 170 hr at 800°C and 216 hr at 850°C (386 hr total). The other crucible was exposed to Cu-Mg-U/$MgCl_2$ for 192 hr at 850°C. Uranium losses were about 50% in the first run and about 20% in each of the other two runs. One crucible was sacrificed for metallographic examination and chemical analyses. Metallographic examination revealed no detectable corrosion except for the formation of a metal surface film 5 to 15 mils thick. Electron microprobe and X-ray diffraction analyses of this film indicated no evidence of the presence of U_6Fe or U_2Fe even though these compounds are known to form under similar conditions (see Corrosion of Croloy 16-1 by Cu-Mg-U/Salt Systems, below). However, the analyses did show the presence of a uranium phosphide (either UP or U_3P_4) in the metal film. The source of the phosphorus for this reaction is the small amount (approximately 0.4 w/o) that is added to cast iron for strengthening purposes. If this is the major mechanism for uranium loss, it is expected that continued use of a single crucible would result in smaller losses over an extended period; however, this might have an adverse effect on the strength of the crucible. Work on the containment of Cu-Mg-U/halide salt systems in cast iron crucibles has been temporarily discontinued and will be resumed when similar tests on other candidate materials of construction have been completed.

Corrosion Resistance of Cast CB-30 Stainless Steel to Cu-Mg-U/Salt Systems. Cast CB-30 stainless steel[25] in the form of crucibles[26] is also being tested for containment of Cu-Mg-U/$MgCl_2$ systems. Two crucibles have been tested. One crucible was exposed to a Cu-9 w/o Mg-2 w/o U/$MgCl_2$ system at 850°C in three runs for a total exposure time of 600 hr with no visual evidence of corrosion or deterioration. The second crucible, exposed for 200 hr under similar test conditions, evidenced comparable results.

Uranium analyses of the metal phases for three of the four runs are presented graphically in Figure I-11. Of the three runs presented on this figure, two runs (CuMg-9 and CuMg-9B) were performed with new crucibles. The results of these two runs indicate probable solute instability, with losses of about 10 and 20%, respectively, of the solute uranium. The results of the third run (CuMg-9A), performed by reusing the crucible previously used in run CuMg-9, indicated an apparent uranium loss of about 5%. Reuse of the crucible appears to result in a more stable uranium solution, probably because of the formation of a protective film which is, at least, somewhat adherent.

[22] Analytical Group.

[23] Composition (w/o): 3.48 C, 2.12 Si, 0.405 P, 0.125 S, 0.46 Cr, balance Fe.

[24] The halide salts are $MgCl_2$ and 50 m/o $MgCl_2$-30 m/o NaCl-20 m/o KCl.

[25] Chemical composition (w/o): 0.168 C, 0.33 Mn, 1.93 Si, 18.96 Cr, 0.10 Ni, balance Fe.

[26] Crucible dimensions: 4½-in. OD by 6½ in. high by ¼-in. thick wall, cast with four integral mixing baffles about 5/16 in. wide extending 7/16 in. into the crucible.

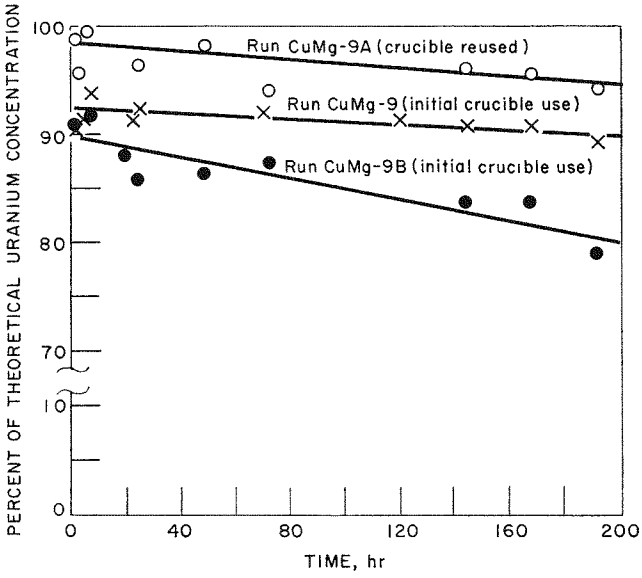

308-400

FIG. I-11. Stability of Uranium Solute in Cu-Mg-U/$MgCl_2$ System in CB-30 Stainless Steel Crucibles.

Temperature: 850°C
Time (each run): 192 hr
Metal Phase:
Weight (each run): about 2,100 g
Composition: Cu-9 w/o Mg-2 w/o U
Salt Phase:
Weight (each run): about 500 g
Composition: 100% $MgCl_2$

In run CuMg-9A, a fine black precipitate was noticed in the salt phase at the metal/salt interface. Several samples of this precipitate were analyzed by X-ray diffraction with inconclusive results: the presence of the $MgCl_2$ matrix precluded identification of the precipitate. An X-ray spectrochemical analysis of this precipitate showed the presence of uranium, copper, magnesium, and iron. After water dissolution of a salt sample to remove the matrix phase, the insoluble material was identified as UO_2 and MgO. However, the water dissolution may have caused the oxidation of some other uranium compound. A sample taken at the metal phase/crucible interface and analyzed by X-ray diffraction showed the presence of UN (major phase) and U_6Fe (minor phase).

Since the formation of UN was unexpected, a run was conducted to determine if the presence of nitrogen gas, as an impurity in the cover gas (argon) used in the corrosion tests, could cause loss of uranium from solution. This run was conducted with an alumina crucible using tantalum accessories to eliminate the possibility of a reaction between the uranium in the Cu-9 w/o Mg-2 w/o U/$MgCl_2$ system being tested and the nitrogen present in steel. Pure nitrogen (at 10 psig) rather than argon was used as the cover gas in an effort to accentuate the problem that could arise from a nitrogen gas impurity in argon. The results of this run which was conducted at 850°C for 98 hr are shown in Figure I-12. In this run, samples were taken only during the early and final portions of the run. The analytical data indicated that the uranium was rapidly lost from the liquid metal solution. Salt samples taken at the same time evidenced a corresponding decrease in the uranium concentration of the salt phase, which indicated that the UN formed was not in solution in either phase.

It is concluded that nitrogen presnt in the gas phase can cause the loss of uranium from solution as can the formation of U_6Fe.

In an effort to determine if nitrogen contamination of the cover gas had been a problem in previous solution stability tests of Cu-Mg-U/$MgCl_2$ systems, probable sources of nitrogen contamination were examined. These were inleakage of air and desorption of nitrogen from graphite accessory equipment (secondaries and receivers). Two solution stability runs were conducted utilizing the same Cu-Mg-U/$MgCl_2$ system. In the first run, the only materials in contact with the liquid metal-molten salt system were alumina, tantalum, and tungsten (these materials are believed to be inert to the process solution); the usual graphite accessory equipment was used. In the second run, the graphite accessories were eliminated.

The analytical results of the two runs indicated that the uranium solute concentration was essentially stable at a concentration slightly less (by 3.0 and 4.4%, respectively) than the calculated theoretical concentration; however, these values are still within the accuracy of the analysis.

Conclusions based on the results of these tests are as follows. (1) The reaction of uranium with nitrogen in the cover gas probably has not been a major problem under the conditions used. (2) The formation of UN resulted from reaction of uranium with the crucible. (3) The major mechanisms for uranium loss were formation of UN and formation of U_6Fe. The loss of plutonium in similar runs may be more extensive than that of uranium since Pu_6Fe forms at a lower temperature (~400°C vs. ~810°C) than does U_6Fe. Work on these two alloys has been temporarily suspended pending testing of other materials which, at this time, appear promising.

Corrosion of Croloy 16-1 by Cu-Mg-U/Salt Systems. Croloy 16-1[27] is a ferritic stainless steel that is available both as tubing and as pipe. This alloy is similar in chemical composition to type 405 stainle

[27] Chemical composition: 15 w/o Cr, 1 w/o Ni, 1 w/o Mn, balance Fe and minor constituents.

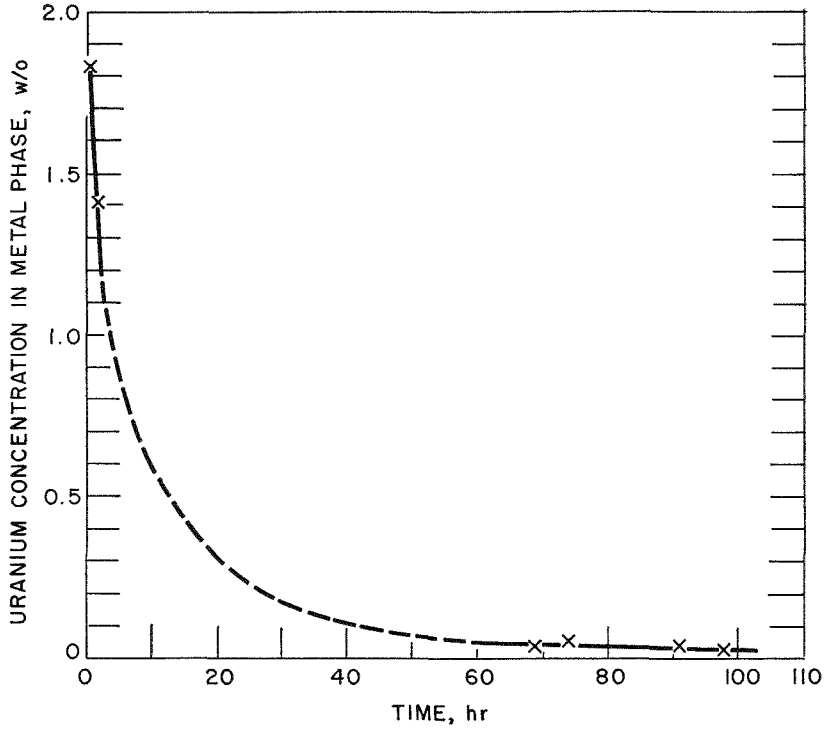

308-414

FIG. I-12. Stability of Cu-Mg-U/$MgCl_2$ System in a Nitrogen Atmosphere.
Temperature: 850°C
Time: 98 hr
Metal Phase:
Weight: 2400 g
Composition: Cu-9 w/o Mg-2 w/o U
Salt Phase:
Weight: 500 g
Composition: 100% $MgCl_2$
Atmosphere: N_2 at 10 psig
Crucible: Alumina
Agitator and thermowell: Tantalum

steel[28] which is not readily available in fabricated forms. Because of favorable experience in the containment of many molten metal/salt systems by type 405 stainless steel, Croloy 16-1 is currently being tested for possible utilization as a process transfer line material for molten Cu-Mg/salt systems.

Two corrosion tests of Croloy 16-1 were previously reported (ANL-7225, pp. 39–40). The following corrosion rates were observed for specimens exposed to the metal phase (Cu-9.7 w/o Mg-2 w/o U): 4 to 16 mils/197 hr at 800°C, salt phase, 50 m/o $MgCl_2$-30 m/o NaCl-20 m/o KCl; 2 to 10 mils (generally observed) and up to 100 mils (localized areas) in 191 hr at 850°C, salt phase, $MgCl_2$. Metallographic examination indicated that the mode of attack was by the formation of a surface reaction film. Electron microprobe analysis of this film showed the presence of U_6Fe.

A Croloy 16-1 transfer line (1.00-in. OD by 0.120-in. thick wall) was used in several engineering demonstration runs of the salt transport process (see section I.B.2.). The transfer line was exposed to Cu-Mg-U/$MgCl_2$ and Zn-Mg-U/$MgCl_2$ salt systems at temperatures of around 800°C for about 60 hr and was used for approximately 200 salt transfers between the two metal solutions. Examination of this line after exposure indicated very little corrosion on the inside of the tube exposed to the molten salt. The end exposed to the Cu-Mg-U phase showed about 36 mils of corrosion whereas the end exposed to the Zn-Mg-U phase showed about 80 mils of corrosion. It is concluded that Croloy 16-1 possesses adequate corrosion resistance to Cu-Mg-U/$MgCl_2$ systems to allow its use in

[28] Chemical composition: 13 w/o Cr, 1 w/o Mn, 0.2 w/o Al, balance Fe and minor constituents.

TABLE I-6. Corrosion of Low-Carbon Content Molybdenum and TZM Alloy by Cu-Mg-U/Halide Salt Systems

Coupons were exposed as agitator blades (2 in. long by ¾ in. wide by 0.070 in. thick) attached to a tungsten agitator shaft rotating at 250 rpm in test solutions contained in an alumina crucible (volume, 2400 ml).

Coupon composition: Molybdenum of low carbon content (0.003 w/o); TZM, a molybdenum alloy containing titanium (0.5 w/o) and zirconium (0.08 w/o).

	Run CuMg-				
	14	22	15	21	26
Alloy Tested	Mo	Mo	TZM	TZM	TZM
Metal Phase					
Weight (g)	2400	2000	2700	2000	3500
Composition (w/o)	89 Cu-9 Mg-2 U	66 Cu-33 Mg-1 U	89 Cu-9 Mg-2 U	89 Cu-9 Mg-2 U	89 Cu-9 Mg-2 U
Salt Phase					
Weight (g)	500	500	500	500	500
Composition (m/o)	100 $MgCl_2$	50 $MgCl_2$-30 NaCl-20 KCl	100 $MgCl_2$	100 $MgCl_2$	50 $MgCl_2$-30 NaCl-20 KCl
Time (hr)	200	192	200	133	192
Temperature (°C)	850	700	850	850	760
Observed Depth of Corrosion (mm)					
Metal phase	<0.01	0.02	0.01	0.02	0.02
Metal/salt interface	0.01	0.11	<0.01	0 05	0.03
Salt phase	<0.01	0.19	<0.01	0.01	0.03
Vapor phase	0.01	0.02	<0.01	[a]	0.02

[a] Not tested.

exploratory engineering runs, but it may not be adequate for eventual process use. Other materials will be tested for this application.

Containment of Cu-Mg/$MgCl_2$ Systems in Silicon Carbide Crucibles. Silicon carbide is being considered as a possible crucible material for pyrochemical processes because it is relatively inexpensive, easily available and apparently inert to process solutions. The Carborundum Corporation is now developing a high-density form of silicon carbide which may eliminate the salt leakage problem that has previously prevented the use of silicon carbide in process application. Leak tests of a high-density silicon carbide crucible (6-in. OD by 5-in. ID by 4-in. height) were carried out. In the first test, it held water for 72 hr without noticeable leakage. In another test, this same crucible also successfully contained a Cu-9 w/o Mg/$MgCl_2$ salt system for 171 hr at 850°C without noticeable salt or metal leakage. The crucible will now be retested in a uranium solution stability experiment.

Corrosion of Type 304 Stainless Steel in Cu-Mg-U/$MgCl_2$ Systems. Type 304 stainless steel was tested for corrosion resistance to a Cu-9 w/o Mg-2 w/o U/$MgCl_2$ salt system in a 192-hr run at 850°C. The material was tested as 0.031-in. thick agitator blades. Four blades were located on the shaft so that each blade was exposed to one of the following phases: metal, salt, metal/salt interface, and vapor. Inspection of the coupons after exposure showed the following. The metal-phase sample had completely disintegrated. Portions of the sample exposed at the metal/salt interface evidenced attack in excess of 16 mils (the half-thickness of the specimen). The sample exposed to the salt phase was still intact and metallographic examination indicated the formation of a 4-mil thick reaction film (probably an intermetallic compound) of unidentified composition. The reaction film tended to be nonadherent and, therefore, would be ineffective in preventing further corrosion. The vapor phase sample evidenced a similar reaction film to a depth of only about 0.2 mil.

It is concluded that type 304 stainless steel is not a desirable container material for Cu-Mg-U/$MgCl_2$ systems at 850°C.

Corrosion of Tenelon Steel by Cu-Mg-U/$MgCl_2$ Systems. Tenelon[29] steel (18 w/o Cr, 15 w/o Mn, 0.75 w/o (max) Ni, 0.1 w/o C, balance Fe and minor alloying elements), which is austenitic in structure (as is type 304 stainless steel), is currently being tested as a candidate material for containment of Cu-Mg-U/$MgCl_2$ systems.

Tenelon was tested as agitator blades, which were used to stir a Cu-9 w/o Mg-2 w/o U/$MgCl_2$ salt system for 192 hr at 850°C. Four specimens, 0.077-in. thick, were used; each specimen was located on the stirrer shaft so that it was exposed to a separate phase.

Metallographic and chemical analyses were per-

[29] Product of United States Steel Corporation.

formed to determine the extent of corrosion. Corrosion rates of the various coupons and their locations were as follows: vapor phase, none detected; metal/salt interface and salt phase, ~3 mils; metal phase, ~5 mils (general) and ~12 mils (localized). The salt and metal phases were analyzed for manganese. None was detected in the salt phase; the amount found in the metal phase (~0.5 g) would account for an attack of about 5 mils on the coupon (if uniform dissolution is assumed), an amount that is in agreement with the measured value. Uranium analyses during the run were inconclusive; the indicated loss (~3.8%) may be real, but the difference is within analytical variation.

It is concluded that even though Tenelon stainless steel possesses some usefulness in containing Cu-Mg-U/$MgCl_2$ systems, it will be slowly attacked, probably by both the dissolution of the contained manganese and the formation of a uranium intermetallic compound.

Corrosion Resistance of Low-Carbon Content Molybdenum and TZM Alloy to Cu-Mg-U/Halide Salt System. Both molybdenum of low-carbon content (0.003 w/o) and TZM alloy (0.5 w/o Ti, 0.08 w/o Zr, balance Mo) are being tested for corrosion resistance to Cu-Mg-U/halide salt systems. These alloys are being tested because of their good high-temperature properties, reported corrosion resistance to a variety of molten salts and liquid metals,[30] and good fabrication properties.

Specimens of these materials, as agitator blades, were exposed to Cu-Mg-U/halide salt systems. The test conditions and results are presented in Table I-6. In the TZM runs conducted with Cu-9 w/o Mg-2 w/o U/$MgCl_2$ at 850°C, and the one run performed with Cu-9 w/o Mg-2 w/o U/$MgCl_2$-30 m/o NaCl-20 m/o KCl at 760°C, the alloy performed well. In four of the five runs, corrosion rates were low; the corrosive attack appeared principally at the ends of the rotating agitator blades. In the remaining run, carried out with Cu-33 w/o Mg-1 w/o U/$MgCl_2$-30 m/o NaCl-20 m/o KCl system at 700°C, molybdenum specimens exposed to metal/salt interface and salt phase were severely corroded. The reason for the observed high corrosion rate is unknown since the lower temperature and decreased copper concentration were expected to reduce the corrosiveness of the system. The possibility that the ternary salt is more corrosive to molybdenum than is pure $MgCl_2$ is currently being investigated.

It is concluded that TZM alloy and molybdenum may be usable as a material of construction for salt transport separations, but more extensive testing of the two materials is required. TZM and molybdenum crucibles (4¾-in. OD by 6½ in. high by 0.075 in. thick) are currently being fabricated for testing.

[30] F. B. Nair and J. Z. Briggs, *Corrosion Resistance of Molybdenum and Molybdenum Base Alloys*, Climax Molybdenum Company of Michigan Technical Note, January 1964.

TABLE I-7. Corrosion of Low-Carbon Content Molybdenum and TZM Alloy by Zn-Mg-U/Halide Salt Systems

Coupons were exposed as agitator blades (2 in. long by ¾ in. wide by 0.070 in. thick) attached to a tungsten agitator rotating at 250 rpm in test solutions contained in an alumina crucible (volume, 2400 ml).

Coupon composition: Molybdenum of low carbon content (0.003 w/o); TZM, a molybdenum alloy containing titanium (0.5 w/o) and zirconium (0.08 w/o).

	Run SRP-		
	23	24	25
Alloy Tested	TZM	TZM	Mo
Metal Phase			
Weight (g)	1200	1200	3200
Composition (w/o)	35 Zn-64 Mg-1 U	87 Zn-10 Mg-3 U	94 Zn-5 Mg-1 U
Salt Phase			
Weight (g)	500	500	500
Composition (m/o)	100 $MgCl_2$	100 $MgCl_2$	50 $MgCl_2$-30 NaCl-20 KCl
Time (hr)	200	195	192
Temperature (°C)	850	750	700
Observed Depth of Corrosion[a] *(mm)*			
Metal phase	<0.01	0.07	0.26
Metal/salt interface	<0.01	0.07	0.23
Salt phase	<0.01	0.01	[b]
Vapor phase	<0.01	[b]	0.01

[a] The corrosion mechanism appears to be a dissolution of the molybdenum.

[b] Not tested.

b. CONTAINMENT OF Zn-Mg-U/HALIDE SALT SYSTEMS

Corrosion Resistance of Low-Carbon Content Molybdenum and TZM Alloy to Zn-Mg-U/Chloride Salt Systems. Molybdenum of low carbon content and TZM alloy are also being tested for containment of Zn-Mg-U/halide salt systems. In these tests, molybdenum and TZM coupons in the form of agitator blades were exposed to Zn-Mg-U/chloride salt systems. The test conditions and results of tests performed to date are presented in Table I-7.

The low corrosion rates of TZM alloy exposed to the Zn-64 w/o Mg-1 w/o U/$MgCl_2$ system at 850°C and to the Zn-10 w/o Mg-3 w/o U/$MgCl_2$ system at 750°C are considered very encouraging and further testing of TZM alloy will be performed. The reason for the high

corrosion rates observed for molybdenum exposed to the Zn-5 w/o Mg-1 w/o U/$MgCl_2$-30 m/o NaCl-20 m/o KCl system at 700°C is uncertain. However, the high rate is believed to be due either to the increased zinc concentration of the metal phase or to increased corrosiveness of the ternary salt. These effects will be investigated further.

In these tests, the TZM and molybdenum coupons exposed to the metal phases lost their normal room-temperature ductility. The reason for this loss in ductility is not fully understood, since metallographic examination revealed no observable molybdenum leaching, structural changes, or obvious interstitial element pickup. Hardness tests taken before and after exposure showed no measurable difference on any sample. It is suspected that this apparent loss of ductility is a result of increased notch sensitivity of the metal after wetting by the liquid metal phase.

Corrosion Resistance of Croloy 9M to Zn-Mg-U/$MgCl_2$ Systems. Croloy 9M is a ferritic stainless steel similar in composition to Croloy 16-1 except for the lower chromium content (9 w/o vs 16 w/o). This material was tested for possible application as a transfer line in salt transport separations. The Croloy 9M was exposed to a Mg-35 w/o Zn-2 w/o U/$MgCl_2$ system at 850°C for 100 hr as agitator blades; one blade was exposed to the metal phase, one to the metal/salt interface, one to the salt phase, and one to the vapor phase. Corrosion of the samples from the metal phase and metal-salt interface was severe (penetrations of 1.1 and 0.9 mm, respectively) whereas that of the samples from the salt and vapor phases was slight (0.04 mm and 0.03 mm, respectively). These results suggest that Croloy 9M is an acceptable material for use with molten $MgCl_2$ but not for liquid zinc-magnesium alloys, except for very short periods of time.

C. PROCESS EQUIPMENT DEVELOPMENT—SKULL RECLAMATION PROCESS

(G. J. Bernstein, R. K. Steunenberg, P. Fineman)

At the conclusion of the EBR-II melt refining operation, a residue (skull) containing uranium remains in the processing crucible. A process has been developed and successfully demonstrated for reclaiming the uranium from the skull and removing a large fraction of the included fission products (ANL-7225, pp. 42–47). The recovered uranium is returned to the melt refining process as make-up material. The skull is initially converted into a free-flowing oxide powder in a skull oxidation furnace, which is now in use in the EBR-II Fuel Cycle Facility (see ANL-6900, pp. 116, 118–120). Plant-size equipment for processing the skull oxides in the Fuel Cycle Facility has been built and tested by this Division. The equipment is sized for operation on about 5.8 kg of skull oxide (~5 kg of uranium oxide), which is equivalent to the amount of skull material produced in about seven normal melt refining skulls.

The skull reclamation process consists of the following operations. (1) The oxidized skull material is charged to a molten halide salt flux, the salt phase is contacted with liquid zinc to extract the noble metal fission products, and the zinc phase is removed. (2) The salt phase is then contacted with a magnesium-rich Zn-Mg alloy which reduces the uranium oxides to metal. Metallic uranium, which has a very low solubility in the Zn-Mg alloy, precipitates from solution. The salt and the supernatant alloy, which contain most of the remaining fission products, are transferred off as wastes. (3) The uranium product is redissolved in a zinc-rich Zn-Mg alloy and the solution is transferred to a mold. (4) The resulting U-Zn-Mg ingot is retorted to remove zinc and magnesium, and the metallic uranium product is consolidated by melting.

Two furnaces are required for the process: (1) a reduction furnace where the noble metal extraction, oxide reduction, and uranium redissolution steps are performed, and (2) a retorting furnace where solvent metals are vaporized from the uranium and the uranium sponge is melted. Although installation of the reduction furnace and retorting furnace in the Fuel Cycle Facility has been postponed (ANL-7225, p. 46), the retorting furnace will be used at Argonne, Illinois, to investigate retorting operations in other pyrochemical processes.

1. Skull Oxide Reduction Furnace (W. Miller, J. Lenc, J. Wolkoff, R. Paul, P. Kelsheimer,[31] E. Johnston)

In the preceding semiannual report (ANL-7225, pp. 43–44) the results of the direct examination[32] of the skull oxide reduction furnace at the conclusion of the first series of runs (SRR-2 through SRR-10) were reported. That examination revealed an accumulation of flux and oxides on the interior surface of the tungsten crucible wall. This material was removed manually in preparation for the next series of runs (SRR-11 through SRR-18; ANL-7225, pp. 44–47). Following the completion of the latter series, an attempt was made to recover accumulated material by a method suitable for remote operation. A recovery procedure involving chemical treatment was tested. The furnace was charged with a Zn-13 w/o Mg alloy (30 kg) and sufficient salt mixture (70 kg of 47.5 m/o $MgCl_2$-47.5 m/o $CaCl_2$-5 m/o CaF_2) to almost fill the tungsten crucible so as to provide contact with most of the interior surface of the crucible. This alloy and salt mixture were agitated for several hours at 800°C and then discharged. Approximately 350 g of uranium was removed with the zinc-magnesium alloy, an amount that represented about 1.1% of the total uranium charged in the last series of runs. An equivalent amount was subsequently removed during a direct manual cleanout of the furnace after the inert-atmosphere enclosure in which it is located was returned to air. Overall accountability of the 32.5 kg uranium charged in the eight runs was about 97.8%. Accountability of less than 100% is attributed to possible bias in obtaining small representative samples of large volumes of non-homogeneous process streams. Recovery of uranium in the product stream of runs that closely followed the process flowsheet was about 92.6% and is adequate for the process (see ANL-7225, pp. 46–47). This uranium recovery from skull oxides combined with melt refining pouring yields of 93% would result in an overall uranium recovery of greater than 99%.

Direct examination of the furnace revealed that foaming and overflow of a portion of the salt flux had occurred during the chemical treatment or wash run. This salt had solidified in the annulus between the tungsten crucible and the Hastelloy C furnace shell. Consequently, when the furnace cooled cracks developed in the Hastelloy C furnace body and in the tungsten crucible which are attributed to stresses resulting from the presence of the solid salt layer and the greater contraction of Hastelloy C as compared with tungsten.

The foaming and overflow of the salt is attributed to the fact that an unusually large quantity of salt was used which may not have been entirely free of moisture. Under standard flowsheet conditions such foaming would not occur. The mechanical performance of the equipment during the two series of runs was reliable and reproducible.

Testing of the reduction furnace and auxiliaries was considered completed after run SRR-18. Since a decision had been made earlier to postpone installation of the skull reclamation equipment in Idaho, the furnace is not being rebuilt at the present time.

2. Recovery of Uranium Product by Retorting (J. Lenc, W. Miller, J. Wolkoff, M. Slawecki,[31] R. Paul, P. Kelsheimer,[31] E. Johnston)

In the EBR-II Skull Reclamation Process, the final process stream from the skull oxide reduction furnace is about 8 liters of a Zn-12 w/o Mg-12 w/o U solution weighing approximately 36 kg and containing about 4 kg of uranium. Retorting equipment has been developed for recovering uranium from this solution in a form suitable for use as a supplementary feed material for the melt refining process. Recovery of the uranium is achieved by distilling off the zinc and magnesium. To date, development of this retorting equipment has been directed specifically toward uranium recovery in the reprocessing of EBR-II fuel. A similar recovery procedure may be applicable to other pyrochemical fuel reprocessing schemes currently under consideration. The plant-scale (4 to 4.5 kg U) retorting equipment has been previously described (ANL-7175, pp. 18–22).

In recent work, twenty-two additional runs (PSR-26 through PSR-47) were completed in the plant-scale retorting unit located in the large argon-atmosphere enclosure. The approximate composition of the charge material was Zn-12 w/o Mg-1 to 12 w/o U and total charges ranged from about 11 to about 37 kg. All runs were conducted at a nominal pressure of 10 torr in thixotropically cast beryllia crucibles. The bulk of the volatile zinc and magnesium metal was distilled at temperatures of 650 to 750°C. Vaporization of the re-

[31] Design Group.

[32] The inert-atmosphere enclosure in which the equipment was located was returned to an air atmosphere to permit direct examination and maintenance of equipment, after which the enclosure was returned to an argon atmosphere.

TABLE I-8. Performance of Thixocast Beryllia Crucibles[a] in Retorting Runs

Crucible Identification	Number of Retorting Runs
Original Thixocast BeO[b]	10
BeO No. 1	7
BeO No. 7	10
BeO No. 8	6
BeO No. 9	6
BeO No. 14	6
Total	45

[a] Purchased from The Brush Beryllium Company of Elmore, Ohio.

[b] The first plant-scale thixocast beryllia retorting crucbile purchased from The Brush Beryllium Company prior to their subcontract arrangement with this Division to investigate variables in the fabrication of plant-scale retoring crucibles (ANL-7225, p. 49).

maining volatile material and liquation of the uranium product were achieved by increasing the temperature to 1150–1200°C for about 45 min. The average distillation rate in the recent runs ranged from about 30 to 50 g/min.

Satisfactory containment of the zinc and magnesium vapors within the retorting apparatus was achieved in all of the twenty-two latest runs. Of the total zinc and magnesium (459 kg) distilled in these runs, only 1.27 w/o escaped from the graphite enclosure. Of this amount, 0.87 w/o was condensed on the Fiberfrax insulating sleeve and 0.4 w/o was unaccounted for. In these runs, essentially all of the retorted product was in the form of a consolidated ingot which was dumped out of the beryllia crucible with ease. Small quantities of product material which adhered to the inner surface of the crucible were recycled to succeeding runs.

The twenty-two current runs were conducted in four different thixotropically cast (thixocast) beryllia crucibles.[33] Nine of the runs (PSR-26 through PSR-34) were made in the same crucible, designated by the fabricator as BeO No. 7, that had been previously used in one run (PSR-25, ANL-7225, p. 50). One of the runs (PSR-35) was made in a crucible, designated BeO No. 1, that had been used in six previous runs (PSR-14, -16, -21, -22, -23, and -24, ANL-7225, p. 49). Of the twelve remaining runs of the recent series, six runs (PSR-36 through PSR-41) were made in a crucible designated BeO No. 14 and six runs (PSR-42 through PSR-47) were made in a crucible designated BeO No. 9.

A tabulation of the number of retorting runs conducted in the various thixocast beryllia crucibles tested to date is shown in Table I-8. All six of the crucibles listed in this table have performed successfully in containing the bulk of the retorted uranium product and are still intact. After each retorting run, a small quantity of uranium was found in the annular space between the beryllia crucible and its graphite secondary container. The presence of uranium in this annulus is attributed to seepage of the Zn-Mg-U retorting solution through the crucible wall. In a series of six runs (PSR-42 through PSR-47) conducted in the same thixocast crucible (BeO No. 9) using full-scale (about 35 kg) charges, the total weight of uranium found in the annulus amounted to about 65 grams or approximately 0.31 w/o of the total retorted product.

Summary. The reliable operation of the retorting furnace has been established in the course of the 45 runs made with unirradiated uranium-containing charges. The containment of the zinc and magnesium vapors within the distillation apparatus has been satisfactory. Of the 12 plant-scale beryllia crucibles which were to be supplied by The Brush Beryllium Company under their development contract (see ANL-7225, pp. 49–50), five have been tested, as indicated in Table I-8. The crucibles that have been tested were found to be durable, and the release of the retorted uranium ingot was readily achieved. The slight amount of solution seepage is not considered significant from a process standpoint; the uranium found in the annulus could be recovered if necessary. Since the plant-scale beryllia crucibles appear to be satisfactory for their intended use in retorting operations, the development contract with The Brush Beryllium Company is being terminated.

3. Removal of Uranium from Metal Crucible by Hydriding (J. Lenc, W. Miller)

In the current reference flowsheet for pyrochemical reprocessing of fast reactor core and blanket material (Figure I-1), about 50 kg of uranium product will be accumulated in one of the process crucibles. The bulk of the uranium is expected to be in the form of a precipitate enveloped in a matrix of residual magnesium possibly covered by a thin layer of flux. This material is expected to adhere tenaciously to a metal crucible.

The use of a hydriding procedure is being considered for removing the uranium from the crucible. Removal by melting is presently not feasible since molten uranium will react with metallic crucibles suitable for the

[33] A product of The Brush Beryllium Company, Elmore, Ohio.

pyrochemical process. Dissolution of the uranium as a Zn-12 w/o Mg-12 w/o U solution which could be transferred from the metal crucible into a beryllia retorting crucible is undesirable because of the large quantity of zinc-magnesium that would have to be removed by retorting.

Previous experiments (see ANL-7055, pp. 68, 70) showed that under certain conditions it is possible to break up a uranium-rich mixture by hydriding the uranium and thereby facilitate removal of the material from a metal crucible. If removal of uranium-rich material from the crucible following a hydriding step can be demonstrated for the current reference flowsheet, only the relatively small amount of magnesium and residual flux present would have to be removed by retorting. Equipment for the preparation of uranium precipitates and the testing of hydriding procedures is being set up.

4. Absorption of Molten Salts by Fiberfrax (W. Miller, R. Paul)

In the course of plant-scale reduction furnace runs it was found that molten salts readily wet Fiberfrax[34] and are absorbed while molten metals do not wet (see ANL-7225, pp. 43, 45–46). A simple trap made of Fiberfrax was used in some of the runs to remove the small amount of residual flux which transfers with the final liquid metal product. An application for salt absorption in a molten salt-molten metal process may lie in its use to remove small quantities of residual flux in crucibles which contain molten metal product solutions.

Several tests have been performed to measure the absorption of molten salt by Fiberfrax. Cylinders (rods) of low-density Fiberfrax (0.3 g/cm³), 17 in. long and ⅝ in. in dia., were cut from flat stock by core drilling. The rods were outgassed under vacuum at 700°C and then supported vertically over a molten salt bath with one end submerged in the bath to a depth of 1 in. The salt consisted of 62 m/o $CaCl_2$-38 m/o NaCl in which 1 w/o each of $PbCl_2$ and $CdCl_2$ was dissolved. The rods and the salt bath were maintained at 700°C. Following a given period of submergence, the rods were withdrawn from the bath and cooled. Each rod was sectioned into wafers which were weighed to determine salt content. The quantity of salt found in the bottom section of each rod was assumed to be the maximum quantity of salt which the rod could hold and is designated as the saturation quantity. The salt content at saturation was 6.5 g salt/g Fiberfrax or 2.0 g salt/cm³ Fiberfrax. The distribution of salt along two low-density Fiberfrax rods after immersion periods of 5 and 10 min is shown in Figure I-13. Wafers cut from the ends of the rods will be examined for evidence of any segregation of lead and cadmium salts which would indicate some form of chromatographic separation.

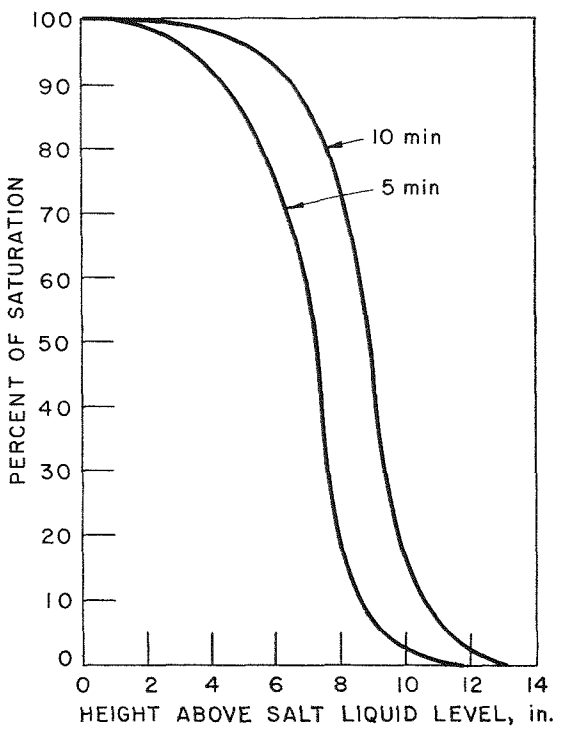

308-412

Fig. I-13. Absorption of Salt by Low-Density Fiberfrax.
Rod Dimensions: ⅝-in. dia. by 17 in. long; 2 rods
Fiberfrax Density: 0.3 g/cm³
Salt Composition: 62 m/o $CaCl_2$-38 m/o NaCl containing 1 w/o each of $PbCl_2$ and $CdCl_2$
Saturation: 6.5 g salt/g Fiberfrax
Immersion Time: 5 or 10 min
Temperature: 700°C

A similar test was made with a higher density Fiberfrax rod (0.5 g/cm³), 29 in. long and ⅝ in. in dia., which was immersed for 22 hr. Examination of samples cut from the rod showed that the limiting height to which the salt would travel had not been reached. The distribution of salt in the higher density Fiberfrax rod is shown in Figure I-14. Measurement of the quantity of salt in the lowest section showed the saturation content was 3.5 g salt/g Fiberfrax or 1.7 g salt/cm³ Fiber-

[34] A mineral fiber material consisting of approximately 51% alumina and 49% silica manufactured by Carborundum Co. The material used in the tests was molded from the fiber by Refractory Products Co.

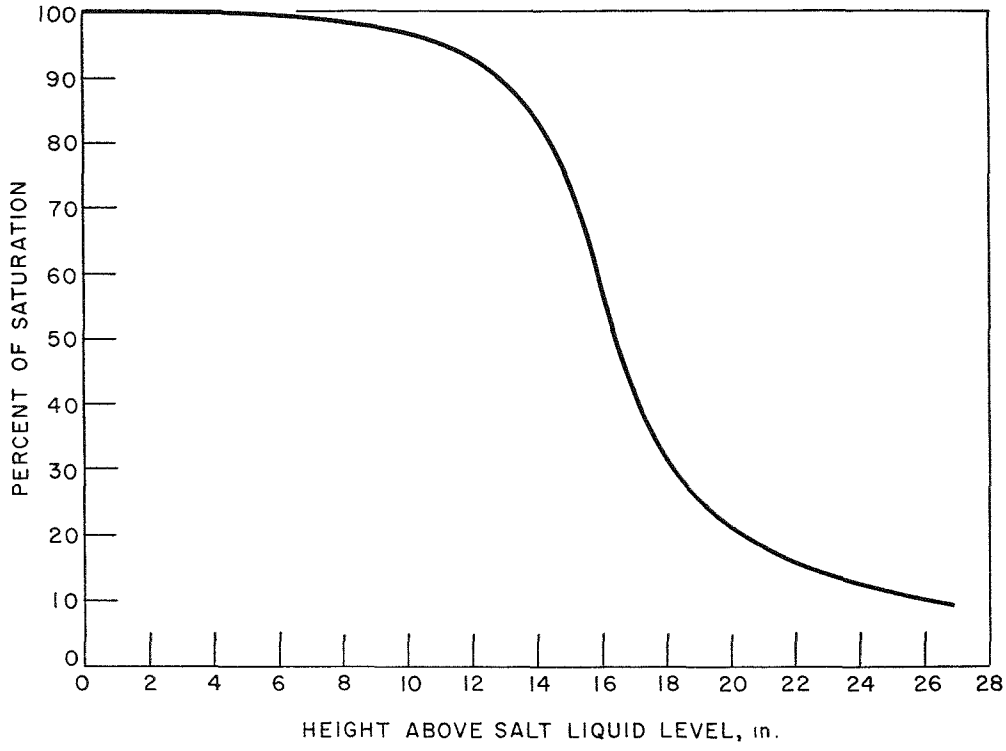

308-404

FIG. I-14. Absorption of Salt by High-Density Fiberfrax.
Rod Dimensions: ⅝-in. dia. by 29 in. long
Fiberfrax Density: 0.5 g/cm³
Salt Composition: 62 m/o $CaCl_2$-38 m/o NaCl containing 1 w/o each of $PbCl_2$ and $CdCl_2$
Saturation: 3.5 g salt/g Fiberfrax
Immersion Time: 22 hr
Temperature: 700°C

frax. The less dense Fiberfrax was found to hold more salt at saturation on a volume basis as well as on a weight basis. Additional tests are planned to obtain information on rates of salt absorption and to measure the performance of Fiberfrax rods in removing a molten salt layer from the surface of a molten metal.

D. FUEL CYCLE FACILITY OPERATIONS (C. E. STEVENSON, M. J. FELDMAN, D. C. HAMPSON)[35]

In order to meet the fuel requirements of the Experimental Breeder Reactor-II, process operations in the adjacent Fuel Cycle Facility (FCF) were increased. For the six-month period ending October 1966, 83 discharged reactor subassemblies were processed and 70 subassemblies were refabricated for return to the reactor.

A continuation of the study of the variables of time and temperature in the melt-refining process indicated that 2.5 to 3.0 hr of liquation at 1400°C are required for more than 98% removal of alkali, alkaline earth, and rare earth fission products. The removal of cerium is the limiting factor; a removal of as low as 77% was observed in a 2-hr liquation period at 1300°C.

In the removal of Vycor glass molds from injection cast fuel elements, a small amount of fuel alloy accompanies the crushed glass. Arrangements have been made with the Idaho Chemical Processing Plant to recover the uranium from this fissium alloy by HNO_3 leaching.

Post-irradiation examination of Mark IA fuel [13.5-in. long pin, enriched uranium (~52 a/o ^{235}U)-fissium alloy] has indicated a somewhat higher rate of swelling than that observed for the Mark I fuel [14.22-in. long

[35] Idaho Division.

pin, enriched uranium (~48 a/o ^{235}U)-fissium alloy], and approximately the same maximum burnup limitation. Marked differences have been observed in the swelling behavior of various batches of recycled fuel alloy, which appear to be related to the process steps which precede casting. Causes for this behavior are not yet understood but various possibilities are being examined.

A summary of operating and maintenance experience with the electromechanical manipulators and cranes used in the Facility shows generally excellent performance. Over several years of use, the time of actual operation per manipulator unit for each of the various motions (grip, rotation, hoist, bridge travel, and carriage travel) has varied from 120 to 640 hours (the grip and grip rotation show the least usage, and the bridge travel shows the largest). A wide variety of repairs has been effected, either remotely or after removal from the cell.

1. Summary of Process Operations in the Fuel Cycle Facility (M. J. Feldman, D. C. Hampson)[35]

Process operations were carried out at an increased rate as compared with the preceding period (ANL-7225, pp. 54–55), which was the capacity of the Facility with the manpower then available. Maintenance efforts were required for the repair of manipulators and process equipment. The cooling system for the Air Cell storage pits was extended by remote installation of the necessary piping, and the number of pits containing inserts for the storage of subassemblies was increased from 4 to 9 (ANL-6605, pp. 26–27). Process operations are summarized in Table I-9.

TABLE I-9. Summary of Fuel Cycle Facility Process Operations
(*May 1966 through October 1966*)

Operation	No. of Units
Irradiated subassemblies cleaned of sodium and dismantled	83
Fuel elements decanned, including process rejects	7802
Melt refining ingots produced from discharged reactor fuel	47
Total melt refining ingots produced, including recycled material	79
Injection casting operations	78
Injection castings produced	8000
Acceptable cast pins produced	7077
Fuel elements assembled and welded	7596[a]
Fuel elements passing leak test	7161[a]
Fuel elements bonded and passing bond test	6132[a]
Subassemblies fabricated	70

[a] Including 151 fuel elements fabricated at Argonne, Illinois (less than 151 in subsequent steps; see ANL-7225, p. 55).

2. Processing Irradiated Fuel by Melt Refining (R. M. Fryer)[35]

Volatile and chemically active fission products are removed from discharged fuel by holding the molten fuel alloy in contact with a ZrO_2 crucible and separating the purified alloy from the dross (or skull) formed by pouring the alloy from the crucible. Melting is effected by induction heating of a graphite susceptor which supplies heat to the crucible.

a. EFFECT OF MELT-REFINING VARIABLES ON FISSION PRODUCT REMOVAL

In a continuation of earlier studies (ANL-7125, p. 54) aimed at defining minimum process conditions for melt refining, the effect of liquation temperature on fission product removal was investigated. A series of two-hour runs was made with irradiated fuel (average burnup, 0.25 to 0.85 a/o) in which the liquation temperature was varied between 1300 and 1400°C. As shown by the results listed in Table I-10, cesium and barium were removed to the extent of 99.9% or more at 1350°C. Only 89 to 97% of the cerium was removed at this temperature; a temperature of 1400°C was required for 99.9% removal of cerium in this series of runs. At 1300°C, only cesium was removed to a high extent (99.5%).

Additional analytical data from run MR-47 indicate that technetium acts similarly to molybdenum, ruthenium, palladium, and rhodium during melt refining, in that its concentration is but little affected. The

concentration of technetium was slightly higher in the refined ingot than in the charge, indicating that the technetium did not react with the ZrO_2 crucible.

In another series of melt-refining runs conducted at a liquation temperature of 1400°C, data on fission product removal have been obtained for various liquation periods. The analytical results show 98% or better removal of barium, cesium. and iodine for liquation periods of 0.25 to 4.0 hr. Data for cerium indicate that its removal is time-dependent at this liquation temperature in that 2.5 to 3.0 hr are required for quantitative (>98%) removal. Figure I-15 is a graph of the cerium removal data.

Although it is not possible to relate these results directly to previous work on melt refining, the general conclusion is that these results confirm the original conditions specified for melt refining, i.e., a 3-hr liquation period and a 1400°C liquation temperature are required to assure adequate fission product removal (ANL-6696).

TABLE I-10. Effect of Variations in Liquation Temperature on Fission Product Removal in Melt Refining

Charges: 10.1 to 11.3 kg which consisted of 0.5 to 1.1 kg make-up alloying material (uranium and noble metals), balance decanned irradiated fuel (except 0.9 kg reject castings in run MR-34)
Liquation Period: 2 hr

Run No.	Ave. Burnup (a/o)	Liquation Temp. (°C)	Fission Product Removals (%)		
			Cerium	Barium	Cesium
MR-4[a]	0.25	1400	99.9	>99.9	>99.9
MR-33	0.82	1350	96.5	99.9	>99.9
MR-34	0.67	1350	88.8	>99.9	>99.9
MR-47	0.85	1300	77.0	96.6	99.5

[a] Data previously presented (ANL-7125, Table I-18, p. 55).

b. PERFORMANCE OF MELT-REFINING FURNACE INDUCTION HEATING SYSTEM

A several-turn, solid copper spiral around the melt-refining furnace assembly induces the heating effect in the graphite susceptor. Previously, failure of the coil was observed and was probably due to shifting of packed insulation (ANL-7125, p. 56). This resulted in a crack forming in the furnace insulation which allowed the susceptor, which operates at 1600 to 1800°C, to radiate heat to the coil, thereby causing it to melt.

During the course of current plant operations, two more melt-refining furnace assemblies have failed due to arcing from the induction coils. The failure of these two units is attributed to a different cause than was the failure of the first two furnaces. Examination of the furnaces showed an apparent loss of electrical in-

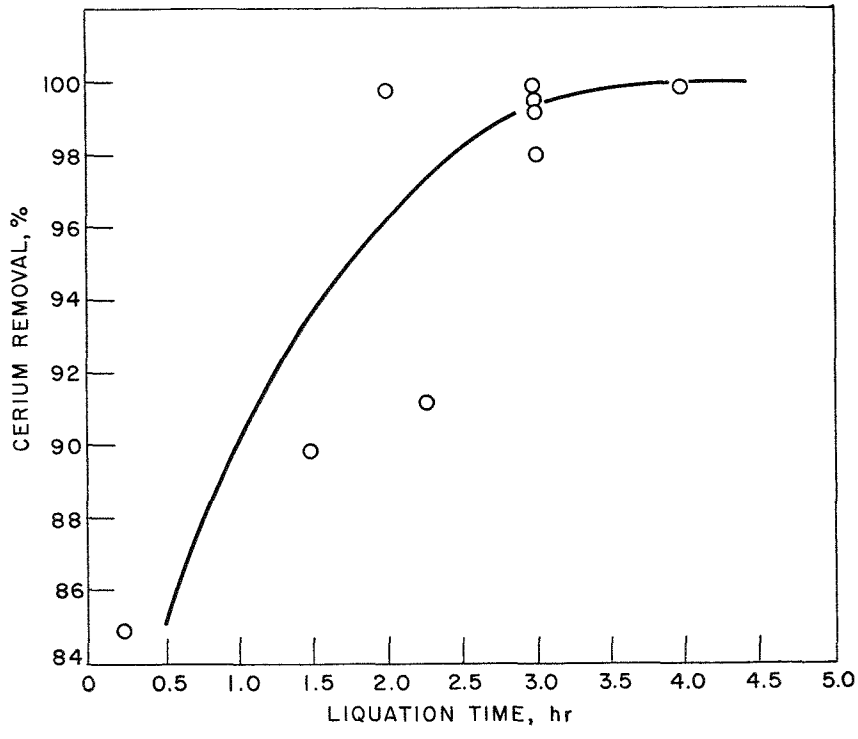

308-403

Fig. I-15. Effect of Variations in Liquation Period on Cerium Removal in Melt Refining. Liquation Temperature: 1400°C

sulating properties of the induction coil supports; however, the cause of failure has not been definitely determined. The number of runs does not appear to be the governing factor; one furnace had operated for 30 runs and the other for 50 runs prior to failure. The failure could be the result of deposition of condensable sodium (some 15 to 50 g of sodium is associated with a kilogram charge of fuel) or fission products that were not contained by the Fiberfrax fume trap which rests over the crucible during melt refining. An effect of sodium deposition is suggested by a closer correlation with the amount of sodium-bonded fuel melt refined in each furnace (220 kg in one and 260 kg in the other), indicating that increased electrical loss through condensing sodium may be the cause of the failure. New furnace assemblies have since been built and installed, in which ceramic coil supports surround the steel supports near the coils.

3. Reclamation of Fuel Alloy Scrap Present in Crushed Glass Molds from Injection Casting Operations (V. G. Eschen, N. J. Swanson)[35]

Precision-bore Vycor[36] glass tubing is employed for molds in the injection or pressure casting of ingots of refined uranium-fissium alloy as received from the melt-refining operations (ANL-6925, pp. 76–79). After the casting is completed and the alloy has cooled and solidified, the glass is removed from the cast fuel pins by the impact of a pneumatically operated hammer, which breaks the glass away from the cast rod and allows the latter to drop through a slot onto deflecting rails. The broken glass falls through a chute and is collected in 3½-gal steel waste cans. About 1 to 2 percent of fuel alloy (short pieces of casting and excess material at the lower end) is lost from the production stream via this route. The loss is estimated by a material balance obtained by weighing the charge, the finished rods, and the sheared ends.

From the beginning of radioactive operations at the FCF (September 1964) until July 1, 1966, a total estimated to be about 24 to 25 kg of refined alloy had been accumulated with the glass mold scrap. All of this material was contained in 36 waste cans (the alloy limit per waste can was 1 kg) that were stored in the Argon Cell.

Arrangements were made for the Idaho Chemical Processing Plant (ICPP) to recover the alloy scrap and to dispose of the glass waste. The ICPP proposes to leach the uranium from the alloy scrap from the broken glass with nitric acid. To reduce overall shipping and processing costs, the 36 cans of scrap mixture were consolidated into 17 cans. The consolidation was possible because advantage was taken of the high boron (which acts as a nuclear poison) content in the glass, which makes it possible now to accumulate up to 3 kg of scrap alloy in a waste can. The cans of scrap mixture (alloy scrap plus broken glass) are shipped to the ICPP in 3-ton, lead-shielded casks. Shipment of the 17 cans of scrap mixture to the ICPP was completed on September 4, 1966.

The glass scrap being generated currently is accumulated in steel waste cans as before. However, the alloy limit of 3 kg is being applied and as soon as this limit is reached, or the can is filled to two-thirds capacity (an operational limit imposed by ICPP), the can is capped. Future shipments to ICPP will occur at intervals of about 6 months when about 12 filled cans have been accumulated. A 12-can shipment is expected to be processed within three weeks. The ICPP requires that all alloy received be cooled at least 120 days following removal from the reactor. Therefore, several cans of glass scrap will be retained in the Argon Cell at all times.

At the current FCF production rate, the quantity of alloy associated with the crushed glass has averaged several kg per month. In an effort to minimize this scrap stream and to develop the FCF into a more completely integrated plant, steps are under way to develop a glass-alloy separator (ANL-6925, p. 82). A prototype separator has been designed and built and will be tested in the mockup area before in-cell installation. This separator consists of a ball mill and a particle classifier and is operated in the following manner. Crushed glass bearing the uranium alloy is added to the ball mill, which is then operated until all of the glass has been pulverized to particle sizes much smaller than those of the contained alloy. The mixture is then dumped onto a screen which permits passage of the glass dust but retains the alloy pieces. The two streams are routed to separate containers for subsequent handling. It is expected that the prototype unit may be sufficiently developed to be used for pilot-plant tests with radioactive glass and alloy scrap mixture during the next year.

[36] Vycor is the trade name for high-silica glass manufactured by Corning Glass Works, Corning, New York.

4. Swelling of EBR-II Fuel as a Result of Irradiation (J. P. Bacca, J. H. Cook)[35]

a. BEHAVIOR OF MARK IA FUEL

Post-irradiation examinations have been conducted on 13 EBR-II subassemblies that utilized type Mark IA fuel elements. The Mark IA element (ANL-7225, p. 55) uses a U-5 w/o fissium alloy fuel pin measuring 0.144 in. in dia. by 13.5 in. in length. The alloy has a nominal ^{235}U enrichment of 52 a/o. For comparison, the EBR-II Mark I fuel element employs a U-5 w/o fissium alloy fuel pin 0.144 in. in dia. by 14.22 in. in length and has a nominal ^{235}U enrichment of 48 a/o. The fuel element jacket assembly is the same for both types of elements except for the length of the restrainer plug-end. This closure is 0.72 in. longer in the Mark IA element than in the Mark I type.

The fuel-burnup capability of the Mark IA element was expected to be greater than that of the Mark I type because of the greater gas-plenum volume (approximately 33% more volume at room temperature) incorporated in the fuel element design. This greater volume, into which swollen fuel and displaced sodium can move, was expected to result in significantly lower internal gas pressure within the element, with resultant lower cladding stresses, as burnup of the fuel progressed.

Determination of fuel swelling by eddy current measurement of the increase in sodium level and by void volume was carried out on Mark IA subassemblies at various fuel-burnup increments in the range of 0.58 to 1.22 a/o maximum subassembly burnup (0.46 to 1.06 a/o average subassembly burnup). Swelling values are normally the average of 21 elements sampled according to a standard pattern in a subassembly. Fuel swelling data obtained from changes in sodium level are presented in Table I-11. These data indicate an average swelling for Mark IA fuel in the range of 10% to 14% at 1.2 a/o maximum subassembly burnup. Figure I-16 shows fuel swelling determined by the two methods as a function of burnup. Figure I-17 presents a comparison of irradiation-swelling shown by Mark I and Mark IA fuel. It can be seen that the average Mark I fuel swelling at this same 1.2 a/o burnup is in the range of 4.5% to 7% (ANL-7125, p. 58). Using these data, it has been calculated that, at 1.2 a/o burnup, fuel element internal pressure and resultant cladding stress generated in the Mark IA element are comparable to those generated in the Mark I fuel element. Therefore, the maximum allowable Mark IA fuel burnup has been established at 1.2 a/o maximum subassembly burnup, the same as that allowed for Mark I-fueled subassemblies.

b. VARIATION OF SWELLING RATE WITH PROCESS OPERATIONS

Product analysis data obtained to date indicate that significantly different irradiation swelling rates exist for Mark I and for Mark IA reprocessed fuel produced in the FCF. Swelling variations for the Mark I fuel appear to be related to the origin of the melt-refining batch charge. For the Mark IA fuel, the data are yet too limited to make conclusive statements.

In the FCF operations, reprocessed-fuel melt-refining batches designated "MR" typically utilize furnace

TABLE I-11. Mark IA Fuel Swelling

Subassembly No.	Alloy Source and Number of Fuel Elements Sampled		Irradiation Position in EBR-II Core	Calculated Burnup (a/o)		Fuel Swelling (%)[c]	
	Illinois[a]	Idaho[b]		Maximum	Average	Average	Range
C-165	21	0	4B3	0.58	0.461	2.9	2.0–3.7
C-180	3	25	3A2	0.815	0.674	4.2	2.9–5.9
C-166	21	0	3F2	0.947	0.783	4.9	3.6–6.1
C-217	1	20	4D2	1.06	0.84	5.3	3.5–9.6
C-186	11	11	4F3	1.09	0.865	6.1	4.2–8.4
C-196	1	20	3B1	1.114	0.929	10.2	5.4–12.2
C-185	20	0	3F1	1.125	0.930	7.2	4.9–9.1
C-197	4	17	3C2	1.16	0.96	11.5	8.0–13.8
C-198	1	20	3E2	1.16	0.96	10.9	6.7–13.6
C-184	11	10	3D2	1.197	0.99	10.4	5.4–13.8
C-175	21	0	2C1	1.22	1.02	14.0	12.3–15.3
C-179	19	9	2D1	1.22	1.02	11.5	6.3–14.8
C-169	27	0	1A1	1.22	1.06	12.2	9.7–14.7

[a] Fuel pins fabricated from virgin alloy by ANL Metallurgy Division in Illinois.
[b] Fuel pins produced in Fuel Cycle Facility from melt refined alloy.
[c] Determined from changes in sodium level (by eddy current measurements).

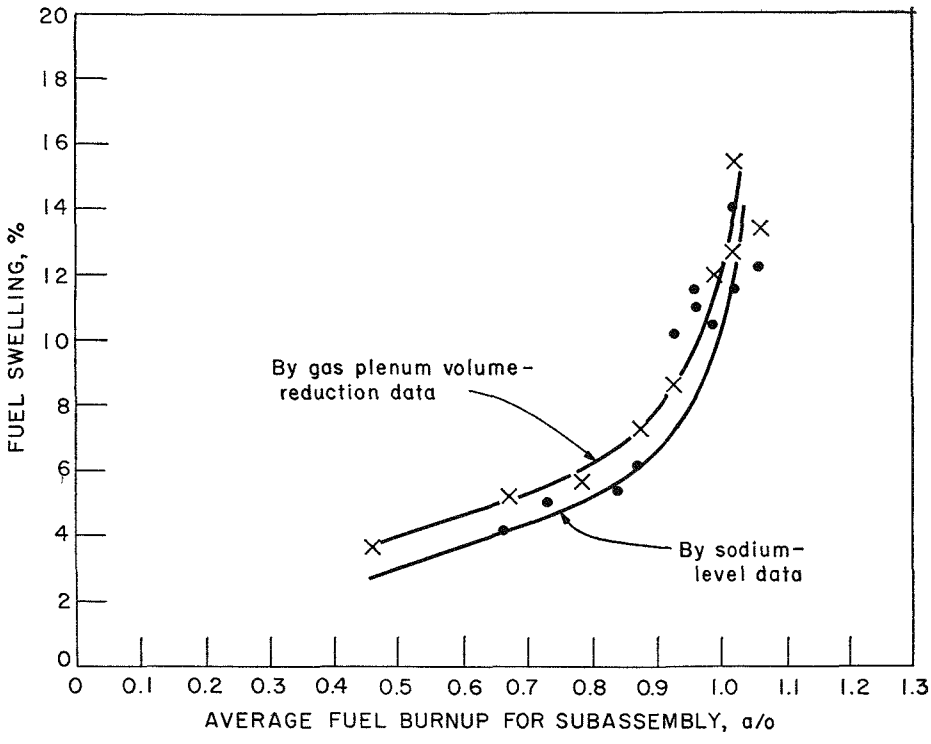

308-481

FIG. I-16. EBR-II Mark IA Fuel Swelling as a Function of Burnup.

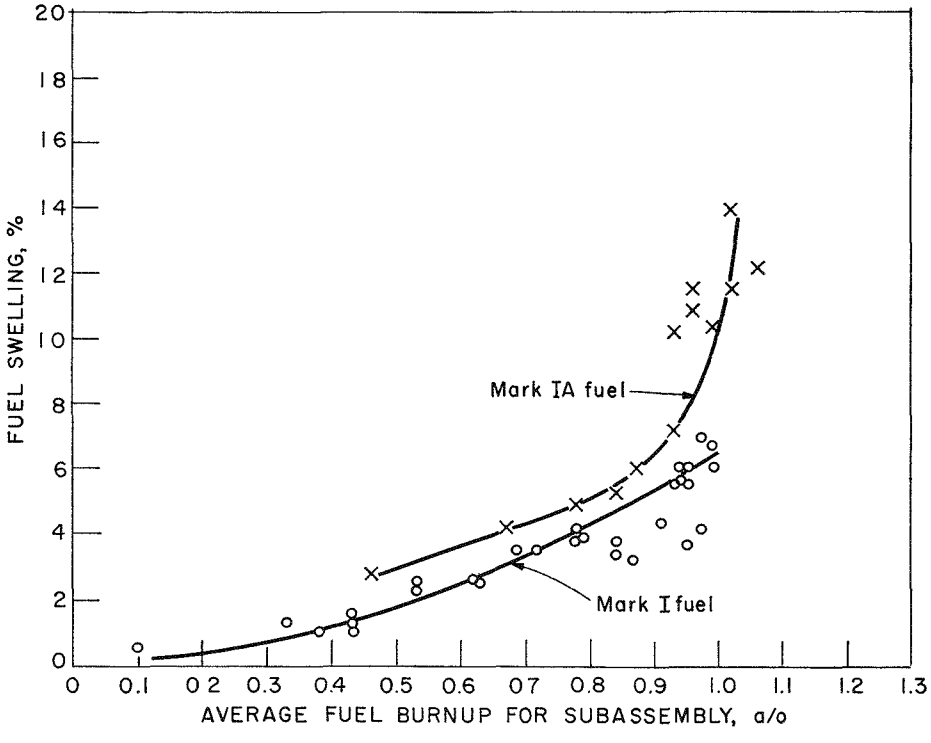

8-476

FIG. I-17. EBR-II Mark I and Mark IA Fuel Swelling as a Function of Burnup (by sodium-level data).

charges comprised of approximately 10 kg of irradiated fuel pins removed from discharged subassemblies and approximately 1 kg of nonirradiated ^{235}U for reenrichment purposes. The refining operation normally consists of maintaining the alloy in the molten state at 1400°C for approximately 3 hr for fission product removal from the alloy. Melt-refining batches termed "MRC" (consolidation batches) typically employ furnace charges consisting of various proportions of fuel-alloy heels from previous injection casting batches, shards (scrap pin-ends), and chopped pin segments prepared from fuel pins rejected because of "out-of-specification" reasons (principally dimensional) at the pin processing station. Because the intent of the "MRC" run is primarily to consolidate the various forms of charged fuel into a composite ingot for subsequent injection casting of new fuel pins, the blending operation normally consists of maintaining the alloy material molten at 1400°C for ¼ to 1 hr instead of the 3 hr as used in the "MR" type refining run.

FCF-produced, Mark I fuel manufactured from "MR" type melt-refining batches indicated irradiation swelling ranging from 5.4% to 8% at 1.2 a/o maximum subassembly burnup (approximately 1 a/o average burnup). Fuel originating in "MRC" type batches indicated 3.8% to 5% swelling at this same burnup. Swelling data obtained to date from FCF-produced, Mark IA fuel indicate this same general trend, with fuel originating in "MR" type batches displaying the higher swelling rate; but these data are as yet not complete. Fuel pins fabricated from virgin alloy material by the ANL Metallurgy Division in Illinois displayed swelling values (see Table I-11) that ranged from 9.7 to 15.3% at 1.2 a/o maximum subassembly burnup. Possible reasons for these differences in swelling characteristics are being studied. Some of the factors being examined include fabrication site of fuel pin, trace element and fissium element content, fabrication history and thermal cycling.

5. Maintenance of Electromechanical Manipulators and In-Cell Cranes (D. M. Paige, J. O. Kleffner, V. N. Thelen)[35]

Transfer operations in the Air and Argon Cells are carried out with eight heavy duty electromechanical manipulators[37] and three 5-ton cranes. Process equipment operation, installation, and removal is also accomplished by this equipment, particularly in the Argon Cell. These devices have now been in regular operation for four years, two years of which have involved operation in a high radiation background. For three years, the six manipulators and two cranes installed in the Argon Cell have been in operation in an argon or nitrogen atmosphere (the last 2 years in argon) containing normally <50 ppm each of water and oxygen, at a temperature of about 95°F. Since most of the trolley units may be interchanged between the Air and Argon Cells, all of the units have operated at least a good part of the time in an inert atmosphere.

TABLE I-12. In-Cell Crane and Electromechanical Manipulator Usage

Type of Unit	No. of Units Operating	Hours of Use for Each Type of Unit									
		Grip		Rotate		Hoist		Carriage		Bridge	
		Past Year[a]	Total[b]	Past Year[a]	Total[b]	Past Year[a]	Total[b]	Past Year[a]	Total[b]	Past Year[a]	Total[b]
Argon cell manipulator	5[c]	560	735	350	590	1450	2375	1300	1985	1900	3150
Air cell manipulators	2	200	250	210	260	750	945	600	770	1100	1355
Average per unit for all manipulators	7		140		120		475		400		640
Argon cell cranes	2					175	500	80	180	80	240
Air cell cranes	1					420	725	200	275	230	300

[a] November 1965 to October 1966.
[b] To October 1966.
[c] Plus one carriage which has been out of service most of the time since startup.

The motions for all units include bridge and carriage travel, and hoist, while the manipulators also have grip rotation and opening-closing motions. Normally, only one motion is performed at any time. The accu-

[37] J. E. A. Graae et al, A Radiation Stable Heavy Duty Electromechanical Manipulator, TID-7599, December 1960.

mulated hours of manipulator operation per unit have ranged from about 120 to 140 for the gripping and grip rotation motions, to 400 for carriage travel, 475 for hoist operation, and 640 for bridge travel. Crane use is somewhat less, with 150 hr of carriage travel, 180 hr of bridge travel, and 400 hr of hoist operation per unit, as summarized in Table I-12. Generally, over half of this operation has been realized in connection with the intensified production operations during the past year, during which the typical manipulator unit has been in operation about 30% of the working hours.

Since these devices contain parts that are operating at rather close dimensional tolerances (telescoping tubes, etc.), wear and occasional maloperation were anticipated. It is very difficult to perform preventive maintenance on this equipment, because of its in-cell location. Manipulator breakdowns can be divided into two classes: (1) those which can be corrected remotely, and (2) those which require (or are thought to require) contact maintenance.

The first type of maintenance operation includes replacement of such items as bus bar pickup brushes, drive units, and grips and forearms. These have all been carried out routinely and with no unusual problems. In short, this phase of maintenance has worked as designed.

The second maintenance category is of great concern since the manipulators have become contaminated (~25 R/hr at 1 ft) to the extent that, even after some cleaning and the use of some shielding (⅛ in. of lead), working time is still only 5 to 10 minutes per person. Experience to date with both electromechanical manipulators and master-slaves has been that even the simplest jobs are very time-consuming when the working time is less than 10 minutes per person, because if those who are not manipulator repair specialists must be used, a good fraction of the time is required to establish technique.

One of the more frequent problems requiring contact repair has been the result of failure of the limit switches used to protect the manipulators from collision and from overrunning various motions. Basically, the faults have been dust between contacts, dust or lack of lubricant causing activators to stick, bending of extended feelers and resulting nonactivation, and improper original assembly. (A return-to-normal spring has been found missing in some cases.) Replacing these bad switches should be a simple job, but it is complicated by several factors among which, in addition to the high radiation background, are included the following. The switches are generally wired in with mineral-insulated cable and tube fittings which require very careful replacement to avoid damage to the seals. Some limit switches require careful adjustment which is difficult to accomplish without a test bridge on which to run the carriage. (The in-cell carriages are much too contaminated to bring to the mockup area.) This problem is being attacked on a long-range basis by considering new designs whereby most of the limit switches can be replaced remotely.

Another problem that is developing is associated with the ball spline telescoping tubes. To date, approximately 3 of the 9 tubes have given indication of trouble (sticking when going up or down). A possible serious effect of sticking is that when a tube sticks on the down travel and then releases suddenly, and its down travel is abruptly checked by the tube stops, this then puts a shock load on the balls, the ball returns, and the tube stops. In one case where it was possible to remove the tubes and to decontaminate them sufficiently for direct examination (from one of the carriages that had not been in the cell for very long), it was found that the ball races were galled and several ball returns were cracked. This particular problem has been temporarily solved for one case by remotely lubricating the ball spline. This seems to solve the problem but may tend to aggravate sticking in the long run since grease tends to collect dust and relubrication is required frequently. To take care of the telescoping tube problem, as well as any other problems of this nature, present plans call for consideration of modification or replacement with tubes of other designs, and provision of a decontamination area in the roof shelter[38] above the cells where a manipulator can be cleaned and completely overhauled. This area may also include a test bridge where a carriage can be tested before returning it to use. To further supplement this work, a complete spare carriage is being obtained so that there will be no loss of operating units in the cells when overhaul is being done. An overhaul will, of course, be expensive since all bearings will need replacement after decontamination.

[38] A metal-walled building enclosing the cell roof hatches, the jib crane and the pivot shield.

II

Fluidization and Volatility Processes[1]

(A. A. Jonke, J. J. Barghusen)

INTRODUCTION

The reaction of fluorinating agents with nuclear reactor fuel materials in fluid-bed systems to produce volatile uranium hexafluoride and plutonium hexafluoride is the basis of fluid-bed fluoride volatility processing. Currently, major attention is being directed toward the demonstration of fluoride volatility processes for low-enrichment UO_2-PuO_2 power reactor fuel clad in Zircaloy. The primary objective of this effort is to develop the technical data required for the design of an all-volatility commercial plant for the reprocessing of power reactor fuels.

The reference process flowsheet (Figure II-1) for the recovery of uranium and plutonium from reactor fuel materials is based on the use of interhalogen compounds to selectively convert the uranium to volatile UF_6 while plutonium is converted to nonvolatile PuF_4. The process involves four principle steps: (1) *decladding:* the fuel elements, Zircaloy-clad UO_2-PuO_2, are immersed in a fluidized bed of inert alumina particles and contacted with HCl gas whereby the cladding is converted to volatile $ZrCl_4$ which is removed from the reactor and subsequently converted to solid ZrO_2 by pyrohydrolysis with steam; (2) *oxidation*: the oxide fuel, which is unaffected by the decladding step and accumulates in the lower portion of the fluid-bed reactor, is contacted with 15 to 25 v/o oxygen in nitrogen at 450°C to form a mixture of U_3O_8 and PuO_2 fines (~20 μ diameter); (3) *uranium fluorination*: uranium is recovered from the oxide fines as volatile UF_6 by reaction of the fines with 5 to 15 v/o BrF_5 in nitrogen at 300°C; and (4) *plutonium fluorination*: the plutonium, which is converted to nonvolatile PuF_4 during the uranium fluorination step, is recovered as PuF_6 by reaction of PuF_4 with fluorine at 300 to 550°C.

The UF_6 produced in the uranium fluorination step is collected in a condenser together with excess BrF_5, bromine, and volatile fission product fluorides. The UF_6 is separated from the fission products and interhalogens by fractional distillation and sorption techniques. Plutonium hexafluoride, produced in the second fluorination step by reaction of PuF_4 with fluorine, is collected in cold traps and then revaporized and passed into a separate vessel for final purification.

Implicit in the application of the BrF_5 process to the reprocessing of spent fuel materials is the need to consider methods for the recycle of the interhalogen. Two different schemes for BrF_5 recycle are being studied. In the first scheme, represented in Figure II-1 (Phase II), the liquid mixture containing bromine, BrF_5, fission product fluorides, and UF_6 is contacted with fluorine gas during the fractional distillation step to convert the bromine component to BrF_3. The BrF_3 product is then fluorinated to BrF_5 in a separate vessel, and the BrF_5 is recycled.

The second scheme involves fluorination of the bromine to either BrF_3 or BrF_5 prior to condensation of the UF_6 product. The extent of fluorination (to BrF_3 or to BrF_5) will depend, in part, on the method employed to recover neptunium from the UF_6 stream. Results of experiments reported here have indicated that neptunium is fluorinated by BrF_5 to NpF_6 which accompanies the UF_6-gas stream.

Process development work on the interhalogen flowsheet is being carried out with UO_2-PuO_2 fuel material containing fission products in a 2-in. dia. fluid-bed reactor. Tests demonstrating the plutonium recovery step are being made in an engineering-scale alpha facility. In addition, bench-scale tests are under way to demonstrate the interhalogen process with highly irradiated fuel materials. Supporting studies are primarily directed toward defining the behavior of neptunium in the process, and toward developing methods for purifying the plutonium product.

[1] A summary of this section is given on pages 5 to 9.

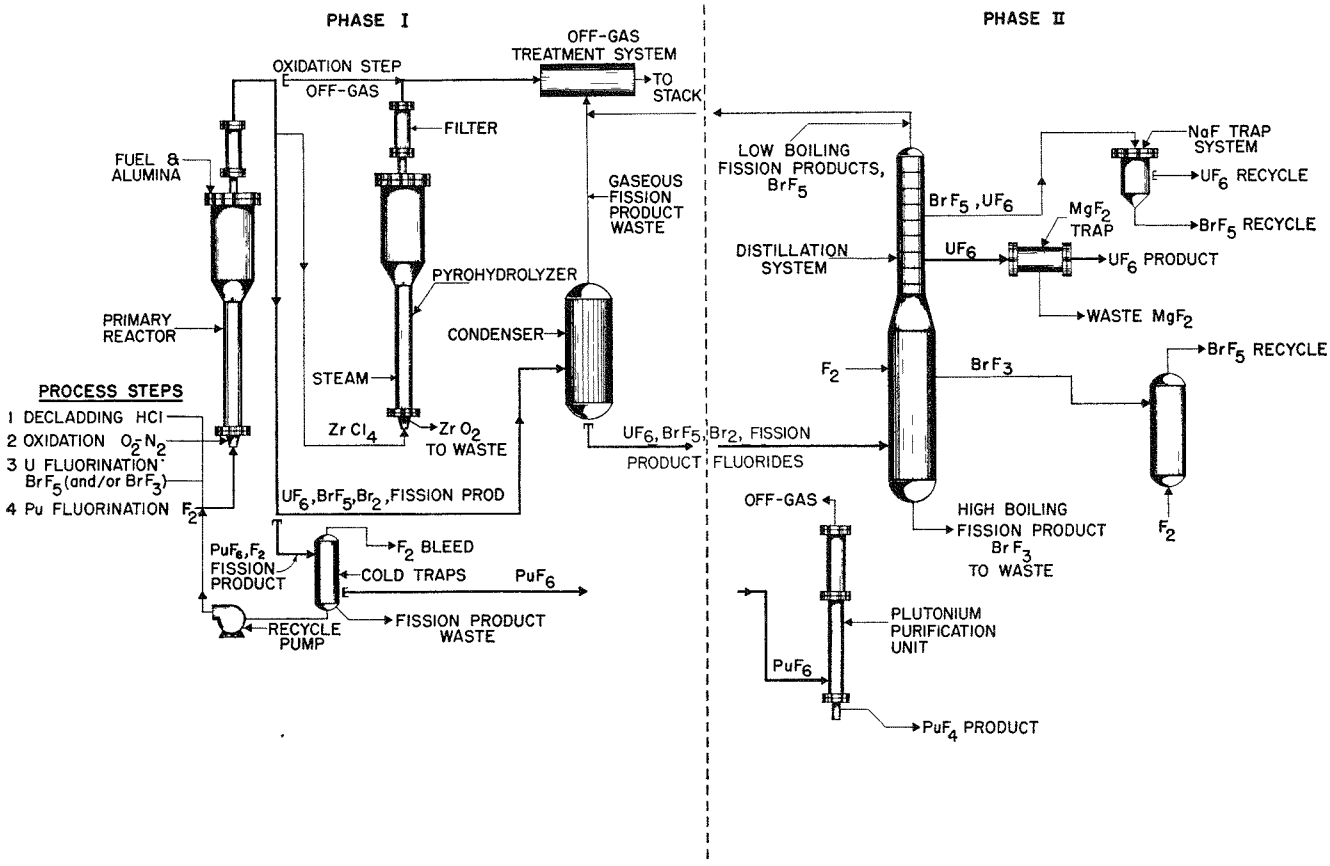

108-9966 Rev. 1

FIG. II-1. Fluid-Bed Volatility Process Interhalogen Reference Flowsheet.

Nominal Process Conditions

Process Step	Reagent	Reagent Concentration (v/o)	Temperature (°C)
Decladding	HCl	60–90	400
Pyrohydrolysis	Steam	3 × Stoich.	350
Oxidation	O_2	15–25	450
Uranium Recovery	BrF_5	5–15	300
Plutonium Recovery	F_2	10 → 90	300 → 550
Uranium Purification (Distillation)	—	—	80–90, 40–50 psia

A. LABORATORY INVESTIGATIONS (M. J. STEINDLER)

1. Fluorination of UO_2-PuO_2-Fission Product Pellets in a 2-inch Diameter Reactor

(L. J. ANASTASIA, P. G. ALFREDSON,[2] G. W. REDDING, M. HAAS)

Fluorination studies are being carried out to define conditions for the fluorination of UO_2-PuO_2-fission product pellets that would insure a minimum retention of uranium and plutonium in a fluidized bed of alumina particles.

Two fluorinating agents are being evaluated for the processing of UO_2-PuO_2-fission product pellets: fluorine and bromine pentafluoride (BrF_5). Of two processing sequences under consideration, one involves oxidation of the fuel pellets to U_3O_8-PuO_2 fines in a separate step followed by fluorination with either fluorine or

[2] Guest Scientist, Australian Atomic Energy Commission.

bromine pentafluoride. By the use of this processing sequence, it is possible to initiate the fluorination step at lower temperatures (300 to 350°C) than in the two-zone concept (fluorination temperature 450°C) which was used in previous experiments (ANL-7125, pp. 62–66, and ANL-7225, pp. 65–68). In the other sequence, which utilizes the two-zone concept, the fuel pellets are oxidized to fine particles in the lower portion of a fluid-bed reactor and the fines are simultaneously fluorinated in the upper portion of the reactor. Results of previous experiments using the two-zone concept indicated that plutonium retention on the alumina bed particles was higher when cesium fluoride was added to the alumina bed than when cesium fluoride was not present in the bed. Since this behavior was not observed in experiments with the two-step process, the inhibiting effect of CsF was attributed to the higher fluorinating temperature employed in the two-zone operation.

This report presents the results of recent experiments to demonstrate the feasibility of alternative processing concepts for the recovery of uranium and plutonium from oxide fuel materials. One concept which was evaluated involved the reuse of an alumina bed to process more than one batch of fuel, thereby reducing plutonium losses in the waste solids. Two techniques were investigated: (1) oxidation of the oxide fuel to U_3O_8 and PuO_2 fines followed by fluorination of the fines with fluorine for each batch of fuel, and (2) oxidation of the fuel followed by fluorination of uranium to UF_6 with BrF_5 for each batch of fuel, and then a single fluorination step with fluorine to recover the accumulated plutonium from several batches. Another concept tested was leaching of the alumina bed to recover plutonium after the uranium has been fluorinated by BrF_5. In addition, the effect of BrF_5 fluorination temperature on subsequent plutonium removal with fluorine was investigated and, in one experiment, the behavior of neptunium was observed during fluorination with BrF_5 and with fluorine.

The rate of reaction for the fluorination of U_3O_8 fines with BrF_5 was fitted to a diminishing sphere model, and results obtained in the fluid-bed reactor were compared with previous thermobalance data (ANL-7225, pp. 78–86). The problems attending the retention of plutonium in fine particles elutriated to cool portions of the fluid-bed reactor are discussed.

a. EQUIPMENT AND PROCEDURES

The major components of the experimental system are the 2-in. dia. fluid-bed reactor, a remote-head diaphragm pump for gas recycle, chemical traps for disposal of excess reactants (BrF_5 and F_2 disposal in soda lime and activated alumina, respectively), and traps (cold traps or NaF traps) for collection of hexafluoride products. Detailed descriptions of these components and of the experimental procedures have been reported (ANL-6925, p. 116 and ANL-7055, p. 110).

The pellets used in these studies (type II) were prepared by blending mixed UO_2-PuO_2 powders and fission product oxides, and sintering the mixture in 6 v/o hydrogen in nitrogen for 6 to 8 hr at 1700°C. These pellets contain nominally 0.4 w/o plutonium as PuO_2, 86 w/o uranium as UO_2, and 1 w/o fission products as the oxides. The type II pellets have been completely described in a previous report (ANL-7225, pp. 65–66). In most runs, the charge consisted of approximately 650 g of UO_2-PuO_2-fission product pellets, corresponding to a 2-in. deep pellet bed, and approximately 1100 g of nominal 48 to 100 mesh alumina, corresponding to a static-bed depth of 12 in. In all runs, about 0.6 g CsF was added to the alumina bed; in run Purse-9 and subsequent runs, about 0.15 g RbF was also added to the alumina. The CsF and RbF were added to the system to simulate more closely the fission product distribution expected from irradiated fuel. For run Purse-9, 0.52 g NpO_2 was also added to the alumina bed.

b. REUSE OF AN ALUMINA BED TO PROCESS SEVERAL BATCHES OF FUEL

The reuse of a single batch of alumina for the processing of three successive batches of oxide fuel was evaluated in runs Pure-19, -20, and -21 and in runs Purse-10, -11, and -12. The objectives of these runs were to test the reuse scheme, to determine if plutonium in the final alumina bed could be reduced to less than 1% of the total charged, and to establish if the recycle-fluorination time normally required for the recovery of plutonium in three separate batches of pellets could be shortened in the reuse experiments.

(1) Reuse Experiments Involving Uranium and Plutonium Volatilization by Reaction with Fluorine

In previous laboratory studies (ANL-6742, p. 13 and ANL-7077, pp. 23–31), the initial fluorination step, in which most of the plutonium was volatilized, was followed by a recycle-fluorination sequence of 5 hr at 450°C, 5 hr at 500°C, and 10 hr at 550°C. The same steps were used in the present experiments (Pure-19, -20, and -21, Table II-1) and consisted of pellet oxidation followed by fluorination with 5 to 16 v/o fluorine and then recycle-fluorination. In the alumina reuse experiments, the pellet to alumina charge ratio was kept constant at about 0.6 to provide a uniform ba[illegible] for comparing the runs. It should be noted that the alumina bed, 1200 g for run Pure-19, was significantly reduced in weight by fluidized-bed samples taken during

TABLE II-1. Operating Conditions for Fluorination of Uranium and Plutonium from UO_2-PuO_2-Fission Product Pellets with Fluorine—Runs Pure-19 to Pure-22

Equipment: 2-in. dia. fluid-bed reactor
UO_2-PuO_2-F.P. pellets: Type II, 0.5-in. dia. by 0.4-in. right cylinders
Alumina bed: Alcoa T-61 alumina, nominal 48 to 100 mesh (−170 mesh removed)
Bed support: Nickel balls
Diluent gas: Nitrogen

	Pure-19	Pure-20	Pure-21	Pure-22
Material Charged to Reactor				
UO_2-PuO_2-F.P. pellets (g)	720.5	649.8	577.7	650.4
Alumina (g)	1200	1115[a]	970[b]	1100
CsF (g)	0.65	0.61	0.53	0.60
Oxidation with 20 v/o Oxygen at 450°C				
Reactor pressure (mm Hg)	1040	975	1015	1050
Superficial velocity (ft/sec)[c]	0.8	0.8	0.8	0.75
Cumulative process time (hr)	0–4	0–4	0–4	0–4
Fluorination with Fluorine at 350°C—Once-Through Flow				
Reactor pressure (mm Hg)	1440	1340	1350	1490
Superficial velocity (ft/sec)[c]	0.65	0.6	0.6	0.6
Fluorine concentration to fluid bed (v/o)	5–15	5–15	5–15	5–16
Cumulative process time (hr)	4–6	4–6	4–6	4–6
Recycle-fluorination with 90 v/o Fluorine				
Reactor pressure (mm Hg)	1360	1350	1360	1420
Superficial velocity (ft/sec)[c]	0.5–0.8	0.5–0.8	0.5–0.8	0.5–0.7
Cumulative process time (hr)	6–16	6–16	6–19	6–21
At temperature of 350°C (hr)	6–9	6–9	6–9	6–9
350° to 550°C (hr)[d]	9–15	9–15	9–15	—
375°C (hr)	—	—	—	9–12
400°C (hr)	—	—	—	12–15
450°C (hr)	—	—	—	15–17
500°C (hr)	—	—	—	17–19
550°C (hr)	15–16	15–16	15–19	19–21

[a] Residual alumina bed plus line clean-out samples from run Pure-19.
[b] Residual alumina bed plus line clean-out samples from run Pure-20.
[c] Calculated for operating temperature and pressure.
[d] Reactor temperature increased 5°C/9 min.

the runs. The processing sequence for each run was similar; however, recycle-fluorination at 550°C was extended from 1 hr in runs Pure-19 and -20 to 4 hr in run Pure-21. Uranium and plutonium concentrations in samples of the fluidized alumina bed taken throughout the course of each of the three runs are shown in Figure II-2.

The final bed from run Pure-21 contained 0.009 w/o uranium and 0.009 w/o plutonium (see Figure II-2). On the basis of the original 1200 g charge of alumina and the total uranium and plutonium fed to the reactor (1680 g and 8.38 g, respectively), these final concentrations correspond to removal from the alumina bed of more than 99.9% of the uranium and 99% of the plutonium charged to the reactor. The plutonium remaining on the alumina bed in this experiment is about one-third the amount of plutonium which would have remained if three separate beds had been used for the processing of three separate charges of fuel.

The specifice surface area of the alumina bed increased from 0.05 sq m/g for the initial alumina bed to 0.23 sq m/g after run Pure-21. The fluoride content of the final bed was 4.4 w/o; the major amount of the fluoride is attributed to fluoride held by compounds of the added fission products. These surface area and fluorine concentration data obtained with Alcoa T-61 alumina are in good agreement with similar data obtained in previous reuse experiments with Norton type RR (high purity) fused alumina[3] and indicate that no significant deterioration of the alumina bed is expected in the reuse of the bed on a process scale.

[3] R. L. Jarry, A. V. Hariharan, J. Fischer, M. J. Steindler, J. J. Stockbar, T. D. Baker, W. H. Gunther, and G. W. Redding, Laboratory Investigations in Support of Fluid-Bed Fluoride Volatility Processes. Part IX. The Fluid-Bed Fluorination of Plutonium-Containing Simulated Oxidic Nuclear Fuel in a 1½-inch-diameter Reactor, ANL-7077, December 1965, pp. 23–31.

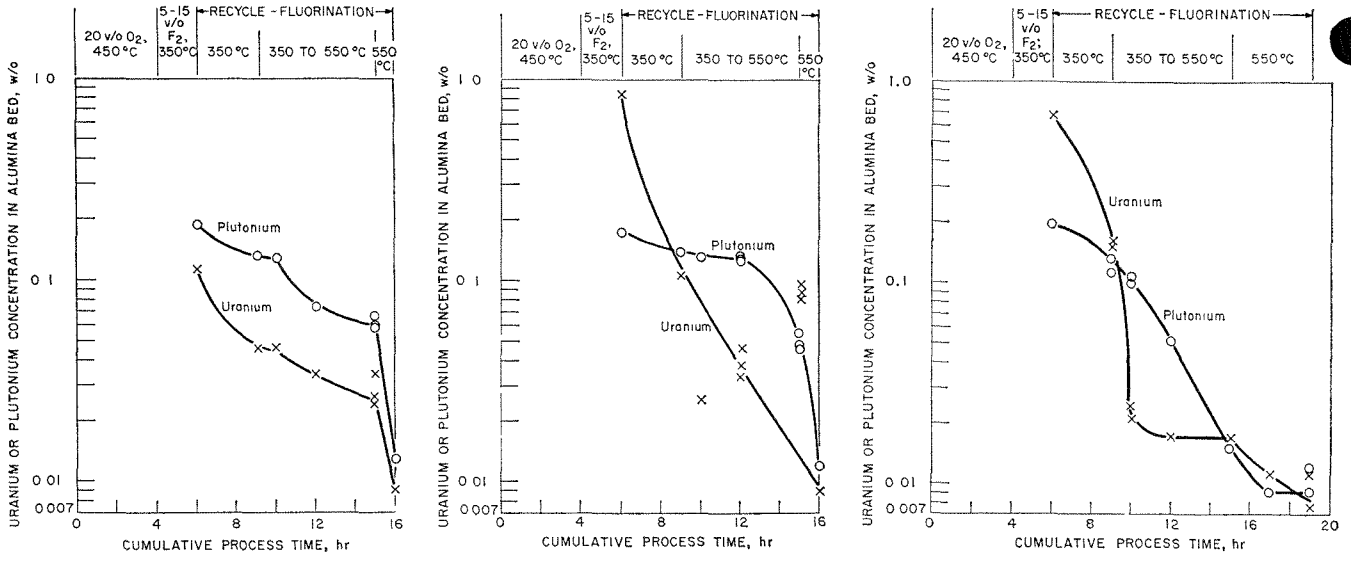

Pellet Batch 1. Run Pure-19 | Pellet Batch 2. Run Pure-20 | Pellet Batch 3. Run Pure-21

308-530

FIG. II-2. Uranium and Plutonium Concentrations in Reused Alumina Bed.

TABLE II-2. OPERATING CONDITIONS FOR FLUORINATION OF URANIUM AND PLUTONIUM WITH BrF_5 FOLLOWED BY FLUORINE—RUNS PURSE-8 TO PURSE-12.

Equipment:	2-in. dia. fluid-bed reactor
UO_2-PuO_2-F.P. pellets:	Type II, 0.5-in. dia. by 0.4-in. right cylinders
Alumina bed:	Alcoa T-61 alumina, nominal 48-100 mesh (−170 mesh removed)
Bed support:	Nickel balls
Diluent gas:	Nitrogen

	Purse-8	Purse-9	Purse-10	Purse-11	Purse-12
Material Charged to Reactor					
UO_2-PuO_2-F.P. pellets (g)	654.3	655.9	654.6	655.6	647.5
Alumina (g)	1100	1100	1100	1150[a]	1200[b]
CsF (g)	0.6	0.6	0.6	0.6	0.6
RbF (g)	—	0.15	0.16	0.15	0.16
NpO_2 (g)	—	0.52	—	—	—
Oxidation with 20 v/o O_2 at 450°C					
Reactor pressure (mm Hg)	1000	1010	950	1020	1000
Superficial velocity (ft/sec)[c]	0.8	0.7	0.8	0.8	0.8
Cumulative process time (hr)	0–4.0	0–4.0	0–4.0	6.0–10.0	12.0–16.0
Fluorination with BrF_5					
Reactor pressure (mm Hg)	1060	1250	1170	1170	1120
Superficial velocity (ft/sec)[c]	0.7	0.7	0.7	0.7	0.7
BrF_5 concentration to fluid bed (v/o)	10–11	9	8–10	9–10	9–10
Temperature (°C)	400	300	300	300	300
Cumulative Process Time (hr)	4.0–5.7	4.0–6.1	4.0–6.0	10.0–12.0	16.0–18.0
Recycle-fluorination with 90 v/o F_2					
Reactor pressure (mm Hg)	1300	1300	[d]	[d]	1360
Superficial velocity (ft/sec)[c]	0.5–0.9	0.6	—	—	0.3–0.5
Cumulative process time (hr)	5.7–16.7	6.1–17.1	—	—	18.0–36.0
At temperature of 300°C (hr)	5.7–8.7	6.1–9.1	—	—	18.0–28.0
300 to 550°C (hr)[e]	8.7–13.7	9.1–14.0	—	—	28.0–33.0
550°C (hr)	13.7–16.7	14.1–17.1	—	—	33.0–36.0

[a] Residual alumina bed from run Purse-10 plus 50 g alumina mixed with CsF and RbF.
[b] Residual alumina bed from run Purse-11 plus 50 g alumina mixed with CsF and RbF.
[c] Calculated for operating temperature and pressure.
[d] Residual plutonium was fluorinated in run Purse-12.
[e] Reactor temperature increased 10°C/12 min.

(2) Reuse Experiments: Fluorination with Bromine Pentafluoride Followed by Recycle-Fluorination with Fluorine

In runs Purse-10, -11, and -12 the pellets were oxidized and uranium was selectively removed by fluorination with BrF_5. The plutonium that had accumulated from the three batches of pellets was then fluorinated with fluorine during a single recycle-fluorination in run Purse-12. The charge for each run was approximately 650 g of UO_2-PuO_2-fission product pellets and 0.6 g CsF and 0.15 g RbF. For runs Purse-11 and -12, the cesium fluoride and rubidium fluoride were mixed with 50 g alumina prior to being added to the residual bed from the preceding run. The operating conditions for runs Purse-10, -11, and -12 are listed in Table II-2.

As a basis for the calculation of the time that would be required to fluorinate two-thirds of the plutonium to PuF_6 at 300°C, a reaction rate constant (diminishing-sphere model) was estimated from the data of runs Purse-4, -5, and -6 (ANL-7225, pp. 70–73). From this constant, a recycle-fluorination sequence consisting of 10 hr at 300°C, 5 hr from 300 to 550°C, and 3 hr at 550°C was chosen for the recovery of plutonium in run Purse-12. Uranium and plutonium concentrations in the alumina bed for runs Purse-10, -11, and -12 are shown in Figure II-3.

Only 25% of the plutonium in the alumina bed was fluorinated during the initial 5 hr of recycle-fluorination at 300°C, and virtually no plutonium was fluorinated during the subsequent 5 hr at 300°C. However, during 6-hr recycle-fluorination at 300 to 550°C (Figure II-3), the plutonium concentration was reduced from 0.3 w/o to 0.009 w/o. These results indicate that a shorter recycle-fluorination sequence totaling 11 hr and consisting of 5 hr at 300°C, 5 hr from 300 to 550°C, and 1 hr at 550°C would be sufficient to reduce plutonium in the final alumina bed to desirably low levels.

The concentrations of uranium and plutonium in the final alumina bed were 0.003 and 0.009 w/o, respec-

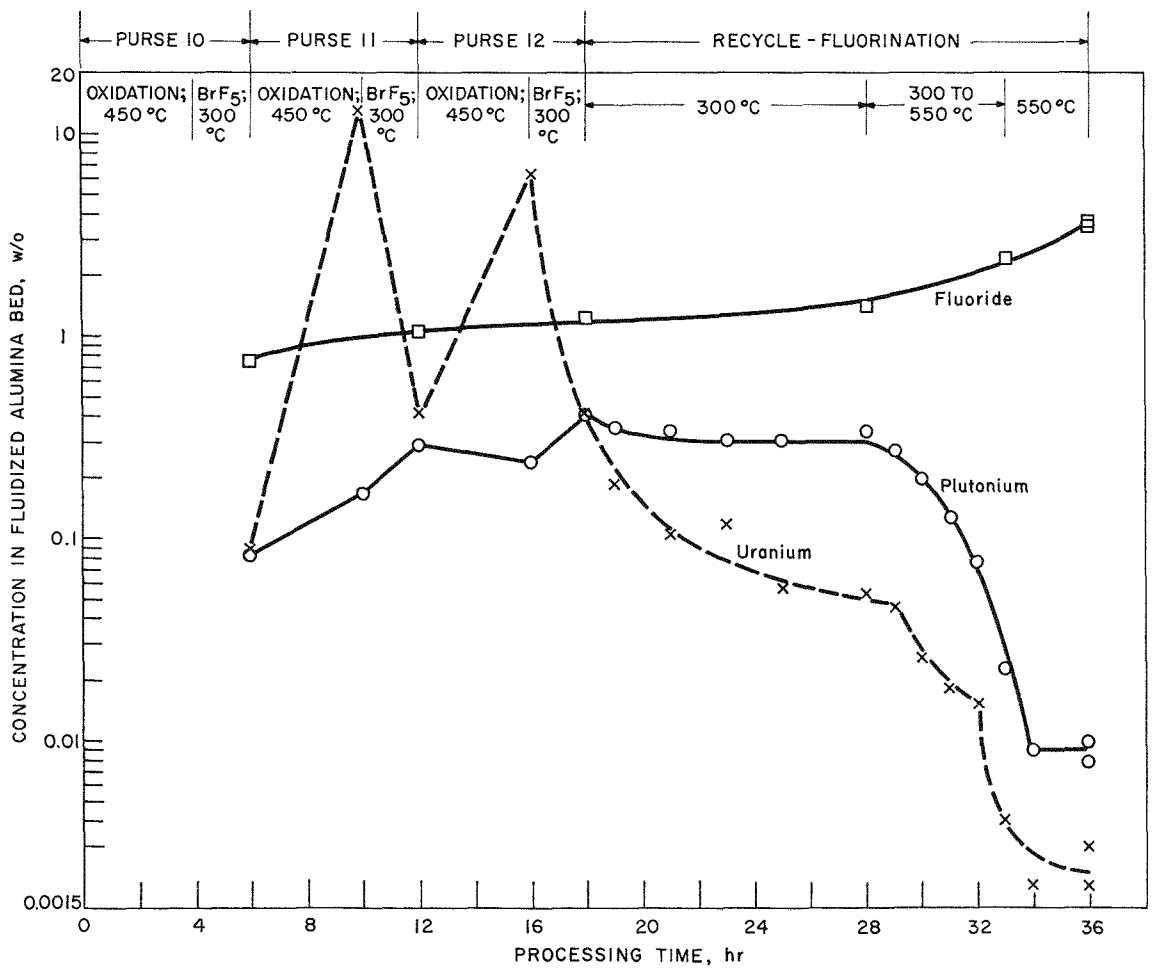

308-424

FIG. II-3. Uranium, Plutonium, and Fluoride in Fluidized Alumina Bed during Alumina Reuse Experiments.

tively. Based on the 1200 g of alumina charged to the reactor, these results correspond to removal of 99.9% of the uranium charge and 99% of the plutonium charge. The fluoride content of the final alumina bed (see Figure II-3) was 3.5 w/o, indicating that an insignificant quantity of alumina was fluorinated to aluminum fluoride in these reuse experiments.

Runs Pure-19, -20, and -21 and runs Purse-10, -11, and -12 have demonstrated that the reuse of a single batch of alumina to process several batches of fuel pellets is a promising method for minimizing total plutonium losses to the inert fluid-bed material and for reducing the total quantity of solid wastes from a fluid-bed fluoride volatility process. Although this principle had been demonstrated in previous alumina reuse experiments,[3] the present tests may be more representative of actual processing conditions since they were carried out with UO_2-PuO_2-F.P. pellets and with a more nearly complete spectrum of fission products. In addition, a relatively economical form of sintered alumina was used rather than the more costly, high-purity type used in the previous tests. Further, the time required to fluorinate the plutonium from three batches of fuel pellets as in runs Pure-19, -20, and -21 (33 hr) was about one-half that required to fluorinate three batches of fuel separately. In the case of the flowsheet based on the use of BrF_5 for fluorination of uranium, it is believed that the recycle-fluorination time can be reduced even further, to 11 hr, to effect a 99% removal of plutonium from the alumina bed.

TABLE II-3. Leaching of Uranium and Plutonium from Alumina Samples

Alumina beds were each sampled after oxidation of PuO_2-UO_2-F.P. pellets and their fluorination with BrF_5 at 300°C. One sample was taken from each of the runs Purse-2, -3, -4 and the samples were combined, thoroughly mixed, and then split into five separate samples for these tests.

Leach solution: 6*N* HNO_3
Temperature: 100°C

	Sample No.	Leaching Time (hr)	U (w/o)	Pu (w/o)	Uranium[a] Leached (%)	Uranium[a] Material balance (%)	Plutonium[a] Leached (%)	Plutonium[a] Material balance (%)
Original sample		—	0 30	0.19	—	—	—	—
Leached samples	1	1	0.001	0.005	97.8	119	97.8	109
	2	2	0.003	0.0006	99.2	119	99.7	108
	3	3	0.0027	0.0004	99.2	108	99 8	100
	4	5	0.0006	0.0002	99.9	115	99.9	97
"As recieved" Al_2O_3		3	<0.001[b]	0.0004	—	—	—	—

[a] Leached (%) $= \left[1 - \frac{M_{solids}}{M_{solids} + M_{soln}}\right]100$ and Material Balance (%) $= \left[\frac{M_{solids} + M_{solution}}{M_{original\ sample}}\right]100$ where M = weight of plutonium or uranium.

[b] X-ray analysis. All other analyses are by wet chemical methods.

c. LEACHING OF ALUMINA BEDS FOR PLUTONIUM RECOVERY

Several experiments were performed to determine the feasibility of recovering plutonium from the alumina fluid-bed material, after uranium recovery in the BrF_5 fluorination step, by leaching the bed material with 6*N* nitric acid. This process alternative is not considered as an integral step in the all-volatility process concept, but was investigated to demonstrate the added versatility in the plutonium-removal step when BrF_5 is used as an agent for the selective volatilization of uranium.

In these experiments, samples of the alumina beds were taken after fluorination of uranium with BrF_5 for 2 hr at 300°C (runs Purse-2, -3, and -4, ANL-7225, pp. 72–73). Three fluid-bed samples were combined, thoroughly mixed, and then split into five separate samples of about 5 g each. One sample was used for chemical analysis of the starting material and four samples were leached 1 to 5 hr with 6*N* HNO_3 at 100°C. Another sample was a blank sample of "as received" alumina which was also leached for 3 hr to determine the extent of cross-contamination from handling of the samples. The results of these leaching tests are shown in Table II-3.

The material balances for uranium and plutonium reported in Table II-3 indicate that some segregation of the original sample may have taken place. Thus, the data for uranium and plutonium leached from the samples are based upon the total uranium and plutonium found in the solutions and in the leached solids. It was not possible to determine the extent of codissolution of certain fission products with the uranium and plutonium, since the quantity of fission products present was below the limits of analysis. Analytical results indicated that less than 0.1% of the alumina dissolved during 2 or 3 hr of leaching.

These tests have demonstrated that the uranium and plutonium in the alumina can be readily leached from the bed material with 6*N* nitric acid at 100°C; greater than 99% of the uranium and plutonium was leached in 2 hr and over 99.9% was leached in 5 hr.

d. FLUORINATION OF UO_2-PuO_2-F.P. PELLETS WITH FLUORINE

Analyses of the results from the Pure series of runs reported previously (ANL-7225, pp. 66–70) and from

runs with BrF_5 as the fluorinating agent (ANL-7225, pp. 70–74) indicated that an initial low temperature of fluorination (below 450°C) is necessary to achieve low plutonium retention on the alumina bed if cesium fluoride is present in the system.

Run Pure-22 has been completed to study the effect on plutonium retention in the final alumina bed of increased recycle-fluorination time at temperatures below 450°C. In this run the recycle-fluorination time at temperatures below 450°C was 9 hr compared with about 5 hr in previous runs. Operating conditions for this run are listed in Table II-1, and the concentrations of uranium and plutonium in the fluidized alumina bed throughout the recycle-fluorination step are shown in Figure II-4. The plutonium concentration in the final alumina bed (0.009 w/o) is the same as that obtained in a similar run, Pure-18 (ANL-7225, pp. 69, 71), wherein the recycle-fluorination sequence totaled 10 hr. Since the recycle-fluorination sequence in Pure-22 totaled 15 hr, it appears that the shorter sequence used in run Pure-18 is more promising for process use.

e. FLUORINATION OF UO_2-PuO_2-F.P. PELLETS WITH BrF_5

(1) Effect of Uranium Fluorination Temperature Upon Plutonium Fluorination

An experiment (Purse-8) was performed to continue the investigation of the effect of the BrF_5 fluorination temperature on the extent of plutonium removal during subsequent fluorination with fluorine. In previous runs (see runs Purse-5 and -7, ANL-7225, p. 71), the BrF_5 fluorination step was carried out at 300°C and 200°C. In run Purse-8, uranium was fluorinated to UF_6 with BrF_5 at 400°C, and the recycle-fluorination sequence consisted of 3 hr at 300°C, 5 hr from 300 to 550°C, and 3 hr at 550°C. Operating conditions for this run are given in Table II-2, and the course of uranium and

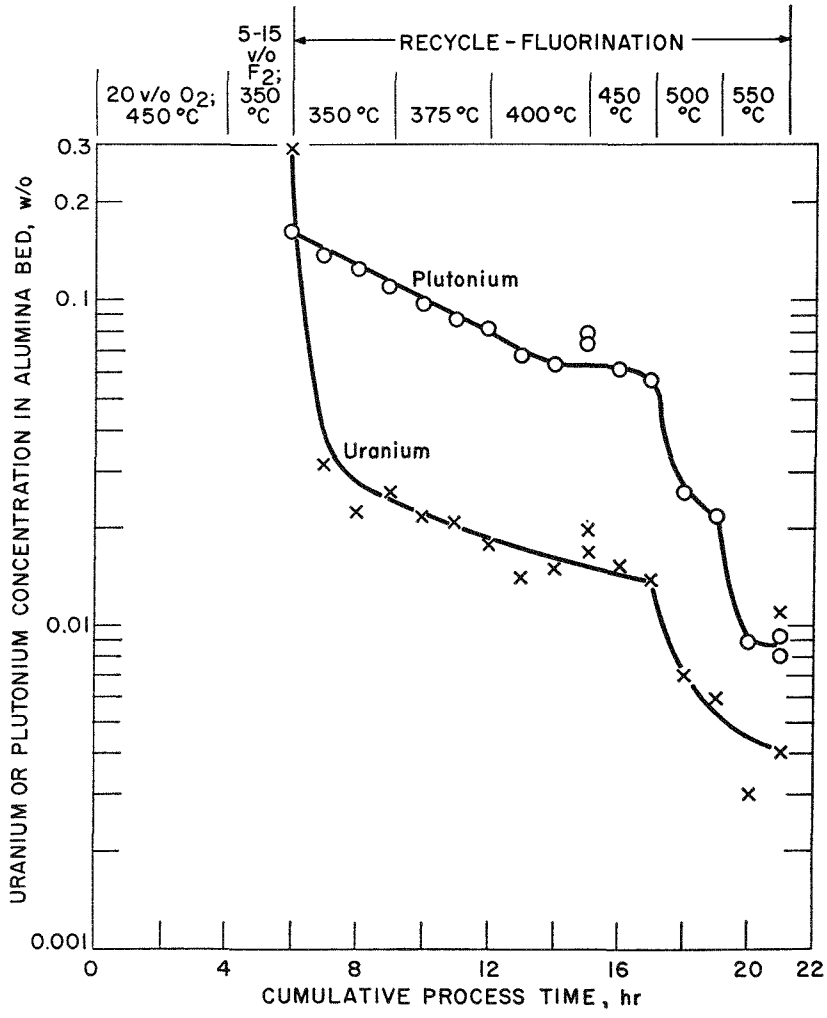

308-409

FIG. II-4. Uranium and Plutonium Concentrations in Alumina Fluidized Bed during 15 Hr of Recycle-Fluorination—Pure-22.

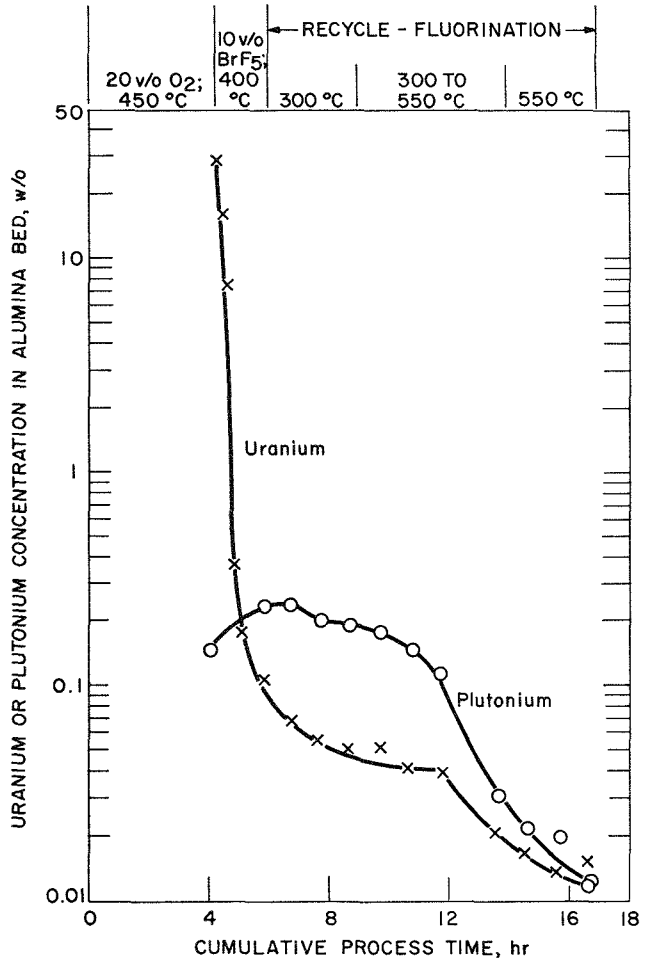

308-402

FIG. II-5. Uranium and Plutonium Concentrations in Fluidized Alumina Bed during Fluorination with BrF_5 Followed by Fluorine—Run Purse-8.

plutonium depletion from the alumina bed during both fluorination steps is shown in Figure II-5.

The average UF_6 production rate observed during the BrF_5 fluorination step in run Purse-8 was 44 lb UF_6/(hr) (sq ft), with peak production rates of about 140 lb UF_6/(hr) (sq ft). The BrF_5 utilization efficiency, based on total fluorine, was 38%. These may be compared with results for fluorination at 200 and 300°C: production rates of 14 and 40 to 45 lb UF_6/(hr) (sq ft) and BrF_5 utilization efficiencies of 8% and 28 to 37%, respectively. The average production rates and BrF_5 utilization efficiencies obtained at 300 and 400°C should be considered as parameters rather than dependent variables because, in these experiments, fixed quantities of pellets were fluorinated in approximately the same times with only slight changes in the total quantities of BrF_5 used.

The recycle-fluorination sequences for removal of plutonium were similar in runs Purse-7, -5, and -8 wherein the uranium had been fluorinated at 200, 300, and 400°C, respectively. The plutonium concentrations in the fluidized alumina beds for these runs are compared in Figure II-6. On the basis of the relative rates of plutonium removal as shown by the curves in Figure II-6 and the final plutonium concentration in the alumina beds, it appears that the temperature at which uranium is fluorinated with BrF_5 does affect subsequent plutonium fluorination. The uranium should be fluorinated at temperatures below 400°C, and on the basis of these data, 300°C appears to be the best temperature.

(2) Fluorination of UO_2-PuO_2-F.P. Pellets in the Presence of Added Cesium, Rubidium, and Neptunium

The recovery of neptunium during fluoride volatility processing of spent fuel may be a significant economic factor in the design of a commercial process; therefore, the reaction of neptunium during the fluorination with BrF_5 and fluorine is of particular interest. For run Purse-9, 0.46 g neptunium as NpO_2 was added to the alumina bed. This amount is about a factor of 40 or more than would be expected in the processing of an equivalent amount of spent BWR fuel irradiated to 10,000 MWd/T; this irradiation level is the basis for fission product addition to the UO_2-PuO_2-F.P. pellets. Excess neptunium was provided so that the concentration of this element would be above the limit of analytical detection in samples of the alumina bed material taken during the run. In addition to neptunium, the alumina bed for this run also contained both cesium and rubidium in proportion to the pellet charge. The fluorination step was carried out at 300°C for 2.1 hr with 9 v/o BrF_5, and the recycle-fluorination with fluorine consisted of 3 hr at 300°C, 5 hr from 300 to 550°C, and 3 hr at 550°C. Operating conditions for run Purse-9 are listed in Table II-2.

Uranium, plutonium, and neptunium concentrations in the fluidized alumina bed during run Purse-9 are shown in Figure II-7. The addition of rubidium, as well as cesium, to the fluidized bed in run Purse-9 did not affect the fluorination of uranium and plutonium from the alumina bed; the final bed from this run contained 0.003 w/o uranium and 0.005 w/o plutonium.

The neptunium concentration in the fluid bed increased during the first hour of fluorination with BrF_5 owing to the rapid depletion of U_3O_8 by reaction to form UF_6. At the end of the BrF_5 step, 0.2 g of neptunium remained in the bed, indicating that approximately one-half of the neptunium had volatilized. This result can be described by a first order rate constant, according to the diminishing sphere model, of 1.6×10^{-3} min^{-1}. This rate constant is about a factor of 10 higher than those observed in boat reactor experiments at

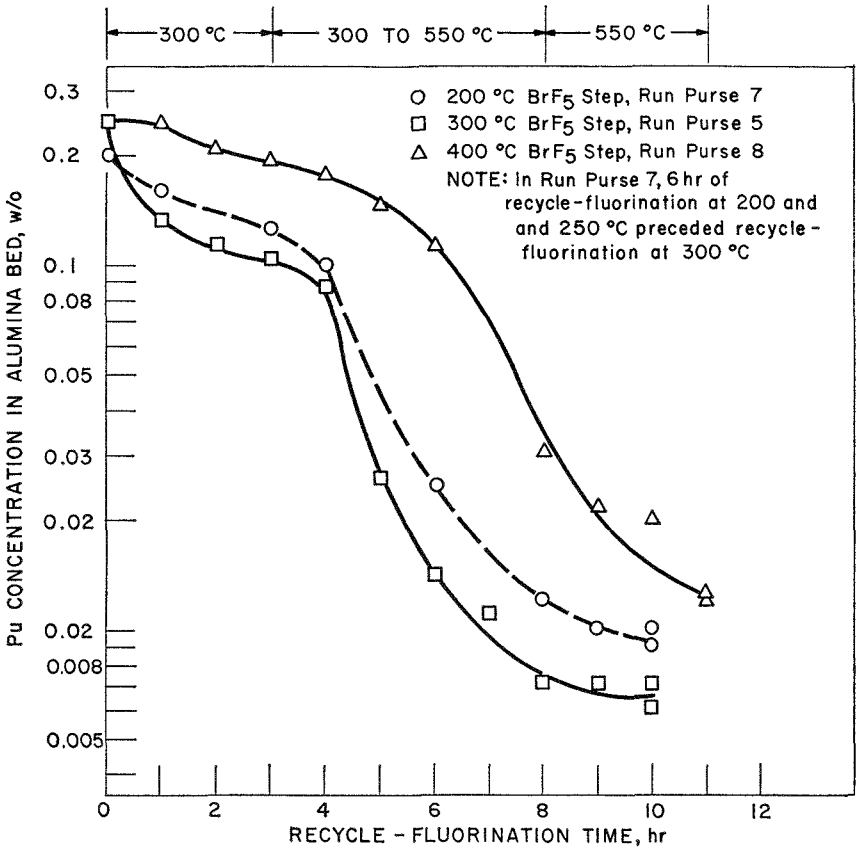

308-474

FIG. II-6. Plutonium Concentrations in Alumina Fluidized Beds Following Fluorination of Uranium with BrF_5.

300°C with 33 v/o BrF_5 at a partial pressure of 250 mm Hg. The difference in reaction rates may reflect a difference in the compounds fluorinated; in the boat tests, NpF_4 was the starting material, while in the fluid-bed experiment, NpO_2 was fluorinated.

The final alumina bed from run Purse-9 contained 0.002 w/o neptunium; approximately one-half of the original neptunium was volatilized with the uranium hexafluoride during fluorination with BrF_5 while the other half was recovered with plutonium hexafluoride during fluorination with fluorine. A total of 95% of the neptunium charged to the reactor was removed from the bed during this run.

f. RATE OF U_3O_8 FLUORINATION WITH BrF_5

Reaction rate constants for the reaction of U_3O_8 with BrF_5 calculated according to a diminishing sphere model are compared below for fluid-bed and thermobalance tests in the temperature range 200 to 400°C.

The integrated rate expression for a first order, irreversible reaction for which surface reaction is the rate-controlling step can be described for a diminishing sphere by:

$$(1 - F)^{1/3} = 1 - k't \qquad (1)$$

where F = fraction of solid reacted
k' = reaction rate constant, min^{-1} (a function of the true rate constant)
t = time, min.

For the reaction of U_3O_8 with BrF_5, the stoichiometry as well as the temperature and pressure dependence for the reaction rate have been reported previously (ANL-7225, pp. 84–86) as

$$5U_3O_8(s) + 18BrF_5(g) \rightarrow 15UF_6(g) + 9Br_2(g) + 20\,O_2(g) \qquad (2)$$

$$\log k' = 0.9 \log P_{BrF_5} - (2000/T) - 0.220 \qquad (3)$$

Under the conditions of the fluid-bed experiments, wherein high concentrations of reactive fines are initially present in the fluidized bed, significant consumption of BrF_5 occurs within the reactor, thus lowering the effective partial pressure of the BrF_5 reagent. Accordingly, the reaction rate constants were corrected using equation 4, which was derived from material balance and reaction rate expressions.

$$k^* = \frac{\Delta(1 - F)^{1/3}}{\Delta t (P_t)^{0.9}}. \qquad (4)$$

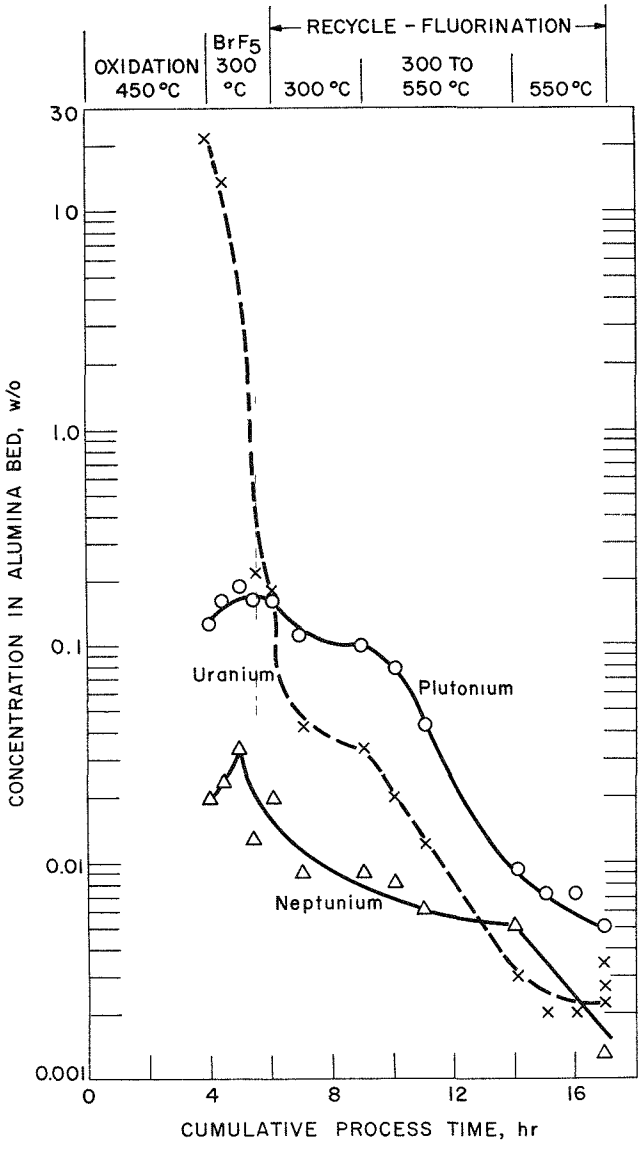

308-406

FIG. II-7. Uranium, Plutonium, and Neptunium Concentrations in the Fluidized Alumina Bed during Fluorination with BrF_5 Followed by Fluorine—Run Purse-9.

where P_t = effective partial pressure of BrF_5 in the fluid-bed reactor. Equation 4 was used to calculate k^* from the experimental data. The rate constants, k^*, were averaged for each temperature and then multiplied by the BrF_5 pressure at the inlet to the reactor in each run to obtain the corrected value of k'.

Rate constants calculated from fluid-bed data, both uncorrected and corrected for depletion of BrF_5, are compared in Table II-4 with those obtained in thermobalance tests. At 200 and 300°C where the rates are relatively low, there is no significant correction for depletion of BrF_5, whereas at 400°C the correction is appreciable. The temperature dependence of the corrected rate constants gives an apparent activation energy of 8.2 kcal/mole. This result is in good agreement with the activation energy of 9.2 kcal/mole obtained in thermobalance work.

g. PLUTONIUM MATERIAL BALANCES

Plutonium material balances for the runs reported above ranged from 87 to 126% and are shown in Table II-5. These runs were conducted so that most of the UF_6 product was collected in cold traps or soda lime traps and most of the PuF_6 product was collected in a sodium fluoride trap at 100°C. The cold traps and soda lime traps were not sampled for plutonium. Previous analyses of the soda lime traps indicated that the concentration of plutonium in these traps was at background level.

TABLE II-4. REACTION RATE CONSTANTS FOR THE REACTION OF U_3O_8 WITH BrF_5 CALCULATED FROM FLUID-BED AND THERMOBALANCE EXPERIMENTS

Reaction Conditions		Rate Constant, $k' \times 10^3$ (min^{-1})		
Temperature (°C)	BrF_5 (mm Hg)	Fluid-bed tests		Thermobalance tests
		Uncorrected	Corrected	
200	116	2.2	2.2	2.4
300	112	9.6	9.5	13
400	110	19	27	41
Activation energy (kcal/mole)		7.0	8.2	9.2

TABLE II-5. PLUTONIUM MATERIAL BALANCES

Run	Pu Charged (g)	Recovered Fines[a]				Total Pu Recovered[b] (g)	Pu Material Balance (%)
		Weight (g)	Pu (w/o)	Pu (g)	Percent of Pu charge		
Pure-19, -20, -21	8.40	23.4	2.72	0.64	7.6	8.09	96.3
Pure-22	2.78	13.9	2.64	0.37	13.2	2.61	93.1
Purse-8	2.81	9.4	3.70	0.35	12.4	3.16	112.5
Purse-9	2.82	15.7	0.34	0.05	1.9	3.56	126.0
Purse-10, -11, -12	8.32	18.0	6.70	1.21	14.5	7.27	87.4
Total (9 runs)	25.13			2.62	10.4[c]	24.69	98.4[c]

[a] These fines are recovered by brushing and rapping the disengaging and filter sections of the reactor at the completion of the run(s).

[b] Includes plutonium recovered in alumina samples and the final bed, reactor fines, and NaF traps. PuF_6 collected in cold traps with UF_6 in runs Pure-19, -20, -21, -22 not included.

[c] Average of nine runs.

The procedure for obtaining a sample from the sodium fluoride trap involved the following steps: the sodium fluoride pellets from the top half of the trap (which is 3 in. in dia. by 24 in. high) were ground in a disc mill. (The gas inlet is located at the top of the trap, and previous analyses have shown that the concentration of plutonium in the lower half of the trap is below background level.) The powder was then riffled several times to reduce the sample size to about 40 g. In runs Pure-19, -20, -21, and -22, a sample was first obtained in this manner and then the remainder of the sodium fluoride pellets which had been removed from the trap were recombined, mixed, and riffled once again to obtain a second sample. The results obtained from these duplicate samples are shown in Table II-6.

TABLE II-6. Analysis of Duplicate Samples Taken from Upper Half of 100°C Sodium Fluoride Trap

Run Pure-	Sample Number	U (w/o)	Pu (w/o)
19	1	11.6	0.095
	2	11.9	0.095
20	1	8.7	0.125
	2	8.5	0.34
21	1	12.1	0.132
	2	11.9	0.133
22	1	13.2	0.099
	2	13.3	0.104

The plutonium analysis for the duplicate sample from run Pure-20 is obviously in error. In this case, the analysis indicates that more than 7 g plutonium was in the trap, whereas only 2.80 g plutonium was charged to the reactor for the run. The reason for this spurious result has not been determined.

In the other runs reported in Table II-6, the agreement between duplicate samples for both the uranium and plutonium analyses was very good and generally within the analytical error. These results show that an effective method of obtaining a representative sample of the sodium fluoride has been used and that reproducible results have been obtained.

Included in Table II-5 is a detailed account of plutonium holdup in the fines recovered from the reactor following each run. These fines do not fall freely from the reactor surfaces but are recovered by vigorous rapping and by brushing of most of the interior surface of the reactor. Thus, plutonium in these fines may constitute a reactor inventory rather than a process loss. The fact that these fines do not readily fall into the bed can be verified by noting the closeness of the duplicate points (Fig. II-2 to II-7) which represent the uranium and plutonium concentrations in the final alumina beds. A pair of duplicate points represents the beds in a fluidized and static condition.

Efforts are now being made to reduce plutonium holdup in the recovered fines since with adoption of the current two-step processing scheme the total quantity of fines has generally increased. In run Purse-9, the fluid-bed filters were heated to about 250°C during the latter portion of both the BrF_5 and recycle-fluorination steps, whereas in preceding runs the normal filter temperature was about 150°C. Higher filter temperatures resulted in a significant reduction in plutonium holdup in the fines for run Purse-9; however, similar results were not obtained in the alumina reuse experiments, runs Purse-10, -11, and -12 during which the filters were heated to 250°C. This may have been caused by elutriation of plutonium during the several oxidation and BrF_5-fluorination steps which preceded the single recycle-fluorination step with fluorine. The extent of possible elutriation after the BrF_5 step in runs Purse-10, -11, and 12 is indicated in Table II-7. These data indicate that almost one-half of the plutonium charge may have been elutriated to cooler portions of the reactor before recycle-fluorination was begun. Since the 18 g of fines recovered after the recycle-fluorination step of run Purse-12 (see Table II-5) contained 1.2 g plutonium, it also appears that blowback of the filters and rapping of the reactor during the run were effective in returning fines containing 2.3 g plutonium to the fluid-bed reaction zone.

Samples of the recovered fines have been fluorinated in boat reactor tests to determine whether plutonium would be removed by fluorination at temperatures used in the recycle-fluorination sequence of runs Purse-10, -11, and -12. Preliminary data from the boat reactor tests have indicated that plutonium concentration was reduced from 6.7 w/o to 0.2 w/o. This result indicates that about 0.4% of the plutonium charged for runs Purse-10, -11, and -12 would be associated with the

TABLE II-7. Plutonium Distribution in the Fluid-Bed Reactor after Selective Fluorination of Uranium with BrF_5

Run Purse-	Total Pu Charged (g)	Pu Removed in Samples (g)	Net Pu in Reactor (g)	Pu in Fluid Bed[a] (g)	Pu elsewhere in Reactor (g)
10	2.78	0	2.78	0.94	1.84
11	5.57	0.066	5.50	3.17	2.33
12	8.32	0.189	8.13	4.60	3.53

[a] Based on chemical analysis of fluid-bed sample and alumina remaining in reactor when sample was taken.

reactor fines in the final bed of run Purse-12 if these fines had been efficiently returned to the reaction zone. Attempts are now being made to determine whether the principal source of plutonium in the fines is derived from elutriation of particles or from the decomposition of PuF_6 in the filter region of the reactor.

2. The Fluorination of Uranium Compounds by Bromine Pentafluoride

(R. L. JARRY, J. STOCKBAR)

a. INTRODUCTION

Bromine pentafluoride is being considered as a fluorinating agent for the fluid-bed fluoride volatility process applied to the reprocessing of spent nuclear power reactor fuel. The reaction of BrF_5 with mixtures of uranium and plutonium compounds converts the uranium to volatile UF_6 while converting the plutonium only to nonvolatile PuF_4. Hence, the use of BrF_5 can achieve a separation of uranium from plutonium in a single fluorination step.

The program to evaluate the selectivity of BrF_5 as a fluorinating agent for mixtures of uranium and plutonium compounds has involved a comprehensive study of the fluorination with BrF_5 of solid reaction mixtures containing uranium and plutonium compounds, fission product element compounds, alumina, and stainless steel or Zircaloy decladding product. Results of these studies were reported in ANL-7055, pp. 114–121 and ANL-7125, pp. 66–68. Reported below is the concluding portion of the study on kinetics of the reactions of BrF_5 with uranium compounds. The kinetics of the reactions of BrF_5 with UO_2 and UO_3 have been determined.

b. EXPERIMENTAL EQUIPMENT AND PROCEDURE

(1) Materials

Uranium Compounds. The characteristics of the UO_2 and UO_3 used in these thermobalance studies are listed in Table II-8. Two sources of UO_2 were used. One of the sources (designated ANL-UO_2) was material prepared in this Division by the reduction of UF_6 using steam-hydrogen mixtures;[4] the second source was high-density sintered UO_2 prepared by Numec[5] (designated Numec-UO_2). The UO_3 was part of a batch previously used in a study of the reaction of UO_3 with SF_4,[6] and was prepared by the thermal decomposition of $UO_4 \cdot 2H_2O$ at a temperature above 300°C. The −170+200 mesh fraction of each of these oxides was used, and the average particle diameter was 81 microns.

TABLE II-8. COMPOSITION AND SURFACE AREA OF URANIUM COMPOUNDS

Compound	Analytical Results		Surface Area[a] (m^2/g)
	Found (%)	Theoretical (%)	
ANL-UO_2			
U	88.3	88.15	0.46
O	12.0	11.85	
Numec-UO_2			
U	88.1	88.15	0.04
O	12.0	11.85	
UO_3			
U	82.7	83.22	0.67
O	16.7	16.78	

[a] Measured by the B.E.T. method using nitrogen.

Bromine Pentafluoride. The BrF_5 used was purified by distillation. Characteristics of this material were previously presented in ANL-7055, p. 115.

(2) Apparatus and Procedure

The Sartorious thermobalance used in this work was described in detail in the preceding semiannual report, ANL-7225, pp. 78–79. Briefly, the thermobalance consists of a vertical tubular reactor 1½ in. in diameter and 20 in. long, and a Sartorious rapid 200 analytical balance equipped with an optical-electronic weight-sensing system and a remote recording output.

The procedure employed in these experiments was the same as that outlined in the preceding semiannual report, ANL-7225, p. 79.

c. RESULTS AND DISCUSSION

(1) UO_2-BrF_5 Reaction

The reaction of UO_2 with BrF_5 proceeds by the formation of UO_2F_2 which, in turn, is fluorinated to UF_6. Experiments were performed in the temperature range 224 to 302°C for the ANL-UO_2 and at 307 to 367°C for the Numec-UO_2. The partial pressure of BrF_5 in

[4] The UF_6 was reduced in a fluid bed of UO_2 particles at 650 to 700°C. The UO_2 particles were then densified to about 96% of theoretical density by sintering in hydrogen at about 1700°C. Additional information on characteristics of this UO_2 may be found in I. E. Knudsen, N. M. Levitz, and A. A. Jonke, Engineering Development of Fluid-Bed Fluoride Volatility Processes. Part 6. Preparation of Dense Uranium Dioxide Particles from Uranium Hexafluoride in a Fluidized Bed, ANL-6902, Dec. 1964.

[5] Specifications for these pellets: O/U ratio, <2.05; sintered in hydrogen at 1700°C; impurities, <0.1%.

[6] C. E. Johnson and J. Fischer, J. Phys. Chem., **65**, 1849 (1961).

the gas phase (26 v/o BrF_5, 74 v/o nitrogen) was 181 torr and the linear velocity of the gas phase was about 0.7 cm/sec. The rate constants obtained are listed in Table II-9 and are shown in the plots of Figure II-8. It is assumed that the products of the reaction are UF_6 and O_2 together with elemental bromine. This assumption is in agreement with the stoichiometry previously discussed (ANL-7225, p. 84). From least squares fits of the Arrhenius equation to the two sets of data, the following equations were obtained:

$$\text{ANL-}UO_2\text{, } \log k' = 1.493 - 1630/T \quad (1)$$

$$\text{Numec-}UO_2\text{, } \log k' = 3.441 - 3060/T \quad (2)$$

From these equations, activation energies of 7.5 and 14 kcal/mole were calculated for the ANL and Numec materials, respectively.

The activation energy of 7.5 kcal/mole for the ANL-UO_2 suggests that the reaction is controlled by the formation of UO_2F_2 and depletion of UO_2F_2 by fluorination. The activation energy for the UO_2F_2 reaction was found previously to be 8.3 kcal/mole (ANL-7225, p. 83). In the case of the Numec-UO_2, the value of 14 kcal/mole suggests the presence of UF_4 as well as UO_2F_2 on the surface of the reacting particles, since previous work (ANL-7225, p. 80) showed that the activation energy for the UF_4 reaction is 16.9 kcal/mole. Rampy[7] has shown that both UO_2F_2 and UF_4 are produced by the reaction of UF_6 with UO_2. Therefore, if in the reaction of Numec-UO_2, the product UF_6 reacts with the UO_2, the solid surface would be an equimolar mixture of UO_2F_2 and UF_4. For such an equimolar mixture, an estimate of the activation energy ($0.5 \times 8.3 + 0.5 \times 16.9$) results in a value of 12.6 kcal/mole, in reasonable agreement with the value of 14 kcal/mole obtained experimentally. Reasonable agreement of theoretical with experimental activation energies had been previously obtained for ⅔ UO_2F_2-⅓ UF_4 mixtures (ANL-7055, p. 119).

The difference in behavior of the two types of oxide probably arises from different degrees of reactivity of the two oxides. A high reactivity of ANL-UO_2 may result in rapid conversion of the surface of the solid to UO_2F_2, so that interaction at the oxide surface with UF_6 to form a mixture of UF_4 and UO_2F_2 would be essentially absent. Sintered oxide (Numec-UO_2) is more slowly fluorinated to UO_2F_2 and therefore some oxide surface is available for contact with UF_6 to form UF_4 and UO_2F_2. To obtain rates comparable to those obtained for ANL-UO_2, higher temperatures are needed for Numec-UO_2; this can be ascribed to the lower reactivity of the sintered UO_2 particles.

Experiments were also performed, using ANL-UO_2, to determine the dependence of the reaction rate on the BrF_5 partial pressure and the linear velocity of the gas phase. The two experiments (at 277°C in Part A of Table II-9) were performed at linear velocities of 0.85 and 1.25 cm/sec, respectively. Values of the rate constant of 0.0312 and 0.0384 min^{-1} which were obtained for these experiments do not indicate a large effect of the linear velocity of the gas phase on the value of the rate constant. Other experiments were performed in which the BrF_5 partial pressure in the gas phase was

[7] G. A. Rampy, USAEC Report GAT-265, June 5, 1959.

TABLE II-9. Rate Constants for the UO_2-BrF_5 Reaction

BrF_5 partial pressure: 181 torr
Total pressure: 1 atm
Linear velocity: 0.7 cm/sec

Temp. (°C)	$k' \times 10^3$ (min^{-1})	
	Exp.	Calc.
A. ANL-UO_2		
224	19.3	18.7
225	23.8	18.9
228	16.8	19.8
230	18.7	20.4
241	25.9	23.8
242	25.4	24.2
253	23 3	28.1
254	22.3	28.5
255	25.3	28.9
262	30.2	31.6
274	33.5	36.7
277[a]	31.2	38.1
277[b]	38.4	38.1
279	43.4	39.0
279	41.6	39.0
279	40.6	39.0
295	47.9	47.1
302	50.1	51.0
B. Numec-UO_2		
307	19.0	14.7
309	16.1	15.3
310	15.7	15.6
326	24.8	21.6
329	18.3	22.9
330	21.3	23.3
333	19.0	24.7
333	19.0	24.7
336	32.5	26.2
339	34.3	27.7
346	30.3	31.5
349	32.0	33.3
354	35.1	36.5
355	51.3	37.1
365	46.7	44.3
367	47.6	45.8

[a] Linear velocity = 0.85 cm/sec.
[b] Linear velocity = 1.25 cm/sec.

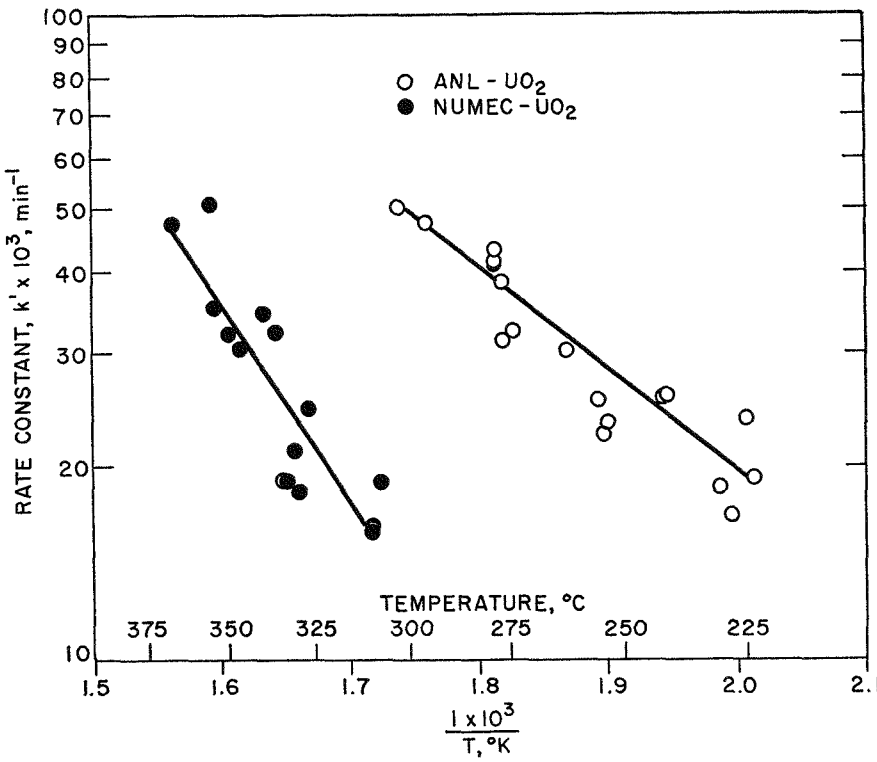

308-531

FIG. II-8. Temperature Dependence of the Rate Constants for the Reaction of BrF_5 with UO_2.
BrF_5 partial pressure: 181 torr
Total pressure: 1 atm
Linear velocity: 0.7 cm/sec

TABLE II-10. DEPENDENCE OF THE RATE CONSTANT, k', ON THE PARTIAL PRESSURE OF BrF_5

Temp. (°C)	P_{BrF_5}[a] (torr)	$k' \times 10^3$ (min^{-1})	Exponent for BrF_5 Pressure Term[b] (n)
A. UO_2-BrF_5 Reaction			
242	74	13.8	
250	74	15.5	
242	181	23.6	
250	181	27.2	
242	369	43.0	
250	369	60.1	0.84
B. UO_3-BrF_5 Reaction			
252	90	12.9	
253	90	12.9	
251	189	26.6	
252	189	31.6	
251	277	41.8	
251	277	41.8	1.05

[a] Total pressure, 1 atm.
[b] For equation $k' = Ae^{-E/RT}P^n$.

TABLE II-11. REACTION RATE CONSTANTS FOR THE UO_3-BrF_5 REACTION

BrF_5 partial pressure: 189 torr
Total pressure: 1 atm
Linear velocity: 0.7 cm/sec

Temp. (°C)	$k' \times 10^3$ (min^{-1})	
	Exp.	Calc.
222	13.7	17.6
226	17.7	18.7
235	22.8	21.5
236	22.8	21.8
251	26.6	27.1
252	31.6	27.5
263	36.6	32.0
264	28.1	32.4
265	28.6	32.8
276	39.1	37.9
278	40.4	38.9
299	50.2	50.3
300	51.6	50.9

74 or 369 torr. The values of the rate constant obtained, along with those for reactions at 181 torr BrF_5 partial pressure (from Table II-9), are listed in Part A of Table II-10. From these data a value of 0.84 was derived for the coefficient, n, of the pressure term in the equation $k' = Ae^{-E/RT}P^n$. Combining this value of n with the previous equation resulted in the following equation representing the temperature and pressure dependence of the UO_2-BrF_5 reaction:

$$\log k' = 0.84 \log P - 1630/T - 0.270$$

where P is expressed in torr.

(2) UO_3-BrF_5 Reaction

The kinetics of the UO_3-BrF_5 reaction were studied over the temperature range 222 to 300°C. The BrF_5 partial pressure was 189 torr in a gas phase containing 27 v/o BrF_5 and 73 v/o nitrogen at a linear velocity of about 0.7 cm/sec. The results are listed in Table II-11 and are shown in the plot of Figure II-9. It is assumed that the products of the reaction are UF_6 and O_2, together with elemental bromine. The following equation representing the temperature dependence of the rate constant was obtained by a least squares fit of the Ar-

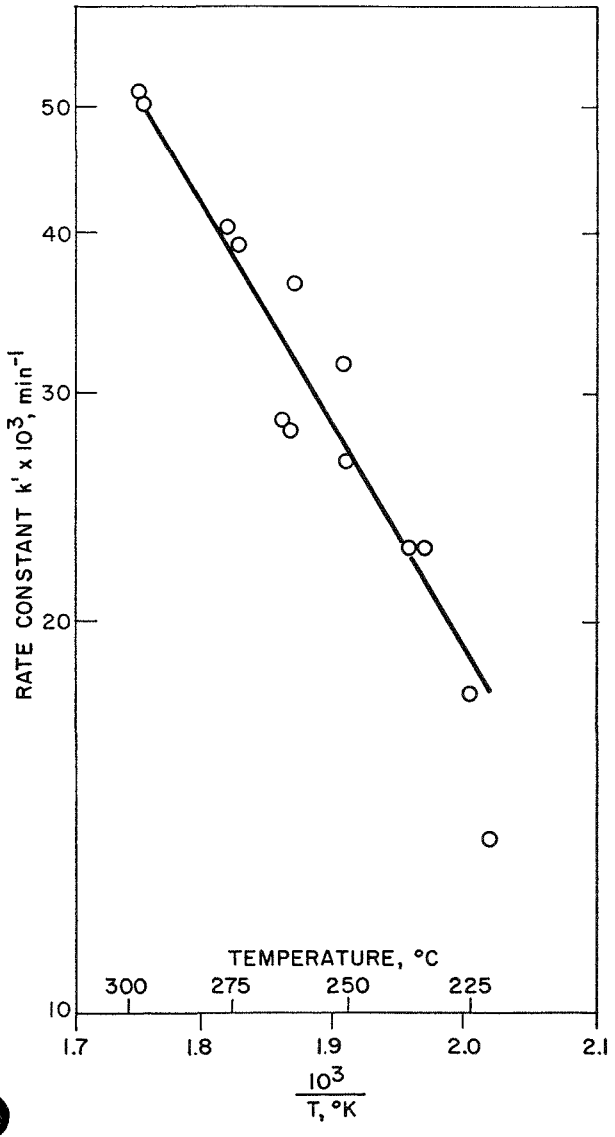

308-411

FIG. II-9. Temperature Dependence of the Rate Constants for the Reaction of BrF_5 with UO_3.

TABLE II-12. RATE EQUATIONS FOR THE REACTIONS OF BrF_5 WITH URANIUM COMPOUNDS

Rate equation:[a] $\log k' = n \log P - (A/T) + B$

	UF_4	UO_2F_2	U_3O_8	UO_2[b]	UO_3
n	0.38	0.71	0.90	0.84	1.05
A	3690	1810	2000	1630	1680
B	4.286	0	−0.220	−0.270	−0.767
Activation Energy (kcal/mole)	16.9	8.3	9.2	7.5	7.7

[a] P in torr, k' in min^{-1}.

[b] High reactivity ANL-UO_2.

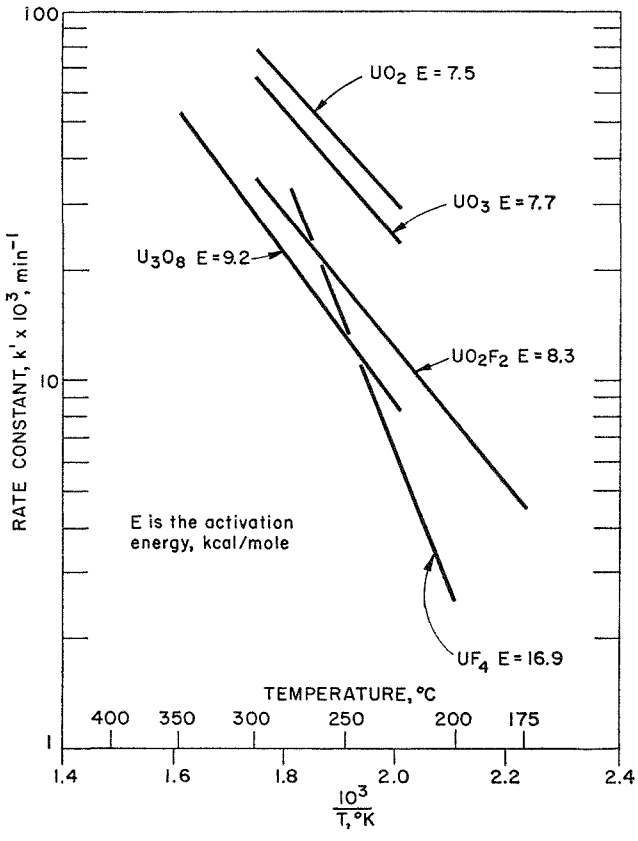

308-401

FIG. II-10. Temperature Dependence of Rate Constants for the Reaction of BrF_5 with Uranium Compounds.

P_{BrF_5} = 250 torr

rhenius equation to the data:

$$\log k' = 1.636 - (1680/T)$$

A value of 7.7 kcal/mole was calculated for the activation energy of the UO_3-BrF_5 reaction.

Several experiments were performed to determine the dependence of the reaction rate on the BrF_5 partial pressure. The data obtained at partial pressures of 90, 189, and 277 torr are listed in Part B of Table II-10. From these data a value of 1.05 for the coefficient n of the equation $k' = Ae^{-E/RT}P^n$ was calculated. Combining this value of n with the previous equation resulted in the following equation representing the combined temperature and pressure dependence of the UO_3-BrF_5 reaction:

$$\log k' = 1.05 \log P - 1680/T - 0.767$$

where P is in torr.

d. SUMMARY OF REACTIONS OF URANIUM COMPOUNDS WITH BrF_5

The experimental work on the kinetics of the reaction of BrF_5 with UO_2 and UO_3 described in this report completes the study of the reaction of BrF_5 with the uranium compounds UF_4, UO_2F_2, U_3O_8, UO_2, and UO_3. The constants for the equations representing the combined temperature and pressure dependence of the rate constant for the various reactions are listed in Table II-12. The temperature dependence of the various reaction rate constants at a BrF_5 partial pressure of 250 torr is shown in the plots of Figure II-10.

3. Tellurium Fluoride Chemistry (D. R. Vissers)

a. INTRODUCTION

The volatile fluorides of fission product tellurium represent a troublesome component in the process off-gas streams from fluoride volatility processing of reactor fuel materials because of the relatively high concentration of radioactive tellurium in the fuel and the chemically inert character of the tellurium fluorides formed in the process. The low maximum permissible concentration, MPC, for airborne, fission product tellurium,[8] which is 1×10^{-8} μCi/ml for both ^{127m}Te and ^{129m}Te, must be considered in the decontamination of process off-gas streams. Little information on the chemistry of tellurium fluorides is available, and consequently, a program on the chemistry of the tellurium fluorides has been established to obtain information on methods for the removal of traces of tellurium fluorides from gas streams. The principal tellurium fluoride species in the fluoride volatility process off-gas is probably tellurium hexafluoride, and small quantities of ditellurium decafluoride, Te_2F_{10}, may also be present.

Various inorganic and organic materials were evaluated to determine their ability to sorb tellurium hexafluoride under static conditions. The sorbents used in this study included soda lime, activated alumina, Linde types 13X and 10X Molecular Sieve, activated charcoal, magnesium fluoride, copper (II) oxide, and metallic copper, aluminum, nickel, and tellurium. The criteria for the sorbent evaluation in this study were: (1) the rate of TeF_6 sorption, (2) the capacity of sorbent for TeF_6, and (3) the quantity of TeF_6 retained on the sorbent.

[8] Maximum Permissible Body Burdens and Maximum Permissible Concentrations of Radionuclides in Air and in Water for Occupational Exposure, U.S. Department of Commerce, National Bureau of Standards Handbook 69, June 5, 1959.

b. EXPERIMENTAL EQUIPMENT AND PROCEDURE

(1) Materials

The tellurium hexafluoride used in this study was obtained from Allied Chemical Company and was purified by fractional sublimation under vacuum to remove lower fluorides of tellurium such as Te_2F_{10}, TeF_4, and $Te_3F_{14}O_2$. The sorbents and chemical trap materials used in this study are listed in Table II-13.

(2) Experimental Equipment

The apparatus consisted of a 97-ml vertical, tubular heated nickel reactor, a general purpose manifold to which were attached a system of cold traps, a calibrated TeF_6 feed cylinder, a vacuum system, and a Booth-Cromer type pressure transmitter with a mercury manometer readout. The manifold, valves, reaction vessel, and all auxiliary equipment exposed to the tellurium hexafluoride were constructed of nickel. A chromel-alumel type thermocouple located within the nickel reactor served as the temperature indicator and regulator signal for the furnace temperature controller.

(3) Procedure

A weighed sample of the sorbent was placed in the reactor and after the system was heated to the desired temperature and evacuated, a measured quantity of tellurium hexafluoride was admitted to the system.

TABLE II-13. REAGENTS TESTED FOR TeF_6 REMOVAL

Material	Source	Designation	Surace Area (m^2/g)[a]
Activated alumina	Alcoa	F-1, −8+14 mesh	295
BPL activated charcoal	Pittsburgh Coke and Chemical Company	−12+30 mesh, BPL	2075
Activated cocoanut charcoal	Sargents	AC-11368	1790
Linde Molecular Sieve	Union Carbide Corporation	1/16 in., Type 13X	280
Linde Molecular Sieve	Union Carbide Corporation	1/16 in., Type 10X	332
Magnesium fluoride	Prepared at Oak Ridge National Laboratory	14–18 mesh	146
Sodium fluoride	Harshaw Chemical Company	Tablets, 1/8 in. by 1/8 in.	<1
Soda lime	Mallinckrodt Chemical Works	4–8 mesh	6.3
Copper metal turnings	Mallinckrodt Chemical Works	—	<0.1
Nickel wool	Brillo Manufacturing Company	Coarse grade	<0.1
Tellurium metal powder	Sargents	—	<1
Aluminum turnings	ANL	2S, clean	<0.1
Copper (II) oxide	Allied Chemical	Reagent wire	<0.1

[a] Measured by B.E.T. method using nitrogen.

The sorption of tellurium hexafluoride was monitored by observing the change of pressure in the system. After sorption was completed, the excess tellurium hexafluoride was collected in a cold trap cooled with liquid nitrogen. The vessel containing the sorbent was then evacuated, at a pressure of $\sim 10^{-2}$ torr, through a cold trap cooled by liquid nitrogen, to determine whether the tellurium hexafluoride could be desorbed from the solid. In some of the experiments, a second reactor vessel heated to 100°C and containing about 10 g of sodium fluoride pellets was placed in series with the principal reactor to collect any hydrogen fluoride which may have been present. Hydrogen fluoride may be introduced into the system by partial hydrolysis of TeF_6.

The initial TeF_6 pressure listed for each of the studies is the pressure of the TeF_6 at 25°C. The characteristics of the Booth-Cromer and mercury manometer readout limited the accuracy of the pressure measurement. Consequently, the maximum sorption could not be reported as 100 percent.

c. SORPTION STUDIES

The capacity of most gas sorbents is principally determined by surface area, pore size distribution, and the chemistry and geometry of the sorbent surface and sorbing gas molecule. For comparative evaluations of the respective sorbents, a sorbed TeF_6 molecule was assumed to occupy the average nitrogen B.E.T. surface area on the sorbent surface of 40 Å^2. The calculated capacity of a sorbent with a surface of one square meter would thus be 4.16×10^{-6} mole, assuming complete coverage by a monolayer of sorbed molecules. The molecular cross-sectional area of the nitrogen molecule was assumed to be 16.28 Å^2 for all of the B.E.T. surface area measurements.

(1) Activated Alumina

A typical gas sorption isotherm at 25°C is shown in Figure II-11 for the sorption of TeF_6 on activated alumina. The isotherm indicates that about 50 percent of the TeF_6 present was sorbed in 30 sec, while after 20 min only 76 percent of the TeF_6 was sorbed. These results indicate that the rate of TeF_6 sorption on activated alumina is high, until about 16 percent of the surface is covered. Several tests were performed in which the ratio of activated alumina to TeF_6 charge was increased so that if the entire quantity of TeF_6 were sorbed, it would occupy only 7.6 percent of the nitrogen-determined surface area of the activated alumina. The results of these tests confirmed the conclusion that the rate of TeF_6 sorption is high at low surface coverage. The studies with the higher ratio of activated alumina to TeF_6 were then extended to higher temperatures. The results of experiments with activated alumina (Table II-14) indicate that activated alumina is a good sorbent for TeF_6 at temperatures below 300°C. After sorption of TeF_6 on activated alumina, nitrogen B.E.T. surface area measurements of the samples were made (Table II-15). Results indicate that only at 500°C does the alumina lose a significant fraction of surface area. No data have been obtained, however, which would indicate whether activated alumina in the absence of TeF_6 would show a similar reduction in surface area. Desorption of TeF_6 at a pressure of 1×10^{-2} torr was slight, indicating that TeF_6 is retained strongly by alumina.

(2) Activated Charcoal

BPL Activated Charcoal. The effects of loading of the charcoal surface by TeF_6 on (1) the kinetics of TeF_6 sorption and (2) the retention of TeF_6 by charcoal were

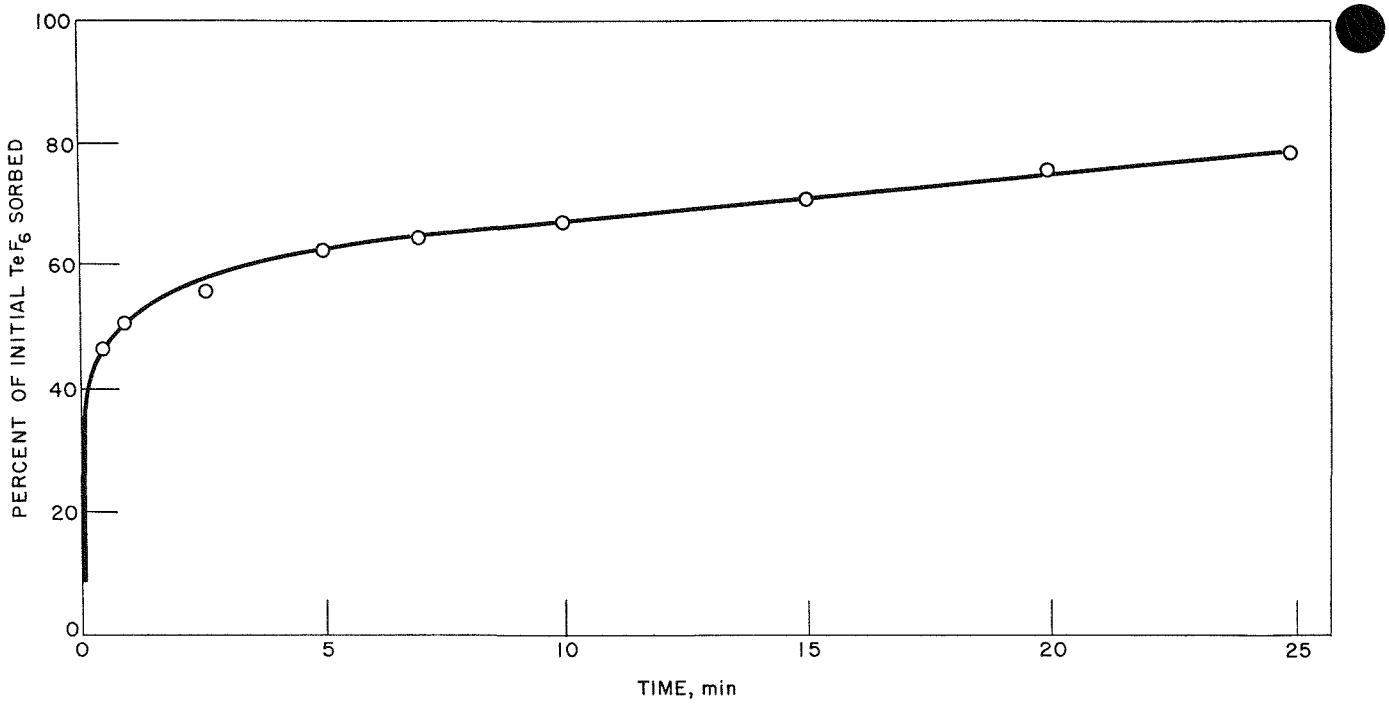

308-432

FIG. II-11. The Rate of Sorption of TeF_6 on Activated Alumina at 25°C.
TeF_6 charge: 4×10^{-3} mole
Initial pressure: 100 torr
Activated alumina charge: 10 g
(TeF_6 monolayer capacity, 1.2×10^{-3} mole/g)

TABLE II-14. THE SORPTION RATE AND RETENTION OF TELLURIUM HEXAFLUORIDE ON ACTIVATED ALUMINA
TeF_6 charge, 2×10^{-3} mole; initial pressure, 200 torr
Activated alumina charge,[a] 22.2 g

Reaction Time (min)	Percent of the Initial TeF_6 Sorbed on Activated Alumina					
	25°C	100°C	200°C	300°C	400°C	500°C
0.5	>97	>99	99	>97	62	37
1.0	>98	>99	>99	>98	66	41
2.0	>98	>99	>99	>98	69	45
5.0	>99	>99	>99	>98	76	50
10.0	>99	>99	>99	>98	85	58
15.0	>99	>99	>99	>98	85	56
20.0	>99	>99	>99	>98	86	56

Temperature of Sorption and Desorption (°C)	Percent of the Initial TeF_6 Desorbed from the Alumina during Evacuation[b]
25	6.5
100	2
200	1.4
300	1.8
400	1.5

[a] The calculated TeF_6 monolayer capacity of the activated alumina was 1.2×10^{-3} mole/g.

[b] The alumina samples were placed under vacuum ($\sim 1 \times 10^{-2}$ torr) for desorption for 1 to 2 hr.

investigated at 25°C. The results of this study are presented in Table II-16. To determine the effect of temperature on the TeF_6 sorption behavior, a series of sorption studies were carried out at 100, 200, 300, and 400°C. The results, reported in Table II-17, indicate that at 25°C charcoal possesses good sorptive characteristics for TeF_6.

Activated Cocoanut Charcoal. To determine how the type of charcoal affects the sorptive properties of the charcoal for TeF_6, a second type of activated charcoal was evaluated briefly as a sorbent for TeF_6. The charcoal used for this study was activated cocoanut charcoal with a monolayer capacity for TeF_6 of 7.43×10^{-3}

TABLE II-15. B.E.T. SURFACE AREA MEASUREMENTS OF ACTIVATED ALUMINA SAMPLES
Reaction time: 20 min

Description of Activated Alumina	B.E.T. Surface Area (m^2/g)	% of Surface Covered with TeF_6
Material as Received	295	—
Reacted at 100°C with TeF_6	297	7.4
Reacted at 200°C with TeF_6	316	7.5
Reacted at 300°C with TeF_6	303	7.4
Reacted at 400°C with TeF_6	316	6.4
Reacted at 500°C with TeF_6	155	~4

TABLE II-16. The Sorption Rate and Retention of Tellurium Hexafluoride on BPL Activated Charcoal at 25°C

TeF_6 charge, 2 × 10^{-3} mole; initial pressure, 200 torr

Reaction Time (min)	Percent of the Initial TeF_6 Sorbed on Activated Charcoal		
	1-g sample[a]	5-g sample[a]	10-g sample[a]
0.5	69	98	>99
1.0	78	99	>99
2.0	86	>99	>99
5.0	93	>99	>99
10.0	94	>99	>99
15.0	95	>99	>99
20.0	95	>99	>99

Sorbent Sample Size (g)	Percent of the Initial TeF_6 Desorbed from the Charcoal during Evacuation[b]
1	36.5
5	1
10	1

[a] The calculated TeF_6 monolayer capacity of the BPL activated charcoal was 8.6 × 10^{-3} mole/g.

[b] The charcoal samples were placed under vacuum (~1 × 10^{-2} torr) for desorption for 1½ hr.

TABLE II-17. The Effect of Temperature on the Sorption Rate and Retention of Tellurium Hexafluoride on BPL Activated Charcoal

TeF_6 charge, 2 × 10^{-3} mole; initial pressure, 200 torr
Charcoal charge,[a] 5 g

Reaction Time (min)	Percent of the Initial TeF_6 Sorbed on Activated Charcoal Sample				
	25°C	100°C	200°C	300°C	400°C
0.5	98	98	27	4	0
1.0	99	>98	29	7	0
2.0	>99	>99	32	7	0
5.0	>99	>99	35	8	0
10.0	>99	>99	38	8	0
15.0	>99	>99	40	8	0
20.0	>99	>99	42	8	0

Temperature of Sorption and Desorption (°C)	Percent of the Initial TeF_6 Desorbed from the Charcoal during Evacuation[b]
25	1
100	3.7
200	35.7

[a] The calculated TeF_6 monolayer capacity of the BPL activated charcoal was 8.6 × 10^{-3} mole/g.

[b] The charcoal samples were placed under vacuum (~1 × 10^{-2} torr) for desorption for about 1 hr.

mole/g. In this study 2 × 10^{-3} mole of TeF_6 at approximately 200 torr was reacted with 5- and 10-g samples of the activated cocoanut charcoal at 25°C. The results of this study showed that only 97 percent of the tellurium hexafluoride present had been sorbed on a 10-g sample of cocoanut charcoal in twenty minutes. During evacuation of the sample chamber for 80 min at 25°C, 31% of the initial TeF_6 was desorbed. Similar results were obtained with the 5-g sample of cocoanut charcoal. These results indicate that cocoanut charcoal does not retain TeF_6 as well as BPL charcoal.

(3) Linde Molecular Sieves

Type 13X Molecular Sieve. The effect of TeF_6 surface loading on the kinetics of TeF_6 sorption and TeF_6 retention by type 13X Molecular Sieve was investigated at 25°C. The results of this study, presented in Table II-18, indicate that TeF_6 is rapidly sorbed on the Molecular Sieve. In another series of sorption studies, the effect of temperature on TeF_6 sorption and retention was observed at 100, 200, 300, and 400°C. At 300°C the TeF_6 sorption was carried out on the 13X Molecular Sieve, both in the presence and absence of the sodium fluoride trap. The sorption studies at 300°C indicated that no significant amount of hydrogen fluoride, derived either from the TeF_6 feed or from interaction between TeF_6 and the sorbent, is present during the sorption step. The results of these studies indicate that the 13X

TABLE II-18. The Sorption Rate and Retention of Tellurium Hexafluoride on Linde 13X Molecular Sieve at 25°C

TeF_6 charge, 2 × 10^{-3} mole; initial pressure, 200 torr

Reaction Time (min)	Percent of the Initial TeF_6 Sorbed on 13X Molecular Sieve Sample		
	1-g sample[a]	5-g sample[a]	10-g sample[a]
0.5	79	99	>99
1.0	84	>99	>99
2.0	91	>99	>99
5.0	>99	>99	>99
10.0	>99	>99	>99
15.0	>99	>99	>99
20.0	>99	>99	>99

13X Molecular Sieve Sample Size (g)	Percent of the Initial TeF_6 Desorbed from the Charcoal during Evacuation[b]
1	36.5
5	1
10	1

[a] The calculated TeF_6 monolayer capacity of the type 13X Molecular Sieve was 1.16 × 10^{-3} mole/g.

[b] The 13X Molecular Sieve samples were placed under vacuum for desorption for 1 hr.

TABLE II-19. The Effect of Temperature on the Sorption Rate and Retention of Tellurium Hexafluoride on Linde 13X Molecular Sieve

TeF_6 charge, 2 × 10^{-3} mole; initial pressure, 200 torr
Type 13X Molecular Sieve charge,[a] 5 g

Reation Time (min)	Percent of the Initial TeF_6 Sorbed on 13X Molecular Sieve Sample				
	25°C	100°C	200°C	300°C[b]	400°C
0.5	99	>97	>91	76, 77	55
1.0	>99	>98	95	79, 79	62
2.0	>99	99	>98	84, 84	70
5.0	>99	>99	>99	92, 92	79
10.0	>99	>99	>99	95, 96	87
15.0	>99	>99	>99	96, 97	90
20.0	>99	>99	>99	96, 97	90

[a] The calculated TeF_6 monolayer capacity of the type 13X Molecular Sieve was 1.16 × 10^{-3} mole/g.

[b] The second of the two numbers represents percent TeF_6 sorbed in the presence of a sodium fluoride trap for hydrogen fluoride.

TABLE II-20. B.E.T. Surface Area Measurements of Linde 13X Molecular Sieve

Reaction time: 20 min

Description of 13X Molecular Sieve Sample	B.E.T. Surface Area (m^2/g)	% of Surface Covered with TeF_6
Material as Received	280	—
Reacted at 100°C with TeF_6	24.3	34
Reacted at 200°C with TeF_6	25	34
Reacted at 300°C with TeF_6	8	34
Reacted at 400°C with TeF_6	13	31

Molecular Sieve is a fairly good sorbent for TeF_6 below 200°C (see Table II-19). Less than 4% of the TeF_6 was desorbed by evacuating the system to 10^{-2} torr for one hour at temperatures up to 400°C.

Comparative nitrogen B.E.T. surface area measurements on the 13X Molecular Sieve before and after TeF_6 sorption are presented in Table II-20. No data are available, however, to indicate changes in surface area of type 13X Molecular Sieve on heating in the absence of TeF_6.

10X Molecular Sieve. Sorption studies of TeF_6 on type 10X Molecular Sieve were carried out by reacting 10- and 20-g samples of the sorbent at 25°C with 2 × 10^{-3} mole of TeF_6 at a pressure of 200 torr. The results of this study showed that both the rate of TeF_6 sorption and the capacity of the sieve material for TeF_6 are comparable to those for type 13X Molecular Sieve. However, the retention of TeF_6 by type 10X Molecular Sieve was very poor.

(4) Magnesium Fluoride and Soda Lime

The sorption properties of 14–18 mesh MgF_2 for TeF_6 were evaluated at 25 and 200°C. It was observed that at 25°C the rate of TeF_6 sorption is rapid until about 10 percent of the surface is covered, while at 200°C the TeF_6 sorption rate is rapid until about 6.6 percent of the surface is covered. None of the TeF_6 sorbed by the MgF_2 was desorbed when the reaction product was evacuated to 10^{-2} torr for 1 hr.

Soda lime was evaluated by reacting 2 × 10^{-3} mole of TeF_6 with 20-g samples of 4–8 mesh soda lime at 25, 100, and 300°C. The results indicated that TeF_6 reacts slowly with soda lime. Therefore, this material is not a good chemical sorbent for tellurium hexafluoride.

d. CHEMICAL TRAPS

Kinetic studies were carried out on a group of reagents of low surface area which might react chemically with TeF_6 to form nonvolatile products. The materials evaluated in this series of tests were copper turnings, nickel wool, copper (II) oxide, aluminum metal, and metallic tellurium.

Copper turnings were reacted with TeF_6 at 400 and 500°C. The results, shown in Table II-21, indicate that TeF_6 reacts rapidly with metallic copper to form nonvolatile products. X-ray diffraction powder patterns showed Cu_2Te and CuF_2 to be the major reaction products.

Samples of nickel wool were reacted at 500°C with TeF_6. The nickel wool in one experiment was prefluorinated with fluorine at 270°C while in the other experiment it was not so treated. The data in Table II-21 indicate that TeF_6 reacts slowly with nickel and that

TABLE II-21. The Reaction Rate of Tellurium Hexafluoride with Copper Turnings and Nickel Wool

TeF_6 charge, 2 × 10^{-3} mole; initial pressure, 200 torr
Quantity of copper metal turnings or nickel wool charged to the system, 10 g

Reaction Time (min)	Copper Turnings		Nickel Wool	
	TeF_6 Reacted at 400°C (%)	TeF_6 Reacted at 500°C (%)	TeF_6 Reacted at 500°C (%)	TeF_6 Reacted at 500°C[a] (%)
0.5	74	98	11	1
1.0	82	99	16	4
2.0	89	>99	28	18
5.0	96	>99	78	80
10.0	97	>99	96	>98
15.0	97	>99	98	>98
20.0	97	>99	98	>98

[a] Nickel wool prefluorinated with fluorine at 270°C.

the rate and extent of reaction are independent of pretreatment of the nickel surface. X-ray diffraction patterns showed NiTe, $NiTe_2$, and NiF_2 to be reaction products.

Copper (II) oxide was found to be essentially nonreactive at 400°C and 500°C with TeF_6. Aluminum metal did not react with TeF_6 at temperatures up to 500°C. Only a slight reaction was noted between TeF_6 and tellurium metal powder at 370°C.

e. SPECTROPHOTOMETRIC STUDIES

Attempts were made to obtain the spectra of tellurium hexafluoride between 2,000 and 10,000 Å on a Cary spectrophotometer. The results of this study indicated that tellurium hexafluoride exhibits no absorption in either the ultraviolet or visible spectrum.

f. DISCUSSION

The results of this survey of materials as sorbents for tellurium hexafluoride indicate that activated alumina, BPL activated charcoal, Linde type 13X Molecular Sieve, magnesium fluoride, and copper metal may be suitable candidate materials for removing TeF_6 from process gas streams.

Although the rate of TeF_6 sorption on activated alumina is high over a wide temperature range (25 to 300°C), the capacity of the sorbent for TeF_6 is less than the capacity of either BPL charcoal or type 13X Molecular Sieve for TeF_6. At temperatures above 100°C, BPL activated charcoal and Linde type 13X Molecular Sieve exhibit a marked decrease in sorption rate and capacity. Therefore, these materials would be much more restricted in application than activated alumina.

Of all sorbents studied, magnesium fluoride had the best retention of sorbed TeF_6. Owing to the low surface area of MgF_2, the material did not exhibit a high capacity for TeF_6. Nevertheless, MgF_2 is a promising material for sorbing TeF_6 from gas streams containing fluorine or BrF_5 since MgF_2 probably does not react with these gases.

Copper turnings show excellent reaction kinetics towards TeF_6 at 500°C and since the reaction products are not volatile, the material appears to be a satisfactory chemical for sorption of TeF_6. The applicability of copper turnings for sorption of TeF_6 from process gas streams may be limited by the susceptibility of copper to air oxidation and fluorination by fluorine.

g. FUTURE STUDIES

Tellurium hexafluoride sorption studies will be carried out in the presence of fluorine, nitrogen, and oxygen in a flow system. In these studies, TeF_6 concentrations similar to those that will be encountered in the fluoride volatility process off-gases will be employed in order to obtain data suitable for recommending methods of off-gas treatment. Analytical techniques to determine ppm quantities of TeF_6 in air are currently being investigated to permit the evaluation of low level flow studies. The analytical procedures will also be used to evaluate the performance of traps used in planned tracer studies.

4. Instrumental Analysis (W. SHINN, M. STEINDLER)

Instrumental methods of analysis are desirable for use in the fluoride volatility processing of nuclear fuels since such methods may avoid problems associated with the sampling of process streams and also avoid difficulties involved in chemical analyses. A successful instrumental method may also be used as a means of controlling certain phases of the process. An experimental program is under way to develop techniques for remote plutonium analysis based on the counting of neutrons derived from (α,n)-type reactions.

A neutron detector for estimating the quantity of plutonium fluorides in laboratory vessels has been constructed. The detector has a sample holder, 5 in. in dia. by 12 in. long, mounted centrally along the axis of a 55-gal drum which contains water for moderation of the fast neutrons emitted from the plutonium fluoride samples. Three proportional counters, each 1 in. in dia. by 12 in. long, containing 10 atm of helium-3 are immersed in the water moderator, and are equally spaced around the sample holder with a distance of 2 in. between each counter and the sample holder.

The water-moderated detector has been calibrated with several compact PuF_4 sources ranging in weight from 0.3602 to 134.5 g. Coincidence corrections, as large as one-third of the gross counting rate of the largest source, are required since the resolving time the detector is 7.35 μsec as determined by a two-source method.[9] Four PuF_4 sources produced a corrected counting rate proportional to the mass of PuF_4 present, and gave a specific neutron counting rate of 20,800 ± 400 counts/(min) (g PuF_4). A 0.0124-g PuF_4 source yielded poor counting statistics owing to the varied and high background of the laboratory. Although quantities of PuF_4 as small as a few milligrams can be accurately measured in small vessels by a detector in a location with a low neutron background, this restriction may prevent ap-

[9] G. Friedlander and J. W. Kennedy, *Nuclear and Radiochemistry*, John Wiley and Sons, N. Y., 1955.

plication of this instrument to analyses of very small quantities of plutonium in process use.

A sample of PuF_6 has been counted in the neutron detector and its weight calculated by assuming that the ratio of neutron activity of the hexafluoride to that of the tetrafluoride is 1.37, the ratio for the corresponding uranium compounds.[10] This procedure predicted 94.6 g which is in excellent agreement with the sample weight of 100.9 g.

Accuracy better than about 5 percent is dependent upon a sample being within two inches of the center of the sample holder—a volume smaller than that of many vessels in which plutonium fluoride determinations are to be performed. In addition, accuracy depends upon knowledge of the sample specific neutron activity, which may be influenced either by alpha activity of the sample or the presence of other materials with the sample. The extent to which fluorides such as NaF or other materials affect neutron activity will be investigated during determinations of laboratory samples for which the plutonium content is known.

Although the detector in its present form does not appear to be suitable for continuous monitoring of process gas streams or for determining plutonium fluoride deposits in fixed equipment, the extent of its limitations is being investigated.

[10] R. H. Stevens and R. C. Smith, USAEC Report K-1586, 1964.

5. Neptunium Fluoride Chemistry (T. Gerding, L. E. Trevorrow)

Neptunium-237 is a valuable constituent of spent power reactor fuels since it can be transmuted to plutonium-238, which has potential use as an isotopic power source. Therefore, it is necessary to consider means for recovering neptunium in the fluoride volatility processing of reactor fuels. An experimental program is under way to evaluate the behavior of neptunium in the various steps of the volatility process. Previous work (ANL-7125, pp. 73–74) has concerned the study of the rate of reaction of NpF_4 with gaseous fluorine. This report describes a study of the reaction of NpF_4 with gaseous BrF_5 to determine the behavior of neptunium when oxidized nuclear fuel is treated with BrF_5. Initial experiments showed that a volatile neptunium compound is formed in the reaction. Additional experiments were carried out to measure the rate of the reaction and to establish the identity of the products.

The rate experiments were carried out in a tube reactor heated by a cylindrical furnace. After the system was heated to the reaction temperature in an atmosphere of flowing nitrogen, a BrF_5-nitrogen mixture at 1 atm was passed over 0.5 to 1 g of powdered NpF_4 contained in a nickel boat. All of the experiments were carried out using a mixture of 33 v/o BrF_5 and 67 v/o N_2. The NpF_4 was prepared by reacting NpO_2 with a mixture of HF and oxygen at 500°C. In most experiments the reaction products and excess BrF_5 were collected in a soda-lime trap for disposal. Several experiments were performed in which the reaction products were collected in a cold trap and subsequently vaporized into a spectrometer cell for examination. The boat containing the powdered NpF_4 was weighed before and after each experiment to determine the weight loss.

The rate data obtained were tested for conformation to the diminishing sphere rate law:

$$(1 - F)^{1/3} = 1 - k't,$$

where k' is the rate constant, F is the fraction of the solid reacted, and t is the reaction time. If values of $(1 - F)^{1/3}$ are plotted versus values of t, the result should be a straight line with a slope which is the rate constant k'. Figure II-12 shows the experimental results plotted in this form. Results obtained at 300, 325, and 350°C yielded straight lines, but the results from two sets of experiments at 400°C produced nonlinear plots. Since the results obtained at temperatures between 300 and 350°C appear to conform to the diminishing sphere rate law, the slopes of the lines shown in Figure II-12 have been used to calculate the rate constants, k', listed in Table II-22. These constants may be compared with the rate constants calculated for the same temperatures and pressures from an equation previously determined for the UF_4-BrF_5 reaction (ANL-7225, pp. 80–82). The rates of the NpF_4-BrF_5 reaction are significantly lower than the rates of the UF_4-BrF_5 reaction. A valid comparison of the rate of the UF_4-BrF_5 reaction with the rate of the NpF_4-BrF_5 reaction, however, requires either values for r_0 and ρ, or the assumption that the ratio

$$\left(\frac{r_{0_U}\rho_U}{r_{0_{Np}}\rho_{Np}}\right) = 1$$

where r_0 = radius of initial spherical particle
ρ = bulk density of solid,

since the observed rate constants, k', are related to true rate constants, k, by $k' = k/r_0\rho_0$. In addition, the surface reactivity must be identical for a meaningful comparison of reaction rates.

The rate constants for the reaction of NpF_4 with BrF_5 at 300, 325, and 350°C follow the Arrhenius equa-

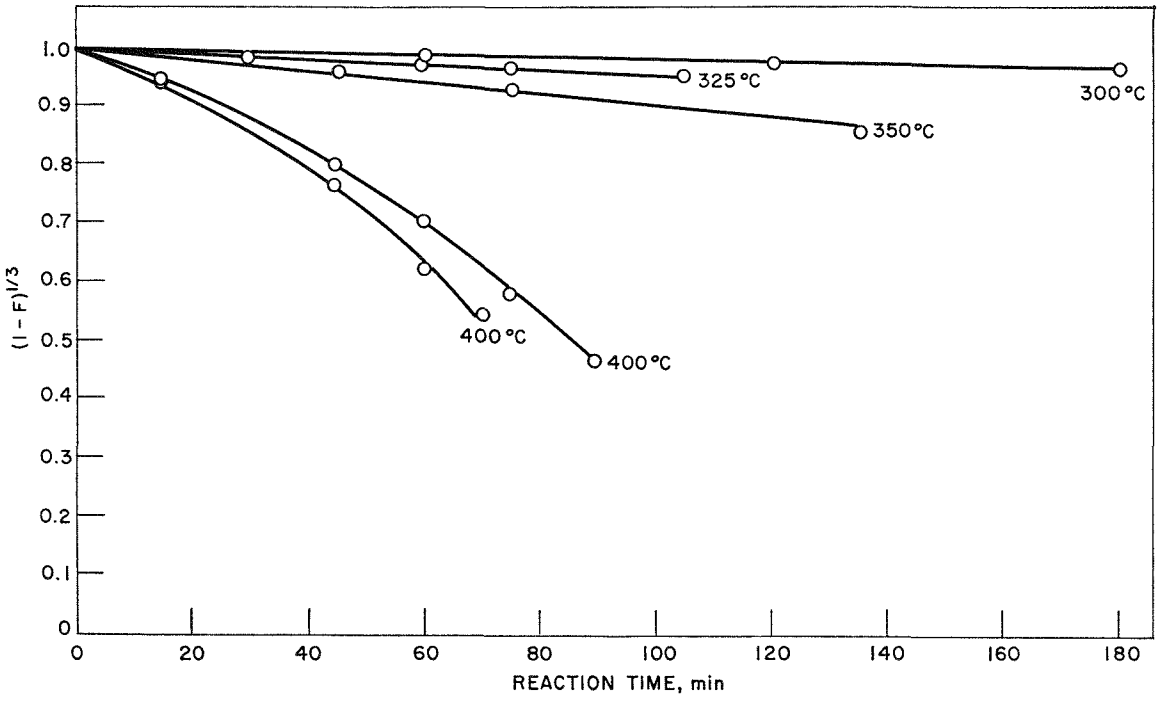

308-425

FIG. II-12. Rate of the Reaction of NpF_4 with BrF_5 Expressed by the Diminishing Sphere Rate Law, $(1 - F)^{1/3} = 1 - k't$.

tion, $\ln k' = -E/RT + A$, as shown in Figure II-13. The activation energy obtained from the slope of the line is 26 kcal/mole. In comparison, the activation energy of the UF_4-BrF_5 reaction is 16.9 kcal/mole.

Solid materials remaining in the boat after partial reaction with BrF_5 were analyzed to determine whether the solid phase is converted to a solid neptunium fluoride intermediate (Table II-23) between NpF_4 and NpF_6. The results of chemical analyses are listed in Table II-23. X-ray diffraction analyses of the solid remaining after treatment of NpF_4 with BrF_5 at temperatures between 325 and 500°C indicated that the only solid present was NpF_4. From this result and the chemical analyses listed in Table II-23, it is concluded that no stable solid neptunium fluoride intermediate is formed in the reaction of NpF_4 with BrF_5.

It has been shown (ANL-7225, pp. 79–81) that products of the reaction of UF_4 with BrF_5 are elemental bromine and UF_6. Attempts to establish, by spectrophotometric methods, the identity of the products formed in the reaction of NpF_4 with BrF_5 have yielded ambiguous results. It has been difficult to determine by visual observation whether bromine is among the products of the reaction of NpF_4 with BrF_5. In some cases a reddish color suggesting the presence of bromine has been observed when the products were condensed in a Fluorothene tube at −78°C, but the color disappeared on warming the contents of the tube to room temperature. Subsequent experiments showed that NpF_6 reacts with bromine at room temperature. When NpF_6 was condensed onto solid bromine at −78°C in a Fluorothene test tube and the mixture was allowed to warm to room temperature (30°C), a reaction producing a solid, nonvolatile material was observed. When excess bromine was present, the reaction occurred rapidly, even at temperatures lower than 30°C. Thus, if NpF_6 and bromine are the products of the reaction of NpF_4 with BrF_5 at 300 to 350°C and if the products are collected together at −78°C, a reaction will occur upon increasing the temperature.

TABLE II-22. RATE OF REACTION OF NpF_4 WITH BrF_5

Gas composition: 33 v/o BrF_5-67 v/o N_2
Total reaction pressure: 760 mm
Apparatus: Boat reactor

Temp. (°C)	Rate Constant[a]	
	k' NpF_4 (min^{-1})	k' UF_4[b] (min^{-1})
300	0.017×10^{-2}	5.8×10^{-2}
325	0.044×10^{-2}	11×10^{-2}
350	0.096×10^{-2}	19×10^{-2}

[a] Calculated from diminishing sphere model.
[b] Calculated for a BrF_5 partial pressure of 250 mm from the equation presented in ANL-7225, p. 80.

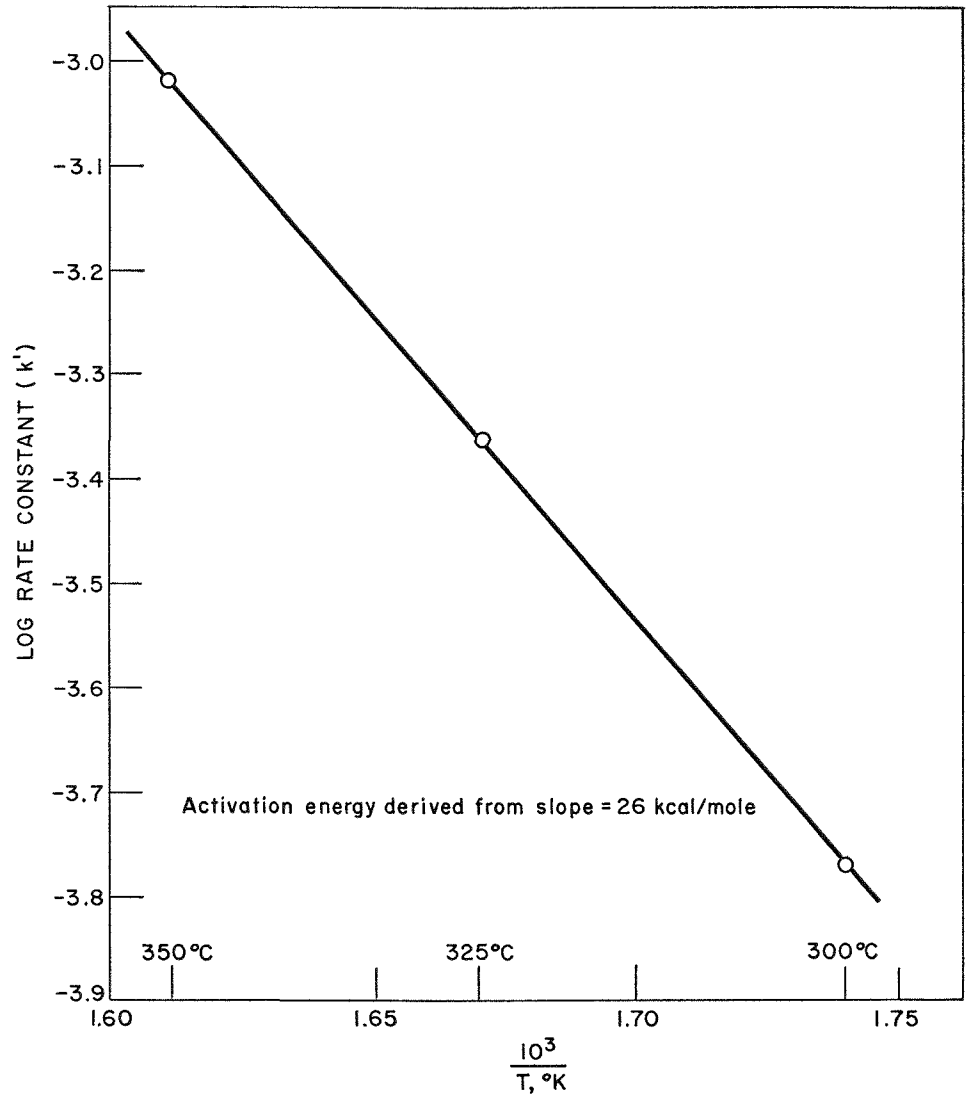

308-428

FIG. II-13. Temperature Dependence of Rate Constant for the Reaction of NpF_4 with BrF_5.
Gas composition: 33 v/o BrF_5-67 v/o N_2
Total reaction pressure: 760 mm
Apparatus: Boat reactor

TABLE II-23. ANALYSIS OF SOLID RESIDUE FROM REACTION OF NpF_4 WITH BrF_5 (33 v/o IN N_2)

Exp. No.	Reaction Temp (°C)	Percent of Initial NpF_4 Reacted	Chemical Analysis of Residue		
			Np (w/o)	F (w/o)	Atom ratio, F/Np
1810F-25	300	15.2	71.2	23.2	4.06
1521F-98	325	76	73.6[a]	23.6[a]	4.0[a]
1810F-17	400	15.6	72.7	24.0	4.12
1810F-20	400	83.5	72.6	23.4	4.02
1521F-93	400	89	74[a]	23[a]	3.8[a]

TABLE II-23.—*Continued*

CALCULATED COMPOSITIONS OF NEPTUNIUM FLUORIDES

Compound	Np (w/o)	F (w/o)	Atom Ratio, F/Np
NpF_4	75.7	24.3	4.00
Np_4F_{17}	74.6	25.4	4.25
Np_2F_9	73.5	26.5	4.50
NpF_5	71.4	28.6	5.00

[a] Average resulting from duplicate analyses.

The reaction between NpF_4 and BrF_3 has been briefly examined. The reaction takes place readily at ~400°C to produce a volatile neptunium fluoride, presumably NpF_6. In one experiment, a mixture of 4 v/o BrF_3 in nitrogen was passed over NpF_4 at 400°C for 45 min and 42% of the NpF_4 was removed from the system. In a second experiment, NpF_4 was contacted with a mixture of 1 v/o BrF_3 in nitrogen at 402°C for 15 min, and 36% of the NpF_4 was removed.

Further work will involve a study of the reactions of interhalogens with neptunium compounds and reactions involving neptunium hexafluoride.

6. Corrosion of Nickel and Nickel Alloys by Fluorides (W. H. Gunther, M. J. Steindler)

In the fluoride volatility processing of power reactor fuel materials, both bromine pentafluoride and fluorine are used as fluorinating agents for the recovery of uranium and plutonium. Bromine pentafluoride is used for the selective fluorination of uranium to UF_6, and in this step several fission product elements are also converted to volatile fluorides and are collected with the UF_6 product in a separate vessel. Purification and decontamination of the UF_6 is carried out by distillation techniques. It has been suggested that a liquid heel of antimony pentafluoride be added to the still pot of the distillation column used to purify the UF_6. This heel will retain niobium and ruthenium pentafluorides and thereby allow recovery of the UF_6. However, BrF_3 could perform the same function, and if sufficient BrF_3 is present in the still pot of the distillation column, the addition of antimony pentafluoride would be unnecessary.

The corrosion of various nickel alloys by equimolar mixtures of UF_6-SbF_5 and UF_6-BrF_3 at about 100°C was briefly studied to evaluate these alloys as materials of construction. The experiments were carried out in a heavy-walled (about ¼-in.) cylindrical Monel vessel of welded construction about 2 in. in diameter and 8 in. long. The vessel was closed at the top by a flange. Two Teflon-gasketed ¼-in. Swagelok fittings, welded to the flange, allowed the nickel coupon holder and a thermocouple well to be raised or lowered during an experiment. The reaction vessel was heated by a 2½-in. dia. electric resistance tube furnace, and the temperature of the fluoride mixture was determined by a Chromel-Alumel thermocouple located in the thermocouple well. The coupon holder was capable of supporting 24 coupons during the reaction. Two coupons each of nickel-200, Monel, and Duranickel-301, and one coupon each of nickel-200 containing areas of nickel-200 weld or nickel-61 weld were exposed in each of the following three locations: the vapor phase, the gas-liquid interface, and the liquid phase. The UF_6-SbF_5 reaction mixture contained 245 g UF_6 and 151 g SbF_5. The pressure at 105°C was about 2400 torr. The UF_6-BrF_3 mixture contained 235 g UF_6, 100 g BrF_3, 0.4 g NbF_5, and 0.23 g SbF_5. The system pressure at 104°C was about 3100 torr. Trace amounts of NbF_5 and SbF_5 were added to duplicate more closely the fluoride mixture expected in the distillation column.

Visual observation of the coupons after exposure to UF_6-SbF_5 revealed them to be free of any appreciable corrosion scale although the surface of the coupons was coated with an oily liquid (possibly SbF_5 or its hydrolysis products). After exposure, the coupons were immersed in hot water and dried prior to weighing. A weight loss of all the coupons was observed. To assure complete removal of any corrosion scale which may have formed on the coupon surface, the coupons were descaled in an equimolar KNO_3-$NaNO_3$ bath for ½ hr at 500°C. The descaling process generally resulted in only small additional weight losses, indicating that if a scale had formed, most of that scale had been removed during exposure to the molten fluoride mixture.

The coupons exposed to the UF_6-BrF_3 mixture showed no visible evidence of reaction except at the gas-liquid interface where a slight darkening of the metals had occurred. Corrosion rates were calculated from the weight gain of the coupons after exposure (assuming that only NiF_2 formed uniformly on the coupon surface), and from the weight loss of the coupons following descaling in an equimolar KNO_3-$NaNO_3$ bath for ½ hr at 500°C.

Corrosion rates, as mils of metal reacted per hour of

TABLE II-24. Corrosion Rates of Nickel and Nickel Alloys by an Equimolar Mixture of UF_6-SbF_5

Temperature: 105 ± 5°C
Pressure: 2400 ± 100 torr
Time: 7.5 hr

Coupon Location	Corrosion Rate[a] (mil/hr)				
	Nickel-200	Monel	Duranickel-301	Nickel-200 Weld	Nickel-61 Weld
Vapor Phase	nil	nil	0.001	nil	0.001
Interface	0.004	0.001	0.002	0.004	0.002
Liquid Phase	0.005	0.001	0.004	0.006	0.006

[a] Corrosion rate calculated from the weight loss of the coupon following descaling in an equimolar KNO_3-$NaNO_3$ bath at 500°C for ½ hr, assuming complete removal of all scale. Corrosion rates are expressed in mils of metal reacted per hour of exposure. Rates reported as nil are less than 0.001 mil/hr.

TABLE II-25. Corrosion Rates of Nickel and Nickel Alloys by an Equimolar Mixture of UF_6-BrF_4

Temperature: 104 ± 5°C
Pressure: 3100 ± 100 torr
Time: 6.8 hr

Coupon Location	Corrosion Rate[a] (mil/hr)				
	Nickel-200	Monel	Duranickel-301	Nickel-200 Weld	Nickel-61 Weld
Vapor Phase	nil (nil)	0.001 (nil)	0.001 (nil)	nil (nil)	[b] (0.001)
Interface	nil (nil)	0.001 (nil)	0.001 (nil)	0.001 (nil)	0.001 (nil)
Liquid Phase	nil (nil)	nil (nil)	nil (nil)	[b] (nil)	[b] (0.001)

[a] Corrosion rates calculated from the weight gain of the coupons assuming that only NiF_2 formed uniformly on the coupon surface. The numbers in parentheses were calculated from the weight loss of the coupons following descaling in an equimolar KNO_3-$NaNO_3$ bath at 500°C for ½ hr, assuming complete removal of all scale. Corrosion rates are expressed in mils of metal reacted per hour of exposure. Rates reported as nil are less than 0.001 mil/hr.

[b] Weight gain data not obtained; before descaling, a weight loss was observed for these coupons.

exposure, for the two experiments are tabulated in Tables II-24 and II-25. In general, the rates of corrosion of the coupons exposed to the UF_6-SbF_5 mixture were lowest in the vapor phase and highest in the liquid phase. Monel showed the best overall resistance to this fluoride mixture. The coupons containing areas of nickel weld corroded at rates similar to the nickel-200 coupons and showed no evidence of increased attack at the welds. All coupons exposed to the UF_6-BrF_3 mixture showed little evidence of corrosion. Microscopic examination of all the coupons revealed that little or no intergranular penetration had occurred.

The results of these experiments indicate that Monel would probably be the best choice as the material of construction for the still pot and the distillation column exposed to UF_6-SbF_5 mixtures at temperatures to 100° C. In the presence of UF_6-BrF_3 mixtures at 100°C, all metals examined showed excellent corrosion resistance and no intergranular attack was determined by the usual microscopic techniques.

7. Development of an Equation to Predict Thermal Decomposition of PuF_6 in Process Gas Mixtures of PuF_6 and F_2 (L. E. Trevorrow, M. Steindler)

In the fluoride volatility processing of nuclear reactor fuels, the sequence of operations performed in a fluidized-bed reactor includes fuel decladding, uranium recovery, and plutonium recovery. The plutonium-bearing fraction of the partially processed fuel (plutonium present in the form of PuF_4) is contacted with fluorine gas at 250 to 550°C, forming PuF_6. The mole ratio of PuF_6 to fluorine in the gaseous mixture flowing from the reactor has an upper limit determined by the equilibrium constant, K_{eq}, of the reaction:

$$PuF_4(s) + F_2(g) \rightleftarrows PuF_6(g). \quad (1)$$

The gas stream from the reactor is rapidly cooled in a gas-cooler section to lower the role of thermal decomposition and then the gas is filtered by metallic filters.

The equilibrium constant, moles PuF_6/moles F_2, decreases with decreasing temperature,[11, 12] and at some point in the cooling section the PuF_6/F_2 ratio in the gaseous effluent exceeds the equilibrium constant, resulting in some decomposition. Thus, although the PuF_6 becomes thermodynamically less stable as the gas mixture cools, the rate of approach to equilibrium (rate of decomposition) also becomes lower.

The problem of thermal decomposition in the cooling section of a pilot-scale facility has prompted a detailed review of all experimental information previously obtained on the rate of thermal decomposition of PuF_6. The data were reviewed with the specific purpose of predicting the amount of thermal decomposition of PuF_6 which would occur in the cooling section of a pilot-scale reprocessing facility. Any prediction, however, must be considered as an estimate only since the data were obtained in laboratory-scale experiments under conditions which do not completely represent those maintained in plant operation. In none of the laboratory experiments were all variables affecting the rate of decomposition completely determined. The results of various types of experiments that have provided information on the rate of thermal decomposition

[11] A. E. Florin, I. R. Tannenbaum, and J. F. Lemons, J. Inorg. Nucl. Chem., **2**, 368 (1956).

[12] L. E. Trevorrow, W. A. Shinn, and R. K. Steunenberg, J. Phys. Chem., **65**, 398 (1961).

of PuF_6 have been previously reported (ANL-6379, pp. 157–159; ANL-6333, pp. 142–148).

In the most extensive series of experiments (ANL-6379, pp. 157–159), the rate of thermal decomposition of PuF_6 was studied by heating PuF_6 vapor in a closed vessel. The results obtained in these experiments can be expressed by a rate equation of concurrent first and zero orders with respect to plutonium hexafluoride pressure:

$$-dp/dt = k_0 + k_1 p, \tag{2}$$

which, in integrated form is

$$p = p_0 e^{-k_1 t} + (k_0/k_1)e^{-k_1 t} - (k_0/k_1), \tag{3}$$

where p_0 is the initial pressure and p the partial pressure after reaction time t. The rate constants, expressed in the form of the Arrhenius equation, are

$$\log k_0 = 7.124 - \frac{3.469 \times 10^3}{T(^\circ\mathrm{K})}, \tag{4}$$

$$\log k_1 = 7.260 - \frac{4.292 \times 10^3}{T(^\circ\mathrm{K})}. \tag{5}$$

The experimental activation energies were 15.9 ± 1.5 kcal/mole for the zero-order reaction, and 19.6 ± 0.7 kcal/mole for the first-order reaction.

Since the reaction rates have been expressed as the rate of change of pressure, the rate constant for the zero-order reaction is dependent on the surface-to-volume ratio, i.e., $k_0 = k_0'$ (s/v). Measurements of absolute surface areas were not obtained; consequently, the values for k_0 derived from the experimental results must be considered to apply only for the ratio of surface area to volume used in these experiments.

Prior to this review, equations 2 through 5 were the only available analytical expressions of the rate of thermal decomposition of PuF_6. Although these equations satisfactorily express the rate of decomposition of PuF_6 in its initial stage, they ignore the back reaction, and are therefore not suitable to express the decomposition rate of PuF_6 in mixtures with fluorine at the low ratios of PuF_6/F_2 encountered in the effluent from a fluidized-bed reactor. Since in earlier experiments (ANL-6333, pp. 142–148) the thermal decomposition of PuF_6 was studied in the presence of fluorine, the results of these experiments have been used to arrive at an expression of the rate of thermal decomposition that is more appropriate for estimating the thermal decomposition of PuF_6 in a PuF_6-fluorine mixture issuing from a fluidized-bed reactor.

The following assumptions were employed in the derivation of the new equation:

1. The rate of decomposition is proportional to the difference between the mole ratio of PuF_6 and fluorine at equilibrium (i.e., K_{eq}) and the mole ratio as it exists in the gas phase.

2. The rate of decomposition increases as a function of the geometric surface-to-volume ratio of the apparatus.

3. There will be no decomposition if the PuF_6/F_2 ratio is less than K_{eq} (i.e., the system contains PuF_4).

4. Significant elemental fluorine is present in the system. If, then

$$\text{Rate} = f(R^t - K_{eq}),$$

where R^t is the PuF_6/F_2 ratio at time t and K_{eq} is the equilibrium ratio at the temperature of the system, we assume

$$R_t = A + (R_0 - K_{eq})e^{-kt} \tag{6}$$

where R_0 is the PuF_6/F_2 ratio at $t = 0$. Considering the boundary condition, i.e., at $t \to \infty$, $R_t \to K_{eq}$, the equation becomes

$$R_t = K_{eq} + (R_0 - K_{eq})e^{-kt} \tag{7}$$

or

$$\ln\left(\frac{R_t - K_{eq}}{R_0 - K_{eq}}\right) = -kt \tag{8}$$

It will be assumed that the dependence of the rate on the surface-to-volume ratio (s/v) is of the form

$$k = k'\left(\frac{s}{v}\right) \tag{9}$$

$$\ln\left(\frac{R_t - K_{eq}}{R_0 - K_{eq}}\right) = -k't\left(\frac{s}{v}\right) \tag{10}$$

If the fraction of PuF_6 decomposed is denoted by F,

$$F = \frac{\text{PuF}_6 \text{ decomposed}}{\text{PuF}_6 \text{ introduced}}, \tag{11}$$

then

$$R_t = R_0\left[\frac{1 - F}{1 + R_0 F}\right]$$

or (12)

$$F = \frac{R_0 - R_t}{R_0[1 + R_t]}.$$

The results of experiments which involved measurements of the decomposition of PuF_6 in the presence of fluorine (ANL-6333, pp. 142–148) were evaluated (1) to derive values for the rate constant, k', (eq. 10) and (2) to obtain values for k' as a function of temperature. It was assumed that the rate constant k' obeys the Arrhenius relation and that the variation of

k' with $T(°K)$ can be expressed as

$$\log k' = A/T + B. \tag{13}$$

$$\log k' = -\frac{3169}{T(°K)} + 5.364 \tag{14}$$

$$E^* = 14.5 \text{ kcal/mole.}$$

It must be emphasized that the quality of the experimental data does not warrant highly precise constants for the above equations. Further, it is probably significant that the activation energy, E^*, falls near the E^*'s derived for k_1 (19.6 kcal/mole) and k_0 (15.9 kcal/mole) for decomposition of PuF_6 in the absence of fluorine. The above equation (10), therefore, should be treated as an empirically derived description of the decomposition of PuF_6 in the presence of fluorine and some PuF_4.

These thermodynamic values can be used to calculate the percentage of the PuF_6 that would decompose in a hypothetical pilot-scale cooler. The temperature of the gaseous mixture of PuF_6 and fluorine will decrease as the mixture proceeds along the length of the cooler. If the cooler is considered to consist of a large number of equal segments, each of length dL, having temperatures T_1, $T_2 \cdots$ then

Total % PuF_6 decomposed
= (decomposition rate at T_1)
(residence time at T_1) +
(decomposition rate at T_2)
(residence time at T_2) + $\cdots$ (15)

$$= \text{decomposition rate at } T_1 \left(\frac{dL}{\text{linear flow rate}}\right) + \text{decomposition rate at } T_2 \left(\frac{dL}{\text{linear flow rate}}\right) + \cdots \tag{16}$$

$$= \frac{1}{\text{linear flow rate}} [\text{decomposition rate at } T_1 dL + \text{decomposition rate at } T_2 dL + \cdots] \tag{17}$$

$$= \frac{1}{\text{linear flow rate}} \int_0^L \text{decomposition rate at } T_n dL \tag{18}$$

The integral can be evaluated if temperature can be expressed as a function of length along the cooler,

$$T = f(L) \tag{19}$$

An example of the thermal decomposition of PuF_6 in a pilot-scale cooler was calculated using equations 10, 14, and 18. The cooler was assumed to have an ID of 8 in., a length of 4.5 ft, and internal fins to give an internal geometric surface/volume ratio of 0.56 cm^{-1}. The temperature of the gas at the inlet was assumed to be 500°C, and the cooler wall was assumed to be maintained at the constant temperature of 50°C. The gas flow rate was assumed to be 45 ft/min, and the inlet PuF_6/F_2 ratio was assumed to be 0.01.[13] A temperature profile for such a cooler was estimated by D. L. Breton of ORGDP,[14] who assumed that the temperature of the cooler is related to the length of the cooler by the equation:

$$\frac{T_{\text{gas}} - T_{\text{wall}}}{T_{\text{gas inlet}} - T_{\text{wall}}} = e^{CL}, \tag{20}$$

where L is the distance from the gas inlet. The gas temperature in the cooler was assumed to decrease from 500°C at the inlet to 100°C at the outlet. The total decomposition in the gas cooler, using the above conditions, is 3.3%, with three-fourths of the total decomposition occurring in the hottest one-fifth of the gas cooler. If the thermal decomposition of PuF_6 in a pilot-scale cooler is calculated using rate equation 3, which ignores the retardation of the decomposition rate by fluorine, the percent PuF_6 decomposed is unrealistic, being very much greater than 100%.

[13] The linear flow rate of 45 ft/min (0.75 ft/sec) is a reasonable operating value for a pilot-scale fluidized-bed reactor. The value of 0.01 is the equilibrium ratio of PuF_6/F_2 at 500°C. This ratio would be obtained at a fluorination efficiency of 100% with one atm of fluorine.

[14] D. L. Breton, ORGDP, private communication, August 1966.

B. ENGINEERING-SCALE INVESTIGATIONS OF FLUID-BED FLUORIDE VOLATILITY PROCESSES

1. Recovery of Uranium and Plutonium from Uranium Dioxide Fuels in the Engineering-Scale Alpha Facility

(N. LEVITZ, G. J. VOGEL, E. L. CARLS, D. GROSVENOR, J. BISHOP,[14a] L. KOPPEL,[15] W. A. MURPHY, R. KINZLER, B. KULLEN, D. RAUE, M. DEERWESTER, W. KREMSNER, J. GERARD[16])

Process studies aimed at demonstrating the main steps of a fluid-bed fluoride volatility reprocessing scheme for UO_2-PuO_2 fuels have continued in the engineering-scale alpha facility. The primary objectives of the experiments are to investigate the possible difficulties in handling PuF_6 on an engineering scale and to determine the feasibility of fluoride volatility process flowsheets. Currently, nonirradiated, synthetic fuel materials containing simulated fission product (F.P.) elements are being employed. Later, experiments may be made with oxide fuel having low levels of radioactive fission product elements.

An Interhalogen Reference Flowsheet (see Fig. II-1 of this report and p. 101 of ANL-7055) is now under development. Head-end steps in the flowsheet include:

1. Decladding.
2. Oxidation-disintegration of the oxide pellets to U_3O_8-PuO_2 fines in a fluidized bed of alumina.
3. Separation of the uranium as UF_6 by reaction with BrF_5.
4. Recovery of the plutonium as PuF_6 by reaction with fluorine.

Experiments simulating the plutonium recovery step (step 4) are now being conducted in the alpha facility pending installation of an interhalogen supply and disposal system. Powdered PuF_4 in alumina, in some cases with added fission product fluorides, is being used to represent the bed which remains after the interhalogen fluorination step (step 3).

The alpha facility, which includes two large alpha boxes, one containing the process equipment and the other containing the off-gas scrubbers and auxiliary equipment, has been described in a topical report.[17] Included in the report is a description of the two pilot plants installed in the larger alpha box, one for fluorination studies and the other for studies on the fluid-bed conversion of uranium-plutonium hexafluorides to oxides. Work on the conversion of hexafluorides to oxides has been deferred until the fluorination studies are further advanced. A third unit, a distillation column intended for studies on mixed UF_6-PuF_6 systems, has been constructed in a mock-up area and shakedown tests with Freon-113 have been performed (see ANL-7225, pp. 108–110). Transfer of this equipment into the alpha facility has been postponed indefinitely.

An automatic data logger is being tested for reliability in the current pilot plant program. The unit, built by the Minneapolis-Honeywell Company, is capable of monitoring 200 variables: 175 thermocouple signals, 19 pneumatic signals, and 6 mv signals. Computer programs designed to accommodate the punched tape output from the data logger are being prepared to facilitate data reduction.

In the current series of experiments, a neutron survey meter has been used to detect the presence of plutonium fluorides in process lines and vessels.

The shakedown program of studies in the alpha facility comprised three fluorination experiments (runs Pu-1, -2, and -3) and three thermal decomposition experiments (runs DUP-4, -5, and -6) using plutonium oxide-uranium oxide-fission product feed material (pellets). Conditions and results of these experiments were discussed in the previous semiannual report, ANL-7225, pp. 103–108. Briefly, the fluorination studies showed that the two-zone oxidation-fluorination scheme used in this earlier work was satisfactory for removing uranium and plutonium from the alumina bed. (Laboratory experiments have shown that the desired high plutonium removal (near 99%) can be achieved if the bed is reused several times.) Satisfactory uranium removal is achieved even with a single use of the bed.

In this two-zone reaction scheme, the fuel pellets reside in the lower portion of the reactor with the alumina grain filling the interstices (a packed-fluidized bed zone). The fuel is pulverized by reaction with oxygen; the resulting fine U_3O_8-PuO_2 material is transported by the fluidizing gas into the unhindered fluidized-bed zone above the fuel where fluorine is admitted, converting the oxides to their corresponding volatile hexafluorides. The hexafluorides are collected together by cold-trapping. Bed sampling during the final period of fluidization indicated that about 97%

[14a] Industrial trainee from Allied Chemical Co.

[15] Consultant from Purdue University.

[16] Co-op student from Purdue University.

[17] G. J. Vogel, E. L. Carls, and W. J. Mecham, Engineering Development of Fluid-Bed Fluoride Volatility Processes, Part 5. Description of a Pilot-Scale Facility for Uranium Dioxide Processing Studies, ANL-6901, December 1964.

of the plutonium and over 99.9% of the uranium was removed from the alumina with a 3-time use of the bed (runs Pu-1, -2, -3). However, samples from the final discharged bed reflected only about a 90% overall removal of the plutonium from the reactor. Each of the individual fluorination experiments also showed this disparity in the plutonium content of samples taken from the bed during fluidization and samples taken from the same bed after it was dumped at the end of a run. This problem is discussed in a following subsection. A material balance for these first experiments with plutonium-bearing material has been completed and is presented below.

The separation of plutonium from a mixture of UF_6 and PuF_6 by thermal decomposition of PuF_6 to PuF_4 in a fluid-bed system proved quite successful; a separation of 99.9% of the plutonium from a mixed uranium-plutonium hexafluoride stream containing approximately 0.4 w/o plutonium was achieved at 300°C. Further laboratory-scale work on thermal decomposition is tentatively scheduled.

a. PLUTONIUM CLEANUP RUNS Pu-3a, -4, AND -5

Neutron surveys of the pilot plant equipment made upon completion of the initial set of oxide fluorination experiments indicated that some plutonium remained in virtually all of the equipment. Deposition of plutonium was attributed to alpha or thermal decomposition of the PuF_6, or to reaction of the PuF_6 with either the materials of construction (mainly nickel) or other system contaminants. A significant quantity of plutonium also remained in the final alumina bed from run Pu-3. In order to recover this plutonium and gain some understanding of the causes of plutonium holdup, a series of fluorination cleanup operations was conducted. All equipment including transfer lines was heated to 300°C, and 100% fluorine was circulated through the system. The bed was refluorinated at temperatures to 550°C to effect further plutonium removal. The length of time a given item of the equipment was at temperature is shown in Table II-26. Exposure at temperature varied from about 10 to 57 hr, principally owing to heater circuit failure for certain components.

The PuF_6 produced in each item of the equipment was collected separately by sorbing it on NaF in individual traps installed just downstream of each piece of equipment. The locations of these traps and the quantities of PuF_6 recovered from each region, determined by analyses of the NaF traps, are shown in Figure II-14 and tabulated in Table II-27.

Neutron surveys of the equipment indicated that the bulk of the plutonium was generally recovered in a few hours, and that little plutonium remained in the system after the cleanup experiments. This was con-

TABLE II-26. PLUTONIUM-CLEANUP RUNS (Pu-4, Pu-5).* SUMMARY OF FLUORINATION TIMES AND APPROXIMATE AVERAGE EQUIPMENT TEMPERATURES

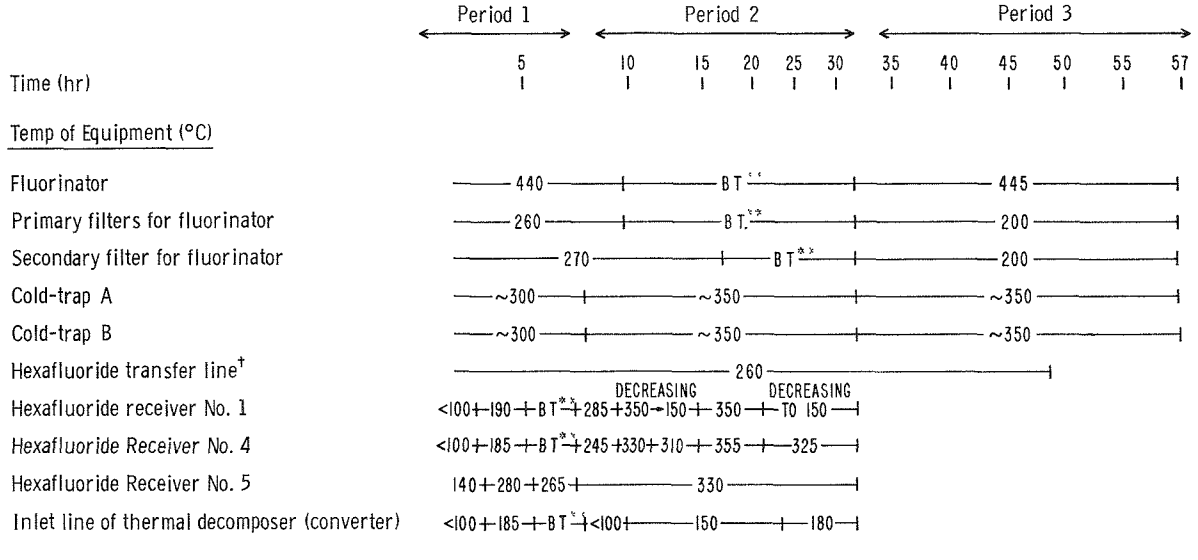

The main fluorinator reaction zone containing the alumina bed was heated to 550°C for 15 hr during the cleanup of the bed (Run Pu-3a) prior to Run Pu-4. The primary filters were heated to about 300°C for the last 6 hr of Run Pu-3a.

*"BT"—At ambient temperature of alpha box; equipment not heated.

†Fluorinated during a separate cleanup period, Period 4 (see Table II-27).

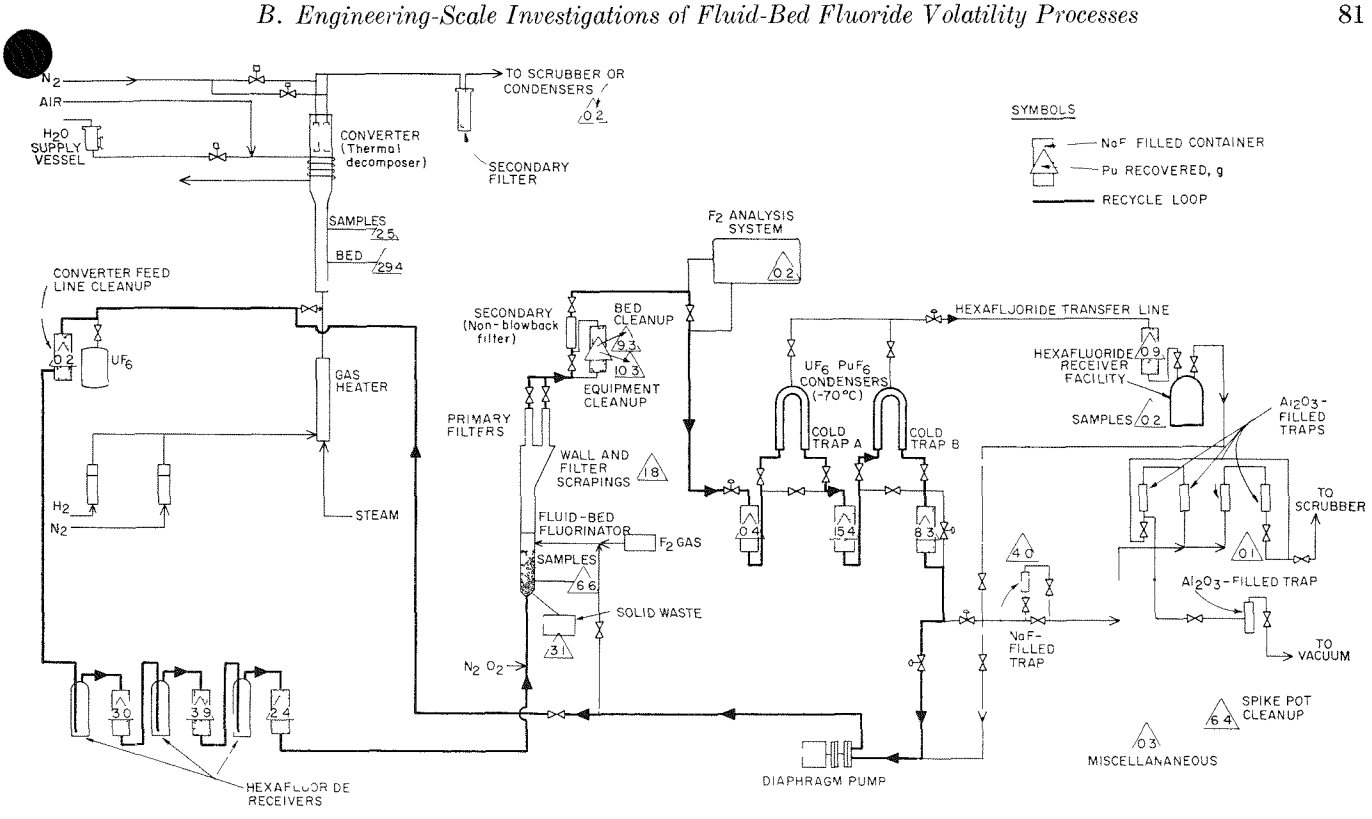

308-475

FIG. II-14. Plutonium Cleanup Fluorination Experiments.

firmed by physical examination of the fluorinator, analysis of wall scrapings, and leach tests on a sectioned hexafluoride product receiver.

On the basis of the cleanup results, the quantities of plutonium that had deposited in the equipment in the course of the initial campaign may be categorized as small, intermediate, or large as follows:

a) Small (~1 g or less)—lines and secondary filter probably as a result of reaction with the nickel equipment.

b) Intermediate (several grams)—product receivers, primary filters.

c) Large (decagrams)—cold traps (see discussion below).

In the work performed to date, it appears that the extent of plutonium removal from the fluorinator is affected by elutriation of fine particles, containing plutonium, from the bed. A characteristic of most fluid-bed systems is elutriation of fines from the bed and deposition of fines on all surfaces not "washed" by the fluid bed. A layer of material is also deposited on the sintered metal filters used to filter the gas leaving the reactor. Also, a fraction of the fines remain suspended in the gas phase. Some of the solids deposited on the filters are returned to the bed during periods of filter blowback. However, material on other surfaces tends to remain static and to be dislodged only by

TABLE II-27. PLUTONIUM DEPOSITS RECOVERED IN CLEANUP FLUORINATION RUNS

	Plutonium Recovered (g)			
	Period 1 of 8 hr	Period 2 of 25 hr	Period 3 of 24 hr	Total for periods 1 through 3, 57 hr
Fluorinator including primary filters	1 8	0.1	0.3	2 2[a]
Secondary filter for fluorinator, and line	0.3	0.1	0.2	24 3
Cold-trap A[b]	4.0	11 4		
Cold-trap B[b]	6 8	1 5		
Hexafluoride transfer line	—	—	—	—
Hexafluoride receivers (total of three)	9 3		—	9.3
Inlet line of thermal decomposer	0 2		—	0 2
Subtotal				36 0
Hexafluoride transfer line (49 5-hr Period 4)				0.9
Total				36.9[a]

[a] An additional 8.1 g was recovered from the filters during the last 6 hr of cleanup run Pu-3a (conducted on the alumina bed from run Pu-3).

[b] Cold-trap A was first in line for runs Pu-1 and Pu-2 and served as a back-up to cold-trap B for run Pu-3. Cold-trap B was first in line for run Pu-3 and served as a back-up to cold-trap A for the first two runs (Pu-1 and -2).

sharp mechanical vibration. Cessation of gas flow allows a fraction of the fines to return to the bed. Since some of the fines are in a cooler portion of the reactor during most of the fluorination period, the plutonium in the fines is not readily fluorinated to PuF_6. Because a fraction of the fines are returned to the bed after fluorination, the concentration of plutonium in the final bed is higher than in grab samples from the fluidized bed.

One possible solution to the problem is to maintain the entire reactor at elevated temperatures for a sufficient time to insure complete fluorination of this material. Filter life, although expected to be affected by this treatment, should not be shortened prohibitively. The cleanup treatment of the filter sections resulted in the recovery of about 8.1 g of plutonium, or about 8% of the input.

Since the cleanup treatment at temperatures of 300°C was successful in all cases except for the cold-traps, which are discussed below, it appears that the plutonium deposited in these process vessels and lines was very reactive and readily recoverable.

Cold-Trap Cleanup. The recovery of plutonium from the cold-traps required the most vigorous treatment. After 8 hr of fluorination at ~300°C, neutron probe surveys indicated that a significant amount of plutonium remained in the traps. Therefore, subsequent cleanup was carried out at temperatures above 300°C. In the second cleanup period, the traps were heated to ~350°C. As indicated in Table II-27, this procedure was effective in recovering the plutonium from the cold-traps. Spectrographic analysis of the contents of the NaF traps showed that considerable molybdenum had also been recovered from the cold-traps along with the plutonium. Interaction, during the oxide fluorinations, of the plutonium in the cold-trap with a molybdenum compound (possibly a relatively high boiling oxyfluoride) is now suggested as a reason for the low yields (~50%) of plutonium from the cold-trap to the product receiver prior to cleanup. The possibility of reaction of PuF_6 with molybdenum compounds or other interfering volatile fission products should be considerably reduced in the new interhalogen scheme, since the bulk of these fission products are expected to be removed with the uranium during fluorination with BrF_5. Further data on molybdenum behavior in these experiments is being obtained.

TABLE II-28. Operating Conditions, Runs Pu-6, Pu-10, and Pu-11

	Run Pu-6	Run Pu-10	Run Pu-11
Charge:			
Wt. of Al_2O_3 (48-100 mesh) before pretreatment with F_2 (g)	6751	4848[a]	6758
PuF_4 (g)	134.2	138.0	135.4
UF_4 (g)	0	41.5	0
CsF (g)	0	41.8	39.2
Gas Flow:			
Total scfm (90 v/o F_2 in N_2)	~0.29	~1.25	~0.29
Make-up F_2 (scfm)	0.1	0.1	0.1
Superficial fluidizing gas velocity for temperature range 300–550°C (ft/sec)	0.2–0.28	0.86–1.21	0.2–0.28
Hours at stated bed temperature			
200°C	3.5		3.5
225°C	2.0		2.0
250°C	1.5		1.5
275°C	1.5		1.5
300°C	1.5	3.0	1.5
325°C	1.5		1.5
350°C	1.5		1.5
375°C	3.0		3.0
400°C	2.0	5.0	2.0
425°C	2.0		2.0
450°C	2.0		4.5
500°C	2.5		2.5
550°C	25.0	6.0	25.0
Hours at stated filter temperature			
~125°C	27.5	7.0	30.0
Increasing to ~300°C	4.5	1.0	4.5
300°C	17.5	6.0	17.5

[a] The final bed from run Pu-6 was reused as the starting bed for this run.

b. FLUORINATION OF PuF_4 AND TRANSFER EXPERIMENTS WITH PuF_6

A new program of fluorination studies was undertaken to develop basic information on the behavior of PuF_6 in the fluorination pilot plant. The experiments were intended to simulate the plutonium fluorination step of the interhalogen reference flowsheet. Known quantities of plutonium as PuF_4 or PuF_6 were employed, thereby avoiding the uncertainty regarding plutonium input encountered with PuO_2-UO_2 pellets.

Three fluorination experiments (runs Pu-6, -10, and -11) were completed employing similar conditions as to quantities of plutonium used, alumina charge, and high (~90 v/o) fluorine concentrations (see Table II-28). The charge in each case consisted of about 100 g of plutonium as PuF_4 and about 6.5 kg of 48-100 mesh prefluorinated alumina, Alcoa T-61 type. Fluorine was used on a recycle basis throughout these experiments. Near the end of each experiment the temperature in the filter zone was raised from the normal 125°C to 300°C to effect recovery of plutonium retained by the fines in this cooler region. This period is designated the cleanup fluorination period. The ma[illegible] differences in conditions between experiments are indicated below:

Run Pu-6: low fluidizing gas velocity, ~0.25 ft/sec; temperature range of fluorination 200 to 550°C; 50-hr duration; collection of the PuF_6 by direct sorption on NaF.

Run Pu-10: 42 g UF_4 + 42 g CsF added to the bed in addition to the PuF_4; relatively high fluidizing gas velocity of ~1.0 ft/sec; bed temperature, 300–550°C; 20-hr duration; collection of the PuF_6 (and UF_6) by cold-trapping in the main cold-traps followed by vapor transfer of the product to a small (weighable) cold-trap.

Run Pu-11: charge composition and product collection system similar to that for run Pu-10, other conditions as in run Pu-6.

Experiments were evaluated mainly on the basis of overall plutonium recovery and material balance.

In addition, two hexafluoride transfer experiments were completed, one with UF_6 alone and the other with PuF_6 alone to show that relatively small amounts of hexafluoride can be manipulated in engineering-scale equipment. Transfer was carried out between a supply vessel and a large inverted U-shaped cold-trap.

(1) Results and Discussion

Fluorination Experiments with PuF_4. The results obtained in the first PuF_4 fluorination experiment (run Pu-6) were considered highly satisfactory. Approximately 99% of the plutonium was fluorinated to PuF_6 and collected in the NaF sorption traps. The residual concentration of plutonium in the alumina bed was 0.005 w/o, representing about 0.25 g plutonium. The overall plutonium material balance was 99.3%.

In the two experiments (runs Pu-10 and -11) made with added CsF, the overall plutonium removal from the alumina was somewhat less than had been obtained in the PuF_4 experiment with no CsF added. The final concentrations of plutonium in the bed were approximately 0.08 w/o. It may be necessary to employ higher ratios of fluorine to plutonium to effect high plutonium recovery when CsF is present. Studies on the interaction of CsF and plutonium fluorides are being pursued in the laboratory program.

Inspection of the fluid-bed reactor after run Pu-11 revealed that the two sintered metal filters in the disengaging zone of the reactor were severely corroded. Apparently, the filters failed during the cleanup fluorination period of run Pu-10 when temperatures in the vicinity of the filters exceeded 375°C. Both filters showed evidence of a nickel-fluorine reaction. The filters used in these experiments were fabricated from sintered Monel powder. A temperature of 300°C is now considered the practical operating limit for such filters in a high-fluorine environment. However, more data on filter behavior and lifetime in such systems is needed.

TABLE II-29. Distribution of PuF_6 in Sodium Fluoride Traps

(Runs Pu-3a, -4, -5, and part of -6)

Trap No.	Superficial Gas Velocity through trap (ft/min)	Trap Temperature Range[a] (°C)	Total Pu Content of Trap (g)	Percent of Pu Found in Given Portion of Trap		
				Inlet third	Middle third	Exit third
1	2	90–96	2.1	99.5	0.2	0.3
2	2	90–96	2.4	93.9	0.4	5.7
3	2	90–96	3.0	94.7	<0.1	5.3
4	2	124–160	4.0	98.2	0.6	1.2
5	2	50–53	6.7	63.1	34.5	2.4
6	6	107–130	17.4	96.3	3.7	<0.1
7	7	80–150	97.4	96.8	3.1	0.1
8[b]	7	100–136	0.8	82.9	7.3	9.8

[a] Range determined from two or three skin temperature measurements.

[b] In series with Trap 7.

PuF_6 Sorption on NaF. Sorption of PuF_6 on NaF at temperatures of 100 to 125°C proved to be a highly efficient method for collection of the PuF_6 product. Performance data on the sorption system are summarized in Table II-29. As indicated in the table, most of the plutonium was sorbed in the inlet third of the NaF bed. At 100°C, the sorption efficiency of the bed for PuF_6 was high, while at 50°C the efficiency was much lower. Sorption efficiency was not affected by gas velocity or the quantity of PuF_6, within the ranges used in these tests. Although the sorption reaction is not reversible and plutonium cannot be readily recovered from the NaF bed, this method for collecting the plutonium generated in the fluorination of fuel materials is much more convenient, for experiment work, than condensation of PuF_6 in refrigerated traps since it offers a simple manner for obtaining material balances.

Transfer Experiments. The first UF_6 transfer experiment served as a shakedown of the equipment train for the next PuF_6 transfer experiment. In the UF_6 transfer experiment, 160.2 g of UF_6 was vacuum transferred from a supply vessel into a large cold-trap (~1 cu ft) maintained at −52°C. The UF_6 was then transferred to a small nickel receiver (800 ml) using nitrogen as a carrier gas. In this operation, the cold trap was heated to 75°C and the UF_6 was swept from the trap in the nitrogen gas stream. The receiver vessel was maintained at temperatures between −38 and −57°C. A small NaF trap was used to collect any UF_6 which passed through the receiver vessel.

Experiments were evaluated on the basis of weight

gain of the receiver and backup NaF trap after transfer. Approximately 123 g UF_6 was collected in the receiver and 35.2 g in the NaF trap; collectively, these numbers represent a UF_6 material balance of about 99% in the transfer operation.

During the PuF_6 transfer experiment, performed under the same conditions, 89.4 g PuF_6 was vacuum-transferred to the large cold-trap. In the second transfer, 74.0 g PuF_6 was collected in the receiver vessel and 13.4 g PuF_6 in the NaF trap. The PuF_6 material balance, taking into account alpha decomposition of PuF_6 at a rate of 2% per day for 8 hr, was 98.4% for the transfer experiment. These results are considered quite satisfactory and demonstrate that relatively small quantities of PuF_6 can be quantitatively transported in engineering-scale equipment provided that the equipment has been properly conditioned (prefluorinated). Additional transfer data are being obtained in the current fluorination program.

(2) Future Work

Studies aimed at demonstrating reliability in the transport of PuF_6 in the engineering-scale alpha facility will be continued. Interhalogen flowsheet studies on oxide pellet materials will commence. Further attempts will be made to exploit neutron detectors as plutonium fluoride monitors. Continued use will be made of the automatic data logger to establish its reliability. Additional time will be spent on the preparation of computer programs for data reduction.

2. Process Development Studies for Uranium Dioxide Fuels (D. Ramaswami, J. Gabor, D. Raue, J. Strand, J. Hepperly)

Engineering-scale studies are being performed in 1½-in. dia. and 3-in. dia. fluid-bed reactor facilities to determine the effects of important process variables on the fluorination of UO_2 fuels by bromine pentafluoride. These studies are being made with uranium-bearing fuels only, rather than with uranium-plutonium fuels, because the safety precautions required for handling plutonium materials would greatly complicate the operations.

a. EXPLORATORY TESTS ON FLUORINATION WITH BrF_5 IN A BENCH-SCALE FLUID-BED REACTOR SYSTEM

Exploratory tests on the fluorination of U_3O_8 with BrF_5 have continued in the 1½-in. dia. fluid-bed reactior. The objectives of the current tests were to determine: (1) the effect of addition of a small concentration of elemental fluorine to the BrF_5 reagent on the fluorination of U_3O_8 and (2) the effect of a small

TABLE II-30. Run Conditions and Amount of Uranium Fluorinated: The Fluorination of U_3O_8 with Mixtures of BrF_5 and F_2

Column diameter: 1½ in.
Bed charge: 270 g of UO pellets[a]
470 g of nominal 48 to 100 mesh alumina[b]
Pellet-bed depth: 1 in.
Fluidized-bed depth: 7 in. (static height)
Diluent gas: Nitrogen

	BrR-16	BrR-17	BrR-18	BrR-19	BrR-20	BrR-21
Oxidation						
Time (hr)	3.0	3.0	3.0	3.0	3.0	3 0
Superficial gas velocity[c] (ft/sec)	0.5	0.5	0.54	0.54	0.54	0.54
Oxygen concentration (v/o)	30	30	30	30	30	30
Temperature (°C)	410	410	460	460	460	450
Fluorination						
Time (hr)	0.58	2.0	2.0	2.0	2.0	2.0
Superficial gas velocity[c] (ft/sec)	0.43	0.50	0.56	0.55	0.55	0.47
BrF_5 concentration (v/o)	49.2	2.1	2.2	0	0	2.6
Fluorine concentration (v/o)	5.7	12.5	12.5	12.8	12.8	0
Temperature (°C)	210–290	200	200	200	200	200
Total BrF_5 feed (g)	880	160	180	0	0	180
UO_2 fluorinated to UF_6 (g)	242	228	221	0	1	17

[a] 280 g UO_2 charged in run BrR-16.
[b] Type T-61, tabular alumina, manufactured by Aluminum Company of America.
[c] At operating temperatures and 1 atm pressure.

concentration of BrF_5 in elemental fluorine on the fluorination of U_3O_8 at low temperatures (~200°C).

(1) Equipment and Procedure

The initial run in the current series of tests (run BrR-16) was made in equipment described previously (ANL-7225, p. 113). The subsequent runs were made with the equipment modified by the installation of sintered metal filters, furnished with an automatic blowback device, in the reactor disengaging section. Previously, the off-gas from the reactor was filtered by a packed bed of −14+28 mesh alumina.

For each run, ~270 g of UO_2 pellets and 470 g of nominal 48- to 100-mesh alumina were charged to the reactor. The pellets were supported on a bed of coarse-grain alumina particles. This bed also served as a distributor for the fluidizing gas. The runs were conducted in two steps: (1) oxidation of UO_2 pellets to U_3O_8 fines with 30 v/o oxygen in nitrogen for 3 hr at 410 to 460°C and (2) fluorination of the U_3O_8 to UF_6 with BrF_5 and fluorine. Operating conditions for the runs are presented in Table II-30.

(2) Results and Discussion

The use of a mixture of 12.5 v/o fluorine and 2 v/o BrF_5 in nitrogen at 200°C (runs BrR-17 and -18) resulted in the fluorination of approximately 225 g UO_2 in each run. In comparison, 12.8 v/o fluorine at 200°C in the absence of BrF_5 was ineffectual as a fluorinating agent. Similarly, in the absence of fluorine the use of 2.6 v/o BrF_5 in nitrogen fluorinated 17 g of UO_2 to UF_6 (run BrR-21).

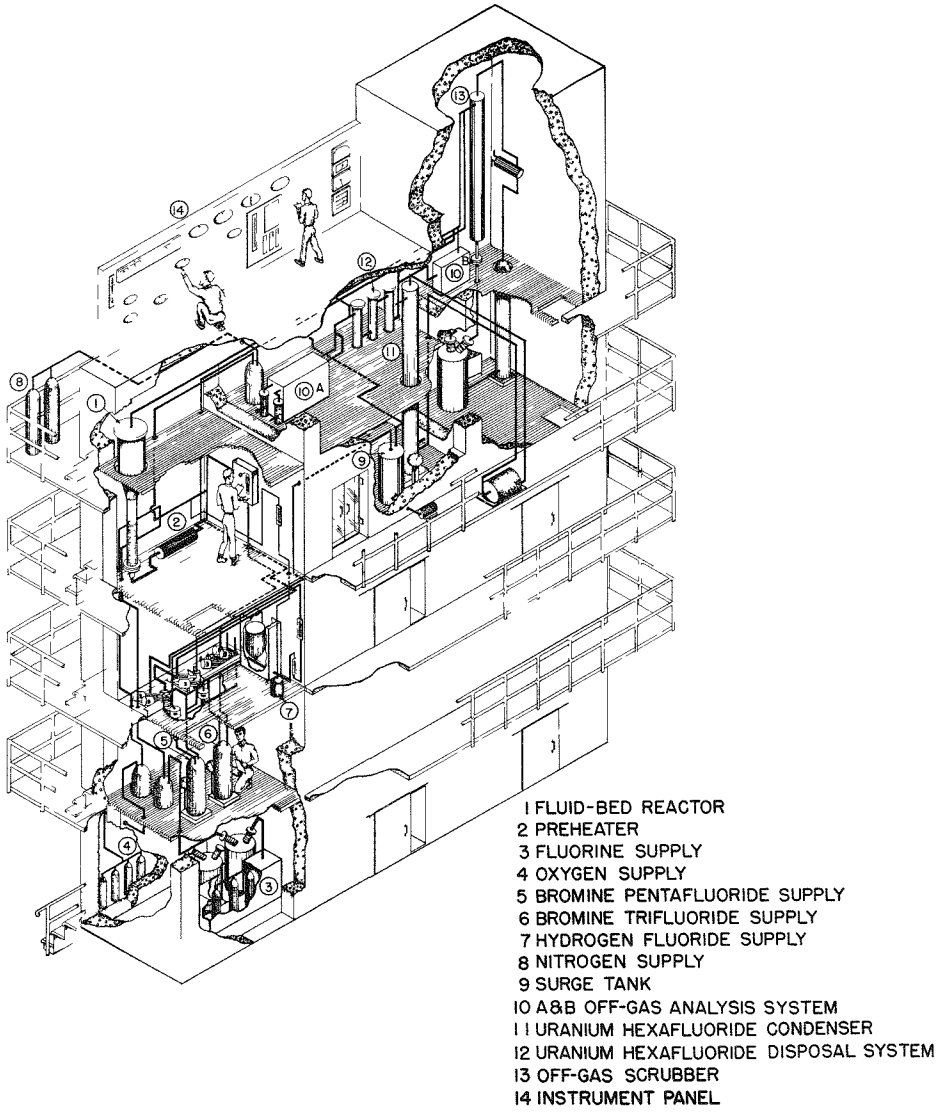

108-9780

FIG. II-15. Bromine Interhalogen Fluorination (BIF) Facility.

These results suggest that the rate of fluorination of U_3O_8 fines by fluorine is affected more by the addition of small amounts of BrF_5 to the fluorine stream than would be expected if the effects were additive. The behavior might be explained by postulating that the bromine produced by reaction of BrF_5 with U_3O_8 is refluorinated by elemental fluorine to BrF_5 which, in turn, reacts further with U_3O_8 to form UF_6.

(3) Future Work

Bench-scale work with the 1½-in. dia. reactor has been suspended, and process studies have been initiated in a 3-in. dia. pilot-scale facility.

b. DEVELOPMENT STUDIES ON FLUORINATION WITH BrF_5 IN AN ENGINEERING-SCALE FLUID-BED REACTOR FACILITY

Development studies have been initiated in an engineering-scale fluid-bed reactor facility to investigate the use of BrF_5 as a fluorinating agent for UO_2 fuels. Since the direct reaction of sintered UO_2 does not proceed readily with BrF_5 alone or in mixtures with oxygen at temperatures up to 400°C, the oxide fuel is pulverized to U_3O_8 fines by reaction with oxygen prior to fluorination.

The objectives of the current work are to determine (1) the feasibility of fluorinating a deep bed of U_3O_8 fines, (2) the production rates of UF_6, (3) the utilization efficiencies of BrF_5, and (4) the reliability of the equipment components in the engineering-scale facility.

TABLE II-31. Operating Conditions for Runs BRF5-1 and BRF5-2

	BRF5-1	BRF5-2
Charge (kg)		
UO_2 (fragmented, −0.5 + 0.132 in.)	2.2	4.4
Fluid bed of sintered alumina[a]	2.9 (−60 mesh)	5.8 (−100 mesh)
Fuel-support bed of sintered alumina[a] (−¼ in., +8 mesh)	3.7	3.7
Blowback		
Blowback frequency for each of the four filters	Once every 32 min	Once every 32 min
Blowback duration, sec	8	8
Oxidation Step		
v/o oxygen in nitrogen	~20	~20
Temperature (°C)	450	450
Gas velocity (ft/sec)	~1.5	~1.5
Time (hr)	6	11
Fluorination Step (BrF_5)		
v/o BrF_5 in nitrogen	~12	~12
Temperature (°C)	300–325	250–275
Gas velocity (ft/sec)	~0.8	~0.8
Time (hr)	2	3
Quantity of BrF_5 (kg)	3.8	5.9

[a] Type T-61, manufactured by Alcoa.

(1) Equipment

The engineering-scale facility basically consists of (1) a reagent feed system, (2) a fluidized-bed reactor, (3) an off-gas analysis system, and (4) an off-gas disposal system. An isometric sketch of the equipment enclosed in ventilated cells is shown in Figure II-15.

The fluidized-bed reactor vessel is the same as that used in the previous studies (ANL-7225, p. 116) and is 3 in. in dia. and 54 in. long. The fluid-bed reactor was cooled by natural air convection. Most of the other equipment has been newly installed.

(2) Operating Conditions

Operating conditions for the first two runs performed in the facility, runs BRF5-1 and BRF5-2, are summarized in Table II-31. For run BRF5-1, the fluid-bed material consisted of 2.9 kg of −60 mesh alumina granules, while for run BRF5-2, a finer grade (−100 mesh) of alumina was used. The UO_2 charge for each run was in the form of −0.5+0.132 in. fragments. The charge for run BRF5-1 was 2.2 kg of fragments; for run BRF5-2, the charge was doubled to 4.4 kg UO_2 fragments. Oxidation of the UO_2 fragments to U_3O_8 was carried out at 450°C using 20 v/o oxygen in nitrogen. The resultant U_3O_8 fines were fluorinated to UF_6 at a fluidizing-gas velocity of ~0.8 ft/sec with ~12 v/o BrF_5 in nitrogen. The fluid-bed temperature during fluorination was about 300 to 325°C for run BRF5-1 and about 250 to 275°C for run BRF5-2.

(3) Results and Discussion

In both runs (BRF5-1 and BRF5-2), the oxidation and the fluorination proceeded without any operational problems. In run BRF5-2, after oxidation, the entire fluid-bed reactor section (4.5 ft) contained the mixture of U_3O_8 fines and alumina. Fluorination of this 4.5-ft deep fluidized bed did not pose any problems under the conditions used for this run.

The average rates of UF_6 production were 65 and 86 lb UF_6/(hr) (sq ft reactor cross section) for runs BRF5-1 and BRF5-2, respectively. Since the bulk of the uranium was fluorinated during the initial two-thirds of the fluorination period, during run BRF5-2 rates approaching 130 lb UF_6/(hr) (sq ft reactor cross section) were probably achieved in that period. This value of UF_6 production rate is significantly higher than that achieved by two-zone oxidation-fluorination of the UO_2 fuels [~80 lb UF_6/(hr) (sq ft); see ANL-

8898, p. 70] and by the fluorination of U_3O_8 fines with fluorine [80 lb UF_6/(hr) (sq ft); see ANL-7225, p. 117].

The utilization efficiency of BrF_5 during the initial period of fluorination in run BRF5-2 was also probably higher than the average utilization efficiency of approximately 60% sustained over the entire fluorination time. These results are considered highly satisfactory for process application.

All equipment in the facility operated smoothly in both runs. The alumina beds were fluidizable throughout the runs, and at the end of the runs the alumina beds drained freely from the reactor. There were no cakes or agglomerates in either bed. All the procedures for handling the BrF_5 in various quantities, ranging from several kilograms to several grams, worked well.

(4) Future Work

Work to determine the effects of important process variables (fluid-bed temperature, BrF_5 concentration, fluidizing-gas velocity, UO_2 mass, and alumina particle size) on the operating characteristics of the equipment, the UF_6 production rates, BrF_5 utilization efficiencies, and off-gas composition during the fluorination will be continued. The finned fluid-bed reactor section will be replaced with a new section equipped with an air-water cooling system for more effective heat transfer. The new reactor section will provide more precise control of cooling and heating of the fluidized bed.

3. Cleanup of Cell Exhaust Air Contaminated with Plutonium Hexafluoride

(R. Kessie, D. Ramaswami, L. Marek)

The toxicity and volatility of PuF_6 requires that a very high degree of air cleanup be provided in the event of an accidental release of PuF_6 in an enclosure. Previous work which has been reported in detail[18] indicates that at a normal moisture concentration in the atmosphere the hydrolysis reaction occurs within the gas phase to produce a fine aerosol (PuO_2F_2 particles of <0.1-μ diameter), but at low moisture concentrations reaction occurs upon solid surfaces exposed to the reactants. The collection of the solid aerosol by two high-efficiency filters in series at 40% of rated flow will limit the proportion of plutonium penetrating the filter to less than one ppm of that released. The kinetics of the surface reaction has been measured in packed beds of glass spheres, and the data have been used to compute filter penetration. The prediction indicates that less than 1 ppm of the released plutonium will penetrate the filter at moisture levels in excess of 0.25 mm Hg. The experimental confirmation of the predicted surface reaction in high-efficiency filters is an objective of the present experiments.

The present series of experiments is being made to determine how each type of reaction (gas-phase and surface reaction) affects filter penetration and to measure plutonium particulate penetration through a series of two filters.

The apparatus used in these experiments is shown in Figure II-16. A disc of filter media is mounted between two glass funnels to form a filter unit. Each unit is tested for DOP (dioctylphthalate) penetration prior to use (see ANL-7125, pp. 96–97). Four units are assembled in a series before the entire assembly is placed in the glovebox. Four filters are required to measure accurately low-level plutonium penetration of the second filter. The function of the third filter is to contain material penetrating the second filter; the fourth filter serves to preclude back-contamination of the third filter. A stream of PuF_6 in dry air is mixed with a moist air stream in a Plexiglas chamber.

Eighteen experimental runs with PuF_6 have been completed. However, analyses of the filters are difficult owing to the small quantity (10^{-9} mg Pu) of plutonium on the filters, and results of these experiments are not available at present.

A second objective of this program is to obtain a numerical computer solution of differential equations describing the mechanisms occurring in filtration which can be used to study the effect of the many variables on the filtration of aerosols. This would be helpful in understanding and planning experiments, particularly where the experiments are difficult and time-consuming. The first parametric study of interest is establishing the effect of particle diameter and gas velocity on the particle penetration of filters at a fixed level of the variables: fiber diameter, fiber spacing, gas viscosity, gas density, gas mean free path, and particle density. The fixed conditions will be those corresponding to the experimental conditions.

Although the computer program has not been completed, sufficient work has been accomplished to indicate that the initial objective should be achieved in several months. The following is an example of the ap-

[18] R. W. Kessie and D. Ramaswami, Removal of Plutonium Hexafluoride from Cell Exhaust Air by Hydrolysis and Filtration, ANL-7066, December 1965.

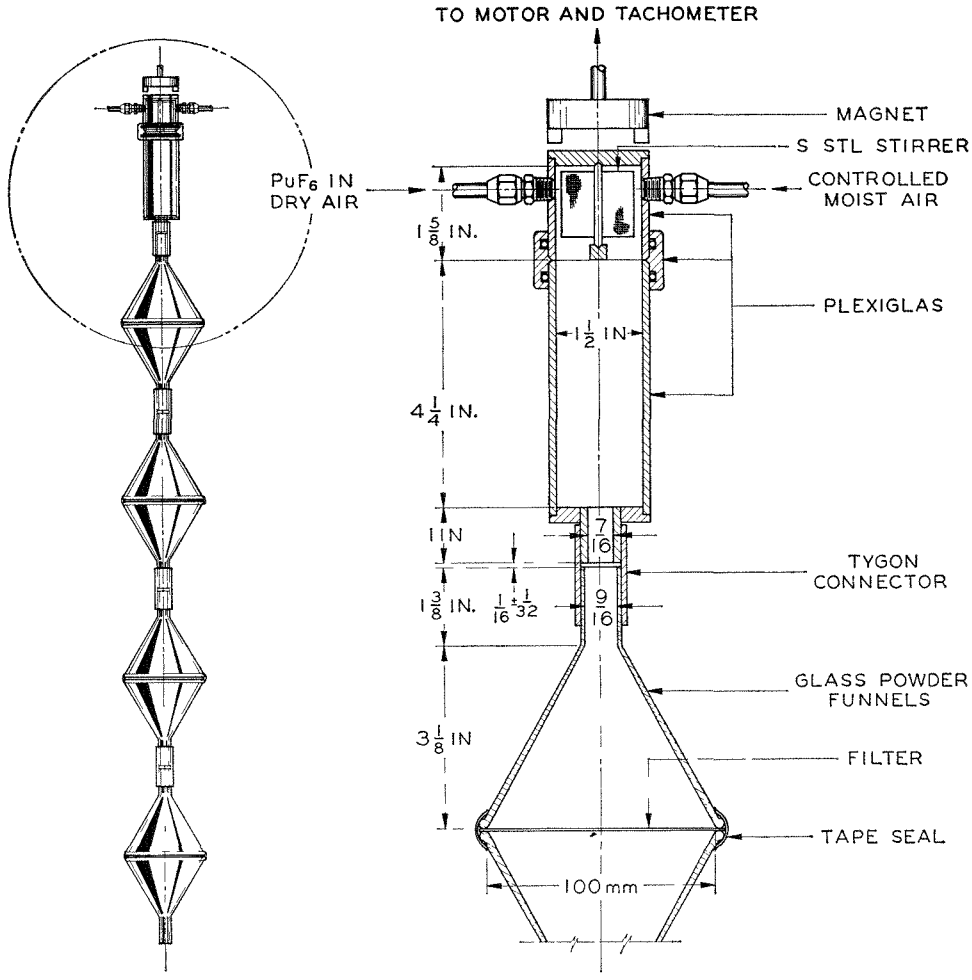

108-9836

FIG. II-16. Equipment for the Study of Plutonium Filtration and Surface Reaction in Filters.

proach used: For the flow field, the Navier-Stokes equations are solved using boundary conditions that include the effect of slip velocity at the fiber surface. These equations are solved using an alternate relaxation and filling technique. The solution is obtained for 2048 points within a hypothetical fiber cell to 0.1% accuracy in a 15-sec computer period. The momentum and drag equations for the particle are solved and, finally, solutions are obtained for the diffusion equations. The momentum and drag equations are such that other particle forces can be readily added. The effects of other particle forces have been tested, in a preliminary way, with central (particle and fiber) electrostatic forces.

4. Bench-scale Fluid-bed Studies with Irradiated Fuels (A. CHILENSKAS, G. POTTS, J. KINCINAS, N. SAITO[19])

A program demonstrating the fluid-bed volatility process with irradiated fuel materials is in progress. Experiments are being conducted in a 1½-in. dia. fluid-bed reactor installed in the senior cave facility of the Chemical Engineering Division. Present work is directed to the determination of the distribution of the actinides and fission products in the process streams in each of the steps of the oxygen-bromine pentafluoride-fluorine process. The fuel charge used was highly irradiated UO_2 pellets, and the bed material was alumina.

a. THE DISTRIBUTION OF THE ACTINIDES AND FISSION PRODUCTS FOLLOWING THE O_2-BrF_5–F_2 PROCESSING OF IRRADIATED UO_2

A series of three runs has been completed using a processing scheme consisting of oxidation of UO_2 to

[19] Guest Scientist from Atomic Fuel Corporation, Japan.

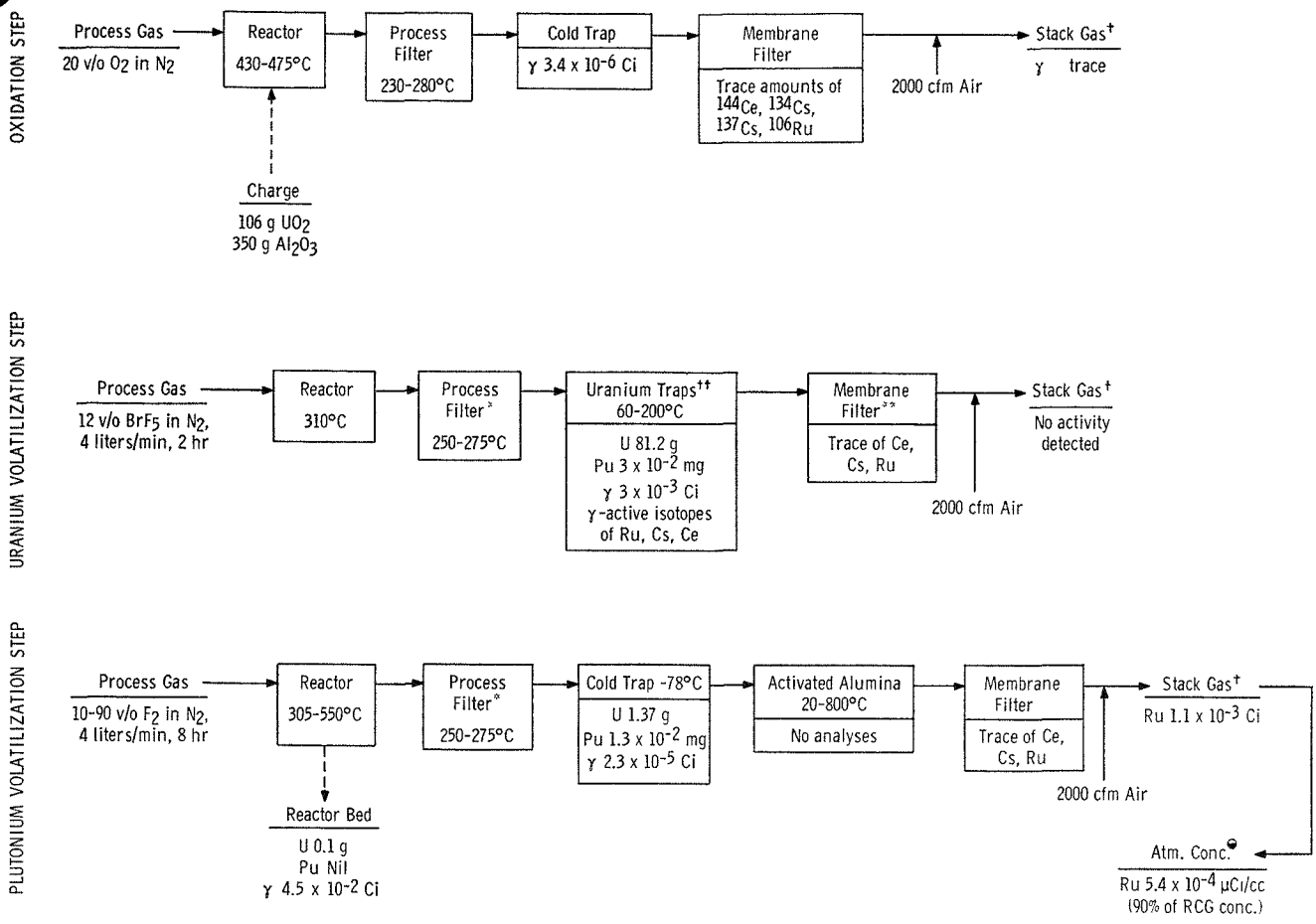

*Sintered nickel, 10-micron pore size, grade G, Pall Trinity Micro Corp.
**Membrane filter, 0.4-micron pore size, Metricel VF-6, Gelman Corp.
† The stack gas passes through an AEC high-efficiency filter and a charcoal filter before it is sampled and discharged to the environment.
†† The uranium traps consisted of two beds of soda lime in series, each 1.75 kg, operated at 105-200°C followed by a bed of activated alumina, 0.9 kg, operated at about 60°C.
● The atmospheric concentrations at ground level below the senior cave stacks are calculated from the stack gas analysis, allowing a dilution factor of 10 from the stack discharge to the ground level. The RCG value represents the percent of the recommended limiting concentration of the radioisotope as proposed in Radioactivity Concentrations Guide, AEC Manual, Chapter 0524, Standards for Radiation Protection, (approved Aug. 12, 1963). Copies can be obtained from AEC Headquarters, Division of Operational Safety, Washington, D.C.

308-485

FIG. II-17. Processing of a Nonirradiated UO_2 Charge Using an Oxygen-Bromine Pentafluoride-Fluorine Scheme in Contaminated Equipment. Run IN-BRF-1.

U_3O_8 at 405 to 475°C, uranium volatilization with BrF_5 at 305 to 315°C, and plutonium volatilization with fluorine at 300 to 560°C. The first of these (run IN-BRF-1) was made using a nonirradiated charge of UO_2 to establish experimental procedures and to determine the levels of activity in the various samples which result from processing in equipment contaminated with radioactive material. The other two runs (BRF-1 and -2) were made with irradiated UO_2 pellets which had been declad mechanically.

The apparatus and procedures employed in these tests were similar to those used in the processing of irradiated uranium alloy fuels (see ANL-7055, p. 156). Prior to the start of these tests, the equipment was modified slightly by the installation of a sintered nickel filter in a separate chamber above the fluid bed. This filter replaced the packed-bed filter previously used.

(1) Run IN-BRF-1

The processing conditions and the distribution of actinides and fission products following the processing of 106 g of nonirradiated UO_2 is shown in Figure II-17. The plutonium and fission product values shown in the figure are attributed to pickup of these materials from the contaminated equipment. It should be noted that the gamma activity movement to the stack gas was negligible during the first two steps of the process, while considerable ruthenium movement (90% of the

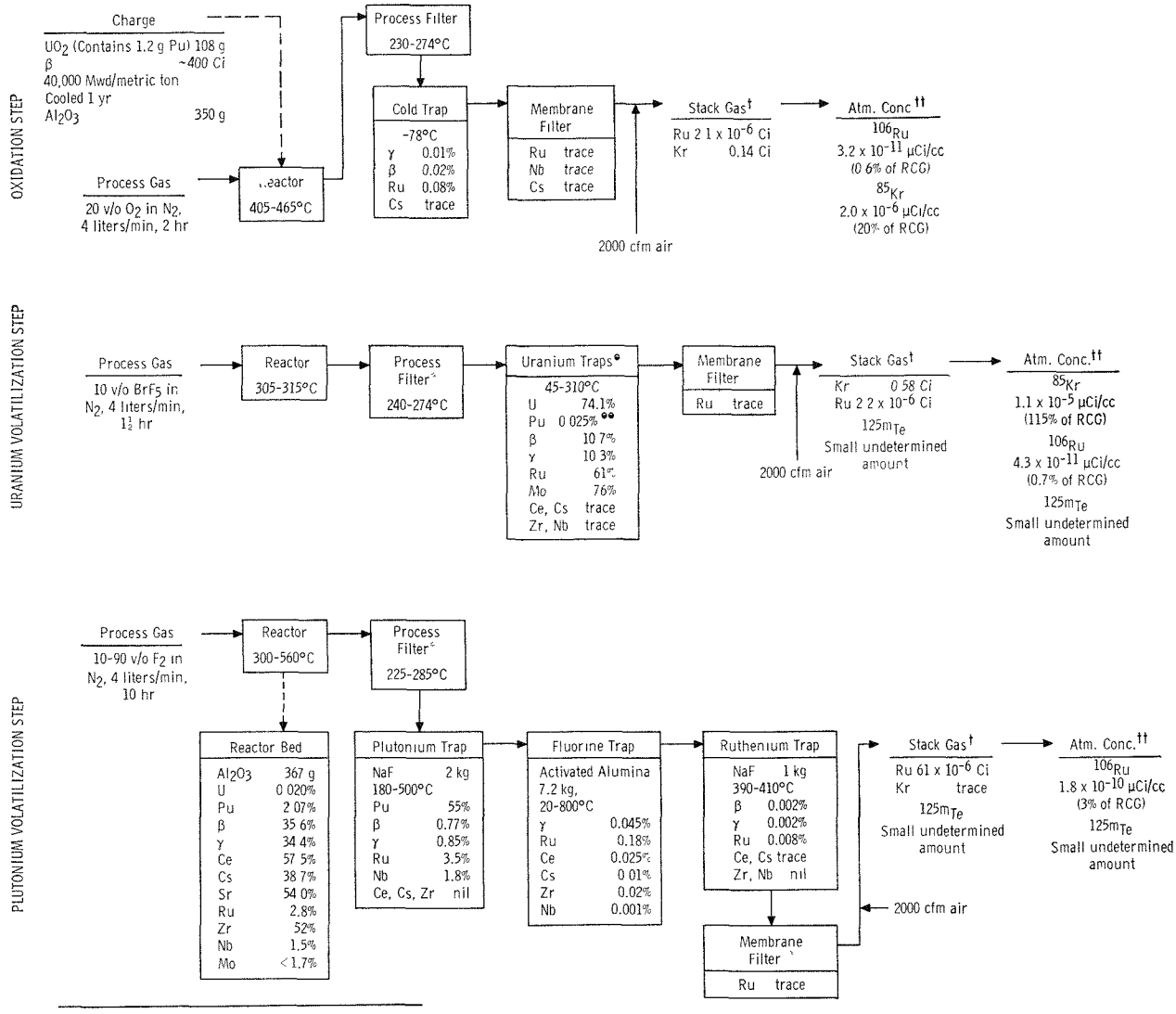

‡Sintered nickel, 10-micron pore, grade G, Pall Trinity Micro Corp.
‡ Membrane filter, 0.4-micron pore, Metricel VF-6 (fluorinated vinyl), Gelman Corp.
† The stack gas passed through an AEC high-efficiency filter and a charcoal filter before it was sampled and discharged to the environment.
†† The atmospheric concentrations at ground level are calculated from the stack gas analysis, allowing a dilution factor of 10 from the stack to the ground level. The RCG value represents the percent of the recommended limiting concentration of the radioisotope as proposed in Radioactivity Concentration Guide, AEC Manual, Chapter 0524, Standards for Radiation Protection (approved Aug. 12, 1963). Copies of the manual can be obtained from AEC Headquarters, Division of Operational Safety, Washington, D.C.
• The uranium traps consisted of two beds in series, the first containing soda lime and the second containing a mixture of soda lime and activated alumina.
•• Run BRF-1 only.

308-483

FIG. II-18. Processing of Irradiated UO_2 Charge Using an O_2-BrF_5-F_2 Process Scheme. Average Values for Runs BRF-1 and -2.

recommended limiting value)[20] was noted during the final step. In general, the levels of activities found in the process beds at the end of the run were such that no significant sample contamination from equipment was indicated.

(2) Runs BRF-1 and -2

The feed material for each run was 108 g of declad UO_2 irradiated to 40,000 MWd/metric ton. Each charge was obtained from the same core loading of the Yankee reactor. The charges for the runs had cooled approximately one year prior to processing. The process conditions and average fission product distributions following each process step are shown in Figure II-18.

The Oxidation Step. Only a small amount of activity volatilized during the conversion of the UO_2 to U_3O_8. The principal volatile activity was krypton-85; about 17% of the total krypton activity was released during this step. It should be noted that the irradiated charges had been declad prior to processing and that the krypton released upon cladding removal is not known. Other

[20] Radioactivity concentration Guide, AEC Manual, Chapter 0524, Standards for Radiation Protection (approved Aug. 12, 1963). Copies can be obtained from AEC Headquarters, Division of Operational Safety, Washington, D.C.

volatile species detected after oxidation were trace[21] amounts of cesium, niobium, and ruthenium. Analysis of the stack gas showed that, in addition to krypton, ^{106}Ru was present at a concentration that was about 0.6% of the recommended upper limit.[20]

The Uranium Volatilization Step. During uranium volatilization by reaction with BrF_5, the principal activities which also volatilized and collected with the uranium in the soda lime and activated alumina traps were 61% of the ruthenium, 76% of the molybdenum, and trace amounts of cerium, cesium, zirconium, and niobium. During this step, 83% of the krypton volatilized. Analyses have not been completed for other fission products, such as neptunium, technetium, and tellurium, which probably form volatile species during the BrF_5 fluorination step. In run BRF-1, 0.025% of the plutonium in the oxide fuel accompanied the uranium and collected in the soda lime trap.

In addition to krypton, small amounts of ^{106}Ru and ^{125m}Te were detected in the stack gas.

The Plutonium Volatilization Step. The volatilization of the plutonium from the reactor was accomplished by the use of fluorine at temperatures from 300 to 560°C. About 0.8% of the gross beta and gamma was volatilized during this step. The major gamma active isotopes found with the plutonium in the NaF trap were ruthenium and niobium (about 3.5% of the ruthenium and 1.8% of the niobium). Small amounts of cesium, cerium, and zirconium (less than 0.1%) collected in the activated alumina trap downstream of the NaF trap. Analyses have not been completed for the other possible product contaminants. The process off-gas contaminants were found to be mainly ruthenium and tellurium. About 3% of the recommended limiting value[20] for ^{106}Ru and a small amount of ^{125m}Te were found in the stack effluent.

Reactor Bed Residues. The average values for retention of actinides and fission products in the final alumina beds were 0.02% of the uranium, 2.0% of the plutonium, 34.4% of the gross gamma, 35.6% of the gross beta, 57% of the cerium, 54% of the strontium, 39% of the cesium, 52% of the zirconium, 1.5% of the niobium, and <1.7% of the molybdenum. Analyses have not been completed for other activities.

TABLE II-32. Comparison of Inactive and Active Runs in which O_2-BrF_5-F_2 Processing Scheme Was Used

	Inactive Run IN-BRF-1	Active Run BRF-1	Active Run BRF-2
Charge			
Uranium (g)	93	91	91
Plutonium (mg)	0	1220	1190
γ (Ci)	0	105	93
Uranium Product			
Uranium (g)	81.8	70.5	64.5
Plutonium (g)	0.03	0.4	N.A.[a]
γ (Ci)	0.003	12.2	8.4
Plutonium Product			
Uranium (mg)	1370	50	300
Plutonium (mg)	0.013	750	755
γ (Ci)	2.3×10^{-5}	1.3	0.5
Reactor Bed			
Uranium (g)	0.097	0.012	0.028
Plutonium (mg)	0	17	45
γ (Ci)	0.045	22.6	44

[a] Not analyzed.

The Activity Contribution to Runs BRF-1 and -2 from Residual Activity in the Equipment from Previous Hot Runs. A comparison of the results for the inactive run (IN-BRF-1) with the results for the two runs with irradiated charges (BRF-1 and -2) is shown in Table II-32. An examination of these values shows that the gamma activity of the samples obtained after processing with a nonirradiated charge is very small when compared to that obtained after processing an active charge. Therefore, the contribution of activity from residual deposits within the equipment can be neglected.

[21] A trace is considered a detectable amount of an element constituting less than 10^{-4}% of the amount present in the charge.

5. Disposal of Gaseous Fluoride Volatility Reagents (J. T. Holmes, C. B. Schoffstoll)

A bench-scale fluidized-bed facility has been used to study the reaction of fluorine with various reactive solids as a means of disposal of fluorine, which is an important reagent in the fluoride volatility flowsheets. The use of a fluidized bed of reactive solids was chosen for the following reasons:

a) Owing to the good heat transfer achieved in fluidized beds, it is possible to carry out highly exothermic gas-solid reactions under nearly isothermal conditions and thereby prevent sintering, which often occurs in packed-bed reactors.

b) The reactive solids can be chosen such that the products of the reaction are solids and nontoxic gases. A solid product is important for ultimate waste disposal if the gaseous reagents contain volatile fission product compounds which also react with the solids.

The current work has been mainly devoted to the disposal of fluorine, using fluidized beds of activated

TABLE II-33. INDEPENDENT VARIABLES STUDIED IN THE DISPOSAL OF FLUORINE IN A FLUIDIZED BED OF ACTIVATED ALUMINA

	Low	High
Bed Temperature	300°C	400°C
Bed Depth-to-Diameter Ratio, L/D	3	6
Particle Size, D_p	48–100 mesh (183 μ)[a]	28–48 mesh (399 μ)[a]
Gas Velocity, V	1.25 V_{mf}[b]	1.65 V_{mf}[b]
Flourine Concentration	5 v/o	10 v/o

[a] Mean particle size.
[9] Minimum fluidization velocity.

alumina (A.A.). The work will be extended to evaluate the use of other solids for fluorine disposal and then, using appropriate solids, for the disposal of other gaseous reagents such as the bromine fluorides, and possibly fission product compounds.

The experimental facility and operating procedure were described previously (ANL-7225, pp. 126–127). A small scrubber containing potassium iodide solution was used to determine the concentration of fluorine in the off-gas from the fluidized bed reactor. An evaluation of the scrubber, over the range 5 to 2600 ppm fluorine in nitrogen, indicated that the scrubbing efficiency was essentially constant over this concentration range. Each experiment was terminated when the fluorine concentration in the off-gas exceeded 1000 to 2000 ppm. The capacity of the activated alumina was determined by chemical analysis of the fluoride concentration in the final fluidized bed. Capacity was defined as the grams of fluorine reacted per gram of activated alumina charged to the reactor. The theoretical maximum capacity is 0.950 g fluorine/g A.A., assuming the following reaction:

$$Al_2O_3 \cdot H_2O + 3F_2 \rightarrow 2AlF_3 + H_2O + 1.5\,O_2\,.$$

After a series of shakedown runs were made to check out the equipment and procedure, a factorially designed set of experiments was used to determine the effect of the five independent variables considered most likely to affect the capacity of activated alumina[22] for fluorine. The variables were: temperature (T), particle size (D_p), bed depth-to-diameter ratio (L/D), fluorine concentration (v/o), and gas velocity (V). For the bed depth to diameter ratio, only the bed depth was varied since the diameter was fixed at 2.07 in. Each variable was studied at the two levels shown in Table II-33. This set of experiments determined the effects of all the variables, the first order interactions (e.g., T, D_p interaction), and experimental error, but did not give any information on the effects of higher order interactions (e.g., T, D_p, L/D interaction). Higher than first order interactions are rather uncommon in physical situations.

[22] Grade F-1 Alcoa activated alumina.

a. RESULTS AND DISCUSSION

No operational difficulties were encountered in any runs. The product beds were always free-flowing and no significant pressure buildups due to deposition of fines on the sintered metal filters were noted. The automatic filter blowback system was not used during any of the runs.

The predried activated alumina is the monohydrate of aluminum oxide ($Al_2O_3 \cdot H_2O$) and therefore some HF was produced by the reaction of the H_2O and fluorine. The HF was not completely sorbed by unreacted activated alumina, and small concentrations of HF were observed in the off-gas from the fluid-bed reactor. The HF concentration was highest during early portions of the run, but never exceeded the concentration of fluorine in the off-gas.

(1) Results of Factorially Designed Series of Experiments

The factorial experimental design is shown on Table II-34. Also included are the experimental values of capacity at breakthrough as defined in the following manner: (1) the point at which the fluorine concentra-

TABLE II-34. FRACTIONAL FACTORIAL DESIGN FOR FLUID-BED DISPOSAL OF FLUORINE WITH ACTIVATED ALUMINA (A.A.)

Run	D_p (μ)	L/D	V ($\times V_{mf}$)	Bed Temp (°C)	F_2 in N_2 (v/o)	Capacity at Breakthrough (g F_2/g A.A.)	
						At 200 ppm F_2 in off-gas	At 99.9% removal of fluorine
5	399	6	1.65	400	5	0.627	0.553
2	399	6	1.65	300	10	0.294	0.283
1	399	6	1.25	400	10	0.660	0.630
8	399	6	1.25	300	5	0.344	0.294
4	399	3	1.65	400	10	0.206	0.183
7	399	3	1.65	300	5	0.153	0.141
3	399	3	1.25	400	5	0.429	0.258
6	399	3	1.25	300	10	0.187	0.174
12	183	6	1.65	400	10	0.740	0.737
11	183	6	1.65	300	5	0.388	0.357
16	183	6	1 25	400	5	0.797	0.797
13	183	6	1.25	300	10	0.412	0.410
10	183	3	1.65	400	5	0.642	0.583
15	183	3	1.65	300	10	0.251	0.23
14	183	3	1.25	400	10	0.676	0.658
9	183	3	1.25	300	5	0.293	0.257

TABLE II-35. EFFECT OF INDEPENDENT VARIABLES ON CAPACITY OF ACTIVATED ALUMINA FOR FLUORINE

Change in Variable	Effect or Capacity (g F_2/g A.A.)	
	At 200 ppm F_2 in off-gas	At <99.9% F_2 removal
Temperature: 300°C to 400°C	0.307	0.280
L/D: 3 to 6	0.178	0.196
Particle Size: 48-100 mesh to 28-48 mesh	−0.162	−0.190
Gas Velocity: 1.25 V_{mf} to 1.65 V_{mf}	Not significant	
Fluorine Concentration: 5 v/o to 10 v/o		
	Mean Capacity at Breakthrough (g F_2/g A.A.)	
	0.443	0.410

tion in the off-gas reached 200 ppm, and (2) the point at which less than 99.9% of the fluorine was removed by the activated alumina. The experiments were made in a random sequence, as shown by the run numbers.

The results of an analysis of variance of the data at both breakthrough points (200 ppm and 99.9% removal) showed that, for the range of the variables studied, bed temperature, A.A. particle size, and bed depth-to-diameter ratio were the only variables which had significant effects on the capacity. Furthermore, these variables were significant at the 99% confidence level. The effects of a change in gas velocity, a change in fluorine concentration, and all first order interactions of the variables were not significant in the ranges studied.

The magnitudes of the effects (g F_2/g A.A.) of each variable are shown in Table II-35. It can be seen that temperature has the largest effect, while bed depth-to-bed diameter ratio and particle size have smaller effects. Changes in gas velocity and fluorine concentration over the ranges studied do not produce significant effects.

The standard deviation for breakthrough at 200 ppm was $\sigma_0 = 0.061$ g fluorine/g A.A. and at 99.9% fluorine removal was $\sigma_0 = 0.058$ g fluorine/g A.A. This means that the observed effects on Table II-35 have 95% confidence limits of about (2) $\sigma_0/2 = \pm 0.06$ g fluorine/g A.A., and that the capacity data of Table II-34 have 95% confidence limits of about (2) $\sigma_0 = \pm 0.12$ g fluorine/g A.A.

The results can be presented as follows:

Capacity (g F_2/g A.A.) at 200 ppm Breakthrough

$$= 0.443 + 0.00307(T - 623) + 0.0593(L/D - 4.5) - 0.000750(D_p - 291)$$

Capacity (g F_2/g A.A.) at 99.9% Removal Breakthrough

$$= 0.410 + 0.00280(T - 623) + 0.0653(L/D - 4.5) - 0.00088(D_p - 291)$$

where T is in °K, and D_p is in microns.

These equations represent the best (least square) linear interpolation over the range of variables studied (Table II-33). The equations should not be used to extrapolate outside of the ranges, and it should not be assumed that the effects of velocity and concentration are not insignificant outside the ranges studied. It can easily be seen that, within the range studied, the maximum capacity can be obtained at $T = 400$°C, $D_p = 183$ microns, $L/D = 6$, any concentration of fluorine from 5–10 v/o, and any gas velocity from 1.25 to 1.65 V_{mf} (compare capacity for run 16 to capacity for other runs in Table II-34).

(2) Mechanism

It is likely that the reaction of activated alumina with fluorine can be characterized by a continuous reaction model since A.A. has a porous structure and a high surface area (260 to 290 m^2/g). The model is shown schematically in Figure II-19. As the reaction proceeds, the reaction rate becomes pore-diffusion limited due to partial plugging of the pores by reaction product. The product, AlF_3, is less dense than the reactant, A.A., and would therefore tend to fill the pores. There is an indication that diffusion through the gas film surrounding the particle does not limit the reaction rate since gas velocity does not appear to have a significant effect on capacity. This model is consistent with the observed effects of all five independent variables.

(3) Experiments at Extreme Conditions

A series of additional runs were made to determine the effect on capacity of operating with conditions out-

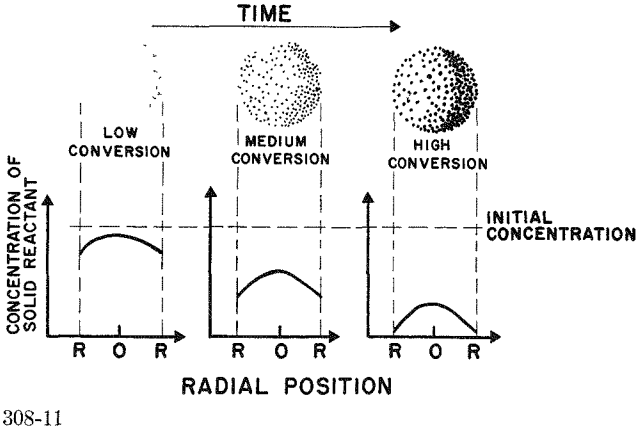

308-11

FIG. II-19. Continuous Reaction Model.

side the range of those used in the factorial design experiment. Since there are practical limitations on the use of smaller particles of activated alumina and on the use of deeper beds (because of the size of the reactor), these variables were not investigated further.

In order to increase the capacity of the bed for fluorine to values greater than those achieved in the planned set of runs, an experiment was conducted at 450°C. This run gave a capacity of 0.803 g fluorine/g A.A., which can be compared with 0.797 g fluorine/g A.A., for run 16, which used the same conditions except for a temperature of 400°C. The difference between the capacities was too small to be statistically significant. It is not surprising that the increase was small since capacities are near the maximum theoretical value of 0.95 g fluorine/g A.A.

Additional runs were made at a higher gas velocity (3.0 V_{mf}) and at higher concentrations of fluorine (30 and 75 v/o) to extend the range of these variables. The higher gas velocity produced a significant but small decrease in the capacity, which is not surprising since high gas velocities often give rise to poor gas-solids contacting. There were no significant effects of 30 or 75 v/o fluorine on the capacity, which is consistent with the previous results obtained using 5 and 10 v/o fluorine.

(4) Comparison of Fluid Beds with Packed Beds

It is interesting to compare the throughput capabilities for the fluid-bed reactor system with that for a packed-bed reactor. Throughput is defined as the feed rate of fluorine in pounds of fluorine per hour per sq ft of reactor cross section. With 183-micron (48-100 mesh) activated alumina and a fluorine concentration of 75 v/o in a fluid-bed reactor, the fluorine throughput rate is about 40 lb/(hr) (sq ft). Throughput rates up to 140 lb/(hr) (sq ft) can be obtained with 28-48 mesh alumina but result in lower capacities. Data obtained earlier for packed beds of activated alumina gave maximum throughputs of about 3 lb/(hr) (sq ft). Above this throughput rate, sintering of the packed bed occurred. It is obvious that if a free-flowing reaction product is desired, the fluid-bed technique will allow much higher fluorine throughput rates. The experiments with packed beds of A.A. gave maximum capacities at breakthrough of about 0.85 g fluorine/g A.A. for runs where bed temperatures were over 1000°C and sintering occurred. The capacities achieved in fluidized beds (up to 0.8 g fluorine/g A.A.) were only slightly lower than the packed-bed capacities.

TABLE II-36. Experimental Conditions for the Disposal of Fluorine in a Fluidized-Bed Facility Using Na_2CO_3 or $CaCO_3$

Temperature	400°C
L/D	6
Particle Size	−60+100 mesh
Fluorine Concentration	10 v/o
Gas Velocity	1.65 V_{mf}

(5) Nature of Solid Reaction Products

The solid reaction products appear to be suitable for waste disposal. The beds were free-flowing at the conclusion of all of the runs. There is no significant change in particle size caused by the formation of a less dense reaction product, or by attrition due to the turbulence of the fluid bed. The bulk density of the product from run 16 was 1.22 g/cc untapped, and 1.36 g/cc tapped.

(6) Other Solid Reagents

Two other solid reagents, soda ash (Na_2CO_3) and limestone ($CaCO_3$), both of which are less expensive than activated alumina, were tested for fluorine disposal in the same facility using the conditions shown in Table II-36. Qualitatively, the results of single experiments with each of the solids were similar to the results obtained with activated alumina. The capacity of soda ash was 0.32 g fluorine/g, and the capacity of the limestone was 0.045 g fluorine/g. These capacities correspond to about 90% and 12% of the theoretical maximum capacities for soda ash and limestone, respectively. It appears that the rate of reaction with limestone becomes diffusion-controlled and that breakthrough occurs before the particle is significantly reacted. The product (NaF) of the soda ash reaction apparently does not hinder the reaction since the reaction product is more dense than the reactant and thus would not tend to produce a resistance to mass transfer. Since sodium fluoride is known to be an effective sorber for certain volatile fluoride compounds, the NaF product from the soda ash reaction may be effective for the removal of volatile fission products associated with the fluorine gas stream.

b. CONCLUSIONS

A fluidized-bed process capable of high fluorine disposal rates has been developed using activated alumina as the reacting solid. The reaction is characterized by an initial period when the fluoride concentration in the reactor off-gas is less than 50 ppm and by a breakthrough period when the concentration rises rapidly. The results of a factorially designed set of experiments indicated that increasing the bed temperature from 300 to 400°C, increasing the bed depth-to-diameter ratio from 3 to 6, and decreasing the particle size from 393 to 183 microns were all effective in increasing the

capacity of the activated alumina for fluorine removal to near the theoretical maximum value. There were no significant effects of varying the fluorine concentration between 5 and 75 v/o or of changing the gas velocity from 1.25 V_{mf} to 1.65 V_{mf}. A higher value of gas velocity (3.0 V_{mf}) decreased slightly the capacity of activated alumina for fluorine.

Solid reactants which are less expensive than activated alumina also are being evaluated. Soda ash is especially promising.

C. BASIC STUDIES OF FLUIDIZED-BED BEHAVIOR RELATED TO PROCESS OPERATIONS (D. RAMASWAMI)

1. Basic Mechanisms of Fluidization (J. D. GABOR, R. E. CARLSON[23])

The effects of walls on the characteristics of particle movement within a fluidized bed are important to the understanding and control of fluidized-bed reactors. For most reactors, heat is either introduced or removed through wall surfaces. Reactor walls also affect the characteristics of gas and particle mixing within fluid-bed reactors. Therefore, knowledge of particle behavior at the walls of a reactor is of practical importance to the design of fluid-bed systems.

Currently, experimental studies are being conducted to determine the effect of column width on fluidized particle movement in a two-dimensional column, i.e., a column of rectangular cross section for which the thickness is so small that a rising bubble is in simultaneous contact with both opposite walls. The results of the current experimental studies have been compared with the previously presented theoretical treatment (ANL-7225, pp. 128–130) for a cylinder (representing a circular bubble) rising through an ideal fluid between parallel walls.

a. EXPERIMENTAL APPARATUS

The trajectories of fluidized particles in a two-dimensional fluidized bed, resulting from the passage of a single gas bubble through the bed, have been observed photographically and have been compared with the theoretical predictions. Two glass columns (one 7.3 cm wide, the other 15.0 cm wide, and both 0.95 cm thick and 51 cm high) were used. Glass beads, 0.27, 0.39, and 0.46 mm in diameter, with black tracer particles, constituted the bed material. The glass beads were supported on a porous metal distributor plate and were fluidized by a gas flow slightly greater than the incipient fluidization velocity. A controlled volume of nitrogen was then injected into the bed through a tube in the center of the distributor plate. The experimental bubble diameter-to-column width ratios (a/d ratios) were varied by regulating the injected nitrogen volume (bubble size) and by using one or the other of the column widths (7.3 or 15.0 cm).

Motion pictures were taken with a Fastax camera using 16 mm Ektachrome (ASA 32) film at 250 to 400 frames per second. The particle trajectories were determined with the aid of a Vanguard Motion Analyzer.

b. RESULTS

The experimentally observed trajectories are compared with the theoretical trajectories for an a/d ratio of 0.63 in Figure II-20. The 7.3-cm wide column and 0.39-mm beads were used for the experimental measurements shown in the figure. The amount of particle movement increases with proximity to the center of the bubble. The particle movement is primarily downward except for particles near the center of the bubble. The rising bubble initially pushes the latter particles upward but rapidly catches up to them. These particles then fall through the bubble into the lens-shaped wake at the bottom of the bubble. The particles are then carried upward in the wake a short distance before being deposited in the bed. This motion is unlike the looping motion indicated by theory for particles near the center of the bubble path. The theory also predicts a greater downward movement near the walls than was experimentally observed. It should be noted that without consideration of the walls (that is, if a bubble was assumed to be rising through an infinite medium), previously developed theories would predict a net *upward* displacement of particles.

The point in time when the center of the bubble was at the same vertical position as a particle is noted as time 0 in Figure II-20. Thus, when the center of the bubble was at $-\frac{1}{4}$ on the X axis (direction of bubble rise), the particle was at the position indicated by the

[23] Co-op student from Northwestern University.

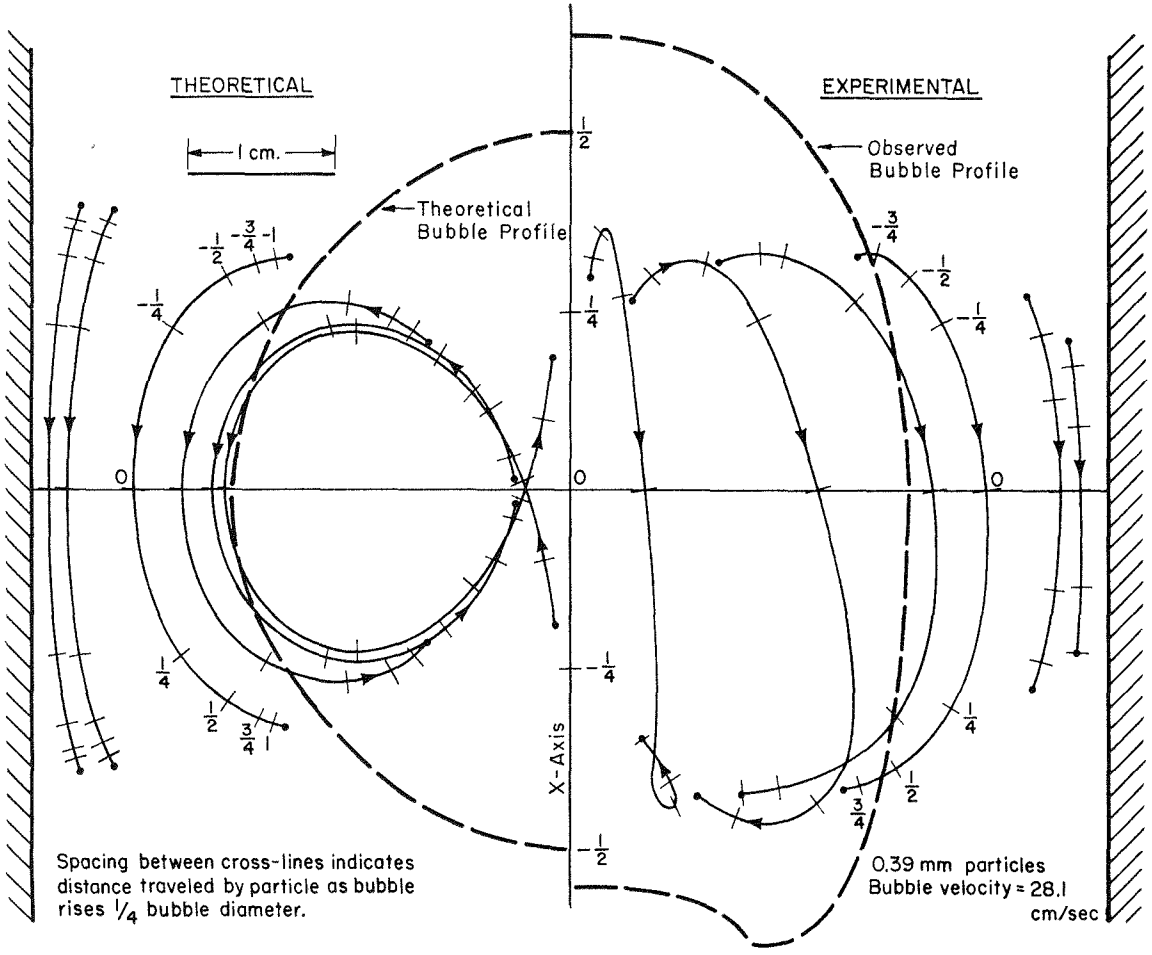

308-196

FIG. II-20. Comparison of Experimental with Theoretical Particle Trajectories for a Bubble with $a/d = 0.63$.

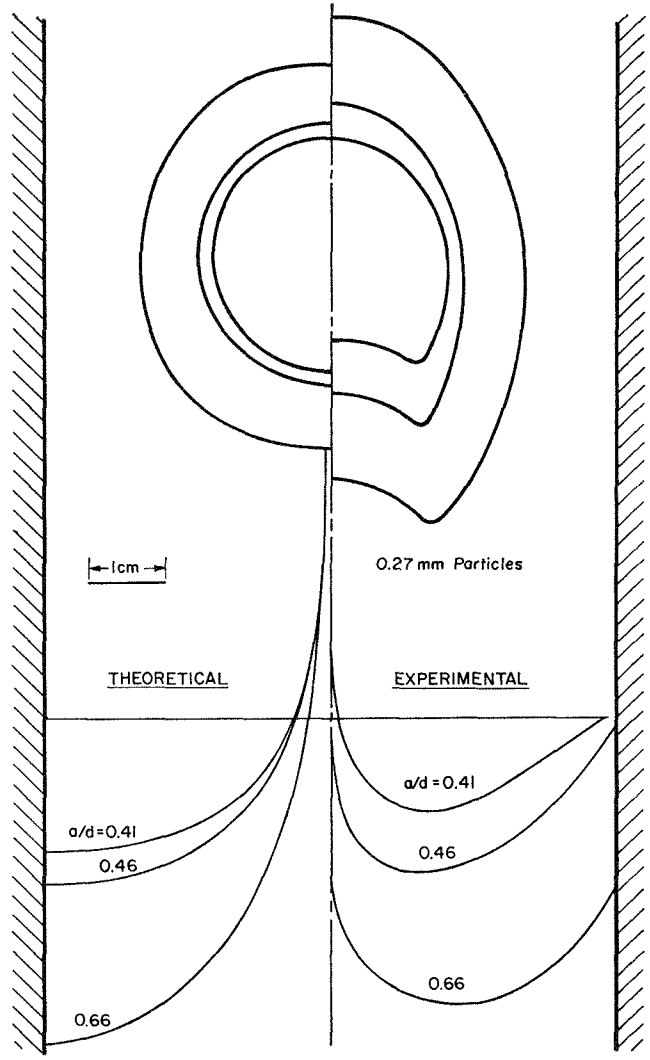

308-225

FIG. II-21. Comparison of Theoretical with Experimental Particle Drift Profiles.

$-\frac{1}{4}$ cross-line. The theory predicts that a particle would be essentially moved from its initial position to its final position as the bubble moves from -1 to $+1$ along the center line. Experimentally, it was found that particle movement was virtually completed as the bubble moved from $-\frac{3}{4}$ to $+\frac{3}{4}$.

Figure II-21 shows the effect of a/d ratio on the particle drift. The initial position of the particles is shown by the solid horizontal line. The theoretical drift profile (left side of the figure) of the particles, in relation to their original positions along the horizontal line, can be compared with the observed drift profile (right side of the figure) for 0.27-mm diameter particles in the 7.3-cm wide column. The drifts for three different bubble sizes resulting in a/d ratios of 0.41, 0.46, and 0.66 are shown.

The data indicate increased particle movement with increased bubble size. The largest observed bubbles had the greatest effect on the particles near the wall, and there was no movement of the particles at the wall for the smallest bubble. This is in contrast to the theoretical prediction, based on an ideal fluid, that the influence of the bubble would extend to the particles at the wall.

It was also concluded from other tests that:

1. Particle movement is primarily in the vertical direction with negligible horizontal movement.
2. The extent of influence by the bubble on particle movement decreases with an increase in particle size.
3. Theory implies that only the a/d ratio would influence the extent of particle motion relative to the bubble; experimental results indicate that both the a/d ratio and the absolute bubble size are significant parameters.

c. FUTURE WORK

Theoretical work will be extended to the case of a chain of rising bubbles and an array of bubbles. Viscosity effects will also be considered.

Future experimental studies will be made to relate particle movement with heat transfer at a wall. A theoretical model appropriate to the planned experiments will also be developed.

2. Mechanism of Heat Transfer Between a Fluidized Bed and the Reactor Wall

(R. D. Patel,[24] L. B. Koppel,[25] J. T. Holmes)

Models proposed to predict coefficients of heat transfer from a gas-fluidized bed to the reactor wall generally require a knowledge of the residence time of fluidized particles at the wall. During the current work, attention has been directed toward improvement of these models and toward experimental verification of the predicted coefficients.

An experimental apparatus (described previously, ANL-7225, pp. 130–131) has been erected and successfully operated to measure both heat transfer coefficients and residence times at the same section of the fluid-bed column wall. Some modifications have been made. In particular, it was found that the previously constructed heater had a large heat loss to the surroundings. This rendered the heat transfer coefficients inaccurate. To circumvent this difficulty, a more elaborate "adiabatic" heater was fabricated, and has been operated very successfully (see Figure II-22). By installing "guard" heaters around the main heater, it was possible to attain nearly adiabatic conditions and negligible heat losses to the surroundings. Thermocouples were mounted in the main and guard heater plates so that their temperatures could be monitored. By adjusting the current to the guard heaters, the temperature of the guard heater enclosure was made to correspond very closely with the main heater temperature. Thus, there was almost no heat loss from the main heater to the surroundings. Data obtained with this heater were very reproducible.

A 35-mm Arriflex motion picture camera driven by a synchronous motor is being used in the particle residence time studies (see ANL-7125, pp. 105–106). The synchronous operation assures a constant time difference between successive frames—important in the subsequent analysis to determine the mean residence time. (Details of the analysis have been published elsewhere.[26])

Preliminary data for residence times and heat transfer coefficients have been obtained for $\frac{1}{8}$-in. acetate spheres fluidized in air. The bed was stirred by a paddle type stirrer to eliminate bubbles. The data indicate that heat transfer coefficients increase as the residence time is decreased:

Air Velocity, based on empty column, ft/sec	Heat Transfer Coefficient, Btu/(hr) (sq ft) (°F)	Mean Residence Time, sec
3.53	18.4	9.2
4.05	24.6	2.4

The mean error in the heat transfer data was about 2%.

Work is continuing on small-particle systems. In

[24] Graduate student from Purdue University.

[25] Consultant from Purdue University.

[26] L. B. Koppel, R. D. Patel, and J. T. Holmes, "Statistical Models for Surface Renewal in Heat and Mass Transfer. Parts I and II". AIChE J. **12**, 941–955 (1966).

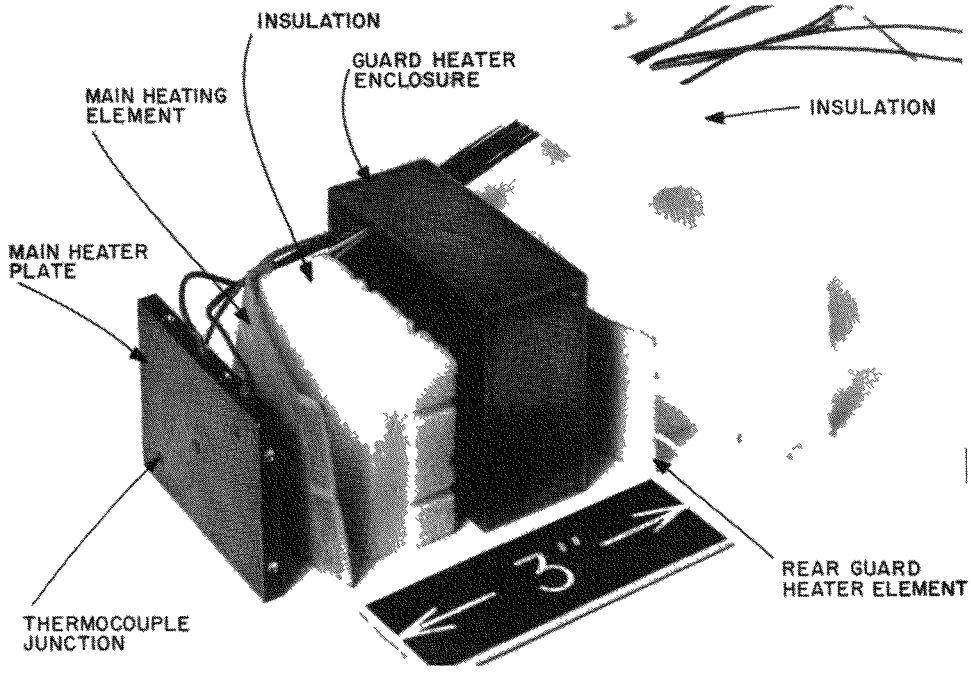

108 9819A

FIG II-22 Exploded View of Adiabatic Heater (Only one guard heating element shown)

particular, two systems of ~30-mesh and ~45-mesh black glass beads and white glass beads are being investigated These particles are more nearly typical of material usually used in a fluidized bed Data are also being obtained for various metal shot particles fluidized in air Particle tagging for residence time studies of these systems will be attempted using fluorescent dyes and ultraviolet lighting

III

Materials Chemistry and Thermodynamics[1]

A. HIGH TEMPERATURE MATERIALS DEVELOPMENT (R. K. Edwards, H. M. Feder, M. Ader)

This program is directed toward the development of nuclear reactor materials that will be subjected to high temperatures. Its objective is to collect basic data on the vaporization and chemical stability of potential fuels, i.e., the oxides, carbides, nitrides, phosphides, and sulfides of uranium, plutonium, and thorium, and their solid solutions; and on the reactions of these materials with other substances. The collected data will be useful for guidance in materials selection; it will also serve to advance knowledge of nonstoichiometry in solids, an important high-temperature phenomenon. Experimentation is carried out quantitatively so as to yield thermodynamic and phase-diagram information. Various complementary methods of investigation are used, according to the requirements of the particular problem.

Studies of the equilibria between vapor and condensed phases of the uranium-urania system, and of the oxidation-reduction equilibria in this system have been concluded. Analogous studies are projected for the U-Pu-O system at U/Pu ratios of interest to fast-reactor fuel use. Some of the specific problems include determinations of (1) the oxygen partial pressures and total vapor pressures by a transpiration method, (2) the phase boundaries of the (U, Pu)$O_{2\pm x}$ phase, (3) the equilibria among the gaseous species (Pu, PuO, PuO_2, and O), and (4) the congruently effusing composition of plutonia. Similar studies on the U-Pu-C system are under consideration. Some mass spectrometric experimentation is being done on the Re-O system in view of the possible use of rhenium as a container material in the U-Pu-O studies. Investigation of the U-UP system by mass spectrometric effusion has been initiated because the available information is uncertain and incomplete.

[1] A summary of this section is given on pages 9 to 12.

1. Condensed Phase Studies (A. E. Martin, F. C. Mrazek)

a. THE URANIUM-URANIA SYSTEM

Final evaluation of the phase-diagram data for the uranium-urania system has been made (ANL-7225, pp. 132–133) and a manuscript has been prepared for journal publication.

b. THE URANIUM-PLUTONIUM-CARBON SYSTEM

A study of selected portions of the uranium-plutonium-carbon system is projected. The primary objective is to establish composition-temperature relations for the phase(s) present in fast-reactor fuels of interest. Definition of the composition-temperature relations is necessary to guide technological developments and also thermodynamic and physical-property studies. A continuing survey of the pertinent literature is in progress. Plans for the modification of facilities for this and for other plutonium studies are fairly well advanced. Sample-pressing, arc-melting, and induction-heating facilities are to be installed in a glovebox having a high-purity inert-gas atmosphere. Metallographic examinations will be conducted in other glovebox facilities available within the Division.

Meanwhile, to gain experience with the special techniques required in working with this system, some simple experiments on the uranium-carbon system have been carried out. Uranium alloys containing 4.5 to 7.6 w/o carbon were prepared in a Zak arc melter equipped with a water-cooled copper hearth and a carbon upper electrode. No difficulties were encoun-

tered. Other alloys were prepared from liquid uranium held in graphite crucibles for about one hour. Two alloys thus prepared at 1590 and 1770°C were analyzed and found to contain 0.36 and 0.60 w/o carbon, respectively. These concentrations are in the range reported[2-6] for the solubility of carbon in liquid uranium. In a similar but longer experiment, a relatively thick uranium carbide layer formed between the crucible and the uranium melt after 22 hours at 1771°C. A comparison of the inner diameter of the crucible before and after the experiment showed that most of the carbide had formed on the uranium side of the original graphite-uranium interface. It was obvious that more carbon had diffused across the interface toward the uranium than had uranium in the opposite direction. These observations agree with those of other workers[7] who studied the growth of the carbide layer between uranium and carbon at 800 to 1100°C, using markers to identify the location of the original interface.

Thermal analysis is likely to be a particularly useful technique for studying U-Pu-C phase relations. For this purpose, a Leeds and Northrup Model 8640 recording optical pyrometer was obtained for use in both ordinary and differential thermal analysis (DTA). The response time of the instrument was found to be satisfactory: the thermal halts associated with the freezing and melting of 4 grams of alumina (m.p. 2050°C) and of 8 grams of platinum (m.p. 1773°C) were easily detected by ordinary thermal analysis both on cooling and heating at 30 to 60 degrees per minute. The progress of the DTA will be automatically recorded as a single curve on an x-y recorder. Although the recording optical pyrometer has not been tested in the DTA mode, there is little doubt that it will operate satisfactorily.

[2] A. I. Snow, CT-954 (1943).

[3] T. H. Carter, CT-609 (1943).

[4] M. W. Mallett, A. F. Gerds, and H. R. Nelson, J. Electrochem. Soc. **99**, 197 (1952).

[5] E. K. Storms, *Thermodynamics, Proceedings of the Symposium on Thermodynamics with Emphasis on Nuclear Materials and Atomic Transport in Solids*, Vol. I, International Atomic Energy Agency, Vienna, 1966, p. 309.

[6] P. Guinet, H. Vaugoyeau, and P. L. Blum, Comptes Rend. **261**, 1312 (1965).

[7] N.S.A. **18**, 19984 (1964).

2. Vaporization Studies

a. DETERMINATION OF COMPOSITIONAL CHANGES BY MASS-SPECTROMETRIC EFFUSION ("TRAVERSE METHOD") (J. W. Reishus, G. E. Gundersen)

In previous reports[8, 9] thermodynamic arguments were used to develop equations relating the changing, relative partial pressures of two vapor species to the composition of a vaporizing binary condensed phase of variable composition. A new experimental technique based on these equations was described. As predicted, it was found possible to evaluate the changing composition of urania from continuous observations of the ion currents of the two major gaseous species, UO and UO_2. A manuscript describing this work is in preparation for journal publication.

b. VAPORIZATION OF URANIUM MONOPHOSPHIDE (J. W. Reishus, G. E. Gundersen)

Investigations are being made of the high-temperature properties of uranium monophosphide, a potentially useful component of nuclear fuels, because the existing information (including the U-UP phase diagram) is uncertain as well as incomplete. In this study the basic quantities being determined are the temperature dependences of the partial pressures of vapor species in equilibrium with uranium monophosphide. The experimental technique involves vaporization of uranium monophosphide within an effusion cell, and analysis of the effusing species by means of a Bendix TOF mass spectrometer. Tungsten was chosen as the container material when it was found (by X-ray diffraction analysis of residues) to be inert to uranium monophosphide up to 2150°C, the maximum temperature of the present experiments. Ionizing electron energies of 15 eV were used in order to avoid fragmentation effects which were observed at higher energies. The compositions of uranium phosphide samples were determined by chemical analysis.[10]

Between 1800 and 2150°C, the primary species vaporizing from uranium monophosphide were found to be U(g), P(g), and P_2(g), as previously reported by Gingerich and Lee.[11] Also in agreement with them, the hypothetical species UP(g) was not observed. Although P_4(g) was observed, its presence was attributed to the vaporization, at relatively low temperatures, of phosphorus which had condensed on the heat shields above the effusion cell. A correction was applied for the effect

[8] ANL-6925, pp. 168–170.

[9] ANL-7225, pp. 135–136.

[10] G. W. C. Milner, D. H. Rowe, and G. Phillips, "The Analysis of Uranium Phosphides," AERE-R-4906, April, 1965.

[11] K. A. Gingerich and P. K. Lee, J. Chem. Phys. **40**, 3520 (1964).

of this secondary vaporization on the observed partial pressure of $P_2(g)$. Minor amounts of UO(g) and $UO_2(g)$ due to slight oxygen contamination (0.27%) of the uranium monophosphide were also detected during the initial heating. The intensities of these species decreased steadily and, generally, became less than $\frac{1}{30}$ that of the U(g) after one hour at temperature.

The preliminary mass spectrometric experiments gave evidence that stoichiometric UP changes composition during vaporization. Continuous effusion from a starting composition $UP_{1.00\pm0.03}$ at 2010°C yielded a much higher concentration of P plus P_2 than U in the vapor, thereby indicating that the monophosphide phase was becoming hypostoichiometric with respect to phosphorus (i.e., UP_{1-x}). Confirmation of the changing vaporization behavior and composition of the residual solid was obtained by an effusion experiment in which over 50% of a sample of initially stoichiometric UP was vaporized at ~2120°C. The rate of loss in weight of the sample was observed to increase steadily over successive time periods. Moreover, metallographic analysis of the quenched residue from this experiment revealed the presence of uranium as a minor phase located at monophosphide grain boundaries. From appearance alone, it could not be decided whether uranium existed as a second phase at the temperature of the experiment, or, alternatively, had precipitated from hypostoichiometric uranium monophosphide on cooling. X-ray diffraction analysis of the residue showed that the lattice parameter of the UP was unchanged from its original value of $a_o = 5.589$ Å.

Baskin and Dusek,[12] on the basis of lattice parameter and metallographic analyses, reported that uranium monophosphide formed a hypostoichiometric phase which appeared to vaporize congruently at about 2000°C. Gingerich and Lee[2] concluded that uranium monophosphide vaporizes congruently between 1477 and 1977°C; however, from extrapolation of their data they inferred that incongruent vaporization would occur at temperatures above 2127°C. Our results, thus far, give no indication of congruent vaporization of monophasic uranium monophosphide. Instead, they suggest that UP, on vaporization, becomes progressively hypostoichiometric until a two-phase mixture, UP_{1-x} (s, sat'd with U)[13] + U(ℓ, sat'd with UP_{1-x}), forms.

Preliminary equations for the partial pressures of U, P, and P_2 over hypostoichiometric UP (possibly the two-phase mixtures) were derived by correlating the data from two types of effusion experiments, mass spectrometric and weight loss.

TABLE III-1. Normalized Mass Spectrometric Measurements of U, P, and P_2 above Hypostoichiometric Uranium Monophosphide

Temperature Range: 2073 to 2423°K

Species	Temperature Dependence, Log I_iT[a]	ΔH (kcal/mole)
U	13.4189 − 26,268/T	120.2 ± 0.3
P	15.6915 − 31,494/T	144.1 ± 1.5
P_2	17.7506 − 37,351/T	170.9 ± 4.2

[a] All ion currents, I_i, in the same arbitrary units. The equations reproduce the values of I_UT, I_PT, and $I_{P_2}T$ to within 1.4, 4.0, and 7.7%, respectively (95% confidence level).

The temperature dependences (1800 to 2150°C) of the U^+, P^+, and P_2^+ ion currents were obtained in three series of measurements for which the starting materials were: (1) 0.1 g of powdered $UP_{1.00\pm0.02}$, preheated for 5 hr at 2000°C; (2) 75 mg of uranium plus 300 mg of a sintered UP disk, preheated 6.7 hr at ~1972°C; and (3) the residue from series 2 plus 36 mg of uranium, preheated 2 hr at ~2040°C. Because the ion currents were found to be reversible with temperature, we may conclude that either a monophasic material of constant composition was present, or that equilibrium between U(ℓ) and UP_{1-x}(s) was always maintained. Furthermore, because of the agreement of the initial ion-current curves for all three series, it is believed that all three came to the same phase composition(s) by vaporization during the preheat periods. The residues from these runs have not been analyzed; however, the residue from a similar run, which gave similar ion-current curves, was found to have a P/U atom ratio of 0.95 ± 0.02. The ion-current data (log I_iT *vs.* $1/T$) for each species was least squared and the three series were combined by normalizing (for different instrumental conditions) at 1961°C, the approximate midrange temperature. The combined equations and derived partial molar enthalpies of vaporization are given in Table III-1.

The partial pressure of an effusing species, p_i, is related to the ion current, I_i, by the equation

$$I_iT = C\sigma_i\gamma_iP_i \qquad (1)$$

where T is the absolute temperature, C is a constant characteristic of the electronics and geometry of the mass spectrometer, σ_i is the ionization cross section, and γ_i is the multiplier efficiency. Otvos-Stevenson[14] cross sections were used in the calculations ($\sigma_U = 55.7$, $\sigma_P = 13.8$, $\sigma_{P_2} = 27.6$). Multiplier efficiencies were estimated on the assumption[15] that ions of equal

[12] Y. Baskin and J. T. Dusek, "Annual Progress Report for 964, Metallurgy Division," ANL-7000, 1964, p. 87.

[13] M. Bowman, Los Alamos Scientific Laboratory, reports that the hypostoichiometric range may extend down to $UP_{0.96}$ at 1900°C (private communication).

[14] J. W. Otvos and D. P. Stevenson, J. Am. Chem. Soc. **78**, 546 (1956).

[15] W. Ploch and W Walcher, Rev. Sci. Instr. **22**, 1028 (1951).

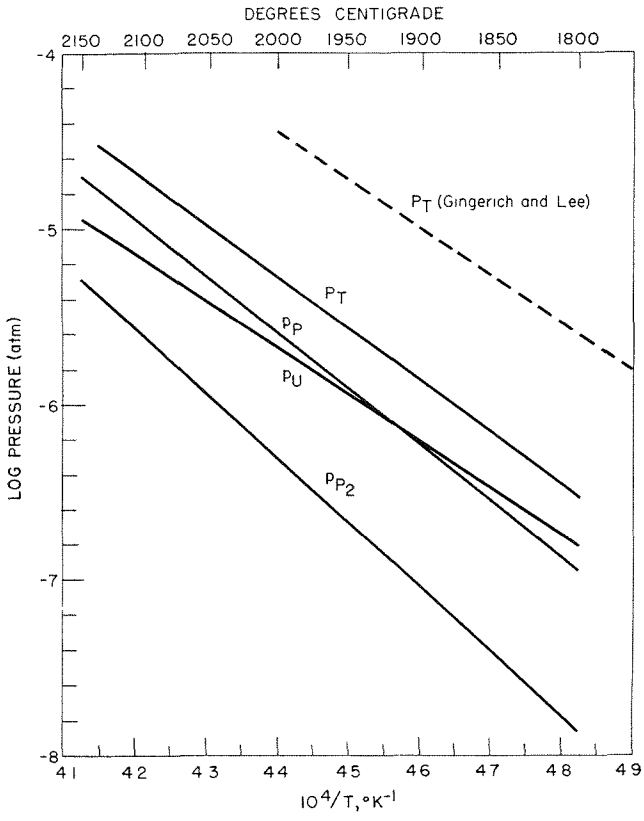

308-416

FIG. III-1. Vapor Pressures over Hypostoichiometric Uranium Monophosphide *vs.* Reciprocal Temperature (2073 to 2423°K).

velocity have equal multiplier efficiencies, i.e., $\gamma_1/\gamma_2 = (M_2/M_1)^{1/2}$, where M is molecular weight. The constant C may be determined by combining the results of experiments in which total mass loss is measured with results of experiments in which the ratios of species in the vapor are measured.

Total weight loss during effusion at about 2000°C was measured for samples comparable to those used in the temperature-dependence experiments. After normalizing the weight losses to the same effusion conditions (time, temperature, orifice diameter), they were found to agree within 10%. The actual weight loss was then used to calculate the constant C in eq. 1. By appropriate substitutions, the partial pressures themselves were ultimately derived.

The combined weight-loss and mass spectrometric measurements led to the tentative partial-pressure equations (2073 to 2423°K):

$$\log p_U \text{ (atm)} = 5.8905 - 26{,}268/T; \quad (2)$$

$$\log p_P \text{ (atm)} = 8.2842 - 31{,}494/T; \quad (3)$$

$$\log p_{P_2} \text{ (atm)} = 10.1451 - 37{,}351/T. \quad (4)$$

The combined uncertainties (95% confidence level) of these pressures are ±4.5, ±7.1, and ±10.8%, respectively. Figure III-1 shows a plot of these equations and includes, for comparison, the total pressures (P_T) from the mass-spectrometric effusion experiments of Gingerich and Lee,[11] and from a summation of the partial pressures reported above. The disagreement with Gingerich and Lee was not unexpected inasmuch as they had reported P(g)/P_2(g) ratios which were clearly nonequilibrium values. Furthermore, they found UO to be a major species during effusion, which indicates appreciable oxygen contamination of their samples, and interaction between uranium monophosphide and their tantalum effusion cells.

The internal consistency of the present results was found to be good. The second-law Gibbs free energy, enthalpy, and entropy of dissociation of P_2(g), calculated from eq. 3 and 4 at 2234°K, the approximate midrange temperature of the experiments, were 15.6 kcal/mole, 117.3 kcal/mole, and 29.4 eu, respectively. These values are in good agreement with corresponding values, 55.1 kcal/mole, 119.2 kcal/mole, and 28.7 eu, calculated from spectroscopic data.[16]

A preliminary value for the enthalpy of formation of uranium monophosphide [$\Delta Hf°$(UP, c)], which thus far is unreported, was estimated using the present results. From eq. 2 and 3 and enthalpy-of-formation data[16] for U(g) and P(g), the value $\Delta Hf°_{2234}$ (UP, c) = −99 ± 4 kcal/mole was derived for the reaction

$$U(\ell) + \tfrac{1}{2} P_2(g) = UP(c).$$

By extrapolation of the mean heat capacity for uranium monophosphide, 13.8 cal/deg/mole[17] for the range 800 to 1200°C, the value $\Delta Hf°_{298}$ (UP, c) = −77 ± 5 kcal/mole was obtained for the reaction

$$U(\alpha) + P(\alpha\text{-white}) = UP(c).$$

Future experiments will be carried out with the mixtures which are definitely biphasic—$U(\ell)$ + UP_{1-x} and UP_{1+x} + U_3P_{4-y}—so that the vaporization behavior of uranium monophosphide can be bracketed.

c. CONTAINER MATERIALS FOR PLUTONIA-CONTAINING SYSTEMS (J. E. BATTLES, G. E. GUNDERSEN)

The question of what container or crucible material to use in projected thermodynamic studies of the Pu-O and U-Pu-O systems is of primary importance because of the possible interaction between samples and their containers. Refractory metals possess desirable properties for the high-temperature work contemplated. For

[16] D. R. Stull and G. C. Sinke, *Thermodynamic Properties of the Elements*, Advances in Chemistry Series, No. 18, American Chemical Society, Washington, D. C., 1956.

[17] J. E. Brugger et al, ANL-7225, p. 154.

example, temperature gradients are minimized relative to refractory oxide crucibles, the conductivity of metals enables direct heating of crucibles by induction or by electron bombardment (as in our mass spectrometer), and the fabrication of parts (such as condenser tubes for transpiration experiments) is facilitated. Estimates of the stability to oxidation of the refractory metals (m.p. °C) tungsten (~3410), rhenium (~3180), tantalum (~3000), molybdenum (~2620) and iridium (~2450) indicated that rhenium might show the most satisfactory combination of properties. The fragmentary thermodynamic data available also indicated that rhenium might be more suitable than tungsten, even though the latter had been used quite successfully in the urania studies. The considerably higher oxygen pressures expected over plutonia-containing systems could cause oxidation of tungsten to volatile oxides. Some simple experiments were made to determine the relative stabilities of rhenium and tungsten.

(1) *Relative Stabilities of Rhenium and Tungsten to Oxidation.* Urania of composition $UO_{2.095}$ (the use of hyperstoichiometric urania simulates the higher oxygen pressures that would prevail if plutonia were present) was heated in a Bendix TOF mass spectrometer to about 1800°C under three sets of conditions:

1. Tungsten effusion cell containing mixed $UO_{2.095}$ and rhenium powders;
2. Rhenium effusion cell containing mixed $UO_{2.095}$ and tungsten powders;
3. Rhenium effusion cell containing $UO_{2.095}$ powder.

In experiments 1 and 2, only tungsten-containing vapor species were observed, which signifies the greater stability of rhenium to oxidation. First detectable at 1150°C, the effusing species were those normally found[18, 19] during vaporization of solid WO_2 and WO_3, namely, the parent vapor species $W_2O_6^+$, $W_3O_9^+$, and $W_4O_{12}^+$, and their associated fragments. In experiment 3 the effusing species, beginning at 980°C, were ReO_2^+, ReO_3^+, $Re_2O_5^+$, $Re_2O_6^+$, and $Re_2O_7^+$.

The results of experiment 3 indicate that even rhenium crucibles, though more stable toward oxidation, will probably react with plutonia-containing phases. Hence, the equilibria among rhenium oxide species becomes relevant in order to know whether the extent of the reaction is tolerable. Because such information is virtually nonexistent a limited study of vapor equilibria in the rhenium-oxygen system was undertaken. Accordingly, the vaporization of rhenium dioxide (ReO_2), which gives rise to numerous oxide species, is being examined mass spectrometrically. The results obtained thus far are discussed below.

TABLE III-2. Approximate Appearance Potentials of Species Vaporizing from Solid ReO_2 at 850°C

	eV[a]
$Re_2O_7^+$	13.1
$Re_2O_6^+$	16.3
$Re_2O_5^+$	~20
ReO_3^+	15.6
ReO_2^+	~19

[a] Correction of −1.0 eV applied; based on appearance potential of H_2O^+ = 12.83 eV.

(2) *Vapor Species Over ReO_2.* Rhenium dioxide was heated to about 850°C in a platinum effusion cell in the Bendix TOF mass spectrometer. The effusing species that were observed at an ionizing electron energy of 25 eV were ReO_2^+, ReO_3^+, $Re_2O_5^+$, $Re_2O_6^+$, and $Re_2O_7^+$. The corrected appearance potentials of these ions are listed in Table III-2. At an ionizing electron energy of 17 eV, the only species observed were $Re_2O_7^+$, ReO_3^+, and $Re_2O_6^+$, with relative ion intensities 90:10:1. At the conclusion of the experiment, X-ray diffraction analysis showed the solid residue in the crucible to be mainly rhenium metal. This result, together with the observation that the vapor phase was predominantly Re_2O_7, suggests that at 850°C vaporization is accompanied by disproportionation according to the equation

$$7\ ReO_2(c) \rightarrow 2\ Re_2O_7(g) + 3\ Re(c).$$

Further experiments will be carried out to obtain values of the enthalpies and entropies of formation of the gaseous rhenium oxides. In addition, iridium, although lower melting than rhenium, will be examined as a possible container material because of its greater resistance to oxidation.

d. THE CONGRUENTLY VAPORIZING COMPOSITION OF URANIA (P. M. Danielson)

A previous report[20] on the congruently vaporizing compositions of urania revealed the necessity for the unambiguous establishment of these compositions as a function of temperature. Accordingly, experiments were made in which approximately 50% of large samples of urania were vaporized from a tungsten Knudsen effusion cell into an ultrahigh vacuum. The compositions of the residues were determined by combustion analysis. Thus, the experiments were conducted in a manner intended to keep the results free from the principal weaknesses of previous studies, namely, (1) insufficient amounts of sample vaporized, and (2) vac-

[18] R. J. Ackermann and E. G. Rauh, J. Phys. Chem. 67, 2596 (1963).

[19] J. E. Battles, Technical Documentary Report No. ML-TDR-64-272, August, 1964.

[20] ANL-7125, p. 122.

TABLE III-3. Compositions of Congruently Vaporizing Urania

Run	Temp. (±10°C)	Composition, O/U Atom Ratio	
		Initial (±0.01)	Residual (±0.004)
4[a]	2290	2.09	1.940
6[a]	2290	1.89	1.948
7[a]	2200	1.92	1.970
8[a]	2230	1.92	1.967
9[a]	2200	1.93	1.971
10[a]	2140	1.90	1.985
11[a]	2026	1.91	1.996
12[a]	2245	1.90	1.962
13	2072	2.09	2.000
16	2238	2.09	1.996
17	2241	2.09	1.978
18	2183	2.09	1.992
19	2172	2.08	1.978
21	2257	1.99	1.960
22	2254	2.09	1.984
24	2275	2.09	1.995
25	2080	2.02	1.990
26[b]	2377	1.98	1.949
27[b]	2366	1.93	1.955
28[b]	2368	1.87	1.934
29[b]	2331	1.87	1.954
30[b]	2332	1.93	1.958
31[b]	2351	1.95	1.958

[a] Reported previously (ANL-7225, p. 137).

[b] Subject to correction because of unresolved possible error in analysis.

uum environments which might have buffered the urania at compositions which did not vaporize congruently. The experimental procedures were discussed in a previous report.[21]

The accumulated data are given in Table III-3, and are plotted as a function of temperature in Figure III-2. The congruently vaporizing compositions were approached from both higher and lower initial O/U ratios, signifying that constant compositions were attained. The results show that the composition of congruently vaporizing urania is not only hypostoichiometric over the temperature range investigated (2026–2377°C), but that it becomes increasingly hypostoichiometric as temperature is increased. Runs 13, 16, 17, 18, 22, and 24 are not included in the figure since the data indicated that the initial O/U ratios were probably too high to allow the samples to reach the congruently vaporizing compositions during the period of the runs. Additional heating of these samples would have left residues too small for accurate combustion analysis.

A control run with a sealed tungsten crucible was made to determine whether or not reduction of urania occurs owing to diffusion of oxygen into tungsten, and whether or not tungsten inclusions were present in the residue owing to reaction or dissolution while at temperature. (The presence of 0.1% of oxidizable tungsten in a 0.5-g sample of the residue can cause a positive error of ~0.004 in the O/U analysis.) A tungsten crucible containing a sintered pellet of $UO_{2.000 \pm 0.004}$ was sealed under vacuum by electron-beam-welding of a tungsten cover. The crucible was leak tested and found to be gas tight. It was heated at 2154°C under conditions simulating those of the previous runs, cooled, and then opened. Combustion of the residue to U_3O_8 showed that, within experimental error, the O/U ratio had not changed. The product from the combustion analysis was analyzed by X-ray fluorescence and found to contain <0.005 w/o tungsten. A portion of the urania pellet was also examined metallographically for tungsten, and the results did not differ markedly from the X-ray fluorescence analysis. The results of this experiment indicate that interaction between tungsten and urania was probably negligible and that the data given in Figure III-2 are valid.

Some additional runs will be conducted to clarify the deviations from the line in Figure III-2, such as the results of runs 4 and 6.

e. TOTAL VAPOR PRESSURE OF URANIUM-BEARING SPECIES AND PARTIAL PRESSURE OF OXYGEN OVER URANIA (M. Tetenbaum, P. D. Hunt)

Measurements of the total pressure of uranium-bearing species over urania by the transpiration method and the simultaneous determination of the partial pressures of oxygen have been completed and the results presented in the previous report.[22] The measurements were conducted with H_2-H_2O gas mixtures which served, by equilibration, to fix the oxygen partial pressures and thereby to control the compositions of the solid phases. It is believed that the currently available data can be fitted by an improved model in terms of vacancies, interstitials, and their energies of formation and interaction. Two manuscripts covering this work are being prepared for journal publication.

f. TRANSPIRATION STUDIES OF THE U-Pu-O AND U-Pu-C SYSTEMS (P. E. Blackburn, S. F. Banaszek, P. D. Hunt)

A review and an evaluation of the literature on the uranium-plutonium-oxygen system has been completed and one for the uranium-plutonium-carbon system is in progress. The objective has been to delineate for these systems questionable or unknown areas of

[21] ANL-7225, pp. 136–137.

[22] ANL-7225, pp. 137–139.

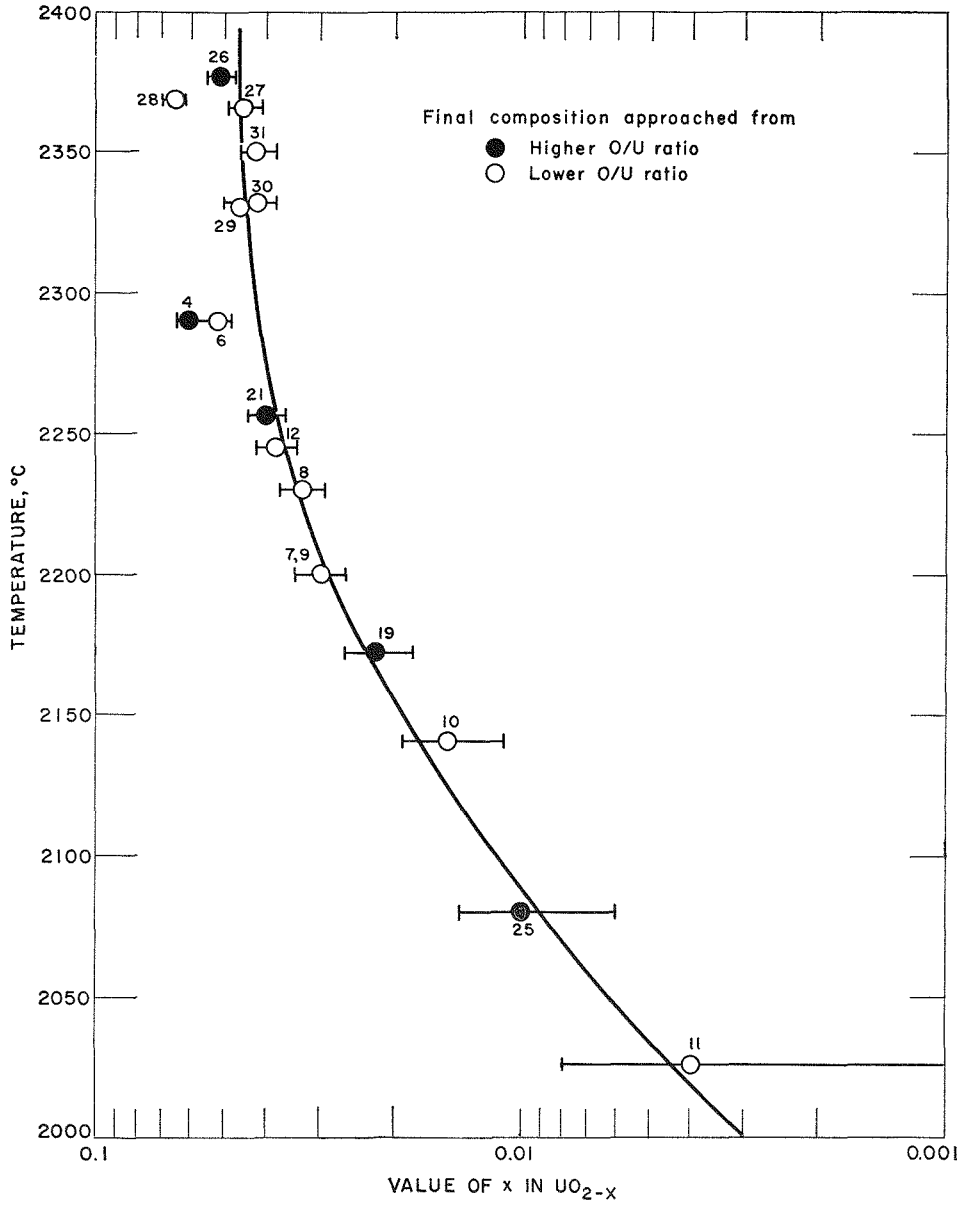

308-420

FIG. III-2. Composition of Congruently Vaporizing Urania *vs.* Temperature. (Numbers at data points indicate run numbers.)

high-temperature thermodynamic study which remain to be investigated.

At the present time it is evident that measurements of the activities of the anionic components in these ternary systems will be helpful in guiding expected fuel technology developments. Accordingly, transpiration studies are projected for both ternary systems within composition ranges which will be relevant to fuel use. The equipment for these studies is being assembled. Blueprints are being prepared for the glove-box facility which will be required for safe handling of plutonium.

While this equipment is being built, an existing transpiration apparatus (previously used for the urania studies in Part e) will be modified for a limited study of the U-C system so that some intended new procedures (such as gas recirculation) can be tested without the encumbrances of handling plutonium. Rhenium, which has a low solubility for carbon and does not form carbides, will be substituted for tungsten in the hot zone. A rhenium condenser tube is being welded in the shop, and a sample container will be machined from rhenium rod now on order. A rhenium furnace tube is on hand. Carbon activities will be determined by passing high-purity hydrogen over uranium carbides and measuring the partial pressures of the carbon-con-

taining gases produced. It is planned to recirculate the gas continuously during the experiment until equilibrium is reached. Three methods for analyzing the carbon-containing gases, principally methane and acetylene, have been considered: infrared spectroscopy, mass spectrometry, and gas chromatography.

At 2000°K the methane concentration in equilibrium with U + UC and 1 atm of hydrogen is about 10^{-6} atm, or 1 ppm. The MSA[23] infrared detector is unsuitable for measuring this concentration of methane since it has a maximum sensitivity of 20 ppm. If the total pressure is increased to 10 atm, the equilibrium pressure of methane becomes 10^{-4} atm, a concentration which could be detected with adequate precision by infrared spectroscopy. However, the problems of working at 10 atm and above 2000°K prompted us to reject infrared detection.

[23] Mine Safety Appliances Co., Pittsburgh, Pa.

Mass spectrometric analysis has also been rejected because of the cost of obtaining an instrument which will detect with adequate precision concentrations of methane as low as 0.1 ppm.

At present it is planned to analyze the transpiration gases by gas chromatography. An available gas chromatograph equipped with a flame ionizer is being tested to determine its sensitivity for methane. The instrument has been modified for introduction of small samples of hydrogen-methane mixtures. Test samples are being prepared by the analytical group.

g. VAPOR DEPOSITION OF TUNGSTEN (J. E. Battles, G. E. Gundersen)

A method has been developed for cladding tungsten-urania cermets with tungsten by vapor deposition from tungsten hexafluoride. A manuscript describing the work is being prepared for an ANL topical report.

B. CHEMISTRY OF FAST REACTOR FUELS (C. E. Crouthamel, P. A. Nelson)

INTRODUCTION

The program on the chemistry of fast reactor fuels was initiated in July, 1966. A group was formed whose chief objective is to determine the chemical behavior of fast reactor fuels upon irradiation in order to form a basis for the development of new fuel with increased burnup capability. A major effort has involved the design of a recirculating helium atmosphere enclosure along with many other modifications for one cell of the Chemistry Division cave complex. It was decided that a cave containing an inert atmosphere would be required for this work. The inert atmosphere will permit prolonged study of fuel specimens and reexamination of specimens after storage. Carbide fuels are especially subject to atmospheric attack. The M-4 cell in the Chemistry Division cave facilities has become available for use in this program, and design work has been completed for installation of an inert atmosphere box and sealed manipulators in this cave. Work on the modification of the cave facilities is scheduled to begin in January 1967.

Another major task has been the evaluation of a group of large complex instruments for application to this program and the generation of detailed specifications for bidding. This has been completed for a spark source mass spectrometer, a solid-state alpha, gamma and X-ray analyzer system, a metallograph, and a shielded electron probe analyzer system.

In addition, the capability for microsampling of irradiated fuel has been developed in the group. And this capability has been extended beyond the standard techniques with the evaporation of microsamples by an optically restricted laser beam. This will augment the electron probe and microdrilling techniques which were already being used. Laser beam microsampling is expected to make especially important contributions to the applicability of the spark source mass spectrometer and the solid-state radiation detector systems in observing the irradiated fuel microstructure. Radiographic techniques and solid state fission and alpha particle track detectors also are being evaluated for their applicability to this program in the elucidation of microstructure detail and also the more widely distributed concentration gradients of alpha active or fissile atoms.

Fast reactor ceramic fuels undergo chemical changes during irradiation which may significantly affect (1) the compatibility of the fuel and jacket, (2) the physical properties of the fuel, (3) the extent of the fuel swelling and, thus, (4) the useful life of the fuel. The relative combined affinities of the fission elements for the anionic elements in the fuel are different from those of the uranium and plutonium from which they were

bred; hence, the oxidizing potential (or carburizing potential, as the case may be) of the fuel will change with burnup. In addition, the fission elements and anionic elements migrate during irradiation under the influence of the large temperature gradients. The neutron flux and energy spectrum vary as a function of location in the reactor causing variations both in the distribution of and total rates of fissioning and neutron capture throughout a fuel element. This complex behavior will be studied by analyzing highly radioactive fuel specimens by both standard and special techniques some of which have been indicated above. All ceramic fuels of interest for the fast reactor program at Argonne, and especially those ceramic fuels irradiated in EBR-II which are prototypes of fuel elements for full-scale fast reactors, will be studied in this program; Pu-U carbides, oxides, and nitrides will be studied as well as other ceramic fuels.

It is desired to develop methods of analysis which will determine both the chemical and isotopic fuel composition as a function of the axial and radial locations within the fuel. In order to determine irregularities in composition at grain boundaries (especially changes in fission product and impurity element content), it will be necessary to utilize microanalysis techniques which will deal with areas of 1 to 100 sq. microns.

Techniques for cutting, grinding, and polishing fuel specimens by means which can be applied in a shielded high-purity helium atmosphere were developed and demonstrated in an air atmosphere. Tests of these techniques and equipment now have been initiated in a high-purity helium atmosphere.

1. Chemical Studies of Irradiated Ceramic Fuels (N. Chellew, M. Adams, C. C. Honesty)

A program is being initiated for the study of irradiated ceramic fuels, particularly uranium-plutonium carbides. The effects to be studied are primarily concerned with the chemical behavior of uranium, plutonium, carbon, and fission products. Initially, measurements of diffusion and gross stoichiometry changes will be attempted. These studies will require the use of a cave for the sample preparations and special analytical instruments.

Fuel-evaluation facility. A cave facility has been designed for the metallographic preparation, examination, and sampling of ceramic fuel specimens. Examination of the problems associated with handling and transporting irradiated fuel, reactive with air and moisture, indicated that this cave should be an inert atmosphere facility and that instruments for chemical analysis of prepared material should be located near the cave. If this is not possible, it would appear necessary to establish good sample communication with the instrument complex. A pneumatic tube system is being considered for operation between the Chemistry Division cave and the Chemical Engineering Division instrument complex. Present plans call for the adaptation of one cell (cell M-4) in the Chemistry Division cave for handling the fuel specimens available for study. Major adaptations to the cell will include the installation of a steel enclosure for the metallographic preparation and sampling procedures in inert atmosphere and providing suitable facilities adjacent to the box for fuel transfer and preliminary wet chemical treatment of fuel samples. The metallographic preparation-sampling enclosure will contain hermetically sealed Model "J" (extended reach) manipulators, three viewing windows, and necessary transfer ports. Areas allocated to fuel transfer and wet chemical operations will each contain one viewing window and a pair of Model "8" manipulators.

At one of the window positions of the inert atmosphere enclosure a periscope unit will be installed with optical relays for use with a low power microscope to be used with microsampling equipment. For correlations of structure with properties found during subsequent work, a high quality shielded metallograph will be required. Specifications for this instrument have been prepared and sent out for bidding. This instrument will be located outside the cave proper. It will be connected to the helium atmosphere cave through a sample transport hole in the cave wall.

Sampling with a microdrill. In the chemical study of ceramic fuels information on fission product and uranium-plutonium distribution in irradiated specimens is important. Microdrilling of defined areas of the fuel specimen appeared to be one of the simpler methods for obtaining analytical samples from which distribution data for selected elements could be obtained. Analyses of cerium, cesium, ruthenium, zirconium, yttrium, strontium, uranium, and plutonium could likely be carried out on individual samples weighing as little as 250 μg. A drilling machine adapted for remote sampling of irradiated ceramic fuels has been designed, constructed and tested.

The drill modified for remote use was a Dumore series-27 microdrill (The Dumore Co., Racine, Wis.) equipped with a motor control which would vary the rotation speed of the electrically driven drill between 0 and 17,000 rpm. The commercial unit contained a

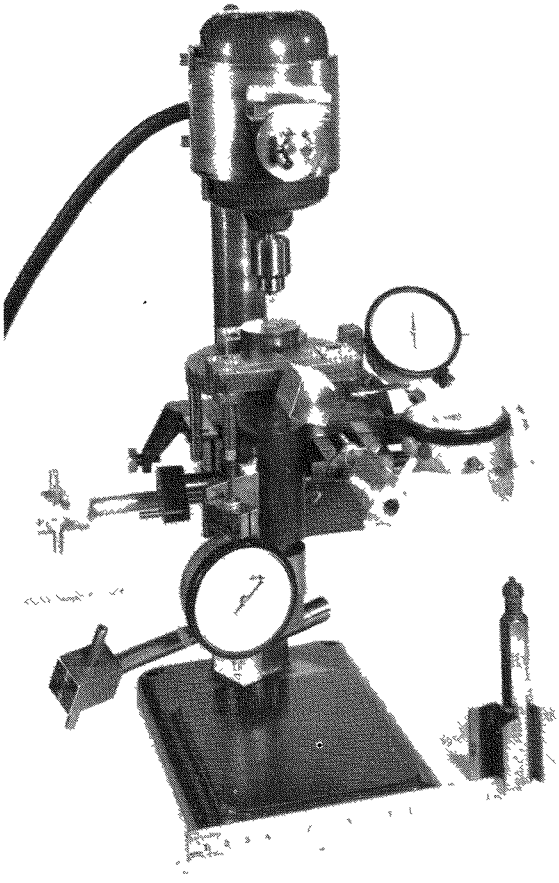

308-125

FIG III-3. Microdrill Adapted for Remote Use.

conventional sample table with provisions for horizontal (x-y) and vertical (z) motions. The z travel was accomplished by use of a counterbalance system for the sample table which required relatively delicate adjustment for in-cell operation. The counterbalance mechanism was modified so that the rate of advance of the specimen into the rotating drill could be sensitively controlled by turning a knob located near the front of the microdrill. Dial gages were provided to measure the amount of all drill table movements to within one mil. Other modifications to the production drill included adapting all control knobs to facilitate their operation with a manipulator, and adding a miniature vise arrangement to the table to permit clamping of Bakelite molds in which the fuel specimens will be mounted (Figure III-3).

Because of the hardness and abrasive nature of ceramic fuels, the drills selected for the initial tests were those typically used for production drilling of hardened tool steels. The spade-type drills employed were fabricated of "Carboloy 883" (reported composition WC 6% Co) with shank diameters of 28 to 40 mils. Since positioning of these small drills in the microdrill chuck would be difficult by remote operation, the drills were first mounted in a ⅛-in. OD brass rod with the use of epoxy resin. The miniature drills were inserted in holes centrally drilled in the rod so that approximately ¼ in. of the cutting end protruded.

Radially sectioned specimens of dense UO_2 used in the drilling tests were first mounted in Bakelite molds with epoxy resin then ground and polished. The tests have provided information on drill life, hole diameters produced by various drills, weight of sample per mil of drill depth, and the capability of the modified microdrill for following a predefined sampling pattern in fuel material.

The tests demonstrated that a ratio of hole depth to drill diameter of at least two could be achieved for 10, 20, and 29 mil drills. Although only one drill broke after about 240 mils of depth travel in the UO_2, dulling of the cutting edge of the flute was evident after each initial test of the drill. Upon extraction of the drill from the work, the powder sample produced was retained on the surface of the specimen as a mound built up around the circumference of the hole. Except for holes in which the ratio of hole depth to drill diameter was as large as three, the holes were regular and within two mils of the nominal drill diameter.

The weight of selected powder samples obtained with drilling was determined with the use of a Cahn microbalance. The weight ratios of samples produced with 10, 20, and 29 mil drills were, respectively, 1:3.3:9.1 at constant hole depth. The similarity of these ratios with those calculated for the cross sectional area of 10, 20, and 29 mil dia. holes (1:4:8.4, respectively) suggests that in sampling by microdrilling the weight of powder sample can be predicted with reasonable accuracy from the drill diameter and the measured hole depth.

Testing of photographic system. A Questar telescope-camera system has been tested as a means of obtaining a magnified image of samples during such operations as microdrilling. Samples can be maintained in focus for viewing as close as 7 ft. At the lowest magnification, 40×, the visual image at this magnification is apparently about 5 to 6 times its real size. The photographic system as used at present has a focal length of 1800 mm and an effective aperture of f/18. Focal length can be changed by simply changing the camera coupling length, the minimum being 1600 mm. Extending the focal length beyond this 1600–1800 mm region gives higher magnification but the effective aperture is decreased to the extent that exposure time, focus, and light become serious problems.

A series of pictures were taken in the senior cave

through the cell windows. As long as the axis of the optical system was perpendicular to the window, resolution was excellent. At increasing angles, resolution decreased rapidly. Beyond about 15° the system would not be usable. A monochromatic light source should allow some improvement. This has not yet been tested.

The system was tested during microdrilling experiments in the open. By proper placement of a small mirror above and behind the specimen, an excellent view of the surface could be obtained during drilling from a distance of about 10 ft. The image was superior to that obtained by the operator at the machine. Rounding of the sharp edges of a 10 mil spade drill was evident after a UO_2 specimen was drilled to a depth of 25 mils.

Preparation of fuel specimens for optical microscopy. For slicing samples from fuel rods, a compact cut-off wheel was designed and constructed. Cutting was with a 4-in. dia. abrasive wheel which was mounted to a gear reduction assembly driven by a fractional horsepower electric motor. Wheel rotation was at about 175 rpm. The cylindrical specimens to be sectioned were held in an "L" shaped vise bed with small setscrews. The vise assembly was hinged so that in operation the movement of a feed handle (designed for remote operation) would carry the work specimen against the abrasive wheel which rotated in a fixed position. This device is illustrated in Figure III-4.

Typically, commercially available high speed cut-off machines usually require use of liquid coolant to produce smooth surfaces and prevent distortion of metallographic structure of the specimen. The coolant used in the preliminary tests was a mixture of hydrogenated terphenyls (a Monsanto product referred to as HB-40), chosen because of low volatility (~1.5 mm Hg at 100°C) and extended liquid range (−25°C to about 350°C). In operation of the cut-off device the amount of wheel coolant spattering was minimized by permitting the wheel to rotate through a slit in a cellulose sponge which was placed in a pan and saturated with the coolant.

Sections removed from the parent specimen have varied between 0.06 and 0.25 in. Thinner sections could be cut if desired.

The cutting rates of ceramic materials with the machine equipped with either an alumina or diamond wheel appeared to be adequate (roughly 5 to 10 min per slice for fuels with cross-sectional areas of about 0.5 cm^2) for cave operation. Particular advantages of using the diamond wheel instead of the alumina wheel in cave operations would be first, its negligible wear would reduce the number of remote wheel changes necessary, and second, the rate of work feed for the machine would not have to be as delicately controlled to prevent binding of the wheel and specimen.

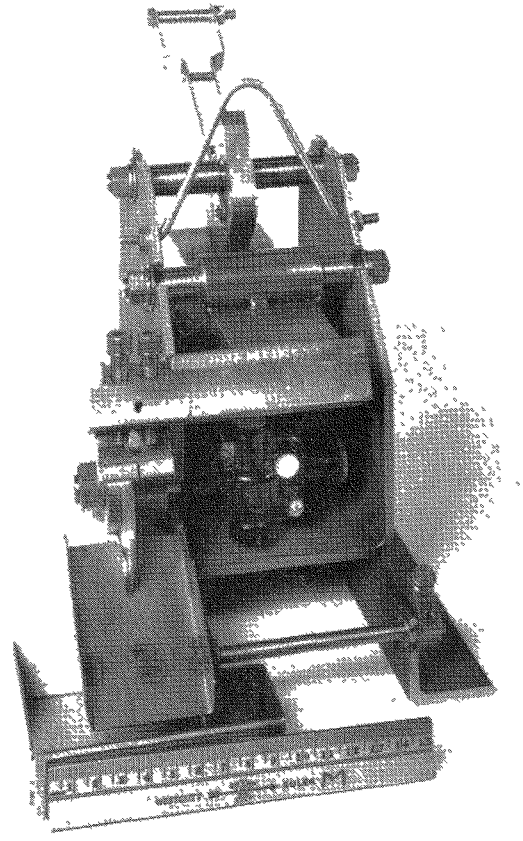

308-136

FIG III-4. Cut-Off Wheel Adapted for Remote Use in Inert Atmosphere Cave.

Specimens of simulated ceramic fuel were mounted in holders fabricated from Bakelite (dia., 1.25 in.; height, ~0.75 in.) which were machined to accept the individual specimens. To prevent fracturing of poorly consolidated grains of the ceramic during subsequent grinding and polishing operations, the specimens were mounted in the Bakelite by vacuum impregnation with a liquid epoxide which cured overnight at room temperature.

Grinding and polishing of UC, UC-5% US and UO_2 was carried out on low-speed rotating wheels (163 rpm) surfaced with selected abrasive material. Buehler "Automet" equipment was used for the grinding step. In "Automet" operation, up to 5 specimens in 1¼-in. mounts are locked securely in a specimen holder for simultaneous grinding. A crank arrangement permits adjustable pressure to be applied between the specimen surface and grinding wheel while the specimen holder is automatically rotated counter to the rotation of the

grinding wheel. Buehler "Whirlimet" apparatus was employed in the polishing step. In operation of this apparatus up to three specimens are placed in a carrier with openings. Clamping of the specimen to the carrier is not necessary. Pressure between the sample and polishing wheel is adjusted by placing appropriate weights over the specimen. As in "Automet" operation, the specimen carrier is automatically rotated in a direction opposite to that of the polishing wheel.

Both "Automet" and "Whirlimet" units have been used in alpha-gamma facilities containing air or nitrogen atmospheres. For our contemplated operation of these units in high purity helium of the Fuel Evaluation Facility, it is important that the procedures to be followed will involve minimal contamination of the helium with liquid media but at the time not seriously hinder optical microscopy of the ceramic specimens which is a necessary preliminary step of the chemical studies. A test of the grinding-polishing operations has recently been completed in which only HB-40 and benzene were used as a specimen lubricant. Both are believed compatible with the helium atmosphere when used sparingly.

The specimens were ground on SiC paper with 240, 320, and 600 grit sizes. Liquid lubricant plus solid material resulting from the grinding operations was collected as a sludge on the inner surface of a bowl which housed the grinding wheel. With the use of the above technique, a liquid disposal system for the grinding equipment was not required.

Polishing of the specimens was carried out on Politex-Pan-W paper (Geoscience Inst. Corp., New York) impregnated with 6 micron Hyprez Diamond Compound (Engis Equipment Co., Morton Grove, Ill.). There was no evidence of liquid spattering or accumulation on areas other than those of the sample surface in contact with the polishing wheel. A final specimen cleaning step by ultrasonic methods with benzene solvent and air drying resulted in some staining of the specimen surface. Vacuum drying of the specimen will be tested as a method of preventing staining.

A three-module glovebox has been adapted for testing of the above-described metallurgical and sampling techniques under pure helium. Several of the pieces of equipment under development for remote use are presently installed in this box. They include cutting, polishing, and mounting devices, an ultrasonic cleaning bath and a simple metallurgical microscope with electrically driven stage and an optical relay for remote viewing.

Laser system for mass spectrometry. A mass spectrometer is being ordered as one of the primary analytical tools for this project. Sensitivity of this instrument is sufficiently high to allow detection of most elements into the region of a few parts per billion on samples of a fraction of a microgram. A double focusing machine commonly used with a spark source was specified because of the high resolution and sensitivity requirements. Rather than use the mass spectrometer with a spark source, however, a laser system is being evaluated. This would have several advantages for our purpose. A laser can be focused optically on the precise spot to be analyzed. It is not deflected by electrostatic fields. Also, the spectrum should be less complex than in spark source excitation work because fewer multiply charged ions should be produced.

A small ruby laser with an optical system suitable for attaching it to a microscope has been obtained. It has been assembled and tested on specimens of UO_2. A single pulse vaporizes a hole in a polished specimen at a precisely determined location. The present laser optical system produces holes from a single light pulse of the order of 4 to 15 microns in diameter and 3 to 10 microns deep. For reference, a hemispherical crater in UO_2 10 microns in diameter would contain about 3 nanograms. This represents 6×10^{12} molecules of uranium dioxide. Because of the low source geometry, the utilization of vaporized material is low, perhaps one in 10^7 ions reaches the photoplate. It is possible that future development work will produce a substantial improvement in the low source geometry. However, only about 5000 ions are required to make a visible line. Thus, a single pulse of the laser will produce sufficient material to record lines for the major components. If trace elements are to be analyzed it will be necessary to strike the same area several times. In Figure III-5 several laser-vaporized craters produced in a UO_2

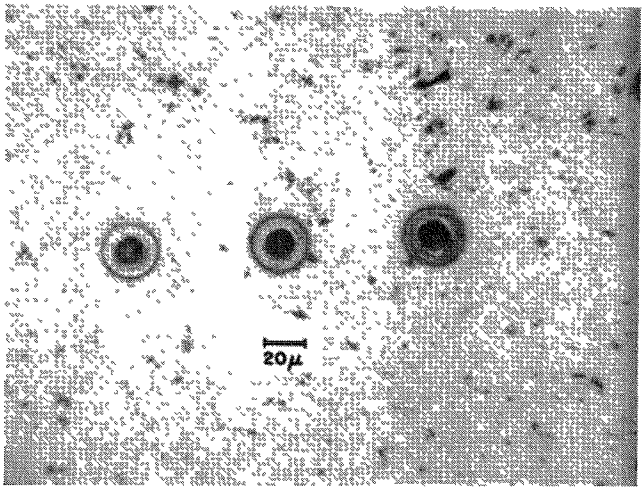

308-396

FIG. III-5. Craters Formed by a Microscope Laser System in a Polished UO_2 Specimen. From left to right, one, two, and four pulses of the laser were directed at the same spot.

matrix are shown. These resulted from one, two, or four flashes in the same spot. The diameter of the holes, about 12 microns, was not significantly increased, but the holes were deepened.

2. Electron Microprobe Application to Irradiated Test Fuel (N. Stalica, C. Seils)

It is expected that the electron probe analyzer will play a key role in the chemical studies of irradiated fuel. Of all the techniques of microanalysis only the laser beam evaporation can approach the 1-micron sample diameters than can be studied with the electron probe. The minimum laser sampling diameter currently appears to be about 5 microns. A shielded probe will be required ultimately for the examination of high-burnup fuel and for the examination of larger fuel samples. This unit has been requested; however, in the interim, it was considered necessary to investigate the limitations in the analysis of irradiated samples using the unshielded Applied Research Laboratories (ARL) EMX electron probe microanalyzer currently in the Chemical Engineering Division. This program has just begun and the first sample selected was a UO_2 fuel pin, 13 percent enriched in ^{235}U, irradiated to approximately 1.0 a/o burnup in the Materials Test Reactor. Reactor exposure was from May 23, 1965, to Nov. 29, 1965. The mounted sample[1] as received was 0.050 in. in diameter and 0.007 in. thick and had an activity level of 40 mR/hr/12 in. gamma and 300 mR/hr/12 in. beta-gamma. When the sample was inserted into the instrument and placed into the analysis position, no radiation was detected at the surface of the instrument (less than 0.1 mR beta-gamma).

Precautions were taken also to contain any loose activity by the vacuum evaporation of a layer of nickel (100 Å thick) on the sample itself and coating of the sample mount with plastic varnish. Swiping of the surface of the sample before and after examination in the electron probe indicated the absence of any loose activity.

Metallographic examination of the sample showed that a white shiny phase existed in some of the fissures and also appeared as small globules less than 1 to 20 microns in diameter dispersed throughout the UO_2. This material has been shown to be stainless steel. An optical image of a portion of the sample at 250× is shown in Figure III-6.

The elemental distribution of a portion of Figure III-6 is shown in Figure III-7 at 900×. An optical image of the area is shown in Figure III-7a; Figures III-7b through 7e are scanning images obtained with the electron probe microanalyzer. The brightness in the specimen current image (Figure III-7b) is inversely proportional to the mean atomic number of the elements present, i.e., UO_2 appears dark gray, stainless steel appears light gray and voids appear as white areas. The relative brightness in the X-ray images for iron (Figure III-7c), nickel (Figure III-7d), chromium (Figure III-7e), and uranium (Figure III-7f) is directly proportional to concentration.

Segregation of chromium can be readily seen in Figure III-7e. The concentration of chromium in this image varied from 3 to 4 w/o in the main portion of the inclusion to almost 100 w/o in the clusters. The average concentrations of iron and nickel in the inclusion were 78 and 18 w/o, respectively.

Twelve small inclusions varying from less than 1 micron to 20 microns in diameter were also examined. All were identified as stainless steel. One of the parti-

308-397

Fig. III-6. Portion of Irradiated UO_2. 250×

[1] The mounted sample was furnished by C. Dickerman and R. Stewart of the Reactor Physics Division. The sample volume was reduced to the practical minimum especially for insertion into the unshielded probe.

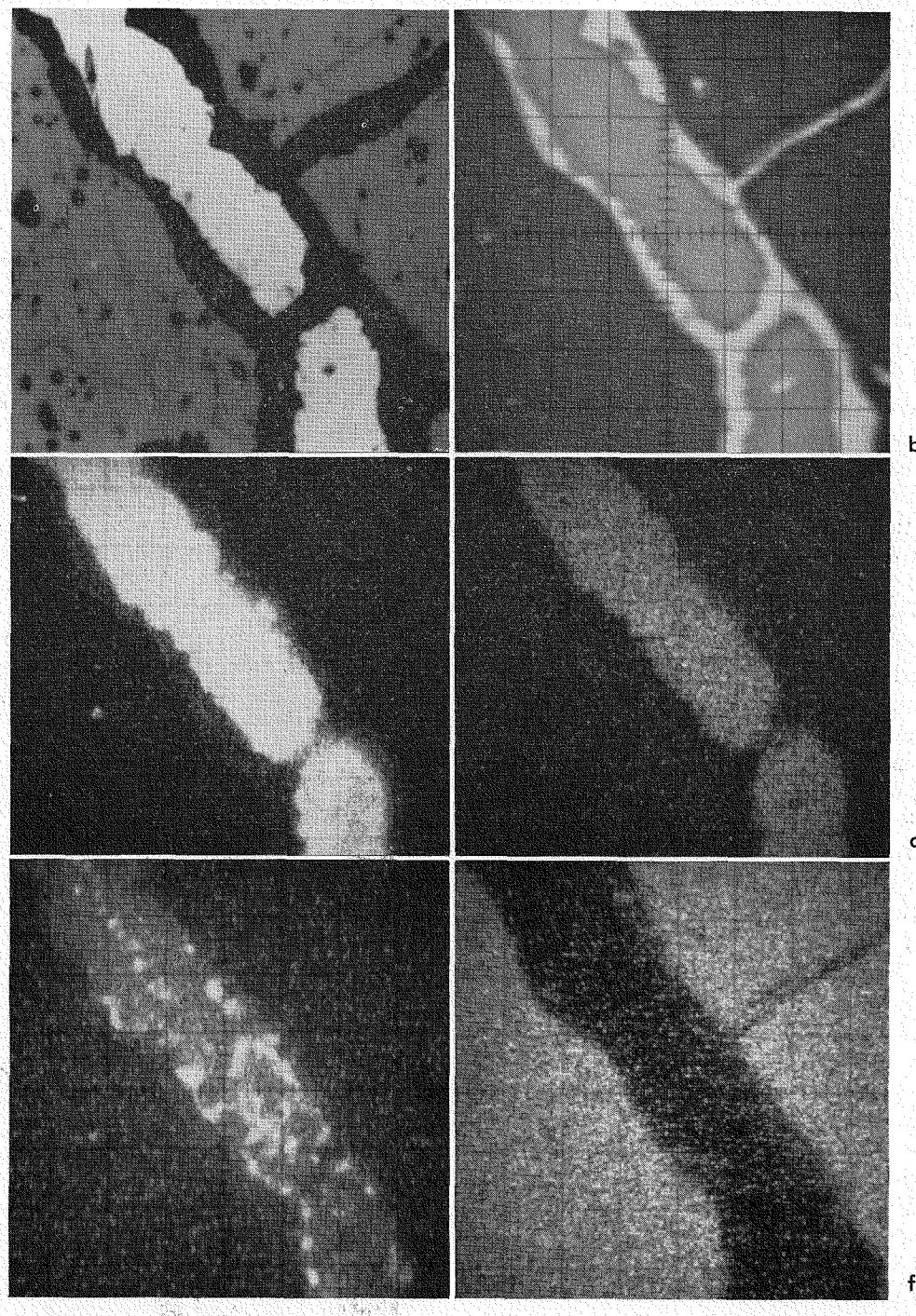

FIG. III-7. Inclusion in Irradiated UO_2 (Enlarged Portion of Fig. III-6). 900×.
a. Optical
b. Specimen Current Image
c. Iron $K\alpha$ X-ray Image
d. Nickel $K\alpha$ X-ray Image
e. Chromium $K\alpha$ X-ray Image
f. Uranium $M\beta$ X-ray Image

cles, about 2 microns in cross section, can be seen in the lower left of Figures III-7a and III-7c.

Studies of samples of higher activity are planned to find the practical limits of activity levels than can be analyzed in an unshielded ARL EMX microprobe. Bradbury et al.[2] have estimated that a gamma level of 200 mR/hr/12 in. is the maximum level for a sam

[2] B. T. Bradbury, J. T. Demant, P. M. Martin, and D. M. Poole, Electron Probe Microanalysis of Irradiated UO_2, AERE-R-4845, 1965.

to be analyzed in the CAMECA electron probe microanalyzer, and that a sample with an activity level of 20 mR/hr/12 in. can be analyzed without difficulty. The gamma activity of the sample analyzed in the ARL EMX instrument had negligible effect on the X-ray detectors because of the design configuration of the magnetic objective lens used in the instrument. The activity levels tolerable in an unshielded ARL EMX instrument are expected to be much higher than the 200 mR/hr/12 in. of the CAMECA instrument.

C. PREPARATION OF REACTOR MATERIALS—CERAMIC FUELS (P. A. Nelson, A. D. Tevebaugh, J. D. Bingle)

The preparation of ceramic fuels is being studied to develop processes which economically fit into appropriate fuel cycles, and to make well-defined fuel compounds for further experimental studies, particularly irradiation studies. At the present time, efforts are being directed toward procedures for preparing uranium and uranium-plutonium carbide fuels.

The fluidized-bed technique appears to be especially attractive for preparation of carbide fuels; it affords efficient gas-solids contacting and the product is a powder which can be fabricated into fuel pellets or densified for vibratory compaction into fuel elements. Two fluidized-bed processes are being developed for preparing monocarbides: (1) carburization of hydrided metal or alloy at 750 to 850°C with methane-hydrogen gas mixtures; and (2) conversion of oxides at 1600 to 1800°C either by reaction with admixed carbon or with a fluidizing gas containing methane. The former problem, which currently requires the larger effort, is discussed below, whereas the latter, which was described in the previous semiannual report, ANL-7225, p. 146, is still in the equipment preparation stage; it will not be further discussed herein.

1. Demonstration of Fluidized-Bed Process for Preparation of (U, Pu)C (E. J. Petkus, P. W. Krause)

A series of twelve runs has been conducted to demonstrate the preparation of high purity (U, 15 w/o Pu)C by the fluidized-bed technique. In each run, 300 g of U-Pu alloy (⅜-in. dia. rods) was hydrided at 250°C to form a powder; this, in turn, was fluidized and reacted at 550 to 800°C with methane-hydrogen gas mixtures to form the monocarbide. These runs were carried out using once-through fluidizing gas flow, in a 1⅝-in. ID reactor which could be manipulated (e.g., for product removal) in a high-purity helium atmosphere glovebox (see ANL-7225, p. 143). This reactor is capable of producing 600 g batches but the batch size was limited to conserve material. The run conditions and product analyses are shown in Table III-4.

In these runs the control of the carbon content and purity of the product were emphasized. Uranium-plutonium monocarbide that is stoichiometric or slightly hyperstoichiometric with respect to carbon is the preferred carbide fuel for fast reactors because: (1) it is more compatible with cladding materials and has lower fission gas release during irradiation than carbide fuels with lower carbon-to-metal atom ratios; and (2) it has higher thermal conductivity than fuels containing a large excess of carbon.[1] The methods for controlling the carbon content of the product in this series of runs were: (1) adjusting the methane concentration in the methane-hydrogen fluidizing gas to prevent formation of free carbon; (2) stopping the reaction after the appropriate extent of carburization had been reached; and (3) treating with hydrogen at the end of the carburization period to remove excess carbon.

The methane concentrations of the inlet and outlet gas streams were determined by infrared analysis. The rate of carburization was determined from the difference between the inlet and outlet methane concentrations and from the gas flow rate. The extent of carbiding during the course of the run was established with an accuracy of ±5 to 10% by integrating the rate of carburization with respect to time. However, chemical analysis of the product yielded a more accurate value (±1%) for the final extent of carbiding, and the values obtained during the run were adjusted accordingly. It was thus possible to plot the extent of carbiding versus

[1] J. H. Kittel et al, "Plutonium Fuel Development for Fast Reactors in the United States," presented at the Nuclear and Metallurgy Symposium of the AIME, October 3–5, 1966.

TABLE III-4. PREPARATION OF (U, 15 w/o Pu)C IN A FLUIDIZED-BED REACTOR
300-g scale, ⅜-in. dia. alloy rods hydrided at 250°C prior to carbiding

Run No.	Carbiding Conditions					Product Analysis (w/o)				X-ray Analysis[c]	
	Temperature (°C)	Pressure (atm)	CH_4 Conc.[a] (v/o)	Carbiding time (hr)	Final H_2 treatment (hr)	Carbon	Oxygen	Nitrogen	Equivalent carbon[b]	Major	Minor
1	750	4	10[d]	6	0	4.11	0.04	—[f]	4.16	MC	βMH_3
2	750	4	10[d]	12	0	4.96	0.016 0.084[e]	—[f]	4.99	MC	none
3	550–750	4	10	11.6	0	4.89	0.049	—[f]	4.95	MC	none
4	750	4	10[d]	11.8	0	4.92	0.077 0.12[e]	—[f]	5.00	MC	M_2C_3
5	800	4	10	10.3	2	4.78	0.073 0.35[e]	—[f]	4.85	MC	none
6	800	1.33 4	10	10.5	2	4.89	0.18	—[f]	5.05	MC	M_2C_3
7	800	4	10	6.8	1.5	4.80	0.058	—[f]	4.86	MC	none
8	800	2	8	6.8	0.5	4.92	0.057	—[f]	4.98	MC	none
9	800	4	—[g]	11.4	2.5	4.76	0.02	0.008	4.79	MC	none
10	800	2	8	7.9	5.5	4.83	0.086	0.013	4.90	MC	none
11	800	2	8	7.0	0.6	4.64	0.12	0.016	4.74	MC	none
12	800	2	8	14.3	6.0	4.70	0.036	0.017	4.74	MC	none

[a] Balance hydrogen.

[b] Oxygen and nitrogen are soluble in (U, Pu)C and replace carbon in the lattice; therefore, the equivalent carbon concentration in weight percent, C_{eq} = w/o C + (12/16) w/o O + (12/14) w/o N.

[c] M = (U, 15 w/o Pu).

[d] Near the end of the run, CH_4 concentration was decreased to 2.5 v/o.

[e] The higher values were assumed to be due to sample contamination. These higher values were not used in the equivalent carbon calculation.

[f] Spurious results; a value of 0.02 was assumed for calculating the equivalent carbon concentration.

[g] Variable as follows: 0 to 0.8 hr, 1.0 w/o; 0.8 to 3.8 hr, 2.6 v/o; 3.8 to 6.5 hr, 5 v/o; 6.5 hr to end of carbiding, 10.0 v/o.

time and to determine the effect of various changes in the reaction conditions on the rate of carbiding.

In one of the early experiments, run 3, it was found that the rate of carbiding was increased by raising the temperature from 550 to 750°C (see ANL-7225, p. 145). Consequently, beginning with run 5, the temperature was maintained at 800°C, the upper operating temperature for this reactor.

The effect of methane concentration on the rate of reaction was investigated in run 9. The reaction rates at 1.0 and 2.5 v/o methane during the initial portion of run 9 were much lower than the rates at 5 and 10 v/o methane during later portions of the run. The effect of an increase in pressure, observed by comparing the carbiding rates for runs made at 2 atm with those made at 4 atm pressure was a slight increase in reaction rate. The effect of the pressure change observed in run 6 is a special case that is discussed below.

In runs 2 through 9, carbiding was interrupted after a period of several hours to rehydride the residual metal in the particles and break up the carbide reaction layer which appeared to be inhibiting further carbiding (see ANL-7225, pp. 144–145). After a carbon content of about 4.0 to 4.2 w/o was reached (stoichiometric monocarbide contains 4.80 w/o carbon), the rate of reaction decreased markedly. Lowering the temperature to 25–400°C at this point in runs 2 through 9 to rehydride the residual metal permitted the completion of monocarbide formation in a few hours. This effect can be seen in the data from run 7 in Figure III-8. The rehydriding portion of the cycle takes only about 1½ hr and would not be a major inconvenience in full-scale operation. The cool-down and heat-up periods are only a few minutes long at temperatures above 600°C where the reaction rate is significant, so that the hydriding period was not included in the carbiding time plotted in Figure III-8.

In all runs the methane concentration in the methane-hydrogen fluidizing gas was such that $(U,Pu)_2C_3$ would be expected to form if the reaction were carried to completion; however, except for run 6 (discussed below), free carbon would not be expected to form. After the carbon concentration in the powder product reached the stoichiometric monocarbide level (4.80 w/o), the rate of carbiding appeared to decrease, and any carbon in excess of the stoichiometric carbon level could be removed at the end of the carbiding period by reaction with hydrogen to form methane. This step

n the process was carried out for runs 5 through 12 and it is illustrated in Figure III-8 in the plots of runs 6 and 7. The infrared analyzer monitoring the off-gas stream indicated the formation and release of a significant amount of methane (0.5 liter in run 7) during the period when the fluidizing gas was pure hydrogen.

In run 11 it was found that a hydrogen treatment at the carbiding temperature prior to reaching the stoichiometric carbon concentration also resulted in the release of carbon in the form of methane, as shown in Figure III-8. This result suggests the presence of a sesquicarbide layer on the outside of the particle, an intermediate layer of monocarbide, and a core of unreacted alloy. (In actuality, the layers are not sharply defined since the particles are very irregular in shape and possess interconnected porosity.) The conversion of this outer sesquicarbide layer to the monocarbide by a hydrogen treatment also resulted in an increase in the rate of carbiding, but by a different mechanism than that which took place with the low temperature hydriding of runs 2 through 9.

Another approach to increasing the rate of carburization was to use a double hydriding cycle prior to carbiding; this was tried in run 5. It is well known that repeated hydriding and dehydriding results in a finer particle size than that from a single cycle. A smaller particle reduces the length of the diffusion path for carbon and therefore, might be expected to be beneficial. However, the desired result was not obtained by using this technique; the reaction rate was lower for run 5 than for the other runs, which had only one hydriding cycle prior to carbiding. A particle size analysis of the product from run 5 showed a substantial portion (14.2 w/o) of large particle agglomerates. These agglomerates were easily broken into fine particles. It appears, therefore, that very fine particles were formed during the two hydriding cycles but that the agglomeration of the particles resulted in a lower carbiding rate than in runs in which a single hydriding cycle was used.

In two of the runs, no attempt was made to increase the rate of carbiding. In run 1, in which the period of uninterrupted carbiding was only 6 hr, the product was only 85% converted to monocarbide. In run 12, the 12.5 hr required to reach to stoichiometric monocarbide carbon content (total carbiding time, 14.3 hr) was a longer time than that used in any of the other runs. Therefore, a hydrogen treatment during carbiding appears to be beneficial, but the best sequence of operation has not been established as yet.

As noted above, the operating conditions during carding in all runs except run 6 were such that free carbon would not be expected to form. During the first 2¾ hr of run 6, the methane concentration in the

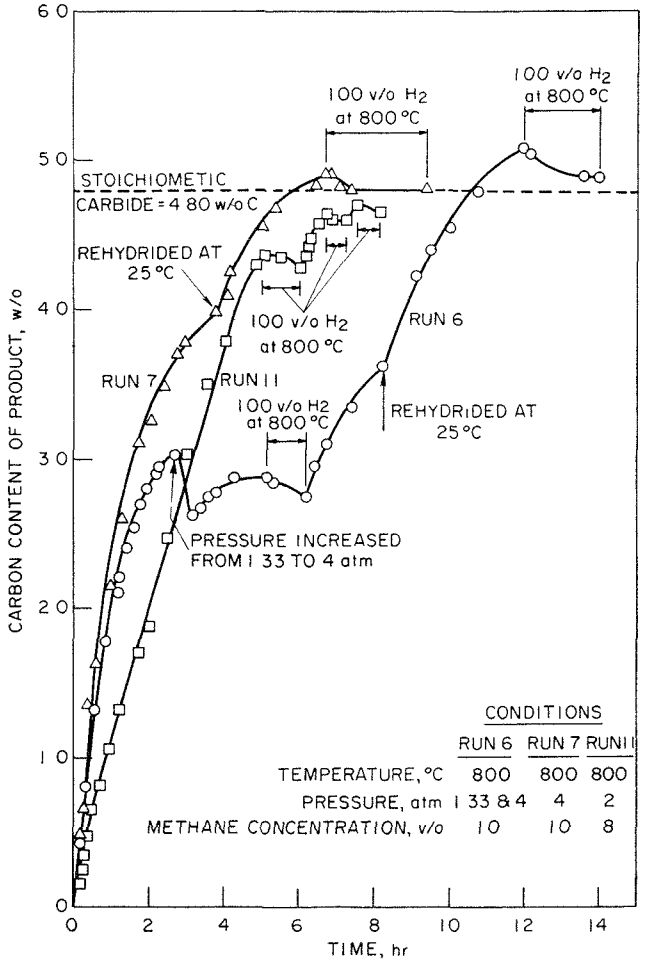

308-335

FIG. III-8. Effects of Process Variables on the Preparation of (U,Pu) C in a Fluidized Bed.

methane-hydrogen fluidizing gas was maintained at 10 v/o at a total pressure of 1.33 atm, conditions which would cause deposition of free carbon by the reaction,

$$CH_4(g) \rightleftarrows C(s) + 2H_2(g),$$

where the equilibrium constant, $k, = p^2_{H_2}/p_{CH_4} = 21.3$ atm at 800°C. A comparison of the rate of carbiding of run 6 with that of run 7 in Figure III-8 indicates the undesirable effect of carrying out the reaction under conditions that produce free carbon. After 2¾ hr, the rate of carbiding in run 6 was considerably lower than that in run 7. Raising the pressure to 4 atm resulted in reaction of the excess carbon to form methane and, ultimately, in an increase in the reaction rate.

An analysis of the data on rates of reaction indicated that it is possible to prepare 100 kg of (U,Pu)C by this process in a period of 10 to 12 hr if the carbiding is carried out at a pressure of 10 atm and a reactor of suitable size (8-in. in dia.) is employed. This rate of

production is sufficient to resynthesize fuel from three 1000 MW(e) nuclear power reactors

The oxygen impurity levels for these products have been low as shown in Table III-4; frequently the two analyses of the product averaged about 0.05 w/o or lower. The two individual oxygen analyses for runs 2, 4, and 5 varied markedly and, therefore, they are listed separately. (Only the lower oxygen values for these runs were used in determining the equivalent carbon contents of Table III-4.) The increase in oxygen content above about 0.05 w/o is almost certainly caused by the introduction of oxygen during sampling prior to analysis. The very low oxygen levels of some runs approach the impurity levels of the alloy feed material, about 0.01 to 0.02 w/o.

Difficulties were encountered in the earlier analyses of the products for nitrogen, and the values originally measured for the first eight runs are believed to be erroneously high. It is now believed that the actual nitrogen content of the first eight runs was similar to that of the last four runs (see Table III-4).

The low impurity levels obtained in these runs indicate that the reactant gases, methane and hydrogen, introduce very small amounts of impurities, a conclusion that is in agreement with calculations based on the flow rates and the impurity contents of the gases.

The carbon content of the last six runs, in which final hydrogen treatment was employed, ranged from 4.70 to 4.92 w/o. It is anticipated that this range will be narrowed even further when process conditions are optimized.

Sieve analyses of the carbide products showed an average particle size of about 40 to 60 μ. This relatively fine material is suitable for fabrication into pellets by pressing and sintering, with no intermediate processing. Preliminary work on pressing and sintering of one batch of this material by Metallurgy Division personnel has shown that densities in excess of 90% of theoretical can easily be obtained.

In summary, the following conclusions have been drawn from these studies on the preparation of (U,Pu)C by the fluidized-bed technique:

a) The operating conditions of pressure, temperature, and methane concentration should be such that free carbon does not form on the particles.

b) The rate of carbiding increases with increasing pressure, methane concentration (within the above restriction), and temperature (at least up to 800°C).

c) After a carbon content of about 4.2 w/o is reached, the rate of carbiding can be increased by treating the bed with pure hydrogen, either at lower temperatures (below 400°C) to cause rehydriding and, apparently, to break up the outer reaction layer, or at the carbiding temperature to remove a higher carbide reaction layer.

d) A final hydrogen treatment is effective in removing any excess carbon from the surface of the carbide particles to yield the monocarbide.

e) It has been demonstrated that a powdered product can be produced which contains less than 1000 ppm oxygen and less than 200 ppm nitrogen; this material is suitable directly for fabrication into pellets by pressing and sintering.

2. Equipment Development for Preparation of Carbides by the Fluidized-Bed Technique (S. Vogler, C. Payne)

An important objective of the work on carbide preparation in a fluidized bed is to adapt the methane-metal reaction process to a fast reactor fuel cycle or to the preparation of a large core loading. In a fuel cycle which involves pyrochemical reprocessing and which produces a metallic product, the fluidized-bed process would require a capacity of 100 kg of core fuel per day for a 3000 MW(e) reactor complex and must be capable of being remotely or semiremotely operated. As discussed previously (ANL-7125, p. 124), the required rate could be obtained with a single 8-in. dia. fluidized-bed reactor. However, several equipment problems and materials handling problems remain to be solved before this objective is reached.

Equipment design and operational concepts that would be applicable to a large-scale process are being tested by preparing UC; plutonium is not being employed in the present studies because of the operational difficulties attendant on its use. The 2½-in. ID semiworks scale (1 kg) fluidized-bed reactor being operated for this purpose was described in the preceding report (ANL-7225, pp. 141–142).

Uranium monocarbide is prepared in this reactor in the following manner. Uranium rods (⅜ in. in dia. by 1 in. long) are cleaned in nitric acid and charged to the reactor through a lock which prevents the admission of air to the system. The uranium is reacted with hydrogen at about 250–300°C to produce finely powdered uranium hydride (UH_3). In the next step, the fine powder, which decomposes to uranium metal at elevated temperatures, is reacted at 750°C and 10 atm pressure with a hydrogen-methane fluidizing gas mixture that usually contains between 5 and 10 v/o methane. The reaction of the uranium metal with methane

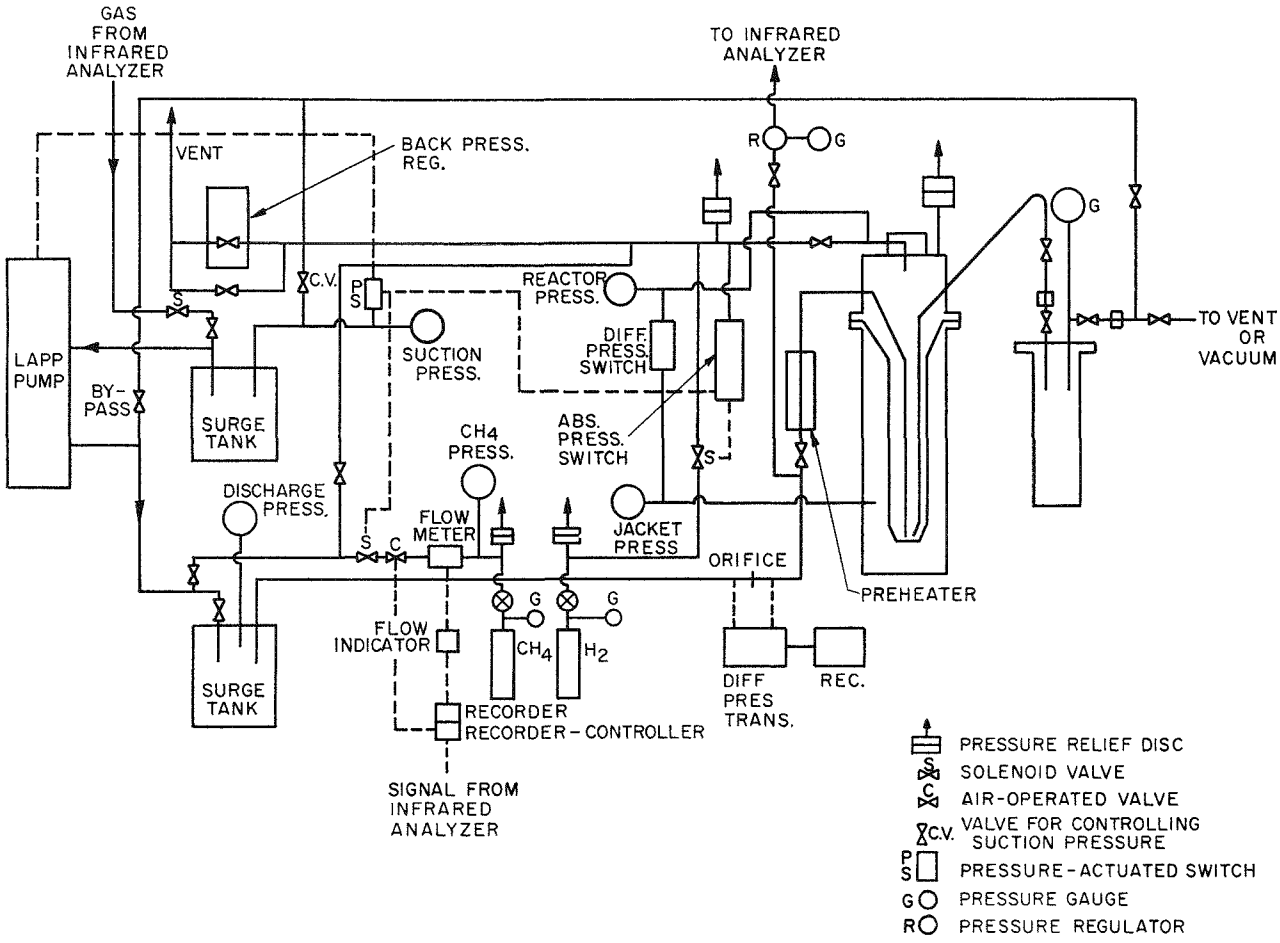

308-473

FIG. III-9. Flow Diagram of Semiworks Fluidized-Bed Reactor.

yields two moles of hydrogen for each mole of uranium reacted:

$$U + CH_4 \rightarrow UC + 2H_2$$

Operation of the reaction with once-through gas flow, described in ANL-7225, pp. 141–142, 143, limited the operating pressure to about 2 atm because of the large flow of gas required at higher pressures. A diaphragm compressor was therefore installed to recirculate the off-gas from the fluidized bed and allow operation at higher pressures. A schematic diagram of the system piping is shown in Figure III-9. The gas is circulated by means of a Lapp diaphragm compressor which is being operated at a pressure of 10 atm. The gas flow rate is measured by an orifice and differential pressure transmitter whose output signal is recorded by a pneumatic recorder. Because of the high specific heat of hydrogen and the large volumes of gas flowing at the higher pressures, it was necessary to install a gas preheater.

The system is maintained at the desired pressure by means of a back-pressure regulator that vents excess gas and a pressure switch that actuates a solenoid valve in case the pressure falls. If a catastrophic pressure drop should occur (as in the event of a ruptured line), a safety pressure switch would be actuated. This switch would immediately turn off the compressor and shut off the hydrogen and methane flow to the system.

As discussed earlier in the section on (U, Pu)C preparations, it is necessary to control the methane concentration in the circulating gas to avoid the deposition of carbon. The methane concentration is controlled in the semiworks system by an electronic recorder-controller equipped with proportional band, rate, and reset controls. The methane concentration of the circulating gas is measured by an infrared analyzer. The signal from the infrared analyzer is fed into the electronic recorder-controller which controls a metering valve for methane additions. The infrared instrument was modified for operation at elevated pressures to allow the sampled gas to be returned to the process system. This modification has made it possible to increase the flow of gas through the instrument, and reduce the response time to methane concentration changes in the circulat-

ing gas. Since this change, control of the methane concentration of the circulating gas has been excellent.

The flow of methane into the system is measured by a thermal flowmeter and recorded on a strip chart. A small tank of known volume supplies the methane to the system; the amount of methane supplied is determined from the pressure drop in this tank. Thus, the extent of carbiding can be determined from a material balance (allowing for methane discharged with the reaction product hydrogen) which results in the following relationship:

$$R = F\left(\frac{1 - C}{1 + C}\right)$$

where R = methane reacted, moles
F = methane added to system, moles
C = methane concentrations, mole fraction

The powdered product is removed at room temperature by pneumatic conveyance using the recirculating system. The use of this system eliminates the need for new gas and thus minimizes contamination of the product.

Four experiments were carried out in which 1-kg batches of UC were prepared at 750°C and 10 atm and in which the equipment was operated in the manner described above. In addition, several tests were made in which the material was only hydrided. The serious problems of poor fluidization, which were discussed in the preceding report (ANL-7225, p. 141), were not encountered in these experiments. However, some channelling and bed agglomeration took place as was evidenced by an occasional erratic change in the pressure drop across the bed and by a rapid increase in rate of carbiding on some of the occasions when the bed was sharply jarred.

It has always been possible to remove the reaction product by pneumatic conveyance without exposing the interior of the reactor to air. However, in one run in which a double hydriding cycle was used, repeated attempts were required to remove the product, presumably because of the poor fluidizing properties of the fine particles that resulted from the two hydriding-dehydriding cycles.

The carbon content of the products of three runs, in which attempts were made to carry the carbiding to completion, varied from 4.56 to 4.78. Difficulty is still being experienced in obtaining oxygen concentrations below about 0.5 w/o in UC (as contrasted to the many low oxygen analyses reported in Table III-4 for (U,Pu)C. Uranium monocarbide is finer than (U,Pu)C and reacts much more rapidly than (U,Pu)C in the glovebox atmosphere (<5 ppm each of H_2O and O_2) in which the sample capsules are filled. However, it may be possible to circumvent this problem by changes in the sampling procedure.

Further work and equipment changes are required before the type of fluidized-bed system used in these experiments is suitable for preparation of (U,Pu)C. However, favorable results were obtained on gas recirculation, control of methane concentration, measurement of the extent of carbiding, and automatic product withdrawal. These results indicate that a fluidized-bed process which is suitable for remote resynthesis of reprocessed fuel can be developed for fast reactor carbide fuels.

3. Thermobalance Studies (S. Vogler, N. Quattropani)

Knowledge of the reaction thermodynamics for the formation of UC and (U,Pu)C by reaction of the metal or alloy with hydrocarbon gases is important to the rational development of processes employing these reactions. A detailed discussion of the reaction thermodynamics involved was presented in ANL-7125, p. 125. It was indicated that excessive carburization of (U,Pu)C by the reaction

$$2(U,Pu)C + CH_4 \rightleftharpoons (U,Pu)_2C_3 + 2H_2$$

can be prevented by maintaining the CH_4 concentration at less than the equilibrium value for this reaction or by driving the reaction to the left as is now being done during the final portions of the demonstration runs described above. The thermobalance experiments are being conducted in order to determine a more precise value of the equilibrium constant for the above reaction than can be obtained by calculations based on currently available free energy data.

A description of the thermobalance equipment and procedure was reported previously (ANL-7055, p. 90). The thermobalance reaction vessel has been modified so that the product can be handled in a controlled atmosphere; this should reduce the presence of impurities in the product and permit better interpretation of the data.

Briefly, the procedure consists of reacting about 3 g of uranium-plutonium alloy with hydrogen in the thermobalance to yield finely divided hydride, and then reacting the hydride with a hydrogen-hydrocarbon mixture. The carburizing gas flow is started as soon as hydriding is complete to prevent sintering as the temperature is raised.

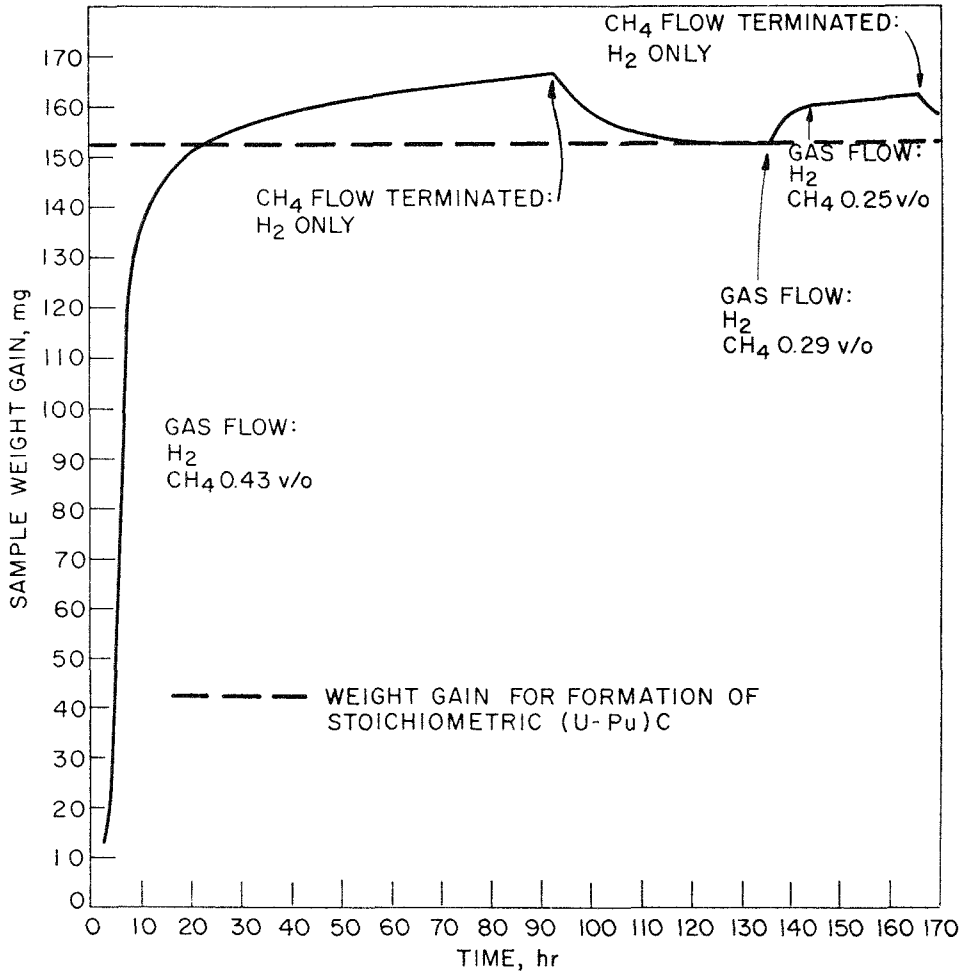

308-334

FIG. III-10. Thermobalance Experiment: U-20 w/o Pu Alloy Reacted with H_2-CH_4 Mixtures at 750°C.

Previous thermobalance experiments with uranium-20 w/o plutonium carbide samples had indicated that at 770°C, the equilibrium methane concentration for the above reaction was approximately 0.75 v/o methane (see ANL-7225, pp. 140–141). However, after making improvements in the equipment, data have been obtained that indicate the equilibrium methane concentration is lower. The data for one such experiment at 750°C are given in Figure III-10. The curve shows that, with an initial methane concentration of 0.43 v/o, the weight gain continued to increase with a slope of 0.3 mg/hr after the theoretical weight gain for stoichiometric monocarbide was achieved. When the methane flow was stopped and hydrogen alone was passed over the sample, the weight immediately decreased and continued to decrease until the weight gain for stoichiometric monocarbide was reached. This would indicate that the weight increase beyond the stoichiometric value was due to the formation of the sesquicarbide, which in turn decomposed to the monocarbide in the hydrogen atmosphere. When methane was again introduced into the gas stream, the weight immediately began to increase. With a gas concentration of 0.25 v/o CH_4, the weight increased at a rate of 0.11 mg/hr. When the methane contribution to the gas flow was terminated a second time, the weight decreased once again.

A preliminary evaluation of this experiment indicates that the equilibrium methane concentration for the system (U,20 w/o Pu)C, (U,20 w/o Pu)$_2C_3$, CH_4, and H_2 is less than 0.25 v/o CH_4 at 750°C. This would yield a ΔG° value of less than -7 kcal/mole of (U,20 w/o Pu)$_2C_3$ at 750°C for the reaction:

$$2(\text{U, 20 w/o Pu})\text{C} + \text{C} \rightarrow (\text{U, 20 w/o Pu})_2\text{C}_3 .$$

(Preliminary data on more recent experiments indicate that the ΔG° value may, indeed, be as low as -9 to -10 kcal/mole.)

The equilibrium methane concentration observed in

the experiment illustrated in Figure III-10 was lower than that observed in previous experiments; this lower equilibrium concentration of methane may be due to greater success in excluding oxygen and water vapor from the system. The fact that the reaction curve leveled out at the calculated weight gain for (U,Pu)C after 125 hr of operation is evidence of the purity of the gas.

D. CALORIMETRY (W. N. Hubbard, H. M. Feder, M. Ader)

The program of the Calorimetric Laboratory is directed toward the determination of thermodynamic properties of substances that are of interest in high temperature chemistry and nuclear technology. Fluorine bomb calorimetry has been developed here in order to obtain the enthalpies of formation ($\Delta Hf°$) of substances not amenable to more conventional types of calorimetry. This method has now been used to determine enthalpy-of-formation values for 25 elemental fluorides and seven binary, high-melting compounds. Bond energies have been systematically calculated for some series of elemental fluorides in an effort to clarify the theoretical bases for the observed variations.

For certain substances, calorimetric reactions are more advantageously carried out in a flow system than in a bomb. A fluorine flow calorimetric system has been constructed for studying such substances. It has been calibrated and is now being used for measurements on uranium monosulfide.

A project has been undertaken to expand the calorimetry program to include compounds of plutonium. A complete calorimetric system—adaptable to oxygen, fluorine, or chlorine combustions—has been installed in a glovebox. An enthalpy-of-solution reaction vessel that can be used with the system is being designed.

A resistance-wire-heated drop calorimeter for measuring enthalpies, relative to room temperature, of substances up to 1500°C has been designed and constructed. It has been used for studies with uranium monophosphide. An electron-bombardment-heated calorimeter has been designed for making similar measurements up to about 2500°C. The components of the latter system have been assembled and are undergoing calibration and testing.

1. The Enthalpy of Formation of Nickel Difluoride (E. Rudzitis, E. H. Van Deventer)

A paper bearing the following title has been published:[1] "Fluorine Bomb Calorimetry. The Enthalpy of Formation of Nickel Difluoride." The abstract is as follows:

"The energy of formation of nickel difluoride was measured by direct combination of the elements in a bomb calorimeter. From these measurements, the standard enthalpy of formation $\Delta Hf°_{298.15}$ (NiF_2, c) was -157.2 ± 0.4 kcal. per mole."

[1] E. Rudzitis, E. H. Van Deventer, and W. N. Hubbard, J. Chem. Eng. Data **12**, 133 (1967).

2. The Enthalpies of Formation of the Diborides of Zirconium and Hafnium (G. K. Johnson)

A paper bearing the following title has been published:[2] "Fluorine Bomb Calorimetry. The Enthalpies of Formation of the Diborides of Zirconium and Hafnium." The abstract is as follows:

"The energies of combustion in fluorine of zirconium diboride ($ZrB_{1.993\pm0.006}$), and hafnium diboride, ($HfB_{2.003\pm0.006}$), were measured in a combustion bomb calorimeter. These results, when combined with the enthalpies of formation of ZrF_4, HfF_4, and BF_3 which were previously obtained by similar techniques, gave $\Delta Hf°_{298.15}$ values of -77.9 ± 1.5 and -78.6 ± 2.1 kcal $(g.f.m.)^{-1}$ for $ZrB_{1.993\pm0.006}$ and $HfB_{2.003\pm0.006}$, respectively."

[2] G. K. Johnson, E. Greenberg, J. L. Margrave, and W. N. Hubbard, J. Chem. Eng. Data **12**, 137 (1967).

3. The Enthalpy of Formation of Carbon Tetrafluoride (Tetrafluoromethane) (E. Greenberg)

The need for a determination of the enthalpy of formation of CF_4 by direct combustion of graphite in fluorine, and preliminary work on the project have been discussed.[3] Calorimetric measurements are under way. A high-pressure, two-chambered bomb[3b] and quartz-crystal thermometry (see part 11) are being used. The system was calibrated by combustions in oxygen of standard benzoic acid. The standard deviation of the mean of a series of eleven calibrations was 0.02%, which is slightly higher than the values, <0.01%, normally expected with a conventional bomb and a platinum resistance thermometer. Whether the poorer precision is attributable to the quartz-crystal thermometer or to the new two-chambered bomb is unclear. However, an error analysis indicated that the precision of calibration was not the limiting error and, therefore, that the new bomb and thermometer would be satisfactory for the combustion of graphite in fluorine. The lack of any serious discrepancy between the results obtained for the different sample sizes (0.6 and 1.2 g benzoic acid) adds confidence that there are no significant systematic errors attributable to the use of the new bomb and thermometer.

[3] (a) ANL-7125, p. 133; (b) ANL-7225, pp. 149–150.

Blank experiments were carried out to determine the thermal effect of expansion of fluorine from the storage chamber into the combustion chamber. The measured energy is the sum of an endothermic effect due to expansion of fluorine into the evacuated combustion chamber, and the exothermic effect due to reaction of fluorine with the bomb walls and/or any adsorbed moisture. By suitable preconditioning of the bomb and subsequent handling in an inert-atmosphere box, the exothermic effect can be kept small and reproducible. Preliminary calculations of the data from six blank experiments indicate a net measured energy which is endothermic by about 1 to 2 cal per experiment. The energy of reaction with the bomb walls has thus been reduced to less than 6 cal, the magnitude of the energy absorbed by the expansion of fluorine.

Calorimetric combustions of both pyrolytic and natural graphites are in progress. These experiments have shown excellent reproducibility and insensitivity to sample size; it is highly probable that a value of $\Delta Hf^\circ(CF_4)$ of acceptable accuracy will be forthcoming. The difference in combustion energy, if real, between natural and pyrolytic graphite is quite small, but in the expected direction.

4. The Enthalpy of Formation of Phosphorus Trifluoride (E. Rudzitis, E. H. Van Deventer)

Experiments have shown that phosphorus trifluoride is a powerful defluorinating agent; some of its possible uses in thermochemistry were discussed previously.[4] These applications require that the enthalpy of formation of PF_3 be known. This value was determined by a calorimetric investigation of the reaction

$$PF_3(g) + F_2(g) \rightarrow PF_5(g). \qquad (1)$$

The reaction was carried out in the two-chambered reaction vessel[5] previously developed for substances which react spontaneously with fluorine. The combustion chamber was charged with an accurately weighed amount of PF_3, and the storage tank with an excess of fluorine. When the interconnecting valve was opened, the fluorine expanded into the combustion chamber and the reaction proceeded spontaneously. Because this reaction occurs in the gas phase, exposed teflon gaskets ignite. Therefore, it was necessary to replace or shield with aluminum all the teflon gaskets.

Commercial PF_3 (nominally 99 v/o) was used after being purified by repeatedly trapping out the less volatile impurities at −78°C, followed by pumping off the more volatile impurities at −196°C. The purified PF_3 had an impurity content of <0.01 v/o as determined by a new analytical technique (see part 8). The same technique was used to demonstrate that no PF_3 remained (limit of detection, 0.01 v/o) after completion of reaction 1.

The values obtained for the energy, enthalpy, and free energy of reaction 1 are, respectively (in kcal mol^{-1}): $\Delta E^\circ_{298} = -151.4 \pm 0.2$; $\Delta H^\circ_{298} = -152.0 \pm 0.2$; $\Delta G^\circ_{298} = -139.8 \pm 0.2$. These values, when combined with an earlier determination[6] of $\Delta Hf^\circ_{298}(PF_5, g)$, yield the following values (in kcal mol^{-1}) for formation of PF_3 according to eq. 2:

$$P(\alpha\text{-white}) + 3/2\ F_2(g) \rightarrow PF_3(g) \qquad (2)$$

[4] ANL-7225, pp. 152–153.

[5] R. L. Nuttall, S. S. Wise, and W. N. Hubbard, Rev. Sci. Instr. **32**, 1402 (1961).

[6] P. A. G. O'Hare and W. N. Hubbard, Trans. Faraday Soc. **62**, 2709 (1966).

$$\Delta Ef^\circ_{298} = -228.5 \pm 0.4$$

$$\Delta Hf^\circ_{298} = -228.8 \pm 0.4$$

$$\Delta Gf^\circ_{298} = -223.8 \pm 0.4$$

The experimental determination of $\Delta Hf^\circ(PF_3, g)$ represents two accomplishments with respect to fluorine bomb calorimetry: the combustion of a lower fluoride to a higher fluoride, and the bomb calorimetric measurement of an all-gas reaction.

5. Thermochemistry of Plutonium Compounds (G. K. Johnson)

The previous report[7] discussed the reasons for undertaking a program on calorimetry of plutonium compounds, the work that has been done in this field, work that is needed, and appropriate calorimetric techniques. Since then, most of the equipment required for initiating such a program has been acquired. A rotating bomb calorimeter, gas-charging and -discharging manifold, balances, and other auxiliary equipment have been assembled within a glovebox in the Division's alpha radiation facility. The manifold is connected to a vacuum system and to pressure tanks which supply fluorine, chlorine, oxygen, and argon. The entire system and the proposed operating procedures have undergone an extensive safety review, and exploratory combustions of plutonium in chlorine have started.

A solution calorimeter capable of functioning as a part of the rotating bomb calorimeter is being designed. This calorimeter, when finally completed and tested, will greatly expand the number of possible reactions which can be employed to obtain thermochemical properties of plutonium compounds.

[7] ANL-7225, pp. 150–151.

6. The Thermochemistry of Uranium Compounds (J. L. Settle, P. A. G. O'Hare)

The considerations leading to the construction of a trial apparatus for examining the combustion behavior of fluorine-sensitive substances (e.g., uranium compounds) in a fluorine flow calorimeter were discussed previously.[8] Satisfactory combustions of uranium monosulfide (US) were obtained in a trial flow system, while some of the problems associated with combustions in a bomb calorimeter were avoided. As a result, a flow calorimetric system was designed and is now completely assembled. A quartz-crystal thermometer (see part 11) is used to measure temperature. Electrical calibrations of the calorimetric system indicate that the precision of the energy measurements is about 0.01%. A preliminary series of combustions of US in fluorine is in progress. If the flow calorimeter proves to be well suited to this study, it will be used in an extensive program involving the thermochemistry of uranium compounds.

[8] ANL-6925, p. 182.

7. Bond Energies in the Chalcogen Fluorides and Oxyfluorides (P. A. G. O'Hare, H. M. Feder)

In this report, earlier bond-energy calculations[9] are updated and extended.

a. SULFUR FLUORIDES

For the electron impact dissociation reaction

$$SF_6(g) + e^- \rightarrow SF_5(g) + F^- \qquad (3)$$

Curran[10] has measured $\phi_{\text{kinetic}} = 0.23 \pm 0.05$ eV and $A_o(F^-) = 0^{+0.05}_{-0.00}$ eV. These values, combined with $E_a(F) = 3.448 \pm 0.005$ eV[11] and the plausible assumption that the internal excitation energy of the SF_5 fragment is small, yield D_1, the primary bond dissociation energy in SF_6:

$$D_1 = D(SF_5\text{—}F) = 3.218 \pm 0.071 \text{ eV}$$
$$= 74.2 \pm 1.6 \text{ kcal mol}^{-1}$$

The enthalpy of formation of the SF_5 fragment was calculated from the equation

$$\Delta Hf^\circ(SF_5, g) = D_1 - \Delta Hf^\circ(F,g) + \Delta Hf^\circ(SF_6, g) \qquad (4)$$

in which $\Delta Hf^\circ(F,g) = 18.9$ kcal mol^{-1} [12] and

[9] ANL-7125, pp. 135–137.

[10] R. K. Curran, J. Chem. Phys. **38**, 780 (1963).

[11] R. S. Berry and C W. Reimann, J. Chem. Phys. **34**, 1069 (1961).

[12] D. D. Wagman et al, "Selected Values of Chemical Thermodynamic Properties, Part I," N.B.S. Technical Note 270-1, U.S. Department of Commerce, National Bureau of Standards, Washington, D. C., October, 1965.

$$\Delta Hf^\circ(SF_6, g) = -291.8 \pm 0.2 \text{ kcal mol}^{-1}.$$[13]

Thus,

$$\Delta Hf^\circ(SF_5, g) = -236.5 \pm 1.6 \text{ kcal mol}^{-1}.$$

In the stepwise dissociation of SF_6, the dissociation energy of the second bond, D_2, was calculated from eq. 5:

$$\begin{aligned} D_2 &= D(SF_4\text{—}F) \\ &= \Delta Hf^\circ(SF_4, g) + \Delta Hf^\circ(F,g) - \Delta Hf^\circ(SF_5, g) \end{aligned} \quad (5)$$

A value of -182 ± 4 kcal mol^{-1} was selected for $\Delta Hf^\circ(SF_4, g)$ on the basis of the results of two investigations.[14, 15] Substitution in eq. 5 gives

$$D_2 = 73.4 \pm 4.3 \text{ kcal mol}^{-1}.$$

Within the quoted uncertainties $D_1 = D_2$; also,

$$D_{12} = D_1 + D_2 = 147.6 \pm 4.0 \text{ kcal mol}^{-1}.$$

This result depends only on $\Delta Hf^\circ(SF_4)$ and $\Delta Hf^\circ(SF_6)$. Kay and Page[16] using a magnetron technique, reported $D_1 = 86.1 \pm 3$ kcal mol^{-1}, $D_2 = 35.1 \pm 1$ kcal mol^{-1}, and, thus, $D_{12} = 121.2 \pm 3$ kcal mol^{-1}. This value is in serious disagreement with the value $D_{12} = 147.6 \pm 4.0$ kcal mol^{-1}. Unless $\Delta Hf^\circ(SF_4, g)$ or $\Delta Hf^\circ(SF_6, g)$ is in error by 20 to 30 kcal mol^{-1}, which seems improbable, the data of Kay and Page must be faulty.

The enthalpy of the reaction

$$SF_4(g) \rightarrow SF_2(g) + 2\,F(g), \quad (6)$$

which is equivalent to $D_3 + D_4$, was calculated from eq. 7:

$$\begin{aligned} D_{34} &= \Delta Hf^\circ(SF_2, g) + 2\,\Delta Hf^\circ(F,g) \\ &\quad - \Delta Hf^\circ(SF_4, g) \\ &= 151.8 \pm 4.5 \text{ kcal mol}^{-1} \end{aligned} \quad (7)$$

The value $\Delta Hf^\circ(SF_2, g) = -68 \pm 2$ kcal mol^{-1} (see part 7.d.) was used in eq. 7.

Finally, the enthalpy of the reaction

$$SF_2(g) \rightarrow S(g) + 2\,F(g),$$

which is equivalent to $D_5 + D_6 = D_{56}$, was calculated from eq. 8, in which $\Delta Hf^\circ(S,g) = 65.9 \pm 0.5$ kcal mol^{-1}.[17]

$$\begin{aligned} D_{56} &= \Delta Hf^\circ(S,g) + 2\,\Delta Hf^\circ(F,g) \\ &\quad - \Delta Hf^\circ(SF_2, g). \\ &= 171.7 \pm 2.2 \text{ kcal mol}^{-1} \end{aligned} \quad (8)$$

b. SELENIUM FLUORIDES

None of the individual bond strengths in SeF_6 have been measured directly. Values for D_{12}, D_{34}, and D_{56} were deduced from thermochemical data.

The sum of the first two bond dissociation energies (D_{12}) is given by the equation:

$$\begin{aligned} D_{12} = D_1 + D_2 &= \Delta Hf^\circ(SeF_4, g) \\ &\quad + 2\,\Delta Hf^\circ(F,g) \\ &\quad - \Delta Hf^\circ(SeF_6, g) \\ &= 122.0 \pm 2.0 \text{ kcal mol}^{-1} \end{aligned} \quad (9)$$

in which $\Delta Hf^\circ(SeF_6, g) = -267.0 \pm 0.1$ kcal mol^{-1} [13] and $\Delta Hf^\circ(SeF_4, g) = -182.8 \pm 2.0$ kcal mol^{-1}.[18] If it is assumed that $D_1 = D_2$ (by analogy with SF_6), a value of -225 ± 1 kcal mol^{-1} can be estimated for $\Delta Hf^\circ(SeF_5, g)$. In part 7.d., $\Delta Hf^\circ(SeF_2, g)$ is estimated to be -75 ± 3 kcal mol^{-1}; from equations similar to eq. 7 and 8 we derive

$$D_{34} = 145.6 \pm 3.5 \text{ kcal mol}^{-1},$$

and

$$D_{56} = 164.0 \pm 3.0 \text{ kcal mol}^{-1}.$$

$\Delta Hf^\circ(Se,g)$ was taken to be 51.2 ± 1 kcal mol^{-1}.[19]

c. TELLURIUM FLUORIDES

The following values were calculated for the successive bond dissociation energies of TeF_6; the method used has been given in parts 7.a. and 7.b.

$$D_{12} = 137.8 \pm 2.1 \text{ kcal mol}^{-1}$$

$$D_{34} = 170.0 \pm 3.0 \text{ kcal mol}^{-1}$$

$$D_{56} = 179.4 \pm 2.2 \text{ kcal mol}^{-1}$$

In addition to $\Delta Hf^\circ(F,g) = 18.9$ kcal mol^{-1},[12] the following enthalpies of formation (kcal mol^{-1}) were used in the calculations: $\Delta Hf^\circ(TeF_6, g) = -327.2 \pm 0.6$,[13] $\Delta Hf^\circ(TeF_4, c) = -241.7 \pm 2.0$,[15] $\Delta H_{sub}(TeF_4) = 14.5$,[20] $\Delta Hf^\circ(TeF_2, g) = -95 \pm 5$ (see part 7.d.), and $\Delta Hf^\circ(Te,g) = 46.6 \pm 1.0$.[10] If one assumes $D_1 = D_2$, by analogy with SF_6, then $\Delta Hf^\circ(TeF_5, g) = -277 \pm 2$ kcal mol^{-1}.

[13] P. A. G. O'Hare, J. L. Settle, and W. N. Hubbard, Trans. Faraday Soc. **62**, 558 (1966).

[14] J. D. Vaughn and E. L. Muetterties, J. Phys. Chem. **64**, 1787 (1960).

[15] M. J. Nichols, Ph.D. Thesis, University of Durham, England, 1958.

[16] J. Kay and F. M. Page, Trans. Faraday Soc. **62**, 1042 (1964).

[17] H. Mackle and P. A. G. O'Hare, Tetrahedron **19**, 961 (1963)

[18] A value of -194 ± 2 kcal mol^{-1} for $\Delta Hf^\circ(SeF_4,\ell)$, recalculated from ref. 15, was combined with $H_s(SeF_4,\ell) = 11.2$ kcal mol^{-1} [R. D. Peacock, J. Chem. Soc. 3617 (1953)].

[19] J. Berkowitz and W. A. Chupka, Argonne National Laboratory, private communication.

[20] J. H. Junkins, H. A. Bernhardt, and E. J. Barber, J. Am. Chem. Soc. **74**, 5749 (1952).

TABLE III-5. Bond Dissociation Energies of the Chalcogen Fluorides

in kcal mol^{-1}

	SF_6	SeF_6	TeF_6
D_{12}	147.6	122.0	137.8
D_{34}	151.8	145.6	170.0
D_{56}	171.7	164.0	179.4

The bond dissociation energies derived in parts 7.a., 7.b., and 7.c. are summarized in Table III-5. The nonmonotonic variation in the bonding of the chalcogen hexafluorides has been noted and discussed previously.[9] The main point to be deduced from Table III-5 is that the anomaly in the hexafluorides also extends to the tetra- and difluorides. That is, the energy liberated in the formation of each successive bond between selenium and fluorine is smaller than in the similar reactions of fluorine with either sulfur or tellurium.

d. CHALCOGEN OXYFLUORIDES

(i) *SO_2F_2*. From electron impact studies, Reese et al[21] have shown that the sums of the S=O bond energies in SO_2 and SO_2F_2 are identical; thus

$$\Delta Hf^\circ(SF_2, g) = \Delta Hf^\circ(S,g) + \Delta Hf^\circ(SO_2F_2, g) - \Delta Hf^\circ(SO_2, g). \quad (10)$$

In addition to the value $\Delta Hf^\circ(S,g) = 65.9 \pm 0.5$ kcal mol^{-1},[17] the following values (kcal mol^{-1}) were inserted in eq. 10: $\Delta Hf^\circ(SO_2F_2, g) = -205.2 \pm 2.0$[21] and $\Delta Hf^\circ(SO_2, g) = -70.9$.[12] Substitution in eq. 10 gives

$$\Delta Hf^\circ(SF_2, g) = -68.4 \pm 2.0 \text{ kcal mol}^{-1}.$$

Data for the oxyfluorides SOF_2 and SOF_4 would be valuable, but they are not available.

(ii) *$SeOF_2$*. A value of -126.0 ± 1.0 kcal mol^{-1} has been derived for $\Delta Hf^\circ(SeOF_2, \ell)$ based on Nichols'[15] measurements. The Clausius-Clapeyron equation, in conjunction with vapor pressure measurements reported by Dagron,[22] had been used to calculate

$$\Delta H_v(SeOF_2, \ell) = 10.6 \pm 0.1 \text{ kcal mol}^{-1}.$$

Thus, $\Delta Hf^\circ(SeOF_2, g) = -115.4 \pm$ .. kcal mol^{-1}. The enthalpy of reaction 11 is estimated to be -40 ± 3 kcal mol^{-1} by analogy with the enthalpies of formation of the monoxides from other selenium compounds.

$$SeF_2(g) + \tfrac{1}{2} O_2(g) \rightarrow SeOF_2(g), \quad \Delta H = -40 \pm 3 \text{ kcal mol}^{-1} \quad (11)$$

Therefore,

$$\Delta Hf^\circ(SeF_2, g) = -75 \pm 3 \text{ kcal mol}^{-1}.$$

Feber[23] has estimated $\Delta Hf^\circ(SeF_2, g)$ to be -80 kcal mol^{-1}.

If it is assumed (by analogy with SO_2F_2) that the sum of the Se=O bond strengths in SeO_2F_2 is equal to the sum of the bond strengths in SeO_2, namely 201.4 ± 1.0 kcal mol^{-1},[10, 12, 24] then

$$\Delta Hf^\circ(SeO_2F_2, g) = 2\,\Delta Hf^\circ(O,g) + \Delta Hf^\circ(SeF_2, g) - 201.4 = -157.2 \pm 3.1 \text{ kcal mol}^{-1}. \quad (12)$$

e. TELLURIUM DIFLUORIDE

The enthalpy of dissociation of $TeF_2(g)$ has been estimated by analogy. For both $SF_2(g)$ and $SeF_2(g)$ one finds

$$D(MF_2) = 2.2\,\bar{D}(M\text{—}F)_{MF_6} \quad (13)$$

Since $\bar{D}(Te\text{—}F)_{TeF_6} = 81.2 \pm 2.0$ kcal mol^{-1},[10] one estimates $D(TeF_2)$ to be 179 ± 5 kcal mol^{-1}. By substitution in an equation analogous to eq. 8, one obtains $\Delta Hf^\circ(TeF_2, g) = -95 \pm 5$ kcal mol^{-1}. Feber[23] has estimated $\Delta Hf^\circ(TeF_2, g)$ to be -104 kcal mol^{-1}; use of this value rather than our own estimate does not change the conclusions about the significant variations in Table III-5.

[21] R. M. Reese, V. H. Dibeler, and J. L. Franklin, J. Chem. Phys. **29**, 880 (1958).

[22] C. Dagron, Compt. Rend. **255**, 122 (1962).

[23] R. C. Feber, "Heats of Dissociation of Gaseous Halides," LA-3164, November, 1964.

[24] J. R. Soulen, P. Sthapitanonda, and J. L. Margrave, J. Phys. Chem. **59**, 132 (1955).

8. Separation of Volatile Fluorides by Fractional Volatilization (E. Rudzitis)

In connection with calorimetric studies of volatile, inorganic fluorine compounds, it became necessary to separate components of gaseous mixtures and to determine limits of detection of the components. Known separations by fractional distillation[25,26] and gas chromatography[27-32] were not sufficiently sensitive or

[25] P. L. Allen and J. F. Ellis, UKAEA Report IGR-R, CA-216, 1957.

[26] N. C. Orric and J. D. Gibson, Anal. Chem. **25**, 1100 (1953).

[27] A. Engelbrecht, E. Nachbaur, and E. Meyer, J. Chromatog. **15**, 228 (1964).

[28] G. Iveson and A. G. Hamlin, *Gas Chromatography 1960*, R. P. W. Scott, Ed., Butterworths, London, 1961, p. 33.

[29] T. R. Phillips and D. R. Owens, ibid., p. 308.

[30] R. S. Juvet, Jr., and R. S. Fisher, Anal. Chem. **37**, 1752 (1965).

[31] R. A. Lantheaume, ibid., **36**, 468 (1964).

[32] O. Rochefort, Anal. Chim. Acta **29**, 350 (1963).

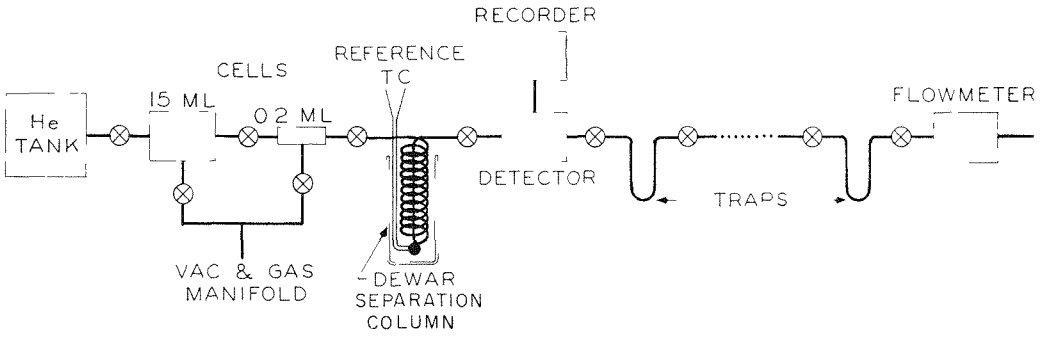

308-41 Rev. 1

FIG. III-11. Gas Separation and Detection Apparatus.

versatile for our purposes, mostly because of limitations imposed by the chemical reactivity and corrosivity of the gases.

A new separation and analytical technique which uses certain features of both gas chromatography and fractional distillation was therefore developed. In common with gas chromatography, the gas mixture is swept by a helium stream through a separation column and into a detector. The separation, however, is accomplished by fractional volatilization in a metal-packed column. The main advantages of the technique are its simplicity (no involved column preparations are needed) and the chemical inertness of an all-metal system which minimizes interactions with reactive substances. The technique, nevertheless, retains the sensitivity of gas chromatography—the total amount of gas taken for analysis does not have to be more than 2 cc-atm. In common with fractional distillation, the proximity of boiling points, i.e., similar volatilities, imposes limitations on the effectiveness of the separations.

a. *Apparatus.* An all-metal system, except for some valve parts made of fluorothene, was assembled. It consisted of a helium source in series with two sample cells, a separation column, a detector, several traps, and a flowmeter. The system is shown schematically in Figure III-11. The components were connected by ⅛-in. dia. copper tubing and Whitey No. 0 valves.

The arrangement of the two sample cells was chosen to facilitate the preparation of standard gas mixtures for calibrations. Mixtures as dilute as 1 part in 10^5 in a total sample of 2 cc-atm could be prepared while keeping the pressure measurements in the convenient range between 0.1 and 100 torr.

The separation column was made of ¼-in. dia. copper tubing, originally 180 cm in length, which was filled with 10- to 20-mesh copper shot, and formed into a helical coil 30 cm long by 5 cm in diameter. The lower end of the coil was connected to the detector, a Gow-Mac 470 Series 30C micro thermal conductivity cell. The power-supply and bridge-control unit, Gow-Mac Model 999-D1, was operated at 9 ma, and the output was recorded on the 1 mV scale of a two-pen potentiometric recorder. Downstream from the detector were several traps, made of ⅛-in. dia. nickel U-tubes, and a flowmeter.

Temperatures along the separation column were monitored by five iron-constantan thermocouples spaced at approximately 30-cm intervals and were recorded on a multipoint recorder. The temperature of the thermocouple attached at the lowest point of the coil served as a reference temperature and was recorded on a 10 mV scale together with the detector output.

b. *Procedure.* Commercial helium, nominal purity 99.9%, is used without further purification. The helium flow rate and pressure are usually adjusted to 10 ml/min at 900 torr through the separation column. When higher sensitivity is desired, the flow rate is decreased to 5 ml/min; on the approach of a peak which might overload the detector, the flow rate is strongly increased for a few minutes to accomplish rapid flushing.

At the start of a run, the output valve is closed (to avoid back-suction of air), and the column is placed in a close-fitting Dewar and cooled by the addition of enough liquid nitrogen to cover the lower quarter of the column. During this time the sample cell(s) are valved off from the rest of the system, evacuated, and filled with gas(es) to be analyzed. After approximately 30 min, when steady temperatures have been achieved, the liquid nitrogen is dumped, the same Dewar is replaced, and helium flow through the sample cells and into the column is begun. At this time, typical thermocouple readings along the column, beginning with the reference thermocouple, are −195, −180, −160, −120, and −75°C. The column gradually and uniformly warms at a rate of about 1°C/min. The gases, which condense along the column according to their vapor pressures and the temperature gradient, repeatedly volatilize and recondense as the helium sweeps them down into the colder portion of the column. This re-

sults in fractionation of the gases, the fractions finally being swept past the coldest point of the column and into the detector.

The separated fractions can be trapped for identification or recycle without interrupting the experiment. Dewars are placed around the U-traps, and the Dewar furthest from the detector is filled with liquid nitrogen. As soon as the most volatile component is swept past the detector, as indicated by a peak on the recorder, the next to the furthest Dewar is filled with liquid nitrogen in order to condense the next most volatile component, and so on. When the experiment is completed, the traps are valved off in the same order.

c. *Results and Discussion.* Because separation in this procedure is based on a repeated condensation-volatilization process which is dependent on temperature alone, it is convenient to use the term "appearance temperature" in the same manner that the term "retention volume" is employed in gas chromatography. Appearance temperature may be defined as the reference temperature which is recorded simultaneously with the initial detector response to a given component. The appearance temperatures of selected components, as found with the apparatus described, are given below (in °C):

N_2, O_2, F_2	−190	CO_2, SF_6	−140
NF_3, CF_4	−175	SeF_6, SF_4	−135
Xe	−170	TeF_6	−130
PF_3	−160	POF_3	−115
BF_3, SiF_4, C_2F_6	−155	S_2F_{10}	−100
PF_5	−145		

The following mixtures have been separated and the minor components, indicated in parentheses, have been detected at concentrations of approximately 1 part in 10^4 in a total amount of approximately 10^{-4} mole: PF_5-(PF_3); CF_4-(C_2F_6); PF_3-PF_5-(NF_3); SF_6-(S_2F_{10}); Xe-PF_3-PF_5-(POF_3). Due to the proximity of their appearance temperatures, the detection of SF_4 in the presence of SF_6 was limited to approximately 1 part in 100.

The semi-empirical nature of the procedure makes it difficult to correlate appearance temperatures with the controllable variables of the separation such as the temperature gradient, rate of warming,[33] length and geometry of the column, and the helium flow rate. But, although the appearance temperatures have no absolute meaning and were not fixed more precisely than to the nearest five degrees, it was found that their relative order, as listed above, remained unchanged even when the variables were changed by as much as a factor of two. The components of an unknown mixture may also be identified by trapping the fractionated gases as described, and analyzing each fraction by infrared spectra or other analytical means.

[33] Improved separations may result from the incorporation of cryogenic temperature programming into the warm-up period, as has been done in gas chromatography [e.g., see C. Merritt, Jr., et al, Anal. Chem. **36**, 1503 (1964)].

9. 1500°C Drop Calorimeter (J. E. Brugger, R. Norris,[34] R. Barnes[35])

The furnace for the 1500°C drop-type calorimeter has been reassembled and is being tested. A number of furnace components were rebuilt to improve the mechanical stability and thermal properties of the unit. Tantalum-sheathed, magnesia-insulated tantalum resistance heaters, and similarly sheathed and insulated Pt-10% Rh/Pt thermocouples, have been installed in place of the ceramic-sheathed assemblies used previously.

Improved circuitry for determining the electrical power dissipated in the copper-block calorimeter during calibration has been taken to the breadboard stage. Meanwhile, reexamination of the temperature-*vs.*-time data taken during electrical calibration has shown that one may detect effects due to the changes with temperature of the calorimeter block (about 0.1%/°C) and the heat leak constant (0.4%/°C). The computational program in current use does not explicitly take these changes into account, nor the fact that the jacket temperature tends to follow that of the block. Because of the latter, the convergence temperature is a function of the temperature offset between the block and the jacket. The convergence temperature can vary by millidegrees per degree offset. In the future, more care will be taken to monitor the jacket temperature and to maintain a steady and high flow rate of thermostated water to the jacket; the computational program will also be improved.

A working model of a device for determining the position of a dropping capsule as a function of time has been built and tested. A photodiode and light source were located on opposite sides of the suspension tape, which was perforated at 1-in. intervals. The signals produced by the pulses of light generated by moving the tape were recorded on a moderately fast, sensitized-paper oscillograph. The device can be adapted to program the closing of the calorimeter shutter and furnace gate for the introduction of gas into the calorimeter chamber after a drop.

[34] Student Aide, Beloit College.

[35] Co-op Student, University of Missouri.

10. 2500°C Electron-Beam-Heated Calorimetric System (D. R. Fredrickson)

The calorimetric system[36] for determining enthalpy increments to 2500°C has been completely assembled.

As mentioned in the last report,[37] a persistent problem has been the stalling of the rotating target when a furnace temperature of 1700°C is exceeded. After numerous tests it was concluded that the problem originated in the shaft and bearings. The housing was modified and the bearings were relocated so that they are further up the shaft. Provision has also been made for additional cooling of the shaft, if necessary: a copper fin brazed to the shaft rotates in a well which can be filled with oil and which is connected to a water-cooled jacket. It has not yet been necessary to use any fluid in the well, since the stalling problem seems to have been solved.

Copper-block calorimeter II[37] has been assembled with its associated optical viewing port and water-cooled shutter. Provision has been made for temperature measurement of the copper block by either a capsule-type platinum-resistance thermometer or a quartz-crystal thermometer which were placed in the copper block at approximately equal distances from the center. An electrical calibration heater has been placed around the receiver well. The heater has a large surface area, which results in a low power density and allows fast heating of the calorimeter without overheating of the heater. Completing this assembly are the constant-temperature water bath, temperature controller, and circulating pump. These components maintain the calorimeter jacket temperature constant within ±0.002°C.

Electrical calibrations of the calorimeter are being carried out with both thermometers. Indications are that the quartz-crystal thermometer will be satisfactory. With its use, the system can be automated for print-out of time-temperature data.

The initial enthalpy measurements will be made on tantalum and tungsten.

[36] See Figure IV-1, ANL-7055, p. 175.

[37] ANL-7225, pp. 154–155.

11. Quartz-Crystal Thermometry (E. Greenberg, J. L. Settle, D. R. Fredrickson)

Resistance thermometry has been employed in the past at this laboratory to obtain the accurate and precise temperature measurements required in calorimetry. A novel technique[38] of measuring temperature, quartz-crystal thermometry, was recently tested. A quartz-crystal thermometer was used in two series of combustions of benzoic acid in oxygen. In one series, the visual read-out temperatures were recorded at arbitrary intervals; in the other, the print-out of the time-temperature data proceeded automatically. The precision of the results obtained in both series, 0.02%, was comparable to that obtained with a platinum resistance thermometer. Reading and recording the data, however, were considerably simplified by the quartz-crystal system, and particularly by the automatic print-out.

After these tests showed the system to be satisfactory, a complete quartz-crystal thermometric system was purchased. Several probes were included: one specially fitted for bomb calorimeter ANL-R2, and one for its isothermal jacket; a short (⅜ in.) one for insertion into copper-block calorimeter II; two for use with the flow calorimetric system; and one for use in the plutonium glovebox calorimetric unit. The thermometers in ANL-R2, the flow calorimetric system, and copper-block calorimeter II have now been used in various studies with very satisfactory results (see parts 3, 6, and 10).

An auxiliary timing device has been built to program the time-temperature data output at varying rates to suit the needs of the experimenter. At present, there are five rates available which range from one set of data each 12 seconds to one set each 120 seconds.

[38] ANL-7020, p. 171.

E. CHEMISTRY OF LIQUID METALS (F. Cafasso, H. M. Feder, M. Ader)

These studies are directed toward a better understanding of the basic factors which influence the chemistry of liquid metals in general, and the particular chemistry of liquid sodium pertinent to its practical use as a reactor coolant. For the sake of clarity and conciseness, the discussions of these studies are conveniently divided into two sections: (1) Fundamental Studies and (2) Liquid Sodium Coolant Chemistry.

1. Fundamental Studies

Significant advances in theoretical methods for treating the properties of liquid metals and alloys have been made in recent years. To parallel these advances, basic physico-chemical data on simple metallic systems which lend themselves readily to theoretical treatment are being collected. Toward this end, experimental measurements are being made of the thermodynamic activity of alkali metals in their liquid binary solutions, of the solubility of rare gases in selected liquid metals, and of the velocity and absorption of high-frequency sound in liquid metal solutions.

a. THERMODYNAMICS OF BINARY ALKALI METAL SOLUTIONS: THE Rb-Cs SYSTEM

(F. Cafasso, L. Jones)

The alkali metals are simple electron-gas-like systems for which the nearly-free-electron model, the pseudo-atom model, and similar approximations should be reasonably valid. The electronic structures and properties of their binary liquid alloys, therefore, should be more amenable to calculation than those of other metal alloys. To test such calculations, precise, experimentally measured, thermodynamic data on alkali metal systems will be required. Accordingly, thermodynamic activities of selected alkali metals in binary liquid solutions are being determined. The method is that of vapor-phase absorption spectrophotometry. This method, previously described[1] in connection with the determination of activities in the Na-K system, compares the absorption of resonance radiation by vapor over an alloy with that over a pure alkali metal. Activities, a_i, are calculated from the relationship $a_i = P_i/P_i^o$, where P_i and P_i^o are the monomeric partial pressures of the ith component over the alloy and over pure metal i, respectively. The activity of rubidium in Rb-Cs alloys has been measured in the current series of investigations.

Absorption measurements were made with the 7800 Å rubidium resonance line. Over the short temperature span of the measurements (42 to 47°C), no variation of activity outside of experimental uncertainty was observed. The measured activities were adjusted to 111°C, the temperature of available enthalpy-of-mixing data, by means of the equation:

$$\frac{\partial \ln a_{Rb}}{\partial T} = -\frac{\bar{L}_{Rb}}{RT^2} \qquad (1)$$

in which $\bar{L}_{Rb}$, the partial molar enthalpy of mixing of rubidium, can be calculated from the data of Yokokawa and Kleppa.[2] Table III-6 gives the activity (a_{Rb}), activity coefficient (γ_{Rb}), the partial molar excess Gibbs energy ($\bar{G}^{xs}_{Rb}$), the partial molar enthalpy of mixing, and the partial molar excess entropy ($\bar{S}^{xs}_{Rb}$) found for rubidium in each of three Rb-Cs alloys.

The two most significant results of this investigation are: (1) the values of γ_{Rb} do not differ from unity by more than their uncertainty, and (2) $\bar{S}^{xs}_{Rb}$ is small and approximately constant at -0.15 ± 0.06 eu. Because γ_{Rb} is so close to unity, the Gibbs-Duhem relationship will require that γ_{Cs} also be near unity. Hence, if enough data were available to compute ΔG^{xs}, the excess Gibbs energy of mixing, there is little doubt that its value would be small. The Rb-Cs system is probably as close to ideal as any liquid metallic solution known.

Since the deviation of the activity coefficient from unity at other compositions is not likely to be larger than the experimental uncertainty, continuation of this study was not considered worthwhile. Consequently, measurements on the Rb-Cs system were discontinued, and a study of sodium activity in selected Na-Rb alloys was begun.

b. SOLUBILITY OF ARGON IN LIQUID SODIUM

(E. Veleckis, R. Blomquist, R. Yonco, M. Perin[3])

The rare gases dissolve in liquid metals as neutral atoms.[4-6] The principal attractive interaction responsible for rare gas solution is believed to arise through the polarization of the rare gas atoms by the ions of the metal. To test this assumption, a quantitative eval-

[1] ANL-6725, p. 107; ANL-6925, p. 95; ANL-7055, p. 80

[2] T. Yokokawa and O. J. Kleppa, J. Chem. Phys. **40**, 46 (1964).

[3] Co-op Student, Northwestern University.

[4] G. W. Johnson and R. Shuttleworth, Phil. Mag. **4**, 957 (1959).

[5] G. W. Johnson, Phil. Mag. **6**, 943 (1961).

[6] ANL-6800, pp. 183–187.

TABLE III-6. Thermodynamic Activities and Excess Thermodynamic Functions of Rb in Rb-Cs Alloys at 111°C

Rb (a/o)	a_{Rb}	γ_{Rb}	$\bar{G}^{xs}_{Rb}$ (cal/g-atom)	$\bar{L}_{Rb}$[a] (cal/g-atom)	$\bar{S}^{xs}_{Rb}$ (eu)
20.3	0.199 ± 0.006	0.98 ± 0.03	−16 ± 23	−75.6 ± 3.0	−0.16 ± 0.06
35.5	0.362 ± 0.010	1.02 ± 0.03	15 ± 23	−49.5 ± 2.0	−0.17 ± 0.06
51.9	0.534 ± 0.016	1.03 ± 0.03	23 ± 23	−27.5 ± 1.1	−0.13 ± 0.06

[a] Calculated from data in ref. 2.

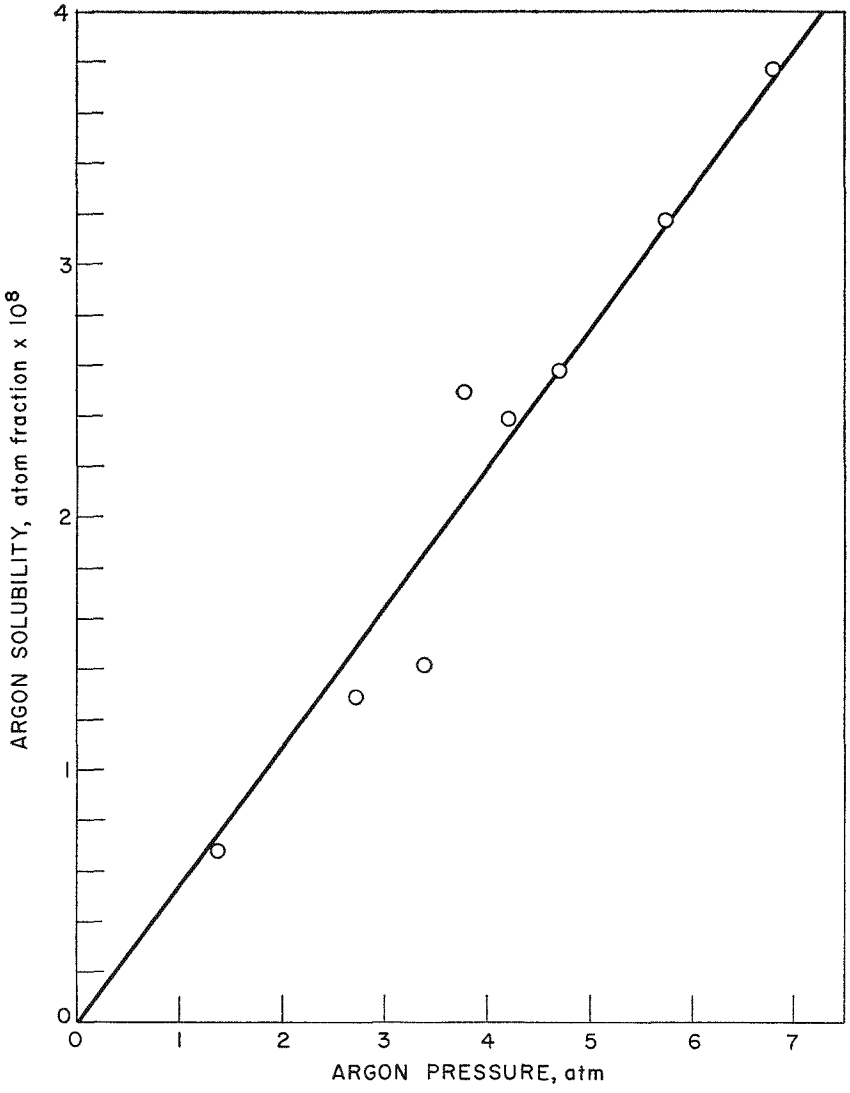

308-480

FIG. III-12. Solubility of Argon in Liquid Sodium at 480°C *vs.* Pressure (Henry's Law).

uation of the polarizability factor is being made by determining the solubilities of several rare gases in a series of alkali metals. The selection of alkali metals as solvents simplifies the evaluation of the repulsive interaction factors.

The argon-sodium system was the initial study in this series, and the results were reported previously.[6] However, subsequent reevaluation of the experimental method indicated that not all of the argon dissolved in the sodium had been recovered for analysis. Consequently, a new series of argon solubility experiments was carried out with the following changes in experimental procedure:

(1) A molecular sieve (Linde type 5A) rather than activated charcoal was used to trap the argon stripped from the sodium by helium sparging. This change was introduced purely for convenience since the efficiency of the trap was not altered.

(2) The method of collection of argon, by recirculation of the argon-helium mixture through a liquid-nitrogen-cooled, molecular sieve trap for 10 minutes, was abandoned. Instead, adsorption of the argon on the molecular sieve bed was effected by permitting the mixture to leak through the cooled trap over a period of 30 minutes and exhausting the unadsorbed helium. This change was made because tests with argon-helium mixtures showed that, at most, only 50% of the argon was recovered by the circulation method. The single-pass, leak-exhaust method, however, gave >99% recovery.

(3) Because of greater sensitivity in the range 10 to 100 ppm argon, gas chromatography, rather

TABLE III-7. Dependence of the Solubility of Argon in Liquid Sodium on Temperature and Pressure

Temperature (°C)	Pressure, P (atm)	Solubility, x (atom fraction $\times 10^8$)	Henry's Law Constant, K_H ($atm^{-1} \times 10^9$)	Weighting Factor
330	6.67	0.286		
330	6.77	0.186	0.353 ± 0.086	2
329	6.80	0.250		
329	6.83	0.251		
380	6.76	0.295		
380	6.80	0.374		
379	6.82	0.282	0.471 ± 0.097	2
379	6.84	0.383		
380	6.84	0.271		
430	6.73	1.80		
431	6.78	2.10	2.76 ± 0.46	3
431	6.80	1.65		
431	6.81	1.94		
481	1.36	0.677		
480	2.72	1.29		
480	3.40	1.41		
478	3.78	2.49	5.49 ± 0.47	6
480	4.22	2.39		
480	4.71	2.58		
480	5.74	3.17		
480	6.80	3.77		
530	3.54	7.03		
530	3.78	7.40		
531	3.91	7.34	19.4 ± 1.2	8
531	6.77	13.8		
530	6.79	13.6		
530	6.80	12.0		

than mass spectrometry, was used to analyze the argon-helium mixtures desorbed from the trap.

The results of twenty-seven solubility experiments are given in Table III-7. The data are subdivided into five sets of measurements, each performed at essentially the same temperature. The sets at 330, 380, and 431°C were obtained at approximately isobaric conditions, ~100 psia argon pressure. For the set at 530°C, two pressures were used, ~100 and ~50 psia. The pressure dependence of the solubility of argon in liquid sodium was determined by measuring solubilities at 480°C as a function of pressure over the range from 20 to 100 psia (1 to 7 atm).

The results of the pressure-dependence test are shown in Figure III-12. The data may be represented by the Henry's law equation, $x = K_H P$. The mean value of the Henry's law constant, K_H, calculated by the method of least squares for the data set at 480°C, was $5.49 \pm 0.47 \times 10^{-9}$ atm^{-1} (95% confidence level). Similar calculations for the remaining data sets gave the mean Henry's law constants listed in column 4 of Table III-7.

The dependence of K_H on temperature is shown in Figure III-13. Because the relative error of the K_H values varies with temperature, each value was weighted in the least-squares calculation of the regression line. The weighting factors were determined by dividing the K_H values by their respective errors and reducing the results by a factor of two. The best regression line may be represented by the equation

$$(330 \text{ to } 530°C) \quad \log K_H = -2.130 - 4542T^{-1}, \quad (2)$$

which reproduces the data with an uncertainty of 18% at the 95% confidence level. From eq. 2 the enthalpy of solution of argon in liquid sodium is 20.8 ± 2.0 kcal/molc.

The present argon solubilities are about 2.5 times larger than those measured earlier; the enthalpies of solution also differ, 20.8 *vs.* 15.8 kcal/mole, but the difference may not be significant.

The solubility and enthalpy of solution of argon in liquid sodium were calculated according to the models proposed by McMillan,[7] Johnson and Shuttle-

[7] W. G. McMillan, BNL-353 (T-63) (1955).

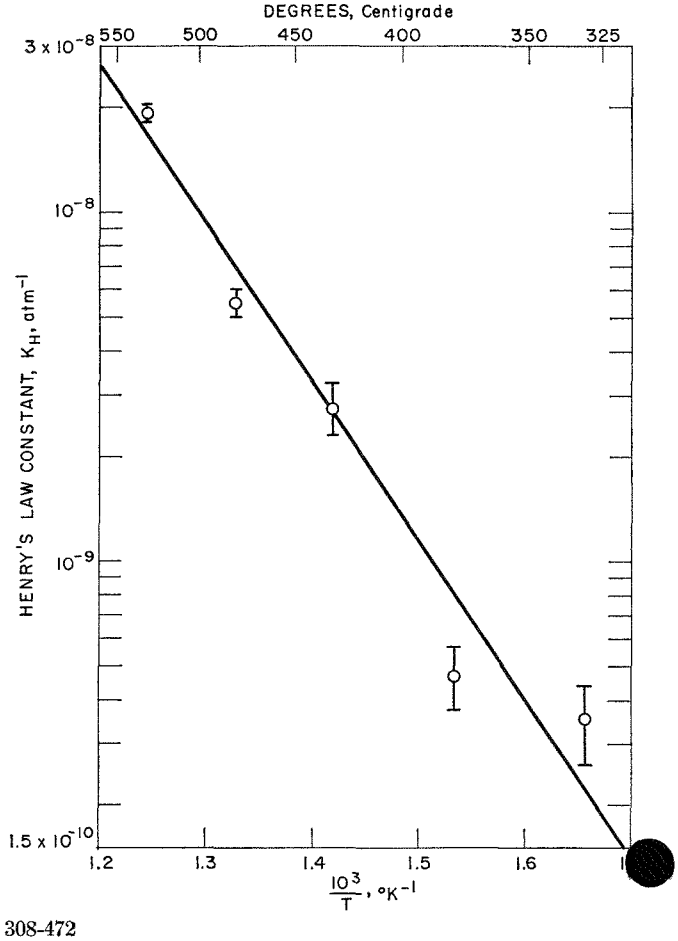

308-472

Fig. III-13. Henry's Law Constant *vs.* Temperature in the Argon-Sodium System (330 to 530°C).

worth,[4] and Pierotti.[8] The first two models yielded solubilities which were several orders of magnitude larger than the measured values, whereas the hard-sphere model of Pierotti yielded solubilities comparable to the measured values. Furthermore, although the enthalpy of solution calculated by either of the first two models was appreciably smaller than the observed, the enthalpy of solution calculated by the hard-sphere model was of the right magnitude. Further study of the solubility of gases in liquid alkali metals is expected to yield data which will permit further refinement of the hard-sphere model.

c. ULTRASONIC MEASUREMENTS IN LIQUID METALLIC SOLUTIONS (F. Cafasso, R. Blomquist)

The existence or nonexistence of distinct molecules in liquid alloys has been the subject of controversy for some time. Because liquid alloys are opaque to the usual spectroscopic methods, resolution of this controversy has been hampered. However, liquid alloys are not opaque to ultrasound. Therefore, the measurement of ultrasonic velocity or absorption in liquid alloys may prove to be useful in detecting the presence of molecules.

To investigate a large number of systems for evidence of molecule formation, it is more expedient to measure sound velocity than sound absorption. Consequently, various systems will be studied by the method of continuous variations in conjunction with ultrasonic velocity measurements. Because it has been claimed that magnesium and tin interact to form molecules with a composition Mg_2Sn, ternary liquid solutions formed by mixing Mg-Cd and Sn-Cd solutions will be studied first. Ultrasonic velocity will be measured as the ratio of magnesium to tin is progressively varied. The ternary solutions will be kept as dilute with respect to total magnesium and tin as is consistent with obtaining significant measurements.

The preliminary experiments are being made with pure liquids. Ultrasonic velocity is being measured by the pulse-echo method which involves the measurement of the time of travel of a short train of acoustic waves in a specimen of predetermined path length. Acoustic equipment for such measurements was previously assembled and tested with water and mercury at room temperature.[9] The performance and reliability of the equipment have now been tested at higher temperatures by measuring the velocity of sound in cadmium and in mercury.

With cadmium much difficulty was experienced before a method for transmission of sound into the liquid was found. For example, no observable sound was transmitted into prefiltered cadmium after it had been melted under dry helium, dry hydrogen, paraffin oil, silicone oil, or molten LiCl-KCl eutectic. Sound transmission into cadmium was finally effected after melting it under mineral oil. The velocity of sound in liquid

[8] R. A. Pierotti, J. Phys. Chem. **67**, 1840 (1963).

[9] ANL-7225, pp. 159–161.

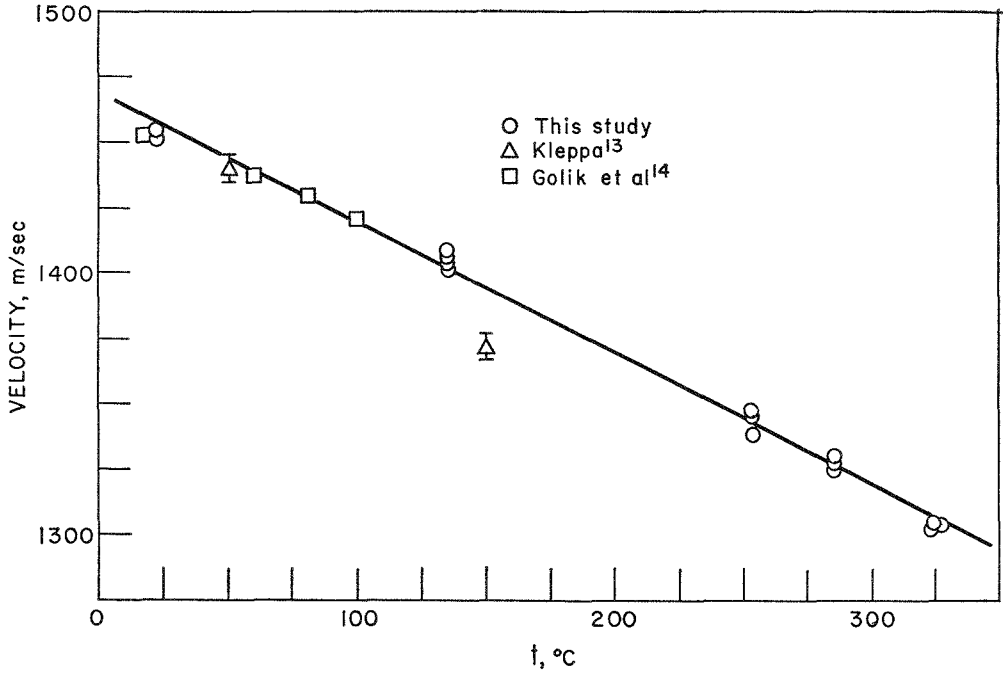

308-477

Fig. III-14. Velocity of Sound in Mercury *vs.* Temperature.

TABLE III-8. Acoustic Velocity and Compressibility Data for Mercury

t (°C)	This Study			Golik et al[a]		Kleppa[b]	
	ρ[a] (g/cm³)	v[c] (m/sec)	$\kappa_a \times 10^{12}$ (cm²/dyne)	v (m/sec)	$\kappa_a \times 10^{12}$ (cm²/dyne)	v (m/sec)	$\kappa_a \times 10^{12}$ (cm²/dyne)
20[d]	13.546	1457	3.48	1452	3.50		
40	13.497	1448	3.53	1445	3.55		
50	13.490	1443	3.56	1441	3.57	1440	3.58
60	13.448	1438	3.60	1437	3.60		
80	13.400	1429	3.65	1430	3.65		
100	13.351	1420	3.71	1422	3.70		
125	13.278	1408	3.80				
150	13.220	1397	3.88			1370	4.03
175	13.162	1385	3.96				
200	13.115	1374	4.04				
250	13.025	1351	4.21				
300	12.881	1328	4.40				
330	12.881	1314	4.50				

[a] Ref. 14.

[b] Ref. 13.

[c] Velocities calculated by means of the empirical equation $v(\text{m/sec}) = (1465.9 \pm 4.5) - (0.46 \pm 0.02)t$.

[d] Hubbard and Loomis[12] and Abowitz and Gordon[15] both report $v = 1451$ m/sec at 20°C, which yields $\kappa_a = 3.51 \times 10^{-12}$ cm²/dyne.

cadmium was determined to be 2247 ± 5 m/sec at 362°C. Filtration was observed not to affect the measured velocity, although it markedly improved the total sound transmission. The measured sound velocity in cadmium is slightly higher than the values, 2200 ± 20 m/sec at 321°C and 2215 ± 1 m/sec at 335°C, reported by Kleppa[10] and Plotskii et al,[11] respectively.

Mercury has been the subject of many ultrasonic studies.[12-15] Despite this attention, the dependence of sound velocity in mercury on temperature has been systemically studied only in the range 20 to 100°C.[14] In the present work it was found that the range of measurements on mercury could be extended to 330°C by maintaining the mercury under mineral oil.

Our results on the variation of sound velocity with temperature are shown in Figure III-14 together with the data of other investigators. The velocity (v) was found to decrease linearly between 22 and 330°C according to the equation

$$v(\text{m/sec}) = (1465.9 \pm 4.5) - (0.46 \pm 0.02)t\ (°\text{C}). \quad (3)$$

The temperature coefficient ($\partial v/\partial t$) of −0.46 ± 0.02 m/sec/deg. agrees with the value of −0.46 m/sec/deg. reported by Abowitz and Gordon.[15] Kleppa[13] reports a temperature coefficient of −0.6 m/sec/deg. on the basis of two measurements at 50 and 150°C; the latter measurement appears to be erroneous (see Figure III-14).

Adiabatic compressibilities, κ_a, of mercury were computed from the data by means of the equation

$$\kappa_a = \frac{1}{\rho v^2} \quad (4)$$

in which ρ is the density. The compressibilities are compared with values reported by Golik et al[14] and Kleppa[13] in Table III-8. No further measurements on mercury are planned.

The present equipment thus appears dependable for the measurement of velocities in liquid metals at temperatures up to 360°C. The velocities of sound in dilute solutions of magnesium in cadmium and of tin in cadmium will be measured next before proceeding to ternary solutions.

[10] O. J. Kleppa, J. Chem. Phys. **18**, 1331 (1950).

[11] I. G. Plotskii, V. F. Taborov, and Z. L. Khodov, Soviet Phys. Acoust. **5**, 202 (1959).

[12] J. C. Hubbard and A. L. Loomis, Phil. Mag. **5**, 1177 (1928).

[13] O. J. Kleppa, J. Chem. Phys. **17**, 668 (1949).

[14] A. Z. Golik, I. F. Kassen, and G. M. Kuchak, Soviet Phys. Acoust. **7**, 202 (1961).

[15] G. Abowitz and R. B. Gordon, Trans. A.I.M.E. **227**, 51 (1963).

2. Liquid Sodium Coolant Chemistry

The chemistry of liquid sodium is being studied to obtain fundamental information on chemical and physical phenomena which may lead to corrosion and, therefore, affect the use of sodium as a heat transfer fluid in nuclear reactors. Structural materials in contact with liquid sodium are known to undergo carburization, decarburization, nitridation, oxidation, reduction, and mass transfer. Of special interest, therefore, are the reactions of elements which enter metals interstitially, e.g., carbon, nitrogen, oxygen, and hydrogen, from contaminants in sodium. In order to reduce the work to manageable proportions, the current investigation has been restricted to the contaminant carbon.

The long-range objective of the program is the collection of sufficient data to understand and possibly control the carburization-decarburization phenomena encountered in sodium systems. The more immediate objectives are:

1) To develop reliable methods for the identification and determination of carbon-bearing species in sodium;
2) To characterize the products of reaction of typi-

cal carbon compounds with sodium at temperatures of practical interest;

3) To identify the mechanism(s) of carbon transport in sodium systems;
4) To develop methods for obtaining carbon-free sodium.

a. PHYSICAL NATURE OF CARBON IN SODIUM

(1) Solubility of Elemental Carbon in Sodium (C. Luner, K. Anderson)

Investigation of carbon transport in liquid sodium has been hampered by inadequate understanding of the transport mechanism and by uncertainties as to the nature and concentrations of carbon species in sodium. Elucidation of the nature and concentrations of the carbon-bearing species is being sought in current studies since such information would furnish a logical basis for the understanding of carbon transport phenomena. The present study has been directed toward the determination of whether or not a true solubility of elemental carbon in sodium exists.

The solubility of elemental carbon in sodium was reported earlier by Gratton.[16] His results were interpreted as showing a large (>10 ppm), temperature- and oxygen concentration-dependent, reversible solubility. However, detailed consideration of the experimental technique used led us to question these conclusions. In particular the experiments seemed inadequate to distinguish between dissolved carbon and small suspended particles. An attempt was made to repeat Gratton's experiment in this Laboratory but with a filtering technique which employed 5μ-porosity stainless steel filters. In contrast to Gratton's results, the carbon content of the filtered samples scattered considerably for a given condition and showed no smooth variation with temperature or time. It was concluded[17] that particulate carbonaceous matter, capable of passing through a 5μ filter, was present in the sampled sodium; the heterogeneity of the dispersion would account for the scatter of the results.

The existence of particulate carbonaceous matter in sodium has since been confirmed by ultracentrifugation,[18] filtration,[19] and dissolution[19] experiments. Therefore, to determine the true solubility of carbon in sodium it is necessary to differentiate between the carbon which has dissolved and the carbon which preexisted in the sample as nonfilterable material. In the present work, the discrimination was accomplished by the use of amorphous carbon labeled with ^{14}C. The use of a radioactive tracer also increased the sensitivity of the measurements many fold; concentrations of ^{14}C-labeled carbon as low as 5 parts in 10^9 parts of sodium could be detected. The radioactive carbon was obtained from New England Nuclear Corporation in the form of a pressed pellet with a specific activity of 2.4×10^6 dpm/mg. It was outgassed *in vacuo* at 1000°C before use. The pellet (135 mg) was added to 300 g of liquid sodium (Reactor Grade, U.S. Industrial Co.) in a stainless steel container. The total carbon content of the sodium charge was 32 ± 5 ppm, as determined by a lengthy series of analyses.

Filtered samples of sodium were withdrawn periodically at various temperatures (168 to 458°C) over a period of four months from the stirred and settled melt. The samples were analyzed for total carbon and radiocarbon.

The total carbon content of the filtered sodium was found to be 9.8 ± 3.2 ppm. No trend with time or temperature was apparent; thus two-thirds of the total carbon in this particular grade of sodium was ascertained to be particulate material which did not pass through a 5μ filter. The remaining third of the carbon, which did pass through the filter, was either dissolved or submicron-sized. In either case, this material was not in equilibrium with solid carbon because radiochemical analyses of the filtered samples indicated the absence of any significant amounts of radiocarbon at all temperatures investigated, even after four months of contact. It thus appears that the true solubility of elemental carbon in liquid sodium is less than 0.005 ppm (the limit of detection for the radiochemical method used) at temperatures up to 450°C.

(2) Zone-Melting Experiments (R. Yonco, E. Veleckis)

The tendency of particulate carbon in sodium to segregate was previously demonstrated[18] by repeated, unidirectional, zone melting of a column of sodium sealed in a fused silica tube. After 240 heating cycles, sodium cores extruded from the middle and bottom sections of the tube were found to contain 3 to 4 ppm carbon whereas the sodium residues adhering to the tube walls were found to be 5 to 10 times more concentrated in carbon. In order to determine the effect of the number of cycles on the apparent segregation of carbon, a zone-melting experiment of only 25 cycles was performed.

The experimental procedure was identical to that described in detail earlier.[18] The procedure, in brief, was as follows: About 25 g of filtered, reactor-grade sodium was sealed under vacuum in a 24-in. long, 10-mm OD, fused silica tube. The tube was mounted vertically in a Fisher Zone Refiner and was heated by a resistance ring which moved downward over the

[16] J. C. Gratton, KAPL-1807, June 30, 1957.
[17] ANL-6925, p. 92.
[18] ANL-7225, p. 156.
[19] ANL-7055, pp. 84, 85.

TABLE III-9. ANALYSES FOR CARBON DISPERSED IN LIQUID SODIUM BY DECOMPOSITION OF Na_2CO_3 AT 550°C

Sample	Ppm Carbon	
	Total (manometric)	Radiocarbon[a] (counting)
1, Filtered	11	<0.01
2, Filtered	11	0.01
3, Filtered	12	0.16
3H, Unfiltered	198	0.02
4, Filtered	12	0.36
5, Filtered	9	0.09
6, Filtered	8	0.07
7H, Unfiltered	13	0.02
7, Filtered	40	0.01

[a] Limit of detection, 0.01 ppm.

length of the sodium column. After 25 cycles the tube was divided into 28 sections. Each section was in turn divided into two parts for analyses: an extruded central core of solid sodium (approx. 8-mm OD) and a sodium residue (approx. 0.13 mm thick) adhering to the tubing walls.

Analysis of the cores and the sodium residues for total carbon showed an apparent radial segregation of carbon toward the sodium-silica interface. The residues were found to be 3 to 20 times more concentrated in total carbon than the sodium cores which contained carbon in the range 3 to 22 ppm. The large random scatter in the analyses of core samples from the top, middle, and bottom of the tube obscured any vertical segregation of carbon which may have existed. A statistical comparison of these results with similar results of the 240-cycle experiment, however, revealed no significant difference between the two experiments in this connection. No improvement in the vertical separation of carbon, therefore, is gained beyond 25 refining cycles.

(3) Casting Experiments (R. HEINRICH)

To determine whether or not radial segregation of carbon towards a sodium-tubing interface occurs in sodium-filled tubes that are not subjected to zone melting, the following simple experiment was done. Molten, unfiltered, reactor-grade sodium was either poured or drawn up into three 10-mm OD fused silica tubes[20] and one clean 304 stainless steel tube (~10-mm OD). After solidification, sodium cores extruded from the four tubes and the sodium residues adhering to the three silica tubes were analyzed for total carbon. Analysis for total carbon in the residue adhering to the stainless steel tube was impractical because of the difficulty of differentiating such carbon from the carbon in the tubing.

Segregation of the carbon impurity occurred; the sodium cores were found to contain 9 to 15 ppm carbon, whereas the sodium residues adhering to the silica tubing were found to be 6 to 9 times more concentrated in carbon. Furthermore, the nature of the surface exposed to sodium did not appear to be an important factor; the extent of the segregation was about the same in the stainless steel and fused silica tubes.

It should be noted that in the 240- and 25-cycle zone-melting experiments reported in Part (2), liquid sodium was filtered into the tubes and allowed to solidify before cycling. It is quite likely, therefore, that the bulk of the radial segregation of carbon in these experiments occurred before the subsequent melt-freeze cycles. However, it is not possible unequivocally to exclude zone melting from having made a small contribution to the segregation. This contribution, if it occurred at all, would be superimposed on the initial segregation.

No further zone-melting or casting experiments are planned. However, the surface activity of the particulate carbon in sodium will be explored as a possible mechanism for the observed segregation.

b. STUDIES OF THE CARBURIZATION AND DECARBURIZATION OF STEEL

(1) Preparation of Stable Dispersions of Carbon-14 in Liquid Sodium (R. HEINRICH)

A potentially serious problem associated with the use of liquid sodium in nuclear reactors is the tendency of metals to carburize or decarburize. Although much research has been done in this area, the mechanism by which liquid sodium acts as a medium for the transport of carbon is not understood. Experience has shown that the bulk of the carbon impurity in sodium is particulate. The ability of sodium to act as a corrodent may therefore be determined by its ability to act as a dispersion medium for particulate solids as well as its ability to act as a solvent for impurities and reaction products. Consequently, a study of corrosion in sodium systems may require information on the formation, stabilization, and destruction of dispersed systems in sodium. Accordingly, it is the aim of this research to prepare labeled, stable dispersions of carbon in sodium and to use them to test the possibility that corrosion in sodium systems may involve a colloidal species of carbon. A variety of methods must be examined to find the proper recipe for the formation and stabilization of a carbon dispersion.

The method first tested involved the decomposition

[20] These tubes were cleaned in hot chromic acid and rinsed in distilled water prior to use. This procedure is identical to that used in the zone-melting experiments.

of ^{14}C-labeled Na_2CO_3 in liquid sodium. A total of 564 mg of ^{14}C-labeled Na_2CO_3 was added in seven small increments (50 to 100 mg) over a 14-day period to 360 g of reactor-grade sodium in a stainless steel (SS) crucible. The sodium was kept at ~550°C and stirred continuously except during brief sampling periods. The additions were made by pressurizing the carbonate, which was sandwiched between two layers of sodium in a 0.25-in. OD SS tube, into the liquid sodium while the tube was submerged. After each addition, at least 24 hours were permitted to elapse before sampling. Filtered samples were taken by pressurizing the sodium into a 0.25-in. OD tantalum tube through a press-fitted, 5μ SS frit; unfiltered samples, by pressurizing the sodium into a 1-mm hole in the side of a closed-end tantalum tube. The samples were analyzed for total carbon[21] and radiocarbon.[22]

The analytical results are given in Table III-9. The total carbon contents found were (except for two samples) not significantly higher than in the starting filtered sodium which contained 9 to 13 ppm carbon. (The relatively high total carbon contents found in samples 3H and 7 are believed to arise from inadvertent contamination introduced when the bottom of the sample tube 3H was welded shut, and from an incompletely cleaned 5μ SS frit in sample tube 7.) The absence of significant dispersion is corroborated by the fact that the maximum radiocarbon content observed (sample 4) was only 0.2% of the maximum possible value. It appears that the Na_2CO_3 settled to the bottom of the crucible and probably decomposed there while in an agglomerated state. Evidence for this conclusion was obtained at the end of the experiment when the bulk of the sodium was decanted from the crucible and the residue was treated with ethyl alcohol. As the sodium reacted, there could be seen several clumps of carbon, each 1 to 3 mm in diameter, or approximately the same bulk size as the Na_2CO_3 increments initially introduced.

Further efforts to disperse finely divided ^{14}C-labeled carbon in liquid sodium will involve wetting, blending, and ultrasonic mixing techniques.

(2) Preparation of Carbon-14-Labeled Steels (C. LUNER)

Another potential method for studying the carbon transfer mechanism involves tracing the migration of radiocarbon present in a steel sample exposed to sodium. Preliminary studies of the availability of suitable specimens and of experimental designs have yielded encouraging results.

[21] Method: combustion in oxygen to Na_2O plus Na_2CO_3, followed by dissolution in dilute H_2SO_4, and manometric determination of the total carbon liberated as CO_2.

[22] Method: same as ref. 21 plus dissolution of the liberated $^{14}CO_2$-$^{12}CO_2$ mixture in a solution containing a scintillator, and determination of radiocarbon by counting in a liquid scintillation spectrometer.

IV

Reactor Safety[1]

(L. Baker, Jr., A. D. Tevebaugh, J. D. Bingle)

The program on reactor safety is concentrated in two areas of research: (1) studies relating to thermal (water-cooled) reactors, and (2) studies relating to fast (sodium-cooled) reactors.

In water-cooled reactors, coolant failure or a severe nuclear excursion could cause the reactor core metals to melt and disperse rapidly in the water. Chemical reactions between the metals and water could result in the release of energy approaching or exceeding the energy released by the fission process during a nuclear excursion. The dispersion of molten materials in the water coolant can also cause an explosive energy release as demonstrated in the SPERT 1 and BORAX 1 destructive tests. Studies of these chemical reactions and physical interactions are being carried out so that realistic estimates can be made of the rates and extents of reactions and interactions occurring during hypothetical reactor accidents.

The reactions of the metals of interest with water are being studied in several ways.[2] Experimental methods include isothermal reaction rate determinations, non-isothermal studies of the reactions with fine metal particles, in-pile meltdown experiments with specimens of typical reactor fuel materials, and heating experiments designed to simulate the conditions experienced by fuel elements during a loss-of-coolant accident. An additional research area consists of calculational studies in which experimental results obtained by several methods are correlated and methods of accident analysis are developed.

In sodium-cooled systems (fast reactors), coolant failure or a severe nuclear excursion could cause melting and rapid dispersion of reactor materials in the sodium. To assess these and other potential problem areas, the following studies relating to the safety of fast reactors are being carried out: (1) transient heat transfer associated with the dispersal of fuel and cladding materials into liquid sodium, (2) in-pile meltdown of typical fast reactor fuel materials, (3) high temperature physical properties of fast reactor materials, (4) fuel migration and segregation in mixed uranium-plutonium compounds, and (5) reaction of sodium with air.

[1] A summary of this section is given on pages 12 to 14.

[2] For the purposes of this report, the studies of the physical interactions (pressure pulse and transient heat transfer) accompanying the dispersal of molten materials in water coolant are discussed together with similar work being done in sodium coolant under Fast Reactor Safety Studies. This is because of the similar nature of the experimental and theoretical work involved in both.

A. THERMAL REACTOR SAFETY STUDIES

1. Isothermal Studies of the Stainless Steel-Steam Reaction

(R. E. Wilson, C. Barnes, Jr.)

Studies of the reactions between molten metals and steam are needed to provide kinetic rate data for predicting, by means of mathematical models, the chemical behavior of core materials during hypothetical reactor incidents. The reaction of molten stainless steel with steam is of particular interest because of the large number of power reactors which employ stainless steel core components.

The reaction of stainless steel with steam has been studied previously by an induction heating meth (ANL-6900, p. 239) over the temperature range 1100 to 1400°C. However, samples heated to 1400°C under-

vent rapid swelling and foaming, and, as the sample disintegrated, all control of temperature was lost because of changes in inductive coupling between the induction coil and the sample. It was concluded that the reaction rate data for temperatures above 1300°C were questionable and that another method of heating the samples was needed. Consequently, most of the experiments at temperatures of 1300°C and above were performed in a high-pressure furnace.

The high-pressure furnace, which is designed to operate at a maximum pressure of 1000 psi and at temperatures up to 1700°C, allows heating of a sample by a method unaffected by sample disintegration. The furnace, which has been previously described (see ANL-6900, p. 242; ANL-6925, p. 187; and ANL-7055, p. 177), is contained in a steel pressure vessel and consists of two zones: an internal steam-filled zone that is surrounded by an alumina tube and an external zone that is argon-filled. The argon-filled zone contains molybdenum heater windings and insulation. The pressures in the two zones are automatically matched to avoid stresses on the alumina tube. Water is introduced into the lower part of the steam zone by a positive-displacement pump and is converted to steam. At the start of an experiment, the sample is elevated from a moderate-temperature section, where reaction with steam is negligible, into the high-temperature section. Some unreacted steam and the hydrogen produced by the metal-steam reaction are continuously removed from the upper part of the steam zone (high-temperature section) through an outlet valve. The extent and the rate of metal-steam reaction are determined by continuously monitoring the amount of hydrogen collected. Upon completion of the experiment, the sample is lowered to its initial position. In these experiments, the samples were contained in alumina crucibles.

Experiments designed to determine the stoichiometry of the stainless steel-steam reaction and an analysis of the thermodynamics of the reaction were reported previously (ANL-7125, p. 152). It was shown in these studies that the average yield of hydrogen was 0.51 ± 0.01 liter (STP)/g and that the reaction product was a mixture of spinel compounds of the type Fe_3O_4, $NiFe_2O_4$, $FeCr_2O_4$, and $NiCr_2O_4$ (theoretical hydrogen yield for complete conversion to spinel compounds: 0.54 liter (STP)/g). The existence of the spinel structure was verified by X-ray diffraction analysis. The thermodynamic analysis indicated that the spinel compounds had a stabilization energy of the order of 5 to 8 kcal/mole in excess of the free energy of formation of the individual oxides: NiO, Cr_2O_3, FeO, and Fe_2O_3. The heat of reaction of type 304 stainless steel with steam was calculated to be 254 cal/g for solid steel forming a solid oxide at 1600°K (1327°C) and 155 cal/g for molten steel forming a molten oxide at higher temperatures.

Additional experiments have been performed in the high-pressure furnace to determine isothermal reaction rates over the temperature range 1300 to 1600°C. These are reported in the following paragraphs. The samples were type 304 stainless steel (16.8 w/o Cr, 8.3 w/o Ni, 1.7 w/o Mn, 73.2 w/o Fe) discs, ¾ in. in diameter and of variable thickness. Steam flow rate through the furnace varied from a minimum of 5 g steam/min (sufficient steam to oxidize a 13 g sample to completion in one min) to a maximum of 12 g steam/min.

a. REACTION RATE AT 1300°C

The results of two experiments in the high-pressure furnace at 1300°C and 1 atm pressure are presented in Figure IV-1 along with the results of two previously reported experiments (see ANL-6900, p. 239) performed by the induction heating method. The data are plotted as volume of hydrogen evolved per square centimeter of sample area vs. time. In the present experiments, as in the induction heating experiments, the trend of decreasing initial reaction rate with increasing heat-up time was observed. The initial reaction rate, which was approximately linear, decreased from about 3.1 to 1.1 ml H_2(STP)/(cm²)(min) as the heat-up time increased from 3 to 9 min. After about 20 min, the reaction rate was linear and ranged from 2.5 to 1.2 ml H_2 (STP)/(cm²) (min) for the four experiments.

The extent of reaction for the 3-min heat-up time experiment (see upper curve in Figure IV-1) is in reasonable agreement with results at 1250°C which have been reported by another research group.[3] Their results were reported in terms of an initial linear reaction rate followed by a parabolic oxidation rate instead of two linear rates as indicated above.

b. REACTION RATE AT 1400°C

No experiments were performed at 1400°C during this reporting period. The results of three experiments at 1400°C and 1 atm pressure were reported in ANL-7125, p. 150. Also reported were one experiment at 2 atm and one at 12 atm which showed that there was no significant effect of steam pressure on the reaction. At 1400°C, the samples underwent a rapid swelling and foaming so that the initial sample shape and surface area changed rapidly. The extent of reaction for experiments at 1400°C and higher is therefore reported in terms of the hydrogen generated per gram of sample instead of per cm² of sample area.

[3] "High Temperature Materials Program Progress Report No. 58A," General Electric Co., Nuclear Materials and Propulsion Operation, GEMP-58A, p. 58 (1966).

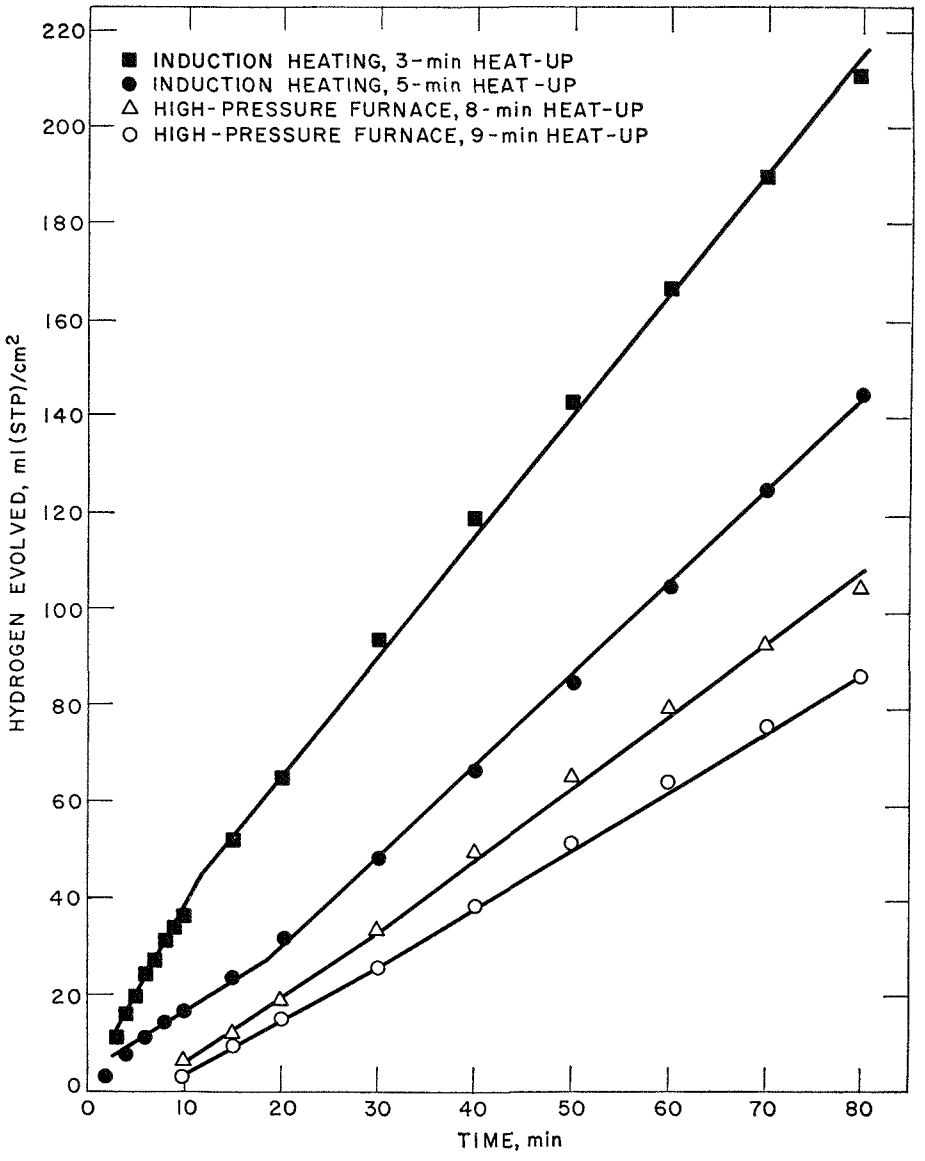

308-545

FIG. IV-1. Effect of Heat-up Time on the Reaction of Type 304 Stainless Steel with Steam at 1300°C and 1 atm Pressure.

c. REACTION RATE AT 1500°C

Two experiments were performed in the high-pressure furnace at 1500°C and one atm pressure. Results are given in Figure IV-2 along with photographs of the reacted samples. One sample of 5.3 g (¾-in. dia. disc, 0.09 in. thick) was completely reacted in 40 min; the other sample of 20 g (¾-in. dia. disc, 0.35 in. thick) was about 85% reacted after 90 min.

d. REACTION RATE AT 1600°C

Two experiments were performed in the high-pressure furnace at 1600°C and one atm pressure. Results are given in Figure IV-3 along with photographs of the reacted samples. Both samples weighed 14 g (¾-in. dia. disc, 0.24 in. thick). Although the two experiments were nominally identical, the observed reaction rates differed markedly. The complexity of the swelling and foaming phenomena is probably responsible for the lack of reproducibility.

Examination of the oxides from the experiments performed at 1500 and 1600°C indicates a similarity in grain structure between samples that reacted to completion (top photographs in Figures IV-2 and IV-3). Although there was a 100°C difference in their reaction temperatures, both had a smooth, foamy texture. The oxides from the 1500 and 1600°C samples that did not react to completion were more nodular in appearance, as can be seen in the bottom photographs of Figures IV-2 and IV-3. This indicates that the reaction rate is probably associated with the texture of the oxide at temperatures above the melting point of stainless steel.

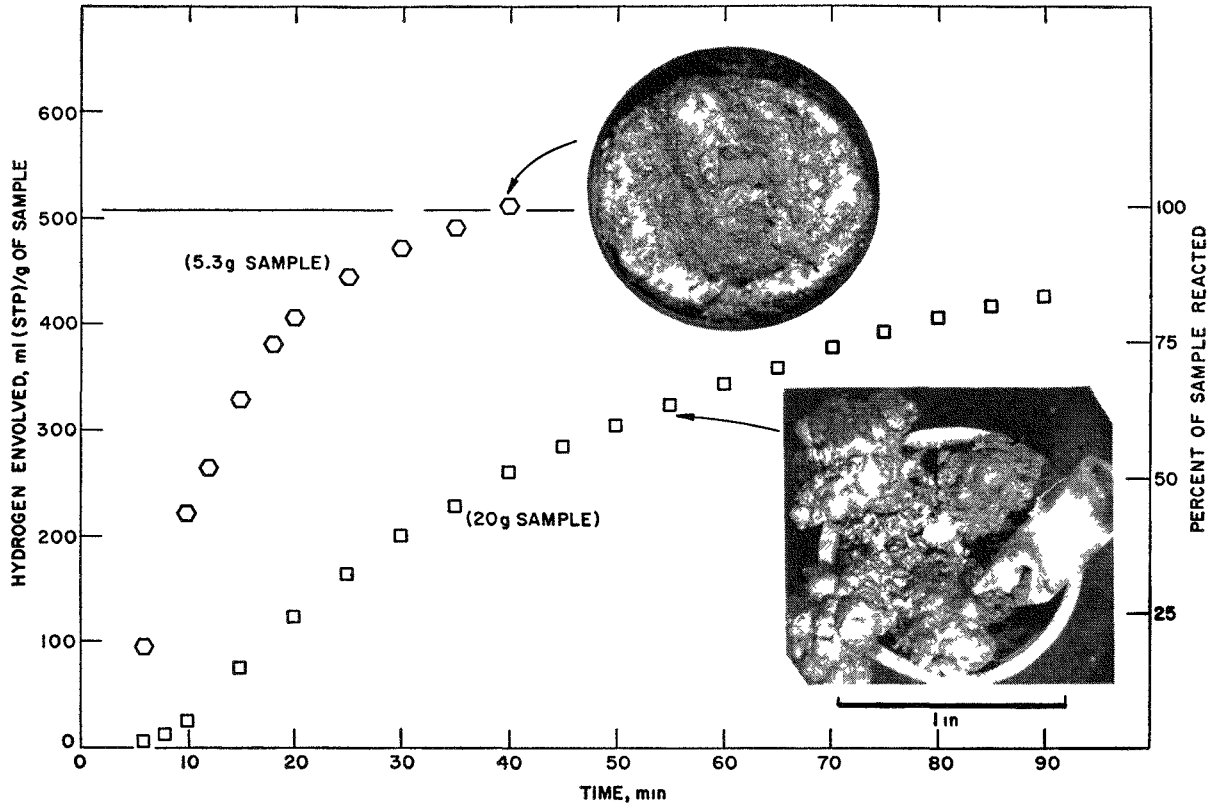

308 570

FIG IV-2 Reaction of Type 304 Stainless Steel with Steam at 1500°C and 1 atm Pressure

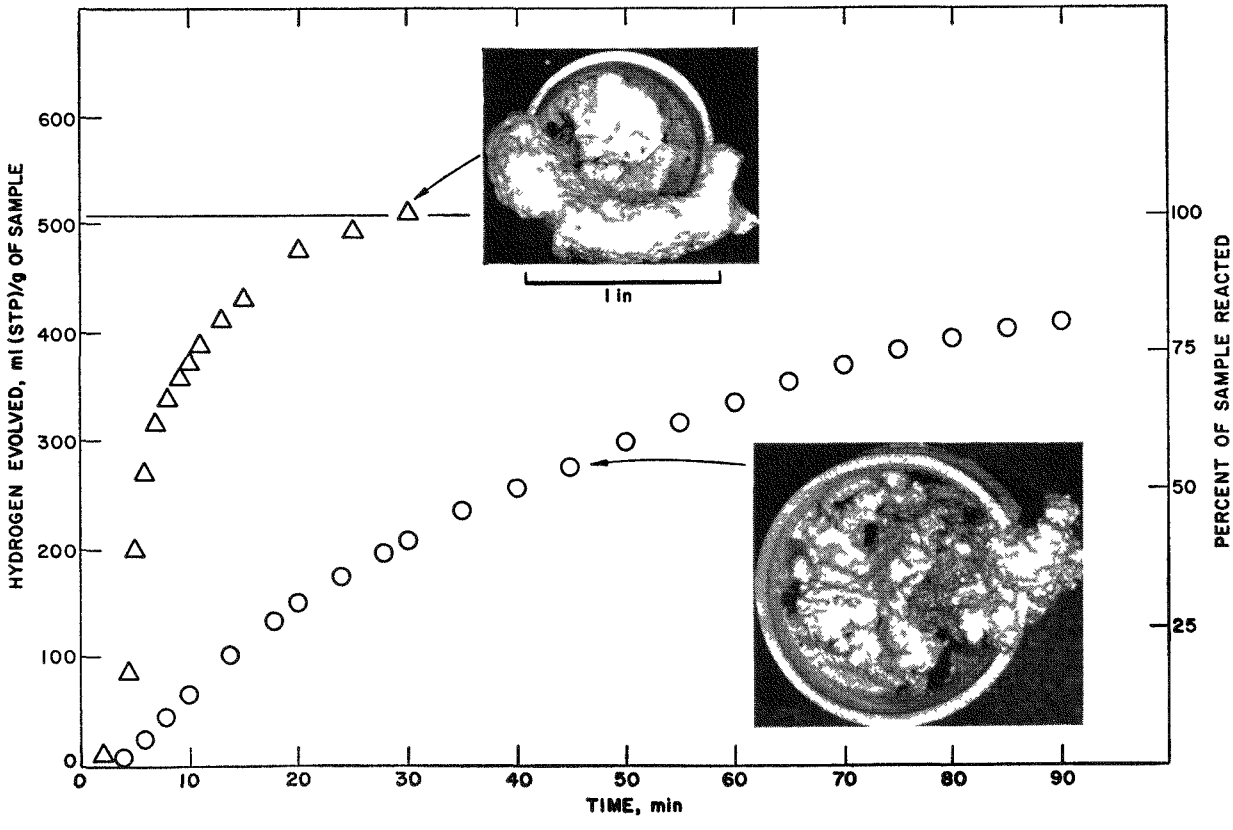

308 568

FIG IV 3 Reaction of Type 304 Stainless Steel with Steam at 1600°C and 1 atm Pressure

2. Isothermal Studies of the Nickel-Steam Reaction

(R. E. Wilson, C. Barnes, Jr.)

Nickel has been proposed as a candidate for the cladding material in some water-cooled test reactors. Consequently, a small experimental program was undertaken to investigate the reaction between nickel and steam at temperatures around the melting point of nickel in order to determine the magnitude of the metal-water reaction. Thermodynamic calculations have shown that, at low hydrogen concentrations (below ~8%) in the steam, the reaction between nickel and steam will proceed, at least up to the melting point of the oxide (2000°C).

Several investigators have reported studies of nickel oxidation at temperatures below its melting point (1455°C). Farber[4] states that the extent of the reaction below the melting point of nickel is not appreciable. Kubaschewski and Hopkins[5] report that the oxidation of nickel in steam over a temperature range of 650 to 1050°C follows a parabolic rate law. Recent experiments by Berry and Paidassi,[6] investigating the kinetics of the nickel-oxygen reaction at 600 to 1400°C, also show that the reaction follows a parabolic rate law.

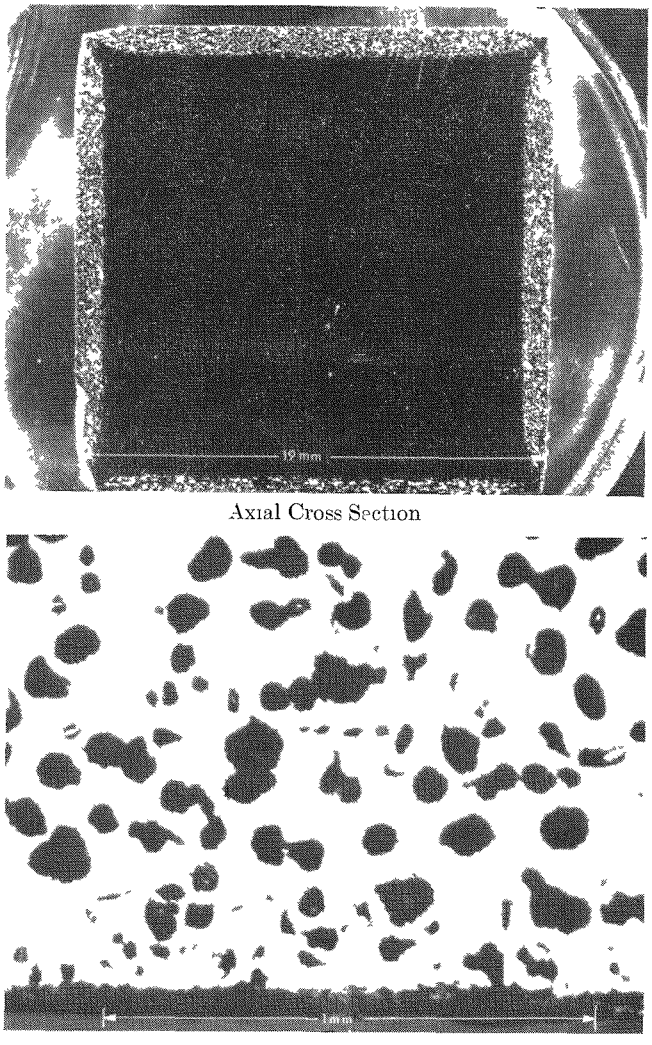

Axial Cross Section

Cross Section of Surface

308-564

Fig. IV-4. Cross Sections of Nickel Sample After Exposure to Steam at 1400°C for 90 min.

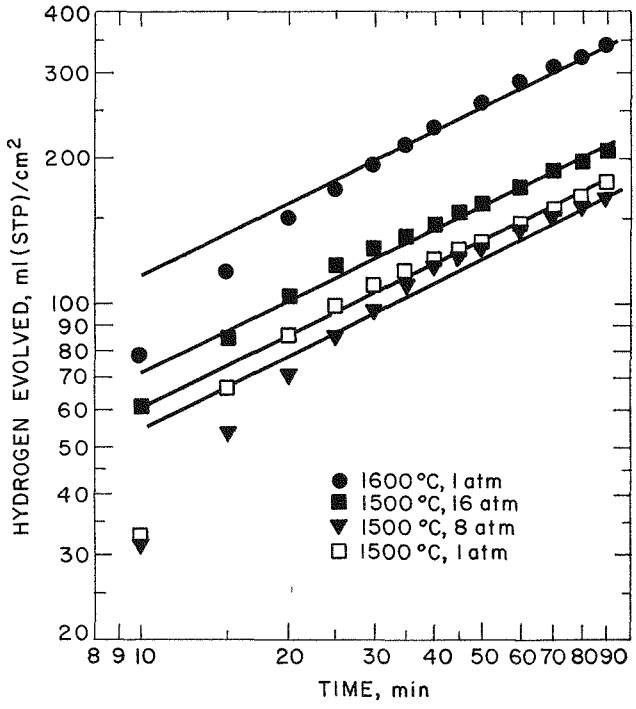

308-544

Fig. IV-5. Hydrogen Evolution as a Function of Time for the Reaction between Nickel and Steam at Various Temperatures and Pressures.

The experiments reported herein were carried out in the high-pressure furnace described in the previous section. The steam flow past the sample was held at 5 g/min for all of the experiments. The samples were cut from Grade A nickel rod in the form of right cylinders (¾-in. dia. by ¾ in. long). They were contained in impervious alumina crucibles during the experiments.

[4] M. Farber, J. Electrochem Soc. **106**, 751 (1959).

[5] O. Kubaschewski and B. E Hopkins, *Oxidation of Metals and Alloys*, 2nd Edition, Academic Press Inc., New York (1962).

[6] L. Berry and J. Paidassi, Compt. Rend., Ser. C, **262**(18), 1353 (1966).

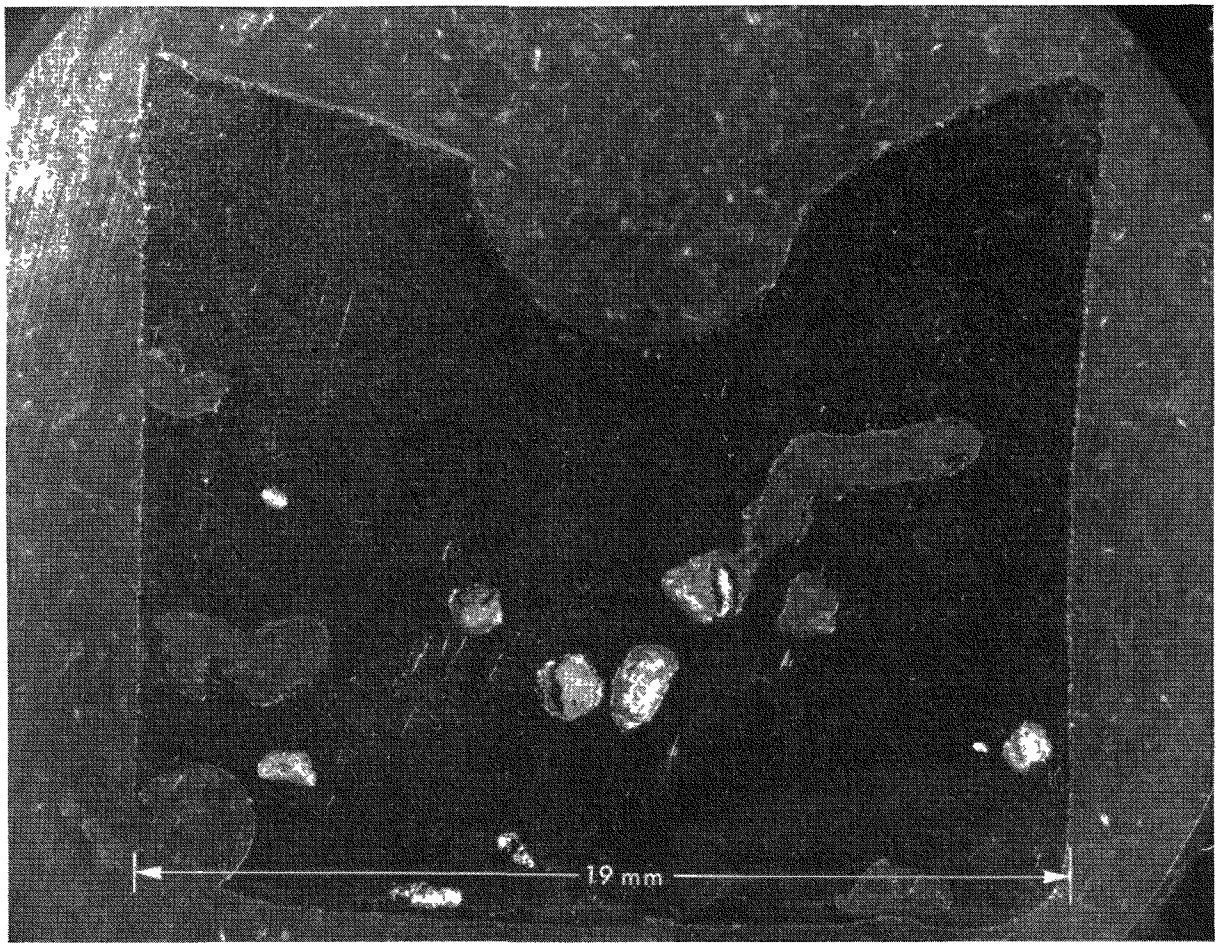

308-541

FIG. IV-6. Cross Section of Nickel Sample After Exposure to Steam at 1600°C for 90 min. (Exposed surface at top.)

The area of the sample exposed to steam during the experiment was assumed to be the original sample area for experiments at 1400°C where the nickel is solid. For experiments at 1500 and 1600°C where nickel is molten, the area was assumed to be that of the inside diameter of the crucible.

The reaction rate at 1400°C was found to be very low. An accurate assessment of the kinetics of the reaction at 1400°C could not be made because of the "background" gas evolution from the furnace which is due to the thermal decomposition of steam into hydrogen and oxygen. However, an average reaction rate for a 100-min experiment was 0.11 ml H_2(STP)/(cm^2) (min) for the nickel-steam reaction.

Cross sections of a sample exposed to steam at 1400°C for 90 min are shown in Figure IV-4. The large cross section shows that, although the corners appear to be intact, the sides of the sample are bowed out due to the formation of voids (the light bands) along the surfaces. An enlargement of one of these areas is also shown in Figure IV-4. The oxide formed by the steam reaction can be seen as a thin dark band at the interface between the metal and the mounting material.

The results of typical experiments at 1500 and 1600°C are shown in Figure IV-5. In the figure the hydrogen evolution (taken as the measure of reaction) is plotted as a function of time. The results indicate that molten nickel follows an approximate parabolic rate law at 1500 and 1600°C.

The low points apparent at short reaction times were probably due to the relatively long time (10 min) required for the samples to reach the reaction temperature in the furnace.

Experiments at 1500°C were performed with steam pressures at 1, 8, and 16 atm and the results in Figure IV-5 indicate that there is no significant effect of pressure on the reaction rate.

Figure IV-6 shows the cross section of a sample exposed to 1600°C steam. In this sample there are large voids. All of the surfaces of internal voids were shiny,

indicating that they were not exposed to steam and that the voids probably formed during freezing of the sample at the end of the experiment. X-ray analysis of scrapings from the sides and tops of the samples after exposure to steam indicated NiO on all surfaces exposed to steam at 1400°C and on the top surface of samples exposed to steam at 1500 and 1600°C. Only nickel and a small trace of $NiAlO_4$ were found on the sides and bottoms of the molten samples (1500 and 1600°C), indicating that those surfaces were effectively shielded from the steam by the crucible.

During the course of these experiments it was noted that NiO appears to be somewhat volatile in a steam atmosphere. Large (3-mm) crystals of NiO were formed on the Al_2O_3 reaction tube in areas removed from the sample-containing crucible.

3. Reaction of Flowing Steam with Zircaloy-2-Clad, UO_2-Core Simulated Fuel Elements (R. E. Wilson, C. Barnes, R. O. Ivins, J. Pavlik)

A series of experiments has been designed to simulate the environment of the fuel in a water-cooled power reactor following a loss-of-coolant accident. In such a situation, the fuel would be subjected to a slowly rising temperature (compared to that of a transient) because of decay heat.

a. EXPERIMENTS WITH LIMITED STEAM FLOW IN THE HIGH-PRESSURE FURNACE

Experiments in the high-pressure furnace were previously completed with simulated fuel elements (using both type 304 stainless steel and Zircaloy-2 as the cladding material) at input steam flow rates of 10 and 20 g/min; these are reported in ANL-7125, p. 153.

The series of experiments using Zircaloy-2-clad, UO_2-core fuel rods has been extended in an attempt to simulate a loss-of-coolant incident under limited steam flow rate conditions similar to those previously considered in analyses using the LOFT reactor as a model (ANL-7125, p. 181). Assuming a steam flow of 1000 lb/hr for the entire LOFT core, the corresponding input steam flow for a single element would be approximately 2.5 g/min. Two experiments were conducted with this input flow rate. In an attempt to simulate

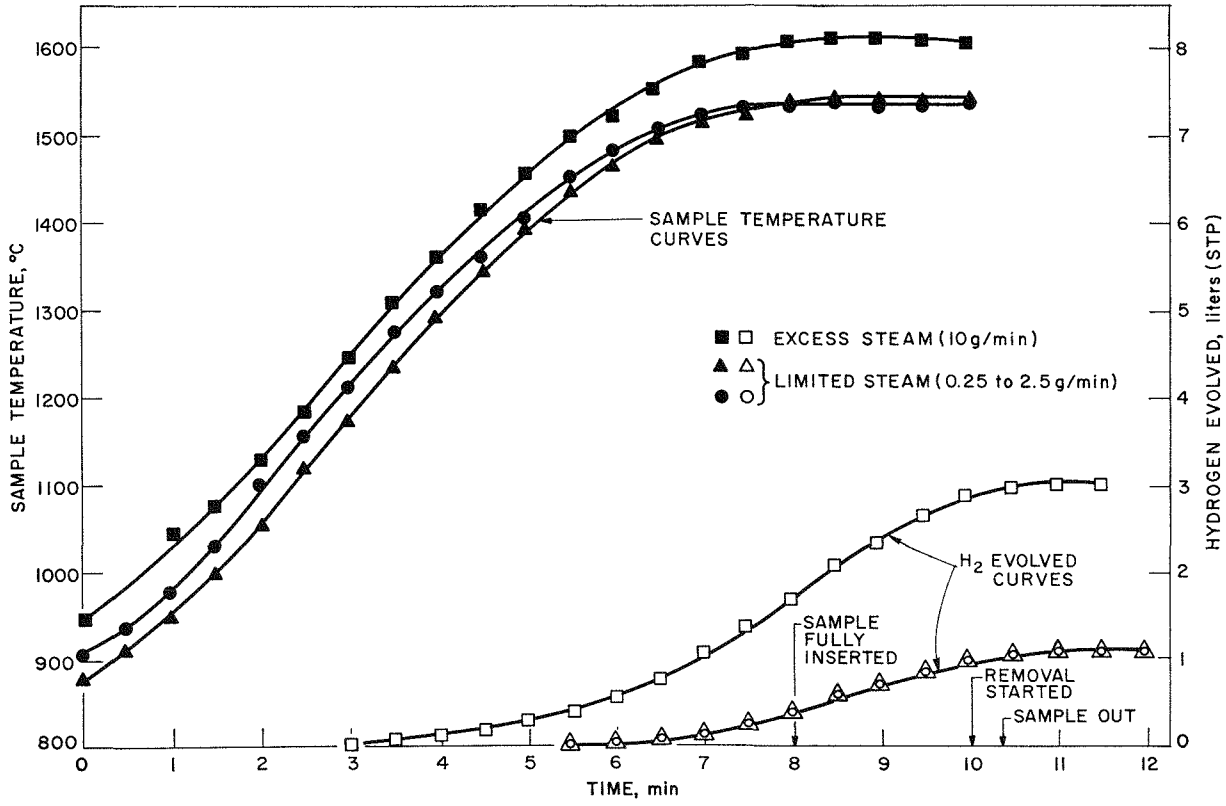

308-543

Fig. IV-7. Experiments in the High-Pressure Furnace with Zircaloy-2-Clad, UO_2-Core Fuel Rods at Various Steam Flow Rates. (Furnace temperature = 1500°C; pressure = 1 atm.)

more steam-limited conditions, one-tenth of this value (0.25 g/min) was used in two subsequent experiments. The experiments were performed in the high-pressure furnace described in the section IV.A.1 of this report.

Each fuel rod (8 in. long by 0.4-in. dia.) consisted of a number of high-density UO_2 pellets clad with Zircaloy-2 tubing having a 27-mil wall thickness. The top and bottom of the tubing were closed with $\frac{3}{16}$-in. thick welded plugs. The 2.5-mil radial gap between the UO_2 and the cladding was filled with helium at a pressure of 20 psia. A fuel rod was raised into the high temperature zone of the furnace (maintained at 1500°C) at a rate of 1 in./min, thus requiring a total of 8 min for complete insertion. After a total residence time in the hot zone of 10 min, the rod was rapidly withdrawn to the original position in the cooler part of the furnace. Evolved hydrogen was monitored for an additional 2 min after the rod had been withdrawn from the hot zone. The amounts of hydrogen evolved for the four experiments were as follows:

Input H_2O Flow (g/min)	H_2 Evolved After 10 min (ml, STP)	H_2 Evolved After 12 min (ml, STP)
2.5	949	1092
2.5	918	1076
0.25	968	1097
0.25	938	1067

From the above data it is obvious that the reaction rate did not change significantly when the input water flow was lowered from 2.5 to 0.25 g/min.

Although metered amounts of water were fed into the furnace, there is no way of measuring the amount of steam flow past the sample. Convection currents of steam are established because of the relatively large reaction chamber (~2-in. ID) in comparison to the size of the steam exit tube (⅛-in. ID). From the data it is concluded that, although different amounts of water were metered into the furnace, steam flow past the hot fuel rod remained relatively constant during the four runs.

The results of two experiments with limited steam flow rates are plotted in Figure IV-7 along with the results of a previous experiment (see ANL-7125, p. 157) in which there was excess steam. The total hydrogen evolved from the experiments with limited steam was about one-third that of the experiment in which there was excess steam.

A photograph of a typical Zircaloy-2-clad fuel rod exposed under limited steam flow rate conditions is shown in Figure IV-8. The white ring of oxide, formed about ⅓ of the way down from the top of the fuel rod, is believed to have been caused by a combination of a vertical temperature gradient (hotter at the top) which would promote reaction at the upper end of the rod, and the limited steam availability which would promote reaction toward the lower end of the rod (steam flow direction upward). The location of greatest reaction is therefore centered at a point below the top of the rod. Previous fuel rod experiments in the high-pressure furnace with a high steam flow rate have resulted in greatest reaction at the top (hottest point) of the rod.

The observation that the location of the maximum reaction point is at a position below the hottest part of the fuel rod suggests that chemical reaction in a

108-9890 Rev-1

FIG. IV-8. Typical Zircaloy-2-Clad, UO_2-Core Fuel Rod after Exposure to Limited Steam Flow at 1500°C.

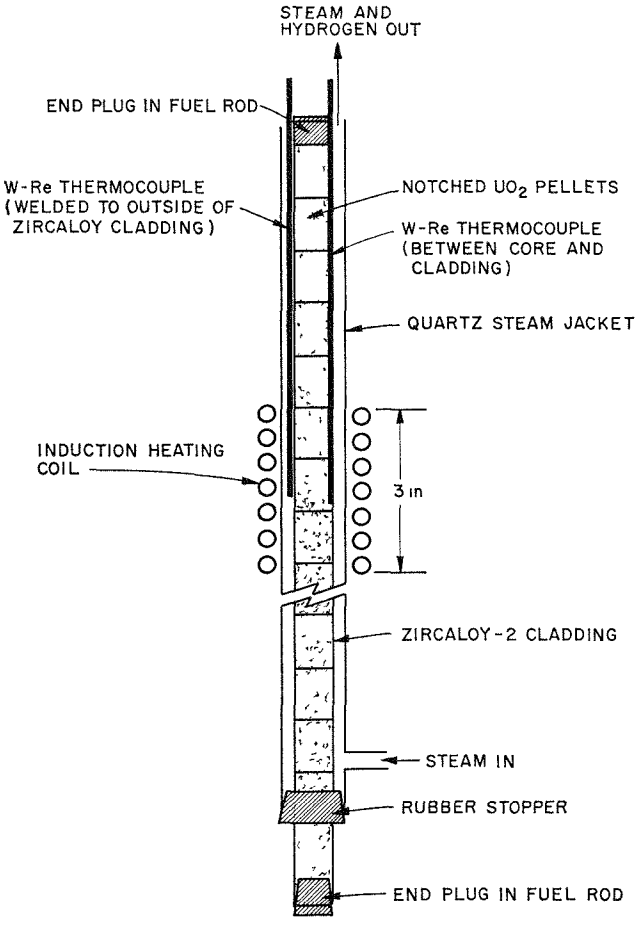

308-542

FIG. IV-9. Apparatus for Induction Heating Experiment Simulating a Loss-of-Coolant Accident.

power reactor loss-of-coolant accident situation would begin at a location somewhat below the center (hottest point) of the reactor under conditions of limited steam availability. As the temperature increased throughout the reactor core because of decay heating, it would be expected that the reaction would propagate to still lower regions of the core while the upper half of the core would be exposed only to the hydrogen produced by reaction at the lower positions.

b. FUEL MELTDOWN EXPERIMENTS BY AN INDUCTION HEATING METHOD

Key unknowns in the analysis of the loss-of-coolant accident for power reactors which use Zircaloy-clad, UO_2-core fuel rods are the effective failure temperature and the mode of failure of the fuel rods. Failure models range from melting and dripping of Zircaloy at 1850°C to the total holdup of the UO_2 by a shell of oxidized zirconium until temperatures reach 2600 to 2800°C where the oxidized cladding would be expected to melt. Uncertainty centers about the ability of partly oxidized cladding to maintain integrity at temperatures above 1850°C, which is the melting point of unoxidized zirconium. Studies in the high-pressure furnace of the behavior of fuel rods under conditions simulating a loss-of-coolant accident were limited to maximum furnace temperatures of 1600°C. Thus, it has not been possible in these experiments to effect melting of the Zircaloy cladding because of the temperature limitation of the furnace. An attempt was made, therefore, using induction heating to observe some of the features of the meltdown and collapse of a single Zircaloy-2-clad, UO_2-core fuel rod. A true simulation of the conditions expected during a loss-of-coolant accident requires a large number of fuel rods to achieve a realistic thermal environment for each rod. The experiment using induction heating of a single rod is recognized as a very rough approximation of the conditions expected in a reactor.

A diagram of the apparatus is given in Figure IV-9, showing arrangement of a Zircaloy-2 tube (27-mil wall thickness) filled with UO_2 pellets, which was located in a quartz steam jacket. An induction coil, 3 in. long, surrounded the quartz tube near the center. The steam flow rate was regulated at 1 g of steam/min. One tungsten-rhenium thermocouple was located within the pellet-cladding gap and another was welded to the outside of the cladding. Thermocouple records could not be interpreted in the preliminary experiment, however, because of interference from the RF field generated by the induction coil. A temperature record was obtained from a Pyroeye two-color pyrometer which was focused on the cladding surface between turns of the induction coil. The record, which was limited to the high range of the instrument, 1900 to 2500°C, indicated a peak temperature of 2140°C. Induction power was turned off a few seconds after the temperature peaked.

The appearance of the fuel rod after the experiment is shown in Figure IV-10 along with a cross section cut from near the center of the heated zone. The appearance of the UO_2 suggested that local melting of the UO_2 had occurred.

Although preliminary in nature, the induction heating experiment showed that there was no tendency for the molten Zircaloy to drip from the fuel rod. The cross section of the fuel rod, Figure IV-10b, indicated that molten Zircaloy was confined between an outer "crucible" of zirconium oxide and the inner surface of the UO_2. There was also evidence for some interaction between molten Zircaloy and the UO_2. The experiment suggested strongly that fuel rod breakup in previous furnace experiments (see ANL-7125, p. 156 and ANL-7225, p. 166) occurred during the cooldown and was not an inherent part of the high temperature failure process.

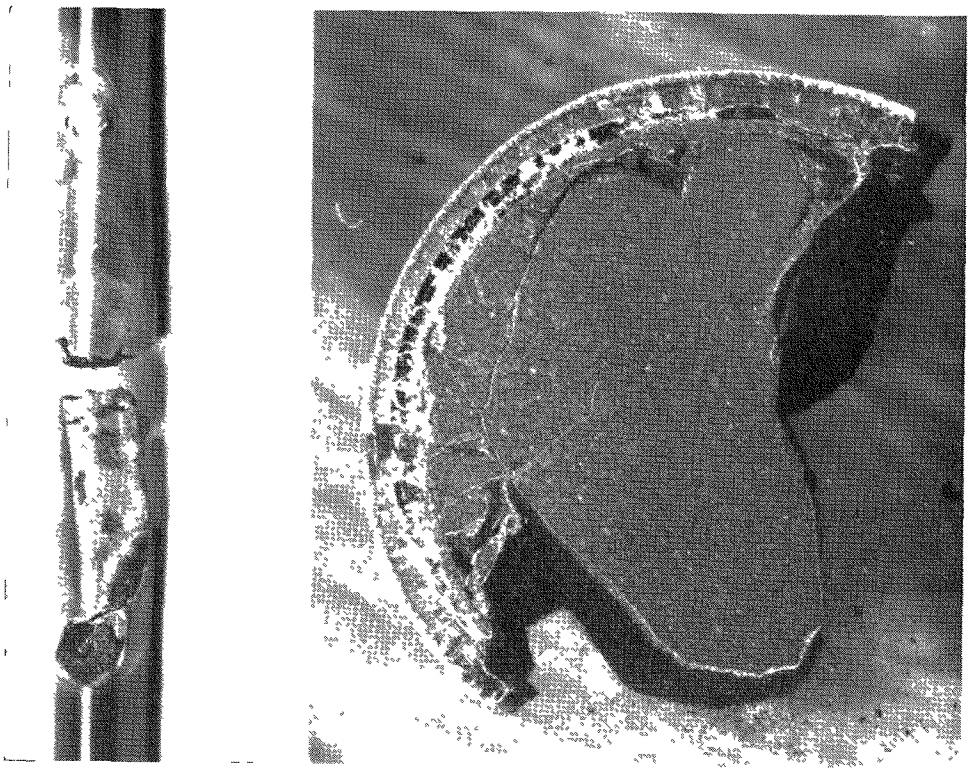

a. Side View of Rod b. Cross-section near Center

308-540

FIG. IV-10. Zircaloy-2-Clad, UO_2-Core Fuel Rod after Induction Heating in Steam to an Indicated Cladding Temperature of 2140°C.

4. Calculation of the Extent of Metal-Water Reaction and Core Heating during a Loss-of-Coolant Accident (CHEMLOC-I Program) (J. HESSON)

Analysis of the effect of the reaction of steam with fuel cladding metal in a loss-of-coolant accident in a water-cooled reactor has continued. The loss-of-coolant accident resulting from a break in a primary-system water pipe has been taken to be the "maximum credible accident" for most of the power reactors built to date. Water loss following the pipe break brings the core into contact with steam. The decay energy in the core is sufficient to cause the fuel cladding to be heated within a few minutes to temperatures at which metal-steam reaction can occur.

In previous analyses using the proposed LOFT (Loss of Fluid Test) reactor as a model, calculations were made for 25-mil thick Zircaloy-clad and 15-mil thick stainless steel-clad, UO_2-core fuel (see ANL-6925, p. 215, ANL-7055, p. 192, and ANL-7125, p. 181). In these analyses the core was divided into 156 equal-volume segments, each of which was assigned to one of 10 groups according to its decay heating rate. The effects of heat transfer in the core by conduction, radiation, and convection, and the effects of unequal steam distribution to the various segments due to hydrogen formation were neglected in the analyses.

a. COMPUTER PROGRAM

The recently developed (see ANL-7225, p. 167) Fortran computer program (designated CHEMLOC-I), which describes the core heating and chemical reaction up to the time of fuel melting, takes into consideration the effects of evaluating the temperatures of the gas, cladding, and fuel separately; the effects of transfer of heat by axial conduction in the cladding and fuel, by radial conduction between cladding and fuel, by radial radiation from cladding to cladding, and by convection between the cladding and the flowing gas; and the effects of changing hydrogen concentration in the steam.

For the analysis, the core is divided into a number of radial zones, each having the same number of fuel rods, as shown in Figure IV-11. The center zone, No. 1, is a cylinder while the remaining zones are annuli. The decay heating varies axially within each zone as well as radially from zone to zone. Steam enters the bottom of

the core at a rate which may be constant or may vary with time.

As the steam flows upward through the core, the concentration of hydrogen increases due to chemical reaction of the steam with the cladding; thus, the cladding in the lower sections of the core tends to be contacted by gas having a higher steam concentration. Since on reaction with the cladding, one mole of water vapor forms one mole of hydrogen, the molar flow rate of gas does not vary with vertical (axial) core position.

A heat and mass balance was made on an elemental section of a fuel rod together with the associated gas flow area. in zone i, of length $\Delta\ell$, and at distance ℓ from the bottom of the core, as shown in Figure IV-12.

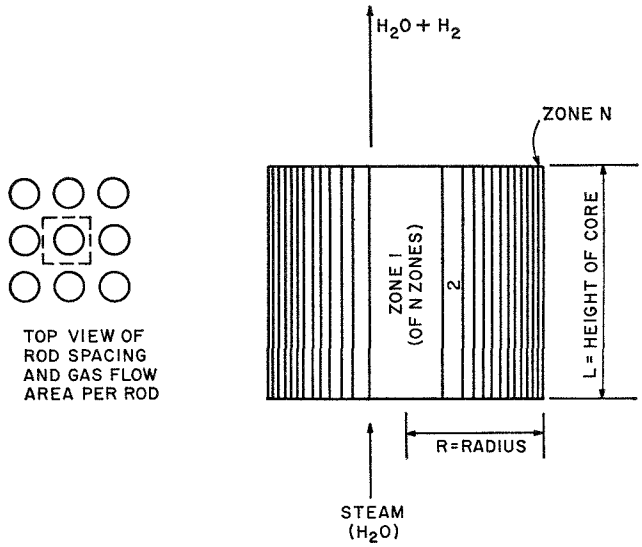

308-549

FIG. IV-11. Reactor Core as Zoned for CHEMLOC-I Calculations.

The heat gain of the fuel per unit length of rod is the sum of the following terms:

q_{di} = decay heat, cal/(sec)(cm);

$-q_{aci}$ = heat transferred from cladding, cal/(sec)(cm);

$A_a k_a \frac{\partial^2 T_{ai}}{\partial \ell^2}$ = net heat gained by axial conduction, cal/(sec)(cm);

where

A_a = cross-sectional area of fuel, cm^2;

k_a = thermal conductivity of fuel, cal/(sec)(cm)(°K)

T_{ai} = temperature of the fuel, °K.

The heat gain of the cladding per unit length of rod is the sum of the following terms:

q_{aci} = heat transferred from fuel, cal/(sec)(cm);

$-q_{ri}$ = heat radiated to zones $i + 1$ and $i - 1$, cal/(sec)(cm);

q_{ri+1} = heat received by radiation from zone $i + 1$, cal/(sec)(cm);

q_{ri-1} = heat received by radiation from zone $i - 1$, cal/(sec)(cm);

q_{si} = heat produced by chemical reaction, cal/(sec)(cm), which may be limited by the chemical reaction rate (kinetic), the diffusion of steam to the reacting surface (dif-

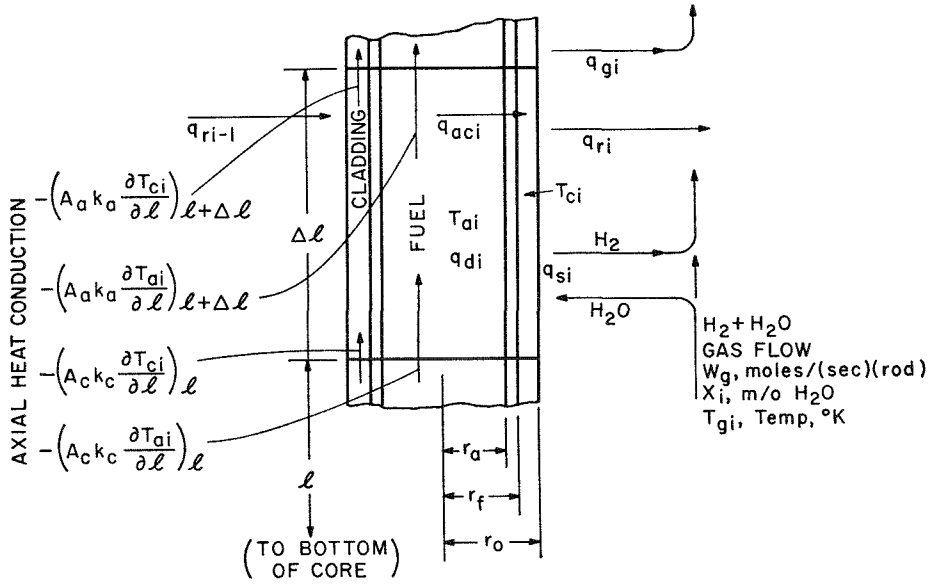

308-548

FIG. IV-12. Section of a Reactor Core Fuel Rod (Zone i) Showing Heat and Mass Transfer.

fusion), or by the complete reaction of the cladding;

$-q_{gi}$ = heat transferred from gas, cal/(sec)(cm);

$k_c \frac{\partial}{\partial \ell}\left(A_c \frac{\partial T_{ci}}{\partial \ell}\right)$ = net heat gained by axial conduction, cal/(sec)(cm),

where

A_c = cross-sectional area of the cladding per rod, cm^2;

k_c = heat conductivity of the cladding, cal/(sec)(cm)(°K);

T_{ci} = temperature of the cladding, °K.

The heat gain of the gas as it flows past a unit length of rod is:

q_{gi} = heat transferred from the cladding, cal/(sec)(cm).

The rate of oxidation of the cladding is:

$$q_{si}/Q_c \text{, g/(sec)(cm)},$$

where

Q_c = the heat of reaction of the cladding, cal/g.

The rate of steam consumption and hydrogen formation in the oxidation of the cladding is:

$$q_{si}/Q_c M_c \text{, moles/(sec)(cm)},$$

where

M_c = grams of cladding reacted per mole of steam, g/mole.

The temperature increase of the fuel is equal to the heat received by the fuel (in time dt) divided by the heat capacity of the fuel, or

$$dT_{ai} = \frac{q_{di} - q_{aci} + A_a k_a \frac{\partial^2 T_{ai}}{\partial \ell^2}}{Cp_a W_a}\, dt, \text{ °K}, \tag{1}$$

where

Cp_a = specific heat of fuel, cal/(g)(°K);

W_a = weight of fuel per unit length of rod, g/cm;

t = time, sec.

The temperature increase of the cladding is equal to the heat received by the cladding (in time dt) divided by the heat capacity of the cladding, or

$$dT_{ci} = \left[q_{aci} - q_{ri} + q_{ri+1} + q_{ri-1} + q_{si} - q_{gi} + k_c \frac{\partial}{\partial \ell}\left(A_c \frac{\partial T_{ci}}{\partial \ell}\right)\right] \frac{dt}{Cp_c W_c}, \text{ °K}, \tag{2}$$

where

Cp_c = specific heat of the cladding, cal/(g)(°K);

W_c = weight of cladding per unit length of rod, g/cm.

The temperature increase of the gas flowing along the cladding is equal to the heat received by the gas (in distance $d\ell$) divided by the heat capacity of the gas flowing past the rod in unit time, or

$$dT_{gi} = \frac{q_{gi}}{W_g Cp_g}\, d\ell, \text{ °K} \tag{3}$$

where

Cp_g = specific heat of the gas, cal/(mole)(°K);

W_g = gas flowing past one rod, moles/(sec).

The reduction in cladding metal radius due to oxidation is equal to the weight of metal oxidized divided by the weight of cladding metal per unit of radius, or

$$d(r_o - r_i) = \frac{q_{si}}{2\pi r_i \rho_c Q_c}\, dt, \text{ cm}, \tag{4}$$

where

r_o = initial radius of cladding, cm;

r_i = radius of unreacted cladding, cm;

ρ_c = density of cladding, g/cm^3.

The change in steam concentration in the gas as it flows along the cladding is equal to the steam consumption divided by the rate of gas flow past the rod in unit time, or

$$dX_i = \frac{q_{si}}{W_g Q_c M_c}\, d\ell, \text{ moles/mole}, \tag{5}$$

where

X_i = steam concentration, moles/mole;

$1 - X_i$ = hydrogen concentration, moles/mole.

The heat generation and heat transfer terms, q_{di}, q_{aci}, q_{ri}, q_{ri+1}, q_{ri-1}, q_{gi}, and q_{si}, previously defined, can be expressed as follows for use in differential equations 1 to 5. (In these expressions and in the previous equations, specific heats, diffusivities, heat and mass transfer coefficients, and thermal conductivities may be functions of temperature; the steam flow rate may vary with time.)

The decay heat in the fuel, per unit length of rod, is:

$$q_{di} = V_a Q_d F(t) f(i)\ 1.5 \sin\left(\frac{0.026\ L + \ell}{1.052\ L}\right)\pi, \text{ cal/(sec)(cm)}, \tag{6}$$

where

V_a = volume of fuel per unit length of rod, cm^3/(cm);

Q_d = reactor operating power, per unit volume of fuel, cal/(sec)(cm^3);

$F(t)$ = ratio of decay heat to reactor power at time, t sec;

$f(i)$ = ratio of average reactor power per cm^3 of fuel in axial zone i to average reactor power per cm^3 of fuel;

$1.5 \sin\left(\frac{0.026\,L + \ell}{1.052\,L}\right)\pi$ = ratio of reactor power per cm^3 of fuel at distance, ℓ cm, from bottom of core in zone i to average reactor power per cm^3 fuel in zone i;

L = height of core, cm.

The heat transferred from the fuel to the cladding, per unit length of rod, is:

$$q_{aci} = (T_{ai} - T_{ci}) \frac{2r_f h_{ac}}{1 + r_f \frac{h_{ac}}{4k_a}}, \text{ cal/(sec)(cm)}, \quad (7)$$

where

r_f = inside radius of cladding, cm;

h_{ac} = heat transfer coefficient between fuel and cladding, cal/(sec)(cm^2)(°K).

The heat radiated radially from the cladding of a rod in zone i to zones $i + 1$ and $i - 1$, per unit length of rod, is:

$$-q_{ri} = A \frac{4\pi^2}{N_r} (2i - 1)\, r_o \sigma \varepsilon (T_{ci})^4, \text{ cal/(sec)(cm)} \quad (8)$$

where

A = geometrical factor for radiation;

N_r = number of rods per zone;

r_o = outside radius of rod, cm;

ε = emissivity factor for radiation of rod surface;

σ = radiation constant, 1.37×10^{-12} cal/(sec)(cm^2)(°K^4).

The heat radiated radially to the cladding of a rod from zone $i + 1$, per unit length of rod, is:

$$q_{ri+1} = A \frac{4\pi^2}{N_r} i r_o \sigma \varepsilon (T_{ci+1})^4, \text{ cal/(sec)(cm)}. \quad (9)$$

The heat radiated radially to the cladding of a rod in zone i from zone $i - 1$, per unit length of rod, is:

$$q_{ri-1} = A \frac{4\pi^2}{N_r} (i - 1) r_o \sigma \varepsilon (T_{ci-1})^4, \text{ cal/(sec)(cm)}. \quad (10)$$

The heat transferred from the cladding to the flowing gas, per unit length of rod, is:

$$-q_{gi} = -(T_{ci} - T_{gi}) S_r h_g, \text{ cal/(sec)(cm)}, \quad (11)$$

where

S_r = surface area of cladding per cm of rod, cm^2/cm;

h_g = heat transfer coefficient cladding to gas, cal/(sec)(cm^2)(°K).

The heat produced by chemical reaction, per unit length of rod, is:

q_{si} = the lesser of

$$2\pi r_i \rho_c Q_c \frac{K}{r_o - r_i}\left[\exp -\left(\frac{\Delta E}{RT_{ci}}\right)\right] \quad (12)$$

or

$$2\pi r_o M_c Q_c h_d \rho_g X_i \text{ (diffusion equation)} \quad (13)$$

or

$$0 \text{ when } (r_o - r_i) \geqslant (r_o - r_f) \text{ (100 \% reaction), cal/(sec)(cm)}, \quad (14)$$

where

K = reaction rate law constant, cm^2/sec;

ΔE = activation energy, cal/mole;

R = gas constant, 1.987 cal/(mole)(°K);

h_d = mass transfer coefficient, cm/sec;

ρ_g = gas density, moles/cm^3.

Chemical reaction rate constants for the zirconium-steam reaction, reactor power distribution in the core and fission product decay heat generation, and initial core temperatures have been previously discussed (ANL-6925, p. 215 and ANL-7055, p. 192). Chemical reaction rate constants for stainless steel-steam reactions have also been discussed (ANL-7125, p. 181).

The specific heat of steam-hydrogen mixtures is taken as:

$$Cp_g = XCp_s + (1 - X)Cp_H, \quad (15)$$

where

X = mole fraction steam in mixture;

Cp_s = specific heat of water vapor, cal/(mole)(°K);

Cp_H = specific heat of hydrogen, cal/(mole)(°K).

The heat conductivity of steam-hydrogen mixtures is taken as:

$$k_g = Xk_s + (1 - X)k_H, \quad (16)$$

where

k_s = heat conductivity of steam, cal/(sec)(cm)(°K);

k_H = heat conductivity of hydrogen, cal/(sec)(cm)(°K).

The heat and mass transfer coefficients, h_g and h_d, for gas (steam-hydrogen) in laminar flow along fuel rods were discussed in the previous semiannual report (ANL-7225, p. 168).

It was shown in ANL-7225 that the Nusselt number for heat transfer, Nu, and that for mass transfer, Nu$_d$, for fully developed laminar flow along fuel rods in square and triangular arrays, could be obtained from the simple model of a "half" annulus surrounding a cylinder. The inner radius of the half annulus is r_o (the radius of the cylinder) whereas the outer radius r' of the half annulus is determined so that the flow area associated with each rod is equal to the actual area. With a square array of rods.

$$r' = p/\sqrt{\pi} \quad \text{or} \quad 0.564\,p \tag{17}$$

and with a triangular array of rods

$$r' = p/2\sqrt{\frac{2\sqrt{3}}{\pi}} \text{ or } 0.525\,p \tag{18}$$

where p is the distance between centers.

Based on this annulus model, the Nusselt numbers for heat transfer and for mass transfer were evaluated. The relationships between the heat and mass transfer coefficient and Nusselt numbers are:

$$h = \frac{\mathrm{Nu}k_g}{r' - r_o}, \text{ cal/(sec)(cm}^2\text{)(°K)} \tag{19}$$

and

$$h_d = \frac{\mathrm{Nu}_d D_g}{r' - r_o}, \text{ cm/sec.} \tag{20}$$

Values of Nu or Nu_d based on $(r' - r_o)$ computed for various ratios of r'/r_o for fully developed laminar flow in half-annuli are given in Table IV-1.

In the computer program, provisions are made to include other oxidizable surfaces, such as cans around subassemblies, and to include the heat capacity effects of materials, such as control rods, in addition to the fuel, fuel cladding, and cans.

The CHEMLOC-I program was developed for integrating differential equations 1 to 5 to solve for T_{ai}, T_{ci}, T_{gi}, $r_o - r_i$, and X_i as a function of zone, i, distance, ℓ, from the bottom of the core, and time, t, for steam flow rates which are constant or which vary with time. In the CHEMLOC-I program, the number of zones, N_i, may be varied up to 25 and the number of rod length increments, $\Delta\ell$, may be varied up to 100. The time increments, Δt, may also be varied.

The computer readout includes the following for preselected time intervals.

1. Steam flow rate (may be variable).
2. T_a = fuel temperature;
   T_c = cladding temperature;
   T_g = gas temperature;
   $r_o - r_i$ = thickness of cladding metal oxidized;
   X = mole fraction of steam in the gas mixture for all zones and preselected rod length intervals.
3. a) Average thickness of all can metal (other oxidizable surfaces) oxidized;
   b) Fraction of all can metal oxidized.
4. a) Average thickness of all cladding metal oxidized;
   b) Fraction of all cladding metal oxidized.
5. Average fraction of hydrogen in gas leaving core.
6. Heat of combustion of hydrogen times rate of hydrogen leaving core.
7. Sensible heat in gas times rate of gas leaving core.
8. Accumulated hydrogen released from core.

TABLE IV-1. Nusselt Numbers as Functions of Ratios of Radii for "Half" Annuli

$\frac{r}{r_o}$	$\mathrm{Nu} = \frac{h}{k_g}(r' - r_o)$ $\mathrm{Nu}_d = \frac{h_d}{D_g}(r' - r_o)$
1.0	2.056
1.1	2.096
1.2	2.134
1.3	2.173
1.4	2.212
1.5	2.252
1.6	2.292
1.67[a]	2.230
1.7	2.332
1.8	2.372
1.9	2.413
2.0	2.452
2.2	2.532
2.4	2.612
2.6	2.691
2.8	2.769
3.0	2.846

[a] Corresponds to spacing for core of LOFT reactor.

b. LOFT CALCULATIONS

The LOFT core was used as a model for the initial CHEMLOC-I calculations. The LOFT core consists of 3328 UO_2-core fuel rods each 0.39 in. in dia. by 3 ft long with 0.025-in. thick Zircaloy-2 cladding. The rods are spaced on a square lattice with 0.58 in. between centers. The core was divided into 13 radial zones. Previously reported values (ANL-6925, p. 215) were used for the power distribution as a function of core location and the decay heating as a function of time.

Computer calculations were made for an initial core temperature of 285°C, and for an initial core temperature distribution corresponding to the equilibrium temperature at operating power (ANL-7055, p. 192). Calculations were made for constant steam flow rates of 100, 1000, 5000, 7500, and 10,000 lb/hr and for a variable steam flow rate starting at 3600 lb/hr and decreasing exponentially with time.

Figure IV-13 (a, b, and c) shows typical computed results for the concentration of hydrogen in the gas leaving the top of the core from the various zones as a function of time. The data are for initial core temperatures and steam flow rates as indicated. The crossing of the lines at zone 9 is caused by the increase in enrichment at zone 9. When the core is initially at a temperature corresponding to operating power, the core is sufficiently hot for considerable steam-zirconium reaction to take place immediately (complete steam utilization in zones 1, 2, and 3, for example). The cladding is assumed to have an initial oxide film corre-

Percent Hydrogen in Steam Leaving Top of Core

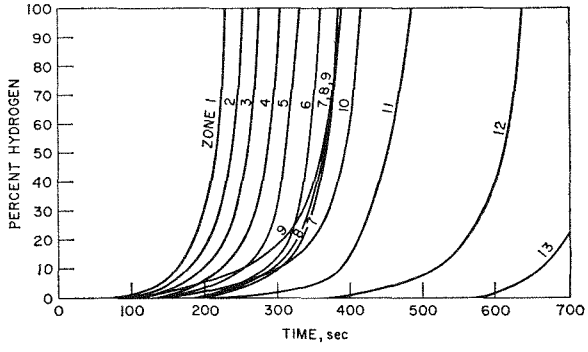

a

Temperature Profile Map (Approx. 10% of core at or above 2800°C)

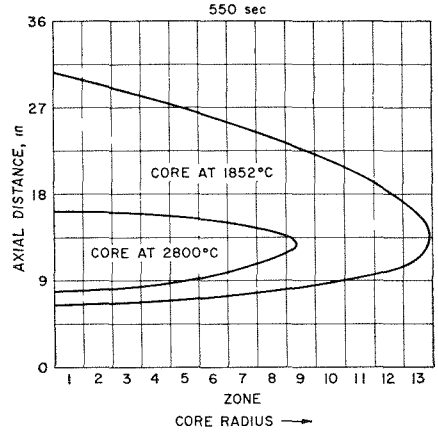

d

Initial Core Temperature 285°C, Steam Flowrate 1000 lb/hr

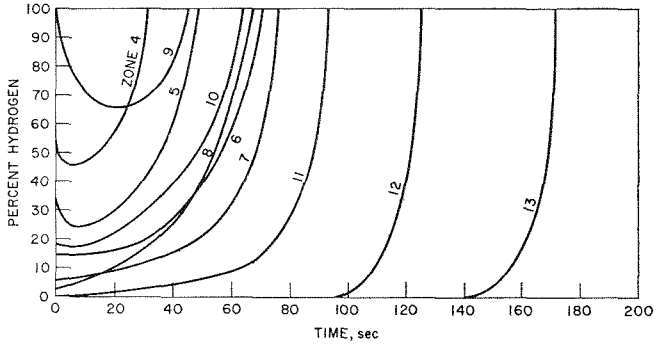

b

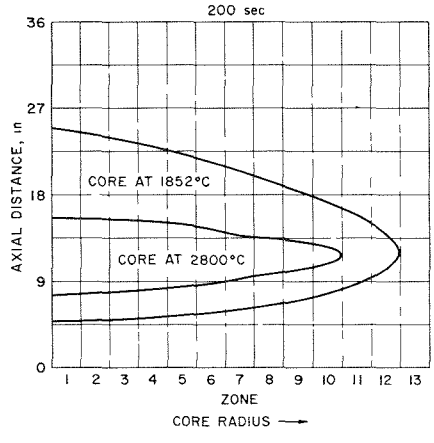

e

Initial Core Temperature—That Corresponding to Operating Power; Steam Flowrate 1000 lb/hr

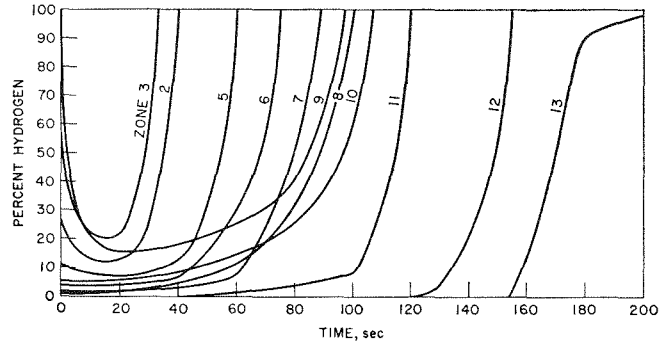

c

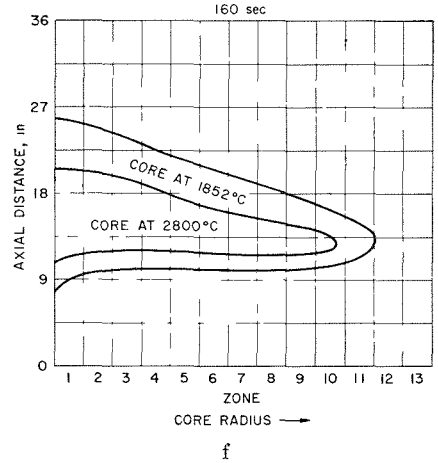

f

Initial Core Temperature—that Corresponding to Operating Power; Steam Flowrate Initially 3600 lb/hr (Decreasing exponentially)

308-333

FIG. IV-13. Typical Data Excerpts from CHEMLOC-I Computations for a Loss-of-Coolant Incident.

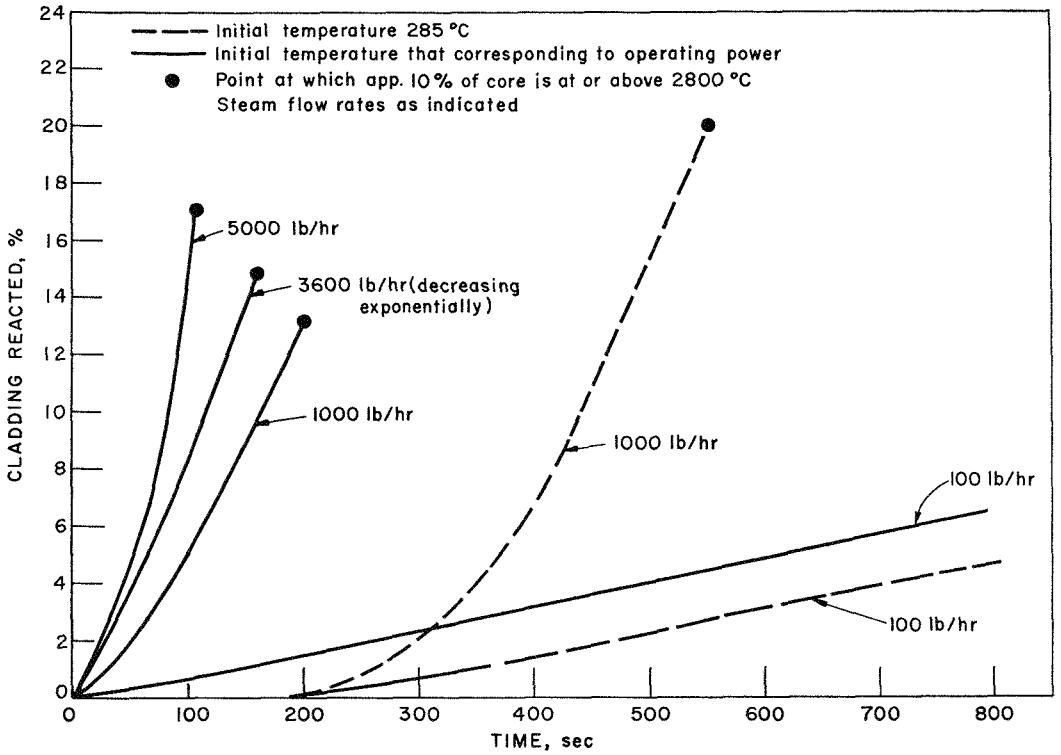

08-332

FIG. IV-14. LOFT Cladding Reacted as a Function of Time for Various Temperature and Steam Conditions. (CHEMLOC-I calculations.)

sponding to 10^{-4} cm of metal; this causes an initial rapid oxidation since the chemical reaction rate is inversely proportional to the oxide thickness. As the oxide film increases, the oxidation rate decreases and then increases as the temperature increases.

Figure IV-13 (d, e, and f) shows temperature profile maps of the core for the conditions of Figure IV-14 (a, b, and c, respectively). Contour lines are shown for 1852°C (m.p. of zirconium) and 2800°C (m.p. of UO_2) at the time when approximately 10% of the core volume is at or above 2800°C.

The computer calculations indicate that for an initial core temperature of 285°C, constant steam flow rates of 7500 and 10,000 lb/hr are sufficient to avoid extensive heating of the core. Figure IV-14 shows the percent of cladding reacted as a function of time for various other cases calculated.

The LOFT calculations using the CHEMLOC-I program have yielded somewhat greater extents of cladding reaction than the values determined in the earlier analyses (ANL-6925, p. 215 and ANL-7055, p. 192). For example, at a steam flow rate of 1000 lb/hr at an initial core temperature of 285°C, the CHEMLOC-I calculations indicated 6.8 and 15.5% reaction at times of 400 and 500 sec, respectively, whereas the previous, less precise calculations had given 5.0 and 9.5% reaction under corresponding conditions. The difference is due to the inclusion in the CHEMLOC calculations of the effects of heat transfer in the core and the unequal steam distribution.

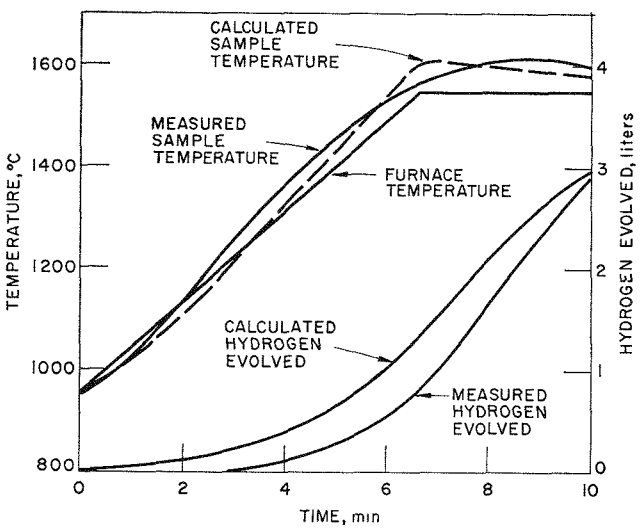

308-556

FIG. IV-15. Calculated Temperature at Top of Single Zircaloy-2-Clad Fuel Rod and Hydrogen Evolution from the Rod: Furnace Experiment. (Steam flow rate: 10 g/min.)

Extension of the present calculations to longer periods of time requires assumptions regarding the mechanism of core meltdown. Development of a meltdown model (CHEMLOC-II) is in progress.

c. SINGLE FUEL ROD CALCULATIONS

A simplified version of the CHEMLOC-I program was used to compute the hydrogen evolution and the rod temperature for a single fuel rod inserted in a furnace in a flowing steam atmosphere. In this case the steam flow rate and furnace temperature were the input data for the computation. Calculations were made for an experiment (previously reported in ANL-7125, p. 155) in which a Zircaloy-2-clad fuel rod, 10 in. long by ⅜ in. in dia., was exposed to a steam flow rate of 10 g/min. Figure IV-15 shows a comparison of the computed and experimental results. The excellent agreement illustrates the applicability of the CHEMLOC program to single-rod calculations.

5. Loss-of-Coolant Simulation Experiments in TREAT on Zircaloy-2-Clad, UO_2-Core Fuel Clusters (R. C. Liimatainen, F. J. Testa)

Experiments were continued in TREAT to investigate the safety problems associated with the behavior of Zircaloy-2-clad, UO_2-core fuel rods during a loss-of-coolant incident (see ANL-7225, p. 177). The purpose of the current tests is to obtain information on the chemical and physical changes which occur upon meltdown of the fuel cluster. Specific emphasis is placed on determining the extent of metal-water reaction, the temperatures and pressures produced, and the final particle size distribution of the fragmented fuel. Three experiments have now been performed, each on a progressively longer time scale. The first of these, CEN-217S, was reported previously (ANL-7225, p. 186).

The basic experimental technique consists of loading a "scale-up" autoclave with a fuel rod cluster and water and exposing the entire assembly to a neutron flux in TREAT. The construction of the autoclave, which is essentially an instrumented stainless steel pressure vessel, was previously described in ANL-6925, p. 209. However, in these simulated loss-of-coolant experiments, three fuel rods were used in each experiment and were located *above* the pool of water (instead of being submerged in it). Each fuel rod consisted of 10 sintered, fired UO_2 pellets clad with Zircaloy-2. The fission heat generated in the 10% enriched UO_2 during the TREAT transient causes failure of the fuel rods. To achieve a more realistic simulation of a loss-of-coolant incident,[7] the TREAT reactor power level, and hence, the neutron flux, was held as constant as possible during the experiments. These irradiations are therefore called "flat-top" transients, in contrast to the power excursion type which were studied previously in this program (see, for example, ANL-7055, p. 192).

The arrangement of the fuel cluster and the support structure inside the autoclave is shown in Figure IV-16. The lower part of Figure IV-16 shows a "Calrod" heater (bent into a loop to fit inside the autoclave) which was actually submerged in the water when the whole assembly was inserted into the autoclave. In two of the experiments this electrical heater raised the water temperature from the ambient 30°C to a value of

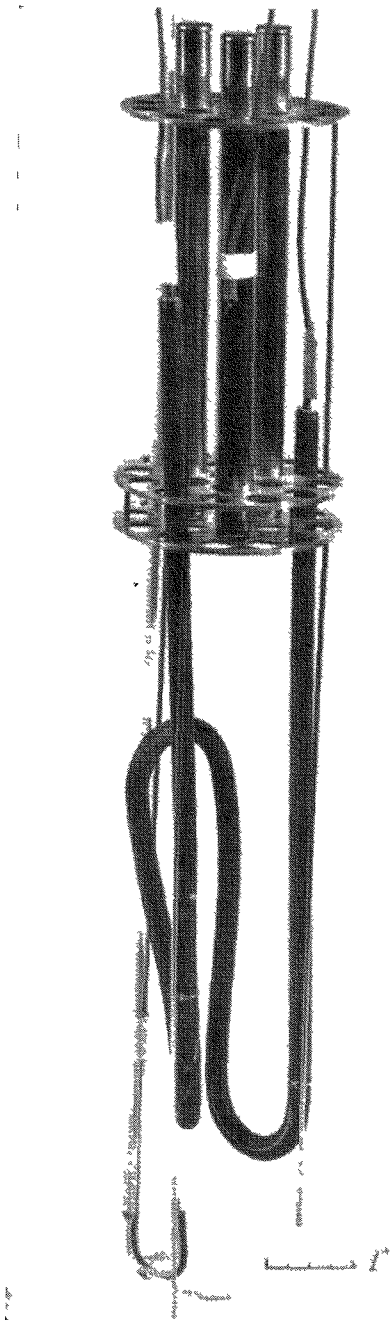

108-9766

Fig. IV-16. Arrangement of Fuel Cluster for Loss-of-Coolant Simulation Experiments in TREAT.

[7] It is recognized that these experiments are not exact simulations of a loss-of-coolant incident. Nevertheless, they do provide considerable insight into the problems involved.

TABLE IV-2. SUMMARY OF RESULTS OF LOSS-OF-COOLANT EXPERIMENTS IN TREAT WITH ZIRCALOY-2-CLAD, UO_2-CORE FUEL CLUSTERS[a]

	Experiment Number		
	CEN-217S	CEN-220S	CEN-223S
Transient			
Location of fuel cluster	Above 30°C H_2O	Above 100°C H_2O	Above 100°C H_2O
Duration of flat-top transient, sec	12	32	50
Average heat generation rate in UO_2,[b] kW/ft	40	20	11
Average reactor power level,[b] MW	40	20	11
Fission energy input, cal/g UO_2	560	770	630
Results			
Metal-water reaction,%	40	44	32
Peak pressure rise, psig	87	750	220
Maximum rate of presssure rise, psig/sec	45	76	3
Final appearance of UO_2 fuel	Complete destruction; fragments and particles; ~½ of cluster dropped into water	Complete destruction; fragments and particles; whole cluster dropped into water	Complete destruction; fragments and particles; whole cluster dropped into water
Average particle size of residue (d_{sv}),[c] mils	91	83	12

[a] Ten sintered pellets of UO_2 (10% enriched in ^{235}U) per rod. Overall rod dimensions, 5.62 in. long by 0.42 in. in dia.; 25-mil thick cladding; 3-mil gap between core and cladding; helium bonded. Three rods with a weight of 254 g of UO_2 and 82 g of Zircaloy-2 per cluster; 750 g of water in autoclave.

[b] The identical values of heat generation rate and reactor power level are coincidental.

[c] $d_{sv} = \dfrac{1}{\sum \dfrac{w_i}{d_i}}$ where w_i = fraction by weight of particles with diameter, d_i, as determined by sieve screen analysis.

100°C just before the TREAT transient was initiated. Thus, in these experiments a 1-atm steam environment was provided for the fuel rods which are located immediately above the water level. A tungsten-rhenium thermocouple was spotwelded to the cladding in the central portion of one of the fuel rods. A second thermocouple with the junction about ¾ in. above the bottom (see Figure IV-16) recorded the bulk water temperature and indicated when the hot fragments from the fuel cluster above had fallen down into the water.

The three experiments which have been completed are summarized in Table IV-2. The runs are arranged from the shortest time of fission heating (12 sec) to the longest (50 sec). (This is the time during which the reactor power is on.) However, in the third test the actual event continued for about 2 min. During the first minute, the nuclear heat generation occurred, and during the second minute the cooling process took place while the pressure in the autoclave was still rising towards its maximum value. The time span of about 2 min, even though quite short, approaches the times that are currently of interest in analyses of loss-of-coolant accidents. With decay heating, under reactor conditions, times from 10 to 15 min are generally of most interest.

Although the first experiment of the series was reported in the previous semiannual report (ANL-7225, p. 186), the results of that experiment are repeated here for the convenience of the reader. The oscillograph records, the particle size distributions, and photographs of the residue of the fuel rod clusters for the three experiments are shown in Figures IV-17, IV-18, and IV-19. One of the most significant features of the experiments is the appearance of the residue; portions of the cladding were present that retained the original cylindrical form of the cladding. These are particularly apparent in the residue from experiment CEN-217S which had the fastest heating rate. Evidently, in this experiment, considerable quantities of UO_2 (apparently largely unmelted) emptied from the Zircaloy cladding before the cladding completely melted. This occurred to a lesser degree in experiment CEN-220S and to a still lesser degree in experiment CEN-223S, where progressively lower rates of fission heating allowed more time for heat transfer between the UO_2 and the Zircaloy.

The best indication of the time of the failure of the fuel rods is given by the time at which the temperature indicated by the cladding thermocouple peaked. Little information, however, is apparently provided by the temperature value itself at the peak. Values of 2430, 1670, and 1570°C, respectively, were recorded for the

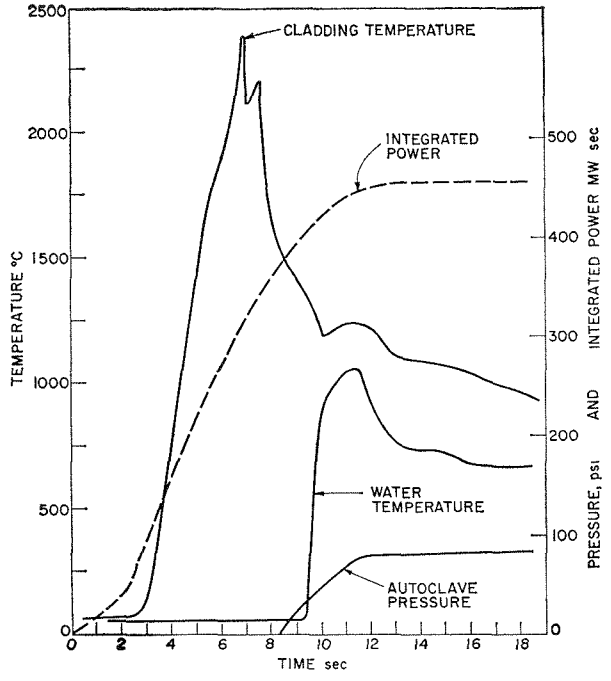

Oscillograph Record

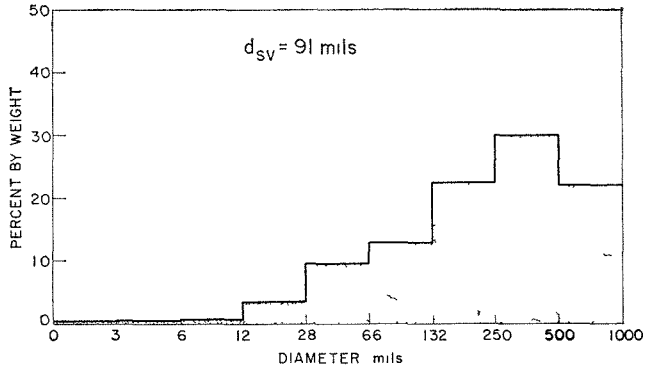

Particle Size Distribution

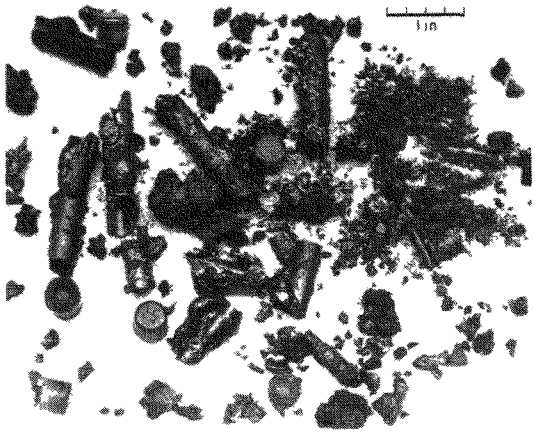

Residue on Upper Support Plate

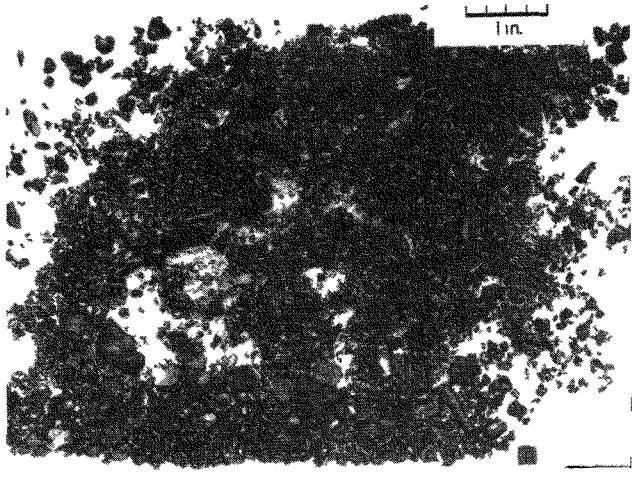

Residue in Lower Water Reservoir

308 567

FIG IV 17 Results of TREAT Loss of Coolant Accident Simulation Experiment CEN 217S (12 sec Flat top transient, 560 cal/g UO_2)

three experiments Table IV-3 gives the conditions of fuel at the time that the maximum temperature was recorded by the cladding thermocouple It is evident from the table that sufficient fission energy had been generated at the probable time of failure to have at least partly melted the UO_2 Another indication that the time of failure of the fuel corresponds to the time of recording of the maximum cladding temperature is that this time coincides within about 1 sec in each experiment with the beginning of significant pressure rise within the autoclave

Considerable information regarding the nature and timing of the collapse can be obtained from the oscillograph records for the three experiments In the first experiment, CEN-217S, there was a very high heating rate, much of the UO_2 emptied from intact tubes cladding, and collapse into the water was probably completed in about 5 sec The 5-sec value is the ap-

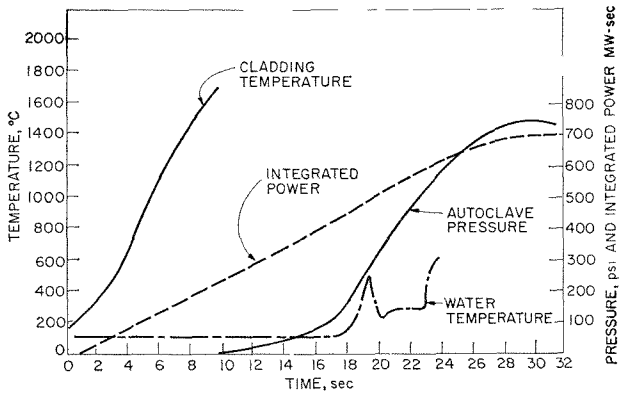

Oscillograph Record

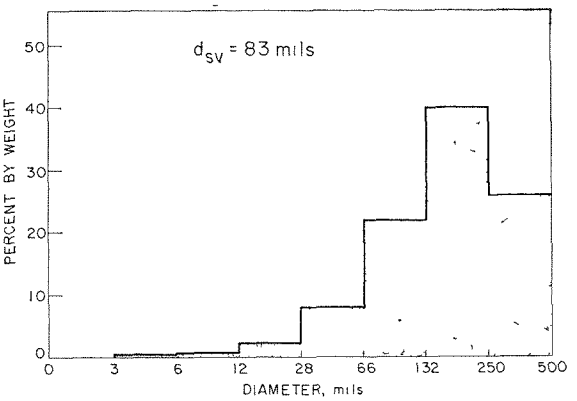

Particle Size Distribution

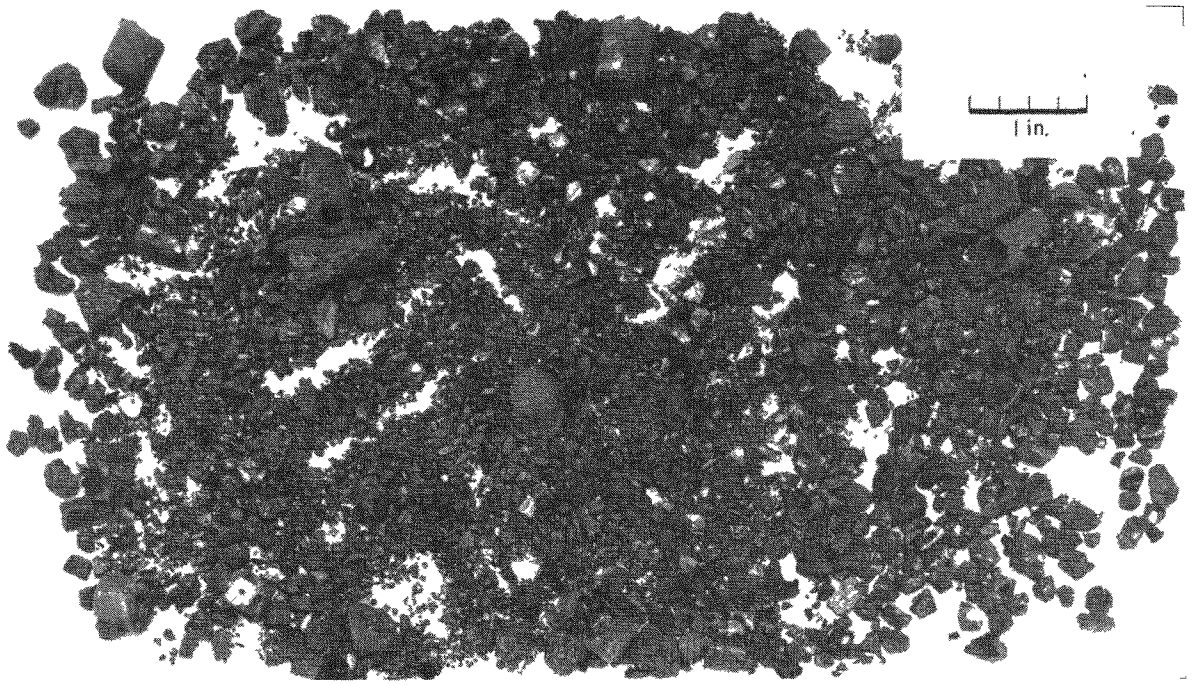

Residue of 3-Rod Cluster (entirely in lower water reservoir)

308-569

FIG. IV-18. Results of TREAT Loss-of-Coolant Accident Simulation Experiment CEN-220S (32-sec Flat-top transient, 770 cal/UO_2.)

proximate time from the recording of the peak cladding temperature to the completions of the pressure rise and water temperature rise (see Figure IV-17). It was only in this experiment (CEN-217S) that the stainless steel support structure did not completely fail. Evidently, the loss of the UO_2 heat source from above the support structure was rapid enough to preclude melting of the structure.

In the second experiment, CEN-220S, there was a more moderate heating rate and indications are that collapse required from 10 to 20 sec. The major indication of collapse was the erratic behavior of the water temperature thermocouple about 10 sec after the time of recording of the peak cladding temperature. Autoclave pressure reached a peak value after another 10 sec had elapsed, suggesting that collapse had been completed.

In the third experiment, CEN-223S, the heating rate was 11 kW/ft for a time of 50 sec. Autoclave pressure, however, rose uniformly for about 130 sec. Indications of water temperature increase were noted during a major portion of this time. It is concluded from this that collapse of the fuel cluster was rather slow and continuous for much of the 130-sec time interval.

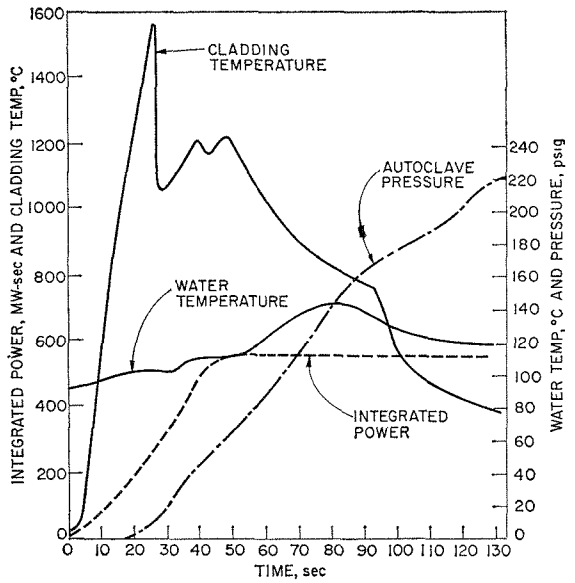

Oscillograph Record

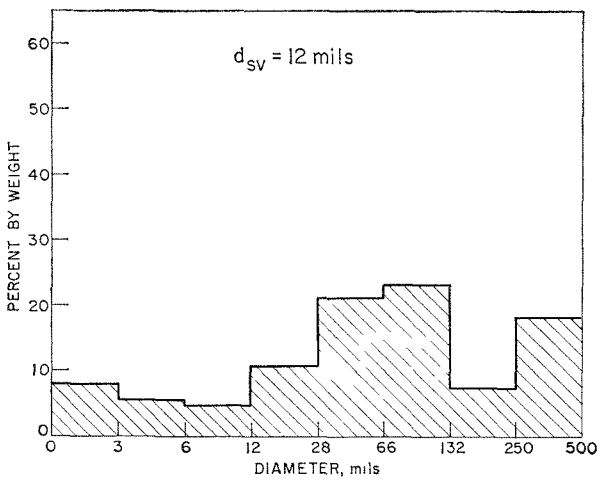

Particle Size Distribution

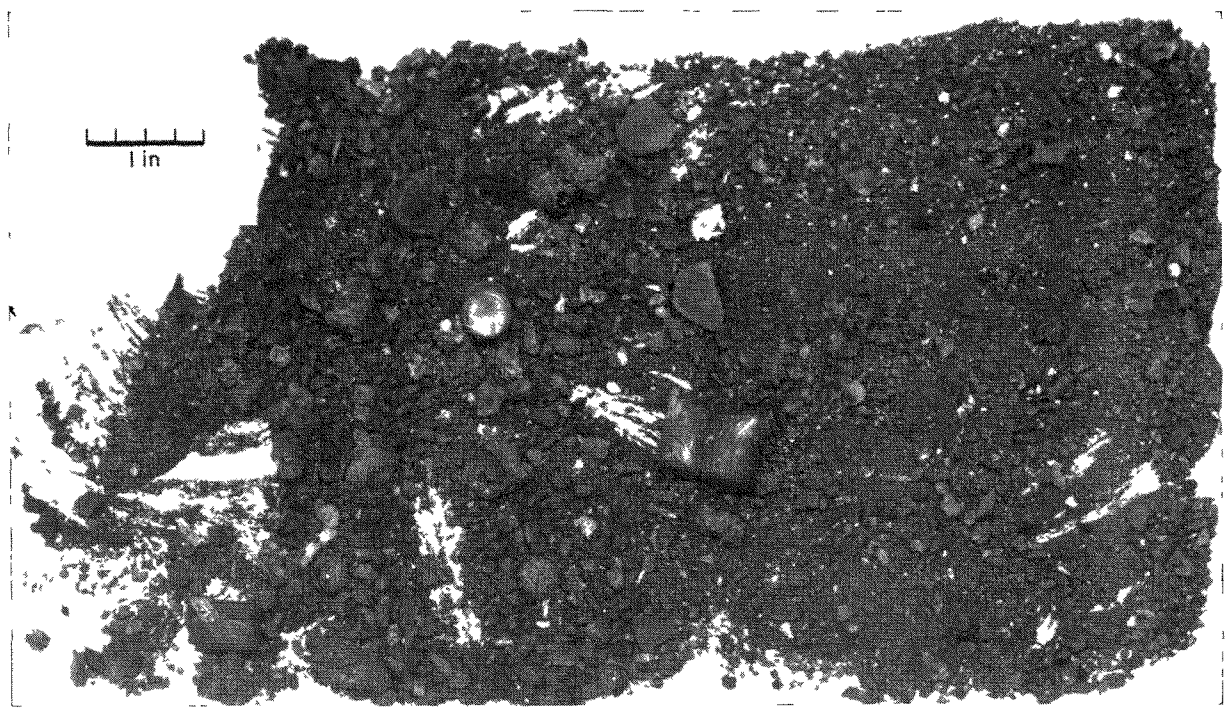

Residue of 3-Rod Cluster (entirely in lower water reservoir)

308-566

FIG. IV-19. Results of TREAT Loss-of-Coolant Accident Simulation Experiment CEN-223S. (50-sec Flat-top transient, 630 cal/g UO_2.)

A significant observation, based upon the particle size distribution of the residues, is the absence of large quantities of very fine particles. This would be a particularly encouraging result if confirmed by additional experiments, since it suggests that molten UO_2 (and molten UO_2-Zr-ZrO_2 mixtures) may not exhibit a marked tendency for spontaneous subdivision on being quenched in water. It is also noteworthy that the pressure-time traces showed no "spike" pressure rises which indicates that no steam explosions occurred as the molten fuel material entered the water pool, at least for the small scale experiments performed in this study.

TABLE IV-3. CONDITION OF FUEL (UO_2) AT THE TIME OF RECORDING OF THE MAXIMUM CLADDING TEMPERATURE IN LOSS-OF-COOLANT EXPERIMENTS IN TREAT

Experiment Number	Average (Constant) Heat Generation Rate[a] (kW/ft)	Peak Recorded Cladding Temperature[b] (°C)	Energy Deposit in Fuel (cal/g UO_2)	Adiabatic Fuel Temp. (°C) and Physical State of Fuel
CEN-217S	40	2430	360	3300 (fuel fully melted)
CEN-220S	20	1670[c]	240	2800 (fuel partly melted)
CEN-223S	11	1570	285	2850 (fuel fully melted)

[a] A heat generation rate of 1 kW/ft is typical of values of greatest interest in loss-of-coolant accident analyses. Such low values cannot presently be sustained in TREAT for a sufficient time to produce fuel failure.

[b] The apparent randomness of the indicated temperature may be associated with the formation of hot spots (and cold spots), which were noted in motion picture studies (see Section IV.A.6. of this report).

[c] The cladding thermocouple may have broken prematurely since the temperature trace was lost at this point (see Figure IV-18).

The total extent of metal-water reaction for the three experiments varied over a range from 30 to 44%. A number of factors complicate any detailed numerical analysis of the metal-water reaction during the experiments. During the initial heating period, the pressure in CEN-217S was 20 psia helium and only about 0.5 psia of water vapor. In the other two experiments, there was about 15 psia of water vapor pressure in addition to 20 psia of helium. There was no forced convection flow in any of the experiments; however, the nature of the assembly of fuel rods suggests that a brisk circulation by natural convection would be established and that there would be considerable steam available for reaction, at least in CEN-220S and CEN-223S. The likelihood of steam being available above the support plate suggests that considerable reaction occurred prior to fuel collapse. The fact that vigorous fission heating continued after much of the fuel had fallen into the water suggests that a sustained reaction (supported by the high rate of fission heating) continued after collapse of fuel into the water. Considering that the entire quantity of fuel had melted and collapsed into the water, a reaction of only 30 to 44% is encouraging from an accident analysis point of view. This result again provides evidence that, upon being quenched in water, Zircaloy-clad fuel is not susceptible to a self-sustained reaction to completion, so long as the cladding is not dispersed in the form of very fine molten droplets.

An analysis of energy sources and distribution was performed for the TREAT loss-of-coolant experiments. The results are summarized in Table IV-4. From the analysis it was concluded that from 20 to 26% of the total energy release was of chemical origin. The remainder was energy generated by fission. The overall thermal efficiency was the fraction of the total energy that was effective in heating and boiling water to reach the quasi-equilibrium state existing at the time of peak autoclave pressure. The remaining energy had been dissipated to the autoclave walls. The efficiency varied from 40 to 70%.

TABLE IV-4. ENERGY CALCULATIONS FOR SIMULATED LOSS-OF-COOLANT EXPERIMENTS IN TREAT

	CEN-TREAT Transient Number		
	217S	220S	223S
Nuclear Source			
Specific fission energy input, cal/g UO_2	560	770	630
Total nuclear energy input, cal	142,000	195,000	160,000
Chemical Source			
H_2 evolved, STP, liters	16.1	17.7	12.9
Heat evolved from Zr-H_2O reaction, cal	51,000	56,000	41,000
Total Energy Release			
Nuclear and chemical, cal	193,000	251,000	201,000
Chemical contribution to total, %	26	22	20
Specific energy input to water, cal/g H_2O	257	334	268
Calculated Final Conditions at "Equilibrium" [a]			
Water temperature, °C	117	257	184
H_2O vapor pressure, psia	26	648	159
H_2 partial pressure, psia	55	86	52
He partial pressure, psia	26	35	30
Total "autoclave" pressure, psia	107	769	241
Observed Final Condition at "Equilibrium" [a]			
Pressure in autoclave, psia (max)	107	770	240
Enthalpy Balance in System[a]			
Total enthalpy increase (H_2O) evaluated at final temperature, cal	78,200	177,500	89,900
Heat lost into autoclave, %	60	30	55
Corresponding thermal efficiency, %	40	70	45

[a] Evaluated at the time of peak autoclave pressure (12 sec in CEN-217S, 30 sec in CEN-220S, and 130 sec in CEN-223S). The fuel is assumed to be cooled to the water temperature.

6. Photographic Studies of Metal-Clad, UO_2-Core Fuel Rods in TREAT

(L. HARRISON,[8] R. C. LIIMATAINEN, F. J. TESTA)

Work has continued in TREAT in the program to determine the high temperature behavior of metal-clad, UO_2-core simulated fuel elements during a reactor transient. Information is sought on the chemical and physical changes which take place upon meltdown of fuels in a nuclear reactor undergoing a power excursion. The previous results have largely been obtained in an opaque autoclave (see, for example, ANL-7225, p. 177). The results obtained in a transparent capsule, reported herein, therefore complement the earlier data in that a visual (photographic) record is a vital part of each in-pile experiment. In particular, it was expected that, in addition to metal-water reaction information, these experiments would provide some insight into such aspects as heat transfer and the actual mechanics of the fuel failure in water.

The in-pile assembly for the photographic experiments was described in ANL-7225, p. 173. As shown in Figure IV-20, the fuel rod, submerged in water, is located within a stainless steel inner capsule having a rectangular cross section and a quartz window. The view in Figure IV-20 is that seen on each frame of the high speed (1000 frames/sec) film that records the transient. The fuel rod is photographed through the quartz window with intense external illumination. However, after the fuel rod attains a high temperature (~1000°C or greater), the light source can be shut off since the incandescence of the fuel rod itself is enough to give proper exposure of the film.

a. EXPERIMENT WITH STAINLESS STEEL-CLAD, UO_2-CORE FUEL

An experiment (Run CEN-221T) was performed with a single, type 304 stainless steel-clad, UO_2-core fuel rod. The results of the experiment are summarized in Table IV-5. The appearance of the fuel rod after the transient (290 cal/g UO_2) is shown in Figure IV-21.

It is apparent from Figure IV-21 that the fuel rod retained its cylindrical form; however, extensive cladding failure had taken place. There is clear evidence that patches of the cladding surface underwent the foaming phenomenon which was found in laboratory experiments where stainless steel-clad, UO_2-core fuel rods were heated to above 1400°C in a steam environment (see, for example, ANL-7125, p. 153). Analysis of the hydrogen evolved indicated that about 2% of the cladding had reacted with water; however, the appearance of the cladding showed that perhaps as much as 10% of the cladding had reacted.

[8] ANL Idaho Division.

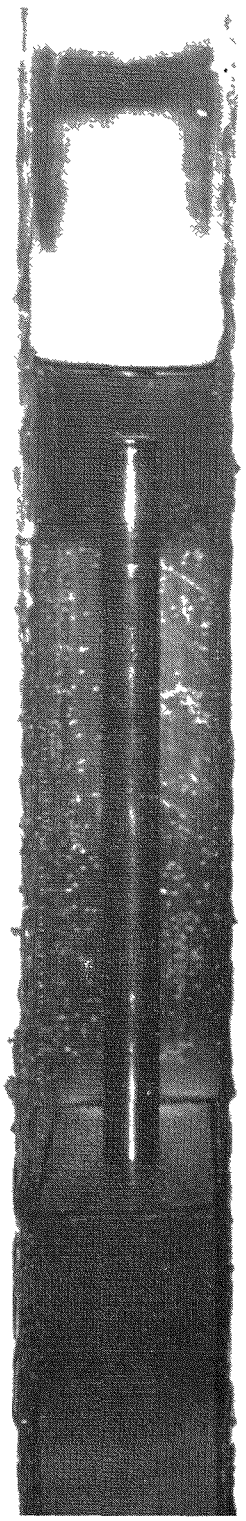

103-7453

FIG. IV-20. Fuel Rod in Photographic Capsule Before TREAT Experiment.

TABLE IV-5. Results from In-Pile (TREAT) Meltdown Experiment with a Type 304 Stainless Steel-Clad, UO_2-Core Fuel Rod Submerged in Water

Rod dimensions, 5⅝ in. long by 0.42 in. in dia.
83 g (10 pellets) of sintered (92% theoretical density) UO_2, 10% enriched.
27 g of type 304 stainless steel (25-mil) cladding.
600 g of H_2O coolant, initially at 30°C.

	Run CEN-221T
Reactor Characteristics	
Integrated power, MW-sec	206
Peak power, MW	352
Period, msec	126
Results	
Peak cladding temp., °C	1,400 (estimated)
Stainless steel-H_2O reaction, %	~10
Final appearance of fuel rod	Rod intact, began to slump, partial melting of cladding
Fission energy input, cal/g UO_2	290
Total fission energy, cal	24,000
Chemical energy, cal	(negligible)
Adiabatic UO_2 temperature, °C	2,800 (melted)
Calculated temperature rise of H_2O, °C	30
Observed temperature rise of H_2O, °C	33

In previous experiments with single, small (½-in. long), stainless steel-clad, UO_2-core fuel pins at energy inputs of about 290 cal/g UO_2, the fuel pins fragmented completely and from 5 to 9% metal-water reaction occurred (see ANL-6900, p. 254). It appears likely that a longer, single vertical fuel rod, such as was used in Run CEN-221T, has a somewhat higher threshold for total failure than does a short fuel pin, although the total extent of metal-water reaction is not greatly different for the two cases.

From the appearance of the fuel rod in Run CEN-221T, it is likely that the cladding temperature had exceeded 1400°C only in localized areas where the cladding had oxidized and foamed. The tarnished nature of the other areas of the cladding indicated that temperatures as high as 1200 to 1300°C were reached although the cladding thermocouple indicated a temperature of only 490°C (Figure IV-21 shows that it was located on an unfoamed area). The thermocouple located in the water indicated a total temperature rise of 33°C. The adiabatic temperature rise of the water calculated from the total energy released was 30°C, as shown in Table IV-5.

The motion pictures of the experiment showed the initial development of nucleate boiling, followed by an apparently localized boiling burnout[9] and the

[9] Transition to film boiling.

103-7449

Fig. IV-21. Fuel Rod after Run CEN-221T.

growth of irregular patches of very hot (luminous) cladding interspersed with cooler (nonluminous) patches. The location of the overheated areas corresponded to the areas of cladding oxidation and foaming apparent in Figure IV-21. It is reasonable to suppose that the spotty nature of the heating was due to irregular contact between the UO_2 pellets and the cladding. Following the nuclear transient, there was a long period of cooling (5–10 sec) during which the irregular variation of the cladding temperature was converted to a vertical temperature gradient where the top portion of the rod was hottest and the lower portion of the rod was cooler. However, there was a *sharp* gradation of luminosity with the top one-third of the rod being luminous and the lower two-thirds nonluminous. The demarcation then gradually progressed upward as cooling continued. This post-transient behavior is understandable in terms of the gradual development of free convection flow about the surface, leading to greatest cooling at the lower portion of the rod.

b. EXPERIMENT WITH ZIRCALOY-2-CLAD, UO_2-CORE FUEL

An experiment (Run CEN-222T) was performed in which a single Zircaloy-2-clad, UO_2-core fuel rod was subjected to three consecutive neutron bursts of progressively higher energy. The conditions and results of the experiment are summarized in Table IV-6.

The first pulsed irradiation resulted in a fission energy input of 165 cal/g UO_2, with a 238-msec reactor period. This corresponds to a maximum, or adiabatic, UO_2-core temperature of 2200°C. Since the UO_2 remained solid, as would be expected, the transient was nondestructive in nature. The Zircaloy cladding attained a peak recorded temperature of 1165°C. Thus, both the core and the cladding were below their melting point.

The second pulsed irradiation resulted in a fission energy input of 305 cal/g UO_2, with a 115-msec reactor period. This corresponds to an adiabatic UO_2-core temperature of 2850°C, with the UO_2 in a fully melted state. The Zircaloy-2 cladding reached a maximum temperature of 1700°C, as indicated by the cladding thermocouple. Thus, the cladding reached a temperature only slightly below its melting point of 1850°C. Although the cladding had not been melted, it appeared from the early part of the motion picture record of the third transient that two small pinholes had developed in the cladding during the second transient irradiation. However, no sign of cladding failure was apparent from the motion picture record of the second transient.

The third pulsed irradiation resulted in a fission en-

TABLE IV-6. Results from In-Pile (TREAT) Meltdown Experiment with a Zircaloy-2-Clad, UO_2-Core Fuel Rod Submerged in Water

Rod dimensions, 5⅝ in. long by 0.42 in. in dia.
83 g (10 pellets) of sintered (92% theoretical density) UO_2, 10% enriched.
27 g of Zircaloy-2 (25-mil) cladding.
600 g of H_2O coolant, initially at 30°C.

	Run CEN-222T, Transient Number		
	I	II	III
Reactor Characteristics			
Integrated power, MW-sec	118	218	248
Peak power, MW	113	443	556
Period, msec	238	115	101
Results			
Peak cladding temperature, °C	1165	1700	2100
Zircaloy-H_2 reaction, %	0	—[a]	7
Final appearance of fuel rod	Intact	Intact, but local cladding failure indicated by film	Some fragmentation but rod shape retained; partial meltdown and cladding distortion
Fission energy input, cal/g UO_2	165	305	347
Total fission energy, cal	13,700	25,300	28,800
Chemical energy, cal	0	—[a]	2,950
Total energy, cal	13,700	25,300	31,750
Adiabatic UO_2 temperature, °C	2200 (solid)	2850 (melted)	3200 (melted)
Calculated temperature rise of H_2O, °C	23	42	53
Observed temperature rise of H_2O, °C	25	43	52

[a] Not determined.

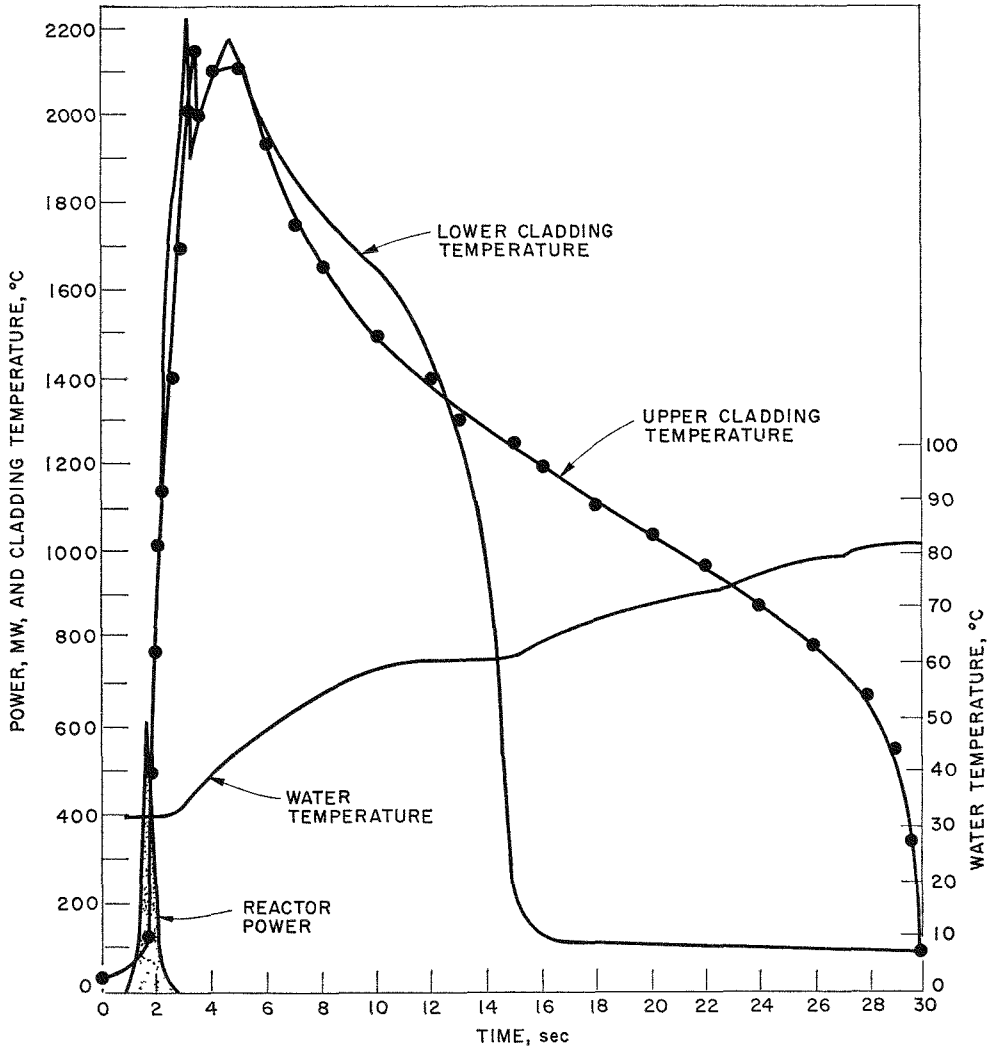

308-562

FIG. IV-22. Oscillograph Record of Run CEN-222T. (Transient III.)

ergy input of 347 cal/g UO_2, with a 101-msec reactor period. The corresponding adiabatic UO_2-core temperature was 3200°C (400°C above the UO_2 melting point). The measured peak cladding temperature was about 2200°C as shown in the oscillograph record in Figure IV-22.

The final appearance of the fuel rod after the third transient irradiation is shown in Figure IV-23. The fuel rod retained its cylindrical form; however, extensive cladding damage did occur. There was an area of "crinkling" or inward deformation of the cladding which may have been due to static or dynamic pressures acting to collapse the softened or melted Zircaloy. Globules of solidified UO_2 were found after the transient which had apparently escaped through cladding defects.

The motion pictures of the third transient irradiation showed a number of interesting features. Early in the transient, when the energy release in the fuel was only 14 cal/g UO_2, two small horizontal streaks were seen to emanate from the lower end of the fuel pin. These streaks appeared to be jets of water vapor and/or fine particulate matter flowing from defects in the cladding which were apparently produced during the second transient irradiation. The jets were discernible for 0.27 sec but probably lasted for a longer period of time. During the period, the bottom end of the fuel rod came out of the hole in the graphite support block and the force created by the jets caused the fuel rod to move against the side of the water container. The jet diameter increased from about 0.07 in. to 0.12 in. during the period while the jets were discernible. The jets eventually became obscured by the general cloudiness of the water in the lower regions of the water column.

When the energy released in the fuel had reached 231 cal/g UO_2,[10] the first of five small drops of incandescent material, apparently molten fuel, escaped from the penetrations in the cladding. Each drop was approximately 0.05 in. in diameter and the incandescence lasted approximately 0.01 sec for each particle. Later, when the nuclear energy release had reached 280 cal/g UO_2, the first of a slightly larger quantity of intensely incandescent material (molten fuel) escaped from the rod through penetrations in the cladding. A sufficient amount of material escaped in 0.02 sec to create an intense white light which obscured all but the upper end of the fuel rod. Many large gas bubbles could be seen approaching the water surface at this time. Material which escaped from the fuel rod was later found, by X-ray spectroscopic analysis, to be UO_2 which contained only a small amount of zirconium.

About one-half second after the initial escape of the molten fuel, the light intensity had decreased to the point where the molten fuel lying on top of the graphite could be seen. At this point, the upper end of the cladding began to become incandescent. At about 0.7 sec after initial fuel escape, additional molten fuel penetrated through the cladding at another location. About 0.3 sec later, a third penetration of fuel occurred as evidenced by a flash of light.

After this third fuel release, the cladding was highly incandescent over its entire length except for a short section at the top of the rod. This region, very likely, was void of fuel because fuel had flowed from it to replace fuel below that had escaped from the cladding. Dark spots were apparent which corresponded to cladding defects which had been sealed by frozen fuel. Although the cladding surface appeared somewhat spotty, surface luminosity was not as irregular as it had been in the motion picture of the stainless steel-clad rod.

The film showed cooling of the rod for about 10 sec. During this period convection currents in the water led to a rather sharp vertical gradient in luminosity. As in the case of the stainless steel-clad rod, cooling progressed from bottom to top. The sudden temperature decrease, probably corresponding to the collapse of film boiling, was indicated (see Figure IV-22) first by the lower thermocouple and, about 15 sec later, by the upper thermocouple.

The fuel rod lost a total of 6.6 g out of an original total of 111 g. Oxygen pickup from cladding oxidation was 0.7 g at the maximum. Total fuel loss from the rod was, therefore, 7.3 g or about the equivalent of one pellet out of a total of ten pellets. Although the total fuel loss was not great, the effects on the motion picture film were very startling because of the extremely high temperature of the escaping fuel.

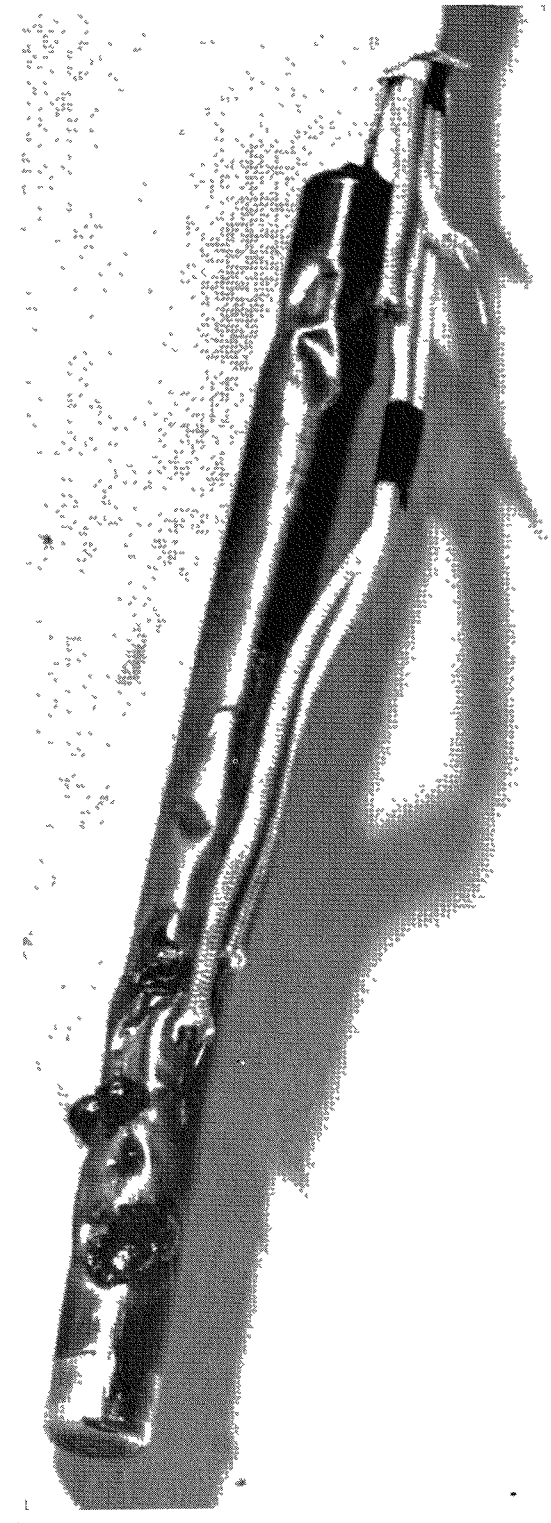

103-7451

FIG. IV-23. Fuel Rod after Run CEN-222T.

[10] Approximately 220 cal/g UO_2 is required to heat UO_2 from 25°C to the melting point of 2800°C, adiabatically. An additional 60 cal/g is required to melt UO_2 completely.

c. SUMMARY OF PRINCIPAL OBSERVATIONS FROM PHOTOGRAPHIC EXPERIMENT

1. The initial heating of the cladding appeared to be very irregular. Cladding temperature appeared to vary by at least several hundred degrees in a patchwork arrangement.

2. Both stainless steel and Zircaloy-2 cladding are very effective in containing molten UO_2. Although there were localized areas of melt-through, the defects became sealed by frozen fuel.

3. Convection currents were established within a few seconds that caused a uniform wave of cooling moving from the bottom to the top of the rod over a period of about 30 sec.

B. FAST REACTOR SAFETY STUDIES

1. Transient Heat Transfer Studies: Measurement of Heat Flux from a Heated Metal Sphere Moving through Liquid Sodium and Water

In order to analyze adequately the consequences of an incident in a reactor (either fast or thermal) in which hot fuel materials may be dispersed into the liquid coolant and result in explosive vapor generation, a knowledge of the manner in which large amounts of energy are transferred from these patricles to the liquid coolant is needed. At present, neither experimental nor thoretical information is available for the calculation of heat transfer that occurs as small particles at very high temperatures are dispersed in liquid sodium or water. Thus, a study of forced convection heat transfer from spheres in both media has been initiated.

a. THEORETICAL STUDIES (J. Hesson, L. Witte)

A detailed literature search and a general theoretical treatment of forced convection film boiling from a very hot sphere were presented in the preceding report (ANL-7225, p. 190). The theoretical expression derived from that treatment considered heat to be transferred across a vapor film from the sphere to the bulk liquid phase by conduction and radiation, with the heat being used partly to form vapor and partly to heat the bulk liquid for the case where the liquid was subcooled. The expression could not be solved in closed form and only numerical methods could be considered for solution.

A special case of the expression was solved analytically for the conditions in which there is no subcooling in the liquid, thermal radiation is negligible, and there is a linear velocity profile across the vapor film. Another special case has now been solved analytically for the conditions in which both vapor generation and thermal radiation are negligible. This case corresponds to extensive subcooling in which nearly all of the heat is transferred into the bulk liquid. The expression for this case is:

$$q/A = \frac{k_\ell \, (\sin^2\phi)\Delta T_B}{(\pi M \eta)^{\frac{1}{2}}} \tag{21}$$

where q/A is the local heat flux, k_ℓ is the thermal conductivity of the liquid, ϕ is the angular coordinate from the direction of sphere velocity, ΔT_B is the temperature difference from the liquid surface (facing the heated sphere) to the bulk liquid, and

$$M = \frac{2}{3}\frac{R\alpha}{U_\infty}, \quad \text{and} \quad \eta = \int_0^\phi \sin^3\phi \, d\phi$$

where R, α, and U_∞ are the sphere radius, the liquid thermal diffusivity, and the sphere velocity, respectively.

In the derivation of equation 21, it was assumed that the flow around the sphere was frictionless and could be described by potential flow theory, and that the distance of penetration of heat into the liquid was small as compared to the sphere radius. It is instructive to integrate equation 21 over the surface of the sphere to various values of the angular coordinate, ϕ. This results in the average heat flux from the sphere where heat transfer is interrupted at the angle, ϕ_s.

$$q/A = \left(\frac{3}{\pi}\right)^{\frac{1}{2}}\left(\frac{2}{3} - \cos\phi_s + \frac{\cos^3\phi_s}{3}\right)^{\frac{1}{2}} \left(\frac{U_\infty \rho_\ell C p_\ell k_\ell}{D}\right)^{\frac{1}{2}} (T_\ell - T_B) \tag{22}$$

where ρ_ℓ, Cp_ℓ, and k are the density, specific heat, and thermal conductivity of the liquid, D is the sphere diameter, and T_ℓ and T_B are liquid surface and bulk liquid temperatures, respectively.

Evaluation of the angular term in equation 22 results in the following:

$$q/A = K\left(\frac{U_\infty \rho_\ell C p_\ell k_\ell}{D}\right)^{\frac{1}{2}} (T_\ell - T_B) \tag{23}$$

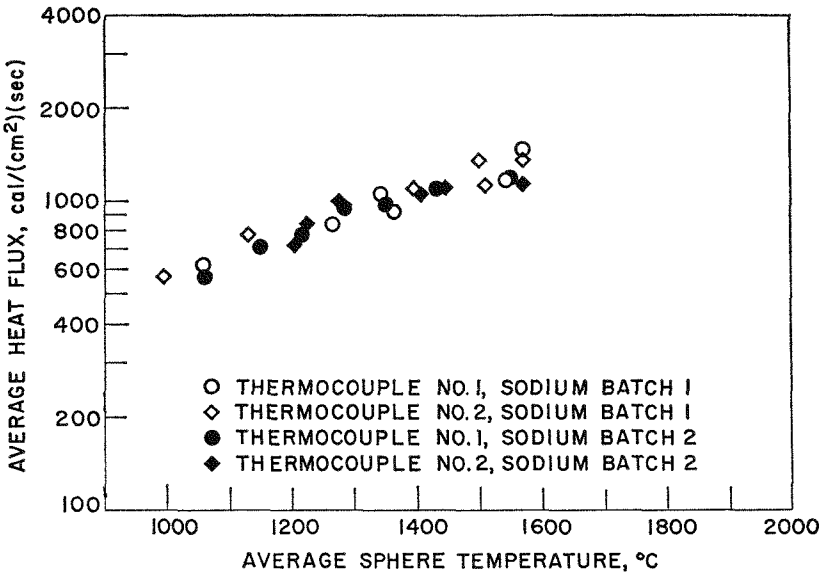

308-561

FIG. IV-24. Average Heat Flux *vs.* Average Sphere Temperature for 1/2-in. Diameter Sphere Moving through Liquid Sodium. (U_∞ = 10 ft/sec; T_{Na} = 300°C.)

where K has the following values for various values of ϕ_s :

ϕ_s	K
0°	0
90°	0.80
120°	1.04
135°	1.09
180°	1.13

The angle, ϕ_s, may be identified with the position of flow separation from the sphere if heat transfer to the fluid in the wake is ignored. From the results of the calculations, it is apparent that most (92%) of the heat transfer occurs up to an angle of 120°. It is also apparent from the calculations that the term K has a value of 1.13 for the case of no flow separation. This result was also obtained by Sideman.[11]

The theoretical development suggests a method of calculating the thickness of the vapor film at any point on the surface of the sphere. The heat flux is given by equation 21 for any angular position on the surface. The heat must flow across the vapor film so that the heat flux must also satisfy the following equation:

$$q/A = \frac{k_v}{\delta_v}(T_w - T_t) \qquad (24)$$

where k_v is the thermal conductivity of the vapor, δ_v is the vapor film thickness, and T_w is the sphere surface temperature. Calculations based upon equating the right-hand sides of equations 21 and 24 should yield a value of the vapor film thickness, δ_v .

[11] S. Sideman, Ind. Eng. Chem. **58**(2), 55 (1966).

b. EXPERIMENTAL STUDIES IN LIQUID SODIUM (L. WITTE, M. SILVERMAN)

The experimental investigation of forced convection film boiling from a sphere to liquid sodium has continued. The motor-driven, swinging-arm apparatus described in ANL-7225, p. 195 has been used to obtain heat fluxes from a ½-in. dia. tantalum sphere to liquid sodium at both 300 and 450°C. Sphere velocities of 6 and 10 ft/sec were employed and initial sphere temperatures ranged up to 1980°C.

The data from the above experiments were reduced by the method of Stolz[12] that accepts as input data a measured temperature-time trace at some internal point in the sphere. The sphere surface temperature and the heat flux are computed from this input. For much of the data the Stolz method proved unsuitable for reducing the initial portion of the data run where extremely high heat fluxes were encountered. Consequently, the initial part of the temperature-time trace for these runs were matched to an analytical solution for convective cooling of a sphere. This "matching" allowed the accurate calculation of the initial part of the data run. The method of Stolz calculated the latter portions of the data run accurately. The two methods of data reduction were then combined and an accurate representation of the entire data run was obtained.

Reproducibility of the data was shown by a series of experimental runs performed in 300°C sodium at a sphere velocity of 10 ft/sec. Two different sphe thermocouple assemblies and two different batches of

[12] G. Stolz, Trans. ASME (Series C) **82**, 20 (1960).

sodium were used. The data are shown in Figure IV-24. Since the data were obtained using thermocouples exhibiting poor response characteristics, the data were evaluated using the relation

$$(q/A)_{avg} = \frac{\Delta H}{A\Delta t} \qquad (25)$$

where $(q/A)_{avg}$ is the average heat transfer rate, ΔH is the change in enthalpy of the sphere because of its encounter with the sodium pool, A is the area of the sphere, and Δt is the time that the sphere was exposed to sodium. The technique for evaluating the change in enthalpy was described in ANL-7225, p. 198. The average heat flux is referenced to an average sphere temperature that is the arithmetic mean of the sphere equilibrium temperatures at entrance and at exit. Although considerable experimental scatter is present in the data in Figure IV-24, good agreement exists between measurements made with different sphere-thermocouple assemblies and in different batches of sodium.

Additional experimental runs were made using thermocouples with excellent response characteristics. For these experiments, instantaneous values of heat flux and the corresponding sphere surface temperatures were calculated. Data points were taken at convenient temperature intervals. The accuracy of the instantaneous heat fluxes was checked by comparing the mean heat flux, found by integrating the instantaneous flux values for each data run, to the average heat flux, found by equation 21. The integrated mean heat flux was found by evaluating the expression,

$$(q/A)_{mean} = \frac{1}{\Delta t}\int_0^{\Delta t} q/A(t)\, dt. \qquad (26)$$

TABLE IV-7. Comparison of Average and Integrated Heat Fluxes

Run	Average Heat Flux Equation 25 [cal/(cm²) (sec)]	Integrated Mean Heat Flux Equation 26 [cal/(cm²) (sec)]
59	788	1055
60	692	672
62	474	568
63	903	1005
64	825	803
66	615	660
67	640	624
68	895	711
70	840	918
71	950	890
74	825	697
75	735	718
76	431	457
77	413	416
79	491	629
80	481	402
81	495	510
82	394	379
83	347	300
84	615	676
85	493	376
86	402	330
87	802	600

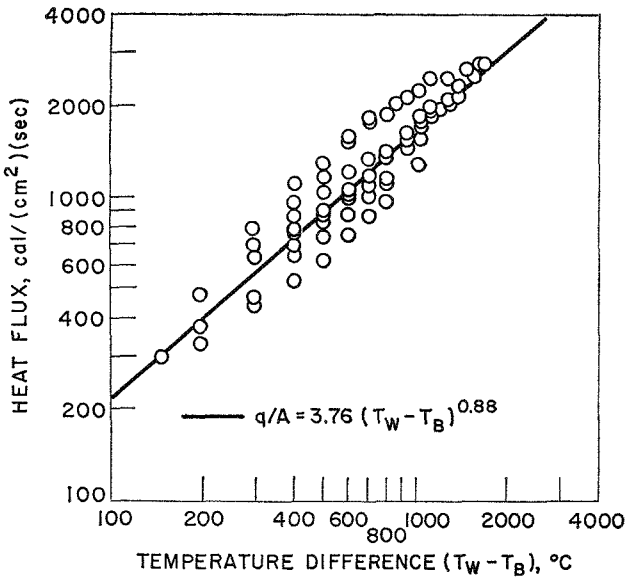

308-560

Fig. IV-25. Heat Flux *vs.* Temperature Difference for ½-in. Diameter Sphere Moving through Liquid Sodium. (U_∞ = 10 ft/sec; T_{Na} = 300°C.)

Table IV-7 shows the results of this comparison for the data runs which were used in the final data presentation. Generally, for most of the runs these two heat fluxes, calculated by independent methods, showed agreement to within approximately 10%.

By plotting the data points on log-log coordinates it was found that the data could be correlated empirically by the following expression:

$$q/A = C(T_w - T_B)^{0.88} \qquad (27)$$

where

q/A = heat flux, cal/(cm²)(sec)
T_w = surface temperature of sphere, °C
T_B = sodium bulk temperature, °C
C = 3.76 cal/(cm²)(sec)(°C)$^{0.88}$ for velocity = 10 ft/sec, T_B = 300°C
C = 2.82 cal/(cm²)(sec)(°C)$^{0.88}$ for velocity = 6 ft/sec, T_B = 300°C
C = 2.96 cal/(cm²)(sec)(°C)$^{0.88}$ for velocity = 10 ft/sec, T_B = 450°C.

A typical plot for a velocity of 10 ft/sec and a sodium temperature of 300°C is shown in Figure IV-25.

The correlation of heat flux with surface temperature of the sphere was also examined. Figure IV-26 shows

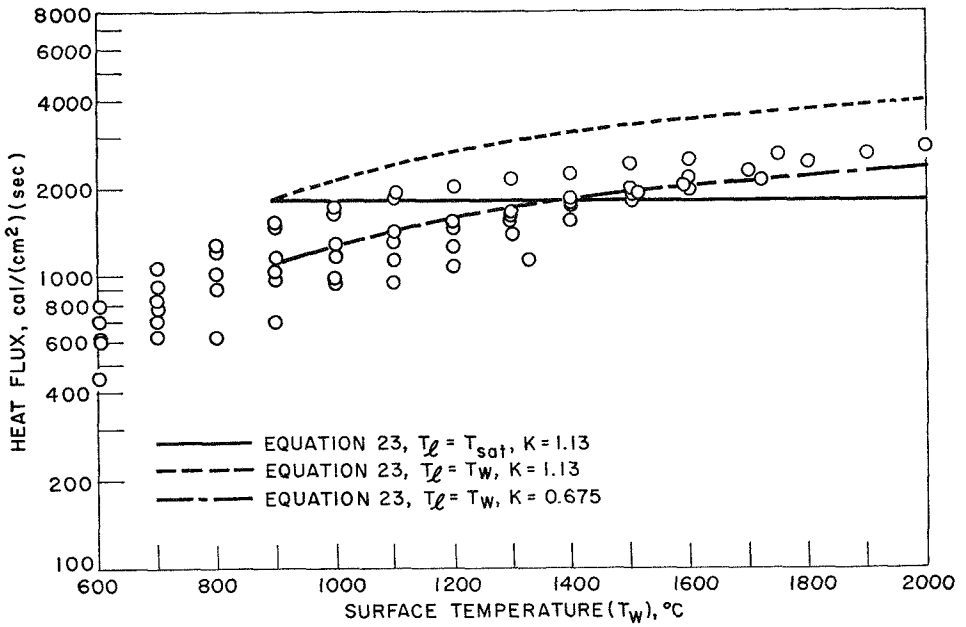

308-559

FIG. IV-26. Heat Flux *vs.* Surface Temperature for 1/2-in. Diameter Sphere Moving through Liquid Sodium. (U_∞ = 10 ft/sec; T_{Na} = 300°C.)

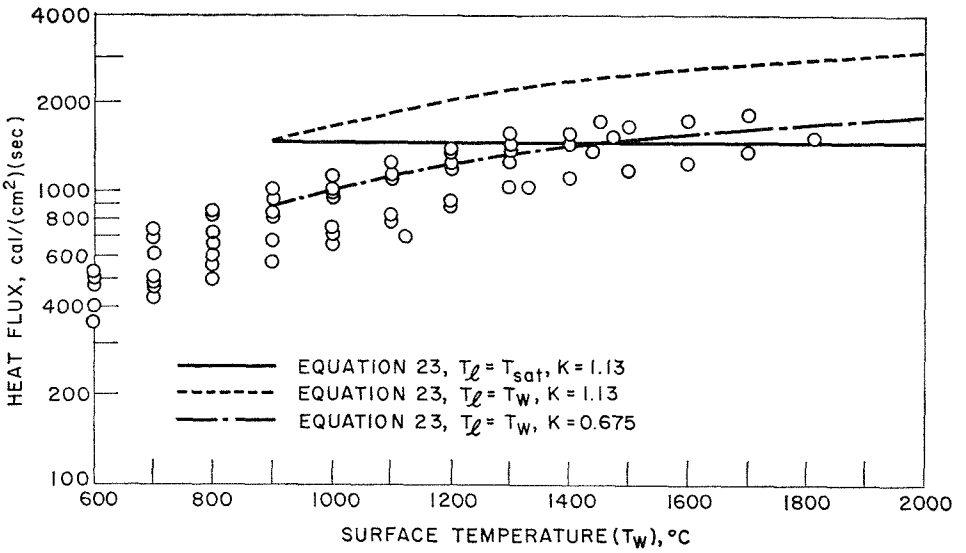

308-558

FIG. IV-27. Heat Flux *vs.* Surface Temperature for 1/2-in. Diameter Sphere Moving through Liquid Sodium. (U_∞ = 6 ft/sec; T_{Na} = 300°C.)

the data obtained at 10 ft/sec in 300°C sodium, Figure IV-27 shows the data obtained at 6 ft/sec in 300°C sodium, and Figure IV-28 shows the data obtained at 10 ft/sec in 450°C sodium. Calculations of heat fluxes based upon equation 23 are compared with the experimental results in the three figures. If it is assumed that the sodium boils at the saturation temperature at one atm pressure, without superheating, then $T_\ell = T_{sat}$ and the straight line in the figures is obtained. However, it is apparent from the figures that the experimental data show an increasing heat flux with increasing surface temperature. If it is assumed that the liquid surface temperature T_ℓ, at the liquid-vapor interface, is the temperature of the surface of the sphere, T_w, i.e., that complete superheating occurs, then the upper curves in the figures are obtained. A good fit to the data is obtained by using a constant fraction (K = 0.675) of the value calculated from equation 23 while substituting

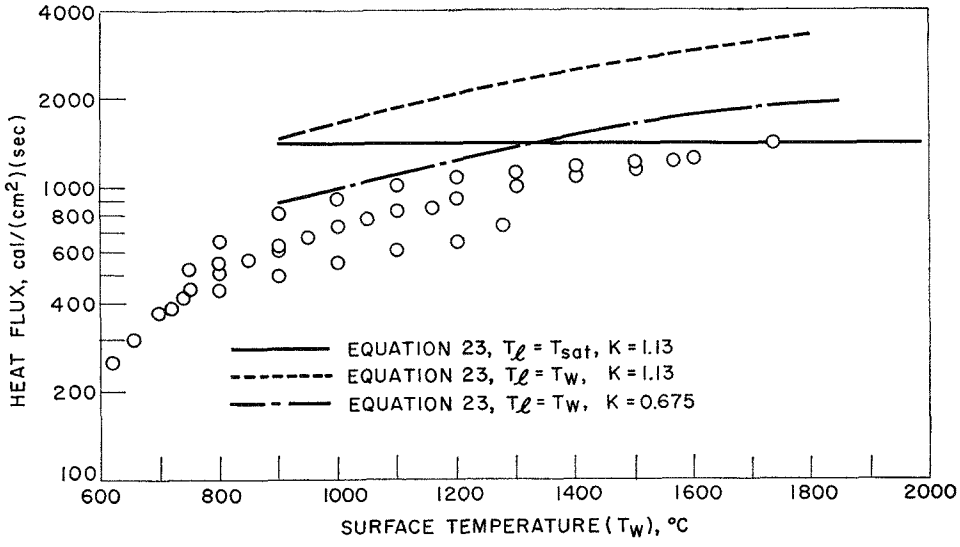

308-547

FIG. IV-28. Heat Flux *vs.* Surface Temperature for 1/2-in. Diameter Sphere Moving through Liquid Sodium. (U_∞ = 10 ft/sec; T_{Na} = 450°C.)

$T_t = T_w$. These heat fluxes are represented by the lower curves in Figures IV-26, IV-27, and IV-28. The fractional value of K requied to correlate the data may be due partly to flow separation near the 90° position on the sphere (see equation 23). It is also likely that somewhat incomplete superheating occurs within the liquid sodium near the liquid-vapor interface and this reduces the value of K to be used in equation 23.

The thickness of the vapor film required to transfer these large quantities of heat is extremely small. For example, the thickness of the vapor film at the 90-degree position on a ½-in. dia. sphere at 1911°C moving at 10 ft/sec was calculated to be 7.6×10^{-6} in. from equations 21 and 24. Although the sphere surfaces were relatively smooth, it is believed that the magnitude of the roughness of the surface greatly exceeded this value. It is possible that protuberances on the sphere surface could extend through the vapor film into the liquid sodium. This would cause the film to become unstable and possibly to collapse completely. This collapse would bring liquid sodium into contact with the sphere's surface which is at a high temperature. The sodium would then tend to assume the sphere surface temperature and could become highly superheated.

The agreement between experimental data and the theory that was developed by assuming superheating of liquid sodium indicates that this theory is adequate to describe the actual physical phenomenon. The physically unrealistic vapor film thicknesses that were calculated also tend to support the theory of superheating.

The results of this study indicate that large quantities of energy can be transferred from extremely hot spherical particles to highly subcooled liquid sodium without vapor formation.

Both experimental and theoretical investigations into heat transfer from moving spheres to liquid sodium are continuing.

c. EXPERIMENTAL STUDIES IN WATER (J. HESSON, J. CASSULO)

In previous transient heat transfer experiments in water, a heated ¼-in. dia. nickel sphere was either pushed or pulled through the water by means of a gravity-operated swinging arm or pendulum with a knife blade attached to the arm (see ANL-7055, p. 206, ANL-7125, p. 194, and ANL-7225, p. 194). The most recent experiments have been conducted with a motor-driven swinging-arm apparatus utilizing a ¼-in. dia. silver sphere. The silver sphere is attached to the end of a 1/16-in. dia. sheathed thermocouple which serves as the arm as well as the temperature measuring device. The motor-driven swinging-arm apparatus is very similar to that used for the studies in sodium and allows a greater range in combinations of velocity and immersion time than does a free-swinging pendulum, since the velocity of the sphere is independent of arm length.

The angular velocity of the sphere is determined through the use of a perforated timing wheel attached to the back of the motor shaft. The wheel separates a light source and a photoconductive cell; as the wheel turns, light intermittently falls upon the photo cell and a blip occurs on a recorder chart. This information, together with the arm length (distance from center of sphere to the center of the axis of rotation), the dis-

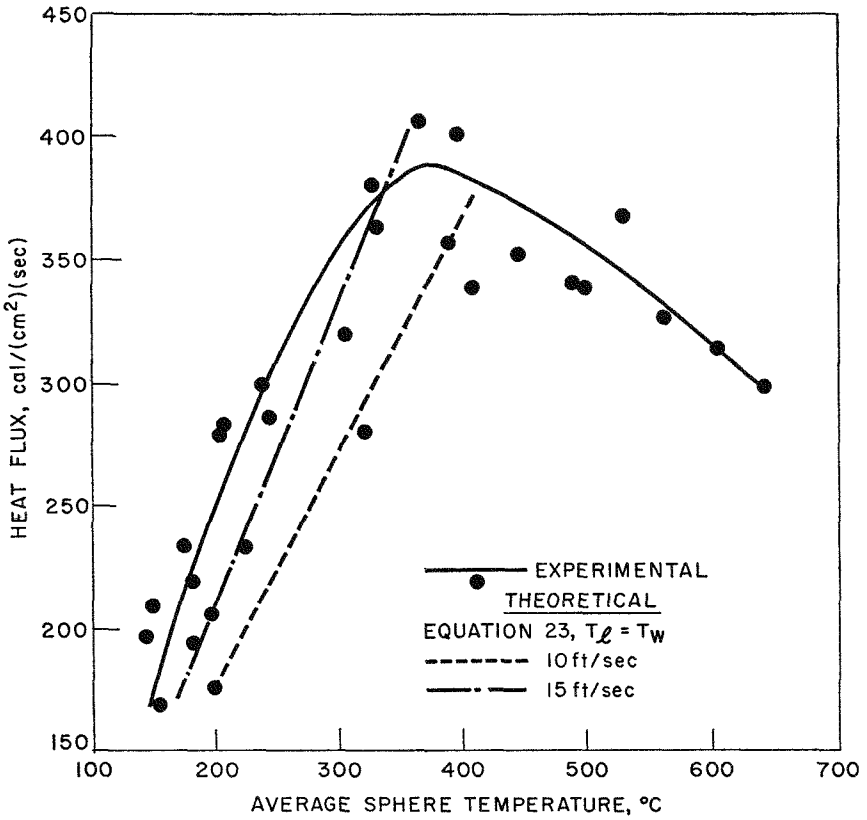

308-546

FIG. IV-29. Heat Flux *vs.* Average Sphere Temperature for a 1/4-in. Diameter Silver Sphere Moving through Water. (U_∞ = 12 to 15 ft/sec; T_{H_2O} = 23 to 25°C.)

tance from the axis of rotation to the water surface, and the temperature history of the sphere as it moves through the water are sufficient to calculate the length of the sphere path through the water, the linear velocity of the sphere in the water, the time of the sphere in the water, and the average temperature of the sphere before it enters and after it leaves the water. From these the heat transfer rate and average temperature of the sphere are calculated.

A silver sphere (rather than the previously used nickel) is being used for the water studies at lower sphere temperatures since silver's high thermal diffusivity yields more nearly uniform sphere and surface temperatures.

Figures IV-29, IV-30, and IV-31 show the results of the experiments utilizing the motorized equipment. For these experiments the water temperature ranged from 23 to 25°C. Figure IV-29 includes data over the sphere velocity range 12 to 15 ft/sec; Figure IV-30, that over the range 15 to 17 ft/sec; and Figure IV-31, that over the range 17 to 19 ft/sec. During these runs arm lengths of from $2\frac{15}{16}$ to $3\frac{1}{16}$ in. were used. The path lengths of the sphere in the water varied from 0.352 to 0.412 ft, and the length of time of the sphere in the water varied from 0.019 to 0.031 sec.

Calculations of heat fluxes based upon equation 23 are compared with the experimental results in Figures IV-29, IV-30, and IV-31. If it is assumed that the water boils at the saturation temperature, 100°C, at one atm pressure, without superheating, the calculated heat fluxes are about ¼ of the observed values. If it is assumed that the liquid surface temperature, T_ℓ, at the liquid-vapor interface, is the temperature of the surface of the sphere, T_w, i.e., complete superheating, then the dashed curves in the figures are obtained. The dashed curves in the figures do represent the experimental data, within a scatter band, up to sphere temperatures of the order 300 to 400°C, suggesting that water is superheated to these temperatures.[13]

At sphere temperatures greater than 300 to 400°C, the heat flux decreases. It is postulated that, in this region, boiling or flashing of the superheated water occurs, resulting in the formation of vapor films which reduce the heat flux. The incidence of boiling of the superheated water is somewhat erratic, causing a scattering of the experimental data. Many of the data points indicate a heat flux greater than values calculated from equation 23. This could be due to effects of

[13] It should be noted that the critical temperature of water is 374°C.

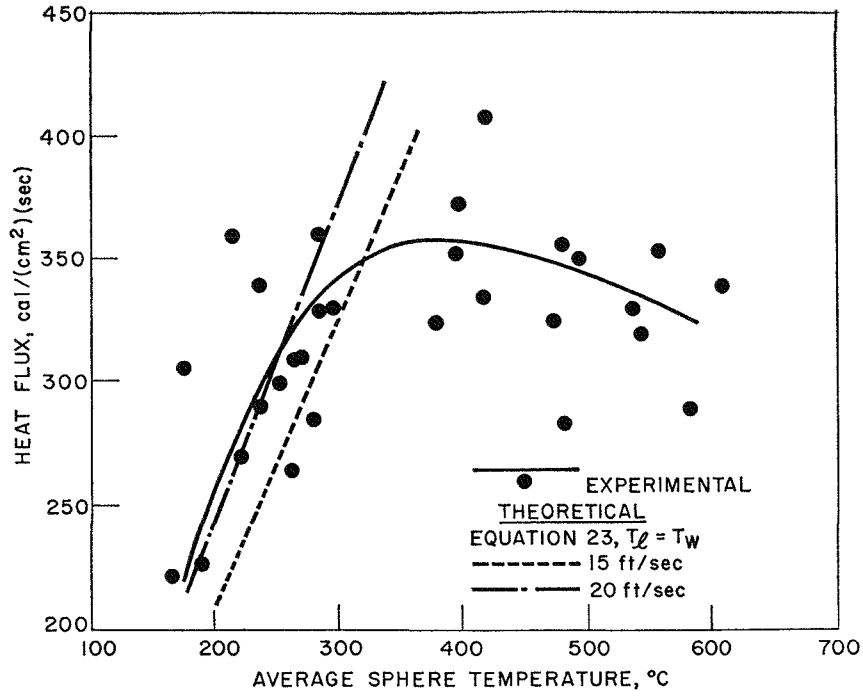

08-555

FIG. IV-30. Heat Flux *vs.* Average Sphere Temperature for a 1/4-in. Diameter Silver Sphere Moving through Water. (U_∞ = 15 o 17 ft/sec; T_{H_2O} = 23 to 25°C.)

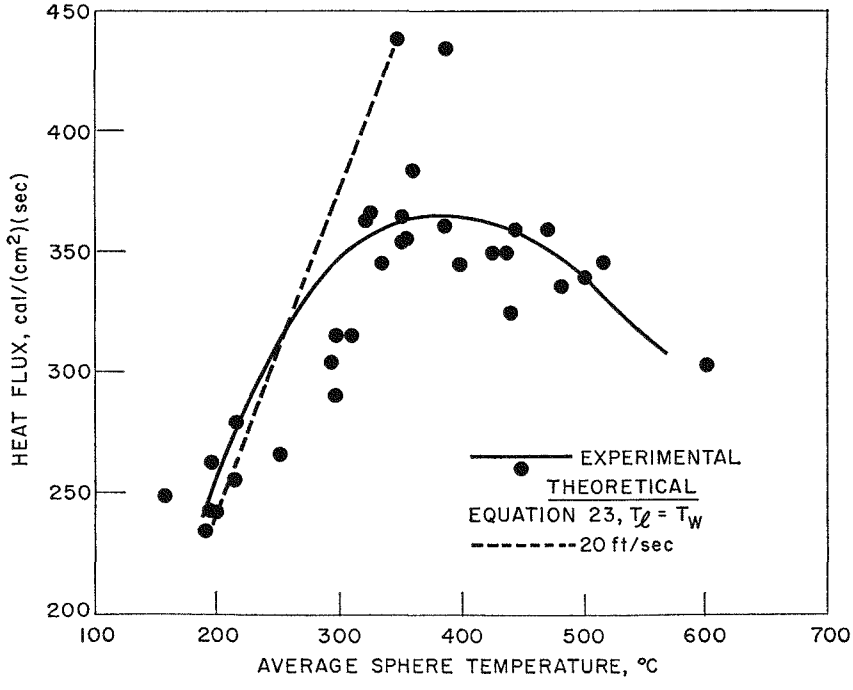

308-554

FIG. IV-31. Heat Flux *vs.* Average Sphere Temperature for a 1/4-in. Diameter Silver Sphere Moving through Water. (U_∞ = 17 to 19 ft/sec; T_{H_2O} = 23 to 25°C.)

turbulence generated in the water layer adjacent to the sphere surface that could be induced by slight irregularities on the sphere surface.

Equation 23 indicates that the heat flux should be proportional to the square root of the sphere velocity. This effect is not evident from the existing data. The data scatter and the limited range of velocity studied thus far have tended to mask effects of velocity. Both the effects of velocity and the role of turbulence are the subject of continuing study.

The thickness of the vapor film which would be required to transfer these large quantities of heat in water is very small. The thickness is calculated to be about 2×10^{-4} in. if it is assumed that the water boils at the normal boiling point.

d. CONCLUSIONS

Studies of energy transfer from very hot spheres to sodium and to water have shown the great importance of superheating. The experimental results indicate that water can remain in the liquid form in contact with a moving sphere at temperatures of the order of 300–400°C before transition to film boiling occurs. In sodium, there was no evidence for the development of film boiling even at the highest sphere temperatures studied (~1800°C). These findings make it clear that future attempts to understand the overall process of explosive vapor generation must take the superheating phenomenon into account. Future studies will be aimed at determining the conditions required for vapor formation at lowered sphere velocities.

2. TREAT Studies of Fuel Meltdown in Sodium (J. BOLAND,[14] R. C. LIIMATAINEN, F. J. TESTA)

Work has been initiated to obtain information from TREAT experiments on fuel meltdowns in a sodium environment at high energy inputs. This information would be useful in evaluating potential problems that could be encountered in the operation of sodium-cooled fast reactors. The work thus far has progressed through conceptual planning, design of equipment, and completion of construction of the in-pile assembly. Preliminary testing and calibration are now in progress. When this is completed, actual meltdown experiments in TREAT will begin.

Figure IV-32 shows the autoclave assembly being used for the studies. The autoclave assembly has double containment. In an experiment, nine rods, five of which are fueled with UO_2, are located in an environment of liquid sodium during a reactor transient. As shown in Figure IV-32, there are four thermocouples (W/Re) to measure the liquid sodium temperature, a variable impedance transducer to measure transient pressures, and a linear motion transducer to measure the sodium expulsion. The autoclave has a design rating of 6000 psi at 600°F. The ultimate strength of the autoclave, however, is 50,000 psi at 600°F.

A sketch of one of the fuel rods that will be used in the meltdown experiments is shown in Figure IV-33. The nominal OD of the fuel rod is 0.29 in. with an overall rod length of 12 in. The fuel rod is divided into two sections, a lower fueled section and an upper unfueled section. Each fuel rod is made up of 10 sintered UO_2 pellets, 10% enriched in ^{235}U, in the fueled section, clad with 15-mil type 304 stainless steel. There is a gas annulus (helium bonded) between core and cladding.

The upper unfueled section of the fuel rod simulates a reactor blanket region. A feature of particular interest is that the cladding in this section of each rod will have different wall thicknesses. The wall thicknesses were chosen to collapse at specific external pressures (at 1000, 3000, and 5000 psi). This should give additional information on the peak pressures attained during the transient. Should some cladding sections collapse and others not, this data would serve to give upper and lower limits to the pressure and would be an independent measurement to compare with that indicated by the pressure transducer.

In addition to giving information on peak pressures, the hollow cladding has another purpose. When the high pressure causes its collapse, a void volume is provided for the sodium. Should the piston stick and the liquid sodium undergo thermal expansion in the confined volume, this additional free volume will help in preventing autoclave rupture during the meltdown experiments.

Figure IV-34 shows the top view of the 9-rod fuel cluster. As stated above, five of the rods will be fueled, whereas the other four will be "dummy" rods. The dummy rods as well as the rupture disc spacer (shown in Figure IV-35) are designed to collapse in the event that the piston jams in the cylinder and the autoclave pressure exceeds 5000 psi, thus giving additional free volume for sodium expansion.

A sketch of the main components in the autoclave measuring system is shown in Figure IV-35. Measurements will be made of sodium temperatures, transient pressures, and rate and distance of sodium expulsion.

The piston is made of a molybdenum-30% tungsten

[14] ANL Idaho Division.

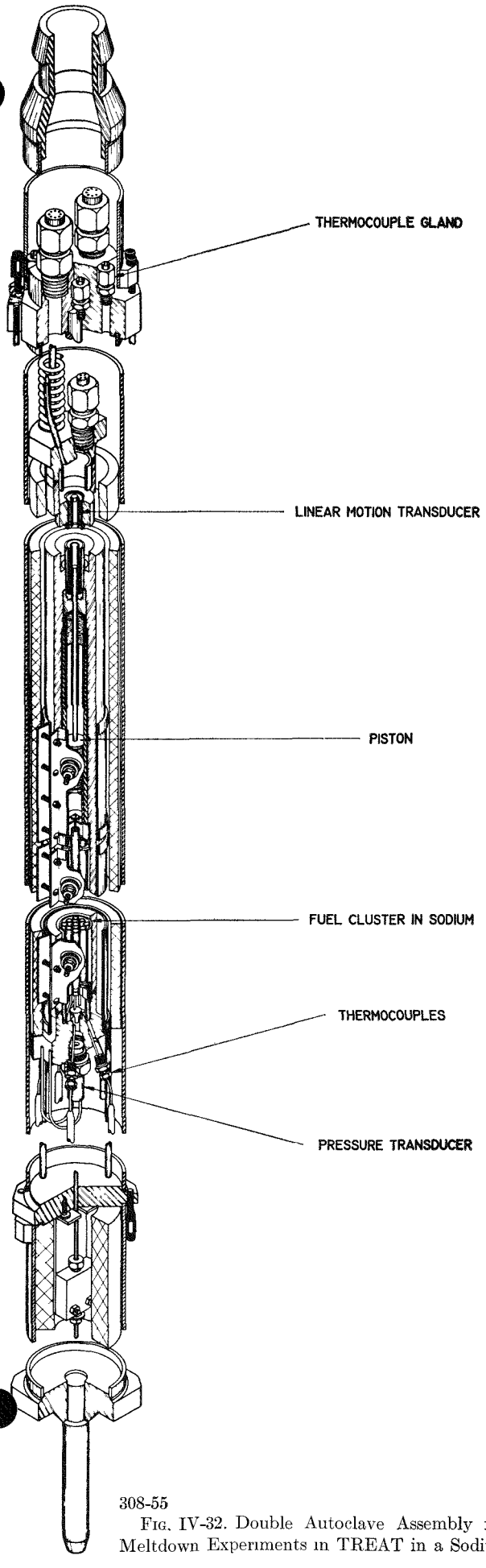

308-55

FIG. IV-32. Double Autoclave Assembly for High Energy Meltdown Experiments in TREAT in a Sodium Environment.

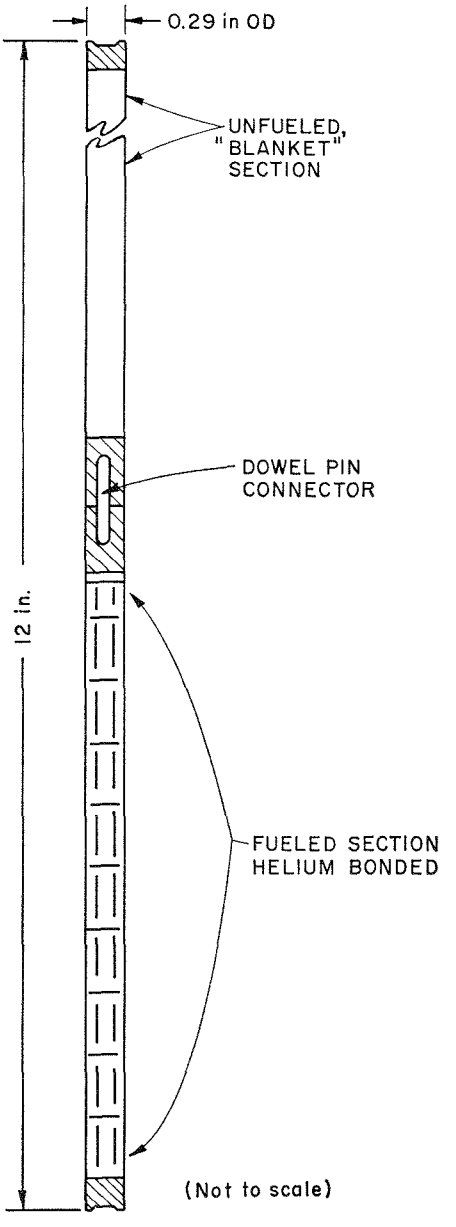

308-553

FIG. IV-33. Fuel Rod for High Energy Meltdown Experiments in TREAT in a Sodium Environment.

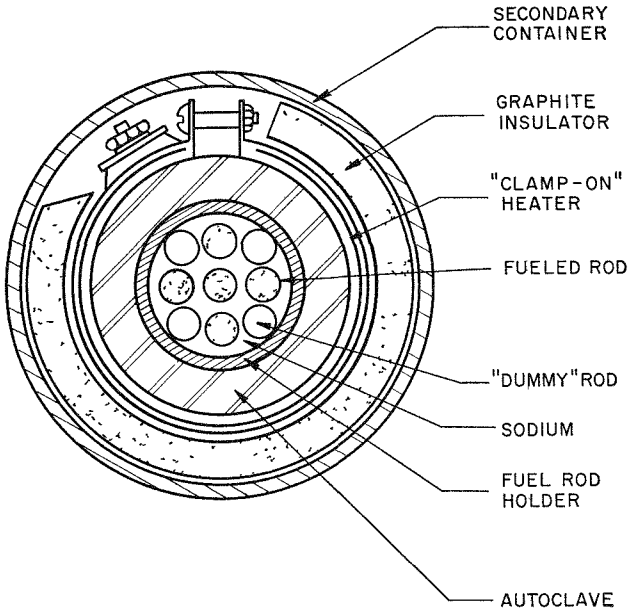

308-552

FIG IV-34. Top View of 9-Rod Fuel Cluster for High Energy Meltdown Experiments in TREAT in a Sodium Environment

alloy. The surrounding walls of the cylindrical chamber, through which the piston moves, are made of type 304 stainless steel. This inner wall has a fine-honed surface to minimize friction. The annulus, or gap, between the piston and the cylinder is 1.5 mils at room temperature. Out-of-pile tests are being performed to verify the performance of the piston.

The shock absorber shown in Figure IV-35 is designed to cushion the shock between the moving piston and the linear motion transducer, after the connecting rod has completed its stroke. The porous-metal shock absorber was tested on a compressive load machine; it began to yield when the applied load reached 4250 lb, and a force of 5500 lb caused a total compression of ¼ in. Using 4800 lb of force (average) and a displacement of ¼ in., the total energy absorbed is equivalent to 32 calories. This kinetic energy would be produced if the pressure acting on the piston were 5000 psi, sustained during the period which the piston moves over its maximum stroke of 4 in. Additional energy absorbing capacity is available in the shock absorber, since the maximum compression is about ½ in.

In the initial series of out-of-pile tests of the equipment, a gas pulse is being used to drive the piston. The gas is injected into the bottom of the autoclave from a high-pressure source through a quick opening valve (solenoid or explosive type).

The first in-pile test will be an irradiation in TREAT to establish the relationship between the reactor integrated power and the fission energy generated in the fuel rod. Meltdown experiments will then be made at various energy levels.

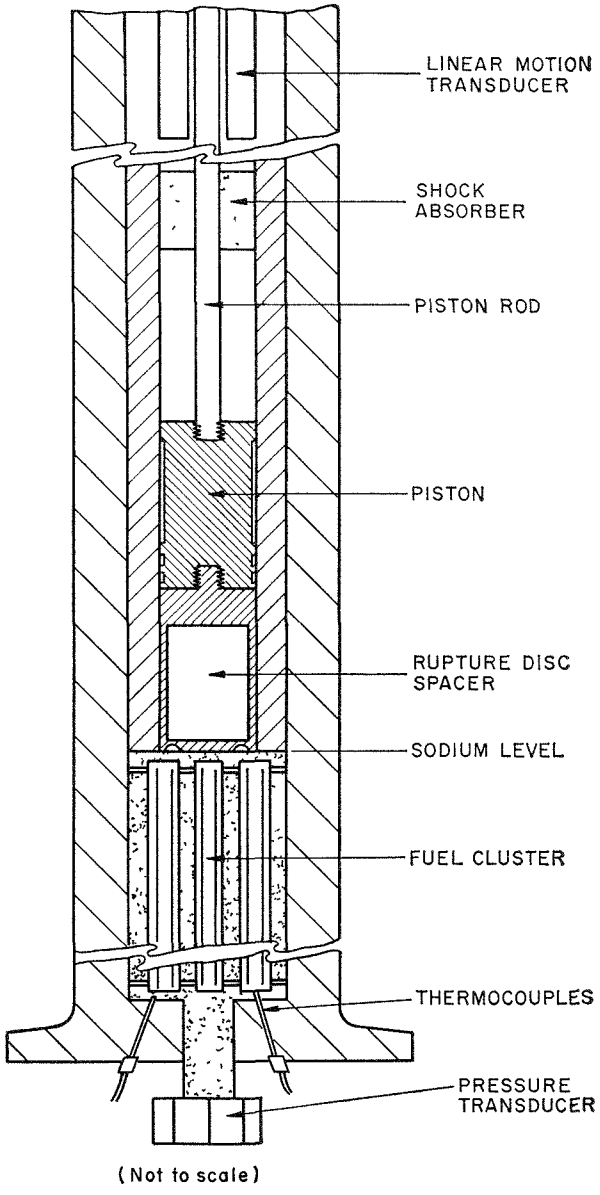

308-551

FIG IV-35. Autoclave Measuring System for High Energy Meltdown Experiments in TREAT in a Sodium Environment.

3. High Temperature Thermal Properties of UO_2 (L. LEIBOWITZ, L. W. MISHLER)

Work is continuing on the program to measure the heat capacity of liquid uranium dioxide, an important quantity in fast reactor safety calculations. Initial experiments were designed to test the suitability of

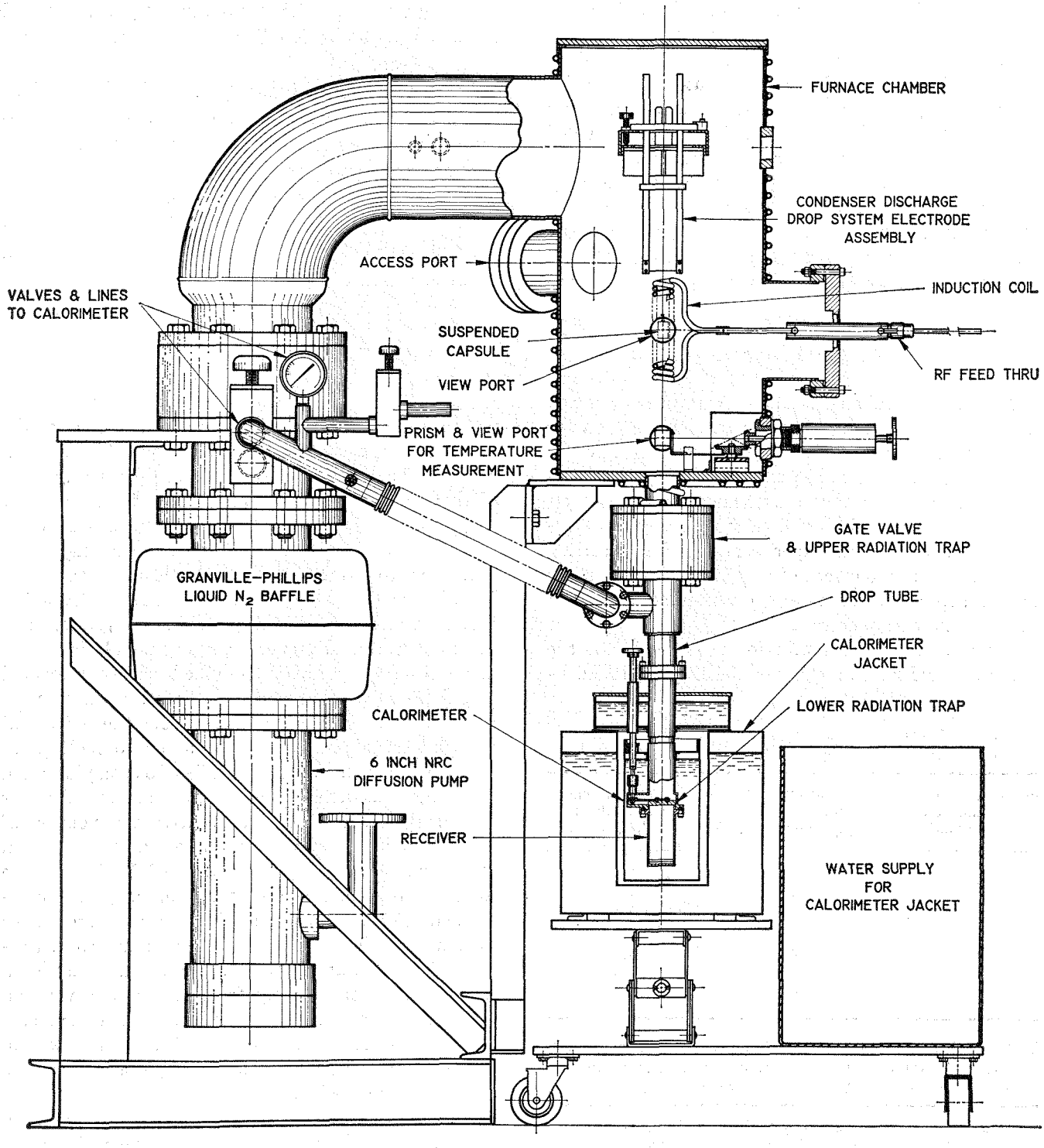

308-172

FIG. IV-36. High Temperature Calorimetric System for Measurement of the Heat Capacity of Liquid Uranium Dioxide.

tungsten as a container for the UO_2 at temperatures above 3000°C. A series of tests (ANL-7225, p. 198) has shown that tungsten will indeed behave satisfactorily. Several designs of capsules for holding the liquid oxide have been prepared and tested. These have varied from simple crucibles with lids to complex double walled containers with black body holes.

While experiments were in progress to test materials, fabrication methods, and design for sample capsules, the design of the entire calorimeter system was also

proceeding. The final design is shown schematically in Figure IV-36. The encapsulated oxide will be heated inductively and temperatures measured through a magnetically shuttered Varian Associates sight port by means of a Pyrometer Instrument Company automatic optical pyrometer. Black body holes will be provided in the capsule for temperature measurements.

The capsule containing the UO_2 will be suspended by a tungsten wire which in turn is to be connected, via appropriate electrodes, across a high voltage condenser bank. When dropping of the capsule into the calorimeter is desired, the condenser discharge will vaporize the tungsten suspension wire extremely rapidly and allow the capsule to fall. This simple scheme insures a vertical drop.

The calorimeter to be used, with suitable modifications, is a commercial adiabatic calorimeter manufactured by the Parr Instrument Company for bomb calorimetry. A precision Dymec quartz thermometer will be used to follow the calorimeter temperature.

Construction and necessary calibrations are presently in progress as is final testing of coil design and condenser discharge operation.

4. Fuel Migration Studies (M. G. Chasanov, D. F. Fischer)

The effect of fuel migration and segregation in mixed uranium-plutonium fuels can be an important factor in safety considerations for large fast reactors. Investigation of the migration of plutonium and fission products in a thermal gradient is planned for mixed fuels such as uranium and plutonium oxides, carbides, oxycarbides, and nitrides. Experiments are being carried out to evaluate the extent of migration that can occur and to help in understanding the mechanisms involved in the migration processes.

Radial and axial redistribution of fissile and fertile material could have an effect on the Doppler broadening shut-down mechanism and, in addition, could materially change the localized physical properties of the material, e.g., an increase in PuO_2 content in a small area of a PuO_2-UO_2 fuel could lower the melting point of that area. Changes resulting from fission product migration could also affect the physical properties of the fuel as well as its interaction with cladding.

In order to estimate the importance of the change in Doppler coefficient and melting point for a PuO_2-UO_2 fuel in which substantial plutonium migration had taken place, some Doppler coefficient calculations were made based on a rather simplified scheme presented in GEAP-3888.[15] The equations presented there were modified to reflect current ideas about the individual contributions of plutonium and uranium to the Doppler coefficient. For example, in GEAP-3888 each plutonium atom was considered to contribute a positive Doppler coefficient of 2⅓ times the negative contribution of each uranium atom; we have chosen them to be equal (based on newer data presented in ANL-7120[16]). The calculations compared the change in the Doppler coefficient for a fuel in which migration has taken place to that for a fuel with uniform plutonium concentration. The calculations were made for the case of a reactor excursion starting from zero power with an initial fuel temperature of 750°K to a final temperature of 2200°K at the position of average power in the pellet. For the many simplifying assumptions, see the original discussion.[15]

Tables IV-8 and IV-9 present the results of such calculations for both radial and axial linear plutonium

TABLE IV-8. Change in Doppler Ratio due to Radial Linear Concentration Gradients in a Cylindrical Pellet with 20% Average Plutonium Enrichment

Plutonium Enrichment at Centerline	% Decrease of $\frac{\Delta K_{Dopp}\text{ (migration)}}{\Delta K_{Dopp}\text{ (no migration)}}$	Fraction of Pellet Radius above Melting Point
0	4	0
10	1	0
20	0	0
30	1	0
40	4	0.15
50	9	0.30
60	16	0.43

TABLE IV-9. Change in Doppler Ratio due to Axial Linear Concentration Gradients in a Cylindrical Pellet with 20% Average Plutonium Enrichment

Plutonium Enrichment at Axial Midplane	% Decrease of $\frac{\Delta K_{Dopp}\text{ (migration)}}{\Delta K_{Dopp}\text{ (no migration)}}$	Fraction of Pellet Height Above Melting Point
0	12	0.08[a]
10	3	0
20	0	0
30	3	0
40	12	0.12

[a] Outermost zones above melting point.

[15] F. L. Leitz, editor, "Sodium Cooled Reactors Program, Fast Ceramic Reactor Development Program, First Quarterly Report, October–December 1961," GEAP-3888, pp. 147–15[illegible] (1963).

[16] D. Okrent, "Summary of Intercomparison Calculations Performed in Conjunction with Conference on Safety, Fuels, Core Design in Large Fast Power Reactors," Proceedings of the Conference, ANL-7120, p. 3 (1965).

gradients in a fuel pellet with an average plutonium enrichment of 20% In the case of the radial gradient, it appears that the decreases in the Doppler ratios are not large, exceeding 10% only when the concentration at the center of the pellet is more than 10 times that at the outer periphery and reaching a maximum of 16% when the outer boundary is depleted of plutonium For the case of the axial gradient, the Doppler ratio decrease is about three times that for the radial gradient at comparable central enrichments While parabolic gradients instead of linear gradients would yield larger changes in the Doppler ratio, they too would probably not cause decreases large enough to markedly affect the Doppler shutdown capability

At the recent International Conference on Fast Critical Experiments and Their Analysis (held at Argonne on October 10-13, 1966), P Greebler of General Electric reported[17] that " the Pu-239 Doppler effect in large, dilute fast power reactors can be virtually disregarded " However, this conclusion is yet to be demonstrated in a large, dilute fast power reactor The continuing trend on the part of reactor physicists toward lower and lower positive values for the Doppler coefficient for ^{239}Pu makes it increasingly likely that even severe separations between the fissile and fertile components of fuel will not compromise the Doppler shutdown capability Other adverse effects of migration and segregation must be considered to be more significant

The change in local composition of portions of the pellets in these calculations coupled with changes in the local temperatures produced by fissioning indicated that portions of the pellet could be at temperatures above the melting point of the PuO_2-UO_2 solutions The data of Chikalla[18] was used to estimate what fraction of the pellet would be above the melting point for the appropriate local composition From Tables IV-8 and IV-9 it can be seen that, while the Doppler ratio itself may change little, sizable portions of the pellet could be above the melting point of the material in these zones For the radial gradient, the inner portions could become molten For the axial gradient, a linear gradient with most of the plutonium in the outer regions could result in molten regions near the ends of the pellet, concentration of plutonium in the central portions could lead to melting there Of course, such behavior is dependent on the extent of migration of plutonium and the magnitude of the transient These calculations merely serve to indicate that such redistribution of the fissile material, while not changing the Doppler characteristics significantly, could alter the physical properties of the fuel and affect safety considerations

The thermal gradient apparatus to be used in the migration studies has been employed in a series of preliminary experiments to test the equipment and to determine its behavior during extended use The equipment itself has been described earlier in ANL-7225, p 200 For these preliminary studies, pellets of UO_2-CeO_2

TABLE IV 10 Experiments in Thermal Gradient Furnace with Urania Ceria Pellets

Pellet dimensions $\frac{3}{8}$ in in dia by $\frac{1}{2}$ in long

Ceria Content (m/o)	Heating Time (hr)	Thermal Gradient[a] (°C/cm)	Weight Loss (w/o)
15	100	1100	4 1
15	514	890[b]	3 8
30	100	1050	3 4
30	504	1060	14

[a] The temperature at the top of the pellet was approximately 2100°C

[b] Lower gradient due to changed heat shield geometry

308-563

Fig IV-37 Longitudinal Cross Section of a UO -30 m/o CeO Pellet Heated in Thermal Gradient of 1050°C/cm for 100 hr

[17] P Greebler et al Implications of Recent Fast Critical Experiments on Basic Fast Reactor Design Data and Calculational Methods ANI 7320 (in press)

[18] T D Chikalla, 'The Liquidus for the System UO PuO_2 , HW 69832 (1961)

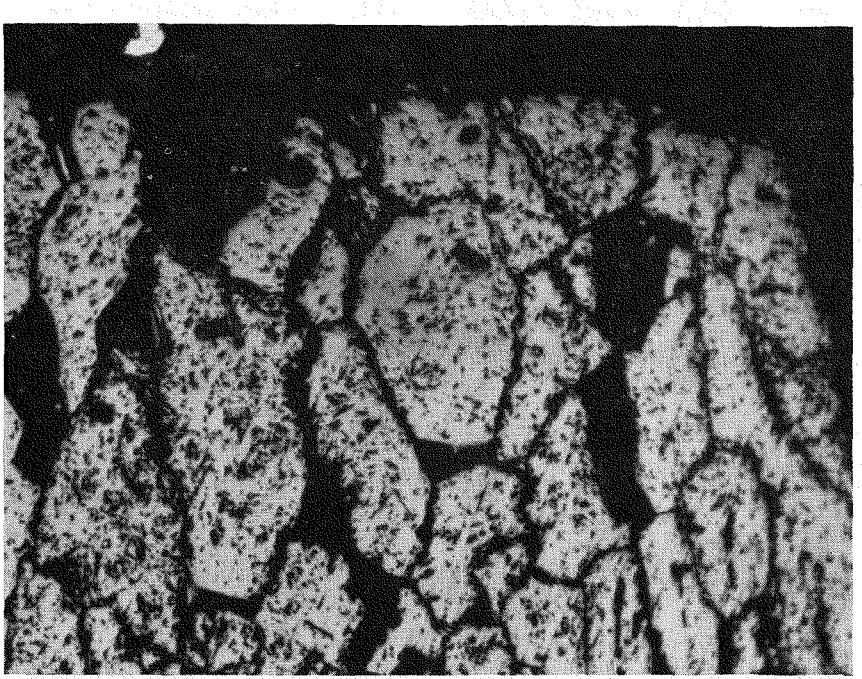

Top Portion

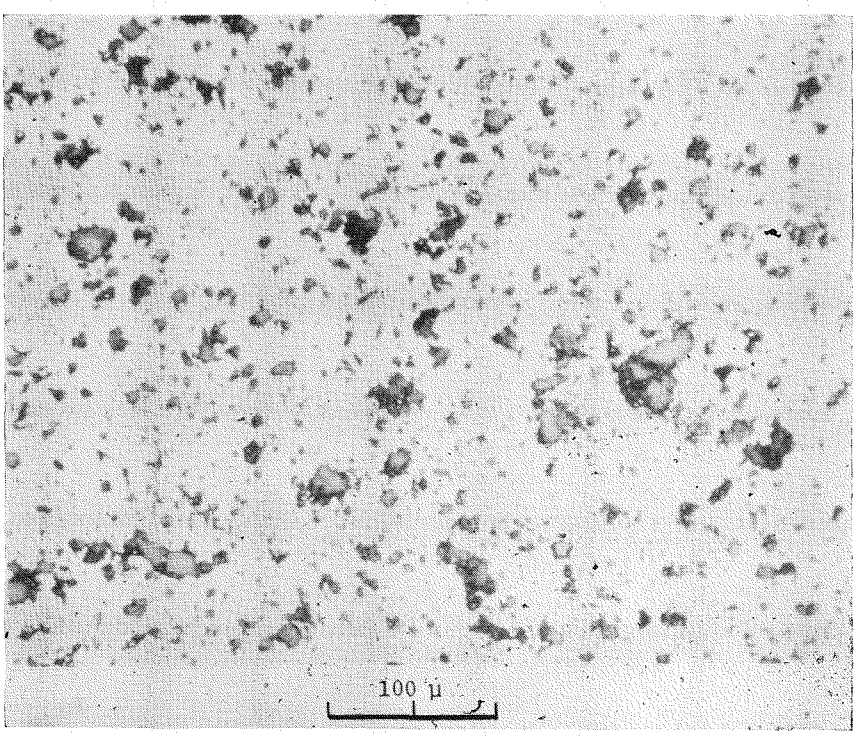

Central Portion

308-565

FIG. IV-38. Longitudinal Cross Sections of a UO_2-30 m/o CeO_2 Pellet Heated in a Thermal Gradient of 1060°C/cm for 504 hr.

solid solution material were continuously heated in the apparatus for periods up to approximately 500 hr. The experiments completed to date are summarized in Table IV-10. The pellets have been submitted for electron microprobe analysis for cerium and uranium.

These experiments have demonstrated the reliability of the apparatus for extended operation. Tungsten foil heaters proved satisfactory and the same foil could be used in several experiments. Thermal gradients in the samples of the order of 1000°C/cm were readily maintained.

Ceramographic examination of the heated pellets indicated pore migration toward the hotter end of the samples had occurred. Figure IV-37 is a longitudinal

cross section of the UO_2-30 m/o CeO_2 pellet that had been heated for 100 hr. The increase in porosity near the top of the sample is quite evident in the figure; unheated samples show a more uniform distribution of pores and in general, pores of much smaller size. Associated with this porous region near the top of the samples are evidences of columnar grain growth. Figure IV-38 shows a portion of the longitudinal cross section near the top of the UO_2-30 m/o CeO_2 pellet which had been heated for 504 hr. A portion of the central part of the same heated pellet is also shown for comparison. The difference in porosity and grain size is quite evident.

Table IV-10 indicates loss of material through evaporation from the heated pellets. Deposits of recondensed material were found on the outer periphery of the pellets; these whisker-like growths contained uranium, cerium, and small amounts of tungsten. X-ray examination of these materials gave the same type structure (fcc) as the original pellet, but the lattice parameters corresponded to a more uranium-rich solid solution. Coating of the pellets with a metallic film of tungsten may be required to reduce the evaporation rate. Evaluation of such a procedure is in progress.

Upon completion of these preliminary experiments, the equipment will be moved into a plutonium glovebox. Modification of an existing glovebox is under way to accommodate the thermal-gradient apparatus.

5. Sodium-Air Reactions (R. E. Wilson, T. Krolikowski, L. Leibowitz, J. Pavlik)

Safety analyses for sodium-cooled reactors require knowledge of the temperatures and pressures generated during sodium combustion in air. Combustion of both pools and sprays have to be considered. It was pointed out previously (ANL-7055, p. 208) that, regardless of the burning mechanism, the maximum pressures and temperatures are limited by the thermodynamic properties of the system. Theoretical calculations have shown (ANL-7225, p. 201) that the maximum pressure of 9.1 atm is generated at a sodium-to-oxygen ratio (g atoms Na/mole O_2) of 7, and that the maximum temperature of 1987°C is generated at a sodium-to-oxygen ratio of 5 in dry air. The peak values in air with 100% humidity at 25°C are predicted to be lower.

A major experimental effort is now being made to study the reaction of sodium sprays in air. Pressure generation rates, peak pressures and temperatures, and the nature and post-reaction behavior of the reaction products will be studied as functions of the initial conditions.

The apparatus consists of a pneumatically operated piston spray injector that will spray 15 g of molten sodium into a reaction chamber of known volume in a period of about 20 msec. The initial temperatures of the sodium, the water content of the air in the reaction chamber, and the sodium-to-oxygen ratio will be varied to determine their relative importance. A photograph of the apparatus is shown in Figure IV-39.

A glass chamber is being used to permit the evaluation of the sodium spray in the absence of reaction. The chamber will be filled with cold nitrogen to quench the sodium spray rapidly. This chamber will be replaced with a steel vessel fitted with view ports for periments made in air.

The spray injector head forms the bottom of the reaction chamber. Under the injector is located the pneumatic drive apparatus. The top flange contains the two pressure transducers (one of high- and one of low-speed response) and the entrance port for several thermocouples. The thermocouples will be located at several points inside the chamber in order to ascertain both the average temperature and the peak temperatures obtained. The transducers are protected from direct sodium impingement by a baffle attached to the top flange.

The sodium injector is shown in Figure IV-40. The lower piston is driven by nitrogen introduced through a large orifice solenoid valve from a ballast tank. This piston pushes the upper piston to drive the molten sodium upward into the reaction chamber through a discharge disc containing suitable orifices. Different orifice sizes and geometries are obtainable by changing the discharge disc.

Loading of the sodium injector is done in a helium-filled glovebox. The injector is assembled with both pistons in the lowest position and the assembly heated to a temperature above the melting point of the sodium. Molten sodium is poured in, and the assembly sealed by means of a copper gasket and a copper rupture disc. The assembly is then cooled and attached to the reaction chamber. At this point, the injector assembly is reheated to the desired initial conditions. The chamber is filled with the desired atmosphere and the sodium injected. After the reaction is over, the residue may be analyzed.

Preliminary tests of the injector system using water as the driven fluid have been made. Figure IV-41 shows a typical spray pattern obtained from a circular pattern of 0.030-in. orifices.

Errata

In ANL-7225, p. 172, Eq. 17 should read:

$$D = 4.125 \times 10^{-5}\, T_f^{1.75}/P$$

Also on p. 172, in column 2, paragraph 1, sentence 4 should read: The calculated average rates at 1 and 10 atmospheres for $r = 0.018$ cm are, respectively, 3.5×10^{-5} and 3.9×10^{-5} moles H_2O/sec.

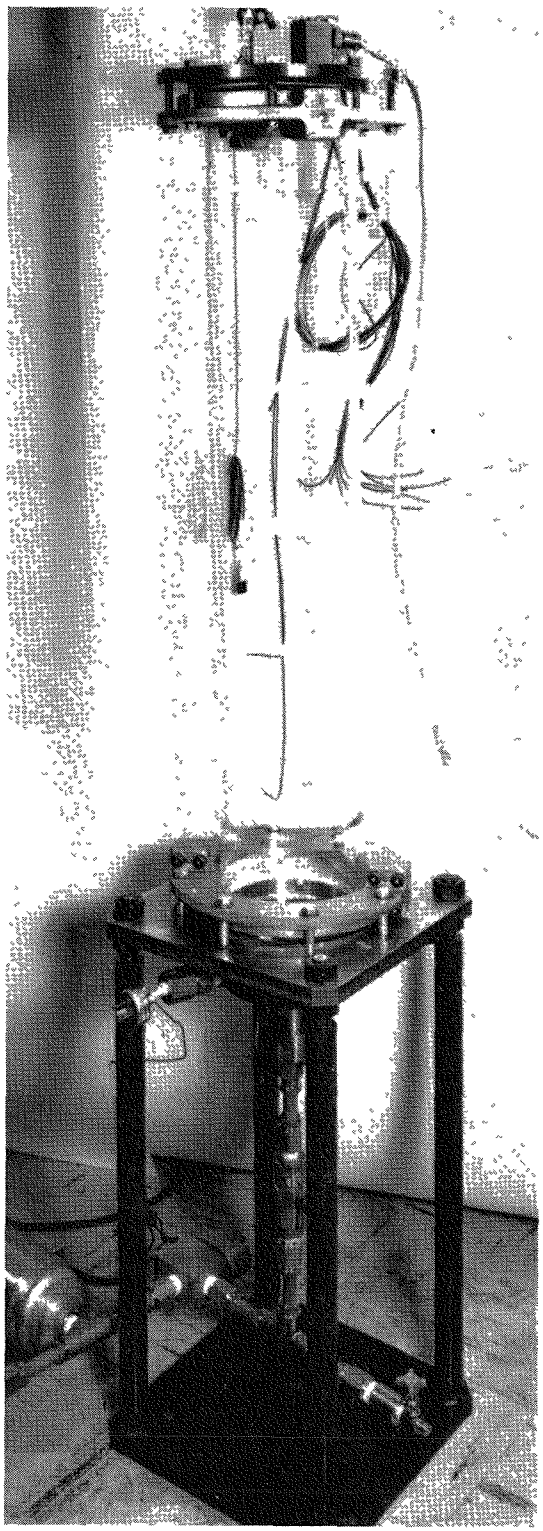

308-307

FIG. IV-39. Sodium-Air Reaction Apparatus.

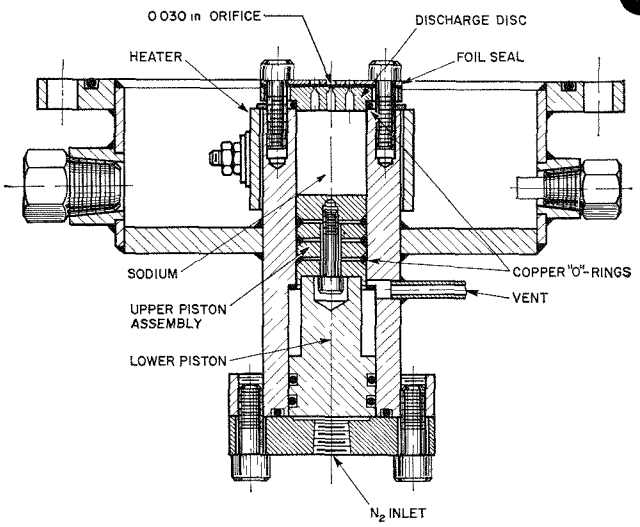

308-550

FIG. IV-40. Cross Section of Sodium Spray Injector for Sodium-Air Experiments.

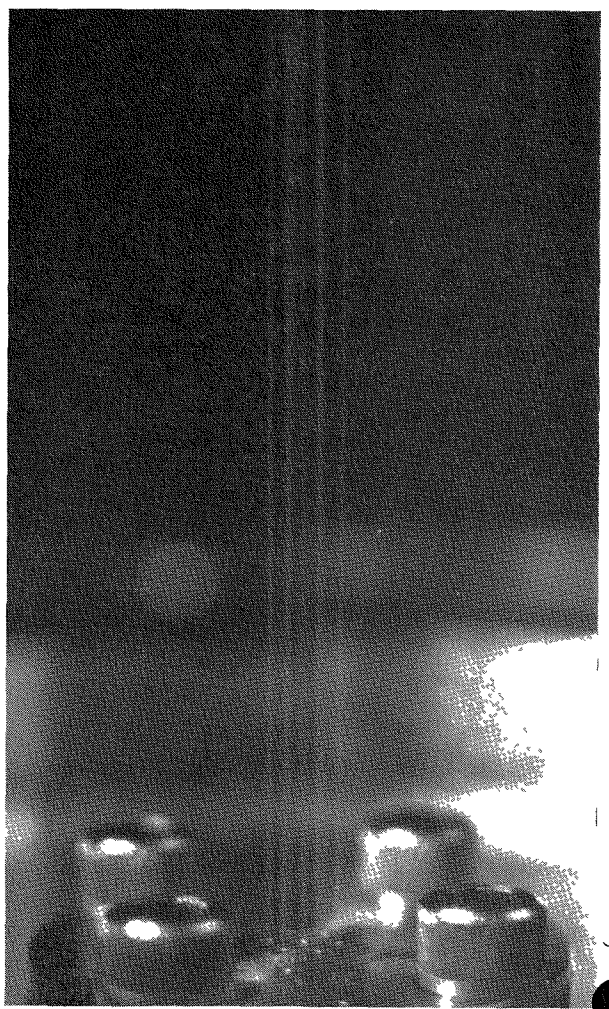

308-557

FIG. IV-41. Spray Pattern from Sodium Spray Injector Using Water as a Test Fluid. (0.030-in. orifices.)

V

Energy Conversion[1]

(E. J. Cairns, A. D. Tevebaugh, J. D. Bingle)

Work is continuing on the development of regenerative electrochemical systems. In the strictest sense a thermally regenerative electrochemical system is one in which thermal energy (heat) is converted into electrical energy by means of an electrochemical reaction; it is an energy system closed with respect to mass. In the systems studied in this laboratory a galvanic cell would function in the low temperature isothermal leg of a Carnot cycle to form a cell product and produce electrical energy. In the high temperature isothermal leg, the cell product would be decomposed into the cell reactants, which would be separated and returned to their respective electrode compartments of the cell. The two isothermal legs would be connected by an adiabatic countercurrent heat exchanger. In actual practice, imperfections in these cyclic operations would not allow the maximum Carnot efficiency to be achieved. The Carnot cycle efficiency limitation represents the price paid for converting random kinetic energy (thermal energy) into directed energy (electrical) and regardless of the method of regeneration, e.g., thermal or electrical, the Carnot cycle efficiency is the maximum theoretical efficiency of the cycle.

In a system using anode metal A and cathode metal C as reactants, the operation of the system can be represented by the equations:

Cell Reaction at T_1 :

$$A_{(\ell)} + C_{(\ell)} \rightarrow AC \text{ (dissolved in } C)_{(\ell)} \qquad (1)$$

Regenerator Reaction at T_2 :

$$AC \text{ (dissolved in } C)_{(\ell)} \rightarrow A_{(g)} + C_{(\ell)} \qquad (2)$$

where $T_2 > T_1$. Reaction 1 is carried out electrochemically as follows:

Anode Reaction:

$$A_{(\ell)} \rightarrow A^+ + e^- \qquad (3)$$

Cathode Reaction:

$$A^+ + C + e^- \rightarrow AC \text{ (dissolved in } C)_{(\ell)} \qquad (4)$$

The electrolyte is usually a fused salt containing A^+ ions in order to support high rates of electrochemical reaction at both electrodes.

Two types of cells are being studied in this laboratory: (1) the lithium hydride cell and (2) bimetallic cells. The hydride cell consists of an anode of liquid lithium metal, an electrolyte of molten lithium halides, and a hydrogen gas cathode. The cell oxidizes lithium metal to lithium ions at the anode and reduces hydrogen gas to hydride ions at the cathode to form the cell product lithium hydride. The bimetallic cells have two liquid metal electrodes in contact with a molten salt electrolyte. The cell reaction is the oxidation of the anode metal to produce metal ions in the electrolyte, while at the cathode the metal ions in the electrolyte are reduced to form a cathode alloy. High cell voltages are obtained by selecting anode and cathode metals which interact strongly, but not so strongly that regeneration is difficult.

The conversion of heat into electrical energy by means of thermally regenerative galvanic cells utilizes a method which relies on no moving parts such as rotating machinery. It is expected that, with proper design, realistic overall thermal efficiencies of 12 to 20% can be obtained in a practical, engineered system with the lithium hydride cell and with selected bimetallic cells.

In addition to serving in an energy conversion capacity, some bimetallic cells are well suited to the purpose of energy storage (as high-rate secondary cells). These secondary cells could accept electrical energy from a nuclear reactor energy depot (being considered by the military services) at a high rate, enhancing the usefulness of the energy depot concept. Other potential applications for high-rate secondary bimetallic cells are as pulse power sources for fusion research, sonar, communications, and military vehicle propulsion power, when used in combination with fuel cells.

The overall efficiency of thermally regenerative gal-

[1] A summary of this section is given on pages 14 to 15.

vanic cells is limited by the Carnot cycle efficiency, which should be maximized within the limits set by technology. This means that the highest practical regenerator temperature should be used, together with the lowest achievable cell operating temperature. Previously, there was the hope that ferrous alloys would be suitable for the construction of relatively low-temperature regenerators (for the systems sodium-bismuth and sodium-lead), but since corrosion experiments have shown that only refractory metals are suitable, emphasis has shifted toward systems compatible with high temperature regeneration (above 1000°C) where refractory metals can still be used. Such a system is lithium-tin, with a lithium halide electrolyte.

A. LITHIUM HYDRIDE CELL

The lithium hydride system is in principle one of the simplest thermally regenerative systems. The separation of hydrogen from the liquid phase takes place spontaneously, allowing a clean separation of phases. There is, however, an appreciable vapor pressure of the fused halides under the conditions of regeneration, causing some concern over the long-term gas phase transport of electrolyte to cooler parts of the system. This problem might be minimized by appropriate use of hydrogen-permeable metal diaphragms of vanadium, although this solution of the problem would decrease the efficiency by a few percent.

The cell emf is largest at the lower end of the range of operating temperatures, but the minimum temperature of operation will probably be determined by the hydrogen transport properties of the diaphragm-type anode (currently made of vanadium), and by the freezing point of the electrolyte. The selection of suitable low-melting electrolytes for the lithium hydride cell is guided by phase-diagram studies of candidate systems.

1. Electrolyte Studies

a. PHASE DIAGRAMS AND THERMODYNAMICS

(C. E. Johnson, E. J. Hathaway)

Thermal analysis techniques have been used to define the liquidus-solidus equilibrium temperatures for the LiH-LiCl-LiI ternary system and the component binary systems. The ternary system is of interest because of its potential application as the electrolyte in the lithium hydride cell. Details of the experimental techniques and description of the apparatus have appeared elsewhere.[2]

All experiments were run under a hydrogen pressure of 1 atm. Reagent grade lithium chloride and lithium iodide were obtained from Mallinkrodt Chemical Co. The lithium chloride was purified with chlorine gas using the method of Maricle and Hume.[3] The lithium iodide was purified using a modification of the method of Laitinen et al[4] in which the anhydrous halogen acid was used to remove the last traces of water from the molten salt. The melting points of the purified salts were 606.8°C and 467.9°C, respectively. Lithium hydride was prepared by contacting high purity liquid lithium metal with purified hydrogen at 750°C. The lithium hydride melting point was 686.4°C. Temperatures were measured with Pt/Pt 10% Rh thermocouples which had been calibrated against the melting points of N.B.S. pure Zn (m.p. 419.5°C) and N.B.S. pure Al (m.p. 660.0°C).

The liquidus temperature-composition data measured for the LiH-LiCl, LiH-LiI, and LiCl-LiI binary systems are given in Figure V-1. Each of these systems is a simple eutectic with no apparent indication of the formation of solid solutions. The LiH-LiCl binary has a eutectic at 34.0 m/o LiH that melts at 495.6°C; the LiH-LiI binary has a eutectic at 23.5 m/o LiH that melts at 390.8°C; and the LiCl-LiI binary has a eutectic at 66.0 m/o LiCl that melts at 368.0°C.

The diagram of the ternary crystallization surface (Figure V-2) consists of three areas: one each for pure lithium hydride, lithium chloride, and lithium iodide. Liquidus temperature data for five different LiCl:LiI mole ratios radiating from the lithium hydride corner of the ternary diagram were used to construct the surface; these are given as Series I through V of Table V-1. One other cross section was also investigated, that of LiH:LiCl at a mole ratio 34:66; these data are given as Series VI of Table V-1. Inspection of Figure V-2

[2] C. E. Johnson, S. E. Wood, and C. E. Crouthamel, Inorg. Chem. **3**, 1487 (1964).

[3] D. L. Maricle and D. N. Hume, J. Electrochem. Soc. **107**, 354 (1960).

[4] H. A. Laitinen, W. S. Ferguson, and R. A. Osteryoung, J. Electrochem. Soc. **104**, 516 (1957).

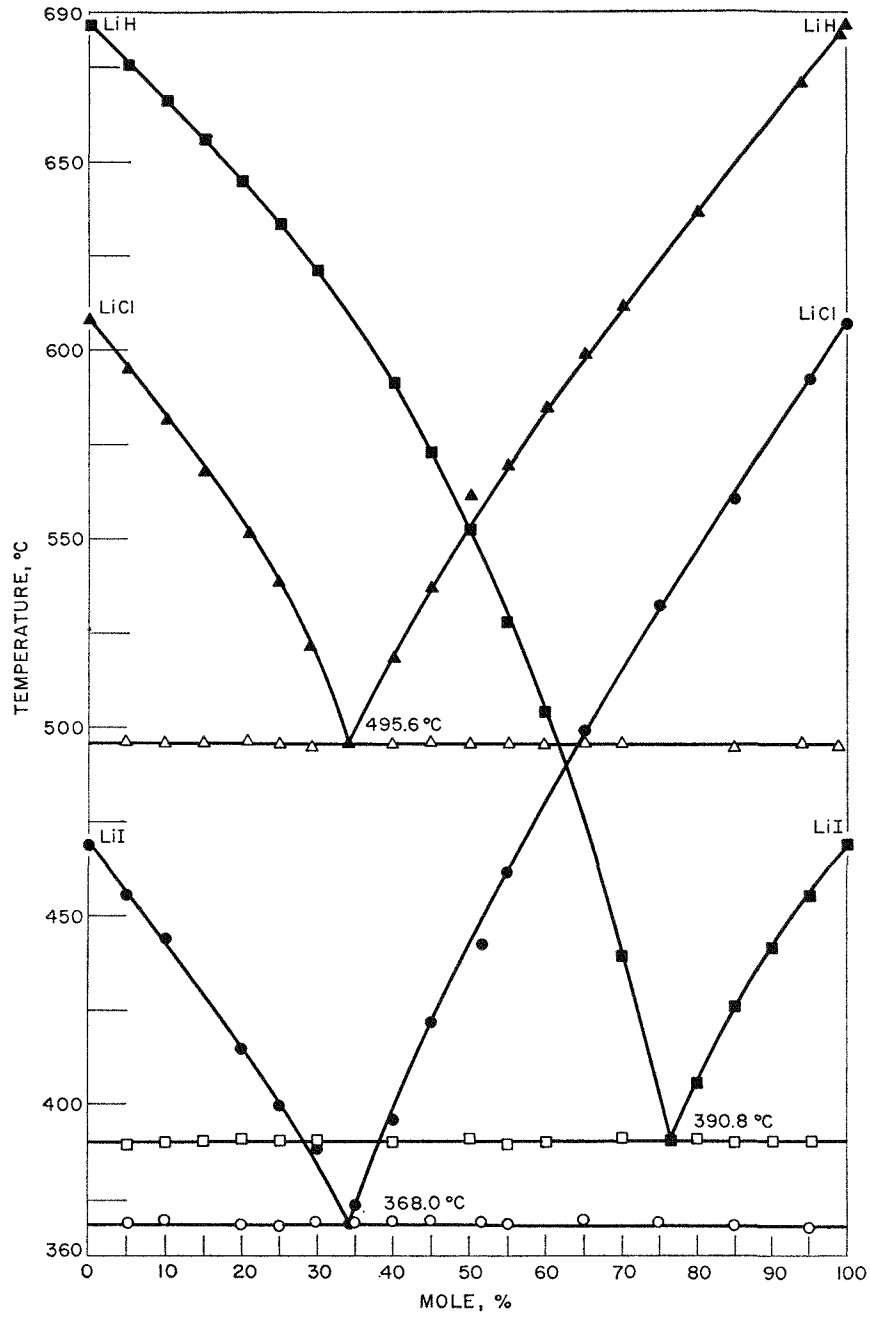

308-430

FIG. V-1. Binary Systems LiH-LiI, LiCl-LiH, LiCl-LiI. [under 1 atm of H_2(g).]

indicates that the system is eutectic with the eutectic composition being 14.3 m/o LiH, 27.7 m/o LiCl, 58.0 m/o LiI, melting at 332.9°C.

b. CONDUCTIVITY OF LITHIUM HYDRIDE-LITHIUM HALIDE MIXTURES (C. E. JOHNSON, J. PECK)

Thermodynamic analysis of the solid-liquid equilibrium data of the binary lithium hydride-lithium halide (Cl^-, Br^-, I^-) systems has indicated that these systems all show positive deviations from ideality (see ANL-7225, p. 216; also Ref. 5). A model which assumes pairwise association of lithium halide molecules was developed to account for these deviations. However, contrary to previous observations concerning the apparent low conductance of lithium hydride,[5] recent information[6] indicated that lithium hydride is highly ionic in nature. This necessitated further ex-

[5] C. E. Johnson, S. E. Wood, and C. E. Crouthamel, J. Chem. Phys. **44**, 884 (1966).

[6] Private communications from M. Bredig, Oak Ridge National Laboratory.

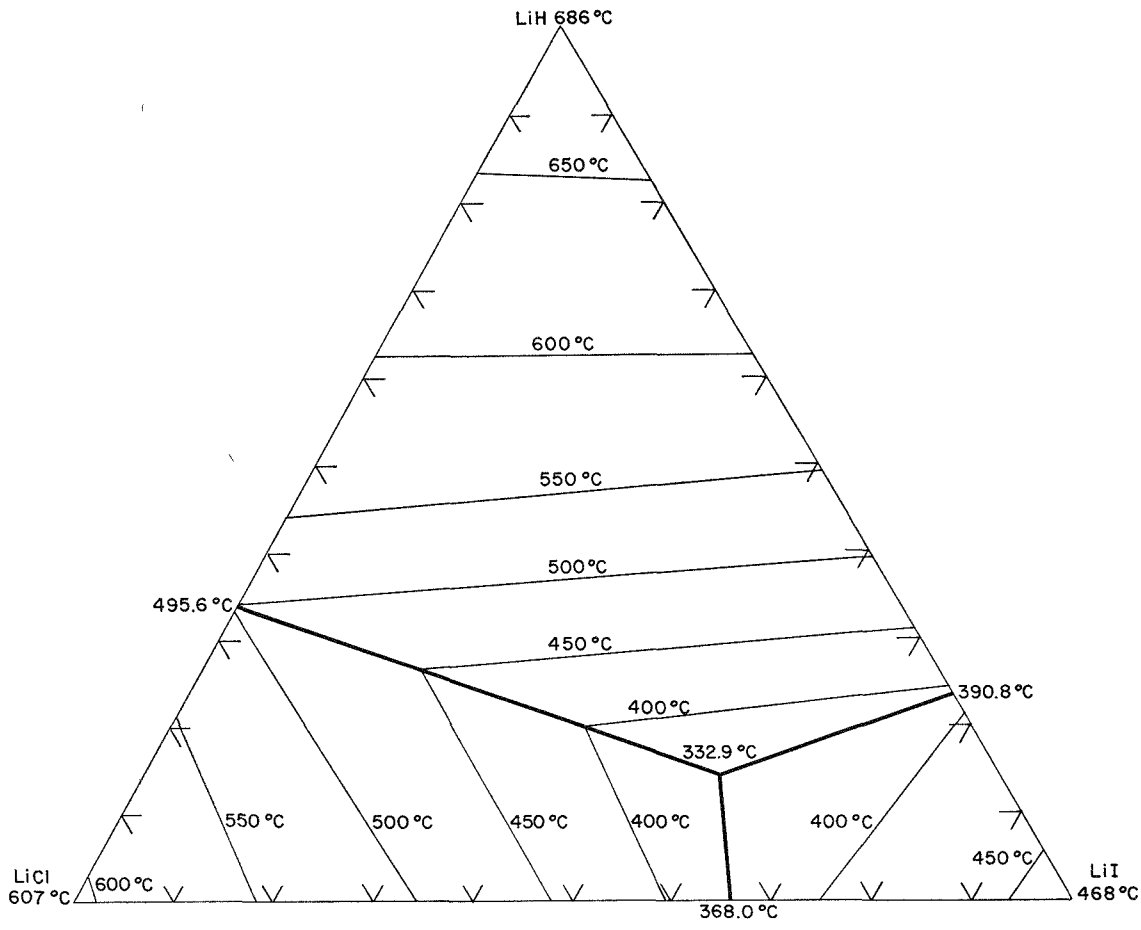

308-399

FIG. V-2. LiH-LiCl-LiI Ternary System.

TABLE V-1. CRYSTALLIZATION TEMPERATURES FOR LiH-LiCl-LiI

Series I Mole Ratio LiCl:LiI 1:9		Series II Mole Ratio LiCl:LiI 3:7		Series III Mole Ratio LiCl:LiI 1:1		Series IV Mole Ratio LiCl:LiI 7:3		Series V Mole Ratio LiCl:LiI 9:1		Series VI Mole Ratio LiH:LiCl 34:66	
m/o LiH	Temp (°C)	m/o LiH	Temp (°C)	m/o LiH	Temp (°C)	m/o LiH	Temp (°C)	m/o LiH	Temp (°C)	m/o LiI	Temp (°C)
0.0	442.0	0.0	385.0	0.0	442.0	0.0	515.5	0.0	567.0	0.0	495.6
10.0	411.1	5.0	367.4	5.0	430.2	10.0	488.7	10.0	545.8	20.0	452.3
20.0	379.6	10.0	352.7	10.0	420.4	20.0	464.6	20.0	524.3	30.0	428.1
25.0	415.9	15.0	339.5	15.0	412.9	30.0	457.9	30.0	485.2	40.0	403.2
30.0	442.7	20.0	367.0	20.1	404.0	35.0	495.2	40.0	518.4	50.0	363.0
35.0	475.5	25.0	419.1	25.1	433.5	40.0	515.7	50.0	559.4	54.7	343.2
45.0	532.1	30.0	451.9	35.0	489.0	50.0	552.8	60.0	587.8	56.0	340.1
55.0	564.4	40.0	509.7	45.0	534.5	60.0	488.5	70.0	612.5	58.0	332.7
65.0	608.7	50.0	556.8	55.0	578.5	70.0	614.2	75.0	625.6	65.0	360.8
75.0	632.5	60.0	590.5	65.0	609.4	80.0	637.2	85.0	647.3	77.1	400.2
85.0	653.5	70.0	620.1	75.0	629.5	89.4	660.4	89.6	657.3	90.0	440.8
100.	686.0	80.0	639.6	85.0	650.4	100.	686.0	100.	686.0	100.	468.0
		90.0	663.2	100.	686.0						
		100.	686.0								

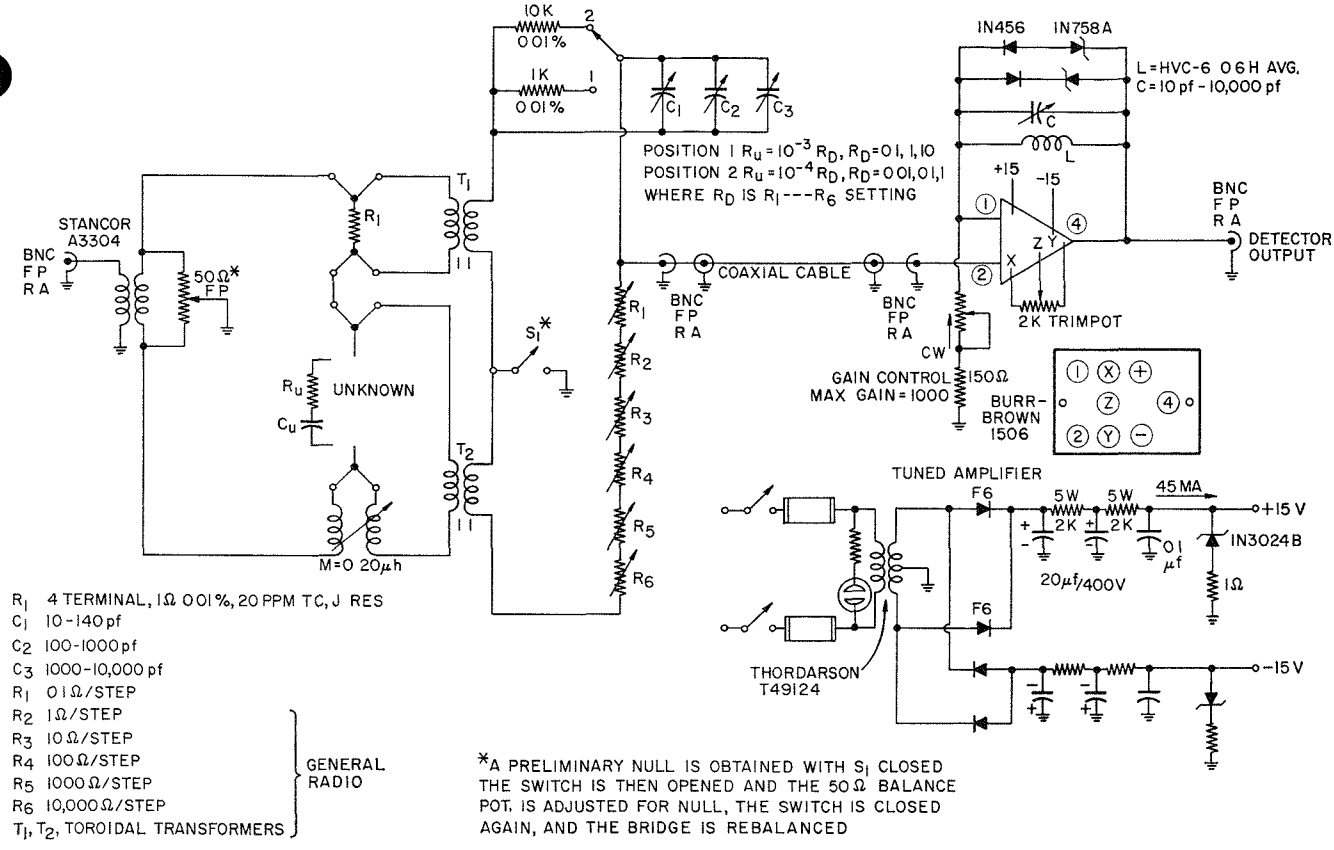

308-398

FIG. V-3. Low Resistance Bridge.

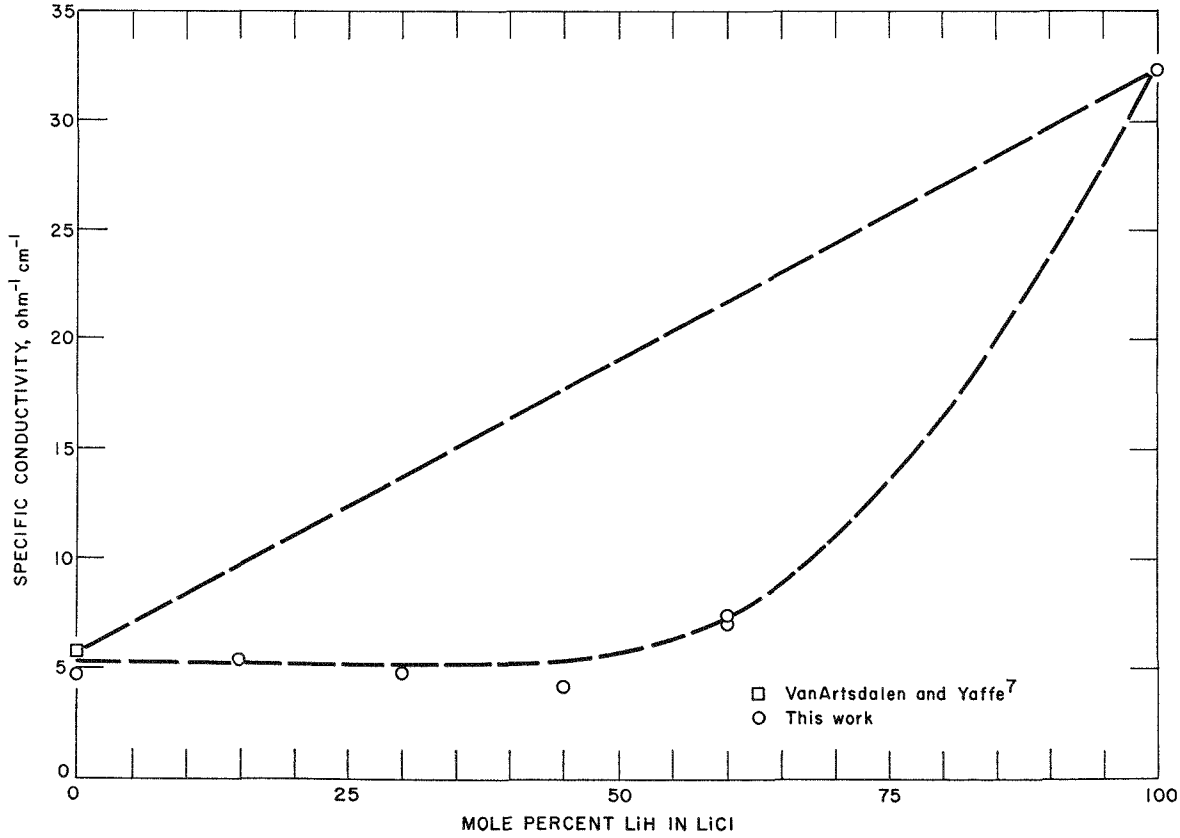

308-427

FIG. V-4. Specific Conductivity of LiH-LiCl System.

perimental work (reported below) which confirmed the high conductivity for lithium hydride. It is now postulated that the lithium halides are present in lithium hydride-lithium halide binary systems as associated ions of the type LiX_2^-. The present interpretation corresponds to that given previously but with the present emphasis in terms of the ionic nature of the melt.

If such associated ions are present in the electrolyte, a significant change in the normal character of the conductivity of the electrolyte might result. Therefore, electrical conductance measurements are being made in an attempt to determine the nature of the species present in these fused salt solutions.

Electrical conductance measurements have been made on selected compositions of the LiH-LiCl binary system, using the parallel-electrode conductivity cell. In this technique,[7] the resistance between two parallel molybdenum electrodes dipping into the melt is measured as a function of frequency and depth of immersion. Fused salts have very low resistivities; for example, the resistivity of LiCl at 650°C is 0.169 (ohm) (cm), whereas that of the best conducting aqueous system is >1 (ohm) (cm). Thus, a very sensitive bridge is needed for accurate measurement of the electrolyte resistance. Such a transformer bridge, built by J. Bobis of the ANL Electronics Division, has been incorporated into the apparatus. A schematic diagram of this bridge is given as Figure V-3.

In Figure V-4 the specific conductivity of the selected LiH-LiCl binary mixtures at 620°C is plotted as a function of composition. The value for pure lithium chloride at 5.77 ohm^{-1} cm^{-1} in Figure V-4 is taken from the data of Van Artsdalen and Yaffe.[8] The other value for pure lithium chloride (4.70 ohm^{-1} cm^{-1}) is our experimental result. Since a duplicate experiment has not been run on pure lithium chloride, it is not yet possible to comment on the discrepancy between these two values. The value for pure lithium hydride (32 ohm^{-1} cm^{-1}) was determined in this laboratory and checks reasonably well with extrapolations of the data given by Moers.[9]

Duplicate experiments were carried out for the 60 m/o LiH-LiCl mixture with fair agreement between runs: 7.10 and 7.35 ohm^{-1} cm^{-1}. As can be seen from Figure V-4, the deviations from ideality in the system are large and positive. This is consistent with the concept of the formation of $LiCl_2^-$ discussed above.

[7] H. R. Bronstein, A. S. Dworkin, and M. A. Bredig, J. Phys. Chem. **66,** 44 (1962).

[8] E. R. Van Artsdalen and I. S. Yaffe, J. Phys. Chem. **59,** 118 (1955).

[9] K. Moers, Z. Anorg. Allegem. Chem. **113,** 179 (1920).

2. Raman Investigation of the LiH-LiCl System (E. L. Gasner, T. F. Young)

Considerable uncertainty exists in our knowledge of the degree and nature of molecular association present in molten LiH-LiCl. The cryoscopic studies described earlier[2] strongly suggest the presence of polymer species, and this position is supported by the recent conductivity results reported above. Unfortunately, cryoscopic and conductivity measurements can provide no conclusive proof of molecular association. The discovery of vibrational Raman spectra would provide unambiguous proof of the existence of polymeric species and woud give information as to their nature and their concentration and temperature dependence. Therefore, a Raman spectral investigation of the LiH-LiCl system has been initiated.

The physical and chemical nature of the LiH-LiCl system poses difficulties and severe and exacting requirements upon all parts of the experimental apparatus: (1) the molten LiH-LiCl mixture reacts with all known window materials, (2) hydrogen atmosphere is required in order to prevent dissociation of the LiH, (3) the sample must be maintained at temperatures of 500 to 800°C, and (4) any polymeric species present (such as Li_2Cl_2, Li_2Cl^+, or $LiCl_2^-$) would probably have bonding which was more nearly ionic than covalent. Ionic bonding results in low specific Raman intensities.[10] Hence, the apparatus as as whole, while capable of handling molten LiH-LiCl, should have a sensitivity comparable to the sensitivity attainable with conventional samples.

All of the experimental difficulties described above appear to have been overcome. A versatile and highly sensitive laser-excited Raman spectrophotometer has been designed and constructed (see ANL-7225, pp. 219–221). A novel sample cell, the 45° mirror cell, has now been designed, constructed, and tested.

The design and operation of the 45° mirror cell is illustrated in Figure V-5. A metal sample cell is used to contain the melt. A slot, 1 in. long by ⅛ in. wide, in the lid of the sample cell is used to permit the entrance of the laser light and the exit of the Raman light. A stainless steel 45° mirror (4 in Figure V-5) immersed in the melt causes the laser beam to pass horizontally down the length of the melt. A large 45°

[10] G. Herzberg, *Molecular Spectra and Molecular Structure. I. Spectra of Diatomic Molecules*, D. Van Nostrand Co., Inc., Princeton, N.J., 1945, p. 88.

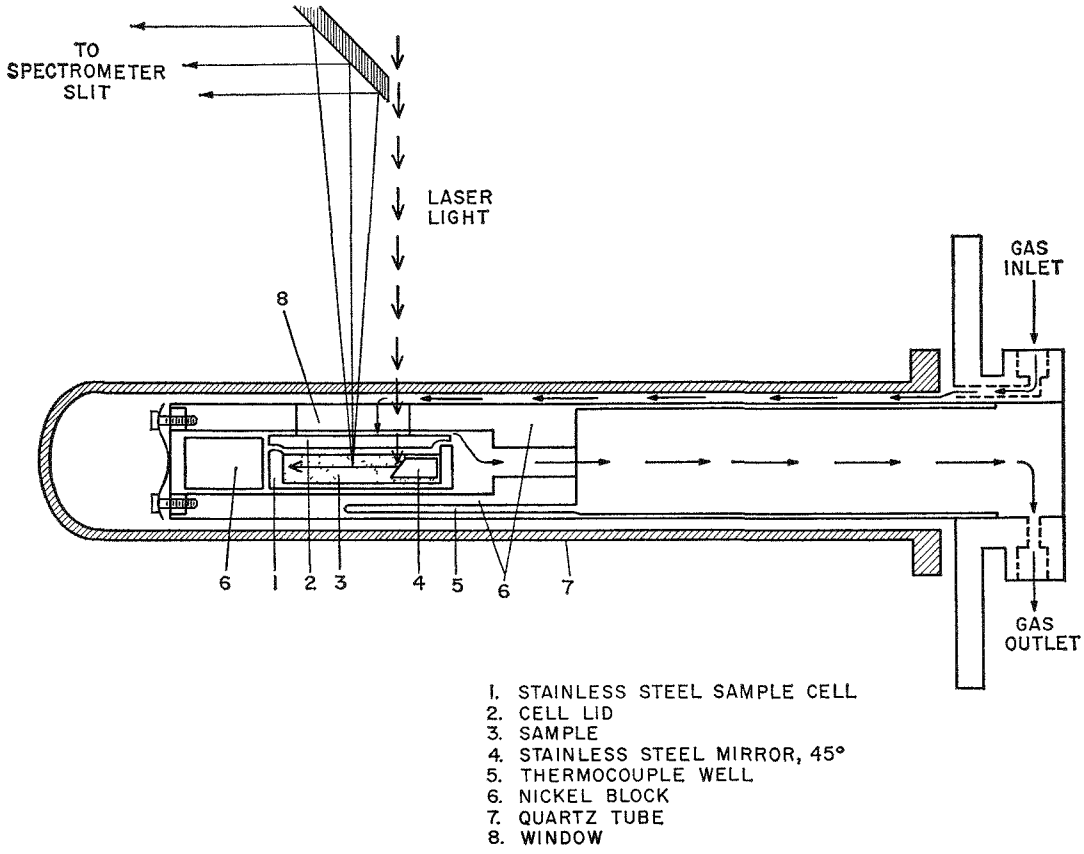

308-421

FIG. V-5. Sample Cell and Its Peripheral Apparatus.

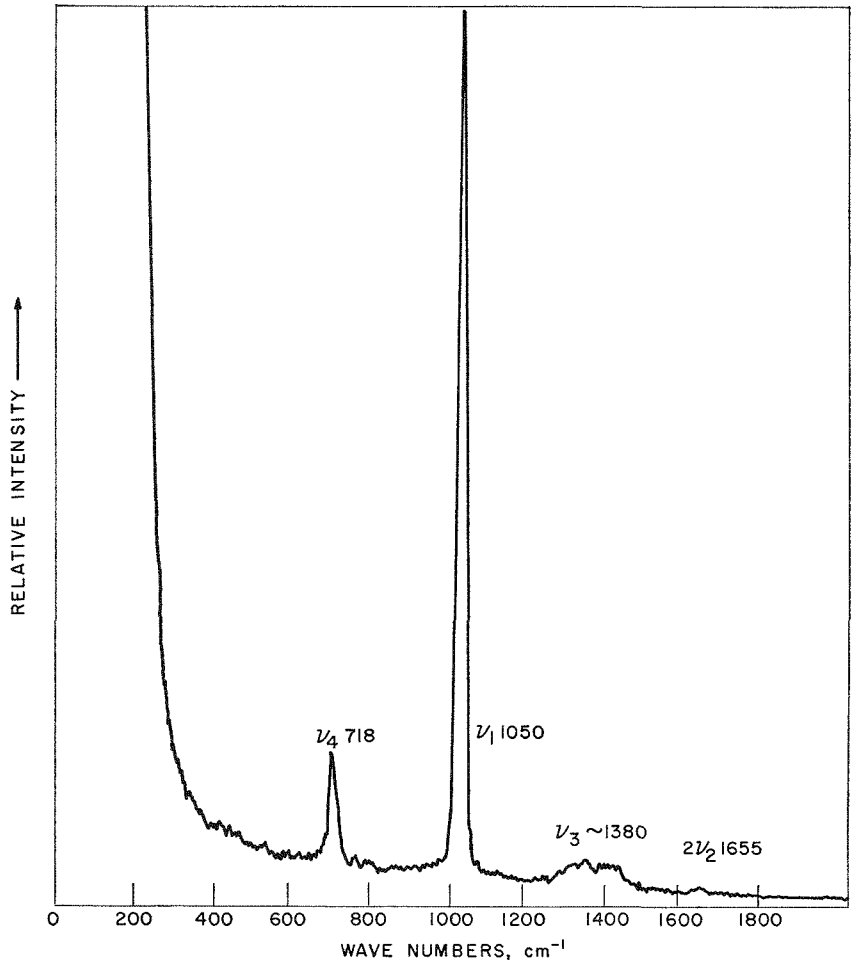

308-417

FIG. V-6. Raman Spectrum of Molten $NaNO_3$-KNO_3 Eutectic Mixture (250°C).

mirror outside the furnace allows the Raman light originating from the horizontal "rod" of illuminated sample to be focused on the vertical entrance slit of the spectrometer.

The sample cell (1 in Figure V-5) is surrounded by a nickel block (6). A small wedge-shaped hole in the nickel block provides for the necessary passage of light (8). The nickel block is enclosed in a quartz tube (7) in order to provide a controlled atmosphere around the sample. Passage of a continual stream of purified hydrogen, in the direction indicated by the arrows, tends to prevent corrosive vapors of the sample from reaching the quartz jacket. The entire sample region is surrounded by a tube furnace which can be operated at temperatures up to 1000°C.

The effectiveness of the 45° mirror cell has been tested at 250°C with a molten $NaNO_3$-KNO_3 eutectic mixture. An example of the spectrum attainable with the molten nitrate sample is given in Figure V-6. This spectrum was obtained using a very high scanning speed (325 cm^{-1}/min) and a short time constant (t.c. = RC = 1 sec). In spite of the use of such a short time constant, the line at ~1650 cm^{-1} is clearly visible above the background noise. Molten nitrates were investigated previously by Janz and James[11] using the conventional Hg arc excitation with the Hg arcs surrounding a transparent quartz sample cell. This favorable sample geometry would be expected to give an intense Raman signal. Janz and James, however, while able to detect the 1650 cm^{-1} line photographically, were unable to observe this line when using photoelectric detection. One may therefore conclude that the special Raman apparatus developed in this laboratory will allow the investigation of molten LiH-LiCl to be performed with at least the same sensitivity as can be achieved elsewhere with conventional samples.

Raman spectral investigations of molten LiH-LiCl mixtures are under way. Samples have been maintained at 500°C for many hours with no appreciable discoloration of the quartz sample envelope or of the 45° mirror immersed in the melt. Results are too sketchy to warrant comment at this time.

[11] G. J. Janz and D. W. James, J. Chem. Phys. **35**, 739 (1961)

B. BIMETALLIC CELLS

Bimetallic cells have the capability of operating at very high current densities with only minimal losses due to non-ohmic overvoltages. This means that very high energy-density bimetallic systems can operate at reasonable efficiencies, both as secondary cells and as thermally regenerative galvanic cells.

Three main areas of research are being actively pursued:

1. Emf studies of bimetallic systems. These studies yield emf data as a function of composition and temperature, from which thermodynamic properties of the bimetallic system can be calculated. The selection of promising systems for engineering development is made on the basis of these data.
2. The selection of low-melting electrolytes for bimetallic cells is made using the phase diagram data for appropriate binary and ternary halide systems. The phase diagrams and their thermodynamic interpretation guide other portions of the research activity, such as the Raman investigation.
3. Vapor pressures and vapor phase compositions are necessary for the evaluation of the suitability of bimetallic systems for use in the thermally regenerative mode of operation. One component (preferably the anode metal) should be much more volatile than the other, in order to obtain adequate separation in a simple, single stage regenerator. Thermodynamic analysis of the data indicates that perhaps intermetallic compounds are present in the liquid phase.

Two systems, sodium-bismuth and sodium-lead, have entered the engineering development phase, and are being studied both as thermally regenerative galvanic cells and as secondary cells. The engineering work will soon include cells with lithium anodes, for instance, lithium-tin. In preparation for this work, corrosion studies are under way at high temperatures where regenerators are expected to operate (1000–1300°C).

1. Emf Studies and Thermodynamics (M. S. Foster, G. H. McCloud)

Thermodynamic properties of binary alloys are readily determined from the open-circuit voltages of reversible concentration cells without transference, i.e., from cells of type 1:

A(liquid)/electrolyte containing

A ions/A dissolved in B

The physical state of the cathode is usually a liquid alloy of A in B, although alternatively it may also consist of two phases—a solid compound of A and B and a liquid B saturated with the compound. The electrolyte may be either liquid or solid. Any solubility of A in the electrolyte may result in mixed conduction in the electrolyte by the transport of electrons as well as A ions. The effect of mixed conduction is to lower the cell voltage below that which would otherwise exist. Erroneous values for calculated thermodynamic quantities would then result because the cell is no longer a reversible concentration cell without transference. The solubility of A in the electrolyte will also cause irreversible (non-electrochemical or non-current producing) transfer of A from the anode to the cathode, reducing the current efficiency of the cell.

a. BIMETALLIC CELLS WITH LITHIUM ANODES

In cells where the anode metal A is lithium and the electrolyte is a molten LiCl-LiF mixture of eutectic composition, the small solubilities of the metal in the salt are not sufficient to cause significant voltage losses due to electronic conduction. However, irreversible transfer does cause noticeable voltage losses which increase linearly with time. The voltage decrease due to irreversible transfer is minimized by using a reference electrode (bismuth saturated with solid Li_3Bi) which is not sensitive to the addition of lithium. The solubility of the solid compound (Li_3Bi) in the electrolyte does not lead to significant voltage losses with time. The results from several cells with lithium anodes have been discussed previously (ANL-7125, p. 215) and are considered to be of sufficient accuracy for the calculation of the thermodynamic properties of the lithium-containing alloys.

b. BIMETALLIC CELLS WITH SODIUM ANODES

In cells where the anode metal A is sodium and the electrolyte is a molten NaI-NaCl-NaF mixture of eutectic composition, the sodium has an appreciable solubility in the salt. Electronic conduction in the molten salt saturated with sodium is 10–20% of the total conductivity (see ANL-7225, p. 216). In addition, the solubility of sodium is large enough to lead to high mass transfer rates of sodium which preclude the observations of stable cell voltages. When attempts are made to use a reference electrode of bismuth saturated with solid Na_3Bi, the solubility of Na_3Bi in the electrolyte is sufficiently large to again result in appreciable mass transfer and rapidly falling cell potentials.

The transfer of sodium through the electrolyte is significantly reduced by the use of a solid electrolyte such as a single crystal of sodium chloride. The mobility of dissolved sodium atoms, *per se*, is considerably less in the crystal than in a liquid electrolyte. Further, any transfer due to the combined mobility of electrons and sodium ions will be reduced in the crystal because of a decreased mobility of the sodium ions.

However, voltage loss at open circuit depends on the relative electronic and ionic conduction and is not easily ascertained. In the molten electrolyte saturated with sodium, the mobilities of both the electrons and sodium ions (as well as that for neutral sodium atoms) are high. In the solid, both of these are greatly reduced, but the exact reduction for each is not known. If in the solid, as compared to the liquid, the mobility of the ion is reduced by a larger factor than the mobility of the electron, the voltage losses for cells with solid electrolytes would be larger than those for cells using a liquid electrolyte.

The extent of the voltage loss for cells with solid electrolyte has been estimated by operating a cell of type 2:

$$Na(\ell)/NaCl(s)/40\ a/o\ Na\ in\ Pb(\ell)$$

The potential of two such cells was observed at various temperatures. The results, along with the best (least-squares fit) curve for the data, are given in Figure V-7. As indicated on the figure, the standard deviation of the points from the curve is 4 mv.

The cell potential was also independently calculated from the activity of sodium in 40 a/o Na-Pb at 700°C as determined by A. K. Fischer of this Division from a measurement of the total vapor pressure of the alloy (see section V.B.3 of this report). In this calculation, it was assumed that the vapor phase consisted entirely of sodium monomer, and the known vapor pressure of pure liquid sodium was used in the calculation along with the equilibrium constant for dimerization of sodium in the vapor phase. Using the value obtained for the activity of sodium in the alloy, 0.0456, the potential of a type 2 cell was calculated to be 0.259 volt at 700°C (Figure V-8).

In Figure V-8, the curve representing the present data is compared with data of other investigators,[12-16]

[12] M. F. Lantratov, Russian J. Inorg. Chem. **4**, 927 (1959).

[13] K. Hauffe and A. L. Vierk, Z. Elektrochem. **53**, 151 (1949).

[14] B. Porter and M. Feinleib, J. Electrochem. Soc. **103**, 300 (1956).

[15] A. G. Morachevskii, J. Applied Chem. USSR **31**, 1252 (1958).

[16] A. F. Alabyshev and A. G. Morachevskii, Russian J. Inorg. Chem. **2**, 313 (1957).

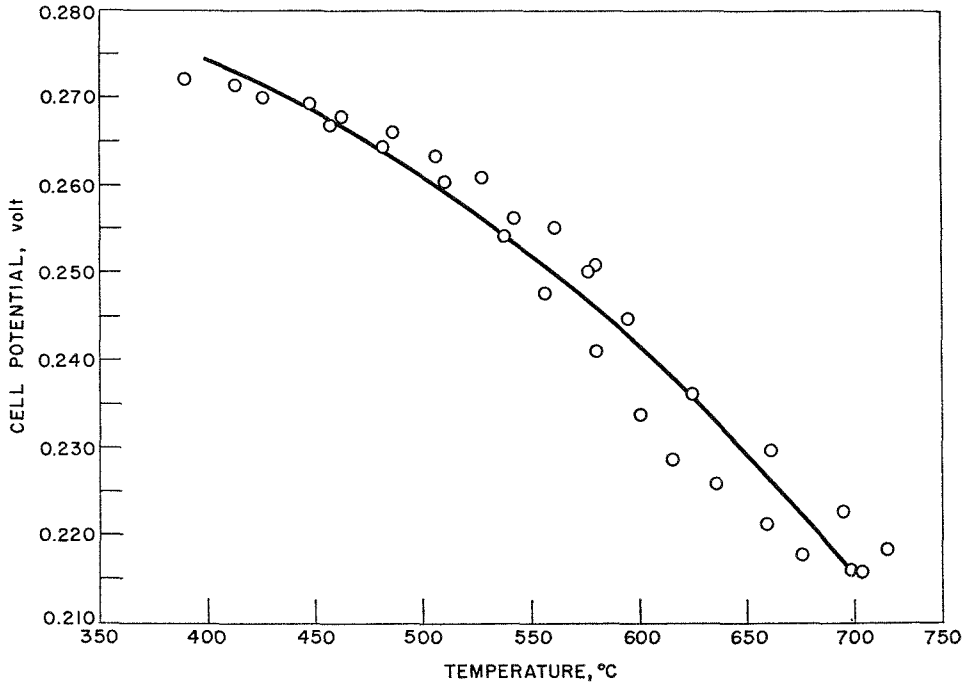

308-478

FIG. V-7. Observed Potentials for the Cell: Na(ℓ)/NaCl(s)/40 a/o Na in Pb(ℓ). (Standard deviation = 4 mv.)

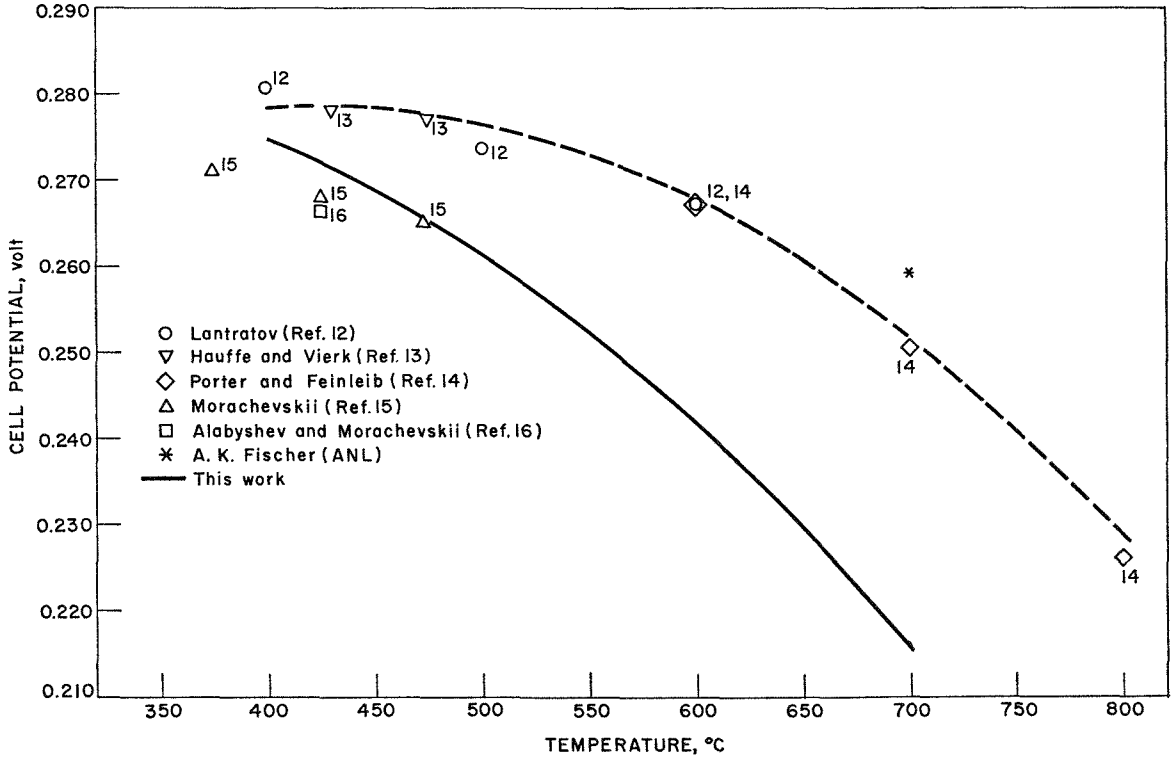

308-419

FIG. V-8. Potentials Reported for Sodium-Lead Cells. (Standard deviations = 4 mv.)

most of whom used solid glass electrolytes. The upper curve in the figure is the best (least-squares fit) curve for the data of Lantratov,[12] Hauffe and Vierk,[13] Porter and Feinleib,[14] and the datum point of Fischer. Some of the cell potentials reported in the literature[15, 1] are less than those observed in this laboratory and were not used in the least-squares curve in Figure V-8. These potentials were probably low because of

TABLE V-2. LITHIUM-SELENIUM CELL POTENTIALS AT 580°C

	First Cell				Second Cell	
Cathode Composition (a/o Li)	~0	5	10	15	~0	5
Observed Potential (volts)[a]	1.318	1.263	1.220	1.216	1.086	0.926
Calculated Li-Se Potential (volts)[b]	2.005	1.950	1.907	1.903	1.773	1.613
Li-Te Potential (volts)[c] (Ref. 17)	—	1.797	1.763	1.745	—	—

[a] Observed for type 4 cell:

$$Bi(\ell) \text{ saturated with } Li_3Bi(s)/LiCl\text{-}LiF(\ell)/Li \text{ in } Se(\ell)$$

[b] Calculated for type 5 cell:

$$Li(\ell)/LiCl\text{-}LiF(\ell)/Li \text{ in } Se(\ell)$$

[c] Calculated for type 3 cell:

$$Li(\ell)/LiCl\text{-}LiF(\ell)/Li \text{ in } Te(\ell)$$

the difficulty of making solid glass electrolytes which give identical potentials for the same cell. It has been estimated that if a dozen glass electrolytes were used, an identical number of potentials, ranging over 10–15 mv, could be expected.

Since each of the two curves in Figure V-8 has a standard deviation of 4 mv, it is difficult to ascribe a real difference between them over the temperature range 375 to 500°C. However, at 700°C the difference, which is the voltage loss at open circuit for cells of type 2, does appear significant. This difference will be verified by further work utilizing a different technique.

c. LITHIUM-SELENIUM AND LITHIUM-TELLURIUM SECONDARY CELLS

Certain applications for batteries require that power be delivered at a high rate for relatively short lengths of time, which are separated by longer periods of essentially no load. During the longer periods, the battery might be electrically recharged using some other source of energy, such as a thermoelectric generator, which by itself is not capable of delivering power at the required rate for the "on" cycle. For applications such as these, it is not necessary to restrict consideration to cells which are thermally regenerative since regeneration is accomplished electrically. Bimetallic cells in general are ideally suited for these applications since they have a low internal resistance and very little over-voltage from other than resistive sources. Therefore, it is profitable to consider bimetallic cells which would not normally be chosen for study as thermally regenerative cells, but which are expected to have high voltages and high current densities.

Previously, a type 3 lithium-tellurium cell:

$$Li(\ell)/LiCl\text{-}LiF(\ell)/Li \text{ in } Te(\ell)$$

was reported[17] to have an open circuit potential of no less than 1.67 volts where the cathode alloy was >61 a/o Te (up to saturation of tellurium with solid Li_2Te). It was expected that if selenium were substituted for tellurium, an even higher voltage would be obtained. Such a cell has been studied.[18]

In the lithium-selenium cell, neither tungsten nor Mo-30 w/o W alloy could be used as an electrode contact. Specimens of these materials disintegrated when held in contact with liquid selenium at 550°C for six days. Therefore, platinum electrical leads were used from the lithium-selenium alloy and tungsten electrical leads were used from the anode, which was liquid bismuth saturated with solid Li_3Bi. A correction was made for the thermoelectric potential developed because of the difference in electrical leads. The potential of the anode alloy had previously[19] been measured against pure lithium. Therefore, the potentials observed for the type 4 cell:

$$Bi(\ell) \text{ saturated with } Li_3Bi(s)/LiCl\text{-}LiF(\ell)/Li \text{ in } Se(\ell)$$

could be corrected to those expected for the type 5 cell:

$$Li(\ell)/LiCl\text{-}LiF(\ell)/Li \text{ in } Se(\ell)$$

Two cells of type 4 were operated at 580°C until failure. The first failed because of loss of selenium by volatilization and possible solubility[20] in the electrolyte. The second cell failed when the porous BeO crucible used to contain the lithium-selenium alloy cracked. The large discrepancy between the results of the two cells (see Table V-2) indicates that the second cell probably failed in part before any measurements were taken. The lithium content of the lithium-selenium alloy was fixed by passing a constant current between the electrodes (type 4 cell) for a given length

[17] M. S. Foster and C. C. Liu, J. Phys. Chem. **70**, 950 (1966).

[18] These studies were accomplished with the aid of J. J. Seidler, M. Husian, and J. L. Kerian, students at the ANL-AMU Summer Engineering Practice School.

[19] M. S. Foster, S. E. Wood, and C. E. Crouthamel, Inorg. Chem. **3**, 1428 (1964).

[20] A solubility of 0.0077 w/o was measured for selenium in molten CsCl at 650°C; if the solubility of selenium in molten LiCl-LiF is of a similar order of magnitude, loss of selenium by dissolution in the electrolyte will not be a significant factor.

of time and assuming 100% efficiency for the transfer.

Comparison of the calculated voltages for a type 5 lithium-selenium cell with a type 3 lithium-tellurium cell in Table V-2 indicates that the former will have ~0.2 volt higher potential at open circuit. However, in view of the difficulties in operating such a cell, it is anticipated that the lithium-tellurium cell will prove more useful in practice.

2. Electrolyte Studies (C. E. Johnson, E. J. Hathaway)

a. ELECTROLYTES FOR CELLS WITH SODIUM ANODES

Solid-liquid phase equilibria have been determined by thermal analysis techniques for the NaF-NaCl-NaI ternary system. This mixture has potential application as the electrolyte in a regenerative bimetallic cell employing sodium as the anode material.

The apparatus used in this work has been described in detail elsewhere.[2] Analytical grade sodium fluoride, sodium chloride, and sodium iodide obtained from Mallinckrodt Chemical Co. were used in the experimental program. The salts were filtered through a porous quartz frit prior to use. The melting points of the salts were 990.0, 801.0, and 659.3°C, respectively.

The liquidus temperature-composition data measured for the NaF-NaCl, NaF-NaI, and NaCl-NaI binary systems are given in Figure V-9. Each of these systems is a simple eutectic with no indication of solid solution. The NaF-NaCl binary has a eutectic at 33.0 m/o NaF that melts at 680.4°C; the NaF-NaI binary has a eutectic at 18.0 m/o NaF that melts at 597.1°C; and the NaCl-NaI binary has a eutectic at 38.5 m/o NaCl that melts at 572.9°C.

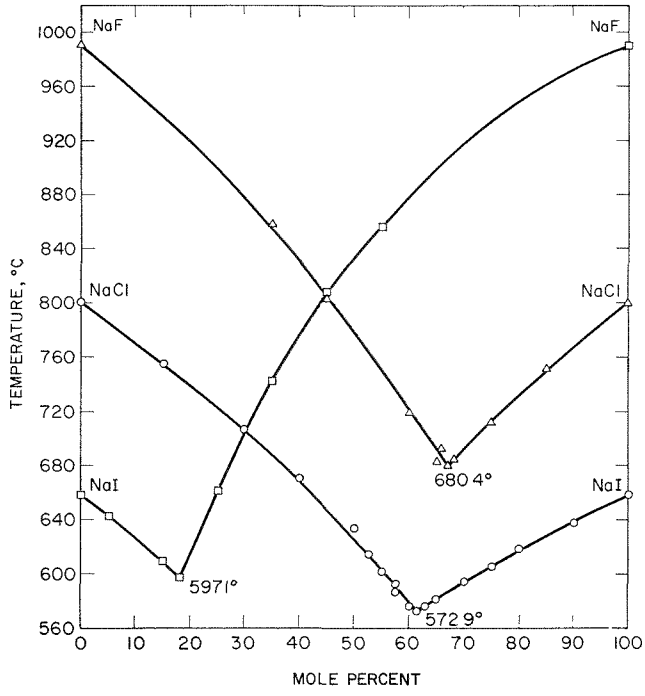

108-9691 T-1

Fig. V-9. Binary Systems NaF-NaCl, NaCl-NaI, NaI-NaF.

The diagram of the ternary crystallization surface (Figure V-10) consists of three areas: one each for pure sodium fluoride, sodium chloride, and sodium iodide. Liquidus temperature data for five different NaCl:NaI mole ratios radiating from the sodium fluoride corner of the ternary system were used to construct this surface; these are given as Series I through V of Table V-3. One other cross section, that of NaI:NaF at a mole ratio fo 85:15 was also investigated in order to completely describe the area of the minimum; these data are given as Series VI of Table V-3. The dashed lines of Figure V-10 is an extrapolation of the experimental data up to the melting point of pure sodium fluoride. Inspection of the data of Figure V-10 indicates that the system is eutectic with the eutectic composition being 15.2 m/o NaF, 31.6 m/o NaCl, 53.2 m/o NaI, melting at 529.4°C.

b. ELECTROLYTES FOR CELLS WITH LITHIUM ANODES

There are distinct advantages in the operation of a bimetallic cell at lower cell temperatures. Increases in Carnot cycle efficiency, lower corrosion (resulting in increased cell life times), and lower anode metal solubility in the electrolyte (reducing the possibility of inefficiencies caused by irreversible transfer of anode metal) all could be realized by operation at lower cell temperatures. Further, it has been considered advantageous to use electrolytes containing only a single cation. This limitation was imposed so that reactions between the active metal in the cell and the electrolyte could not take place. Such reactions would decrease the efficiency of thermally regenerated cells and would complicate both the collection and interpretation of data. Therefore, an extensive survey has been made of various binary and ternary lithium salt systems with the objective of seeking a low-melting electrolyte for a bimetallic cell using a lithium anode.

This evaluation was restricted to an examination of those lithium salt systems consisting of the following anions F^-, Cl^-, Br^-, I^-, OH^-, CO_3^{-2}, PO_4^{-3}.

The hydroxide salt is attractive because of its low melting point (450°C). However, in a cell where lithium metal is present, it is likely that either of the

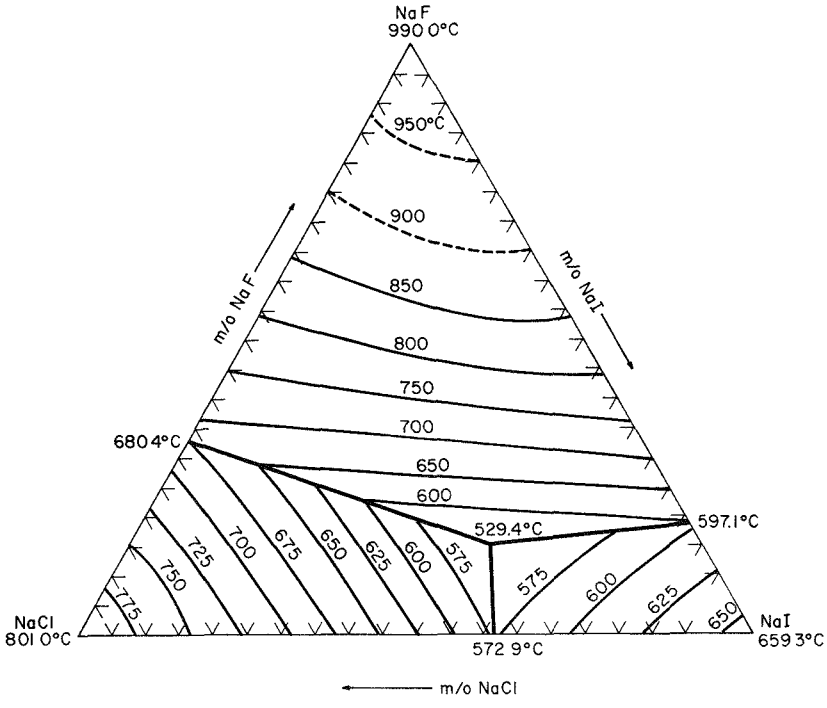

108-9690 T-1

FIG. V-10. NaCl-NaF-NaI Ternary System.

TABLE V-3. CRYSTALLIZATION TEMPERATURES FOR NaF-NaCl-NaI

Series I Mole Ratio NaCl:NaI 1:4		Series II Mole Ratio NaCl:NaI 2:3		Series III Mole Ratio NaCl:NaI 3:2		Series IV Mole Ratio NaCl:NaI 7:3		Series V Mole Ratio NaCl:NaI 4:1		Series VI Mole Ratio NaI:NaF 8.5:1.5	
m/o NaF	Temp (°C)	m/o NaF	Temp (°C)	m/o NaF	Temp (°C)	m/o NaF	Temp (°C)	m/o NaF	Temp (°C)	m/o NaCl	Temp (°C)
0.0	617.3	0.0	579.5	0.0	668.7	0.0	706.0	0.0	739.2	0.0	609.5
5.0	603.0	5.0	569.3	5.0	652.6	5.0	693.3	5.0	721.5	15.1	586.7
10.0	585.9	10.2	556.2	10.0	637.1	10.0	688.4	10.0	706.8	25.0	567.6
15.0	571.1	15.0	539.5	15.0	623.8	14.9	661.6	15.0	690.2	35.0	562.8
20.0	597.8	20.0	567.5	20.0	608.4	20.0	645.2	19.9	673.4	45.0	604.0
25.0	655.5	25.0	634.2	25.0	633.0	24.9	626.7	25.0	656.7	55.0	646.9
30.0	707.9	25.0	642.2	30.1	669.6	30.0	663.7	30.0	665.4	65.0	683.2
35.0	735.4	30.0	688.0	34.9	710.3	35.0	711.0	35.0	697.0	75.0	720.1
40.0	767.5	35.0	725.7	40.0	751.7	40.0	738.5	40.0	724.5	100.0	801.0
45.0	803.4	40.0	761.5	45.0	778.5	45.0	771.7	45.0	763.2		
50.0	835.5	45.0	793.5	50.0	805.6	50.0	803.6	50.0	803.2		
55.0	848.4	50.0	821.5	55.0	835.5	55.0	828.3	55.0	820.0		
100.0	990.0	55.0	843.8	60.0	855.2	60.0	852.8	60.0	844.3		
		100.0	990.0	100.0	990.0	100.0	990.0	100.0	990.0		

following reactions could take place, bringing about gross changes in the electrolyte characteristics:

(1) $LiOH + 2Li \rightarrow$

$$Li_2O + LiH \quad \Delta F^o_{750} = -40 \text{ kcal/mole}$$

(2) $LiOH + Li \rightarrow$

$$Li_2O + \tfrac{1}{2}H_2 \quad \Delta F^o_{750} = -25 \text{ kcal/mole}$$

The lithium oxide melting point is approximately 1700°C, an undesirably high temperature.

Lithium carbonate may undergo the following reaction:

(3) $Li_2CO_3 + 2Li \rightarrow$

$$2Li_2O + CO \quad \Delta F^o_{750} = -35 \text{ kcal/mole}$$

Phosphate salts would appear to be compatible with the cell environment, but the melting point of

this salt appears to be considerably higher than the stated literature value of 837°C. Attempts to melt this salt have been unsuccessful up to temperatures of 1050°C.

Thus, only the halides have been given detailed consideration. Experiments are presently in progress to determine temperature-composition data which will define the liquidus-solidus equilibrium surface for the LiBr-LiI binary and the LiF-LiCl-LiI ternary systems.

3. Liquid-Vapor Equilibrium of Cathode Alloys

Problems involving liquid-vapor equilibria are intimately involved with the design of a thermally regenerated bimetallic galvanic cell. One such problem is the determination of the range of pressure under which a cell may operate successfully. Another problem is the selection of the cathode composition and the regeneration temperature which will provide the most favorable regeneration path. These matters have been treated generally and also specific answers have been given for the sodium-bismuth system in previous reports (ANL-7055, pp. 221–225, ANL-7125, pp. 220–226, and ANL-7225, pp. 218–219). One important point which may be recalled is that a pressure of at least 240 torr is needed to avoid depositing solid Na_3Bi in the regenerator of a sodium-bismuth cell.

In the present report, a thermodynamic analysis is given for the results for the sodium-bismuth system, together with the assembled data for the sodium-lead system.

TABLE V-4. Activities and Activity Coefficients for the Liquid Sodium-Bismuth System at 900°C (1173°K)

Atom Fraction Sodium (x_{Na})	Sodium Activity (a_{Na})	Sodium Activity Coefficient (γ_{Na})	Calculated Bismuth Activity Coefficient (γ_{Bi})
0.100	2.23×10^{-4}	2.23×10^{-3}	9.88×10^{-1}
0.200	1.11×10^{-3}	5.47×10^{-3}	9.29×10^{-1}
0.332	3.28×10^{-3}	9.76×10^{-3}	7.37×10^{-1}
0.400	6.44×10^{-3}	1.59×10^{-2}	6.22×10^{-1}
0.500	1.41×10^{-2}	2.82×10^{-2}	3.66×10^{-1}
0.600	2.65×10^{-2}	4.37×10^{-2}	1.96×10^{-1}
0.750	1.58×10^{-1}	2.11×10^{-1}	4.03×10^{-3}
0.775	5.48×10^{-1}	7.08×10^{-1}	9.97×10^{-5}
0.800	6.97×10^{-1}	8.73×10^{-1}	4.23×10^{-5}
0.900	8.63×10^{-1}	9.59×10^{-1}	2.33×10^{-5}

TABLE V-5. Excess Partial Molar Entropy at 1173°K of Sodium in the Liquid Sodium-Bismuth System

Atom Fraction Sodium (x_{Na})	$\Delta\bar{S}^E_{Na}$ (cal/mole)
0.50	−2.15
0.60	−5.61
0.75	−6.43
0.775	+2.70
0.80	+1.51
0.90	+0.45

a. THERMODYNAMICS OF THE SODIUM-BISMUTH SYSTEM (A. K. Fischer, S. A. Johnson, S. E. Wood)

The total pressure and transpiration techniques used to study the sodium-bismuth system have been described earlier (ANL-7055, pp. 221–223 and ANL-7125, pp. 221–222). Our reported data for total pressure and vapor densities in the sodium-bismuth system, derived using these techniques, have been used to calculate the activities and activity coefficients for sodium. A series of values for these quantities was obtained across the full composition range at a temperature of 1173°K. A graphical Gibbs-Duhem integration based on sodium yielded activity coefficients for bismuth. The measured activities and activity coefficients for sodium and the calculated activity coefficients for bismuth are shown in Table V-4.

Since the total pressure data were available as a function of temperature and since vapor from the sodium-rich liquids was essentially pure sodium, it was possible to calculate, from total pressure data on the sodium-rich liquids, values for the chemical potential of mixing for sodium ($\Delta\mu^M_{Na} = RT \ln a_{Na}$). These chemical potentials were fitted to a quadratic function of temperature with the aid of a computer. The derivatives of the resulting equations with respect to temperature were then used to calculate excess partial molar entropies of sodium for each composition at a temperature of 1173°K. These entropies are shown in Table V-5.

An interesting feature of Table V-5 is the large negative partial molar excess entropy at 0.75 atom fraction sodium. Such a negative excess entropy may be taken as indicative of short range order above the melting point of the system. When it occurs as it does here, at the stoichiometry of a compound existing in the solid phase, it becomes tempting to speculate on the possible persistence of the compound in the liquid state. Such a possibility has been rejected by some metals physicists in the past, although recently pieces of experimental evidence have appeared which tend to support the idea. For example, the results of nuclear magnetic resonance studies on the indium-bismuth system have been found

to be consistent with the existence of an intermetallic compound in the liquid state.[21] Some success in correlating activity data on the basis of a dissociated molecular liquid model has also been achieved by Schmahl and Sieben[22] for the Mg-Pb and Mg-Sb systems, and by Högfeldt[23] for the Tl-Hg, Tl-Pb, and Bi-Cd systems. For the sodium-bismuth system, we found that by assuming the existence of the compounds Na_3Bi and NaBi, the thermodynamic data could be correlated by means of a quasi-ideal solution treatment. Such a treatment assumes that the species of the solution, as distinguished from the components, behave ideally. In our case, four species are involved: Na, Bi, Na_3Bi, and NaBi.

The reason for taking Na and Bi as species is plain. The selection of Na_3Bi as a species is based on the experimental observations (1) that the excess chemical potentials for the two components change markedly in the composition region corresponding to Na_3Bi, and (2) that the partial molar excess entropy of sodium has a large negative value at this composition. Furthermore, the phase diagram shows the formation of Na_3Bi in the solid phase. The inclusion of NaBi as a species is supported by (1) the fact that the compound exists in the solid phase as shown by the phase diagram and (2) the need to introduce a 1:1 complex to make the $\Delta\mu^E$ curves from the quasi-ideal treatment consistent with the features of the experimentally determined curves, particularly in the limiting cases of pure components.

The activity coefficient of sodium, γ_{Na}, may be expressed in the quasi-ideal context by

$$\gamma_{Na} = \frac{1 + K_1(2x'_{Na} - x'^2_{Na}) + K_2(4x'^3_{Na} - x'^4_{Na})}{1 + K_1 + K_2(3x'^3_{Na} - 2x'^3_{Na})} = \frac{x'_{Bi}}{x_{Bi}}$$

The expression for the activity coefficient of bismuth is

$$\gamma_{Bi} = \frac{1 - x'_{Na}}{(1 - x_{Na})(1 + K_1x'_{Na} + K_2x'^3_{Na})} = \frac{x'_{Bi}}{x_{Bi}}$$

where

x'_i = mole fraction of the species indicated by the subscript

x_i = mole fraction of the component indicated by the subscript.

K_1 and K_2 are the equilibrium constants for the formation of the compounds NaBi and Na_3Bi, respectively:

$$Na + Bi \rightleftharpoons NaBi \qquad K_1 = \frac{x'_{NaBi}}{x'_{Na}x'_{Bi}}$$

$$3Na + Bi \rightleftharpoons Na_3Bi \qquad K_2 = \frac{x'_{Na_3Bi}}{x'^3_{Na}x'_{Bi}}$$

The values for these equilibrium constants are related to the limiting values of the activity coefficients as the composition approaches the pure components. Thus, γ_{Na} reduces to $1/(1 + K_1)$ in the limit of $x'_{Na} = 0$ and γ_{Bi} reduces to $1/(1 + K_1 + K_2)$ when $x'_{Na} = 1$. From a preliminary plot of the experimental values for the activity coefficients, tentative values for K_1 and K_2 were obtained. These were refined by successive approximations so that, ultimately, the values $K_1 = 300$ and $K_2 = 2 \times 10^5$ were found to yield theoretical curves which agree well with the experimental data. These curves, plotted as $\Delta\mu^E/4.57T$ vs. x_{Na}, are shown in Figure V-11. The ability of this treatment to fit the data is not taken as proof that the postulated compounds exist in the liquid state, but rather as another example, in addition to those of References 22 and 23, of the ability of a simple model to correlate thermodynamic data.

b. LIQUID-VAPOR EQUILIBRIA IN THE SODIUM-LEAD SYSTEM (A. K. Fischer, S. A. Johnson)

The possibility of utilizing the sodium-lead system in a regenerative bimetallic emf cell has been proposed, and some cell work has already been done. As one aspect

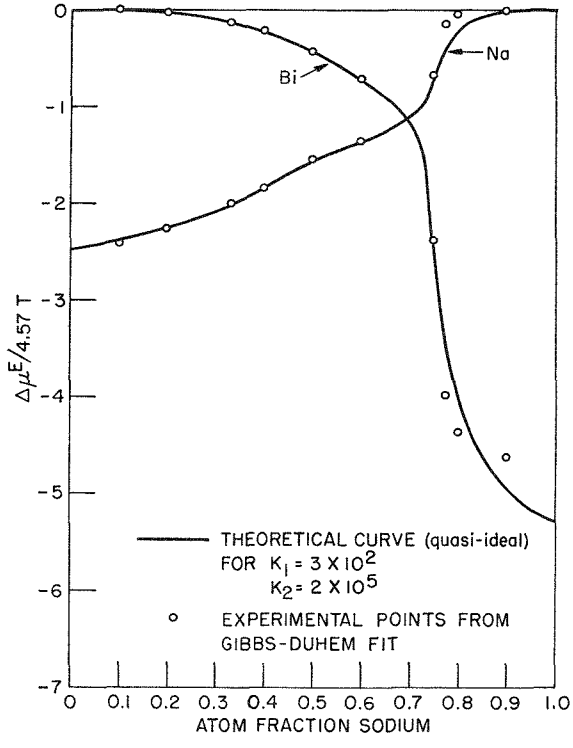

308-272

Fig. V-11. Excess Chemical Potentials of the Components in the Sodium-Bismuth System at 1173°K.

[21] E. F. W. Seymour and G. A. Styles, Proc. Phys. Soc. **87**, 473 (1966).

[22] N. G. Schmahl and P. Sieben, "Physical Chemistry of Metallic Solutions and Intermetallic Compounds", Volume 1, National Physics Laboratory Symposium No. 9, Her Majesty's Stationery Office, London, 1959 Paper 2K.

[23] E. Högfeldt, Rec. Trav. Chim. **75**, 790 (1956).

of the experimental effort necessary for this cell, the liquid-vapor equilibrium relationships in the sodium-lead system have been studied. The general procedure followed was the same as for the sodium-bismuth system: total vapor pressures were measured by the quasi-static method as a function of temperature for a series of compositions; also, the vapor composition and density were measured by transpiration experiments on three lead-rich liquids at a temperature close to 1123°K, the projected regeneration temperature.

The total pressures are presented in Table V-6 and the transpiration data in Table V-7. The equations derived from Table V-6 were solved for the total pressure at a temperature of 1126°K, the temperature of the transpiration experiments. The results constitute the column labelled $P_{1126°K}$ in Table V-6. These values were combined with the total pressures calculated from the transpiration experiments in order to construct the pressure-composition diagram for the sodium-lead system at 1126°K, Figure V-12. It is seen that the vapor over a probable cathode alloy in a sodium-lead regenerative cell contains an appreciable fraction of lead, so that regeneration of the sodium-lead cell is likely to require refluxing and fractionation.

TABLE V-6. Total Vapor Pressures for the Na-Pb System as Measured by Quasi-static Method

$$\log P = -A/T + B$$

Atom Fraction Sodium in Liquid (x_{Na})	Temperature Range of Measurements (°K)	A	B	Root Mean Square Error in log P	$P_{1126°K}$ (torr)
0.1517	1181–1271	6541.24	6.38436	0.01133	3.75 ± 0.09
0.3009	1066–1204	6621.37	7.10098	0.00875	16.6 ± 0.4
0.3994	948–1122	6656.69	7.46188	0.01078	35.5 ± 0.9
0.4992	958–1140	6348.62	7.60320	0.00378	92.2 ± 0.8
0.6028	1015–1146	5981.29	7.50208	0.00424	154.9 ± 1.5
0.6997	838–1147	5744.27	7.50703	0.00582	254.4 ± 3.3
0.7997	1063–1144	5423.23	7.38649	0.00174	371.6 ± 1.4
0.8998	753–1103	5310.81	7.42567	0.00693	511.8 ± 8.0

An examination of the data will be made to determine if the thermodynamic functions of this system may be treated in a manner similar to that used on the sodium-bismuth system.

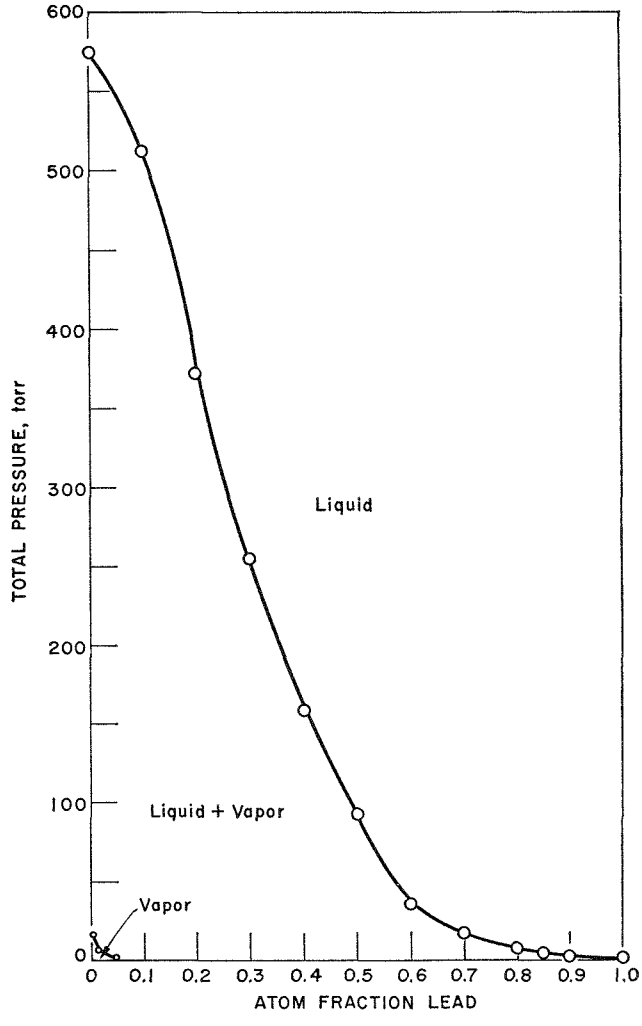

308-429

Fig. V-12. Pressure-Composition Diagram for the Na-Pb System at 853°C.

TABLE V-7. Transpiration Experiment Results on the Sodium-Lead System at 1126°K

Atom Fraction Sodium in Liquid (x_{Na})	Melt Temperature (°K)	Vapor Density		Partial Pressure (torr)			Total Pressure (torr)	Atom Fraction Sodium in Vapor (y_{Na})
		Sodium (g/ℓ)	Lead (g/ℓ)	P_{Na}	P_{N_2}	P_{Pb}		
0.300	1126.1 ± 0.7	(5.47 ± 0.21) × 10^{-3}	(2.33 ± 0.14) × 10^{-4}	16.4	0.11	0.066	16.6 ± 0.6[a]	0.996
0.200	1124.9 ± 1.3	(2.23 ± 0.07) × 10^{-3}	(3.06 ± 0.08) × 10^{-4}	6.76	0.018	0.102	6.88 ± 0.21	0.985
0.100	1125.9 ± 1.3	(7.35 ± 0.13) × 10^{-4}	(3.51 ± 0.21) × 10^{-4}	2.24	0.002	0.112	2.35 ± 0.15	0.950

[a] This value agrees well with the total pressure observed by the quasi-static method. In Table V-6, the total pressure for this composition at 1126°K is given as 16.6 ± 0.4 torr.

4. Laboratory-scale Bimetallic Cells (H. SHIMOTAKE, G. ROGERS)

a. SODIUM-BISMUTH CELL

An experimental sodium-bismuth cell without a thermal regenerator was built and placed in operation on December 9, 1964 (see ANL-7055, p. 226) and was kept in long-term operation as a secondary cell until the unit was shut down by an accidental short-circuit in the heating element after approximately 17 months of operation (see ANL-7225, p. 221). During operation, the cell temperature was kept between 535 and 650°C, with an average temperature of 550°C. The average open circuit voltage was 0.66 volt with 30 a/o sodium-bismuth cathode alloy; however, with pure bismuth cathode metal, an open circuit voltage of 1.22 volts was obtained. The cell was electrically discharged and recharged about once every two days. A current efficiency of approximately 87% was achieved. The cell itself, including the frozen electrolyte insulator-pressure seal, showed no sign of failure. Upon disassembly, inspection of the interior revealed surprisingly little corrosion, with only 50 μ dissolution of stainless steel from the cell housing. X-ray analysis indicated that there was no decomposition of the electrolyte salt mixture.

The cell has been cleaned, recharged with electrolyte and sodium-bismuth alloy, and will be put back into operation. This time, a thinner electrolyte layer will be used to minimize the internal resistance of the cell.

b. THE SODIUM-LEAD CELL APPARATUS

An experimental sodium-lead cell apparatus (see ANL-7125, pp. 228–229) with attached thermally operated regenerator, was built and operated intermittently for a total of approximately 150 hr. Experiments were terminated because of the development of linear fractures in the flanges. The fractures were caused by fatigue of the flange material, a stainless steel, due to repetitive heating-cooling cycles.

During operation of the regenerative cell apparatus, circulation of the cathode alloy became erratic. Because of this difficulty, a separate regenerator study was performed, which is described in the following section.

5. Regenerator Studies (H. SHIMOTAKE, G. ROGERS)

In a thermally regenerative bimetallic cell system, the circulation of liquid metal between the cell and the regenerator depends on thermal convection. During operation of the sodium-lead emf cell apparatus with attached thermal regenerator (apparatus described above), it was noticed in every run that after approximately 3 hr of continuous operation, the circulation rate of liquid metal descreased and finally stopped. Tilting, mechanical vibration, pressurizing, or depressurizing of the apparatus did not succeed in reinitiating circulation. However, when the apparatus was left for an hour under argon gas, circulation resumed.

Causes for stoppage of the circulation were sought and an experiment was conducted using a device identical to the one shown in Figure VI-13 on p. 227 of ANL-7055. It consists of a vertical cylindrical reservoir connected to a vertical regenerator by means of tubes forming a loop for the continuous recirculation of the alloy by thermal convection. The upper part of the regenerator is provided with a sodium vapor condenser. A tube that connects the condenser with the reservoir allows condensed sodium liquid to return to the reservoir.

The first set of data was taken with argon cover gas, which suppressed distillation of the sodium in the regenerator. After 24 hr of operation without stoppage of circulation, pressure was lowered to approximately 5 mm Hg for a second run. Circulation then stopped after 2 hr, 55 min. Tilting, pressurization, or rocking did not reinitiate circulation. However, when the apparatus was left under argon cover gas for approximately two hours, circulation resumed. The third run was made under vacuum. This run lasted for 3 hr 10 min, at which time the circulation stopped again. A series of radiographic photographs was taken during the experiment (using a portable ^{192}Ir source) to determine the liquid metal level and possible plugs in the circulation lines. The result indicated that under vacuum the liquid level in the regenerator section intermittently became considerably lower than expected. A corresponding increase of the liquid level in the reservoir was suspected. This intermittent fluctuation of the liquid level could be caused by (1) intermittent discharge of the sodium condensate in the return line to the reservoir, or (2) periodic violent boiling, i.e., "bumping" of the liquid metal in the regenerator section. A temporary halt of circulation caused by liquid level fluctuation results in depletion of the sodium content of the liquid metal in the regenerator section and increases the density of the liquid metal in this section, thus upsetting the necessary density gradient required to maintain the thermal convection.

Based on the above findings, modifications have been made in the regenerator. The changes include: (1) a

larger sodium condensate return line (from ¼ in. to ⅝ in. ID), (2) larger and slanted circulation lines (from ¼ in. to ⅜ in. ID), and (3) a higher hydrostatic head (from 2¼ in. to 8¼ in.). The modified unit was charged with 30 a/o sodium-lead alloy and was placed in operation with the still temperature at 800°C and the reservoir temperature at 550°C under a condenser pressure of approximately 5 mm Hg (absolute). Although some signs indicative of erratic circulation appeared during the first few days, continued degassing of the liquid metal improved the stability of the circulation. After approximately three days of operation, stable circulation and condenser pressure patterns were established. The unit was successfully operated for 935 hr without interruption, at which time the experiment was terminated. The present design is considered adequate for the operation of thermally regenerative sodium-lead cells.

6. Engineering Material Corrosion Studies (H. Shimotake, J. Kargol)

Candidate construction materials for thermally regenerative bimetallic emf cell systems are being evaluated with respect to corrosion by the liquid metals of interest. Since the highest temperature of the cell system at the regenerator exceeds 800°C for sodium-lead and sodium-tin systems and exceeds 1000°C for sodium-bismuth and lithium-tin systems, it is logical that corrosion studies are required for the development of a long-life bimetallic cell. Very little information on corrosion by heavy metals at temperatures above 800°C is available in the literature.

a. STATIC CORROSION TESTS

Static corrosion tests were conducted on various materials by immersing coupons of test materials in liquid metals. These coupons were usually cut from sheet stock of the material to be tested. The coupons and liquid metal were placed within a crucible fabricated from molybdenum-30 w/o tungsten, an alloy which is considered to be nearly inert to attack by bismuth, tin, and lead. A summary of all of the static tests results obtained at temperatures up to 1000°C was reported previously (ANL-7225, pp. 222–224).

Some additional static corrosion results were obtained at temperatures as high as 1300°C using a molybdenum-wound furnace. A capsule made of tantalum (the test material) containing molten tin and helium gas was kept at 1300°C in the furnace for a period of 150 hr. Metallographic examination of the capsule showed only slight dissolution, to the extent of 50 μ.

A second tantalum capsule containing molten 30 a/o lithium-tin was kept at 1300°C for 150 hr. This capsule showed similar attack. This capsule is still undergoing detailed metallographic examination.

b. DYNAMIC CORROSION TESTS

Dynamic corrosion tests have been conducted using thermal convection loops fabricated of selected test materials. The loops are constructed of ¼ in. pipe (0.54-in. OD and 0.364-in. ID) in the form of parallelograms about 10 in. high and 6 in. wide. Electric resistance heaters are used to maintain the four sections of each loop at different prescribed temperatures, setting up thermal convection circulation of the liquid metal within the loop.

The results of the previous dynamic corrosion tests conducted were reported in ANL-7225, pp. 224–225. These results indicated that neither stainless steel nor low carbon steel is suitable for use in a sodium-bismuth cell system at temperatures above 800°C with a temperature difference of more than 250°C between the cell and the regenerator. Because of the severe nature of the dynamic corrosion of the ferrous alloys by the liquid metals, special efforts were made to fabricate loops from some refractory metals. A loop (Loop 10) fabricated of work-hardened molybdenum-30 w/o tungsten tubing developed linear fractures after 2488 hr of exposure to liquid bismuth in an argon atmosphere with cold and hot leg temperatures of 700–900 and 1050°C, respectively. The fractures were caused by lack of annealing after the welding of loop joints had been performed. Since no chemical attack or corrosion was found between the liquid metal and the loop material, this material presents an encouraging picture.

A tantalum loop (Loop 16) protected from air oxidation by a type 316 stainless steel sheath tube, was constructed and charged with 30 a/o sodium-lead alloy. This loop was operated with a hot leg temperature of 1050°C and a cold leg temperature of 750°C for 932.5 hr, at which time a leak developed in the area where the stainless steel sheath was directly exposed to the liquid metal.

Still another tantalum loop (Loop 20) containing 30 a/o lithium-tin alloy has been in operation for 110 hr in an argon-filled enclosure. The cold and hot leg temperatures are 950 and 1050°C, respectively. No external signs of corrosion have appeared thus far.

Although information obtained so far on the corrosion resistance of refractory metals by heavy metals is limited, the outlook for the refractory metals is encouraging. Adequate choice of materials based on the corrosion data supported by proper design and advanced fabrication methods should solve the construction materials problem.

VI

Nuclear Constants[1]

(D. C. Stupegia, A. D. Tevebaugh, J. D. Bingle)

The fast neutron program is directed toward the measurement of neutron cross sections which are needed in calculations of the breeding gain of fast reactors, and toward the use of these data to test theories of nuclear reactions. Current progress is reported for (1) neutron capture cross sections of reactor, structural, and control materials, and (2) capture-to-fission cross-section ratios of fissile and fertile species.

[1] A summary of this section is given on page 15.

A. RADIATIVE CAPTURE (D. C. Stupegia, M. Schmidt, A. A. Madson)

Neutron radiative capture cross sections are being measured as a function of neutron energy between 5 keV and 3 MeV. The capture reaction is one which absorbs neutrons unproductively in reactors; therefore capture cross sections are needed in order to evaluate the behavior of various materials in a reactor.

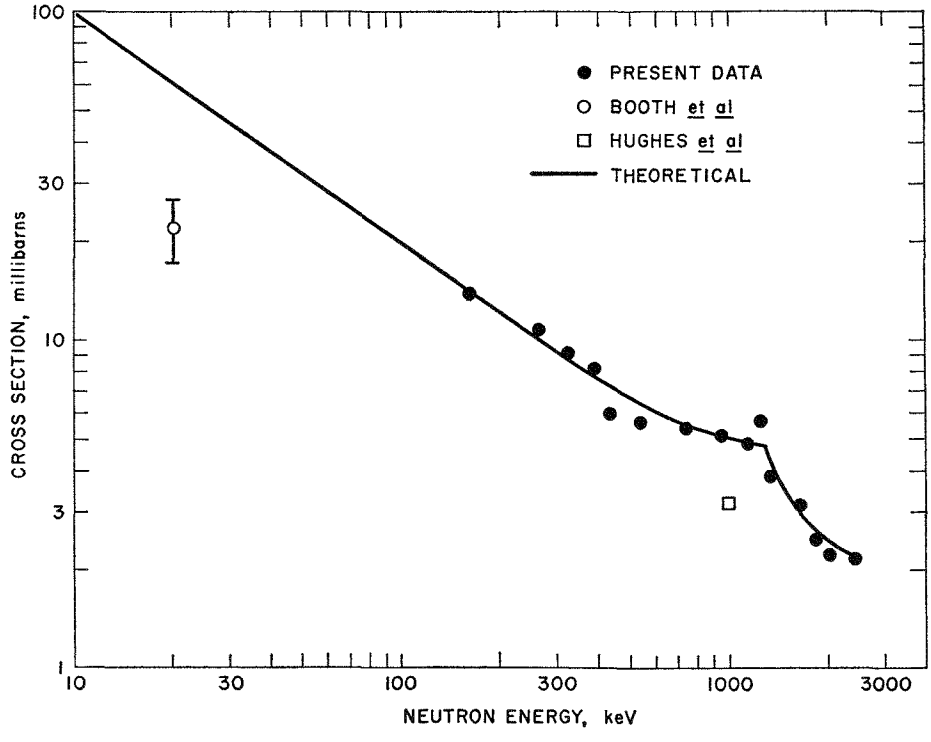

308-410

Fig. VI-1. Radiative Capture Cross Section of Potassium-41.

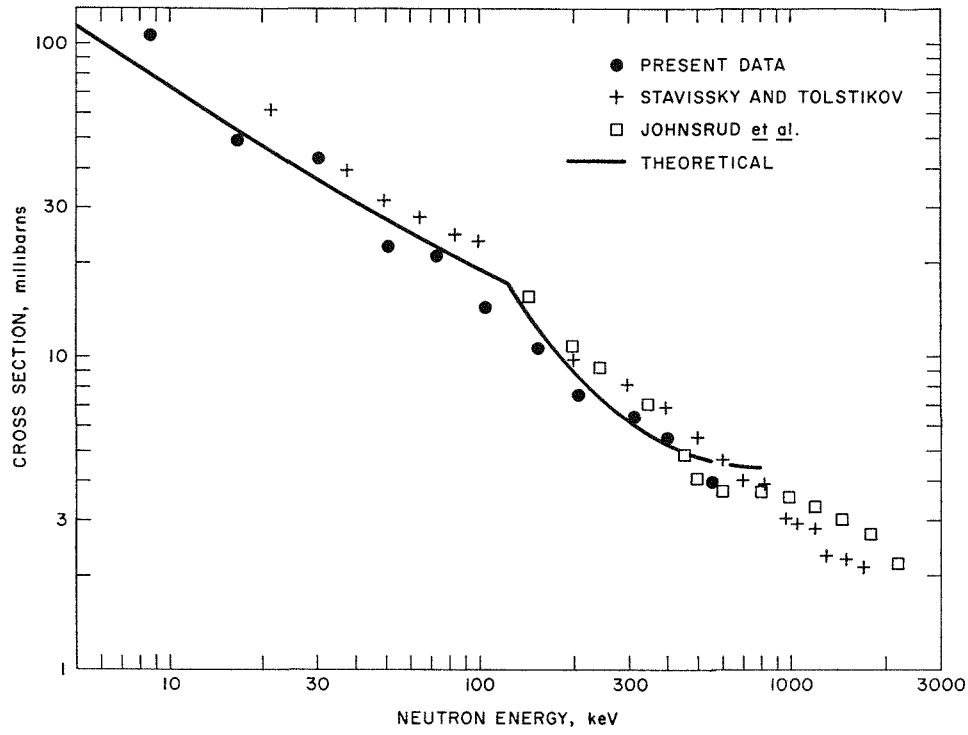

308-415

FIG. VI-2. Radiative Capture Cross Section of Manganese-55.

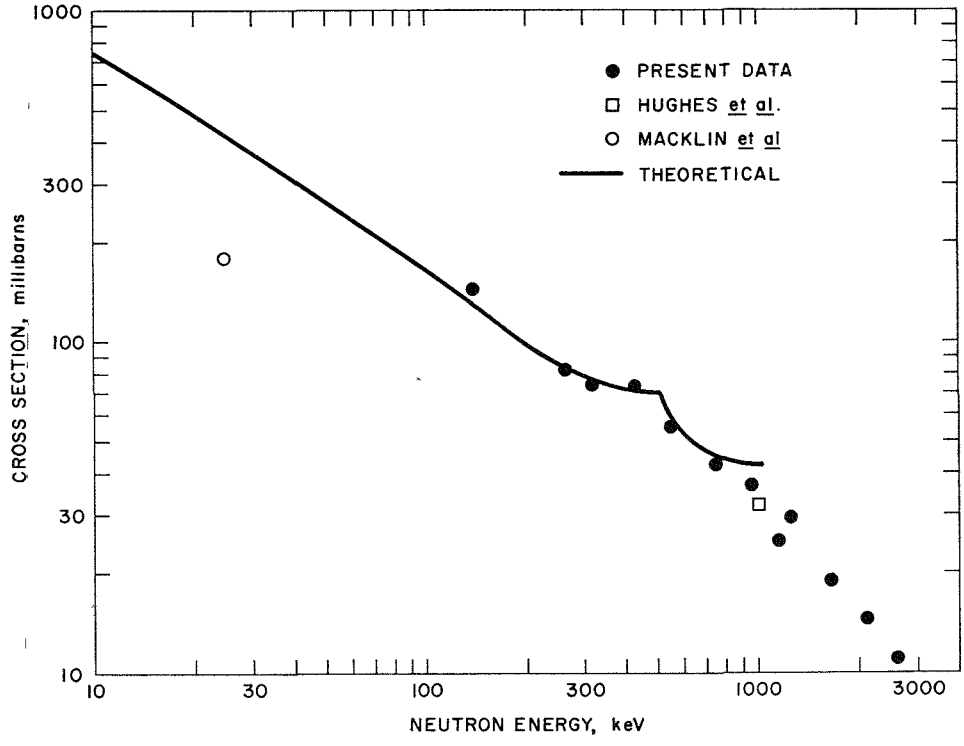

308-413

FIG. VI-3. Radiative Capture Cross Section of Rubidium-85.

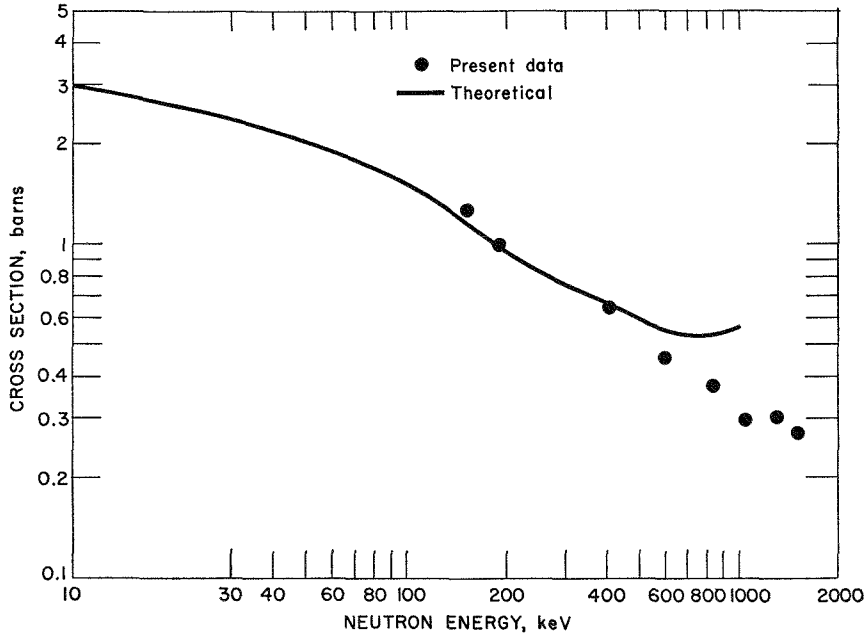

308-426

FIG. VI-4. Radiative Capture Cross Section of Neptunium-237.

The experimental method is the neutron activation technique in which a sample is irradiated in a monoenergetic neutron beam and counted with a beta or gamma ray counter. Monoenergetic neutrons are produced by bombarding lithium or tritium targets with protons from the Van de Graaff accelerator.

Measurements of the radiative capture cross sections of ^{41}K, ^{55}Mn, ^{85}Rb, and ^{237}Np have been completed. The data are shown in Figures VI-1 to VI-4, along with the results of other workers[2–6] when available. The standard deviations of the cross-section values are approximately $\pm 8\%$, and the neutron energy spreads for the present data are generally wide enough so that the spreads of adjacent points just overlap.

The experimental results have been compared with calculations using the statistical model of the compound nucleus, which gives compound nuclear cross sections averaged over resonances. The curves given in the figures were calculated using the model in the form given by Moldauer[7–9] in which the average compound nuclear cross section for capture of neutrons of energy E is given by

$$\sigma_{\text{cap}} = \pi^2 \lambda\!\!\!^{-2} \sum_{J\pi} \frac{2J+1}{2I_o+1} \langle \Gamma_o^{J\pi} \rangle \rho_{J\pi} \frac{\langle \Gamma_{\text{cap}}^{J\pi} \rangle}{\Gamma^{J\pi}} S^{J\pi}$$

where $\lambda\!\!\!^{-}$ is the deBroglie wavelength of the neutron; I_o is the spin of the ground state of the target nucleus; $\langle \Gamma^{J\pi} \rangle$ is the average total width of compound states with spin J, parity π, and density $\rho_{J\pi}$, at excitation energy $U + E$, where U is the neutron separation energy in the compound nucleus; $\langle \Gamma_o^{J\pi} \rangle$ is the average partial width for emission of elastic neutrons; and $S^{J\pi}$ is the width fluctuation correction factor.

The calculations also include the variation of radiation width and level density with excitation energy and spin of the compound nucleus, and the variation of neutron widths from level to level.

The experimental data are accurately predicted by the theory for ^{41}K, ^{55}Mn, and ^{85}Rb, at least up to neutron energies at which the energy levels of the target nucleus are known. In the case of ^{237}Np, the range over which the comparison can be made is limited because the lower energy data have not yet been measured.

[2] R. Booth, W. P. Ball, and M. H. MacGregor, Phys. Rev. **112**, 226 (1958).

[3] D. J. Hughes, R. C. Gorth, and J. S. Levin, Phys. Rev. **91**, 1423 (1953).

[4] Yu. Ya. Stavissky and V. A. Tolstikov, At. Energ. **10**, 508 (1961).

[5] A. E. Johnsrud, M. G. Silbert, and H. H. Barschall, Phys. Rev. **116**, 927 (1959).

[6] R. L. Macklin, N. H. Lazar, and W. S. Lyon, Phys. Rev. **107**, 504 (1957).

[7] P. A. Moldauer, C. A. Engelbrecht, and G. J. Duffy, Nearrex: Computer Code for Nuclear Reaction Calculations, ANL-6978.

[8] P. A. Moldauer, Rev. Mod. Phys. **36**, 1079 (1964).

[9] P. A. Moldauer, Phys. Rev. **135**, B642 (1964).

B. CAPTURE-TO-FISSION RATIOS IN EBR-II (D. C. Stupegia, A. A. Madson)

In calculating the breeding gain of a reactor one needs to know the distribution of neutron energies in the reactor, and the fission, scattering, and absorption cross sections as a function of neutron energy for the various materials used in the reactor. When sets of data as complete as this are lacking, or highly difficult to obtain, it is useful to obtain the ratio of the capture and fission cross sections of the fissile or fertile species in a given reactor spectrum. The object of this program is the measurement of the ratio of the capture and fission cross sections of ^{233}U, ^{238}U, ^{239}Pu, ^{240}Pu, and ^{242}Pu as a function of position in EBR-II.

The general experimental approach to this work is to measure the number of fissions in each sample by beta and gamma counting of the fission product ^{137}Cs, and to measure the number of captures by mass spectrometry. In order to obtain a sufficient build-up of the capture and fission products, samples of uranium and plutonium were placed in subassemblies in EBR-II over a year ago (see ANL-7055, p. 232). All sample-containing subassemblies will have received sufficient irradiation by about February 1967, and will be removed from the reactor and returned to Argonne by that time.

In the meanwhile, the major work in this program has been directed toward the development and testing of analytical and radioactive counting techniques needed for analysis of the samples. In particular, alpha and beta counters are being assembled and tested for use in the assay of alpha-active capture products and in the determination of fission product ^{137}Cs. Further, uranium and plutonium samples are being irradiated in CP-5 under conditions simulating those of EBR-II samples. These samples will be used to test the dissolution, chemical separation, and counting procedures which will be applied to the EBR-II samples.

Finally, for a logical extension of the capture-to-fission ratio work, suitable samples of ^{238}Pu and ^{241}Pu have been recently acquired. It is intended that samples of these two isotopes, which were not available earlier, will be irradiated in EBR-II and their capture-to-fission ratios determined.

VII

Analytical Research and Development[1]

(R. P. Larsen, R. J. Meyer)

The program for the development of analytical methods for the determination of burnup of fast reactor fuels and for the measurement of fast fission yields is continuing. A method for determining burnup by a total rare earth analysis is being developed. After separation from interferences by precipitation and ion exchange, the rare earths are determined by a complexiometric titration. Using lanthanum as a stand-in for the rare earth fission products, the compatibility of the separation procedure and titration has been demonstrated.

A neutron activation method for the determination of fission product praseodymium-141 in irradiated nuclear fuels has been developed. Separation from uranium and other fission products is effected by precipitation and ion exchange; the assay is accomplished by neutron activation using manganese-55 as an internal flux monitor.

[1] A summary of this section is given on page 15.

A. TOTAL RARE EARTHS FOR MONITORING BURNUP (R. J. Meyer, R. D. Oldham)

A method for determining burnup by means of a total rare earth analysis is under development. After the rare earths are separated from interferences, a photometric titration with ethylenediaminetetraacetic acid (EDTA) is performed using arsenazo as the indicator. The advantages of and prerequisites for this method of burnup analysis, as well as a more detailed description of the titration, were reported in ANL-7125, p. 241. The results reported there indicate that, providing a satisfactory procedure for separating interferences can be established, 500 μg of rare earths (the rare earth content of 200 mg of 1% burnup fuel) can be determined with an accuracy of $\pm 0.5\%$.

Since several of the other elements present in an irradiated fuel, e.g., uranium, zirconium, and yttrium, will either form colored complexes with arsenazo, or react with EDTA, the titration must be preceded by a separation which isolates the rare earths from those constituents. In addition, such anions as fluoride and phosphate, which form strong complexes with the rare earths, must be absent.

From the data obtained by Korkisch and Tera[2] it appeared that the separation of the rare earths from all interferences could be made by absorbing the rare earths on Dowex-1 from a nitric acid-methanol solution and eluting them with dilute nitric acid. A detailed description of the anion exchange procedure was reported in ANL-7225, p. 229. The results reported there indicate that the separation is compatible with the EDTA titration and that the recovery of the rare earths is quantitative.

For samples having burnups of 0.5% or less, the use of ion exchange alone to separate the rare earths becomes impractical. At a burnup of 0.5% the amount of uranium in the aliquot is 500 mg, and the ion exchange column must, of necessity, be large and unwieldy. In such cases, a preliminary separation to remove the bulk of the uranium is desirable. Precipitation of the rare earths using calcium fluoride as a carrier accomplishes this separation. Results reported in ANL-7225, pp. 229–230, showed that the rare earths were quantitatively precipitated and that less than 0.5% of the uranium was carried on the precipitate.

However, when the precipitation procedure was checked for compatibility with the titration, the re-

[2] J. Korkisch and F. Tera, Anal. Chem. **33**, 1264 (1961).

sults were high and erratic. This strongly indicated that a contaminant, such as iron, was being introduced. This interference was overcome by performing the titration in the presence of diethyldithiocarbamate,[3] a reagent which forms strong complexes with elements having insoluble sulfides.

[3] J. Fritz, R. Oliver, and D. Pietrzyk, Anal. Chem. **30**, 1111 (1958).

The compatibility of the combined precipitation and anion exchange separation with the modified titration was checked using known amounts of lanthanum. For 6 trials the relative standard deviation was a very acceptable ±0.9% and there was no observable bias.

Work is now proceeding on testing of the entire procedure with a mixture of rare earths which will simulate the relative amounts expected in an irradiated fuel sample.

B. DETERMINATION OF THE FAST FISSION YIELD OF PRASEODYMIUM-141 BY NEUTRON ACTIVATION ANALYSIS (R. J. Meyer, K. K. Pillay[4])

Praseodymium-141 (stable) is a potentially useful burnup monitor for both fast and thermal reactor fuels. It has a high fission yield, the half lives of its volatile precursors, xenon and cesium, are very short, and it is not a constituent of virgin or reprocessed fuels. To date, however, there have been no analytical techniques which could provide the combination of sensitivity, selectivity, and accuracy required for the determination of praseodymium-141 in irradiated fuel. Consequently, neither the fast nor thermal fission yield of this nuclide has been measured, nor has it been considered as a burnup monitor.

A method for the determination of praseodymium-141 was reported in ANL-7225, pp. 230–232. In this method, praseodymium is separated from interferences by solvent extraction, precipitation, and ion exchange, and then detected by neutron activation using manganese-55 as the internal flux monitor. The method had been tested on synthetic uranium-fission product mixtures and found to be satisfactory.

However, when the method was applied to actual fuel samples (EBR-I, Mark III loading), the praseodymium was contaminated with cesium-137, yttrium-90, and promethium-147. The presence of cesium-137 is undesirable because it is a radiation hazard in subsequent handling of the praseodymium. Promethium-147 and yttrium-90 are serious interferences in the counting of the activation products. Promethium-148, formed on activation of promethium-147, has gammas at both 0.91 and 1.48 Mev which interfere with the assay of manganese-56 (0.845 Mev) and praseodymium-142 (1.57 Mev). Yttrium-90 has a gamma at 1.7 Mev which interferes with the assay of praseodymium-142.

The separation procedure has been revised to eliminate these difficulties. The major separation from uranium is now effected by a fluoride precipitation using lanthanum as a carrier. Separation from cesium-137 is effected by a lanthanum hydroxide precipitation in the presence of cesium hold-back carrier. Further separation from promethium and yttrium is effected by a second cation exchange separation.

A synopsis of the revised procedure is given below.

1. Lanthanum carrier, cesium hold-back carrier, and praseodymium-142 tracer (19.2 hr) are added to the fuel solution.
2. The rare earths are separated from the bulk of uranium and zirconium by precipitating the rare earth fluorides with excess hydrofluoric acid.
3. The rare earth fluorides are dissolved in a nitric acid-saturated boric acid mixture and the rare earth hydroxides precipitated using ammonium hydroxide.
4. The hydroxide precipitate is dissolved in concentrated hydrochloric acid and passed through a Dowex 2 × 10 (200 to 400 mesh) ion exchange column to remove the residual amount of uranium.
5. The eluant is evaporated and fumed repeatedly with perchloric acid to eliminate ruthenium.
6. The individual rare earths are separated by a double cation exchange (Dowex 50W × 12) separation using α-hydroxyisobutyric acid as the elutriant.
7. Residual cerium is removed from the praseodymium fraction on a column packed with a mixture of lead dioxide and Dowex 1 × 2 (200 to 400 mesh) resin.
8. The praseodymium recovery is determined by counting the praseodymium-142 activity in the collected fraction and comparing it with a standard.

[4] Resident Research Associate.

9. The internal flux monitor, manganese-55, is added to both the samples and standards and they are irradiated in a thermal neutron flux.
10. The praseodymium and manganese are precipitated using a mixture of ammonium chloride, ammonium hydroxide and ammonium persulfate.
11. The sample and standards are gamma-assayed for manganese-56 and praseodymium-142 and the weight of praseodymium-141 in the sample is calculated from the results.

Several samples of EBR-I fuel material have been subjected to the first eight steps of the revised procedure. The praseodymium recovery was satisfactory, about 75%, and the praseodymium was free of cesium-137, yttrium-90, and promethium-147.

To establish the fast fission yield of praseodymium-141, it will be necessary to relate the praseodymium content of the fuel to that of a fission product whose yield is known, namely, cesium-137. The cesium-137 analyses, as well as additional praseodymium analyses, are now in progress.